Lecture Notes in Biomathematics

Managing Editor: S. Levin

87

P. Dallos C.D. Geisler J.W. Matthews
M.A. Ruggero C.R. Steele (Eds.)

The Mechanics and Biophysics of Hearing

Proceedings, Madison, WI, 1990

Springer-Verlag

Lecture Notes in Biomathematics

Managing Editor: S. Levin

87

P. Dallos C.D. Geisler J.W. Matthews
M.A. Ruggero C.R. Steele (Eds.)

The Mechanics and Biophysics of Hearing

Proceedings of a Conference held at the
University of Wisconsin, Madison, WI, June 25–29, 1990

Springer-Verlag
Berlin Heidelberg New York London
Paris Tokyo Hong Kong Barcelona

Editorial Board

Ch. DeLisi M. Feldman J.B. Keller M. Kimura
S. Levin (Managing Editor) R. May J.D. Murray G.F. Oster
A.S. Perelson L.A. Segel

Editors

Peter Dallos
Auditory Physiology Laboratory and Department of Neurobiology
and Physiology, Northwestern University
Evanston, IL 60208, USA

C. Daniel Geisler
Department of Neurophysiology and Department of
Electrical and Computer Engineering
University of Wisconsin-Madison,
Madison, WI 53706, USA

John W. Matthews
Computer Systems Laboratory, Washington University
St. Louis, MO 63110, USA

Mario A. Ruggero
Department of Otolaryngology, University of Minnesota
Minneapolis, MN 55414, USA

Charles R. Steele
Division of Applied Mechanics, Stanford University,
Stanford, CA 94305, USA

Mathematics Subject Classification (1980): 92-06

ISBN 3-540-97473-3 Springer-Verlag Berlin Heidelberg New York Tokyo
ISBN 0-387-97473-3 Springer-Verlag New York Heidelberg Berlin Tokyo

This work is subject to copyright. All rights are reserved, whether the whole or part of the material is concerned, specifically the rights of translation, reprinting, re-use of illustrations, recitation, broadcasting, reproduction on microfilms or in other ways, and storage in data banks. Duplication of this publication or parts thereof is only permitted under the provisions of the German Copyright Law of September 9, 1965, in its current version, and a copyright fee must always be paid. Violations fall under the prosecution act of the German Copyright Law.

© Springer-Verlag Berlin Heidelberg 1990
Printed in Germany

Printing and binding: Beltz Offsetdruck, Hemsbach/Bergstr.
2146/3140-543210 – Printed on acid-free paper

Introduction

This compendium represents the proceedings of a five-day symposium held at the University of Wisconsin, Madison between June 25 and 29, 1990. The remarkably rapid progress of hearing science during the past twenty years has been punctuated by two series of international symposia. One series began as meetings whose purpose it was to bring physiologists and psychophysicists together. These triennial meetings continue to the present time at various locations in Europe. A second series of meetings has been designed to enhance interchange among neurobiologists, biophysicists and mathematical modelers dealing with cochlear function. The present volume is the latest in this second series.

In the late seventies and early eighties hearing science entered a revolutionary state in which many fundamental tenets of the cochlea's functioning required reassessment. Key discoveries, among them outer hair cell influence upon cochlear output, otoacoustic emissions, outer hair cell motility and multiplicity of schemes of producing cochlear tuning in different species, provided the rungs of the ladder upon which we climb. The frame of the ladder was made of new and refined techniques applied to cochlear measurements that permitted new views of the system. The assimilation and invention of techniques for measuring low-level motion and force, intracellular measurements *in vivo* and a bewildering array of *in vitro* methods, including those examining single channel properties and cell motility, yielded a cornucopia of data . The emerging view of the mammalian cochlea, based on these methods and experiments, is that of a highly nonlinear distributed feedback system, in which outer hair cells provide local mechanical feedback to the basilar membrane-tectorial membrane complex under stimulus and efferent control to produce the remarkable frequency selectivity and sensitivity of the auditory periphery.

Being an extraordinarily complex mechano-hydraulic and bio-electric system, the cochlea has fascinated physicists and engineers since Helmholtz' time. The past decade's developments in the laboratory were paralleled by advances in computing and modeling. An additional element that made recent modeling efforts particularly valuable is a new and highly developed communication process among experimenters and modelers. To this end, symposia have been organized with the avowed purpose of bringing these two species together and fostering their intermarriage. The Madison meeting continues a series of such international symposia focused on cochlear function. It follows in the spirit of the first of these meetings at Delft in 1983 (*Mechanics of Hearing,* Edts. E. de Boer and M.A. Viergever, Delft University Press, Delft, 1983) as well as the previous meeting at Keele in 1988 (*Cochlear Mechanisms*, Edts. J.P. Wilson and D.T. Kemp, Plenum Press, New York, 1989). The tradition of these symposia will continue, providing the periodic overviews and summaries that are so necessary in a rapidly advancing discipline.

As the table of contents indicates, we achieved an excellent balance between theoreticians and experimentalists, reflecting the healthy state of the field. It is also apparent that many ingredients necessary for understanding cochlear function are present in this volume. We begin with experiments and models pertaining to the physiology and motility of individual hair cells and address one of the key issues: what is the relevance of motility to cochlear mechanics? The book continues with several papers on general cochlear physiology and with a major section on otoacoustic emissions. The study of these emitted sounds, whose origin is in the cochlea, has been one of the most profitable avenues of recent inquiry. Another productive line of research, measuring macromechanical movements with ever increasing precision, dates back to Békésy's work and is producing some of the most definitive information about cochlear function. Our compendium closes with two sections on general and nonlinear cochlear models.

The symposium on The Mechanics and Biophysics of Hearing was supported by the National Institute of Deafness and other Communication Disorders (DC00009-01) and by the National Science Foundation (BNS-8919879). We thank the Department of Neurophysiology, University of Wisconsin for its hospitality and the departmental staff for their untiring efforts on the conference's behalf. Particular thanks are extended to P. Heinritz, R. Klipstein and R. Sorensen . The conference logo was designed by C. Dizack. The editors dedicate this volume to the memory of the late modeler-experimenter, Juergen Tonndorf who passed away last year.

August, 1990

Peter Dallos
C. Daniel Geisler
John W. Matthews
Mario A. Ruggero
Charles R. Steele

Introduction III

CONTENTS V

1. Hair Cell and Cilia 1
Calcium ions and the adaptation of the transducer current in turtle cochlear hair cells 2
M.G. Evans, R. Fettiplace and A.C. Crawford
Structural abnormalities in inner hair cells following kanamycin-induced outer hair cell loss 10
C.M. Hackney, D.N. Furness and P.S. Steyger
Modelling input-output characteristics of the inner hair cell 18
J.W. Horst and P.C. de Jong
Calcium ions promote rapid mechanically evoked movements of hair bundles 26
F: Jaramillo, J. Howard and A.J. Hudspeth
Modulation of voltage responses to 100 Hz tones by high frequency tones in cochlear hair cells 34
M. Kössl and I.J. Russell
Movements and mechanical properties of ampullary hair bundles and of their kinocilium 42
A. Rüsch and U. Thurm

2 Hair Cell Motility 51
The effect of cytoplasmic turgor pressure on the static and dynamic mechanical properties of outer hair cells 52
W.E. Brownell and W.E. Shehata
The nonlinearity of outer hair cell motility: implications for cochlear physiology and pathology 61
B.N. Evans, R. Hallworth and P. Dallos
Fast outer hair cell motility: how fast is fast? 69
J. Santos-Sacchi
Elastic behavior of the outer hair cell wall 76
C.R. Steele

3. Relevance of Motility to Macromechanics 85
A model for cochlear vibrations based on feedback from motile outer hair cells 86
C.D. Geisler and X. Shan
Does the cochlear amplifier produce reactive or resistive forces? 96
P.J. Kolston and G.F. Smoorenburg
The basilar membrane nonlinear input-output function 106
G.K. Yates
Active cochlear feedback: Required structure and response phase 114
J.J. Zwislocki

4. Electrophysiology 121
Spontaneous activity of auditory afferent neurones in the spiral ganglion of the pigeon 122
A.W. Gummer
Two-tone rate suppression in auditory nerve fibers: Time course of suppression and excitation in peri-stimulus time histograms 132
K.G. Hill and A.R. Palmer
Further evidence for tuning mechanisms of high dynamic order in lower vertebrates 139
E.R. Lewis, M.G. Sneary and X. Yu
Observations on structure and function of the olivocochlear projections in cat 147
M.C. Liberman
The sting is in the tail 154
V.F. Prijs, J. Keijzer, R. Schoonhoven and H. Versnel

5. Emissions 163
Can basilar membrane tuning be inferred from distortion measurement? 164
A.M. Brown and S.A. Gaskill
Changes in stimulus frequency otoacoustic emissions produced by two-tone suppression and efferent stimulation in cats 170
J.J. Guinan, Jr.
Growth functions of tone burst evoked and distortion-product otoacoustic emissions in humans 178
F.P. Harris and R. Probst
Sound induced changes in electrically evoked cochlear emissions 186
A.E. Hubbard, H.H. Nakajima, E.S. Olson and D.C. Mountain
Chaotic dynamics of otoacoustic emissions 194
D.H. Keefe, E.M. Burns, R. Ling and B. Laden
Observations on simultaneous SFOAE and DPOAE generation and suppression 202
D.T. Kemp, D.N. Brass and M. Souter
Components of the $2f_1$-f_2 distortion product in the earcanal of the bobtailed lizard 210
G.A. Manley, C. Köppl and B.M. Johnstone
Active and passive ADP components in mammalian and avian ears 219
S.J. Norton and E.W. Rubel
A generalized Van der Pol-oscillator cochlea model 227
M.P.M.G. Van den Raadt and H. Duifhuis
Quantitative evaluation of limit-cycle oscillator models of spontaneous otoacoustic emissions 235
C.L. Talmadge, G.R. Long, W.J. Murphy and A. Tubis
Actively and passively generated acoustic distortion at $2f_1$-f_2 in rabbits 243
M.L. Whitehead, B.L. Lonsbury-Martin and G.K. Martin
Effects of tympanic membrane modification on distortion product otoacoustic emissions in the cat ear canal 251
M.L. Wiederhold
Spontaneous otoacoustic emission generators behave like coupled oscillators 259
H.P. Wit

6. Macromechanical Measurements 269
Measurement of middle ear transfer function in cat, chinchilla and guinea pig 270
L. Décory, R.B. Franke and A.L. Dancer
Helmholtz revisited: direct mechanical data suggest a physical model for dynamic control of mapping frequency to place along the cochlear partition 278
E.L. LePage
Measurements of basilar membrane tuning and distortion with laser Doppler velocimetry 288
A.L. Nuttall, D.F. Dolan and G. Avinash
In vivo measurement of basilar membrane stiffness 296
E.S. Olson and D.C. Mountain
Two-tone distortion products in the basilar membrane of the chinchilla 304
L. Robles, M.A. Ruggero and N.C. Rich
Systemic injection of furosemide alters the mechanical response to sound of the basilar membrane 314
M.A. Ruggero and N.C. Rich

7. General Cochlear Models 323
Modeling the noise damaged cochlea 324
J.B. Allen
Wave propagation modes and boundary conditions for the Ulfendahl-Flock-Khanna (UFK) preparation 333
E. de Boer
On dipoles and the radiating membrane 340
J.S.C. van Dijk
Approximate evaluation of cochlear model tuning from the wave development graph 348
S.M. Novoselova
The fractal doubly stochastic Poisson point process as a model for the cochlear neural spike train 354
M.C. Teich, R.G. Turcott and S.B. Lowen
The impedance of the organ of Corti 362
G. Zweig

8. Nonlinear Models 371
Implementation of a nonlinear wave-digital filter cochlear model 372
D.H. Friedman
Nonlinear transmission line model can predict the statistical properties of spontaneous otoacoustic emissions 380
M. Furst
Mathematical analysis of a nonlinear model for hybrid filtering in the cochlea 387
J.L. Goldstein
Automatic gain control in cochlear mechanics 395
R.F. Lyon
Non-linearity in a computational model of the response of the basilar membrane 403
R. Meddis, M.J. Hewitt and T.M. Shackleton
Level dependence of the latency of cochlear transients 411
S.T. Neely

Section 1

Hair Cell and Cilia

CALCIUM IONS AND THE ADAPTATION OF THE TRANSDUCER CURRENT IN TURTLE COCHLEAR HAIR CELLS

M.G. Evans, R. Fettiplace and A.C. Crawford.

The Physiological Laboratory,
University of Cambridge, Cambridge, CB2 3EG, UK.

Introduction

If a maintained displacement is imposed upon the ciliary bundle of a hair cell, many of the transducer channels that initially open in response to the stimulus eventually close. This process of adaptation of the transducer current has been investigated in several preparations, by delivering test steps to the bundle following a conditioning step to induce adaptation. The results of such experiments have shown that even after the transducer current has declined extensively from its initial peak value, the transducer channels can still be re-opened by further displacement of the cell's ciliary bundle towards the kinocilium (Corey & Hudspeth. 1983a,b; Eatock, Corey & Hudspeth, 1987; Assad, Hacohen & Corey, 1989; Crawford, Evans & Fettiplace, 1989). There is therefore no evidence that transducer channels enter a true inactivated state.

If the relationship between transducer current and displacement is examined before and after an adapting step, the activation curve of the transducer is found to shift to more positive displacements (Corey & Hudspeth, 1983a; Eatock, Corey & Hudspeth, 1987) and the slope of the activation curve to become steeper (Crawford, Evans & Fettiplace, 1989).

Recently, it has become apparent that intracellular calcium ions play an important role in controlling the process of adaptation both in the hair cells of the bullfrog's sacculus (Eatock, Corey & Hudspeth, 1987; Assad, Hacohen & Corey, 1989) and in cochlear hair cells of the turtle (Crawford, Evans & Fettiplace, 1989). Here we extend these observations on the role of calcium on adaptation, by measuring transducer currents under whole-cell patch clamp in isolated hair cells of the turtle's cochlea.

Materials and Methods

Hair cells were isolated from the basilar papilla of *Pseudemys scripta elegans* by the methods described fully in Art & Fettiplace (1987) and Crawford, Evans & Fettiplace (1989). After plating out onto coverslips coated with concanavalin A to immobilize the cell's body, the ciliary bundle was manipulated using a glass stylus

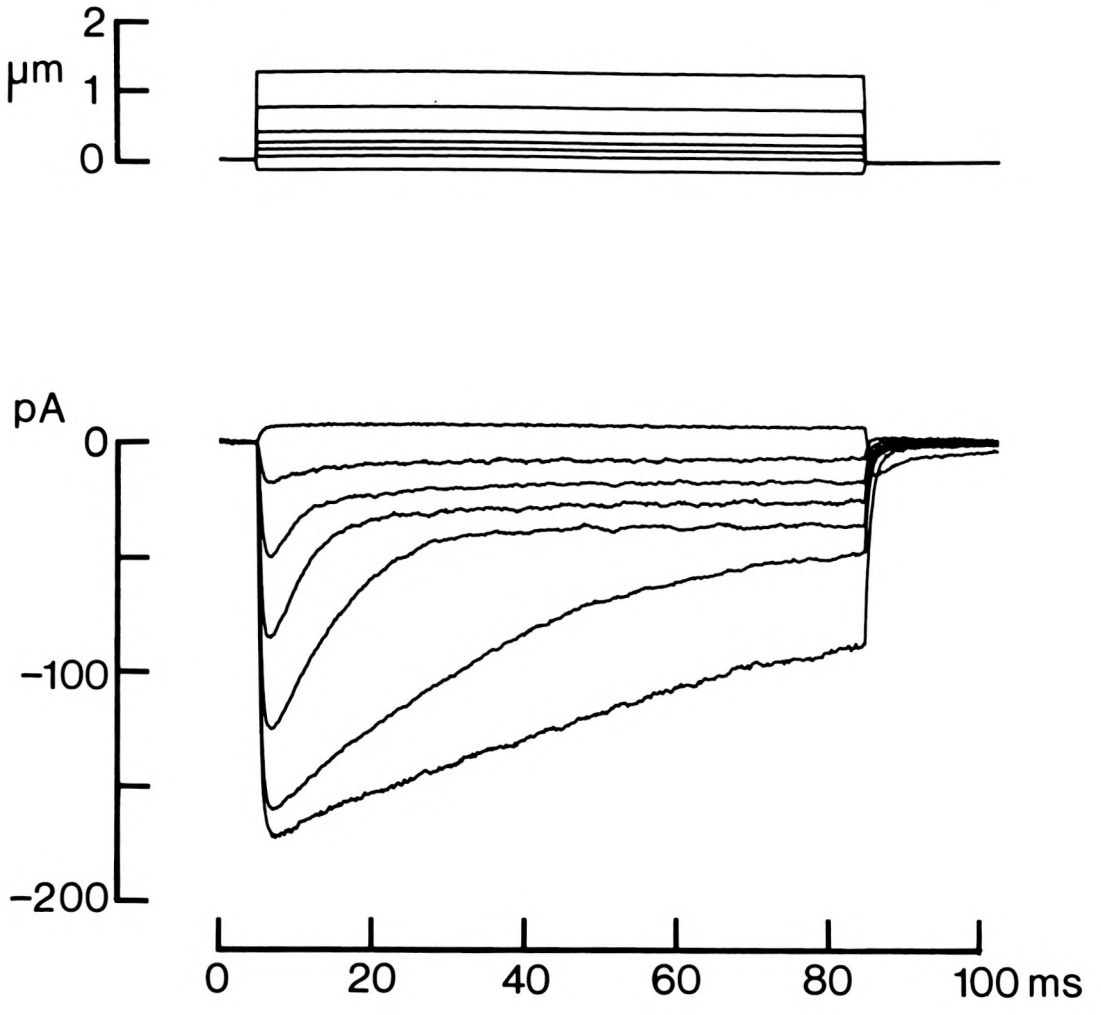

FIGURE 1 Decline or adaptation in transducer currents during 80 ms displacements of the ciliary bundle. Stimulus monitor is shown above with displacements towards the kinocilium displayed as positive. Holding potential -74 mV. Between 20 and 160 responses averaged for each trace. Note that the time course of adaptation is level dependent.

attached to a piezo-electric bimorph. Details of the stimulation equipment and its calibration are also given in Crawford, Evans & Fettiplace (1989). The cell's bundle could be stepped from one position to another in less than 100 μs. All experiments were started in a saline (the control solution) containing (in mM) NaCl, 130; KCl, 4; $CaCl_2$, 2.8; $MgCl_2$, 2.2; NaHEPES, 5; glucose, 4; pH 7.6. Experiments were performed at 18–23° C using at temperature-controlled microscope stage (Crawford & Fettiplace, 1987).

Transduction currents were measured using the whole-cell patch-clamp technique of Hamill, Neher, Marty, Sakmann & Sigworth (1981). Patch pipettes were usually filled with a solution containing (in mM) KCl, 125; $MgCl_2$, 3; K-HEPES, 5; EGTA, 5; Na_2ATP, 2.5; pH adjusted to 7.2 with KOH. For experiments where the membrane potential was clamped to depolarized levels, the patch pipette was filled with a solution based on CsCl rather than KCl, in order to block the potassium currents of the basolateral membranes.

The ionic environment of the cell was changed using the rapid U-tube superfusion system of Krishtal & Pidoplichko (1980) and Fenwick, Marty & Neher (1982).

Under the best conditions, when the U-tube was positioned close to the cell, the calcium concentration at the cell's membrane could be lowered to a new value within 500 ms. Solutions containing reduced concentrations of calcium were calibrated using a calcium-sensitive electrode (WPI).

Results

EFFECTS OF DEPOLARIZATION ON ADAPTATION

A typical family of transducer currents, produced in response to a range of steps imposed upon a cell's ciliary bundle is shown in Fig.1. These records were obtained in control solution (2.8 mM $CaCl_2$; 2.2 mM $MgCl_2$) and at a holding potential of - 74 mV. Such a holding potential is a little more negative than the normal resting potential of these cells (- 50 to -55 mV). In this and all subsequent records inward transducer currents are plotted downwards, and the stimulus monitor above the current records shows a displacement towards the cell's kinocilium (the excitatory direction) as positive. Note that i) the responses to equal steps towards and away from the kinocilium are highly asymmetrical, ii) the onsets and offsets of these currents occur within a millisecond or two, and iii) the currents for the larger steps towards the kinocilium relax back from their peak values (adaptation).

An example of transducer currents measured in another cell when the holding potential was clamped to +66 mV is shown in Fig. 2B. For comparison, control records from the same cell when held at a potential of -74 mV are shown in Fig. 2A. The pipette solution in this experiment contained CsCl as the principal cation to suppress the opening of voltage- and calcium-activated potassium channels that normally populate the baso-lateral membranes of these cells (Art & Fettiplace, 1987) as they do in the hair cells of the bullfrog's sacculus (Lewis & Hudspeth, 1983). The principal effect of depolarizing the cell to positive membrane potentials is to invert the direction of current flow, since the reversal potential for the transducer current lies close to a potential of 0 mV (Corey & Hudspeth, 1979; Crawford & Fettiplace, 1981). While there are several other effects of depolarizing the cell, one of the most striking is the disappearance of adaptation at positive membrane potentials. Similar observation have been made by Assad *et al.* (1989) in the hair cells of the bullfrog's sacculus. One explanation for this effect is that calcium ions normally enter the stereocilia along with the transducer current (Ohmori, 1985), and then induce adaptation by acting at an intracellular site. Thus depolarizing the cell reduces the driving force on calcium entry and hence removes adaptation.

Further evidence in favour of this hypothesis comes from recent experiments where cells were filled through the patch electrode with the rapid calcium buffer BAPTA (Crawford, Evans & Fettiplace, 1989). This agent should reduce or prevent changes in the intracellular calcium concentration which would otherwise occur due to calcium entry through the transducer channels on stimulation. Its effects are indeed consistent with the hypothesis that adaptation is regulated by intracellular calcium; BAPTA removes or greatly slows the rate of adaptation as compared to that seen in control cells filled with normal intracellular solution.

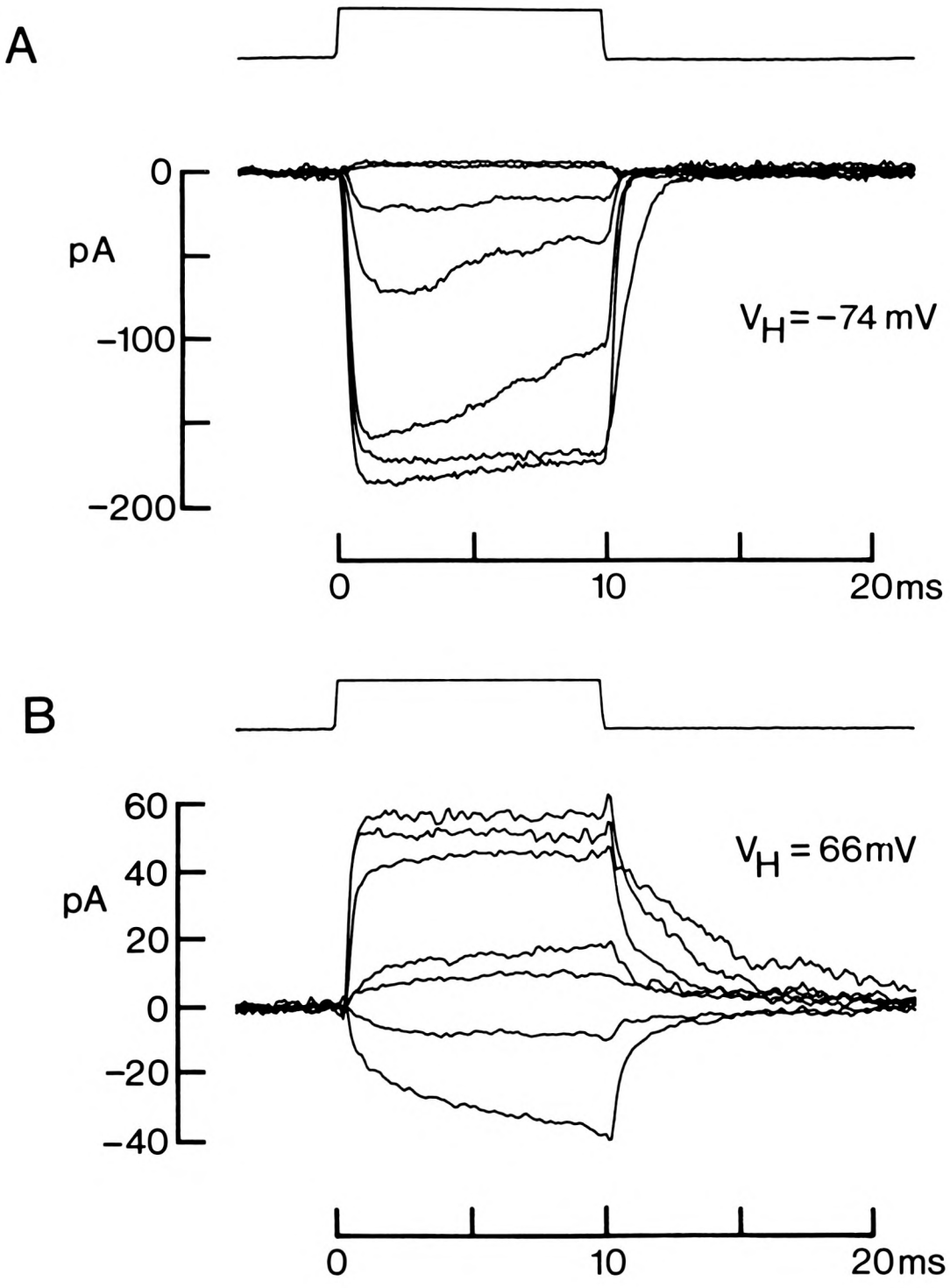

FIGURE 2 Effects of depolarization on the form of the transducer current. Families of currents at holding potentials of -74 mV (A) and +66 mV (B). Time course of displacement step is shown above the traces; the amplitudes, the same for the two families were (in m): 0.05, 0.1, 0.25, 0.5, 0.75. Note that the polarity of the current is reversed and adaptation is lost in B.

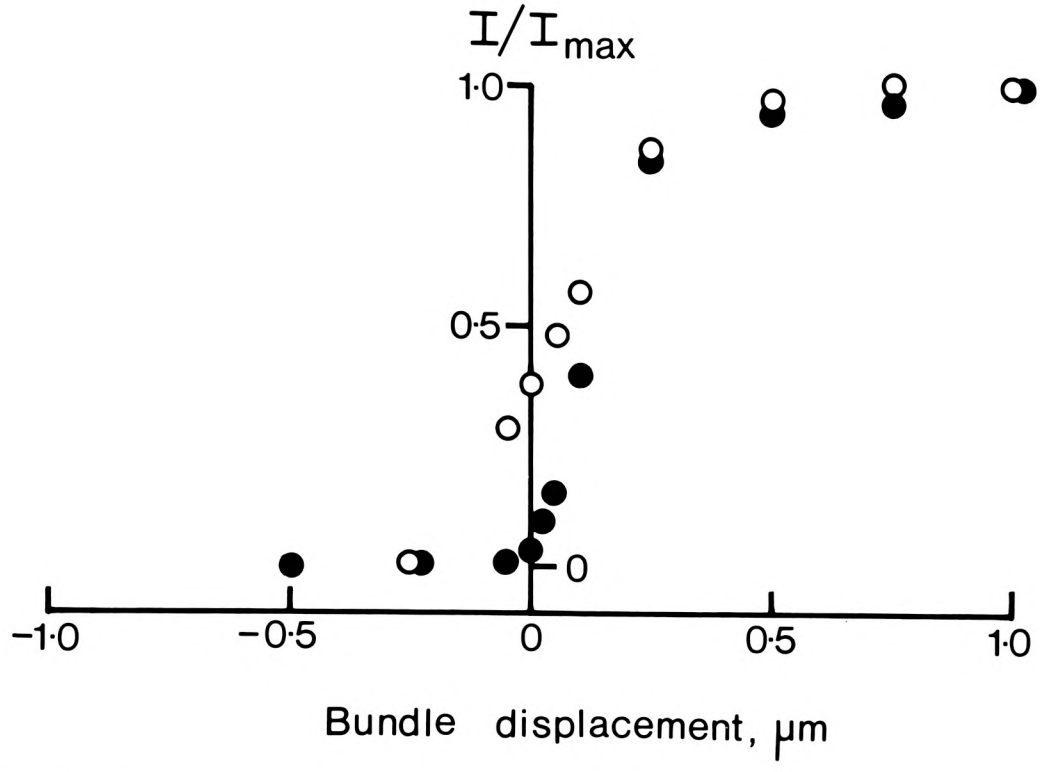

FIGURE 3 Peak current-displacement relationships constructed from the traces shown in Fig. 2. The ordinate is the current, I, scaled to its maximum value, I_{max}. Holding potential -74 mV (filled circles) and +66 mV (open circles). Note that the activation curve is shifted to more negative displacements by depolarization.

Apart from the loss of adaptation, depolarization produces two other important changes. Firstly, the rate at which the transducer current turns off is considerably slowed at depolarized potentials (compare Figs. 2A & 2B). This action is especially striking at the termination of the stimulus. The second feature is that the activation curve of the transducer (the relationship between transducer current and bundle displacement) is altered by depolarization. This effect is illustrated in detail in Fig. 3 which shows normalized current-displacement curves for the cell of Fig. 2 measured at -74 mV (filled circles) and again at +66 mV (open circles). Depolarization both shifts the activation curve to more negative displacements and reduces the gradient of the steepest part of the curve. The combined effect of these changes is to alter the fraction of the transducer conductance that is turned on at the resting position of the bundle; in the cell of Fig. 3 only about 10% of the transducer channels are open when the bundle is undisturbed, while at +66 mV this fraction rises to about 40%.

EFFECTS OF REDUCED EXTRACELLULAR CALCIUM

It has been reported that reducing the external calcium concentration slows the rate of adaptation of the microphonic current in bullfrog's saccular hair cells (Eatock *et al*, 1987). This observation is of some importance since in the mammalian cochlea at least, the calcium concentration of the endolymph is only about 30 M (Bosher & Warren, 1978). We have investigated this action using a rapid perfusion system to

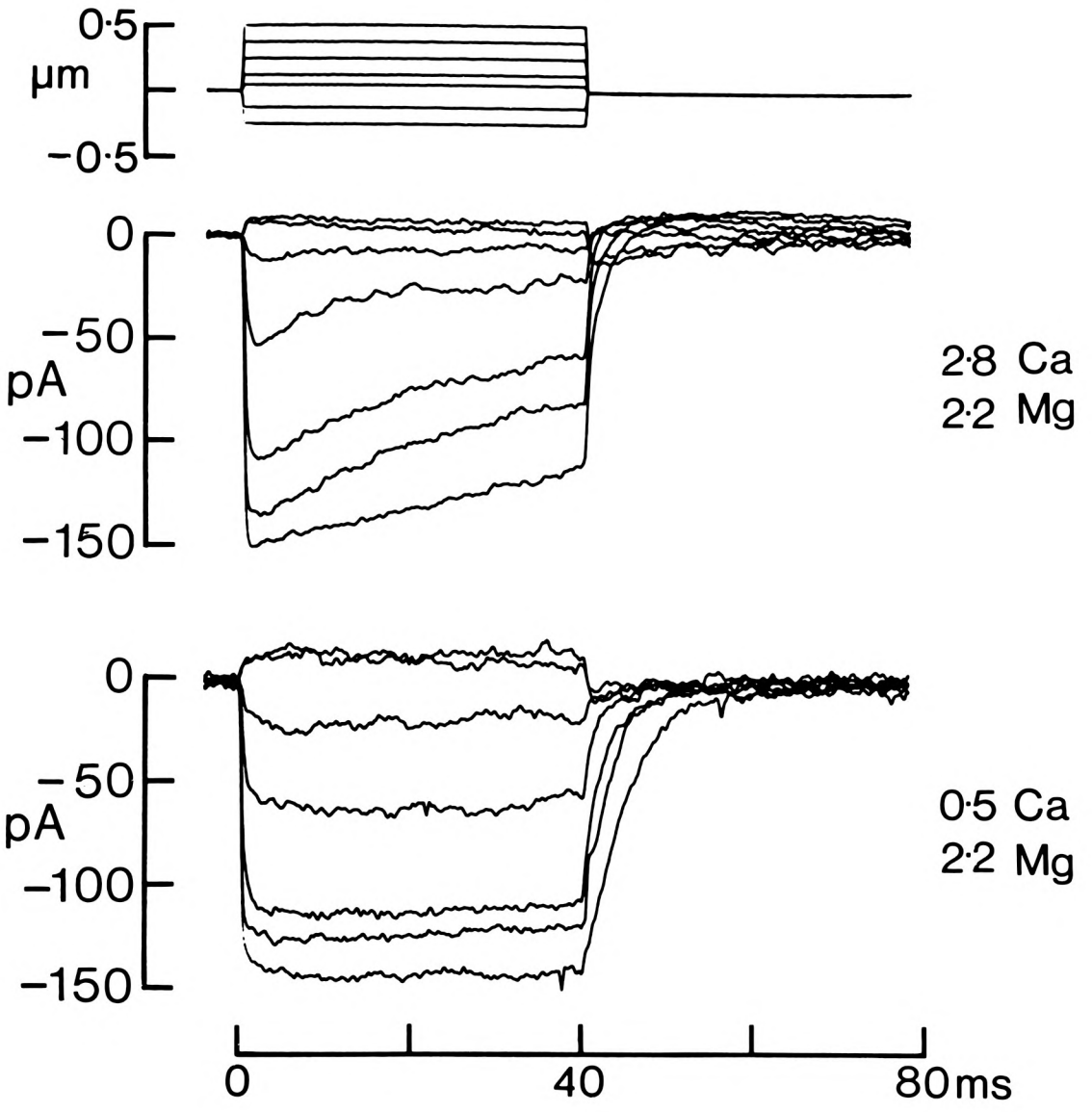

FIGURE 4 Effects of reducing the extracellular calcium concentration on adaptation of transducer currents. The stimulus monitor shown at the top applies to both sets of currents below. Upper current family obtained in normal saline containing 2.8 mM Ca^{2+}; lower family in 0.5 mM Ca^{2+}. Although not shown, the effects of reducing the calcium concentration were completely reversible. Note that adaptation is lost at the lower calcium concentration.

lower reversibly the extracellular calcium concentration around single hair cells under voltage clamp.

Fig. 4 illustrates an experiment where the calcium was reduced from plasma values (2.8 mM) in the records of Fig. 4A, to 0.5 mM in the records of Fig. 4B. Lowering the calcium concentration does indeed remove adaptation, at least over a time scale of 40 ms. Moreover other changes take place that are also reminiscent of those that occur when a hair cell is depolarized. Thus the kinetics of offset of the transducer current are slowed in the lower calcium solution (see Fig. 4B). While not evident from Fig. 4 the form of the transducer's activation curve was in many cells altered when the calcium concentration was lowered. As in cells depolarized to positive membrane potentials, the transducer's activation curve was shifted to more negative displacements and the slope of the curve became more shallow.

Discussion

Three lines of experimental evidence point to the conclusion that adaptation is regulated by the intracellular concentration of calcium: adaptation can be removed or greatly slowed i) by lowering the extracellular calcium concentration, ii) by filling cells with a strong calcium buffer, or iii) by depolarizing the hair cell towards the equilibrium potential for calcium ions. There seems little else to explain actions ii) and iii) above, but the effects of reducing extracellular calcium are more equivocal. We are inclined to think that the actions of reduced extracellular calcium are indeed mediated via a fall in the *intracellular* concentration of this ion, because these actions are so similar to the effects of depolarization both with regard activation and to the loss of adaptation.

Recently it has been suggested that displacement of the ciliary bundle activates the transducer channels through elastic elements or 'gating springs' (Howard & Hudspeth, 1987, 1988). On this view, the process of adaptation would correspond to a time-dependent fall in the tension in the gating springs. While the physical identity of the gating springs is uncertain, the most popular candidates are the links connecting the tips of the stereocilia together and first described by Pickles, Comis & Osborne, (1984). Unfortunately these structures are extracellular ones and therefore unlikely to be the site at which calcium controls adaptation. One way round this problem is to suggest (Howard and Hudspeth, 1987) that the control is exerted at the point of attachment of the tip-link to the stereocilium. Thus a rise in calcium concentration within the stereocilia would somehow cause the attachments to slide down the cilia and thus relieve the tension in the gating springs

But we also have to explain why it is that as adaptation proceeds, the transducer's activation curve becomes steeper, and conversely why it is that if adaptation is prevented the activation curve flattens out. The latter action is certainly also controlled by intracellular calcium since it occurs when the hair cell is depolarized. One possible explanation is that the intracellular calcium concentration controls not only the resting tension in the gating springs but also their stiffness. If the force to open a channel is developed by stretching a gating spring in series with it, then the stiffer the spring the smaller the displacement needed to achieve the opening force. If this idea is correct, a rise in $[Ca^{2+}]_i$ would have to increase the stiffness of the

gating spring, and a fall in $[Ca^{2+}]_i$ to reduce it. However it is not easy to see how $[Ca^{2+}]_i$ could affect the properties of extracellular structures like the tip-links.

References

Art, J.J. & Fettiplace, R. (1987). Variation of membrane properties in hair cells isolated from the turtle cochlea. *J. Physiol.* **385**, 207-242.

Assad, J.A., Hacohen N. & Corey, D.P. (1989). Voltage dependence of adaptation and active bundle movements in bullfrog saccular hair cells. *Proc. Natl. Acad. Sci. USA.* **86**, 2818-2922.

Bosher, S.K. & Warren, R.L. (1978). Very low calcium content of cochlear endolymph, an extracellular fluid. *Nature* **273**, 337-378.

Corey, D.P. & Hudspeth, A.J. (1979) The ionic basis of the receptor potential in a vertebrate hair cell. *Nature* **281**, 675-677.

Corey, D.P. & Hudspeth, A.J. (1983a). Analysis of the microphonic potential of the bullfrog's sacculus. *J. Neurosci.* **3**, 942-961.

Corey, D.P. & Hudspeth, A.J. (1983b). Kinetics of the receptor current in bullfrog saccular hair cells. *J.Neurosci.* **3**, 962-976.

Crawford, A.C., Evans, M.G. & Fettiplace, R. (1989). Activation and adaptation of transducer currents in turtle hair cells. *J. Physiol.* **419**, 405-434.

Crawford, A.C. & Fettiplace, R. (1981). Non-linearities in the responses of turtle hair cells. *J. Physiol.* **315**, 317-338.

Crawford, A.C. & Fettiplace, R. (1987). A substage cooling attachment for Zeiss IM microscopes. J.Physiol. 396, 13P.

Eatock, R.A., Corey, D.P. & Hudspeth, A.J. (1987). Adaptation of mechanoelectrical transduction in hair cells of the bullfrog's sacculus. *J. Neuroscience* **7**, 2821-2836.

Hamill, O.P., Neher, E., Marty, A., Sakmann, B. & Sigworth, F.J. (1981). Improved patch-clamp techniques for high-resolution current recording from cells and cell-free membrane patches. *Pflgers Archiv* **391**, 85-100.

Howard, J. & Hudspeth, A.J. (1987). Mechanical relaxation of the hair bundle mediates adaptation in mechanoelectrical transduction by the bullfrog's saccular hair cell. *Proc. Natl. Acad. Sci. USA* **84**, 3064-3068.

Howard, J. & Hudspeth, A.J. (1988). Compliance of the hair bundle associated with gating of mechanoelectrical transduction channels in the bullfrog's saccular hair cell. *Neuron* **1**, 189-199.

Fenwick E.M., Marty, A. & Neher, E. (1982). A patch-clamp study of bovine chromaffin cells and of their sensitivity to acetylcholine. *J. Physiol.* **331**, 577-597.

Krishtal, O.A. & Pidoplichko, V.I. (1980). A receptor for protons in the nerve cell membrane. *Neuroscience* **5**, 2325-2327.

Lewis, R.S. & Hudspeth, A.J. (1983). Voltage- and ion-dependent conductances in solitary vertebrate hair cells. *Nature* **304**, 538-541.

Ohmori, H. (1985). Mechano-electrical transduction currents in isolated vestibular hair cells of the chick. *J.Physiol.* **359**, 189-217.

Pickles, J.O., Comis, S.D. & Osborne, M.P. (1984). Cross-links between stereocilia in the guinea-pig organ of Corti, and their possible relation to sensory transduction. *Hearing Res.* **15**, 103-112.

STRUCTURAL ABNORMALITIES IN INNER HAIR CELLS FOLLOWING KANAMYCIN-INDUCED OUTER HAIR CELL LOSS

Carole M. Hackney, David N. Furness and Peter S. Steyger

Department of Communication and Neuroscience
University of Keele, Keele, Staffs., ST5 5BG, U.K.

Introduction

The aminoglycoside antibiotic kanamycin has been widely used in studies of the comparative function of inner (IHC) and outer (OHC) hair cells of the mammalian cochlea. Administration of this drug has been used to produce dose-dependent selective OHC loss in certain regions of the cochlea whilst leaving IHCs apparently intact as judged by Nomarski light microscopy (LM). In guinea pig (Harrison and Evans, 1977), and also in cat (see e.g., Kiang et al, 1986), loss of frequency selectivity and elevated thresholds have been reported in afferent nerve fibres of IHCs from regions of total OHC loss, whilst in chinchilla, elevation of threshold without loss of frequency selectivity has been found (Dallos and Harris, 1978). These results are considered consistent with other data which suggest that whilst the IHCs are the primary sensory receptors of the mammalian cochlea, the OHCs are involved in some way in the active mechanical enhancement of the IHC response (see e.g., review by Patuzzi and Robertson, 1988).

However, in order to support this interpretation of the ototoxicity experiments, the physiological responses recorded in Type I afferents from regions of OHC loss must be assumed to come from IHCs and nerve fibres which have not been directly affected by the kanamycin regime themselves. It is thus essential to ensure that the IHCs and associated afferents are not subtly damaged in regions of kanamycin-induced OHC loss. To investigate this, electron microscopical studies have been performed, yet the results have been somewhat contradictory in different species. Ultrastructural analysis of the kanamycin-damaged chinchilla cochlea has suggested that although IHC damage occurs where the adjacent supporting cells are missing, in general, the IHCs appear normal in regions of OHC loss (Ryan et al, 1980). In cat, IHCs have also been reported to be normal in regions of total OHC loss (Kiang et al, 1986). However in guinea pig, Hawkins (1977) found some evidence for damage to the IHCs and their stereocilia when higher doses of kanamycin were used. We ourselves have found, using scanning electron microscopy (Furness and Hackney, 1986), that although the stereocilia of the IHCs and their fine intrastereociliary linkage systems appeared predominantly intact after a similar kanamycin dose regime to that employed by Harrison and Evans (1977), preliminary observations using transmission electron microscopy (TEM) revealed alterations to the IHC somata and their terminals in regions of OHC loss (Hackney and Furness, 1987). An immunohistochemical investigation of the distribution of actin and tubulin in cochlear segments following kanamycin administration also suggested that changes might be occurring in the organisation

of these cytoskeletal proteins in both OHCs and IHCs in basal regions of the cochlea (Hackney et al 1989).

In this paper, we report further results obtained using both TEM and the immunofluorescent localisation of tubulin which indicate that alterations in the IHCs and their afferent nerve terminals should be taken into account when interpreting the data obtained in earlier physiological experiments.

Methods

Pigmented guinea pigs, 6 to 8 weeks old, were given 400 mg/kg/day kanamycin for 8 days and allowed to recover for 2 weeks prior to sacrifice. At least one animal was kept from each litter as a control. Cochleas were then prepared in one of two ways.

For cell counting and correlated TEM, the cochlea was fixed by perfusion with 2.5% glutaraldehyde in 0.1 M sodium cacodylate/2 mM calcium chloride buffer (pH 7.4) for 2 h, and postfixed using 1% osmium tetroxide in buffer for 1 h. The cochlear shell was partially removed and the cochlea dehydrated via an ethanolic series. Infiltration of resin was carried out over a period of three weeks, using a vacuum embedding oven. The embedded whole cochlea was sliced into hemiturns using a Malvern 2A Microslice with an annular diamond blade. The segments were examined using Nomarski light microscopy, and the hair cells counted to produce a cytocochleogram. Ultrathin sections were cut at 50 - 70 nm from selected areas, stained using uranyl acetate and lead citrate and examined in a JEOL 100CX TEM at 100 kV.

For immunolabelling, the cochlea was fixed using 4% paraformaldehyde in 0.1 M phosphate buffer for 2 h. The cochlear shell was removed and the tissue permeabilised with 0.25% Triton-X 100 for 30 min. Following pre-blocking for 30 min with neat bovine serum albumin (BSA), the cochlea was incubated for 20 h in a monoclonal rat anti-yeast-tubulin antibody (Sera-Lab - dilution 1:200) in phosphate buffer containing 1% BSA, and then washed and incubated in FITC-conjugated goat anti-rat secondary antibody (Sigma - dilution 1:20) for 5 h. Cochlear segments were then dissected out and observed using a Leitz Dialux microscope with epifluorescence optics. Hair cell counts were also obtained from these segments using Nomarski microscopy.

Results

PATTERNS OF KANAMYCIN-INDUCED HAIR CELL LOSS

Hair cell counts from kanamycin-damaged cochleas have shown a wide variation in the degree of hair cell loss produced in different guinea pigs, even siblings, despite using identical dose regimes. Fig. 1 shows representative counts from a control cochlea (Fig. 1a), from one showing only a small degree of hair cell loss following kanamycin administration (Fig. 1b) and from two others where hair cell loss was much greater (Fig. 1c, d). Ultrastructural and immunocytochemical investigations have been concentrated on cochleas showing total basal OHC loss and relatively unaffected IHCs at the LM level, for comparison with previous physiological experiments (as in Figs. 1c and 1d). TEM has been used to compare the structure of IHCs in the relatively undamaged apical regions with IHCs in the highly affected basal regions. The structure of surviving OHCs has also been examined for comparison to determine whether the pattern of IHC damage, when present, is similar to that of OHCs in the early stages of degeneration.

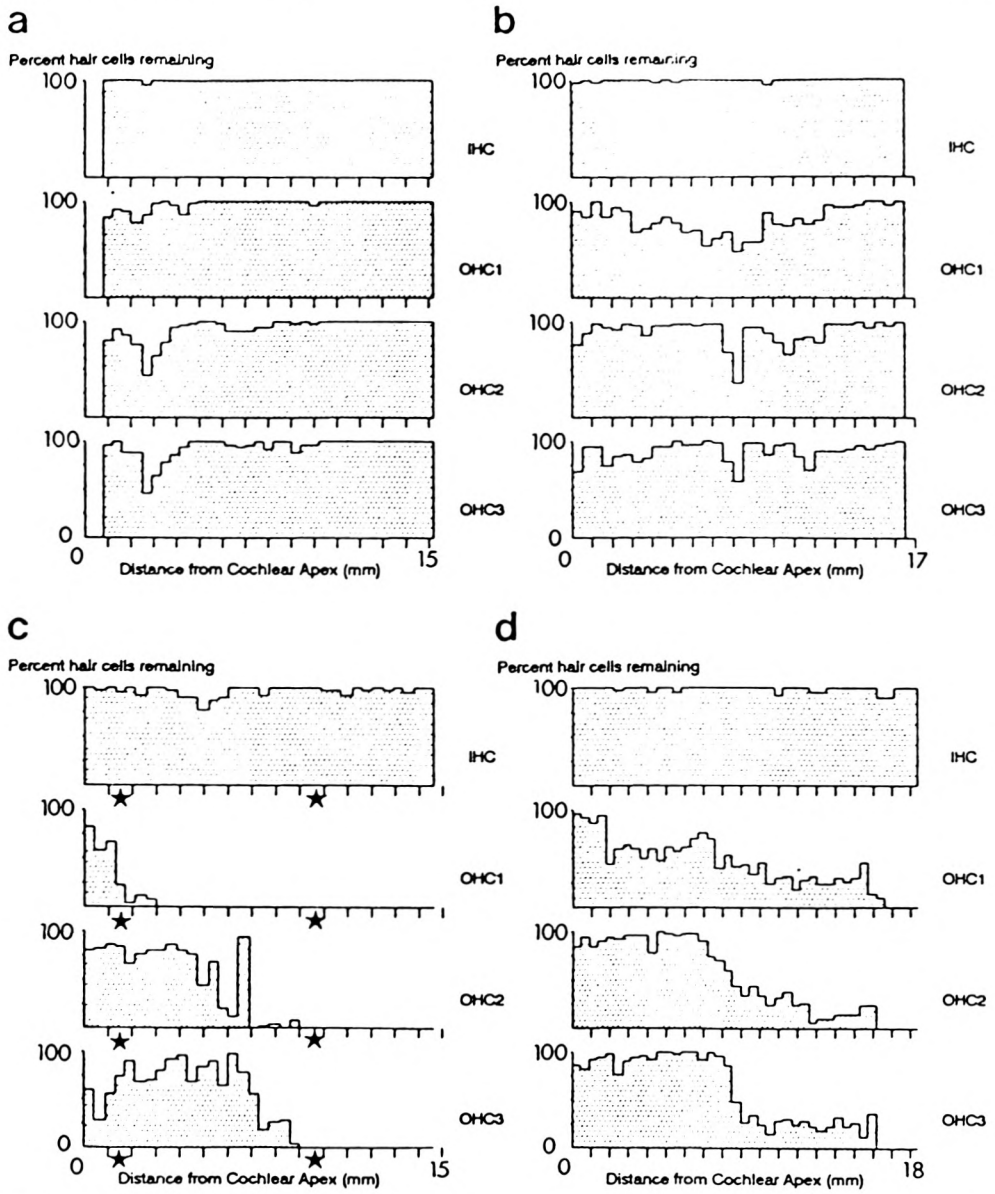

FIGURE 1 Cytocochleograms of a control (a) and three kanamycin damaged cochleas (b - d). Note the relatively small degree of hair cell loss in (b), and the pattern of total basal OHC loss demonstrated by (c) and (d). Areas examined by TEM from (c) are shown (*). The example shown in (d) was labelled for tubulin.

STRUCTURAL CHANGES IN THE OHCS

Surviving OHCS in regions of partial OHC loss frequently show evidence of increased cytoplasmic density and, in some cases, fusion of stereocilia with the apex (Fig. 2a). However, the damage to the OHC most often occurs below the reticular lamina leaving the apical region of the cell comparatively intact (Fig. 2b). The distribution of tubulin as revealed by immunofluorescent localisation appears normal in many of the surviving OHCs in regions of partial OHC loss, with readily identifiable fibrillar staining around the cuticular plate and in the cell body (Fig. 3a). However, some OHCs show labelling which is reduced and sometimes completely missing, even when the cell is still present and appears normal in bright field microscopy. Many show an altered fibrillar pattern with the fluorescence becoming more diffuse, again without appearing abnormal in bright field (Fig. 3a, b). In some, the patterns may be altered in the cell body whilst the apical region is unchanged.

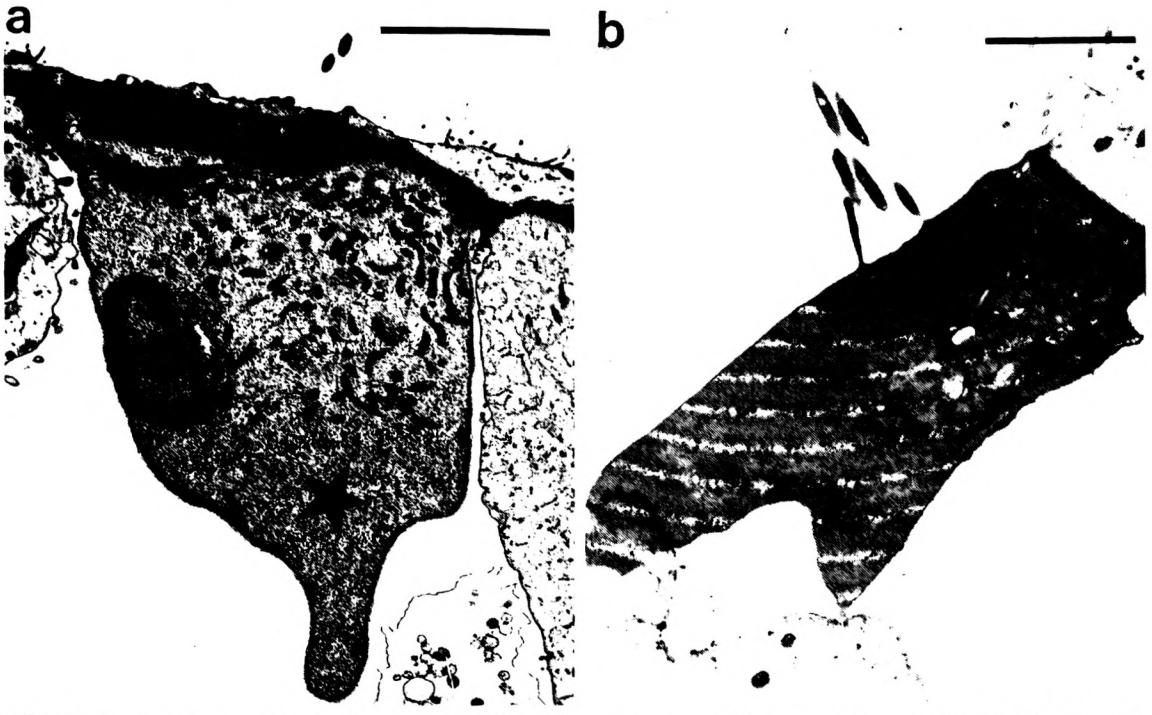

FIGURE 2 (a) Example of a damaged OHC. Note the area of high cytoplasmic density (*star*). The stereocilia have fused with the apex and Hensen's body appears to be abnormal. Scale bar = 5 μm. (b) An OHC with loss of the major part of the cell body but with the apex remaining. Scale bar = 2 μm.

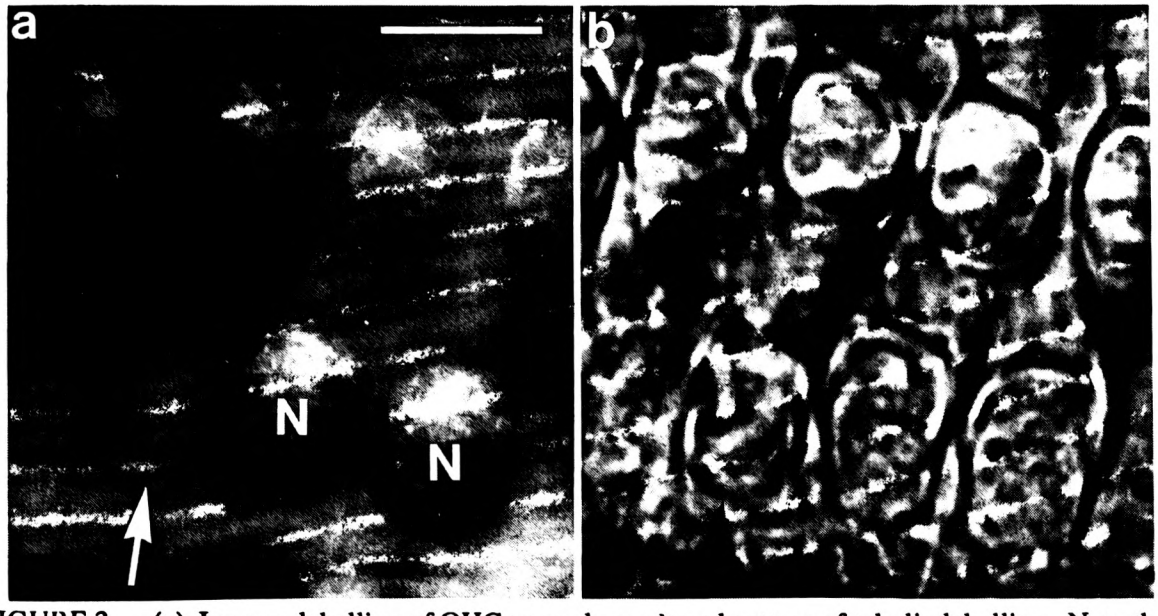

FIGURE 3 (a) Immunolabelling of OHCs reveals an altered pattern of tubulin labelling. Note the normal bright filamentous patterns (N) and one cell where the pattern is more diffuse (arrow). (b) The cell with altered tubulin labelling appears normal in the bright field view (arrow). Scale bar = 10 μm.

STRUCTURAL CHANGES IN THE IHCS

Ultrastructural analysis of basal regions where total OHC loss has occurred, reveals evidence of an effect on the IHC system. The most marked alteration is to the afferent nerve fibres innervating IHCs, which show expanded terminals, apparently empty of cytoplasm, when compared with controls (Fig. 4a, b). In addition to nerve terminal swelling,

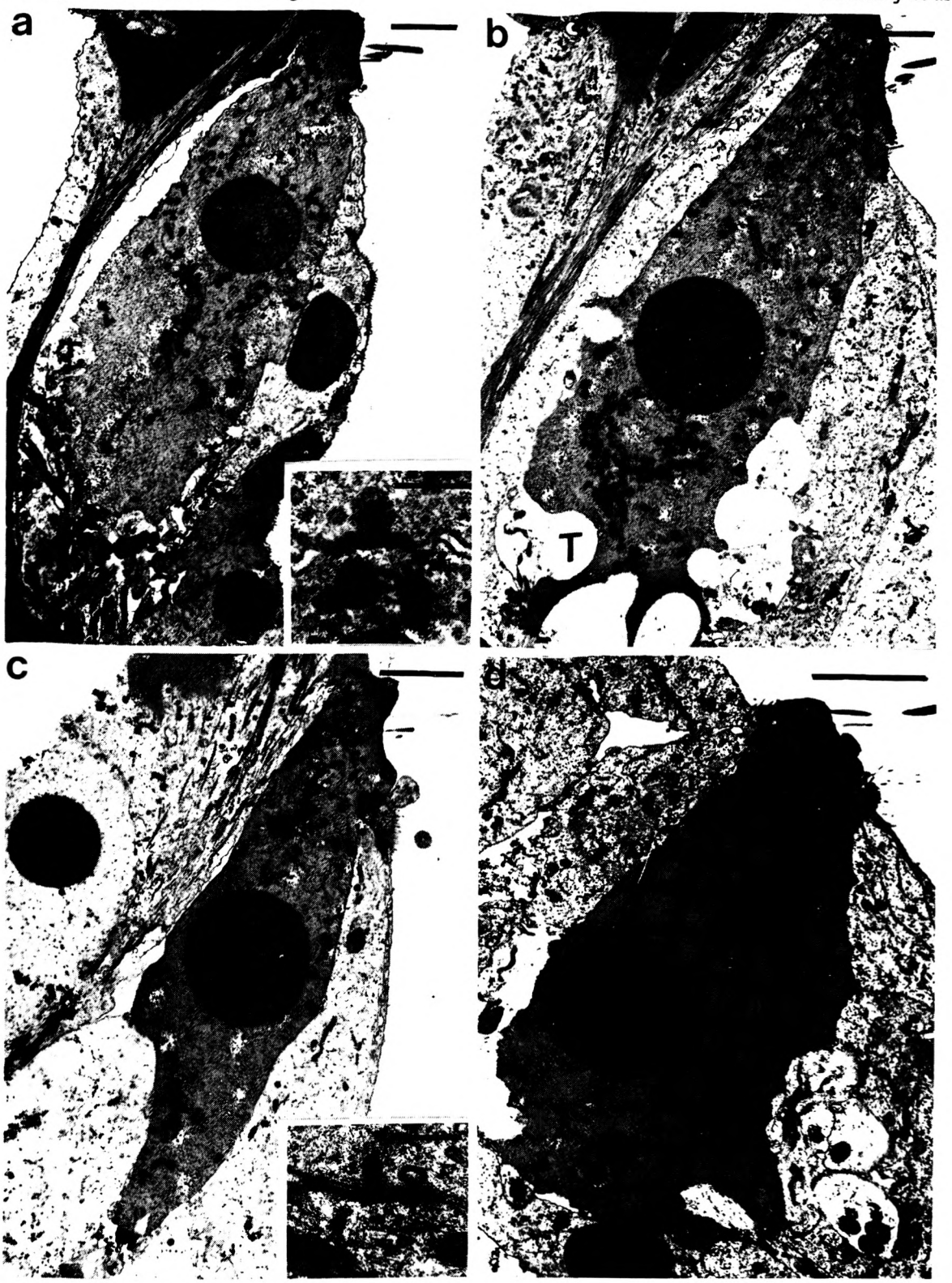

FIGURE 4 IHCs from control (a) and kanamycin (b - d) damaged cochleas. (a) The normal flask shaped IHC body has well preserved terminals at the base (T and inset). (b) An IHC from a region of total OHC loss (the basal region noted in Fig. 1c) shows swollen nerve terminals (T). (c) An IHC from the apical region (noted in Fig. 1c) appears relatively normal with no indication of damage at the base of the cell. Inset: An afferent terminal from this region appears normal. (d) A damaged cell shows increased cytoplasmic density, stereocilia fused with the apex, and distortion of the cell body. Scale bars = 5 μm. Inset scale bars = 0.5 μm.

IHCs may themselves be damaged. Fig. 4d shows an example of an IHC from a region of total OHC loss which reveals distortion of the cell body, an increase in cytoplasmic density and fusion of stereocilia with the apex of the cell. The IHC shown in Fig. 4d occurred adjacent to damaged supporting cells. In contrast, in the apical region of cochleas showing these basal changes, both the IHCs and their nerve terminals appear relatively normal, or show damage which is less marked than in the basal regions (Fig. 4c). Many of the terminals in this region appear very similar to those in most control material from either basal (Fig. 4b) or apical regions. However, it should be noted that in some instances, swollen nerve terminals and distorted IHCs have been found in both controls and in the apical regions of some kanamycin-damaged cochleas. In these instances, damage to the IHCs occurs in both apical and basal regions, and there are other signs, such as cytoplasmic changes and blebbing of the apical surface which may indicate that the cochlea was hypoxic at fixation. Moreover the preservation of the hair cells and supporting cells usually appears poorer than in rapidly fixed material. Thus, only if the apical regions of a cochlea appeared intact and free of blebs, and the cells remaining in all regions appear well-fixed, has a cochlea been included in this study.

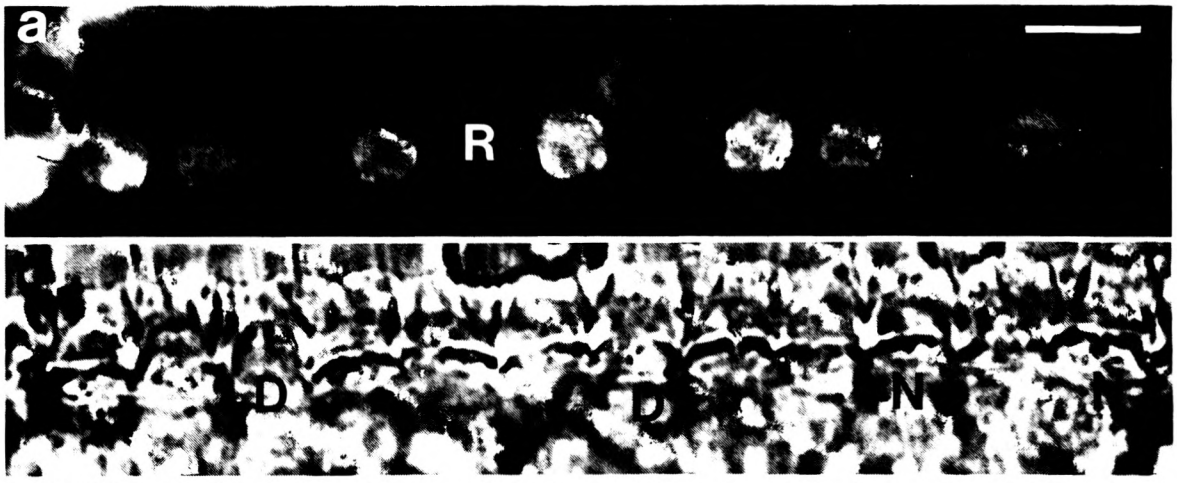

FIGURE 5 (a) Immunolabelling shows evidence of alteration of tubulin in some IHCs, mainly in the form of loss of labelling intensity (R). b) In the bright field view of the same area it can be seen that some of the IHCs which show reduced labelling appear normal (N), whilst others are clearly damaged or absent (D), in comparison with the adjacent normal-appearing cells in which labelling is unaltered. Scale bar = 10 μm.

Immunolabelling has also revealed possible changes in the cytoskeleton of IHCs in kanamycin-damaged cochleas. The tubulin network in some individual IHCs shows a reduced intensity of labelling compared to adjacent IHCs, whilst the IHC may still be present and appears normal in bright field (Fig. 5). Such an effect is confined to regions of total OHC loss. These changes differ from those seen in the OHCs, where various stages in the loss of the fibrillar pattern have been observed, in that the pattern of tubulin staining in IHCs seems to be retained but the staining intensity varies.

Discussion

In the pigmented guinea pigs we have used, differing patterns of hair cell loss have been produced using the same dose regime of kanamycin. This variability of response presumably also occurs at the ultrastructural level making the exact extent of the

ultrastructural damage to the remaining hair cells difficult to predict in these animals. Our results suggest that a number of changes may be occurring at the subcellular level that would not be revealed by a conventional cytocochleogram. For instance, alterations in the cytoskeleton of the OHCs may affect their mechanical characteristics well before hair cell loss occurs. Similarly, we have observed changes to the IHCs and their afferent nerve fibres in regions of total OHC loss which call into question the degree of functional integrity of the surviving IHC system. The presence, in particular, of widespread damage to the IHC afferent terminals suggest that their function may be impaired.

The observation of many apparently normal terminals in apical regions suggests a similar relationship between *position* in the cochlea and degree of afferent damage as is seen for the degree of loss of OHCs in some cochleas, i.e. the basal region is affected more substantially than the apical region. Indeed, the distribution of terminal damage seems to correlate with the distribution of altered responses of nerve fibres seen in physiological studies since normal terminals are found apically from which normal fibre responses would probably have been recorded, and damaged ones basally where the altered responses were found. The most likely outcome of swelling of afferent terminals is the elevation of the thresholds of affected nerve fibres, as has been demonstrated previously following noise-induced swelling of the afferent terminals (Robertson, 1983).

Our findings are in contrast to those of Ryan et al (1980) and Kiang et al (1986) who did not report such alterations and who considered IHCs to be generally normal in regions of total OHC loss. However, the damage in their animals may have been less extreme because of different drug regimes and species differences. It is also possible that any damage could be temporary, and could thus disappear with differing survival times in different species. Indeed, Robertson (1983) noted that noise-induced swelling of afferent nerve terminals was reversible. The most extreme effects we have observed in IHCs occurred where supporting cells were also damaged, a finding which is consistent with that of Ryan et al (1980). Interestingly, IHC degeneration resembles the less severe forms of OHC degeneration, suggesting that a similar process is occurring to a lesser extent.

The alterations in cytoskeletal organization which result from chronic kanamycin administration may suggest a direct impairment of IHC function at the level of the cell itself in addition to the changes observed in the afferent terminals. Alterations in the tubulin distribution, particularly in the integrity of the microtubular networks, are likely to affect both the mechanical properties and neurotransmission in these cells. We have postulated several possible functions for the microtubules in IHCs (Steyger et al, 1989; Furness et al, 1990). They may provide structural support of the apex and thus determine to some extent its response to mechanical stimulation. They could also be responsible for the transport of neurotransmitter vesicles from the apical region, where the synthetic apparatus of the cell is mainly located, to the synaptic region (Furness and Hackney, 1988; Hackney and Furness, 1989). The disruption of microtubules could therefore potentially cause an alteration in the response of the transduction mechanism and/or it could lead to a change in synaptic vesicle transport, which might in turn affect the neurotransmission of the IHC response. However, the variable staining intensity of the IHCs could also be the result of imperfect penetration of the antibody into the cells during immunolabelling and so some care must be taken in interpretation of this result, although in control cochleas, penetration appears to be relatively even. More definite changes occur to the tubulin networks of surviving OHCs in other regions of the cochlea. Here, it is not simply reduced intensity of labelling but also a change in the nature and pattern which indicates that the distribution and form of the tubulin has altered.

It is clear that complex structural changes occur in the organ of Corti following the administration of kanamycin. Damage to the IHC system in regions of total OHC loss could provide an alternative or additional explanation for the altered physiological responses obtained from nerve fibres originating in regions of total OHC loss. Whether the lesions observed in the IHC system are sufficiently extensive to be responsible for the physiological effects reported, or whether even more subtle changes produce the alterations in function, still remains to be established.

Acknowledgements

This work has been supported by the Wellcome Trust and an MRC studentship to PSS.

References

Dallos, P and Harris, D. (1978) Properties of auditory nerve responses in absence of outer hair cells. J. Neurophysiol. 41, 365-383.

Furness, D.N. and Hackney, C.M. (1986) Morphological changes to the stereociliary bundles in the guinea pig cochlea after kanamycin treatment. Brit. J. Audiol. 20, 253-259.

Furness, D.N. and Hackney, C.M. (1988) Cytoskeletal organisation in the apex of cochlear hair cells. In: Auditory Pathway - Structure and Function (Eds: Syka, J and Masterton, R.B.) Plenum Press, New York and London, pp 23-28.

Furness, D.N., Hackney, C.M. and Steyger, P.S. (1990) The organization of microtubules in cochlear hair cells. J. Electron Microscop. Tech. 15, 261-279.

Hackney, C.M. and Furness, D.N. (1987) Hair cell ultrastructure in the normal and kanamycin treated cochlea. Brit. J. Audiol. 21, 319.

Hackney, C.M. and Furness, D.N. (1989) Observations on the cytoskeleton and related structures of mammalian hair cells. In: Cochlear mechanisms: Structure, function, and models (Eds: Wilson, J.P. and Kemp, D.T.) Plenum Press, New York and London, pp 11-20.

Hackney, C.M., Furness, D.N. and Steyger, P.S. (1989) Ultrastructural and immunohistochemical observations on the effects of chronic doses of kanamycin on cochlear hair cells. Abstracts of the 26th Workshop for Inner Ear Biology, p 40.

Harrison, R.V. and Evans, E.F. (1977) The effects of hair cell loss (restricted to outer hair cells) on the threshold and tuning properties of cochlear fibres in the guinea pig. In: Inner ear biology (Eds: Portmann, J. and Aran, J.M.) INSERM, Paris, pp 105-124.

Hawkins, J.E. Jr. (1977) The condition of inner hair cells after aminoglycoside intoxication. In: Inner ear biology (Eds: Portmann, J. and Aran, J.M.) INSERM, Paris, pp 327-334.

Kiang, N.Y.S., Liberman, M.C., Sewell, W.F. and Guinan, J.J. (1986) Single unit clues to cochlear mechanisms. In: Cellular mechanisms in hearing (Eds: Flock, A. and Wersall, J), Elsevier Science Publishers, Amsterdam, Oxford and New York, pp 171-182.

Patuzzi, R. and Robertson, D. (1988) Tuning in the mammalian cochlea. Physiol. Rev. 68, 1009-1082.

Robertson, D. (1983) Functional significance of dendritic swelling after loud sounds in the guinea pig cochlea. Hearing Res. 9, 262-278

Ryan A.F., Woolf, N.K. and Bone, R.C. (1980) Ultrastructural correlates of selective outer hair cell destruction following kanamycin intoxication in the chinchilla. Hearing Res. 3, 335-351.

Steyger, P.S., Furness, D.N., Hackney, C.M. and Richardson, G.P. (1989) Tubulin and microtubules in cochlear hair cells: comparative immunocytochemistry and ultrastructure. Hearing Res. 42, 1-16.

MODELLING INPUT-OUTPUT CHARACTERISTICS OF THE INNER HAIR CELL

J. Wiebe Horst and Piet C. de Jong

ENT Clinic, Research Department
University Hospital, Groningen, The Netherlands

Introduction

The transduction in the cochlea contains several nonlinear stages. Single-fiber recordings, however, sometimes are predominantly linear, whereas other recordings show strong nonlinear aspects. Horst et al. (1985, 1986b, 1990) have demonstrated that the type of stimulus used is very critical. In particular the short term spectral content in relation with the instantaneous amplitude of the stimulus turned out to be an important factor. Using a set of stimuli with relatively simple amplitude spectrum but strong variations of the waveform envelope they found very level-dependent responses. The majority of their data (collected from neurons with high spontaneous discharge rates) could be adequately described by the involvement of an input-output (IO) function, which was linear at low and intermediate stimulus levels and compressive at higher stimulus levels. The data collected from neurons with low spontaneous rates behaved differently at low levels (Horst et al., 1986b). That is, at low levels they could be described with an expansive IO function.

Whereas it is not ruled out that cochlear IO-functions can change with level, it seems more elegant to model hair-cell transduction with a single (not level dependent) IO-function. The sigmoid curve (expansive for low input, compressive for high input) is a good candidate. First we will show that the transduction in the cochlea after the initial filtering by means of a single sigmoidally shaped IO curve is fairly adequate to describe responses to multicomponent complex stimuli. This applies both to the responses in the temporal and the spectral domain. This same IO curve, however, can not take care of the rate-level curve of pure-tone stimuli. We conclude in the Discussion that in order to adequately describe responses to pure tones as well as complex stimuli, another element has to be added which takes care of adaptation-like processes. This additional element has to be sandwiched between two nonlinearities. The last nonlinearity is essential to describe responses to nerve fibers with low spontaneous activity.

The Model

It is argued above that the sigmoid curve is a reasonable choice for the case of the low-spont. neurons (Fig. 1). Our working hypothesis is that the difference between IO curves for neurons with high and neurons with low spontaneous activity is the horizontal position. Thus the IO curve for a neuron

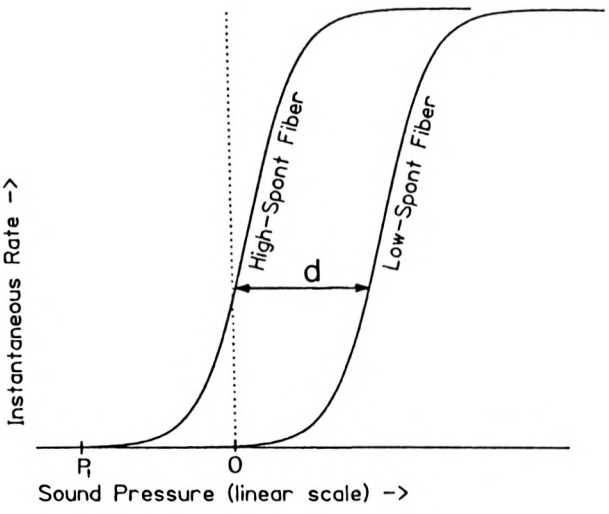

FIGURE 1 A first approximation of the input-output curves for high- and low-spont. nerve fibers. The intersection of the zero-input line and the IO function is the spontaneous rate. At small stimulus intensities the response of the high-spont. fiber is linear, whereas the response of the low-spont. fiber is expansively nonlinear.

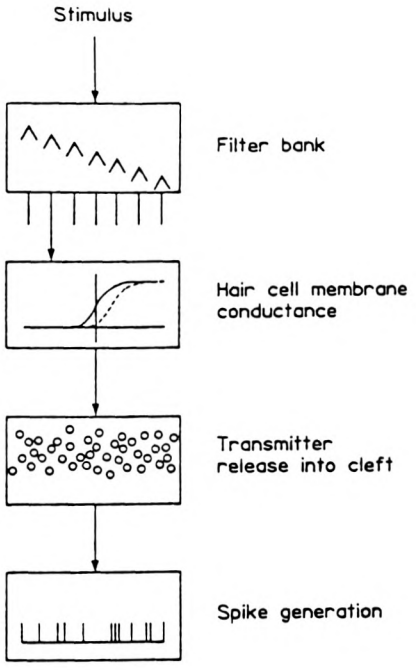

FIGURE 2 Working model consisting of a linear combination of a filter bank, nonlinear IO curve representing the conductance of the hair-cell apical membrane, chemical synapse, and a stochastic process producing action potentials.

with high spontaneous activity is generated from the low spont. case by a simple translation to lower input and vice versa. This behavior is simulated by our initial model. It is the series combination of four stages, as shown in Fig. 2. The first stage is a linear filter. The second stage represents the change of hair cell receptor membrane conductance. The third stage represents the generation and release of neurotransmitter. The fourth stage takes care of the generation of action potentials. Our starting assumption was that the third and fourth stage are fairly transparent. Therefore, we first focused on the output of the second stage. The model leaves several options for the actual choice of the shape of each stage. In this paper we used the filter characteristics according to Patterson (1974). The third stage (a set of difference equations) and the last stage (the generation of action potentials according to a Poisson process) are modeled according to Meddis (1986).

The shape of the curve was chosen as a combination of a hyperbole describing the compressive part (according to Meddis, 1986) and a power function describing the expansive part. The basic case is described by

$$y = 0 \qquad x \le x_t$$
$$y = v\{(wx+p)/p\}^P \qquad x_t \le x < = 0$$

and

$$y = g(x+a)/(x+a+b) \qquad x > 0$$

In the cases described here we used $a=5$, $b=300$, $g=2000$. The values for v and w were chosen so that y and its derivative are continuous at $x=0$. For the low-spont. case x has to be replaced by x-d, where d describes a horizontal shift of the IO curve.

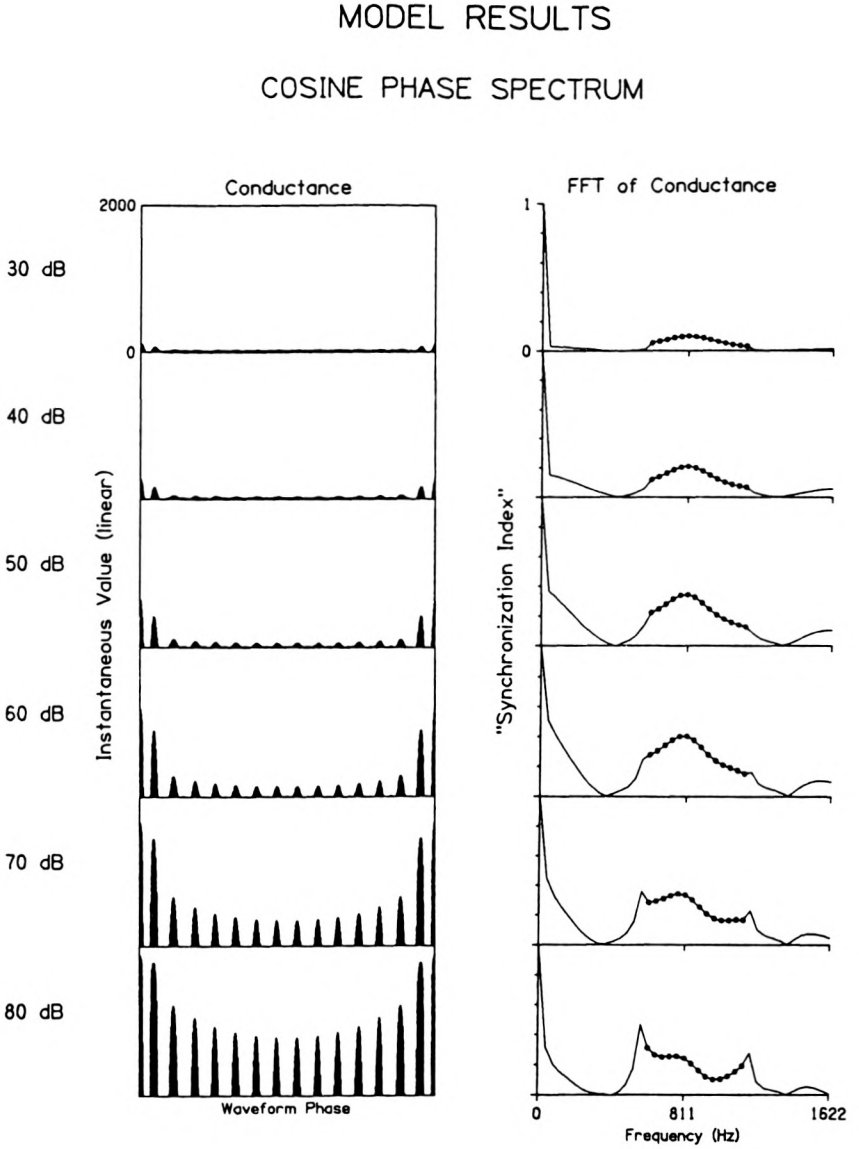

FIGURE 3 Model responses to an octave-bandwidth harmonic complex with all components in cosine phase and $N = CF/F_0 = 20$. Intensities are expressed in dB per component. 30 dB corresponds to rms = 1. $Q_{10} = 1.2$; $d = 0$, representing a high-spont. neuron.
Left: the conductance plotted as a period histogram.
Right: the spectra of the "period histogram". Filled circles indicate responses to frequencies present in the signal. Amplitudes are normalized with respect to the DC components.

Results

OUTPUT OF THE SECOND STAGE

Responses of the second stage to complex stimuli are shown in Fig. 3 for the case of a stimulus with flat amplitude and phase spectrum and a bandwidth of 1 octave. The left column shows the output waveform, the right column its spectrum for the case of $d = 0$, i.e. high spontaneous activity. The spectra shown are normalized with respect to the DC component. This is the way to determine synchronization indices for period histograms. We will use here the same terminology. Then, we can regard the conductance at zero input as spontaneous activity. In the left column we see at low levels an increase of synchronization with level. First, there is spontaneous activity, then it becomes

modulated with increasing amplitude. In the spectra this shows as increasing synchronization. At higher levels the response attains the character of a half-wave rectified response. This is a consequence of the asymmetry of the sigmoid curve with respect to $x=0$. Amplitudes reach values between 1000 and 2000. This agrees with single-fiber data, where we often found instantaneous rates of several thousands spikes/s. So we do need the large dynamic range of the proposed IO curve to adequately describe the large ratios between maximum instantaneous rate $y(\infty)$ and spontaneous rate $y(0)$. In the present case this is 2000/33. The part of the spectrum around CF remains roughly the same at intermediate levels. Then, as level goes up further, the response envelope gradually flattens as a consequence of the compressive shape of the IO function. The spectral counterpart is an enhancement of the spectral edges.

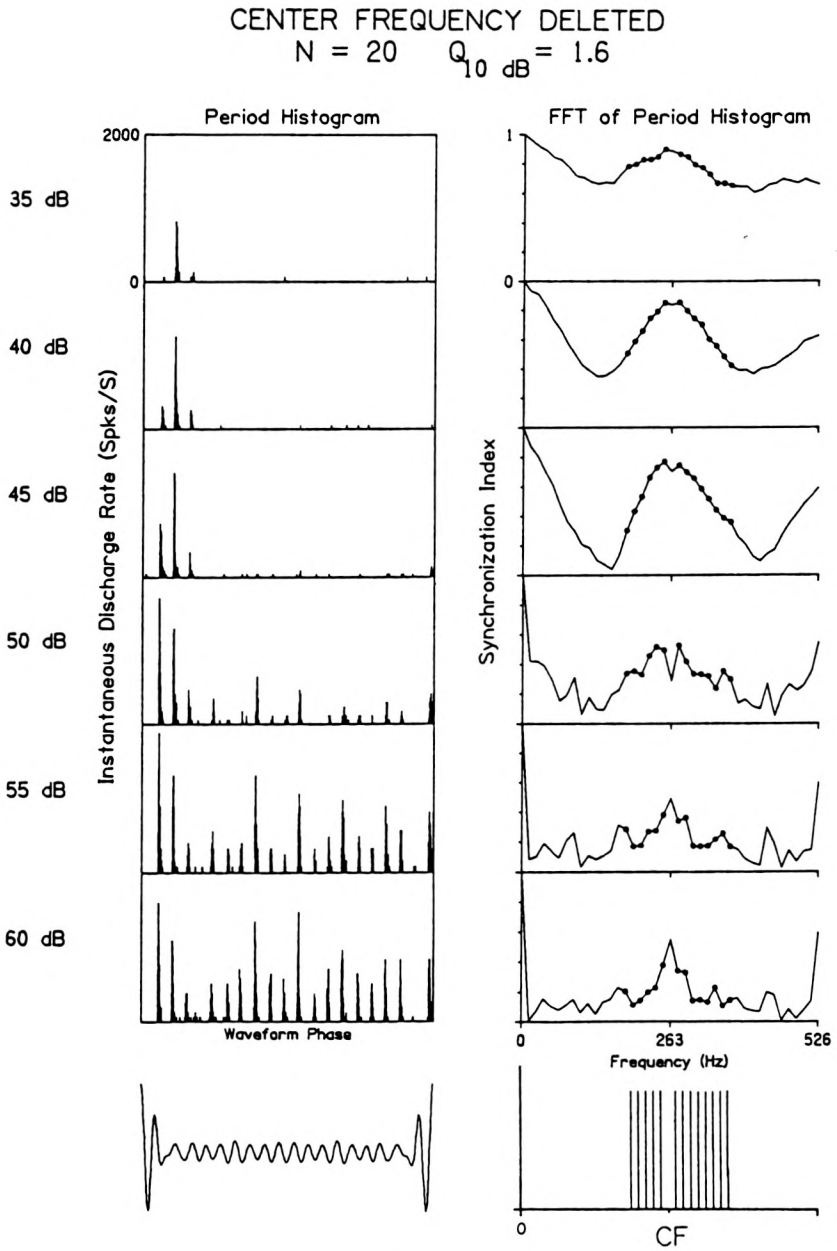

FIGURE 4 Single-fiber responses from a low-spont. neuron to an octave-bandwidth harmonic complex with all components in cosine phase and the center frequency component deleted. CF = 263 Hz, $Q_{10} = 1.7$, spont. rate = 0.0 spikes/s. Stimulus waveform and spectrum are shown for comparison.

This is due to the fact that the part of the stimulus waveform between the crests contains mainly information of the spectral edges (Horst et al. 1986a, 1990, Wit and Horst, 1986).

The strong level dependence of the responses is apparently caused by the property of the cochlear transduction to put more or less emphasis on different amplitudes of the stimulus (Horst et al., 1985, 1990). As a consequence responses will vary more or less with level dependent on the degree to which the spectral content is less or more evenly distributed over the various amplitudes within the stimulus period. Thus a noise-like stimulus will produce fairly constant response spectra over a large level range (Horst et al., 1988, 1990). On the other hand, the change in shape of the waveform envelope with level should not be underestimated. All this is adequately simulated by the model.

Some special cases of uneven distribution of the spectral content of the stimulus over the stimulus period are produced by manipulating the level of

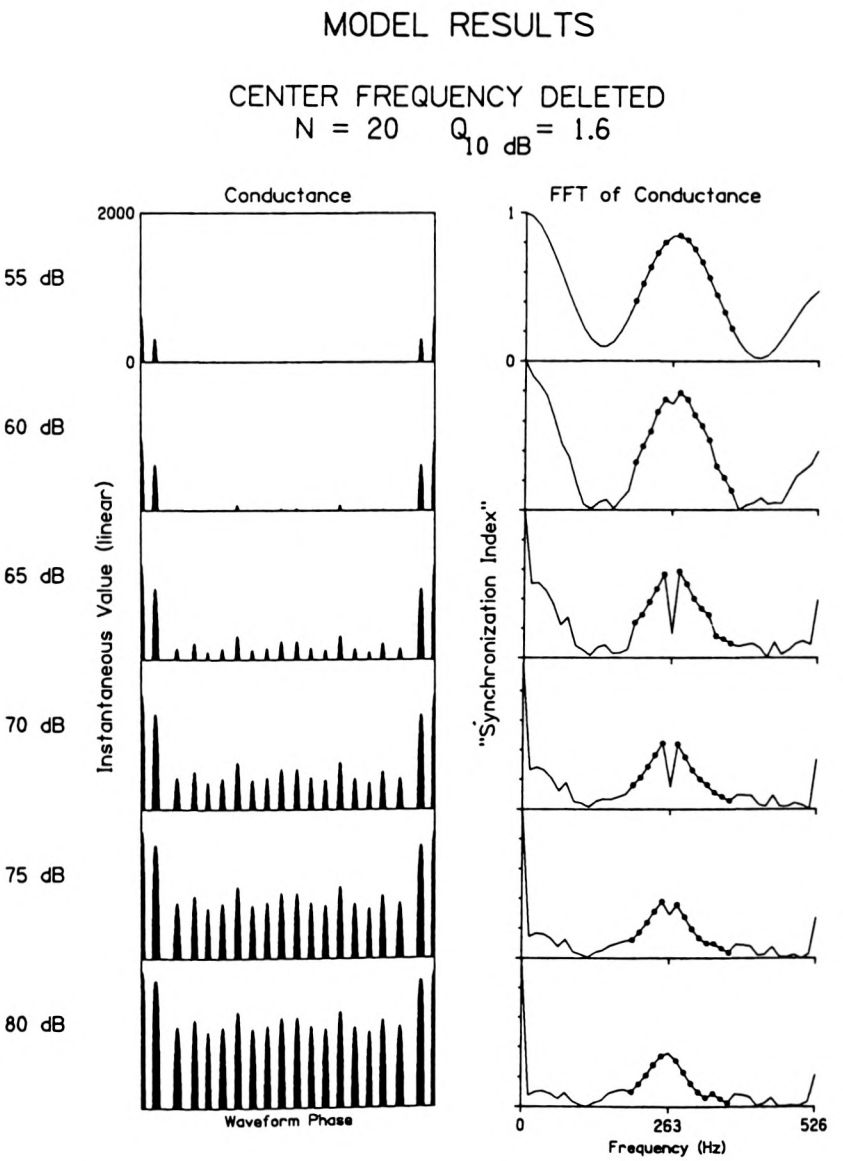

FIGURE 5 Model responses simulating the case of the low-spont. neuron of fig. 4. Parameter values were: p = 10, d = 50.8.

one spectral component. This can be done by deleting as well as by amplifying that component. Fig. 4 shows single-fiber responses to a stimulus with the center component deleted, for the case of a neuron with low spontaneous activity. These data were collected in an investigation reported by Horst et al. (1986b, 1990). An interesting aspect of the response at low stimulus levels is the synchronized response in a very limited part of the period histogram and the almost complete absence of spikes in the remaining part of the period histogram. As described by Horst et al. (1986b) these responses can be interpreted as resulting from an expansive IO curve. The consequence for the spectrum for low stimulus levels is synchronization at the frequency of the deleted component. There is only a small range of stimulus levels around 50 dB where the response spectrum looks more or less linear (note that the responses are reproduced here in steps of only 5 dB), i.e. there is no response at the frequency of the missing component. At high levels the spectrum becomes dominated by the missing component.

These responses can be understood by regarding the input stimulus of the hair-cell as consisting of two parts: The high crests mainly carrying information on the auditory filter shape, and the low-amplitude part between the crests consisting of an CF component added in counterphase. At low levels the additional CF component is suppressed, leaving only a response to the high crests. At high levels the crest response is compressed and as a consequence response to the additional out-of-phase CF component dominates the output. The model produces similar responses (Fig. 5) showing a dip in the response spectrum at CF in a only limited frequency range. Although there is a considerable response at CF at the highest stimulus level, no strong domination occurred in this case. More abrupt changes of the response spectrum can be realized by trying other shapes of the IO curve. However, instead of limiting this investigation to the shape of the IO curve, we will show in the following that it is important to take the next stages of the model also into consideration.

Fig. 6 shows output of the second stage of the model in response to a pure tone. At low stimulus levels (30 dB) the response consists mainly of modulation of the "spontaneous rate". That is, synchronization occurs before the average response increases. This is of course in agreement with the single-fiber responses. Fig. 6 also shows "Synchronization Index" SI and "Average Rate" AR for each level. A comparison with single-fiber data is possible by interpreting the AR in terms of actual spikes/s. Then, it is clear that the average rate grows too much for high input levels. This is a consequence of the large ratio between $y(\infty)$ and $y(0)$, which is needed for the responses to the multi-component complexes. At high input levels the pure tone response degenerates to a square wave, so $AR \approx 0.5y(\infty)$. For more realistic rate-intensity curves the next stages of the model had to be taken into account. Detailed description of responses of the last two stages falls beyond the scope of this paper.

Discussion

The purpose of this paper is to show that with relatively few and simple assumptions several aspects of auditory processing can be simulated. We specified the shape of an IO function for the instantaneous discharge and were able to produce response waveforms for complex stimuli and rate-intensity curves.

Sachs and Abbas (1974) and Sachs, Winslow and Sokolowski (1989) provided a model which chiefly produces a mathematical description of the

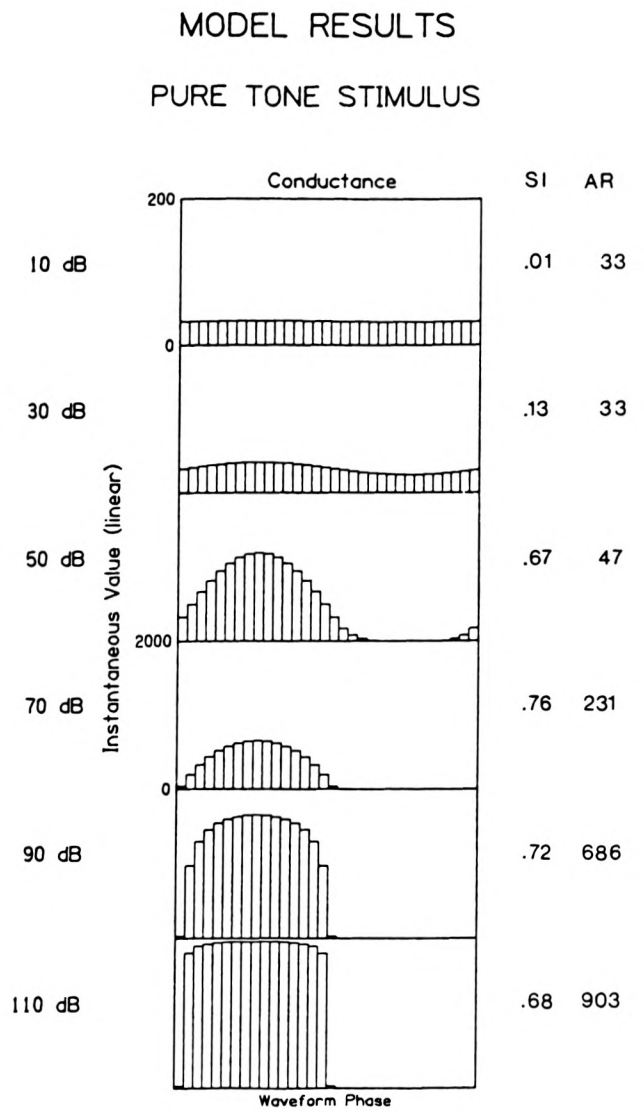

FIGURE 6 Model responses to a pure tone for the case of a high-spont. neuron (d = 0). Note the two different scales used in the left column. To the right of each panel the synchronization index SI and average rate AR are shown. Note that synchronization starts with modulation of the spontaneous rate, in other words SI starts increasing before AR.

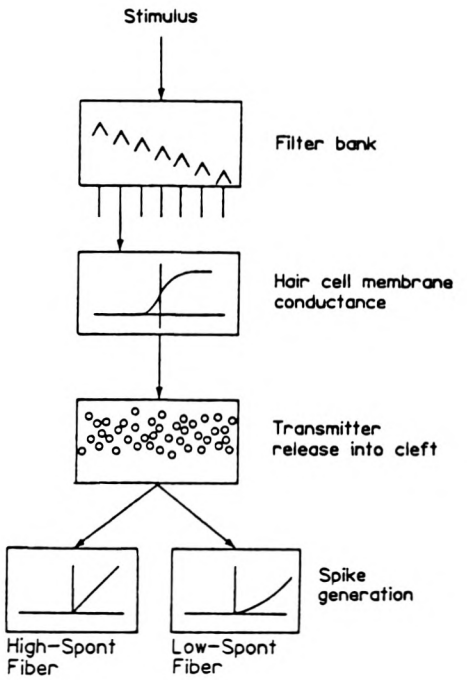

FIGURE 7 Final version of the model. The chemical synapse is sandwiched between two nonlinearities. The last nonlinearity represents the reduced ability of low-spont. neurons to produce spikes in response to small amounts of transmitter in the synaptic cleft.

rate-intensity curves. Our model goes a step further as it relates the IO function for instantaneous rate to the rate-intensity curve. The IO function was thought to be produced by the conductance of the hair-cell membrane; the effect of further processing by the hair-cell nerve-fiber synapse was originally assumed to be fairly linear. Geisler (1985) provided an IO function for instantaneous rate to describe responses of two-tone stimuli. It was not used for predicting rate-intensity curves. In that case, however, it would not have for produced much dynamics as the spontaneous rate y(0) and the maximum rate $0.5y(\infty)$ did not show much difference. More recently Geisler (1990) related an IO function to rate-intensity curves but this function cannot produce the high instantaneous rates that are observed in response to complex stimuli.

The model results show that a single IO curve cannot produce realistic instantaneous rates for complex stimuli on one hand and realistic rate-intensity

curves for pure-tone stimuli on the other hand. This problem can be solved by taking into account the third stage in the model. Then, the model produces more realistic rate-intensity curves for pure tones whereas the high instantaneous rates and the strong level dependence of responses to multi-component complexes are retained.

Behavior of low-spont. neurons could easily be produced by shifting the IO curve so far along the input axis, that the expansive part of the curve comes into effect for small stimuli. Importantly, the shape of the curve and the shift should not result in a value of $x_t > 0$. That would cause center clipping of the stimulus. McGee (1983) has clearly demonstrated that such responses are unlikely. This means that the model proposed by Greenwood (1988) which does produce center clipping is not adequate for simulating low-spont. fibers.

A shortcoming of the model is the attempt to explain differences in spontaneous rate by a different position of the IO curve. Although Howard and Hudspeth (1988) have actually shown shifts of curves of receptor potential as a function of displacement, it cannot be ignored that both high- and low-spont. fibers can innervate the same inner hair-cell (Liberman, 1982). This indicates that an additional nonlinear IO relation is needed after (or in combination with) the stage responsible for the transmitter release. This means that instead of the one initially proposed nonlinearity we need two different nonlinearities separated by the stage responsible for the transmitter release. A related but more simple model was described by Geisler (1990) consisting of these two nonlinearities but without the stage responsible for the transmitter release. In conclusion the model we propose is shown in Fig. 7.

References

Geisler, C.D. (1985). "Effects of a compressive nonlinearity in a cochlear model," J. Acoust. Soc. Am. 78, 257-260.

Geisler, C.D. (1990). "Evidence for expansive power functions in a the generation of the discharges of 'low-and medium-spontaneous' auditory-nerve fibers," Hearing Research 44, 1-12.

Greenwood, D.D. (1988). "Cochlear nonlinearity and gain control as determinants of the response of primary auditory neurons to harmonic complexes," Hearing Research 32, 207-253.

Horst, J.W., Javel, E., Farley, G.R., (1985). "Extraction and enhancement of spectral structure by the cochlea," J. Acoust. Soc. Am. 78, 1898-1901.

Horst, J. W., Javel, E., and Farley, G. R. (1986a). "Coding of spectral fine structure in the auditory nerve.I. Fourier analysis of period and interspike interval histograms," J. Acoust. Soc. Am. 79, 398-416.

Horst, J.W., Javel, E. and Farley, G.R. (1986b). "Effects of phase and amplitude spectrum in the nonlinear processing of complex stimuli in single fibers of the auditory nerve." In: "Auditory frequency selectivity," edited by Brian C.J. Moore and Roy D. Patterson (Plenum Publishing Corporation, New York and London) pp. 229-239.

Horst, J. W., Javel, E., and Farley, G. R. (1990). "Coding of spectral fine structure in the auditory nerve.II. Intensity-Dependent Nonlinear Responses," Submitted to J. Acoust. Soc. Am.

Horst, J.W., Wit, H.P. and Segenhout, H.M. (1988), "Single-fiber responses to complex sounds in the pigeon." In: "Basic Issues in Hearing," edited by H. Duifhuis, J.W. Horst and H.P. Wit (Academic Press, London) pp. 235-243.

Howard, J. and Hudspeth, A.J. (1988). "Compliance of the hair bundle associated with gating of mechanoelectrical transduction channels in the bullfrog's saccular hair cell". Neuron 1, 189-199.

Liberman, M.C. (1982). "Single-neuron labeling in the cat auditory nerve". Science 216, 1239-1241.

McGee, J. (1983). "Phase-locking as a frequency and Intensity Coding Mechanism in Auditory Nerve Fibers". Unpublished master's thesis, Creighton University, Omaha, Nebraska.

Meddis, R. (1986). "Simulation of mechanical to neural transduction in the auditory receptor," J. Acoust. Soc. Am. 79, 702-711.

Patterson, R.D. (1974). "Auditory filter shape," J. Acoust. Soc. Am. 55, 802-809.

Sachs, M.B. and Abbas, P.J. (1974). "Rate versus level functions for auditory-nerve fibers in cats: tone-burst stimuli." J. Acoust. Soc. Am. 56, 1835-1847.

Sachs, M.B., Winslow R.L. and Sokolowski B.H.A. (1989). "A computational model for rate-level functions from cat auditory-nerve fibers," Hearing Research 41, 61-70.

Wit, H.P. and Horst, J.W. (1986). "Contrast enhancement in frequency spectra of cochlear microphonic responses to complex stimuli". Hearing Research 21, 59-65.

CALCIUM IONS PROMOTE RAPID MECHANICALLY EVOKED MOVEMENTS OF HAIR BUNDLES

Fernán Jaramillo[1], J. Howard[2], and A.J. Hudspeth[1]

[1]*Department of Cell Biology and Neuroscience*
University of Texas Southwestern Medical Center, Dallas, TX 75235-9039, USA
[2]*Department of Physiology and Biophysics*
University of Washington School of Medicine, Seattle, WA 98195, USA

Introduction

The mechanoreceptive organelle of a hair cell, the hair bundle, consists primarily of a bevelled array of hexagonally packed stereocilia. When a mechanical stimulus is applied at a bundle's tip, the individual stereocilia behave as rigid rods that bend at their basal insertions into the cell's apical surface. The 20 or so actin filaments that form the cytoskeleton in this tapered basal region probably contribute much of the bundle's steady-state stiffness, which is approximately 1 $mN \cdot m^{-1}$ for the hair cells of amphibians (Howard and Ashmore, 1986; Howard and Hudspeth, 1987a; Denk *et al.*, 1989), reptiles (Crawford and Fettiplace, 1985), and mammals (Flock and Strelioff, 1984; Russell *et al.*, 1989).

The mechanical behavior of a hair bundle is not, however, fully determined by the passive properties of its constituent stereocilia: four phenomena suggest greater mechanical complexity. First, a hair bundle is less stiff – or more compliant – over the range of positions in which the transduction channels are neither all open nor all closed than it is in either extreme position (Howard and Hudspeth, 1988). This gating compliance is a statistical-mechanical effect that ensues from the reciprocal relation between force applied to transduction channels and their probability of being open (Howard and Hudspeth, 1988; Hudspeth *et al.*, 1989). In a second manifestation of mechanical complexity, hair bundles undergo oscillatory motions both spontaneously and following applied mechanical stimulation. This response has been observed in hair cells of the turtle's basilar papilla (Crawford and Fettiplace, 1985) and the bullfrog's sacculus (Howard and Hudspeth, 1987a; Denk and Webb, 1989). A third, time-dependent behavior is evident when a maintained mechanical force is applied to a hair bundle. Following an exponential timecourse with a time constant of 5-27 ms, the bundle's stiffness declines to about half its initial value (Howard and Hudspeth, 1987a, 1987b; Russell *et al.*, 1989). Because this mechanical relaxation is associated with adaptation of the mechanoelectrical transduction process (Eatock *et al.*, 1987; Howard and Hudspeth,

1987a), both phenomena may ensue from resetting of the gating springs that communicate force to the transduction channels (Howard and Hudspeth, 1987a, 1987b; Hacohen *et al.*, 1989; Hudspeth, 1989). The voltage dependence and Ca^{2+} sensitivity of adaptation (Eatock *et al.*, 1987; Assad *et al.*, 1989) suggest that Ca^{2+} enters through transduction channels and serves as the second messenger that effects adaptation.

The final type of complex mechanical response in hair bundles, and the subject of this communication, may be demonstrated by abruptly deflecting a bullfrog's saccular hair bundle in the positive (excitatory) direction with a flexible stimulus fiber. After an initial displacement in the direction of the applied force, and before the relaxation associated with adaptation, the bundle exhibits a transient movement in the negative direction (Howard and Hudspeth, 1987a, 1988). In a saline solution containing 4 mM Ca^{2+}, this rebound motion occurs roughly 1 ms after the onset of the stimulus, and lasts for about twice that long. Because it is associated with an abrupt decrease in the receptor current, this rebound movement is probably associated with the closure of mechanoelectrical transduction channels. The present study tests the hypothesis (Howard and Hudspeth, 1988) that Ca^{2+} is involved in the rebound and receptor-current decrease.

Methods

Experiments were performed at room temperature (20°-22° C.) on hair cells in saccular maculæ from bullfrogs (*Rana catesbeiana*). The preparations were maintained at pH 7.25 in a standard saline solution containing 110 mM Na^+, 2 mM K^+, 4 mM Ca^{2+}, 118 mM Cl^-, 3 mM D-glucose, and 5 mM HEPES; with adjustments of the Ca^{2+} concentration, the same solution was used during experiments. To provide access to hair bundles for electrodes and stimulus probes, otolithic membranes were detached after 40 min digestion in a similar solution containing 50 $mg \cdot l^{-1}$ subtilopeptidase BPN' (Sigma Chemical Co., St. Louis, MO).

Cells were observed at 500× under a mechanically stabilized microscope (UEM, Carl Zeiss, Inc., Oberkochen, Federal Republic of Germany) equipped with a 40×, water-immersion objective lens and differential-interference-contrast optics. Using previously described procedures (Hudspeth and Corey, 1977; Howard and Hudspeth, 1987a, 1988; Kroese *et al.*, 1989), we made intracellular voltage recordings with bent, conventional, glass microelectrodes (Hudspeth and Corey, 1978), whose resistances were 100-300 MΩ when filled with 3 M KCl. Measurements were made with a high-input-impedance amplifier system (Axoclamp-2A, Axon Instruments Inc., Burlingame, CA), whose headstage was mounted on a damped, leaf-spring micromanipulator. The resistance and capacitance of each cell's membrane were measured by injecting 10-30 pA current pulses through the recording electrode. To estimate the timecourse of the current transient underlying the depolarizing peak of the receptor potential, we digitally filtered each electrical recording by the inverse of the cellular input impedance. This procedure corrected the data of Fig. 2*B* for low-pass filtering by the cells' membranes.

Each hair bundle was stimulated with a horizontally mounted, flexible, glass fiber whose stiffness approximated 0.5 $mN \cdot m^{-1}$ at its tip. The base of the fiber was displaced by a piezoelectrical micromanipulator, whose risetime (10% to 90%) was 500 μs (Corey and Hudspeth, 1980). The position of the probe's tip, which was attached to the

kinociliary bulb in the hair bundle, was monitored by a photodiode projection system described previously (Howard and Hudspeth, 1988).

Stimuli were controlled and data were acquired and analyzed with a computer system (PDP-11/73, Digital Equipment Corp., Maynard, MA) equipped with an interface and software for physiological experimentation (BASIC-23, Indec Systems, Sunnyvale, CA). The mechanical and hydrodynamical properties of hair bundles and stimulus probes, and the resistive and capacitative characteristics of microelectrodes, limited the frequency responses of mechanical and electrical signals at respectively 0.7 kHz and 1 kHz. After appropriate filtering, responses were sampled at an interval of 500 μs.

Results

Application of a force step to a hair bundle rapidly evoked a brief depolarization in a hair cell (Fig. 1). This depolarization, which lasted a few milliseconds in standard saline solution, resulted from a spike of inward transduction current (Howard and Hudspeth, 1987a). During the peak depolarization, the hair bundle transiently reached a local maximum in its excursion, then reversed its direction of motion, producing a retrograde or rebound movement. The bundle thereafter gradually moved in the positive direction, a reflection of its relaxation; with the same timecourse, additional transduction channels closed in the phenomenon of adaptation.

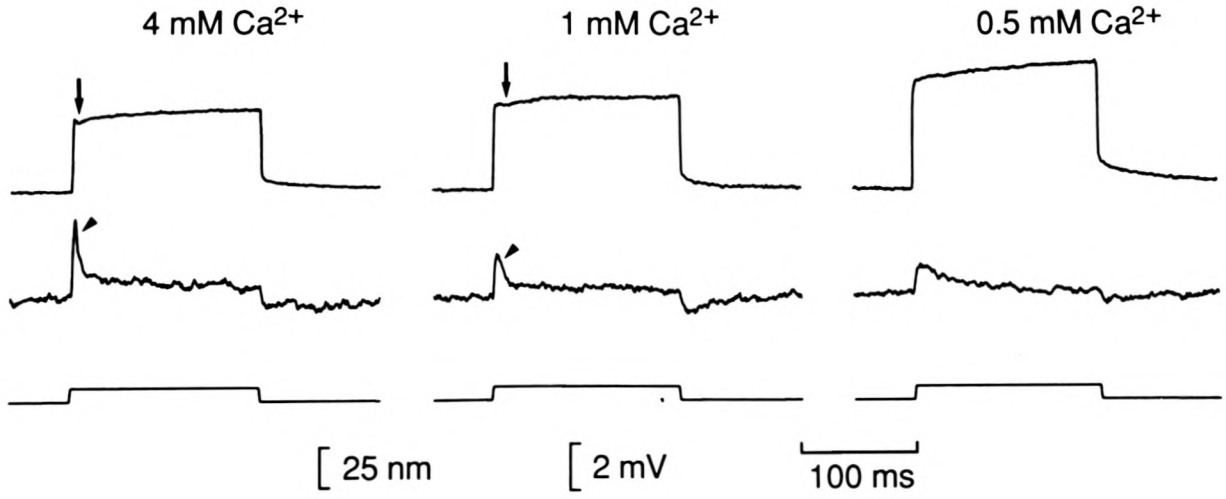

FIGURE 1 Hair-bundle displacements (upper traces) and intracellular electrical responses (middle traces) to mechanical stimuli applied by a flexible glass probe. The responses were obtained from three different cells, which were bathed in saline solutions with the Ca^{2+} concentrations indicated above the panels. Reducing the Ca^{2+} concentration slowed, and eventually obliterated, the rebound bundle motion (arrows) and depolarizing peak in the receptor potential (arrowheads). The base of the stimulus probe was displaced by 100 nm with the timecourse indicated (bottom traces).

The durations of the depolarizing peak and of the accompanying mechanical transient depended upon the extracellular Ca^{2+} concentration. As the Ca^{2+} concentration was progressively lowered from 4 mM, both the depolarization and the transient became slower and less pronounced (Fig. 1). At Ca^{2+} concentrations as low as 0.25 mM, neither the depolarizing peak nor the rebound was detectable. Restoration of 4 mM Ca^{2+} solution consistently restored the timecourse of the mechanical transient to its control value.

The half-widths of the depolarizing peak and of the mechanical transient displayed roughly hyperbolic dependences upon the Ca^{2+} concentration (Fig. 2). The two durations covaried with high significance ($r^2 > 0.99$).

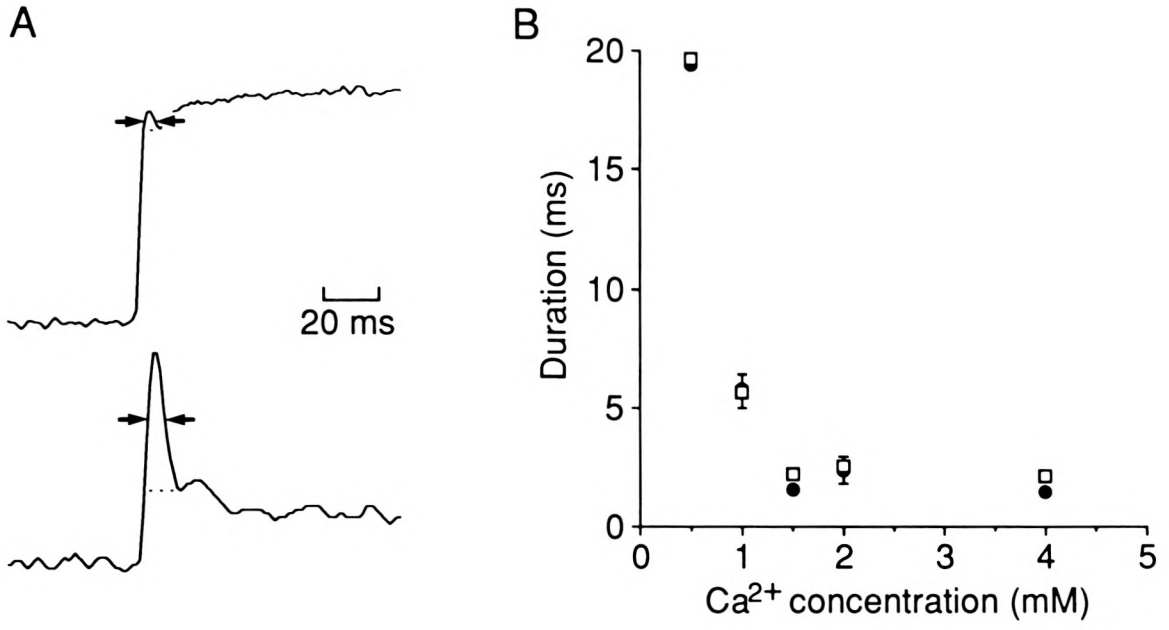

FIGURE 2 *A*, Measurement of the timecourses of the mechanical transient (upper trace) and of the peak depolarization of the receptor potential (lower trace). Each data point corresponds to the duration of the appropriate signal at half its maximal amplitude (between paired arrows). *B*, The dependence upon extracellular Ca^{2+} concentration of the timecourses of the hair bundle's transient motion (●) and of the depolarizing peak (□). The data, which are presented as means and their standard errors, included 2-13 determinations at each Ca^{2+} concentration.

Discussion

The present results extend the earlier evidence (Howard and Hudspeth, 1987a, 1988) for a relation between the rebound hair-bundle motion and the depolarizing peak that follow a step force stimulus. The two phenomena have similar durations, which moreover vary systematically and concurrently with changes in the extracellular Ca^{2+}

concentration. It seems probable that the depolarization and the mechanical transient have a common origin in the workings of the transduction apparatus.

Hair cells in the turtle's basilar papilla also exhibit a brief spike of receptor current in response to abrupt mechanical stimulation (Crawford *et al.*, 1989). When measured after small stimuli in a solution containing 2.8 mM Ca^{2+}, this current relaxation displays a relatively long time constant of 3-5 ms. The response has therefore been compared to the adaptive resetting of the hair cell's operating range described for the frog (Eatock *et al.*, 1987; Howard and Hudspeth, 1988a; Assad *et al.*, 1989; Hacohen *et al.*, 1989). Because it is not accompanied by mechanical relaxation of the hair bundle and its rate is sensitive to the extracellular Ca^{2+} concentration, however, the transient current in the turtle's cells may prove to be related to the faster transient current of the frog's cells.

According to the gating-spring model for mechanoelectrical transduction, deflection of a hair bundle increases the tension in elastic gating springs, which in turn apply forces that open the mechanically sensitive channels (Corey and Hudspeth, 1983; Howard and Hudspeth, 1988; Howard *et al.*, 1988; Roberts *et al.*, 1988; Hudspeth, 1989). There are two general ways in which this transduction process could adapt to stimuli. First, the tension in a gating spring could be reduced during protracted stimulation. This mechanism is thought to underlie the adaptive resetting of the transducer's working range (Eatock *et al.*, 1987; Howard and Hudspeth, 1987a, 1987b; Assad *et al.*, 1989; Hacohen *et al.*, 1989). Second, a channel's probability of being open at a given gating-spring tension could be reduced during sustained stimulation. The data presented here suggest that the decline of the depolarizing transient signifies adaptation by this second mechanism, which may be portrayed by the following kinetic scheme:

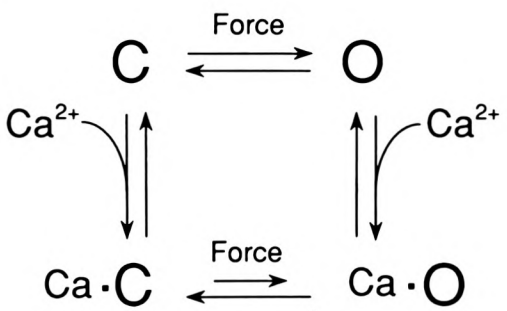

Here **C** and **O** are respectively the closed and open states of a mechanically sensitive channel. Deflection of the hair bundle in the positive direction stresses each gating spring and promotes opening of the associated channel. Ca^{2+} then flows through the channel, carrying a portion of the receptor current. As it accumulates in the stereociliary cytoplasm, Ca^{2+} binds to an intracellular site and stabilizes the channel in its closed state. In addition to reducing the receptor current, closure of the channel's gate exerts additional tension on the gating spring, which in turn pulls the bundle – and the attached stimulus probe – back in the negative direction. The binding of one or more calcium ions to a channel protein thus exerts a chemical force that opposes positively directed mechanical force acting on the hair bundle by driving the channel toward its closed state.

A straightford argument indicates that this scheme is thermodynamically reasonable. The work performed in pulling a hair bundle back 5 nm against the elastic resistance of a

stimulus probe is about 10^{-20} J; the speed of the rebound in high-Ca^{2+} solution indicates that a similar amount of work must be done against viscous drag. For Ca^{2+} alternatively to bind to and detach from a channel protein at kilohertz rates, the K_d of the Ca^{2+} binding site, and hence the intracellular Ca^{2+} concentration, might be expected to be approximately 25 μM (Jackson, 1989). Even in the cochlea, where the endolymphatic Ca^{2+} concentration is only 22-30 μM (Bosher and Warren, 1978; Ikeda *et al.*, 1987), the change in electrochemical potential of a calcium ion as it traverses a transduction channel could contribute a free energy in excess of 10^{-20} J. A substantial rebound motion could therefore be effected by binding of calcium ions to only a few of the roughly 50 transduction channels in a frog's saccular hair bundle.

The functional significance of the bundle's rebound movement remains uncertain. Because it occurs in response to deflections of 20 nm or less, retrograde motion could occur at physiological levels of acoustical and accelerational stimulation. The mechanism that underlies the rebound might also mediate oscillatory motions of hair bundles and the active processes of hair cells that are thought to enhance frequency tuning on the basilar membrane and to produce otoacoustic emissions (for a review, see Patuzzi and Robertson, 1988). Even if they prove to be but epiphenomena of transduction, however, the depolarizing peak and mechanical transient are experimentally useful probes of the mechanoelectrical transduction process.

Acknowledgments

The authors thank Mr. R.A. Jacobs for preparing the figures; he and Mr. J. Dittman kindly provided comments on the manuscript. This research was supported by National Institutes of Health grant DC00241, by the Perot Family Foundation, and by a Fellowship on Sensory Transduction to J.H. from l'Fondation pour l'Etude du Système Nerveux Central et Périphérique.

References

Assad, J.A., Hacohen, N., and Corey, D.P. (1989) Voltage dependence of adaptation and active bundle movement in bullfrog saccular hair cells. Proc. Natl. Acad. Sci. USA 86, 2918-2922.

Bosher, S.K. and Warren, R.L. (1978) Very low calcium content of cochlear endolymph, an extracellular fluid. Nature 273, 377-378.

Corey, D.P. and Hudspeth, A.J. (1980) Mechanical stimulation and micromanipulation with piezoelectric bimorph elements. J. Neurosci. Meth. 3, 183-202.

Corey, D.P. and Hudspeth, A.J. (1983) Kinetics of the receptor current in bullfrog saccular hair cells. J. Neurosci. 3, 962-976.

Crawford, A.C. and Fettiplace, R. (1985) The mechanical properties of ciliary bundles of turtle cochlear hair cells. J. Physiol. 364, 359-379.

Crawford, A.C., Evans, M.G., and Fettiplace, R. (1989) Activation and adaptation of transducer currents in turtle hair cells. J. Physiol. 419, 405-434.

Denk, W. and Webb, W. W. (1989) Simultaneous recording of fluctuations of hair-bundle deflection and intracellular voltage in saccular hair cells. In: Cochlear Mechanisms: Structure, Function, and Models (Eds. Wilson, J.P. and Kemp, D.T.) Plenum Press, New York, pp. 125-132.

Denk, W., Webb, W.W., and Hudspeth, A.J. (1989) The mechanical properties of frog sacculus hair bundles are reflected in Brownian motion measured with a laser differential interferometer. Proc. Natl. Acad. Sci. U.S.A. 86, 5371-5375.

Eatock, R.A., Corey, D.P., and Hudspeth, A.J. (1987) Adaptation of mechanoelectrical transduction in hair cells of the bullfrog's sacculus. J. Neurosci. 7, 2821-2836.

Flock, Å. and Strelioff, D. (1984) Graded and nonlinear mechanical properties of sensory hairs in the mammalian hearing organ. Nature 310, 597-599.

Hacohen, N., Assad, J.A., Smith, W.J., and Corey, D.P. (1989) Regulation of tension on hair-cell transduction channels: displacement and calcium dependence. J. Neurosci. 9, 3988-3997.

Howard, J. and Ashmore, J.F. (1986) Stiffness of sensory hair bundles in the sacculus of the frog. Hearing Res. 23, 93-104.

Howard, J. and Hudspeth, A.J. (1987a) Mechanical relaxation of the hair bundle mediates adaptation in mechanoelectrical transduction by the bullfrog's saccular hair cell. Proc. Natl. Acad. Sci. U.S.A. 84, 3064-3068.

Howard, J. and A.J. Hudspeth (1987b) Adaptation of mechanoelectrical transduction in hair cells. In: Sensory Transduction (Eds. Hudspeth, A.J., MacLeish, P.R., Margolis, F.L., and Wiesel, T.N.) Fondation pour l'Etude du Système Nerveux Central et Périphérique, Geneva, pp. 138-145.

Howard, J. and Hudspeth, A.J. (1988) Compliance of the hair bundle associated with gating of mechanoelectrical transduction channels in the bullfrog's saccular hair cell. Neuron 1, 189-199.

Howard, J., Roberts, W.M., and Hudspeth, A.J. (1988) Mechanoelectrical transduction by hair cells. Ann. Rev. Biophys. Biophys. Chem. 17, 99-124.

Hudspeth, A.J. (1989) How the ear's works work. Nature 341, 397-404.

Hudspeth, A.J. and Corey, D.P. (1977) Sensitivity, polarity, and conductance change in the response of vertebrate hair cells to controlled mechanical stimuli. Proc. Natl. Acad. Sci. U.S.A. 74, 2407-2411.

Hudspeth, A.J. and Corey, D.P. (1978) Controlled bending of high-resistance glass microelectrodes. Am. J. Physiol. 234, C56-C57.

Hudspeth, A.J., Roberts, W.M., and Howard, J. (1989) Gating compliance, a reduction in hair-bundle stiffness associated with the gating of transduction channels in hair cells from the bullfrog's sacculus. In: Cochlear Mechanisms: Structure, Function and Models (Eds. Wilson, J.P. and Kemp, D.T.) Plenum Press, New York, pp. 117-123.

Ikeda, K., Kusakari, J., Takasaka, T., and Saito, Y. (1987) The Ca^{2+} activity of cochlear endolymph of the guinea pig and the effects of inhibitors. Hearing Res. 26, 117-125.

Jackson, M.B. (1989) Perfection of a synaptic receptor: kinetics and energetics of the acetylcholine receptor. Proc. Natl. Acad. Sci. USA 86, 2199-2203.

Kroese, A.B.A., Das, A., and Hudspeth, A.J. (1989) Blockage of the transduction channels of hair cells in the bullfrog's sacculus by aminoglycoside antibiotics. Hearing Res. 37, 203-218.

Patuzzi, R. and Robertson, D. (1988) Tuning in the mammalian cochlea. Physiol. Rev. 68, 1009-1082.

Roberts, W. M., Howard, J., and Hudspeth, A. J. (1988) Mechanoelectrical transduction, frequency tuning, and synaptic transmission by hair cells. Ann. Rev. Cell Biol. 4, 63-92.

Russell, I. J., Richardson, G. P., and Kössl, M. (1989) The responses of cochlear hair cells to tonic displacements of the sensory hair bundle. Hearing Res. 43, 55-70.

MODULATION OF VOLTAGE RESPONSES TO 100 HZ TONES BY HIGH FREQUENCY TONES IN COCHLEAR HAIR CELLS

M. Kössl and I.J. Russell

School of Biological Sciences, University of Sussex, Falmer, Brighton, BN1 9QG, U.K.

Introduction

Inner (IHC) and outer (OHC) hair cells have been ascribed separate roles in mechanosensory transduction in the cochlea. The role of IHCs is assumed to be largely passive in that IHCs respond to the shear displacement between the tectorial membrane and the reticular lamina. The OHCs, on the other hand, may have an interactive role which, through electromechanical feedback of energy to the cochlear partition, enables them to control the shear displacements imparted to the IHCs. The relative gain and phase at which the OHCs feed back energy and the relative mechanical impedance of the major elements (the tectorial and basilar membranes) of the cochlear partition, are crucial to the effectiveness of the feedback process in bringing about the sharp tuning which has been observed in the mechanical properties of the cochlear partition (Sellick et al., 1982) and in the response of hair cells (Russell and Sellick, 1978; Dallos et al., 1982) and auditory fibres. (e.g. Kiang et al., 1965). As a means of exploring some of the properties of the interactive electromechanical processes in the cochlea, we have made intra- and extracellular recordings from IHCs and OHCs in the basal, high frequency turn of the guinea-pig cochlea and measured the voltage responses to a combination of a low frequency (100 Hz) tone and a high frequency tone at frequencies within a bandwith of approximately half an octave above and one octave below the characteristic frequency (CF) of the hair cells.

Methods

A detailed description of the methods of preparation, experimental techniques and stimulus presentation is given in Cody and Russell (1987). Recordings were made from 78 pigmented guinea-pigs (230-320 g) anaesthetized with the neurolept anaesthetic technique (0.06 mg atropine sulphate s.c.; 30 mg/kg pentobarbitone; 4

mg/kg droperidol; 1 mg/kg phenoperidine). The animals were tracheotomized, artificially respired and core temperatures were maintained at 37° C. Intra- and extracellular recordings were made with micropipettes which were advanced through the basilar membrane in the basal high frequency region of the cochlea. The resistances of the pipettes when filled with 4 M KAc were 180-280 Mohms. After capacitance compensation the bandwidth of the pipettes extended to 2-4 kHz. Low frequency voltage responses and dc receptor potentials were digitized and stored on disc using a microcomputer. High frequency ac receptor potentials were analyzed with a two channel lock-in amplifier (EG&G, Princeton, Model 5210) set in quadrature. The in-phase and quadrature outputs were digitized and the phase and magnitude were computed using the microcomputer. No attempt was made to compensate the data for the low pass characteristics of the recording system or the hair cells. All sound levels are in dB re 20 uPa.

Results

The data reported in this paper describe the voltage responses of IHCs and OHCs to 100 Hz tones and the tonic response (dc) and the fundamental (f) component of the phasic response (ac) to high frequency tones. A limited set of results from one animal are shown but they are representative of the responses recorded from all sensitive preparations made in these experiments. The traces in Fig.1 are from an IHC and show the intracellular receptor potentials recorded in response to combinations of a 100 Hz tone at 80 dB SPL and a tone at either CF (18 kHz), 13 kHz or 24 kHz. The first measurable dc response to the 13 kHz tone appears at a greater stimulus level than that required to evoke a dc response at CF. For tones at 24 kHz, the dc responses are not detected until the stimulus level exceeds 90 dB SPL.

The waveform of the response to the 100 Hz tone depends on the frequency and level of the high frequency tone presented with it. The 100 Hz tone evokes a typical asymmetrical, positive, receptor potential which phase-leads the organ of Corti microphonic and OHC responses to the 100 Hz tone by about 90°. When the 100 Hz tone is presented together with a tone at 13 kHz at a level which excites a dc receptor potential, the IHC response to the 100 Hz tone is attenuated, the waveform becomes symmetrical (its phase remains unchanged) and the waveform rides on the plateau of the dc receptor potential (Fig.1). In the presence of a tone at the CF (18 kHz), the response to the 100 Hz tone grows with increasing levels of the CF tone and reaches a maximum at 57 dB SPL (Fig.1), at the shoulder of the steep growth region of the dc-level function (see Fig.2), and then declines with increasing levels above this. For levels of the CF tone at and below 57 dB SPL, the response to the 100 Hz tone is shifted in negative direction with respect to the plateau of the positive dc receptor potential and is characterized by the development of a strong 2f component (Fig.1). For higher levels of the CF tone, the negative phase and the 2f component of the

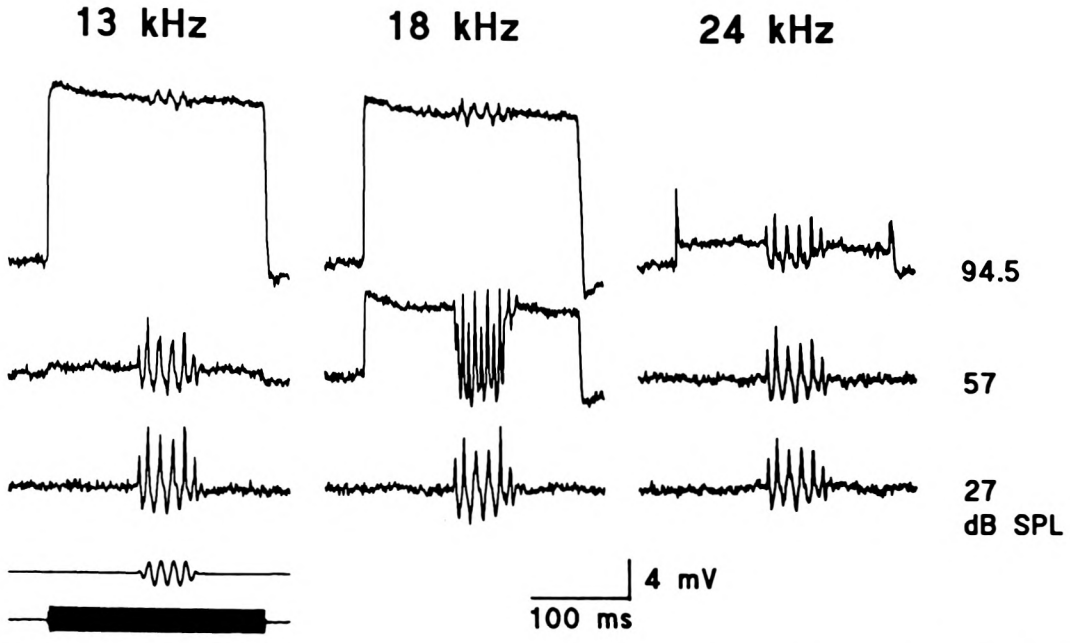

Figure 1 dc and ac voltage responses of an IHC to combined stimulation with a 100 Hz tone and an high frequency tone below, above and at CF (18 kHz) at the sound levels indicated; Resting membrane potential : -40 mV.

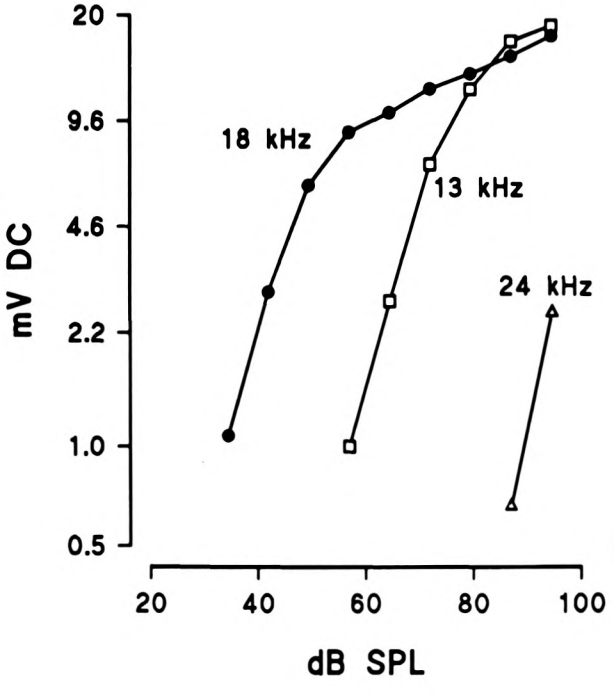

Figure 2 The amplitude of the dc voltage responses of an IHC plotted as a function of sound level at the frequencies indicated. Same cell as in Fig.1.

100 Hz response both decline and the waveform becomes more symmetrical. In the presence of the 24 kHz tone, the response to the 100 Hz tone remains unchanged until the level of the high frequency tone is sufficient to excite a dc receptor potential. At this level, the 100 Hz response develops a 2f component and is shifted in the negative direction with respect to the plateau of the dc receptor potential (Fig.1).

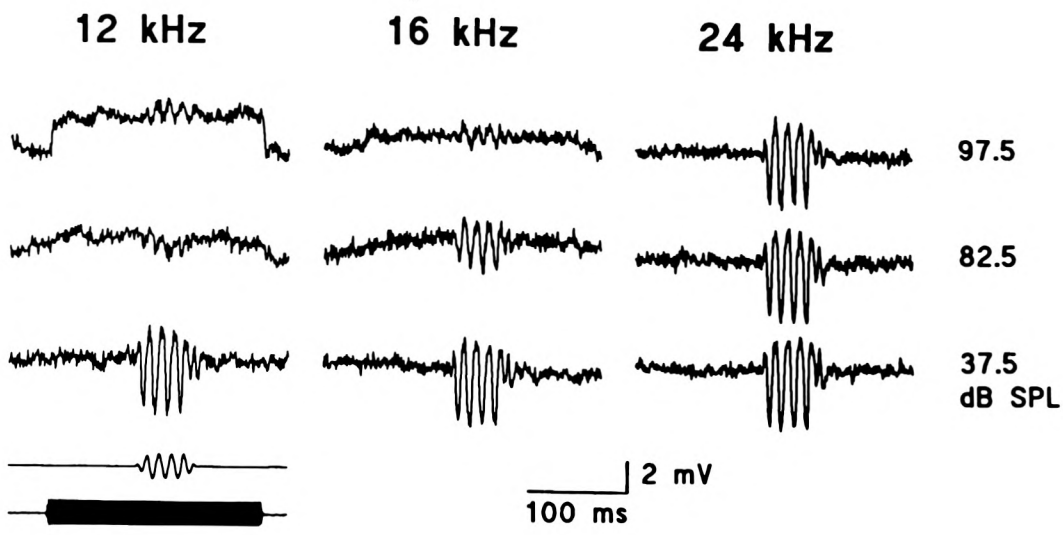

Figure 3 dc and ac voltage responses of an OHC to combined stimulation with a 100 Hz tone at 80 dB SPL and a high frequency tone below, above and at CF(16 kHz).

The responses of an OHC in the same cochlea to combinations of a 100 Hz tone at 80 dB SPL and a tone at CF (16 kHz), below CF (12 kHz) and above CF (24 kHz) are shown in Fig.3. The receptor potentials recorded from the OHC contrast with those of the IHC in that the response to the 100 Hz tone is predominantly negative and the dc receptor potentials generated by OHCs are much smaller than those of the IHCs and are generated only at very high stimulus levels. Furthermore, in contrast to the response of the IHC, no specific influence of the CF tone on the 100 Hz response is apparent. The responses to the 100 Hz tones are influenced only by the level and not by the frequency of the high frequency tone, at levels high enough to evoke a dc receptor potential, the negative phase of the 100 Hz response declines, the waveform becomes more symmetrical and rides on the plateau of the dc response.

In this preparation, an attempt was made to compare, simultaneously, the responses of adjacent IHCs and OHCs to the combination of the 100 Hz and the high frequency tone. This was achieved by making extracellular recordings from the organ of Corti adjacent to an IHC immediately before it was penetrated. By comparison of the extracellular with intracellular recordings made from IHCs and OHCs in this preparation, it was evident that the extracellular dc potentials are dominated by the responses of the IHC and the extracellular ac potentials are dominated by the responses of the OHCs. The magnitude and phase of the extracellular ac component, originating from OHCs, as functions of stimulus level are shown in Fig.4. These relationships are compared with the dc-level functions

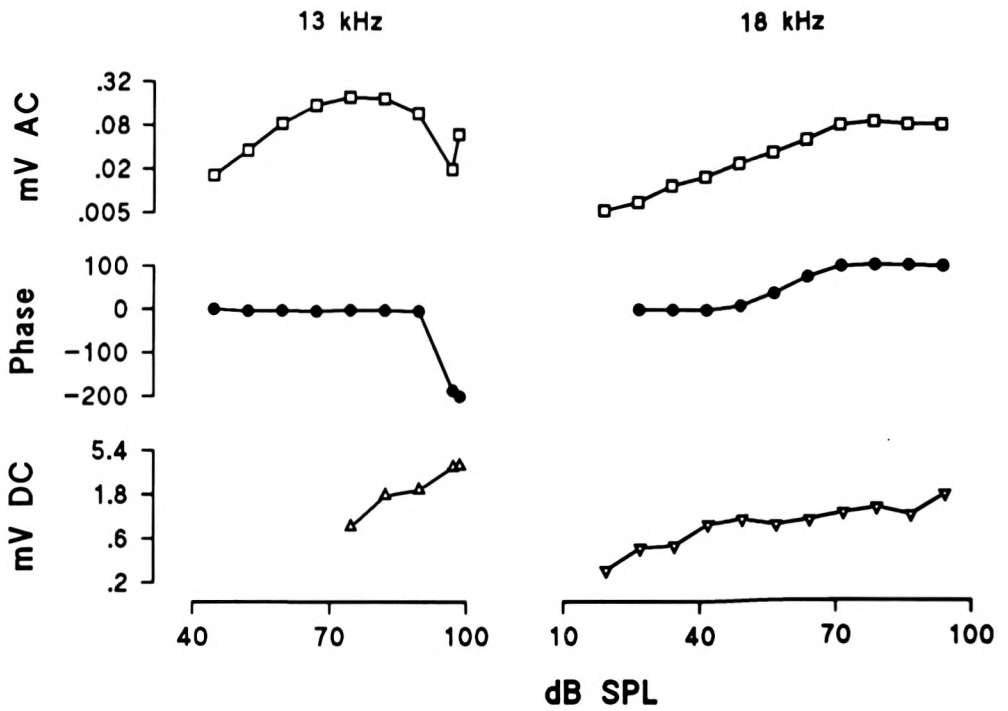

Figure 4 Extracellular responses recorded at a single electrode location from an IHC and adjacent OHCs to tones at 13 kHz and at 18 kHz(CF). Upper trace: magnitude of the fundamental of the OHC ac response; middle trace: phase of the OHC ac response: lower trace: amplitude of the IHC dc response, all as functions of sound level.

recorded extracellularly near the IHC. At 13 kHz, the magnitude-level function of the OHC ac component first grows with increasing level and then declines and shows a second growth phase at high levels. In the example shown, the stimulus levels employed were insufficient to fully explore the second stage. It is evident from data obtained in other preparations, that saturation of the ac response during the second stage of growth was not reached for levels below 105 dB SPL. Throughout the first growth stage, the phase of the ac component remains constant but lags by about 180° during the second stage of growth. There is no measurable dc response of the IHC until the stimulus is increased to a level which causes saturation of the OHC ac response. At CF (18 kHz), the OHC ac-level function and the IHC dc-level function have similar thresholds. Up to 50 dB SPL, the phase of the OHC ac response remains constant and the IHC dc response grows relatively steadily. Above 50 dB SPL the dc response starts to saturate and the phase of the ac response leads progressively and asymptotes to a lead of 90° at 70 dB SPL. At this level the ac response saturates.

Discussion

This paper reports three main findings. The first is that OHCs in the basal turn of the guinea pig cochlea do not generate measurable dc receptor potentials to high frequency tones at low and moderate sound levels (Fig.3). At these levels the ac responses grow, and the phase remains constant and independent of level. It is only at higher levels, when the OHC ac responses are saturated or show a second stage of growth, that the OHCs generate positive dc responses and the phase of the ac response changes with level and either lags or leads the phase at low levels. The second is that, for frequencies below CF, IHCs do not generate a dc receptor potential during the first growth stage of the OHC ac-level function (Fig.4). At CF, the IHC dc- and OHC ac-level functions have similar thresholds and the IHC dc-level function begins to saturate when the phase of the OHC ac response begins to lead. The third finding is that receptor potentials of IHCs to 100 Hz tones are modulated by a simultaneously presented high frequency tone (with a frequency within an octave of CF) in a way which depends on the frequency and level of the higher frequency tone whereas modulation of OHC responses to 100 Hz tones depends only on the level of the high frequency tone.

The finding that OHCs in the basal turn of the guinea-pig cochlea do not generate dc receptor potentials until the ac-level function saturates confirms earlier reports (Russell et al., 1986; Cody and Russell, 1987) and leads to the suggestion that OHCs actively minimize the dc response to optimize the feedback of energy to the cochlea . The proposal that the waveform of the OHC receptor potential is somehow regulated comes from *in vivo* studies on the level-dependence of the waveform of OHC voltage responses to low frequency tones and from a mechanical analog of this, the OHC dc motile response which has been studied in isolated OHCs (Evans et al., 1988).

Experimental evidence is accumulating in support of the hypothesis that OHCs feed back energy to the cochlear partition as a means of overcoming viscous forces which would otherwise damp the mechanical tuning of the hair cells at CF. According to a feedback model of cochlear function (Mountain et al., 1983), the mechanical forces produced by OHCs are governed by the OHC transducer conductance and hence the transducer current or receptor potential. The forces produced by the OHCs are assumed to form one arm of an electromechanical, negative feedback loop which opposes the motion of the basilar membrane for frequencies below CF. At the CF, the phase of the feedback would change by 180° and augment the motion of the basilar membrane. We would extend this hypothesis by suggesting that OHCs generate not only ac forces but also dc forces, one component of which is directed in the radial plane of the basilar membrane. According to this hypothesis, at frequencies below CF, the proposed radially directed forces oppose the generation of dc receptor potentials in IHCs and at the CF they support them. The experimental evidence which leads us to these proposals is that, for frequencies below CF, OHCs generate

ac responses at sound levels 20-30 dB below those which evoke dc receptor potentials in adjacent IHCs. At frequencies below CF, positive dc responses are generated in IHCs only when the OHC ac-level function (and presumably the feedback) has saturated. At CF, the IHC dc and the OHC ac response thresholds are similar, presumably as a consequence of the suggested positive feedback (see Fig.4). The IHC dc response begins to saturate about 40 dB above the detection threshold when the OHC ac response begins to phase lead and the feedback is presumably less effective. The level and frequency dependent modulation of the IHC voltage responses to the 100 Hz tone by the high frequency tone presented simultaneously (Fig.1), provides further support for the hypothesis that OHCs generate dc forces in the radial direction which displace the IHC transfer functions (the peak transducer conductance from resting conductance as a function of sound pressure level) along the level axis. The modulation of the IHC voltage responses to 100 Hz tones by high frequency tones, can be acounted for if the dc responses evoked by the high frequency tones are associated with a level dependent shift in the transfer function equivalent to applying an excitatory bias to the IHC stereocilia bundle for tones at and above CF and an inhibitory bias for frequencies below CF. The responses of OHCs to 100 Hz tones show only a level dependent decrease in the presence of a high frequency tone when the tone is loud enough to generate a dc response from the OHCs (Fig.2). This decrease is seen at all frequencies including CF. There is no increase of the 100 Hz response at CF as in IHCs.

How might IHC stereocilia be biased by the action of the OHCs in a level and frequency dependent manner while the bias of OHC stereocilia is only level dependent? An answer to this question may hinge on the recent finding that the radial stiffness of the tectorial membrane is considerably less than that of the combined radial stiffnesses of the OHC stereocilia (Zwislocki and Cefaratti, 1989) except possibly at CF when the radial mechanical impedance of the tectorial membrane may be similar to that of the organ of Corti (Zwislocki, 1986). If the direction of dc forces exerted by OHCs are only level and not frequency dependent, then as a consequence of changes in the relative mechanical impedances of the tectorial and basilar membranes at CF, these forces could act to produce an outward shear displacement of the tectorial membrane relative to the reticular lamina at CF and a shear displacement in the reverse direction at frequencies below CF which would result in an excitatory versus inhibitory bias of the IHC stereocilia. If the mechanical impedances of the tectorial and basilar membranes are similar at CF, then it might be expected that IHCs would be driven by input from both the tectorial membrane and the basilar membrane and the ac response should reflect this by the presence of a strong 2f harmonic component. Support for this proposal comes from the observation in Fig.1 that the IHC response to the 100 Hz tone in the presence of a tone at CF contains a strong 2f component.

Acknowledgements

This work was supported by the MRC, Wolfson Foundation and Hearing Research Trust. M.K. was supported by a fellowship from the Deutsche Forschungsgemeinschaft. We thank Jim Hartley for excellent electronic technical assistance and Ann Brown, Alan the Cody, Cornè Kros and Alfons Rüsch (the two s'ckrs) for discussion and comments on the manuscript.

References

Cody A.R. and Russell I.J (1987) The responses of hair cells in the basal turn of the guinea-pig to tones. J. Physiol., 383, 551-569.

Dallos, P., Santos-Sacchi J. and Flock Å. (1982) Intracellular recordings from cochlear outer hair cells. Science 218, 582-584.

Evans, B.N., Dallos, P. and Hallworth, R. (1989) Asymmetries in motile responses of outer hair cells in simulated in vivo conditions. In: J.P. Wilson and D.T. Kemp(Eds.) Mechanisms of Hearing. Plenum Publishing, New York, pp.205-206.

Kiang, N.Y-S., Watanabe, T., Thomas, E.C. and Clark, L.F (1965) Discharge patterns of fibers in the cat's auditory nerve. Cambridge, Mass., MIT Press.

Mountain, D.C., Hubbard, A.E. and McMullen, T.A. (1983) Electromechanical processes in the cochlea. In: E. de Boer and M.A. Viergever (Eds.), Mechanics of Hearing, Delft University Press, Delft, The Netherlands, pp. 119-126.

Patuzzi, R.B., Yates, G.H. and Johnstone,B.M. (1989). Changes in cochlear microphonic and neural sensitivity produced by acoustic trauma. Hear. Res. 39, 189-202.

Russell, I.J. and Sellick, P.M. (1978) Intracellular studies of hair cells in the mammalian cochlea. J. Physiol. 284, 261-290.

Russell, I.J., Cody, A.R. and Richardson, G.P. (1986) The responses of inner and outer hair cells in the basal turn of the guinea-pig cochlea and mouse cochlea grown in vitro. Hear. Res. 22, 199-216.

Sellick, P.M. Patuzzi, R.B. and Johnstone, B.M. (1982) Measurement of basilar membrane motion in the guinea-pig using the Mössbauer technique. J. Acoust. Soc. Am. 72, 131-141.

Zwislocki J.J (1986) Analysis of cochlear mechanics. Hear. Res. 22, 155-169.

Zwislocki J.J., and Cefaratti L.K. (1989) Tectorial membrane II: stiffness measurements in vivo. Hear. Res. 42, 211-228.

Movements and mechanical properties of ampullary hair bundles and of their kinocilium

Alfons Rüsch * and Ulrich Thurm

Zoological Inst., University of Münster, D–4400 Münster, F.R.G.

Introduction

For the study of hair bundel movements the semicircular canals provide long, pointerlike bundels. In fish and frogs the stereovilli (=stereocilia) are up to $15\mu m$ long and the kinocilium can be longer than $70\mu m$ (Wersäll, 1956; Nagel and Thurm, 1986). We made use of this pointerlike configuration and the uniform alignment of ampullary hair bundles in order to look for active contributions of hair bundles to the receptor properties, especially the adaptation of the cells. Stimulus dependent motor responses or changes in stiffness of the kinociliums were particularly conceivable with regard to the facts that vestibular hair cells retained a complete ciliary motor equipment throughout the evolution of the vertebrates (Hamilton,1969) and that motility of the kinocilium had occasionally been observed (Brown,1931; Flock et al., 1977). Moreover, the kinocilium of vestibular hair cells also retained to be the only way on which the stimulatory force is conveyed to the stereovilli (e.g. Hillman and Lewis, 1971), the site of mechano-electric transduction as shown by Hudspeth and Jacobs (1979).

Methods

In young eels, *Anguilla anguilla L.*, – chosen because of the transparency of their organ – the left frontal ampulla was exposed, and the whole isolated vestibular organ kept intact (fig. 1). A detailed description of the methods was recently given by Rüsch and Thurm (1989 and 1990). Current injection was done transepithelially according to fig. 1 after the cupula had been sucked off by a micropipette.

In some experiments kinocilia were detached from the stereovilli by lowering the amount of divalent cations, especially calcium. This was achieved by superfusing the hair cells for a few seconds with an artificial endolymph (EN-solution) containing $4\,mM\ EGTA$. After re-infusion of regular EN-solution the kinocilia and the bundle

Present address: MRC Neurophysiology Group, School of Biological Sciences, University of Sussex, Falmer, Brighton BN1 9QG, U.K.

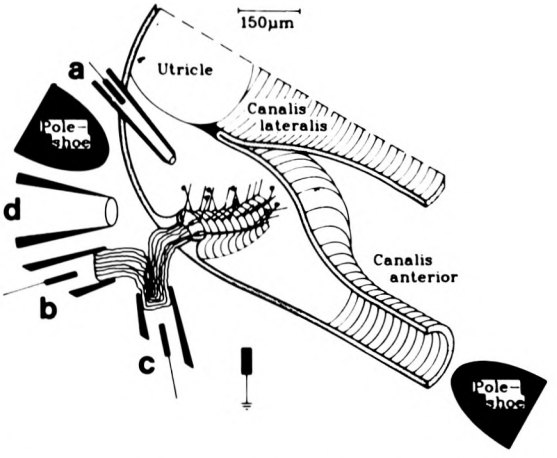

Figure 1: Scheme of the preparation as used in the experiments. With interference optics individual sensory hair bundles could clearly be visualized within the intact ampulla (fig.4a). A microthermocauter was used to make holes into the ampullary wall for micropipettes. The cupula was sucked off with micropipette a. This pipette was also used for infusion of EN-solution and ferromagnetic particles and served as an electrode. Two suction electrodes were used to record from the nerve fibres (electrode b) and to stimulate them electrically (electrode c). Mechanical stimulation of the hair cells was done by electromagnetic displacement of small ferromagnetic particles which preferably attached to the tips of the kinocilia (suspension of particles of Fe_3O_4 with a charged surface). In reality the tips of the two pole-shoes were at equal distance from the crista.
Movements of kinocilia and stereovilli were continuously recorded in the plane of hair-bundle symmetry by a modified videosystem (C1000, Hamamatsu, Japan) or by a pair of photodiodes (for time resolution $\geq 5\,Hz$) attached to an inverted photomicroscope (Zeiss, ICM 405; Normarski optics; 40x objective). Ferrit particles ($\leq 0.5\mu m$) were used also to enhance the contrast of the cilia. The spatial resolution obtained for object shifts was about $150\,nm$ by the video system and $20\,nm$ by the photodiodes. All experiments were done at room temperature (about 20° C).

of stereovilli did not re-connect: detached kinocilia could mechanically be moved without deflecting the stereovilli and the bundle of stereovilli could be deflected without moving the kinocilium (Rüsch and Thurm, 1989).

Results and Discussion

Movements of the kinocilium and the hair bundles

In the intact ampulla the tips of the kinocilia are firmly embedded in the cupula, and no movements could be observed. After removal of the cupula the Brownian motion of the hair bundles could be observed which is similar to irregular pointer-like deflections of a stiff rod hinged at its point of insertion (root mean square displacement of the tips of $65\mu m$ long kinocilia: $x_{r.m.s} = 68nm$).

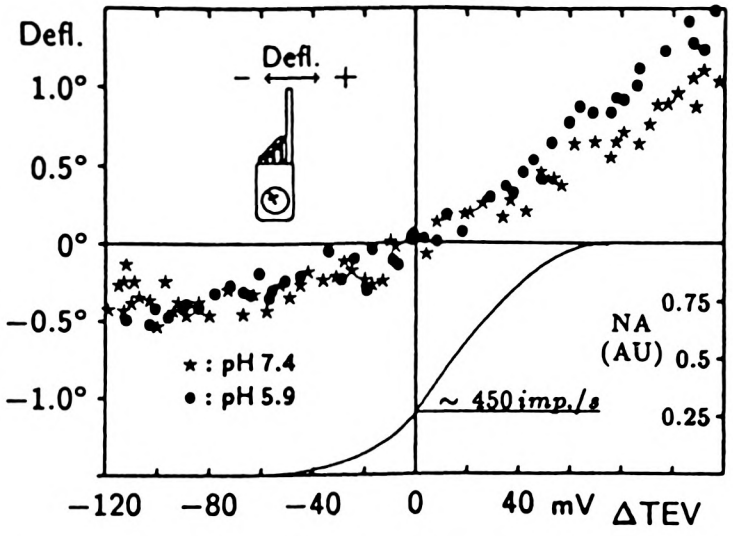

Figure 2: Stimulus-response curve of electrically induced tonic deflections of hair bundles. Deflections of one ampullary hair bundle at pH 7.4 of EN- and artificial perilymph- (PE-) solution and 1 h later at pH 5.9 of EN-solution (PE-solution: pH 7.4) measured at the tip of the kinocilium. The cupula had been removed from the ampulla shortly before this experiment. Deflections measured 450 ms after the onset of the voltage step. Inset in the lower part of the figure: nerve activity versus ΔTEV. Here an eye-fitted curve to the data of different ampulla (with an intact cupula) is plotted instead of the nerve activity of this ampulla which was also recorded during this experiment. This was done because the removal of the cupula reduced the spontaneous nerve activity by up to 50 % - apparently a consequence of disarranging the resting positions of the hair bundles.

Another form of movement was a periodic wriggling of the kinocilium at frequencies between 0.5 and 10 Hz with the bending pattern of swimming sperm flagella. This beating of the kinocilium was powerful enough to deflect the bundle of stereovilli by an angle which would produce a saturating receptor response. If the cupula was still attached, it strongly damped the movement, but could not suppress it. Spontaneous beating of cilia did not occur in fresh preparations but correlated with the deterioration of the preparation during the experiment. In fresh preparations beating of cilia could be elicited by gently pressing onto the tip of a kinocilium. With the cupula still attached, a multitude of kinocilia started and stopped beating simultaneously when a stimulating probe was advanced or withdrawn from the cupula.

One conceivable function of the kinocilium could be that it is part of a feedback-loop controlling the deflection of the stereovilli. Thus, it could contribute to the adaptation of the cell and enlarge the working range of the receptor. This hypothesis is supported by the observation that in all hair cells with a kinocilium the cupula or the otolithic membrane is attached to the tip of the kinocilium only (e.g. Hillman and Lewis, 1971). Mechanical stimuli to the stereovilli could therefore be controlled by the kinocilium if the stimulus induces motor activity in the cilium for example via a rise in intracellular calcium, induced by the receptor current.

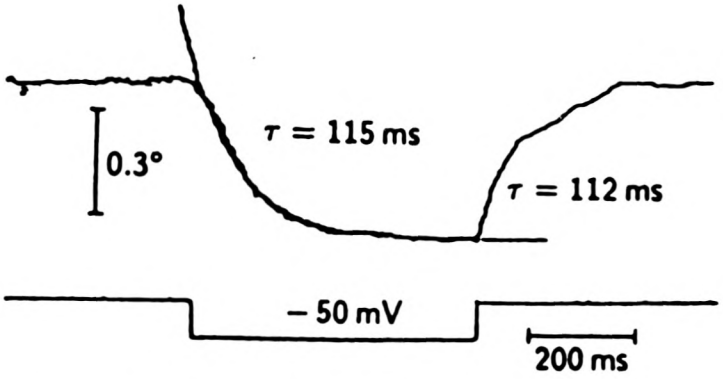

Figure 3: Time course of electrically induced deflections of a hair bundle. upper trace: signal from photodiodes adjusted to measure the movement of the tip of the kinocilium, average of 8 samples. An exponential function has been fitted to the on-reaction. lower trace: transepithelial voltage, command signal.

In order to check on this hypothesis we injected current into the ampulla and polarized the crista transepithelially. Such changes in the transepithelial voltage (TEV) induced pointerlike deflections of the hair bundles in the plane of symmetry of the bundles. The kinocilia moved like stiff rods hinged at their bases (at step-like commands: $\tau = 120ms$, S.D. $\pm 30ms$; n = 6; fig.3; at sinusoidal commands: roll-off frequency $1.3\,Hz$ with a decline of $-4.0\,dB/octave$ S.D. $\pm 0.7\,dB/octave$).

As a control for a possible electrophoretic origin of the movement, current was injected from either side of the ampulla alone or from both sides simultaneously or from one side to the other. No change in the electrically induced deflections was observed.

The angle of deflection was a graded function of the stimulus amplitude (within the range of physiological ΔTEV: $\pm 0.6°$, seldom up to 1°; fig. 2). When the lumen of the ampulla was made positive the deflections of hair bundles were in the positive direction, i.e. towards the kinocilium. Polarization of opposite sign induced deflections in the opposite, i.e. negative direction. At the cellular level this means positive deflections of hair bundles occured at current injection which tends to hyperpolarize the apical cell membrane and depolarize the basolateral membrane, and vice versa. (Within the current path, the regular polarizations of the membranes are opposed.)

The analysis of the responses of 12 hair cells revealed, however, that not for all of them the TEV dependency could be fitted by the above described curve, but that a continuum of different curves resulted with the fig. 2 representing one extreme of this continuum. In the other extreme the negative deflections reversed to positive deflections at more negative ΔTEV. Such forms of response curve were found in 4 out of 12 cells, whereas 6 cells had response curves more or less similar to type 1. The single curves are different overlapping segments of one type of curve. This common curve is non-monotonic and can be roughly approximated by a parabola.

When the kinocilium and the stereovilli were disconnected (fig.4b), changes in TEV induced pointer-like deflections not only of the kinocilium but also of the bundle of stereovilli (fig.5). At a sinusoidal voltage change of $2\,Hz$ both organelles

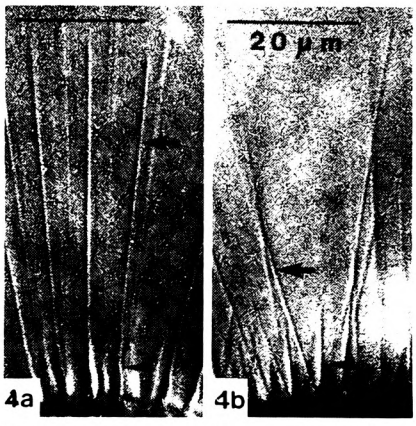

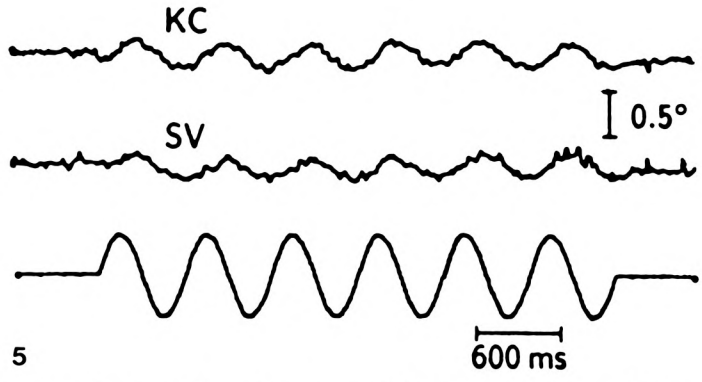

Figure 4: Detachment of kinocilia from the bundle of stereovilli by perfusion with an EGTA-EN-solution ($4\,mM$ EGTA $\sim$ $pCa8$). a. Previous to Ca-deprivation: Intact hair bundles with the (invisible) cupula attached to the tips of the kinocilia. b. Following Ca-deprivation, again in EN-solution: detached kinocilia. The cupula has been removed before. The arrows point towards the kinocilia, the arrow heads mark the bundles of stereovilli.

Figure 5: Electrically induced movements of a bundle of stereovilli and the detached kinocilium. The kinocilium (KC) had been disconnected from the stereovilli. Bottom: command signal (ΔTEV: $2\,Hz$; $100\,mV$ (peak - peak)). Recording of the movement of the kinocilium and the stereovilli by the video system at about $12\,\mu m$ above the crista. Average of 20 samples.

moved with roughly the same angular amplitude and phase relation. In some cells the movement of the kinocilium alone or of both structures together intermittently stopped and re-appeared. Deflections of the kinocilium alone were not observed. Any structural coupling between both structures could be excluded by their independent movement if separately forced by magnetic particles or by a mechanical probe.

This observation of an independent movement of the bundle of stereovilli is inconsistent with the idea that the kinocilium is the motor for the observed deflections. It also suggests that our hypothesis of feedback control through the kinocilium does not fit, at least in its original form. This is further supported by the observation that the electrically induced deflections were neither blocked by an agent that interfers with normal ciliary activity (Ni^{2+}) nor by deprivation of extracellular calcium or a blocker of calcium flux (Mn^{2+}), nor by the long term application of $1\,mM$ CN^-. Only glutaraldehyde (1.6 %) or triton X-100 (1 % in the apical solution) immediately blocked the movements. These results are not in favour for the hypothesis by Assad at al. (1989) which proposed a Ca^{++}– dependent active force development of the stereovilli (cf.also Art et al.,1986).

It seems likely that these deflections are caused by a mechanism which is resident to the cell body and is driven directly by the injected electrical energy. Electrostriction of the cell membrane and electroosmosis are such mechanisms.

However, electroosmosis could not explain the asymmetric, non-monotonic stimulus-response curve (fig. 2).

The electric field across a membrane effects its thickness (electrostriction) and its surface tension via a change in the charge density. As a consequence, the intracellular pressure may change. A rough estimation for these cells according to a formalism by Requena et al. (1975) shows that a voltage change of $100\,mV$ would induce a change in intracellular pressure of about $20\,Pa$ ($= 20\,pN/\mu m^2$). This is apparently enough to move an ampullary hair bundle that can be deflected through 1° by a force of about $2\,pN$ as we detremined.

Electrostriction as well as surface tension are parabolic functions of the membrane voltage. This type of function appears to be particularly appropriate to explain the form of the stimulus-response curves. But our data do not allow to make a final decision about these mechanisms. Results may be complicated by the fact that the apical and basal membrane areas are polarized with opposite sign during transepithelial current injection.

Stiffness of the hair bundles and the kinocilium

We used three different methods to evaluate the stiffness of the hair bundles:
1. Force-clamped deflection: Ferromagnetic particles were attached to the tips of kinocilia by infusing them into the ampulla after the cupula had been sucked off. An electromagnetic field was subsequently used to displace the particle and the hair bundle. The resulting mechanical force was calibrated by applying Stoke's law to the measured velocity of free-floating particles similar in size and close to the fixed particle at the kinocilium.
2. Mechanical relaxation: The time course of mechanical relaxation of a hair bundle from a magnetically induced deflection (see above) was used to calculate the stiffness of the hair bundle. A formalism by Lindeman et al. (1973) was applied.
3. FFT-analysis of thermal motion: In an approach similar to that of Denk et al. (1989) we analyzed the Fourier transforms of the Brownian motion of hair bundles and kinocilia. From these power spectra of motion fluctuations x_{rms}, the root mean square displacement of the tip of the kinocilium was calculated. It is correlated to the translational stiffness K according to $K = (k_B\,T)/x_{rms}^2$.

In the mean of all three methods the rotational stiffness of these hair bundles was $K^* = 5.8 \times 10^{-15}\ N\,m\,rad^{-1}$ (S.D. $\pm 4.1 \times 10^{-15}\ N\,m\,rad^{-1}$). Compared to saccular and cochlear hair bundles, the stiffness of ampullary hair bundles is by factor 2–10 smaller. This difference may correspond to the smaller number of stereovilli in these hair cells (eel ampulla: 20–30 (Nagel, 1986)).

The stiffness of the detached kinocilium was measured by the methods 2 and 3: $K^* = 0.75 \times 10^{-15}\ N\,m\,rad^{-1}$ (S.D. $\pm 0.8 \times 10^{-15}\ N\,m\,rad^{-1}$). In the mean, the contribution of the kinocilium to the stiffness of the complete hair bundle is 15 % . It may vary between 10 and 25 % .

After the disconnection from the stereovilli the kinocilia diverged from the rest of the hair bundle by an angle of 8.0° (S.D. ± 5.0°; n = 44 hair bundles in 2 ampullae; range: 0.0° – 22°).This splitting is accompainied by a step down of the spontaneous nerve activity by 42% (±13%). At the untreated hair bundle this amount of reduction is produced by 1.3° of deflection. 1.2° is the deflection of the stereovilli

which would result from the splaying force according to the ratio of stiffnesses of the kinocilium versus the bundle of stereovilli. The correspondence suggests that the kinocilium exerts a permanent tension onto the bundle of stereovilli.

The infusion of the calcium ionophor A 23 187 ($50-100\mu mol$) into two ampullae did not alter the angle of divergence between the kinocilia and the stereovilli (n = 62 and 17), but in 50 % of the hair cells, the ionophor increased the stiffness of complete hair bundles by 30 % (S.D. $\pm 5\%$). Similar data were obtained from the frog ampulla by Orman and Flock (1983). By disconnecting the kinocilium from the stereovilli we found that the increase in stiffness of the complete hair bundle is mainly due to an increase in stiffness of the kinocilium by a factor 2.4. Changes in the stiffness of the stereovilli remained within the range of uncertainty of the measurements.

With method 2 (relaxation from deflection) we measured the stiffness of the hair bundles during an electrically induced deflection. No changes in the time constants of relaxation were observed. This contrasts with the finding that every deflected state is reached significantly faster if the deflection is electrically induced ($\tau = 120\,ms$) than if it is forced mechanically ($\tau \sim 400ms$). This conspicuous fact would find an explanation if the electrically induced force is initially stronger but decays as the hair bundle approaches the stable position.

We tested the hypothesis whether efferent stimulation of the hair cells can change the mechanical properties of the hair bundles. The success of efferent stimulation, done by electrical stimulation of the whole ampullary nerve, was infered from the off-effect in afferent fibres, i.e. a long-lasting increase in afferent activity after the cessation of efferent stimulation. But neither the resting position of the hair bundles nor their stiffness (i.e. their time course of relaxation from mechanical stimulation) changed during or after repeated efferent stimulation.

Acetylcholine and the following ACh-related drugs were tested whether they changed the stiffness of the hair bundles: muscarine (cholinergic agonist affecting muscarinic receptors), pilocarpine (muscarine-analog), nicotine (cholinergic agonist affecting nicotinic receptors), dimethylphenylpiperazine (nicotine-analog), and adrenaline. Changes in stiffness were never observed as measured by various combinations of the three methods stated above.

We cannot exclude the possibility of an efferent control by a different transmitter or a cotransmitter which were not included in the present work. However, the effectlessness of electrical efferent stimulation makes it unlikely that the mechanical properties of ampullary hair bundles are under (immediate) efferent control.

Acknowledgements: This work was supported by Deutsche Forschungsgemeinschaft (SFB310).

References

[1] Art, J.J., Crawford, A.C. and Fettiplace, R. (1986) Electric resonance and membrane currents in turtle cochlear hair cells. Hear. Res. 22, 31–36.

[2] Assad, J.A., Hacohen, N. and Corey, D.P. (1989) Voltage dependence of adaptation and active bundle movement in bullfrog saccular hair cells. Proc. Natl. Acad. Sci. USA 86, 2918–2922.

[3] Bowen, R.E. (1931) Movement of the so-called hairs in the ampullar organs of fish ears. Proc. Natl. Acad. Sci. USA 17, 192–194.

[4] Denk, W., Webb, W.W. and Hudspeth, A.J. (1986) Optical measurement of the Brownian motion spectrum of hairbundles in the transducing hair cells of the frog auditory system. Biophys. J. 49, 21a.

[5] Flock, Å., Flock, B. and Murray, B. (1977) Studies on the sensory hairs of receptor cells in the inner ear. Acta Otolaryng. 83, 85–91.

[6] Lindemann, C.B., Rudd, G.R. and Rikmenspoel, R. (1973) The stiffness of the flagella of impaled bull sperm. Biophys. J. 13, 437–448.

[7] Hamilton, D.W. (1969) The cilium on mammalian vestibular hair cells. Anat. Rec. 164, 253–258.

[8] Hillman, D.E. and Lewis E.R. (1971) Morphological basis for a mechanical linkage in otolithic receptor transduction in the frog. Science 174, 416–419.

[9] Hudspeth, A.J. and Jacobs, R. (1979) Stereocilia mediate transduction in vertebrate hair cells. Proc. Natl. Acad. Sci. USA 76, 1506–1509.

[10] Nagel, G. (1986) Reizübertragende Strukturen in Bogengangsampullen niederer Vertebraten. Diplomarbeit, Fachbereich Biologie, Universität Münster

[11] Nagel, G. and Thurm, U. (1986): Structures transmitting stimulatory force to the sensory hairs (stereovilli) of vestibular ampullae of lower vertebrates. Verh. Dtsch. Zool. Ges. 79, 228.

[12] Orman, S. and Flock, Å. (1983) Active control of sensory hair mechanics implied by susceptibility to media that induce contraction in muscle. Hear. Res. 11, 261–266.

[13] Requena, J., Haydon, D.A. and Hladky, S.B. (1975) Lenses and the compression of black lipid membranes by an electric field. Biophys. J. 15, 77–81.

[14] Rüsch, A. and Thurm, U. (1989) Cupula displacement, hair bundle deflection, and physiological responses in the transparent semicircular canal of young eel. Pflügers Arch. 413, 533–545.

[15] Rüsch, A. and Thurm, U. (1990) Spontaneous and electrically induced movements of ampullary kinocilia and stereovilli. Hear. Res. (in press).

[16] Wersäll, J. (1956) Studies on the structures and innervation of the sensory epithelium of the cristae ampullares in the guinea pig. Acta Otolaryngol. Suppl. 126, 1–85.

Section 2

Hair Cell Motility

THE EFFECT OF CYTOPLASMIC TURGOR PRESSURE ON THE STATIC AND DYNAMIC MECHANICAL PROPERTIES OF OUTER HAIR CELLS

W.E. Brownell and W.E. Shehata

The Departments of Otolaryngology - Head & Neck Surgery and Neuroscience and The Center for Hearing Sciences, The Johns Hopkins University School of Medicine. Baltimore 21205-2195.

The force generating ability of the outer hair cell (Brownell, et al. 1985) has received a great deal of attention. The effect of the force generator on the movements of the cell, both *in vitro* and *in vivo*, is determined by the mechanics of the cell's microstructure. Outer hair cells provide a pivotal mechanical link between the basilar membrane and the reticular lamina, so that their active and passive mechanical properties should be incorporated when describing cochlear partition movement. We present evidence that the structural features of the outer hair cell are maintained by an interaction between tensile elements associated with the cytoplasmic membrane and the turgor pressure of the cell's cytoplasm. This interaction describes what has been called a hydraulic skeleton (Wainwright, 1970). Maintenance of the turgor pressure is necessary for the hydraulic communication of the pressure gradients responsible for the rapid electromotile response. Aspirin appears to exert its effect on otoacoustic emissions and hearing by weakening the hydraulic skeleton and thereby diminishing the rapid electromotile response.

Methods

Outer hair cells are dissociated from guinea pig temporal bones and maintained in an air-equilibrated media at room temperature. They are plated on the bottom of a recording chamber made from a glass coverslip to which a rubber "O" ring is glued. Video enhanced microscopic images of experimental cells are recorded with a SVHS format video cassette recorder. Morphometric measures of the cell's volume, length and surface area are made by digitizing a single frame of the video tape. The digitized image comprises an array of 512x768 pixels that is stored on disk. If necessary, feature enhancement routines are performed to sharpen object edges (such as the outer hair cell membrane contour). The outline of the cell is traced with a mouse and stored in a file as a series of (X,Y) coordinates. A program then calculates the length, average width, surface area and volume of the outer hair cell. Only turgid cells may be analyzed in this manner because of the underlying assumption that all the cross-sections of the cell are circular.

The recording chamber has a total volume of ~0.5 ml and a continual superfusion of the standard bathing media or test solutions is maintained at a rate of ~0.5 ml/min. A gravity feed is used to deliver the solution through fine polyethylene tubing and it is removed by suction across a filter paper wick through a broken pipette. The superfusion solutions vary with the experiment. The control or standard-bathing solution contains (in mM): 150 NaCl, 5 KCl, 1.5 $CaCl_2$, 1.5 $MgCl_2$, 10 glucose, and 10 HEPES (free acid form). This medium is brought to between pH 7.3 and 7.4 with approximately 2 mM NaOH and has an osmolarity of ~315 mOsm. The osmolarity of all solutions is measured on a WESCOR model

5500 vapor pressure osmometer. Test-bathing solutions contain 0.1-10 mM Na^+ salicylate. The salicylate test solutions are adjusted to be isoosmotic with the standard solution by adjusting the NaCl concentration. Superfusion of high potassium and sugar solutions is achieved by bringing a large (> 10 μm) tip-diameter pipette containing the solutions close to the cell and applying a pressure to the back of the pipette with a syringe. The optical density of the sugar solutions is different than the standard bathing solution and a uniform change in background illumination confirms the presence of the test-solution around the cell in the optical field. The standard-bathing solution continues to flow through the chamber so that removing the pressure from the back of the pipette allows the standard-solution to reperfuse the cell. The sugar solutions contain (in mM): 2.5 $MgCl_2$, 0.06 $CaCl_2$, 0.1 EGTA, 5.0 HEPES, and 300 mM sugar (sucrose, mannitol, sorbitol, dextran). The potassium solution contains (in mM): 140 KCl, 2.0 $MgCl_2$, 0.1 $CaCl_2$, 1.1 EGTA, 10 HEPES.

Tight-seal whole-cell recording pipettes are made with 1.65 mm OD glass (Dagan SA16 or LA16). Pipettes are typically filled with a solution contains (in mM): 150 KCl, 0.5 $CaCl_2$, 5 EGTA, 10 HEPES (free acid), brought to pH 7.2 with KOH. A few experiments were performed with pipettes containing 2 mM of potassium salicylate. The electrodes typically have a tip diameter of approximately 1.0 μm and a tip resistance in the bathing media of between 3-5 MΩ. The pipette is attached to the cell in a tight-seal whole-cell mode, the holding potential is set to the zero-current potential or to -65 mV (whichever is greater) and the cell is stimulated with electrical pulses in voltage clamp. The membrane conductance of the cell is characterized by a series of hyperpolarizing and depolarizing 150-msec duration voltage steps. These are used to generate transient and steady-state current-voltage relationships under different conditions. Voltage-clamp values are corrected for the series resistance of the recording pipette prior to calculation of slope conductance from steady state current-voltage plots. The zero-current potential and whole cell conductance is monitored throughout a given experiment.

Results

The magnitude of the outer hair cell zero-current potential increased over the first two minutes of establishing whole-cell recording as the contents of the pipette exchanged with the cell's electrolytes. Outer hair cells were accepted for analysis if they achieved zero-current potentials of between -25 to -80 mV and had input resistances at the beginning of recording of between 40 to 190 MΩ. Outer hair cells were mechanically rigid and resisted mechanical deformation by probing with pipettes. Their passive mechanical properties resembled those of a stiff rubber rod in contrast to more easily deformed inner hair cells that behaved like water-filled balloons. The accidental rupture of the outer hair cell's plasma membrane by a pipette would result in the cell's cytoplasm spewing from the hole. The pressure gradient driving the cytoplasm was occasionally sufficient to eject the nucleus. This observation provided evidence that the cell's cytoplasm was at a positive hydrostatic pressure relative to the bathing media. Outer hair cells maintained their turgidity and displayed their rapid electromotile response until the zero-current potential declined to zero. This, in some cases, continued for over an hour of whole-cell stimulation.

We found that increasing or decreasing the hydrostatic pressure of an outer hair cell's cytoplasm had dramatic effects on the static and dynamic mechanical properties of the cell. It was possible to collapse a cell by applying a mild suction to the back of the whole-cell pipette. Electromotile responses were either greatly diminished or absent in collapsed cells. A gentle positive pressure applied to the back of the pipette could inflate the cell and bring with it a return of the rapid electromotile response. Changes in the osmolarity of the bathing solution would effect similar changes. Evaporation of the bathing solution resulted in flaccid cells which were refilled by diluting the hypertonic solution with distilled water. Flaccid cells showed diminished electromotility that recovered when the cells regained their turgor

pressure.

ELECTRICALLY INDUCED VOLUME CHANGES

Large shifts in the holding potential changed the outer hair cell's turgor pressure. The cell lost fluid when the holding potential was raised to between +10 and +30 mV and held there for several minutes. The cells crenulated and flattened as they lost turgor. The loss in turgidity was again associated with a diminution of rapid electromotility. Flaccid cells could be restored to their original volume by lowering the holding potential to between -80 and -100 mV. The time course for the increase in fluid with sustained hyperpolarization was similar to that of fluid loss with sustained depolarization. Rapid electromotility returned with the increase in the cell volume. The slow electrically induced changes in volume were considerably different than rapid electromotility which is thought to be isovolumetric and occurs with a time constant that is at least two orders of magnitude shorter.

VOLUME INCREASES

Significant increases in volume were achieved by superfusion with either high-potassium or high-sugar solutions. The outer hair cell profiles in figure 1 show the effect of two superfusions with a high-sugar solution. The volume of the cell increased by over 25% during the high sugar superfusion and returned to its original value with the return of the standard-bathing solution. The magnitude and time course of sugar induced shape changes were virtually indistinguishable from those induced by high extracellular potassium (Brownell et al, 1989).

The shape change appeared to be the passive response of the cylindrical outer hair cell to the increase in volume. The cell's surface area remained essentially unchanged during the volume changes. Volume increases caused the outer hair cell to become shorter as it moved toward a more spherical shape. This was the consequence of the sphere being the geometric shape with the largest volume to surface area ratio. The transmembrane potential change was opposite in sign for the high-potassium and high-sugar solutions. The high potassium solution depolarized the cell while the high-sugar solution hyperpolarized the cell. The difference in sign of the transmembrane potential change was evidence that these volume increases were not a function of membrane potential.

The high-potassium and high-sugar solutions used in these experiments had low calcium concentrations. We superfused outer hair cells with a high-dextran solutions in order to test the hypothesis that the low calcium rendered the cytoplasmic membrane permeable to non-electrolytes of low molecular weight. Dextran is a very large molecule that never crosses an intact membrane. Superfusion with the low-calcium high-dextran solution caused outer hair cells to lose volume even when the solutions were slightly hypotonic. Low molecular weight non-electrolytes (e.g. sugars) are normally present in cytoplasm. Their concentration in the high-dextran solution was zero creating a concentration gradient that could drive the intracellular sugars out of the cell. The volume decrease we observed may be the result of these low molecular weight non-electrolytes moving out of the cell down their concentration gradient. The high-sugar solutions, in contrast, produced concentration gradients that could have driven sugar into the cell.

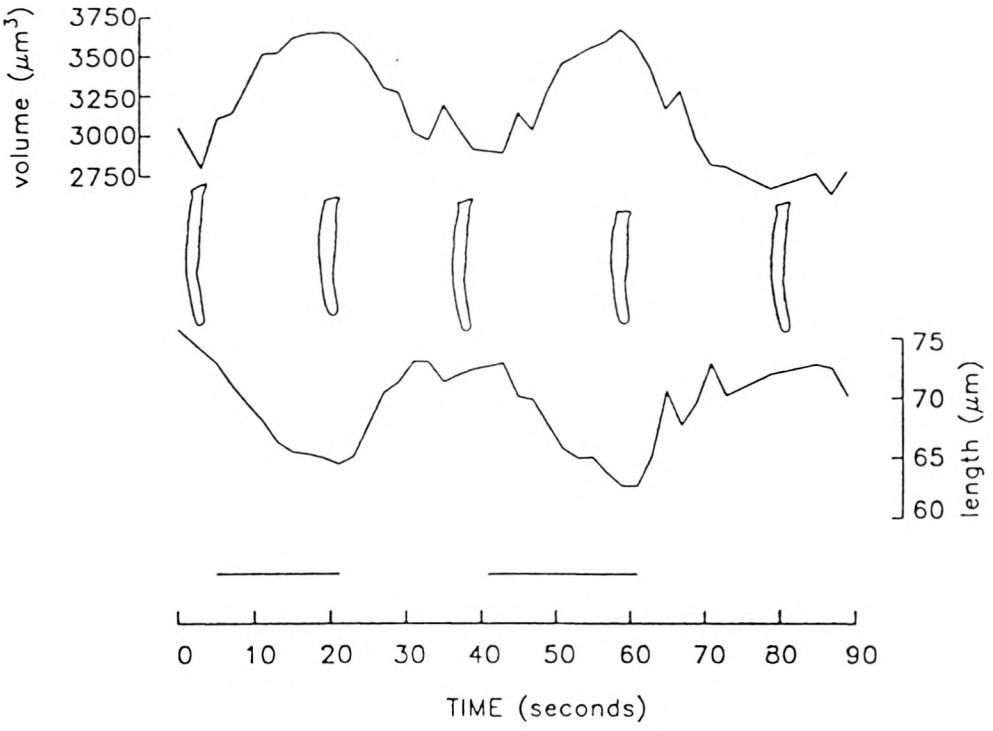

Figure 1 Morphometric analysis of shape changes in response to superfusion with a sucrose solution. The two horizontal bars just above the abscissa indicate the times of the sucrose solution superfusions. Five profiles of the outer hair cell are displayed between the top two traces. The cell volume is plotted in the top trace, the cell length in the bottom trace. The cell volume increases in excess of 25% while its length decreases less than 15 %. The cell surface area remains essentially unchanged.

ASPIRIN INDUCED VOLUME DECREASES

We have exposed over 45 outer hair cells to salicylate while monitoring and stimulating the cells through a whole-cell electrode and all showed a loss of turgor and diminished electromotility. Salicylate intoxicated cells could not be restored to a normal appearance with hyperpolarization. They could, however, be restored to a normal appearance with the recovery of electromotility by reperfusing with the standard-bathing media. Turgor decreases have been obtained with salicylate concentrations as low as 0.1 mM. The 10 mM concentration produced the effect in about three minutes. The lower the concentration the longer it took to observe the change in turgor. Both extracellular and intracellular applications produced the same result. The only difference is that the same salicylate concentration acted faster when administered intracellularly. The response of 11 isolated cells to salicylate superfusion was observed when no pipette was attached to the cell. Morphometric analysis revealed that no significant difference in cell shape resulted from the superfusion alone. Ten more cells were subjected to salicylate superfusion while stimulating transcellularly with a large-bore loose-patch pipette. These cells showed a loss of turgor and diminished electromotility.

Salicylate solutions also produced a change in the conductance of the outer hair cell. Outer hair cell current-voltage plots showed two conductance regions for the steady state response to the voltage pulses. There was a lower conductance region

extending from less than -120 mV to around -20 mV and a higher conductance region for potentials more positive than -20 mV. Eighteen cells were examined before and during exposure to salicylate. The mean slope conductance of the low conductance region was 14.5 ± 9.5 nS. The slope conductance for the high conductance region was 64.0 ± 45.5 nS. Salicylate exposure resulted in an increase in the conductance of the low conductance region to 26.7 ± 11.5 nS but did not markedly alter the high conductance region. The mean difference of the low slope conductance before and during salicylate toxicity was 11.7 ± 10.8 nS. The magnitude of the slope conductance change was not correlated with salicylate concentration unlike the volume decreases that occurred faster with higher concentrations. The conductance change generally took longer to occur than did the loss of turgor and the conductance increase was not reversible. Rinsing with the standard-bathing media failed to reduce the slope conductance even though it restored turgidity and electromotility. The difference in time course and the difference in recovery were evidence that the change in conductance was independent of the change in turgor. The conductance change may represent a general deterioration of the whole-cell recording. Similar increases in slope conductance occurred after a long time in some untreated cells.

SUMMARY OF RESULTS

The outer hair cell is normally turgid and its turgor pressure can be increased either: with mild positive pressure applied through a patch pipette; osmotically by making the bathing media hypotonic; or chemically by increasing the potassium or sugar concentrations of the bathing media. Manipulations that decrease turgor pressure include: mild suction through a patch pipette; hyperosmotic bathing media; subjecting the cell to sustained depolarizing holding potentials in voltage clamp; and ototoxic concentrations of Na^+ salicylate. Associated with the loss in cell turgor is a loss of cell volume and a reduction of rapid electromotility. The change in turgor, cell volume and electromotility produced by each of the manipulations is reversed on restoring the initial conditions.

Discussion

Goldstein and Mizukoshi (1967) were the first to demonstrate the ability of isolated outer hair cells to change shape. They replaced the bathing media, which resembled perilymph, with a high potassium "artificial endolymph" and described the resulting shape change as an increase in cell volume that resembled the increase observed on reducing the osmolarity of the bathing media by dilution with distilled water. Goldstein and Mizukoshi's observations have been confirmed by a number of laboratories which also demonstrated the volume increase to be reversible (Brownell et al, 1989; Dulon et al, 1987; Ulfendahl, 1988; Ulfendahl & Slepecky, 1988; Zenner et al, 1985). The volume increase is most likely the result of an increase in the hydrostatic pressure of the cytoplasm. An increase in the concentration of a solute in the extracellular media leads to an increase in the intracellular concentration of that substance, if the cell's cytoplasmic membrane is permeable it. Unless another substance exits the cell the cytoplasmic osmolarity will increase and with it the

hydrostatic pressure of the cytoplasm. An elastic restoring force associated with the outer hair cell's lateral cortex restores the cell to its elongated shape as the hydrostatic pressure is reduced on restoring the cell to its normal bathing media. While high potassium environments often lead to volume increases in animal cells with conventional cytoskeletons, osmotically balanced sugar solutions do not.

Ototoxic doses of aspirin are known to reduce and to block otoacoustic emissions (Long & Tubis, 1988; McFadden & Plattsmier, 1984). The fact that aspirin blocks both outer hair cell electromotility and otoacoustic emissions is one of the strongest arguments for the role of the outer hair cell in the generation of otoacoustic emissions. The site of action for aspirin's effect on cell turgor may be intracellular since application by dialysis into the cell results in a more rapid loss of cell volume. The lack of a cell shape change in response to superfusion of the salicylate solution alone may indicate that the salicylate takes longer to enter the cell if the transmembrane potential is reduced as is the case for outer hair cells that have been maintained in primary tissue culture (Brownell, 1990).

The distribution of outer hair cell cytoskeletal proteins is highly organized. The cuticular plate and stereocilia contain abundant actin and other long chain molecules. The infranuclear or synaptic region has actin, intermediate filaments and microtubules. There is evidence for circumferentially oriented (Fig. 2 left) actin containing molecules adjacent to the cytoplasmic membrane of the lateral walls (Bannister, et al. 1988; Holley & Ashmore, 1988; Lim et al, 1989). Long chain structural proteins appear to be segregated at the cell's periphery leaving the axial portion of the cell between the nucleus and the cuticular plate relatively free of an internal cytoskeleton. Rapid electromotility is expressed as a longitudinal movement of the cell occurring between the nucleus and the cuticular plate. The cell appears to have mechanisms that maintain the central portion of the cell relatively free of long chain molecules and thereby reduce the impediment to rapid movement that a well formed cytoskeleton would confer.

The outer hair cell must also possess considerable longitudinal compressive strength in order to maintain the structural organization of the cochlear partition (Fig. 2 right). Compressive strength along with the flexibility required for rapid electromotility appear to be provided by a unique hydraulic skeleton (Fig. 2 left). Wainwright (1970) describes a hydraulic skeleton resulting from the interaction between a positive hydrostatic pressure and a flexible elastic cortex with circumferential tensile strength. Our results demonstrate the effect of changing the turgor pressure of the outer hair cell. The volume increases we observe can only result from a significant increase in turgor pressure. The volume decreases reveal that some turgor pressure is required for the pressure gradients associated with the electromotile response to be hydraulically communicated throughout the cell.

The outer hair cell's cytoplasm must be maintained slighty hyperosmotic (Brownell, 1990; Brownell et al, 1989). The mechanism responsible may be related to the unusually high concentration of glycogen in its cytoplasm (Duval & Hukee, 1976; Thalmann, 1975). Glycogen may serve as a reservoir for glucose whose concentration could then be regulated by glycolysis or glycogenesis. Alternatively, soluble glycogen may be the active osmotic agent. The use of sugars to maintain turgor pressure has long been a feature of plant cells.

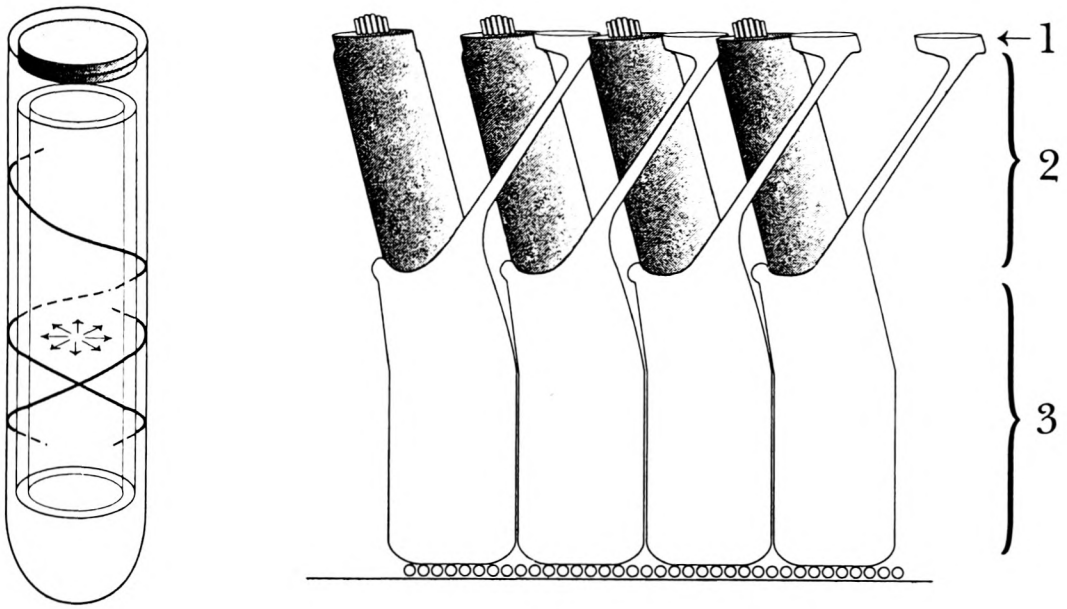

FIGURE 2 LEFT: Schematic of outer hair cell as a pressure vessel. "Circumferential" tensile elements are indicated by oppositely oriented helixes in the lateral walls of the cell. The radially oriented arrows indicate the cytoplasm's positive hydrostatic pressure. The outer hair cell's turgor pressure is most likely based on a slightly hyperosmotic cytoplasm that "inflates" the cell. RIGHT: Drawing showing part of a single row of outer hair cells and associated Deiter's cells as viewed from the otic capsule looking towards the modiolus. The apical or low frequency end of the cochlea is to the left, higher frequencies are to the right. The three longitudinal domains of the organ of Corti are from top to bottom 1) the reticular lamina, 2) the fluid space between the reticular lamina and 3) the Deiter's cell body layer. The reticular lamina is composed of the apical ends of the hair cells together with the ends of the Deiter's cells phalangeal processes that interdigitate between them. The Deiter's cells sit on the basilar membrane (represented by the row of small circles as its constituent fibers project from the plane of the figure).

The outer hair cell's apical end is firmly anchored in the reticular lamina while its basal end rests in a cuplike indentation of a Deiter's cell. The structural integrity of the layer of Deiter's cell bodies is provided by their cytoskeletal elements, the close packing of the cells, and the basilar membrane on which they sit. The outer hair cells and the thin processes of the Dieter's cells bridge the distance across the fluid space in the organ of Corti. The Dieter's cell process contains a cytoskeletal core that extends from the reticular lamina through the cell body to the basal end of the cell where it rests on the basilar membrane. Mechanical probing of the Deiter's cell process reveals that it has little if any compressive strength (Brownell, personal observations). Even if it possessed compressive rigidity the fact that it angles towards the basal end of the cochlear spiral and bends freely about the point of attachment with the Deiter's cell body means that it alone could not prevent the reticular lamina coming closer to the basilar membrane. The separation between the reticular lamina and the Deiter's cell bodies must therefore be maintained by outer

hair cells. The need for outer hair cells to maintain the separation can be appreciated by imagining the vibrations of the cochlear partition during acoustic stimulation. Since it is crucial that the movements be transmitted to the stereocilia anchored in the reticular lamina it is understandable as to why the outer hair cells must have sufficient rigidity to withstand the longitudinal compressive forces associated with such movements. The compressive resisting forces of the outer hair cell acting against the tensile properties of the Deiter's cell processes will contribute to the overall compliance of a given portion of the cochlear partition. The architectonics of the organ of Corti indicate that the outer hair cells play an important role in regulating cochlear partition compliance. Our results suggest that cell volume regulation may play a role in adjusting the mechanics of the cochlear partition by controlling the length of the outer hair cell.

Acknowledgements

J.P. Imredy participated in some of the experiments. Supported by research grant N00014-90-J-1461 from the Office of Naval Research.

References

Bannister L.H., Dodson H.C., Astbury A.F., Douek E.E. (1988) The cortical lattice: a highly ordered system of subsurface filaments in guinea pig cochlear outer hair cells. Prog. Brain Res. 74,213-219.

Brownell, W.E. (1990) Outer hair cell electromotility and otoacoustic emissions. Ear & Hear. 11 82-92.

Brownell W.E., Bader C.R., Bertrand D., de Ribaupierre Y. (1985) Evoked mechanical responses of isolated cochlear outer hair cells. Science 227,194-196.

Brownell, W.E., Shehata, W.E., Imredy, J.P. (1989) Slow electrically and chemically evoked volume changes in guinea pig outer hair cells. In: Biomechanics of Active Movement and Deformation of Cells (Ed: Akkas, N.) Springer-Verlag, New York, pp. 493-498.

Dulon D., Aran J-M and Schacht J. (1987) Osmotically induced motility of outer hair cells: implications for Meniere's disease. Arch. Otorhinolaryngol. 244,104-107.

Duval A.J. III, Hukee M.J. (1976) Delineation of Cochlear Glycogen by Electron Microscopy. Ann. Otol Rhinol. Larygol. 85,234-246.

Goldstein A.J., Mizukoshi O. (1967) Separation of the organ of Corti into its component cells. Ann. Otol. Rhinol. Laryngol. 76,414-426.

Holley M.D., Ashmore J.F. (1988) A cytoskeletal spring in cochlear outer hair cells. Nature. 335:635-637.

Lim D.J., Hanamure Y., Ohashi Y. (1989) Structural organization of the mammalian auditory hair cells in relation to micromechanics. In: Cochlear Mechanisms Structure, Function and Models (Eds: Wilson J.P., Kemp D.T.) Plenum Press, New York, pp. 3-10.

Long G.R., Tubis A. (1988) Modification of spontaneous and evoked otoacoustic emmissions and associated psychoacoustic microstructure by aspirin consumption. J. Acoust. Soc. Am. 84,1343-1353.

McFadden D. & Plattsmier HS. (1984) Aspirin abolishes spontaneous oto-acoustic emissions. J. Acoust. Soc. Am. 76,443-448.

Thalmann R. (1975) Biochemical Studies of the Auditory System. In: Human Communication and Its Disorders (Ed: Tower D.B.) Raven Press, New York, vol 3, pp 31-44.

Ulfendahl M. (1988) Volume and length changes in outer hair cells of the guinea pig after potassium-induced shortening. Arch. Otorhinolaryngol. 245,237-243.

Ulfendahl M., Slepecky N. (1988) Ultrastructural correlates of inner ear sensory cell shortening. J. Submicroscopic. Cytol. Pathol. 20,47-51.

Wainwright S.A. (1970) Design in hydraulic organisms. Die Naturwissenschaften 57,321-326.

Zenner H.P., Zimmermann U., Schmitt U. (1985) Reversible contraction of isolated mammalian cochlear hair cells. Hearing Res. 18,127-133.

Comments and Discussion

LONG

How do the levels of salicylate concentration used in your experiments compare with the levels in the organ of Corti of subjects whose otoacoustic emissions were suppressed by aspirin administration (Long & Tubis, 1988; McFadden & Plattsmier, 1984)?

BROWNELL

Both studies used an aspirin dose expected to produce tinnitus and hearing loss (325 mg/tablet x 12 tablets/day). One of the studies measured a plasma salicylate level of 15-40 mg% (1-3 mM). The concentration of salicylate in perilymph is between 25%-33% the serum level for guinea pigs and rats (Jastreboff, et al. 1986) suggesting the perilymph level for the human studies may have been between .2-1 mM. We superfused with sodium salicylate concentrations that ranged from .1 to 10 mM. All of these concentrations showed an effect on cell turgor and electromotility. The time of onset of cell volume change varied inversely with the log of the salicylate concentration.

Jastreboff, P.J., Hansen R., Sasaki, P.G., Sasaki, C.T. (1986) Differential uptake of salicylate in serum, cerebrospinal fluid, and perilymph. Arch Otolaryngol. Head Neck Surg. 112, 1050-1053.

THE NONLINEARITY OF OUTER HAIR CELL MOTILITY: IMPLICATIONS FOR COCHLEAR PHYSIOLOGY AND PATHOLOGY

Burt N. Evans, Richard Hallworth and Peter Dallos

Auditory Physiology Laboratory (the Hugh Knowles Center) and Department of Neurobiology and Physiology
Northwestern University, Evanston, IL 60208, USA

Introduction

It is now clear that the motile responses of isolated outer hair cells (OHCs) *in vitro* are nonlinear (Evans, 1988; Evans et al., 1989, 1990; Santos-Sacchi, 1989). To further our understanding of the nonlinearity and its physiological significance, we have developed a novel preparation (Evans et al., 1989) that offers several improvements over methods previously used in motility studies. Isolated guinea pig OHCs were prepared by enzymatic digestion in papain followed by gentle trituration. The experimental medium, Leibovitz's L-15 (Gibco), was buffered with 15 mM HEPES, and adjusted to pH 7.35, 320 mOsm. Cells were drawn up by gentle suction into a glass pipette that was heat-polished to a diameter close to that of a hair cell (Fig. 1). The pipette made a resistive seal with the cell body, forming a microchamber. Voltage commands were applied across the cell and the preparation resistance monitored using a current-to-voltage converter. Isolated OHCs were maintained in a separate reservoir and individually transferred to the experimental chamber using a wide-bore suction pipette. Evoked cell length changes were measured by passing the image of the cell's nuclear pole through a

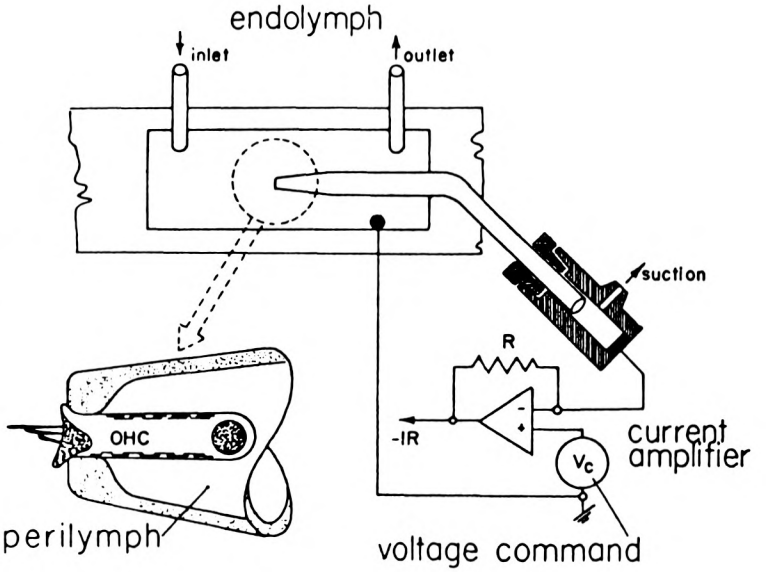

FIGURE 1 Diagram of the experimental setup, illustrating the experimental chamber, the microchamber with a cell in place, and the current-to-voltage converter.

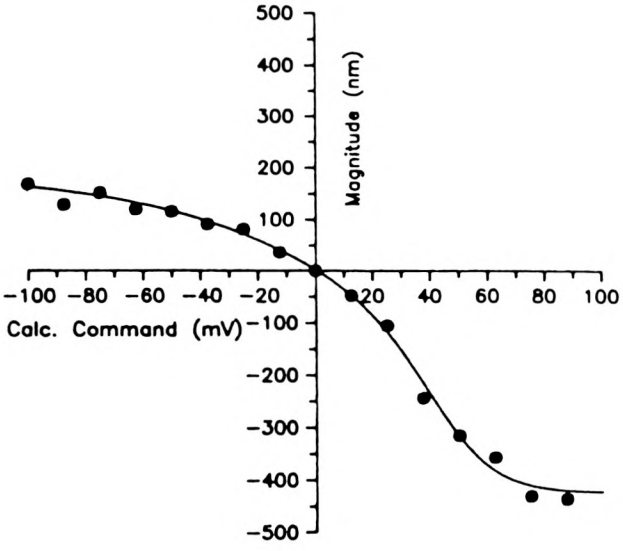

FIGURE 2 The instantaneous step length change of the inserted part of a cell (cell inserted 50%). Internal and external solutions were Leibovitz's L-15 with 15 mM TEA and 2 mM Co added. The abscissa is the computed voltage command applied across the basolateral membrane. The cell length was 55 μm. The fitted curve was generated by an equation of the form :
$k_1/\{1 + e^{a(v-v_0)}(1 + e^{b(v-v_1)})\} - k_2$.

rectangular slit onto a photodiode. All measurements were calibrated by use of an optical lever to translate the cell image by a known amount (Clark et al., 1990).

The method confers several advantages. The microchamber provides a stable platform for the cell as well as isolation from convection and turbulence in the medium. Performing the experiments in a separate bath improves the optical clarity and therefore the sensitivity of the measurements. The method enables us to simulate the natural ionic and electrical environment of the cell. Specifically, we can apply endolymph-like media outside the microchamber to the apical face of the cell. The endolymphatic potential (EP) and the action of the efferents can be simulated by application of DC bias potentials. Finally, since the cell is not penetrated, there is no depressurization of the cell, thus avoiding loss of sensitivity (Holley and Ashmore, 1988). We find that prolonged recordings are possible with this method, sometimes exceeding one hour. A disadvantage of the microchamber method is that we do not know precisely the *resting* membrane potential of the cell. However, for reasons discussed below, we infer that the cell's membrane potentials are often close to those seen *in vivo*.

The Transfer Function of OHC Motility

We assume that the cell length change is a function of the membrane potential (Santos-Sacchi and Dilger, 1988). We will therefore refer to the length change mechanism as the V-M (Voltage-to-Movement) converter. Insertion of the cell into the microchamber effectively divides the cell's membrane into two parts, one inside the microchamber (the internal segment) and the other facing the bath (the external segment). The resistances of the internal and external membrane segments, R_{int} and R_{ext}, are in series, and form a *resistive voltage divider*, in parallel with the seal resistance. The effective voltage command applied across the basolateral membrane is the command voltage multiplied by the voltage divider $R_{int}/(R_{ext} + R_{int})$. In the normal experimental configuration, the cell is inserted as far as the cuticular plate. The cell is therefore partitioned as *in vivo*, and the value of the voltage divider approximates the *in vivo* ratio of basal and apical resistances, α, defined as R_b/R_a, assuming $R_a >> R_b$ (Dallos, 1983). Reasonable values for α range from 0.05 for apical hair cells to 0.15 for basal hair cells.

The voltage divider is experimentally modifiable by extruding the cell part-way out of the microchamber. If the cell is extruded 50% out of the microchamber, the included and excluded membrane areas are equal, and therefore the voltage divider is approximately 0.5, assuming a uniform specific membrane resistance. We used this procedure to examine the transfer function of the V-M converter using known voltage step commands. The media contained 15 mM TEA and 2 mM cobalt to render the membrane resistance constant (Santos-Sacchi and Dilger, 1988). An example of the response amplitude curve is shown in Fig. 2. The curve is nonlinear, saturating abruptly in the contraction direction but gradually in the extension direction. A similar form of the curve has been inferred from previous experiments by one of us, using a different method of stimulation (Evans, 1990b), and is consistent with our earlier reported observations (Evans et al., 1989). Independently, it has been demonstrated that the transfer function is independent of the set point from which step determinations are made (Evans, 1990b). The shape of the curve is the same in media not containing TEA and cobalt. Thus we infer that the nonlinear properties of the cell membrane *per se* play no part in generating the motility asymmetries which we describe here.

The form of the curve suggests strongly that the cells are not seriously depolarized compared to *in vivo*. While the data of Santos-Sacchi (1989) are rather variable, we can reasonably infer that the contraction saturation under voltage clamp, where observed, occurs between 0 mV and +20 mV. We see the contraction saturation at about +80 mV from rest, which suggests that the resting potential for the cell in Fig. 2 was approximately -60 mV.

Sinusoidal Response Characteristics

As would be predicted from the transient response transfer function, the motile response to sinusoidal voltage commands is non-linear, with a DC component in the contraction direction over most of the dynamic range. In this study, the stimulus was a 100 Hz sinusoidal burst presented at an approximately 5/s repetition rate. The stimulus reference (0 dB) level was 125

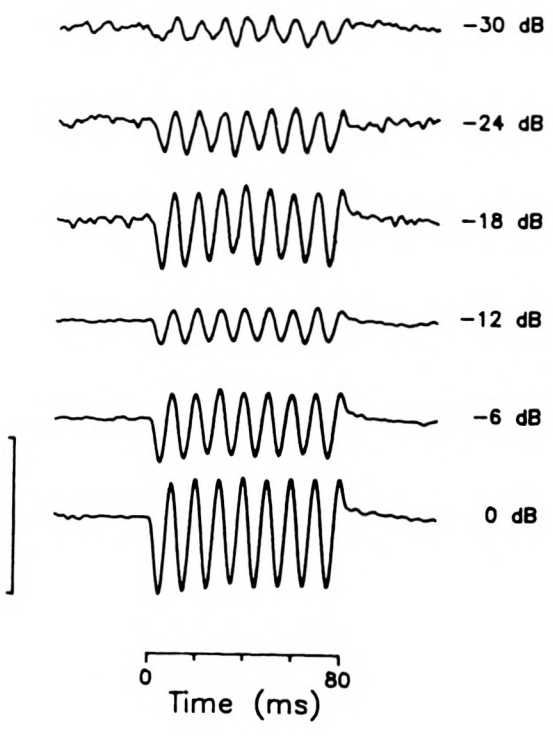

FIGURE 3 Motile responses to sinusoidal stimuli at levels from -30 dB to 0 dB. Amplitude represents the applied voltage command between the bath and the microchamber. Scale bar represents 400 nm for -12, -6 dB and 0 dB waveforms; 100 nm for -30, -24 and -18 dB waveforms. Cell length was 70 μm. The cell was fully inserted into the microchamber.

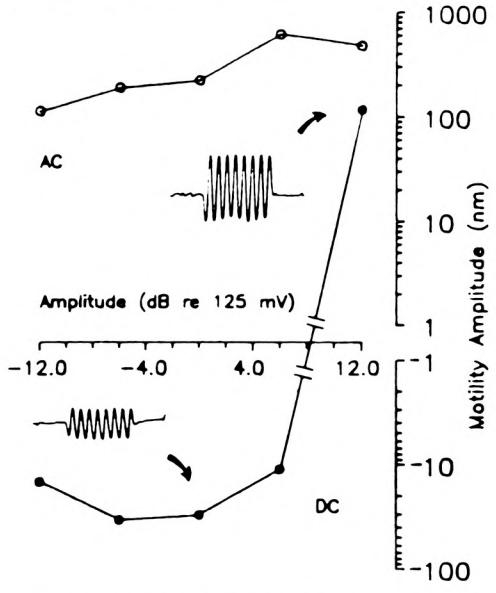

FIGURE 4 An example of the transition to an extension asymmetry generated at high amplitudes, for a cell inserted 50%. Cell length was 60 μm. The abscissa represents the peak amplitude of the voltage command applied between bath and microchamber. The response amplitude is for the inserted half of the cell only.

mV peak between the bath and the microchamber. All motility waveforms are presented with positive length change (i.e., cell extension) on the positive ordinate.

Fig. 3 shows a typical input-output series for a fully inserted cell. The response to sinusoids is nonlinear, showing an asymmetry in the contraction direction and a linear growth of both the AC and DC components with increasing intensity. Note that the DC component is present at the lowest levels we employ, -30 dB. The computed voltage drop across the basolateral membrane at -30 dB was 0.19 mV peak, assuming $\alpha = 0.05$. We estimate the peak receptor potential in third turn OHCs *in vivo* at best frequency to be about 0.05 mV at 0 dB SPL (Dallos, 1986). Thus the OHC motile nonlinearity was observed for command voltages that are clearly in the physiological range.

At higher stimulus levels the nonlinearity was often reversed to an extension asymmetry. Fig. 4 shows an example of the AC and DC magnitude function for higher stimulus levels. The extension asymmetry was consistent with depolarization at the high stimulus levels, the effect of which would be to move the operating point of the V-M converter closer to the contraction saturation (see Fig. 7). Indicative of this is that the extension asymmetry was not seen in TEA-containing media, even at the highest stimulus levels. While the extension asymmetry at high levels is unlikely to be significant in normal function, it has implications for cochlear pathology, which are discussed later.

Biasing Experiments

Modification of OHC resting potentials by efferent stimulation (Brown and Nuttall, 1983; Siegel and Kim, 1982), or by current passing across the cochlear epithelium (Durrant and Dallos, 1974; Mountain, 1980), are known to cause changes in cochlear tuning, sensitivity, and mechanics. The microchamber enables us to simulate the action of these stimuli by applying bias potentials concurrent with the sinusoidal voltage commands.

We have found that while the AC response amplitudes to tones are modifiable to some extent by biasing, the nonlinearity of the sinusoidal response is modified significantly and its direction may even be reversed. For low levels of tone and bias commands (Fig. 5, left), we observed an increase in the contraction asymmetry for depolarizing biases and a decrease in

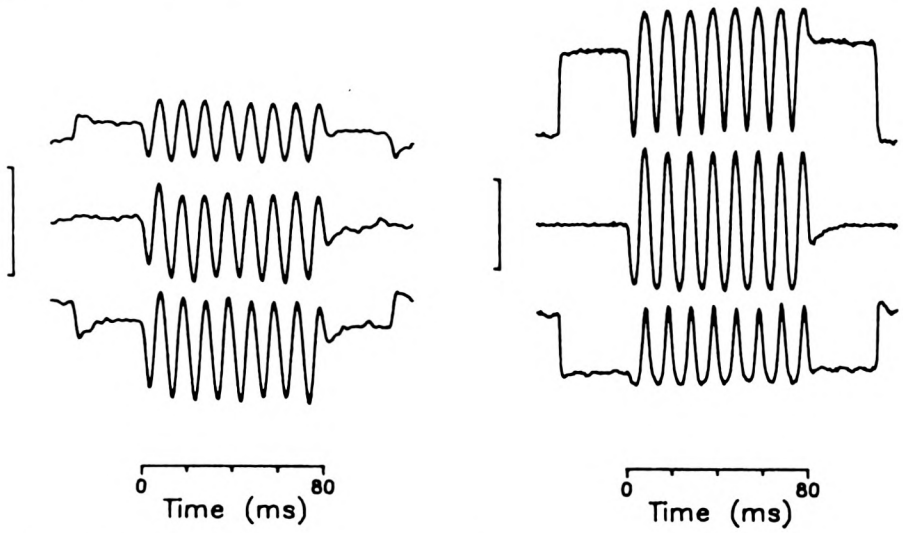

FIGURE 5 The effect of bias on response waveforms. Left: effect of 90 mV (bottom) and -90 mV (top) bias commands (applied between bath and microchamber) on the response of a cell to a 0 dB sinusoidal burst. The response to the burst without a bias is plotted in the center. The cell was fully inserted into the microchamber. Calibration bar represents 100 nm. Cell length was 45 μm. Right: Effects of 180 mV (bottom) and -180 mV (top) bias commands (applied between bath and microchamber) on the responses to a 0 dB sinsusoid. Calibration bar represents 500 nm. This cell was extruded 30% in order to increase the effective basolateral voltage command (by approximately 13 dB). Cell length was 65 μm.

the contraction asymmetry for hyperpolarizing biases. These observations are consistent with translation of the operating point of the V-M converter several millivolts either side of the normal resting membrane potential.

High levels of stimulus and bias command modulated the DC component in a different manner. Fig. 5, right, shows the effects of large bias commands on the nonlinear response to large amplitude sinusoidal commands. In the unbiased case, the response had an extension asymmetry, as described earlier. The effect of bias was to move the cell's resting membrane potential closer to either of the saturation limits, such that a positive bias increased the extension asymmetry while a negative bias reversed the asymmetry to the contraction direction. In neither case was the magnitude of the AC component affected by more than 6 dB.

Endolymph Experiments

In vivo, the OHC is partitioned across the interface between very different fluids, endolymph and perilymph. Previous motility studies have been performed in an artificial ionic environment in which only a single medium was employed. In a series of experiments, the bath medium was replaced with an artificial endolymph. The motile response of the cell to a constant level sinusoid was monitored. We saw either no effect or an increase in the DC/AC ratio (a measure of the nonlinearity) after application of endolymph. As observed in the bias experiments, the DC changes were accompanied by only small changes in the AC magnitude.

The increase in the DC/AC ratio may be understood by assuming that some isolated cells are depleted in internal potassium ions and are therefore depolarized. In this scheme, application of endolymph outside enables the cell to replenish its internal potassium concentration. The effect would be to hyperpolarize the cell, thereby moving the operating

point from a depolarized potential, where the V-M curve is fairly linear, to a more hyperpolarized potential, where the transfer function is more nonlinear. One inference from these observations is that isolated outer hair cells may have an ineffective Na-K ATPase system.

Vulnerability

Overstimulation of outer hair cells can result in loss of the DC component of the motile response without comparable changes in the AC response magnitude. Fig. 6 shows an example of loss of nonlinearity caused by repetitive stimulation. In this experiment we allowed a prolonged recovery time and retested at intervals up to 40 minutes after the initial overstimulation. The cell initially lost DC magnitude, and continued to lose it, eventually resulting in a reversal of the DC direction to extension, all without any significant loss of AC response magnitude.

Our observations are consistent with a progressive depolarization of the cell, possibly due to potassium efflux sufficient to reduce the internal potassium concentration. The operating point of the V-M converter is similarly moved closer to the contraction saturation with time, which then predisposes the cell to generate an extension asymmetry. As would be predicted, we have not observed any sign of these effects in TEA media, despite numerous prolonged experiments at high stimulus levels.

Discussion

In vivo, the linearization of both inner and outer hair cell receptor potentials and loss of sensitivity following high level stimulation has clearly been shown to be correlated with depolarization of OHC resting membrane potentials (Cody and Russell, 1986). Similarly, reduction of the EP also results in reduced sensitivity around best frequency (Sewell, 1984). Other treatments that demonstrably affect the resting membrane potential of OHCs, or might reasonably be expected to modify it, include efferent activation (Brown and Nuttall, 1982; Siegel and Kim, 1982), and transepithelial stimulation (Durrant and Dallos, 1972; Mountain, 1980) all of which modify cochlear mechanics, cochlear tuning, and sensitivity. As we have demonstrated, modification of OHC membrane potentials by small amounts can have substantial effects of the nonlinearity of OHC motility.

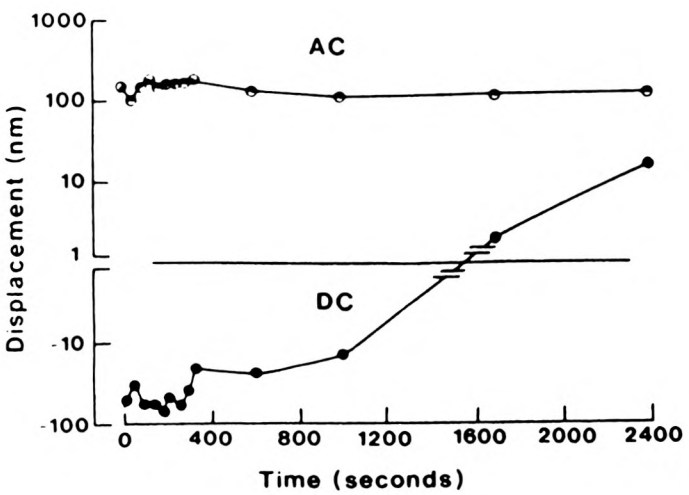

FIGURE 6 Changes of the AC and DC components of the motile response consequent to repetitive stimulation. Each data point represents the averaged response to 32 presentations of a 0 dB stimulus level. The cell was fully inserted into the microchamber. Cell length was 65 μm.

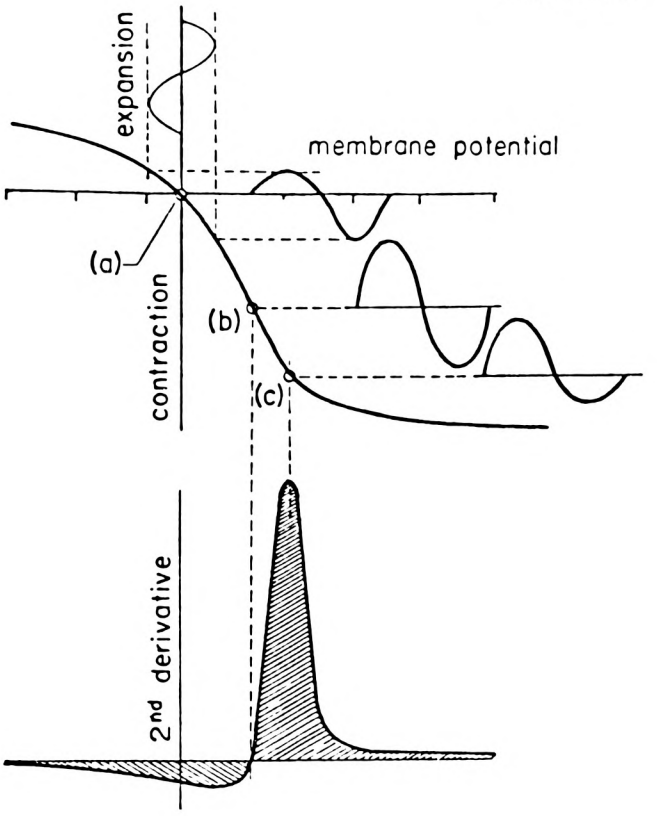

FIGURE 7 Top: hypothetical transfer function of the V-M converter. Cell extension plotted in the positive direction, cell contraction in the negative direction, abscissa represents arbitrary membrane potentials. Bottom: second derivative of the transfer function. It is assumed that the cell is normally operating at point (a). We note that a sinusoid produces a contraction asymmetry about this point. As the cell depolarizes to point (b), the response increases and becomes more linear. Extreme depolarizations, point (c), show a reversal of the asymmetry. Note that the direction and degree of the asymmetry is predicted by the second derivative function.

The demonstration that the OHC motile response is nonlinear at very low stimulus levels suggests strongly that motility could be fundamental to cochlear function. Arguments have been made that the most likely source of cochlear nonlinearities is the forward transduction process of OHCs (Patuzzi et al., 1989; Hudspeth, 1989). The arguments excluding OHC motility have been based on the assumption that the response would be linear in the physiological range (Santos-Sacchi and Dilger, 1988; Santos-Sacchi, 1989). However, our experimental results reveal a significant DC component of the motile response at stimulus levels which are in fact close to those experienced in OHCs near acoustic threshold. As the nonlinear motile behavior can also be observed following application of TEA, as well as under voltage clamp, the nonlinearity must be inherent to the force-generating mechanism itself. Arguments based upon the absence of nonlinearity in the OHC basolateral membrane at low levels (Patuzzi et al., 1989) are therefore insufficient reason to disregard the mechanical properties of OHCs.

The shape of the transfer function implies that low-level asymmetric responses occur where the curvature (or second derivative) of the function is significant. As demonstrated by the biasing experiments, and as illustrated in Fig. 7, small depolarizations increase the nonlinearity of the motile response while increasing the AC gain to a lesser extent: equally, small hyperpolarizing biases decrease the nonlinearity and the gain. At no point within a realistic physiological range would the response be linear, since the curvature of the transfer function is always non-zero except at very depolarized potentials. The asymmetry of the motile response appears to be a delicately balanced phenomenon which is critically dependent on the stability of the cell's membrane potential. It is therefore attractive to consider the mechanical nonlinearity to be fundamental to cochlear sensitivity and tuning.

[Supported by N.I.H. grants NS08635 and NS07223 and the American Hearing Research Foundation].

References

Brown, M.C. and Nuttall, A.L. (1984) Efferent control of cochlear inner hair cell responses. J. Physiol. 354, 625-646.

Clark, B.A., Hallworth, R., and Evans, B.N. (1990) Calibration of photodiode measurements of cell motion by a transmission optical lever method. Pflügers Arch. 415, 490-493.

Cody, A.R. and Russell, I.J. (1985) Outer hair cells in the mammalian cochlea and noise-induced hearing loss. Nature 315, 662-665.

Dallos. P. (1983) Some electrical circuit properties of the organ of Corti: I. Analysis without reactive elements. Hear. Res. 12, 89-119.

Dallos, P. (1986) Neurobiology of cochlear hair inner and outer hair cells. Hear. Res. 22, 185-198.

Durrant, J.D. and Dallos, P. (1972) The effect of dc current polarization on cochlear harmonics. J. Acoust. Soc. Am. 52, 1726-1728.

Evans, B.N. (1988) Asymmetries in outer hair cell electromechanical responses. Abstr., Assoc. Res. Otolaryngol., 11, p 29.

Evans, B.N. (1990a) Fatal contractions: Ultrastructural and electromechanical changes in outer hair cells following transmembranous electrical stimulation. Hear. Res. 45, 265-282.

Evans, B.N (1990b) Mechanical responses of apical and basal outer hair cells. In preparation.

Evans, B.N., Dallos, P. and Hallworth, R. (1989) Asymmetries in motile responses of outer hair cells in simulated *in vivo* conditions. In: D. Kemp and J.P. Wilson (Eds.) Mechanics of Hearing, Plenum, New York, pp 205-206.

Evans, B.N., Hallworth, R., and Dallos, P. (1990) Outer hair cell electromotility: The sensitivity and vulnerability of the DC component. In preparation.

Holley, M.C and Ashmore, J.F. (1988) On the mechanism of a high-frequency force generator in outer hair cells isolated from the guinea pig cochlea. Proc. Roy. Soc. B232, 413- 429.

Hudspeth, A.J. (1989) How the ear's works work. Nature 341, 397-404.

Mountain. D. (1980) Changes in endolymphatic potential and crossed olivocochlear bundle stimulation alter cochlear mechanics. Science, 210, 71-72.

Patuzzi, R.B., Yates, G.K., and Johnstone, B.M. (1989) Outer hair cell receptor current and sensorineural hearing loss. Hear. Res. 42, 47-72.

Santos-Sacchi, J. (1989) Asymmetry in voltage-dependent movements of isolated outer hair cells from the organ of Corti. J. Neurosci. 9, 2954-2962.

Santos-Sacchi, J. and Dilger, J.P. (1988) Whole cell currents and mechanical responses of isolated outer hair cells. Hear. Res. 35, 143-150.

Sewell, W.F. (1984) The effects of furosemide on the endocochlear potential and auditory-nerve fiber tuning curves in cats. Hear. Res. 14, 305-314.

Siegel, J.H., and Kim, D.O. (1982) Efferent control of cochlear mechanics? Olivocochlear bundle stimulation affects cochlear biomechanical nonlinearity. Hear. Res. 6, 171-182.

FAST OUTER HAIR CELL MOTILITY: HOW FAST IS FAST?

J. Santos-Sacchi

Laboratory of Otolaryngology
New Jersey Medical School, Newark N. J. 07103

Introduction

Recent experiments have implicated transmembrane voltage as the driving force of OHC motility (Santos-Sacchi and Dilger, 1988a,b; Iwasa and Kachar, 1989). A voltage dependence of OHC motility clearly implies that a charged voltage sensing particle must reside in the OHC membrane, and as was predicted for voltage dependent ionic channels (Hodgkin and Huxley, 1952), particle movement should occur under an applied transmembrane voltage. Gating currents associated with the movement of the presumed voltage sensor in OHCs have been described by Ashmore (1989).

However, two lines of evidence argue against a voltage-dependent motility mechanism in OHCs. The first is the inability of the OHC to faithfully follow a voltage stimulus in time or frequency; i.e., the speed of the movements have been reported to be unrelated to the time course of voltage clamp stimuli (Ashmore, 1987). The second is the poor temperature dependence of the rate of OHC movement (Ashmore and Holley, 1988). If OHC motility is coupled to a voltage-dependent charge movement across the OHC membrane (hence the observed gating currents), then a temperature dependence with a Q_{10} greater than 2 might be expected as occurs for sodium channel gating currents (Bezanilla and Taylor, 1978; Collins and Rojas, 1982).

This work attempts to explain these discrepancies in the voltage dependency hypothesis of OHC motility.

Methods

OHCs were obtained from the apical turns of the guinea pig cochlea by simple mechanical dissociation. Temperature was adjusted with a Peltier device and measured with a probe placed within 500 um of the cells studied. Voltage step studies were performed with an Axon Instruments A/D and D/A board (Axolab 1100) with associated software (P-Clamp, sampling period down to 3 us). AC studies were performed using a digital signal processing board with custom software (DSP-16; Ariel Corp., NJ), capable of delivering and analyzing pure tone or swept frequency stimuli. Filtered current records were saved to disk for off-line analysis.

Patch electrodes (flint or borosilicate glass) had initial resistances of 3-6 Mohm. The series resistance, i.e., the actual electrode resistance obtained upon establishment of whole cell configuration, typically ranged from 4 to 12 Mohm, and was reduced further by electronic compensation; care was taken to maintain low series resistance values during recording by delivering transient positive or negative pressure into the electrode to maintain an unobstructed orifice. The resistance values are estimated from current transients initiated at the onset of voltage pulses and are corrected for during analysis, so that actual voltages imposed upon the cell are known (Marty and Neher, 1983). The program Clampex (Axon Instruments) was modified to provide a continuous display of clamp time constant, cell capacitance and resistance, and series resistance between data collections. Pipette solutions were composed of 140 mM CsCl, 10 mM EGTA, 2 mM $MgCl_2$, and 5 mM HEPES buffered to pH 7.2. Gigohm seals were obtained at the nuclear level of the cell membrane and electrode capacitance was compensated prior to whole cell recording. Generally, single cells were clamped to holding potentials near -70 to -80 mV using a Dagan patch clamp amplifier. OHC gating currents (nonlinear capacitive currents) were measured by averaging current responses elicited by voltage pulses of alternating polarity (40 mV magnitude) about the holding potential of -80 mV, or by using a P/5 protocol at a holding potential of -120 mV.

Fast OHC movements elicited by voltage clamp with short duration or high frequency stimuli (below video detectability) were measured with a differential photodiode onto which the image of the cuticular plate from the microscope was projected. The frequency response of the differential photodiode is flat out to 2 kHz (measured with a light emitting diode or piezoelectric bimorph). Absolute calibration of cell movements is determined by measuring off the video monitor the cell movement in response to a large steady state or low frequency voltage stimulus.

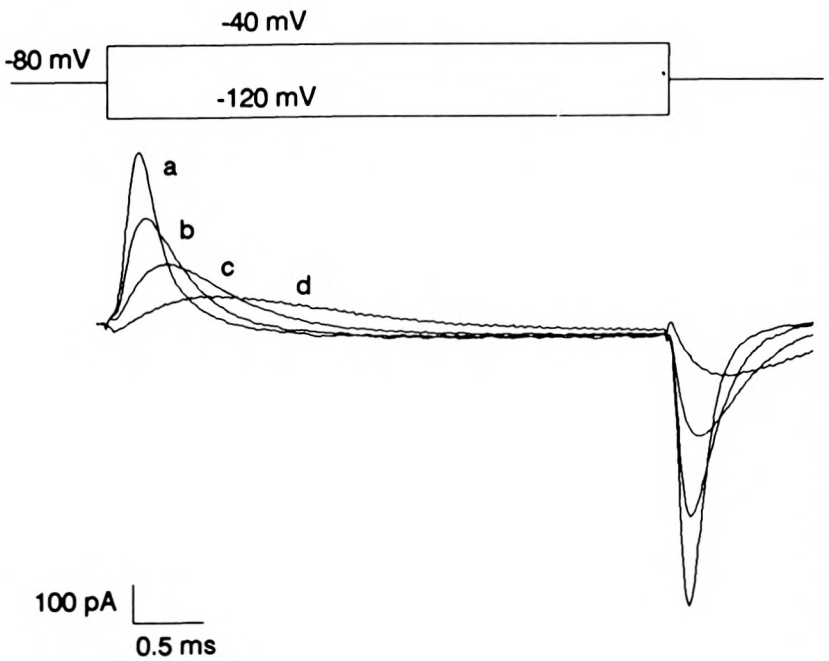

FIGURE 1 Nonlinear capacitive currents generated at the onset and offset of depolarizing voltage step. Linear capacitive currents were removed by averaging 100 X alternating steps of 40 mV above and below a holding level of -80 mV. Cell resistance was 140 Mohm. Charge movement indicates a nonlinear capacitance of 4.5 pF under these conditions. Clamp time constant was varied by adjusting series resistance compensation. Clamp time constant (ms), series resistance (Mohm), gate-on time constant (ms): a) 0.08, 1.38, 0.22; b) 0.15, 4.0, 0.37; c) 0.25, 7.83, 0.52; d) 0.36, 11.8, 1.1. Note parallel shift of gating time constant as clamp time constant is changed. Extracellular solution: 10 mM TEA, 300 nM TTX.

Results

OHCs exhibit a nonlinear charge movement which can be seen under voltage clamp as a transient outward current upon depolarization from negative holding potentials, and an inward current upon repolarization (Fig. 1). Charge movement for the cell in Fig. 1 was equal at the onset and offset of the voltage step, being about 185 fC. The time constants associated with the decaying phase of on and off currents differ, with the off tau being of similar magnitude to the clamp time constant, and the on tau being roughly twice in magnitude. Both time constants are directly dependent upon the clamp time constant, indicating that the kinetics of the gating current are faster than the time limitations imposed by the voltage clamp amplifier. Because of the apical OHC's large capacitance (Santos-Sacchi, 1989b), clamp time constants of only around 100 us have been achieved.

These results may indicate that the speed of OHC mechanical responses are dependent upon the ability of the clamp amplifier to charge the membrane. This is the case, and is demonstrated in the time domain in Fig. 2. The OHC was induced to contract with depolarizing steps to +40 mV from a holding potential of -80 mV, before and after electronically compensating the series resistance. The attendent changes in the clamp time constant is reflected in the rate of onset of the mechanical response, the slower clamp time constant charging the OHC membrane more slowly than the faster clamp time constant. Hence, it would be expected that the mechanical response of the OHC in the frequency domain will display a similar dependence upon clamp characteristics. Fig. 3 illustrates the mechanical response of two OHCs which have been voltage clamped

FIGURE 2 An OHC was held at a potential of -80 mV and stepped to +40 mV for 5 ms duration. Current and mechanical response records were recorded simultaneously, being averaged 200 X. Collections were made with different clamp time constants: a) clamp tau was 0.4 ms; b) clamp tau was 0.19 ms. Boxed portion of traces are enlarged and fitted with single exponentials (smooth curves). a) fitted tau was 0.37 ms; b) fitted tau was 0.23 ms. Scales refer to traces on right.

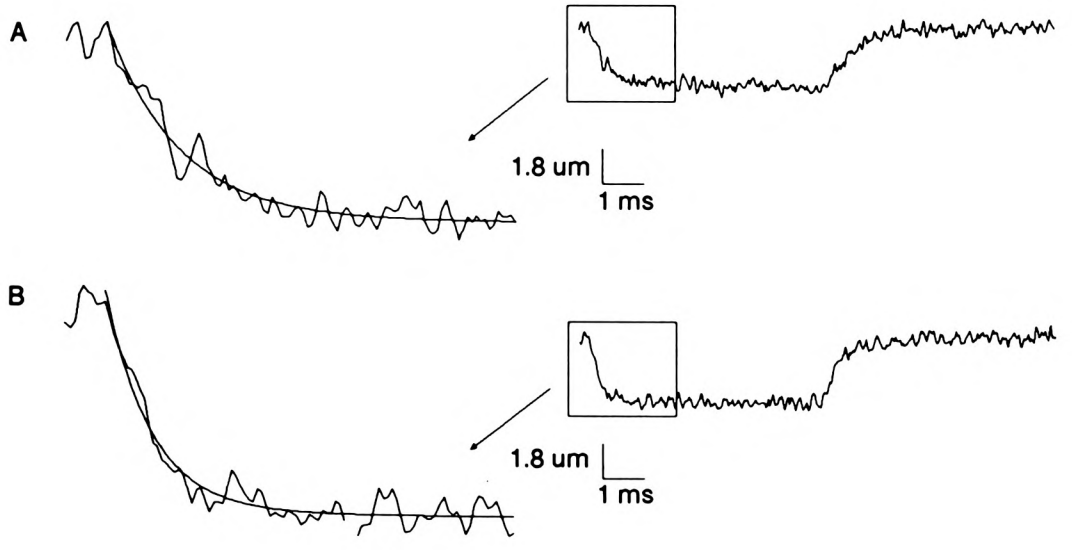

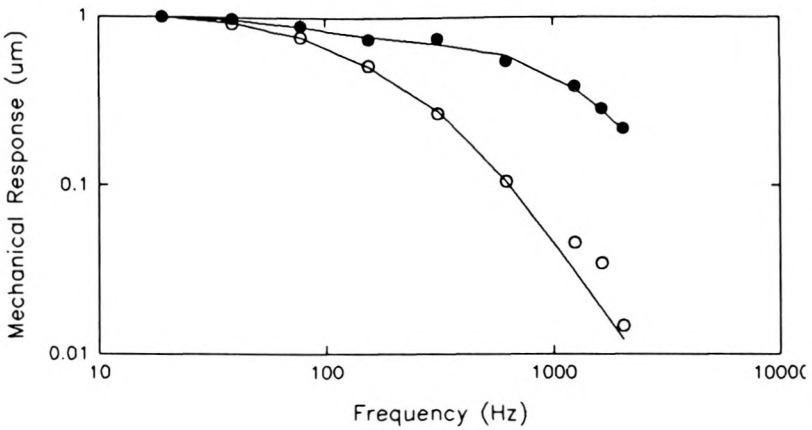

FIGURE 3 Two OHC's were clamped at -80 mV and stimulated with sinusoidal voltage bursts. The fundamental magnitude was obtained by FFT. Open circle (50 mV Pk) data were collected with a clamp tau of 1 ms, and were fit with the sum of two Lorentzians, with time constants of 1.7 and 0.5 ms. Closed circle (40 mV Pk) data clamp tau was 0.2 ms and fit with taus of 1.87 ms and 0.12 ms. Note improved frequency response associated with faster clamp time constant. 20 mM TEA.

at a holding potential of -80 mV and stimulated with superimposed sinusoidal voltages of varying frequency. The clamp time constant dictates the frequency response of each cell's mechanical response. The cell clamped with the poorer time constant displays a precipitous drop in mechanical response as frequency increases. The other cell displays a much better frequency response, the response measuring about 13 dB down at 2 kHz.

The temperature dependence of the gating current time constant was studied in order to determine if it behaves similar to sodium channel gating currents. Figure 4 shows the change in gate-on time constants for two OHCs as the temperature is varied from about 20 to 5°C. At first glance it appears that gating kinetics are slowed down as the temperature is decreased, with a Q_{10} of about 1.5 (Fig. 4a); however, when one takes into account the dependency of gate time constant upon clamp time constant, no relation is apparent (Fig. 4b).

DISCUSSION

The limitations imposed by the whole cell voltage clamp technique can provide us with a distorted picture of some of the properties of the OHC. The apical OHC has a

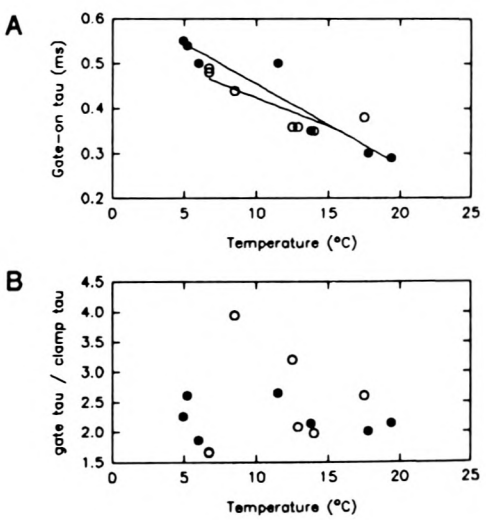

FIGURE 4 Two OHCs were voltage clamped at -80 mV and the single exponential time constant of the non-linear capacitive on current was determined as in Fig. 1. The temperature was varied from about 20 to 5°C and the effects on gate time constant plotted. In Fig. 4a it appears that temperature reduction slows down the kinetics of the gating currents, as is known to occur with sodium channel gating. However, the Q_{10} is only about 1.5. Fig. 4b demonstrates that when the dependence of gate time constant upon clamp time constant is taken into account the temperature dependence is difficult to observe. It appears that cooling the OHC down to 5°C does not slow the gating kinetics sufficiently to overcome the its dependence upon clamp characteristics. 20 mM TEA, 20 mM CsCl, 2 mM $CoCl_2$, no added calcium.

fairly large capacitance, a substantial portion of which is due to a nonlinear voltage-dependent component. The nonlinear contribution saturates with depolarization at about 30% of the cells' linear capacitance when the P/5 protocol at -120 mV holding potential is used (Santos-Sacchi, 1990). Even at a holding potential near the cell's normal resting potential (-70 mV; Dallos, Santos-Sacchi and Flock, 1982), there is a substantial nonlinear contribution. The OHC's capacitance in conjunction with the series resistance limits the voltage clamp's ability to rapidly alter the cell's transmembrane voltage (Santos-Sacchi, 1989b). The fact that the time and frequency response of OHC motility is dependent upon the clamp's ability to charge the membrane indicates that the actual mechanical capabilities of the OHC have yet to be determined. In this regard it is interesting to note that *in vivo* measures of electrically evoked oto-acoustic emissions, presumably due to the activity of OHCs, have been measured in pass bands up to several kHz (Hubbard and Mountain, 1990). Although these investigators suggest, based on Ashmore's data (1987), that the OHC length changes are too low-pass to account for such high frequency phenomena, the data presented here indicate that this may not be the case.

The fact that the time course of the nonlinear capacitive currents is imposed by those of the voltage clamp, also indicates that the kinetics of charge movement in the OHC membrane are faster than can be observed presently. Indeed, an attempt to slow down this charge movement by cooling to 5°C proved unsuccessful. This may indicate that these currents are artifacts of the technique used to collect the data; however, the clearest evidence against this is that Deiter cells possess no nonlinear capacitance. Lower temperatures are being investigated. Nevertheless, if these charge movements are related to the mechanical responses, then it is clear that clamp time constants down to 80 usec with associated fast gating constants (Fig. 1) still cannot validly investigate OHC mechanical capabilities. Ashmore (1989) reported gate time constants ranging from 1 to 2 ms, which is probably indicative of a large series resistance, with attendent slow clamp time constants. Under such clamp conditions (Ashmore and Holley, 1988), it would be difficult to measure a temperature dependent *increase* from 20 to 37 °C in the rate of OHC movement that was due to an effect on the OHC, since the clamp imposes its temporal characteristics.

The OHC appears to alter its length in response to a change in transmembrane voltage. The underlying mechanism may involve the movement of membrane bound molecules bearing charged moieties which is somehow translated into longitudinal forces. This membrane phenomenon can be interfered with, for example, by treatment of the cells with gadolinium ions, which rapidly and reversibly reduce or abolish OHC gating currents and motility (Santos-Sacchi, 1989a; 1990). However, the coupling between membrane phenomena and these longitudinal forces is clearly dependent upon cytosolic volume -- cell turgor. This is demonstrated by several means. Prolonged depolarizations or treatment of OHCs with salycilates produces a slow loss of cell volume, with accompanying reduction of the magnitude of longitudinal motility (Brownell, Shehata, and Imredy, 1989; Brownell, Imredy, and Shehata, 1989; Brownell, 1990). I have observed similar effects during prolonged whole cell voltage clamping, even though cells were maintained at a potential near -70 to -80 mV. In fact, very rapid reversible changes in cell volume can be produced using large tipped patch pipettes. Voltage-dependent longitudinal motility is rapidly abolished during loss of cell turgor

and is restored upon cell volume replacement (Santos-Sacchi, 1990). In sum, the capability of OHCs to mechanically follow transmembrane voltage alterations may be limited by a number of factors including the strength of hydrodynamic coupling between membrane phenomena and longitudinal displacement. As yet, an estimate of this limit is difficult to make with the presently used technology, and it must be concluded that OHC motility is faster than has been reported.

Acknowledgements: Supported by a Research Career Development Award from NIDCD, and NIH grant DC00273. I thank John Callahan and Janet Santos for assistance.

References

Ashmore, J.F. (1989) Transducer motor coupling in cochlear outer hair cells. In: Mechanics of Hearing (Eds: Kemp, D. and Wilson, J.P.) Plenum Press, New York, pp. 107-113.

Ashmore, J.F. (1987) A fast motile response in guinea-pig outer hair cells: The cellular basis of the cochlear amplifier. J. Physiol. (Lond.), 388, 323-347.

Ashmore, J.F. and Holley, M.C. (1988) Temperature-dependence of a fast motile response in isolated outer hair cells of the guinea-pig cochlea. Quart. J. Exper. Physiol., 73, 143-145.

Bezanilla, F. and Taylor, R. (1978) Temperature effects on gating currents in the squid giant axon. Biophys. J., 23, 479-484.

Brownell, W.E. (1990) Outer hair cell electromotility and otoacoustic emissions. Ear and Hearing, 11, 82-92.

Brownell, W.E., Imredy, J.B. and Shehata, W. (1989) Stimulated volume changes in mammalian outer hair cells. Proc. Ann. Int. Cong. IEEE-Eng. Med. Biol. Soc., 11, 1344-1345.

Brownell, W.E., Shehata, W. and Imredy, J.B. (1989) Slow electrically and chemically evoked volume changes in guinea pig outer hair cells. In: Biomechanics of Active Movement and Deformation of Cells (Ed: Akas, N.) Springer-Verlag, New York, pp. 493-498.

Collins, C.A. and Rojas, E. (1982) Temperature dependence of the sodium channel gating kinetics in the node of Ranvier. Quart. J. Exper. Physiol., 67, 41-55.

Dallos, P., Santos-Sacchi, J. and Flock, A. (1982) Intracellular recordings from outer hair cells. Science, 218, 582-584.

Hodgkin, A.L. and Huxley, A.F. (1952) A quantitative description of membrane current and its application to conduction and excitation in nerve. J. Physiol., 117, 500-544.

Hubbard, A.E. and Mountain, D.C. (1990) Haircell forward and reverse transduction: Differential suppression and enhancement. Hear. Res. 43, 269-272.

Iwasa, K.H. and Kachar, B. (1989) Fast in vitro movement of outer hair cells in an external electric field: effect of digitonin, a membrane permeabilizing agent. Hear. Res., 40, 247-254.

Marty, A. and Neher, E. (1983) Tight-seal whole-cell recording. In: Single channel recording (Eds: Sakmann, B. and Neher, E.) Plenum Press, New York, pp. 107-122.

Santos-Sacchi, J. (1990) Reversible inhibition of voltage-dependent outer hair cell motility: effects of gadolinium ions and cytosolic volume alterations. In preparation.

Santos-Sacchi, J. (1989a) Gadolinium ions reversibly block voltage dependent movements of isolated outer hair cells. 19th Annual Meeting, Soc. for Neurosci., Phoenix, AZ, October.

Santos-Sacchi, J. (1989b) Asymmetry in voltage dependent movements of isolated outer hair cells from the organ of Corti. J. Neurosci., 9, 2954-2962.

Santos-Sacchi, J. and Dilger, J.P. (1988a) Whole cell currents and mechanical responses in outer hair cells. Midwinter Meeting, Assoc. for Res. in Otolaryngol., Clearwater, FL, February.

Santos-Sacchi, J. and Dilger, J.P. (1988b) Whole cell currents and mechanical responses of isolated outer hair cells. Hear. Res., 35, 143-150.

ELASTIC BEHAVIOR OF THE OUTER HAIR CELL WALL

Charles R. Steele

Division of Applied Mechanics
Stanford University, Stanford, CA 94305, USA

Introduction

The electromotility of the outer hair cell appears to be a key feature in mammalian cochlear function. The present study was motivated by the conclusion of Brownell (1990) that the normal level of turgor pressure in the cell is necessary for electromotility to occur. The unique feature of the outer hair cell, compared to the inner hair cell, appears to be the development of the cell wall, as discussed by Forge (1989), featuring micropillars discovered by Flock, et al (1987) which connect the plasma membrane and the outermost membrane of the lateral cisterna. The elastic behavior of such a double wall system is therefore of interest. We consider the possibility of an elastic instability of the micropillars, which could be related to the conversion of electrical charge to elastic force.

Linear Elastic Stiffness

For the present study, only the static elastic behavior of a cylindrical cell with a double wall of orthotropic material is considered. The walls are connected by micropillars and the remaining space between the walls is filed with an incompressible fluid. The model shell wall is shown in Fig. 1 and the nomenclature is summarized in Table 1. Following is a summary of results.

EXTERNAL AXIAL FORCE WITH CONSTANT INTERNAL VOLUME

The condition for constant volume contained by a cylindrical shell made of an incompressible material is:

$$\varepsilon_\theta = -\frac{1}{2}\,\varepsilon_x \quad ; \quad \varepsilon_r = -\frac{1}{2}\,\varepsilon_x$$

The result for the axial force is:

$$P = \pi\, r_i\, S_{comb3}\, \varepsilon_x$$

in which the stiffness factor is given in Table 2.

PRESSURE WITHOUT AXIAL CONSTRAINT

The solution for internal pressure without any axial constraint yields this result for the strains:

$$\varepsilon_x = -\frac{p\, r_o}{S_{comb1}}\frac{S_{comb2}}{S_{comb3}} \qquad \varepsilon_{\theta i} = \frac{p\, r_o}{S_{comb1}}\left(\frac{r_o}{r_i} + \frac{S_{comb2}}{2\, S_{comb3}}\right)$$

$$\varepsilon_{\theta o} = \frac{p\, r_o}{S_{comb1}}\left(\frac{r_i}{r_o} + \frac{S_{comb2}}{2\, S_{comb3}}\right) \qquad \varepsilon_z = -\frac{p\, r_o}{S_{comb1}}\left(1 - \frac{S_{comb2}}{2\, S_{comb3}}\right)$$

The pillar strain is rewritten as:

$$\varepsilon_z = -\frac{p\, r_o}{S_{comb1}}\frac{S_{comb4}}{S_{comb3}}$$

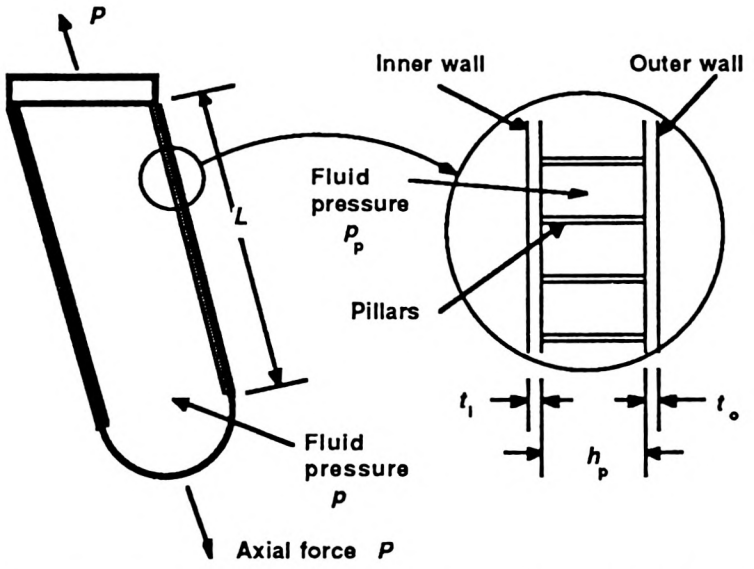

FIGURE 1 Elastic model of outer hair cell, consisting of double walls connected by micropillars. The loads are the internal pressure p and the axial force P. The micropillars can substantially increase the cell stiffness. However, because of fluid between the two walls, both walls carry a significant load with or without the connecting pillars.

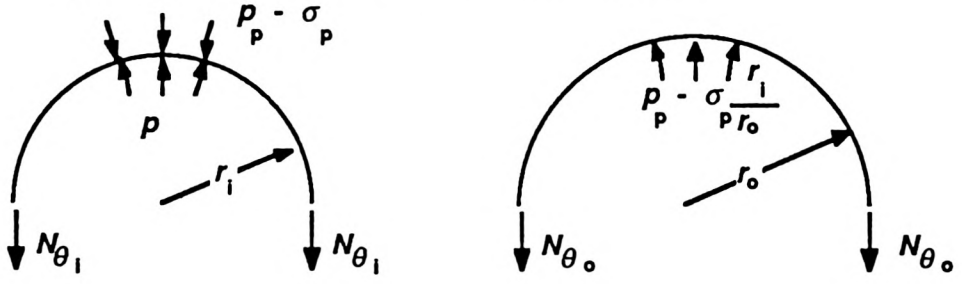

FIGURE 2 Radial forces acting on the inner and outer shell walls. The average tensile stress in the pillars is σ_p. For equilibrium, the pressure on the wall is balanced by the stress resultant in the wall N_θ.

MICROPILLAR FORCE WITHOUT AXIAL CONSTRAINT

The case of a prescribed σ_P, the force per unit area of the inner shell, is considered. This is interpreted as a force exerted by the micropillars inward on the outer wall and outward on the inner wall. The preceding equations give the strains:

$$\varepsilon_x = \frac{\sigma_P h_P}{S_{comb2}} ; \quad \varepsilon_\theta = \varepsilon_z = -\frac{\varepsilon_x}{2}$$

The stiffness of the wall seen by the individual micropillar is therefore the same order of magnitude as the stiffness of the entire cell:

$$k = \frac{\sigma_P s_L s_F}{\delta_P} = 2 \frac{s_L s_F}{h_P^2} S_{comb2}$$

TABLE 1 Nomenclature.

$r_o =$	Radius of outer wall
$r_i =$	Radius of inner wall
$L =$	Length of cylindrical portion of cell
$s_F =$	Spacing between filaments in wall
$s_L =$	Spacing between cross links in wall
$A_F = \pi d_F^2 / 4$	Cross-sectional area of single filament
$A_L = \pi d_L^2 / 4$	Cross-sectional area of single cross link
$A_P =$	Cross-sectional area of single pillar
$t_F = A_F / s_L$	Average thickness of filaments
$t_L = A_L / s_F$	Average thickness of cross links
$c_P = A_P/(s_F s_L)$	Fraction of space between walls occupied by pillars
$t =$	Effective thickness of wall
$h_P = r_o - r_i$	Length of pillars
$\varepsilon_P =$	Strain of pillars
$\varepsilon_z =$	Axial strain of cell wall
$\varepsilon_\theta =$	Circumferential strain of cell wall
$S_{ij} =$	Elastic coefficients for wall
$E =$	Young's modulus
$\nu =$	Poisson's ratio
$w_i =$	Radial displacement of inner wall
$w_o =$	Radial displacement of outer wall
$u_x =$	Axial displacement of cell
$\delta =$	Displacement of contraction of inner and outer cell walls
$\sigma_P =$	Average stress in the pillars per unit area of the inner wall
$p_P =$	Pressure in fluid between walls
$p =$	Internal pressure in cell
$P =$	Axial force on cell

TABLE 2 Stiffness factors combining wall and micropillar properties. Shown are the formulas for two walls of different fiber reinforced construction, the reduced expressions for the case of both walls of the same isotropic elastic material and with the same thickness and the radii nearly the same, and in the last column the present estimate for the effective values for the outer hair cell, with $E\,t$ = 0.1 mN /m. The pillar stiffness dominate all these factors, and in particular makes the second factor positive, which gives cell axial contraction with internal pressure.

	Walls of general properties	Isotropic	OHC (?)
S_{comb1}	$E_P c_P h_P + \frac{r_i}{r_o} S_{22o} + \frac{r_i^2}{r_o^2} S_{22i}$	$E_P c_P h_P + 2\frac{E t}{1-\nu^2}$	$22\,E\,t$
S_{comb2}	$E_P c_P h_P + 2\,S_{12o} - S_{22o} + \frac{r_o}{r_i}(2\,S_{12i} - S_{22i})$	$E_P c_P h_P - 2(1-2\nu)\frac{E t}{1-\nu^2}$	$18\,E\,t$
S_{comb3}	$\frac{1}{2} E_P c_P h_P + 2\,S_{11i} - 2\,S_{12i} - \frac{S_{22i}}{2} + \frac{r_o}{r_i}\left(2\,S_{11o} - 2\,S_{12o} - \frac{S_{22o}}{2}\right)$	$\frac{1}{2} E_P c_P h_P + (5-4\nu)\frac{E t}{1-\nu^2}$	$15E\,t$
S_{comb4}	$4\,S_{11o} - 6\,S_{12o} + 2\,S_{22o} + \frac{r_o}{r_i}(4\,S_{11i} - 6\,S_{12i} + 2\,S_{22i})$	$12(1-\nu)\frac{E t}{1-\nu^2}$	$12\,E\,t$

ACTUAL OUTER HAIR CELL WALL

From the recent examinations of the subplasma lamina by Holley and Ashmore (1988b), the microstructure seems to consist of a lattice of filaments and orthogonal cross links. The filaments form a spiral along the cell, making an angle with the cell axis which has the average value of about 75°. The filaments have the diameter, spacing, and average thickness:

$$d_F = 5 - 8 \text{ nm} \qquad s_F = 40 - 50 \text{ nm} \qquad t_F = 0.4 - 1.3 \text{ nm}$$

while the cross links have:

$$d_L = 2 - 3 \text{ nm} \qquad s_L = 12 - 25 \text{ nm} \qquad t_L = 0.13 - 0.59 \text{ nm}$$

Thus if the filaments and cross links have the same elastic modulus, the lattice is roughly one-third as stiff for stress in the direction of the cross links. For shear stress, however, the resistance is provided by the bending of the filaments and cross links. Since the cross links have greater length and less diameter, their resistance to such shear is less than that of the filaments by a factor of roughly 300. Therefore, for general loading in the plane of the lattice, the primary deformation will be that of bending of the cross links, permitting a relative translation of adjacent filaments. This is the mode of helical spring deformation calculated by Holley and Ashmore (1988b) for the filaments uncoupled from the cross links. From our attempts for a more complete analysis of this deformation, a conclusion is that a significant rotation of the cell will also occur, giving a maximum circumferential displacement about 3 times the axial displacement. Such a rotation has not been reported in the observation of the response of cells. The tentative conclusion is that the membrane connecting the filaments and cross links does supply a significant shear resistance. This would make the wall behave more as an isotropic material than a coiled spring. Therefore, we assume that the wall is isotropic with an effective thickness of t = 1 nm. A lattice with shear panels has zero Poisson's ratio $\nu = 0$. The more

elaborate analysis of the actual lattice does not reveal any substantial difference in behavior from that of the isotropic wall.

The first conclusion is that the pillar stiffness is significant. As emphasized by Brownell (1990) and described by Holley and Ashmore (1988a), increasing the pressure inside the cell causes a radial expansion and an axial *contraction*. This corresponds to $S_{comb2} < 0$, which can occur for the isotropic shell only when the pillar stiffness is significant. Furthermore the conclusion of Brownell that the deformation consists of an increase in volume without an increase in surface area, indicates that the wall strain is small in comparison with that in the axial and circumferential directions. This indicates that the pillar stiffness is actually large in comparison with the wall stiffness. As pointed out in Steele (1989), a filament reinforced vessel will have axial contraction due to internal pressure when the angle between the filaments and the axis is less than 52°. Holley and Ashmore (1988b) report that relatively few of the filaments in the outer hair cell satisfy this condition.

The wall stiffness alone can be computed from the measurements of Holley and Ashmore (1988b) on the stiffness of the demembranated cell with an axial force:

$$\frac{P}{u} = \frac{\pi r}{L} E t \approx 34 \text{ pN/}\mu\text{m}$$

For $L = 50$ μm, and $r = 5$ μm, this gives the value of wall stiffness:

$$E t = 0.1 \text{ mN/m}$$

and, using the nominal thickness of t = 1 nm, the Young's modulus:

$$E = 0.1 \text{ N/m}^2$$

This value is in the range of the rubbery materials, an order of magnitude less than elastin. Such a material would be consistent with the observations that the cell is extremely extensible. The intact cell has the stiffness:

$$\frac{P}{u} = \frac{\pi r}{L} S_{comb3} = \frac{\pi r}{L}\left[\frac{1}{2} E_P c_P h_P + 5 E t\right] \approx 500 \text{ pN/}\mu\text{m}$$

Therefore the relative pillar stiffness is:

$$\frac{E_P c_P h_P}{E t} = 2\left(\frac{500}{34} - 5\right) = 20$$

From the descriptions of Holley and Ashmore (1988b) and Bannister, et al (1987), it seems that this geometric ratio is of the order of unity. Thus the micropillars need to have a modulus of elasticity about 20 times that of the filaments, i.e., of the magnitude of elastin. With such moduli, the combined stiffness terms have the relative values given in Table 2, so the relative strains due to internal pressure are:

$$\frac{\varepsilon_x}{\varepsilon_\theta} = -\frac{S_{comb2}}{S_{comb3}} \frac{1}{\frac{S_{comb2}}{2 S_{comb3}} + 1} = -0.75 \qquad \frac{\varepsilon_z}{\varepsilon_\theta} = -\frac{S_{comb4}}{S_{comb3}} \frac{1}{\frac{S_{comb2}}{2 S_{comb3}} + 1} = -0.5$$

For the cell deformation described by Brownell (1990) consisting of a volume change with no change in the surface area, the ratio of axial to circumferential strain would be – 1.0. The value of – 0.75 obtained from the preceding calculations is at least consistent with the observations. To obtain the magnitude close to unity, the pillar stiffness must be very much larger than that of the walls.

Stability of Micropillars

Due to internal pressure, the both axial and pillar strains are negative, i.e., there is contraction of the wall as well as in the cell length. A critical compression of the pillars will cause buckling instability:

$$\varepsilon_{z\,cr} = -\left(\frac{\pi\, d_P}{4\, h_P}\right)^2$$

which depends on only the diameter to length ratio of the filaments of the pillars. From Lim (1989) it appears that the ratio may be around 10 percent, which would give a critical buckling strain of the order of magnitude of 1 percent. The tugor pressure appears to be adequate to cause such an instability.

We now examine the effect of a lateral force distribution q on the individual filaments of the micropillar, as shown in Fig. 3. For the linear solution, a lateral force will cause a displacement of the filament ends δ which is quadratic with the force. When the filament is acted upon by a compressive force of sufficient magnitude to cause buckling, however, the end displacement may be much larger. The equation governing this behavior may be reduced to the final form:

$$\left[x\left(1 + \frac{1}{\eta}\right) - f \right]\left(1 - f + x\right)^2 = Q^2$$

in which the dimensionless quantities are:

$$x = \eta\,\frac{\delta}{\delta_{cr}} = \frac{k\,\delta}{F_{cr}} \;;\; f = \frac{F_o}{F_{cr}} \;;\; Q = \frac{2\, h_P^2\, q_1}{\pi^2\, F_{cr}\, d_P}$$

The estimates for the relative stiffness of cell wall and micropillars give η about 2. For small values of the transverse load parameter Q, the magnitude of displacement produced is substantially greater for pressure equal or above the critical. This is seen clearly in Fig. 4, which shows the sensitivity dx/dQ at $Q = 0$. Below critical the derivative is zero, equal to infinity exactly at critical, and decreases slowly as the pressure increases above critical.

Conclusions

The present results indicate that the radial micropillars between the OHC plasma membrane and the subplasma lamina is most likely to provide a substantial stiffening of the cell under axial force or internal pressure. The clearest evidence for this is the axial contraction of the cell with an increase in internal pressure described by Holley and Ashmore (1988a) and Brownell (1990). Steele (1989) pointed out that a filament stiffened vessel will have such behavior if the angle of the filaments with the long axis is less than

52°, which is not the situation in the OHC found by Holley and Ashmore (1988b). The most likely resolution seems to be that the pillars are indeed stiff. With turgor pressure these micropillars are in compression, most likely to the point of buckling. The consequence is that a small lateral force on the filaments of the micropillars can cause a significant contraction of the walls. Since the axial strain is of the same order of magnitude as the strain in the wall, the axial displacement is larger by the ratio of cell length to wall thickness, about four orders of magnitude. Therefore small electrostatic charge of the micropillars could produce substantial cell elongation and contraction.

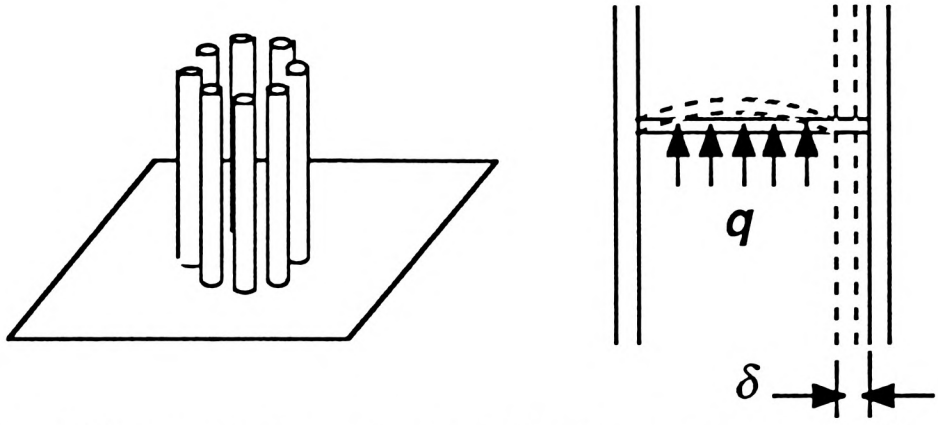

FIGURE 3 If the micropillar consists of individual fibers, as suggested by Lim (1989), a consequence is shown on the right, that a small transverse force distribution q on the individual fibers will cause a contraction δ of the space between the walls. The wall contraction causes an axial displacement of the cell four orders of magnitude larger.

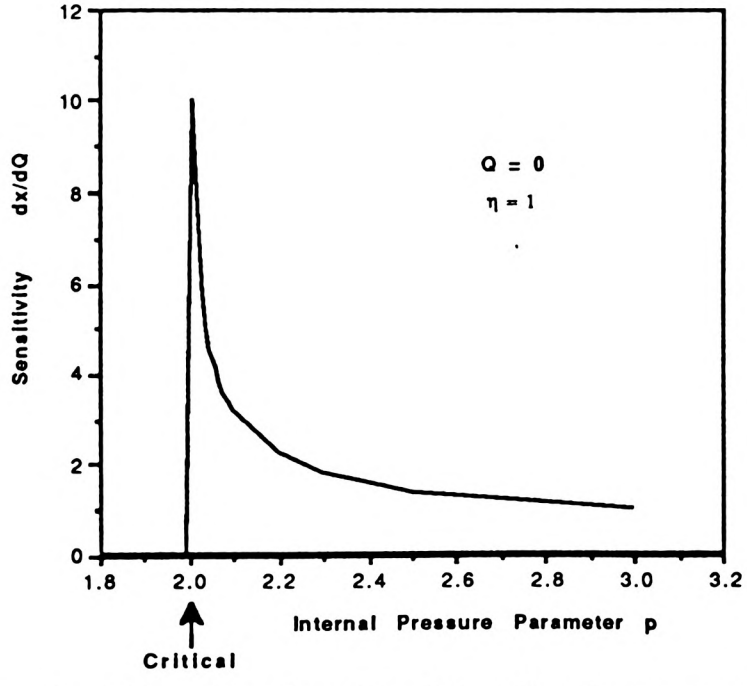

FIGURE 4 Sensitivity of the elongation of the cell to the transverse force on pillar fibers as given by dQ / dx at $Q = 0$. For internal pressure in the cell less than the "critical" the value is zero. Greatest sensitivity occurs exactly at the critical, for which there is a cusp in the curve. For higher values of internal pressure, the sensitivity decreases slowly.

This mechanism is turned off if the internal pressure is less than the critical, which is consistent with the observation of Brownell (1990). The Q - x response relation is nonlinear. For small oscillation in Q about a reference value, for supercritical pressure, the contraction is larger than the cell extension, similar to the response measured by Evans, et al (1989) for low amplitude of electrical stimulation of the cell.. Thus several facts seem to fit into place with the present model for cell wall deformation. The cell dynamic response calculated by Jen and Steele (1987), as shown by Jen (1988), is very similar to the measurements of Ashmore (1987) with the cell stiffness of Holley and Ashmore (1988b), which we have used here. As pointed out by Steele and Jen (1989), the form of the dynamic response should be insensitive as to whether the charge on the wall is a single layer, a double layer, or, as we now suggest, a charge on the filaments of the micropillars.

Acknowledgement

This research was conducted under the support of NIH Grant 2RO1 NS 17662.

References

Ashmore, J.F. (1987) A fast motile response in guinea pig outer hair cells: the cellular basis of the cochlear amplifier. J.Physiol. 388, 323--347.

Brownell, W.E. (1990) Outer hair cell electromotility and otoacoustic emissions. Ear and Hearing, in press.

Bannister, L.H., Dodsen, H.C., Astbury, A.F., Douek, E.E. (1988) The cortical lattice: a highly ordered system of subsurface filaments in guinea pig cochlear outer hair cells. Prog. Brain Res. 74, 213-219.

Evans, B.N., Dallos, P., and Hallworth, R. (1989) Asymmetries in motile responses of outer hair cells in simulated in vivo conditions. In: Cochlear Mechanisms Structure, Function and Models (Eds: Wilson, J.P., and Kemp, D.T.) Plenum Press, New York, pp. 205-206.

Flock, Å, Flock, B, Ulfendahl, M. (1987) Mechanisms of movement in outer hair cells and a plausible structural basis. Arch. Otorhinolaryngol. 243, 83-90.

Forge, A. (1989) The lateral walls of inner and outer hair cells. In: Cochlear Mechanisms Structure, Function and Models (Eds: Wilson, J.P., and Kemp, D.T.) Plenum Press, New York, pp. 29-35.

Holley, M.D., and Ashmore, J.F. (1988a) On the mechanism of a high-frequency force generator in outer hair cells isolated from the guinea pig cochlea. Proc. R. Soc. Lond., B232, 413-429.

Holley, M.D., and Ashmore, J.F. (1988b) A cytoskeletal spring in cochlear outer hair cells. Nature, 335, 635-637.

Jen, D.H. (1988) Microstructure effects in cochlear mechanics. Ph.D. Thesis, Stanford University.

Jen, D.H., and Steele, C.R. (1987) Electrokinetic model of cochlear hair cell motility. J. Acoust. Soc. Am., 82, 1667-1678.

Lim, D.J., Hanamure, Y., and Ohashi, Y. (1989) Structural organization of the mammalian auditory hair cells in relation to micromechanics. In: Cochlear Mechanisms Structure, Function and Models (Eds: Wilson, J.P., and Kemp, D.T.) Plenum Press, New York, pp. 3-10.

Steele, C.R., and Jen, D.H. (1989) Mechanical analysis of hair cell microstructure and motility. In: Cochlear Mechanisms Structure, Function and Models (Eds: Wilson, J.P., and Kemp, D.T.) Plenum Press, New York, pp. 67-74.

Section 3

Relevance of Motility to Macromechanics

A MODEL FOR COCHLEAR VIBRATIONS BASED ON FEEDBACK FROM MOTILE OUTER HAIR CELLS

C. Daniel Geisler[1] and Xueshan Shan[2]

[1]*Departments of Neurophysiology and of Electrical and Computer Engineering,*
[2]*Department of Computer Sciences,*
University of Wisconsin-Madison, Madison, Wisconsin 53706 USA

Introduction

In a previous paper (Geisler, 1986), a model of the effect of outer hair cell (OHC) motility on the movements of a radial strip of the cochlear partition was presented. When that model, slightly modified and extended, is incorporated into a simulation of the entire cochlea, it produces output with characteristics which match, to a surprising degree, those of the observed (or inferred) vibration patterns of the basilar membrane.

The Model Formulation

The basic form of the cochlear simulation used here is the familiar one-dimensional transmission-line model (cf. Geisler, 1976), with the single exception that the impedance of the basilar membrane is modified to include the effects of motile OHCs. A sketch of how these OHC effects are conceptualized, along with a mechanical-circuit diagram, is shown in Fig. 1. This figure is identical to Fig. 2 of the previous paper, with one change: the force F_m generated by the motile forces of the OHC is assumed to be contractile, instead of expansive, when the OHC cilia are deflected in an excitatory direction (away from the modiolus). This new direction is consistent with the recent experimental data of Ashmore (1987).

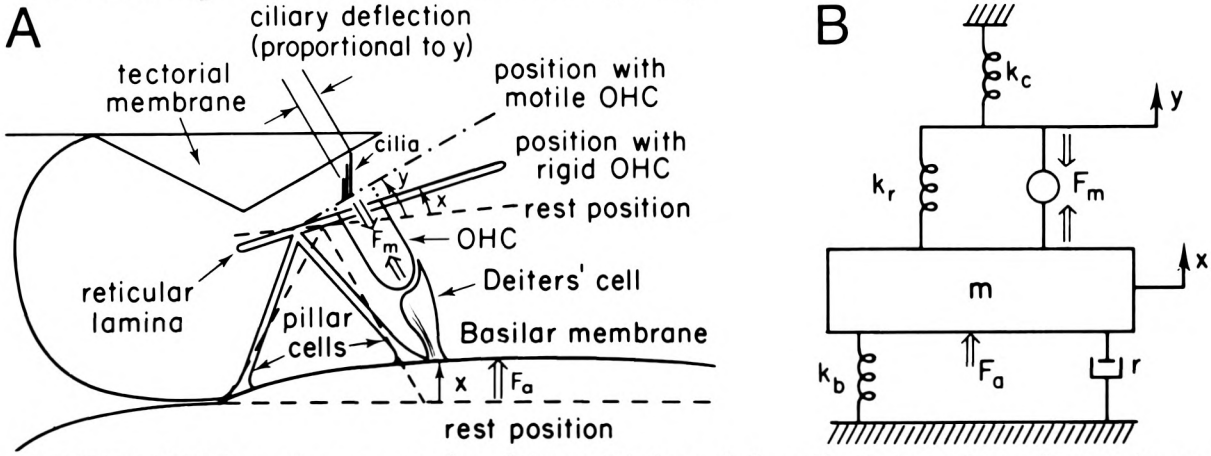

FIGURE 1 (A) Schematic representation of the model. Acoustic force F_a displaces the basilar membrane upwards by x units. The OHC reacts by contracting, exerting motile force F_m on both the basilar membrane and reticular lamina. Total reticular-lamina deflection is y units. Ciliary deflection is proportional to y. (B) Mechanical-circuit diagram of the model; k_b, k_r, and k_c represent springs, m is mass and r is damping.

The equations of the displacements x and y, in Fig. 1B are:

$$F_a = k_b x + m\ddot{x} + r\dot{x} - F_m + k_r(x - y) \quad (1)$$

$$0 = F_m + k_r(y - x) + k_c y \quad (2)$$

where the dots indicate differentiation with respect to time. For purposes of clarity, let us assume at this point only that the contractile OHC motile force is proportional to the displacement y. Thus, in complex notation,

$$F_m = F(\omega)y, \quad (3)$$

where the exact form of $F(\omega)$ is to be specified later.

Simultaneous solution of Eqns. 1-3 yields Eq. 4, which relates the displacement of the basilar membrane x to the acoustic force F_a. Examination of the bracketed

$$F_a/x = k_b - m\omega^2 + j\omega r + \left[\frac{k_r k_c/(k_r + k_c)}{1 + F/(k_r + k_c)}\right] \quad (4)$$

term in this equation shows clearly that the OHC force acts, via a feedback loop, to change the effective impedance of the springs k_r and k_c. Figure 2 shows this relationship in classic feedback format. Of particular significance is the sign of the feedback. It is negative. The original formulation of the OHC model (Geisler, 1986), while formally equivalent, showed the feedback as positive. In its current negative-feedback form, the model is similar in nature to that proposed by Mountain et al. (1983) for ciliary forces.

Based on the work of Ashmore (1987), the OHC motile force was assumed to be composed of a force constant F_0 and a delay of time T. Specifically, the assumed transfer function, in complex notation, is:

$$F(\omega) = -jF_0\exp(-j\omega T). \quad (5)$$

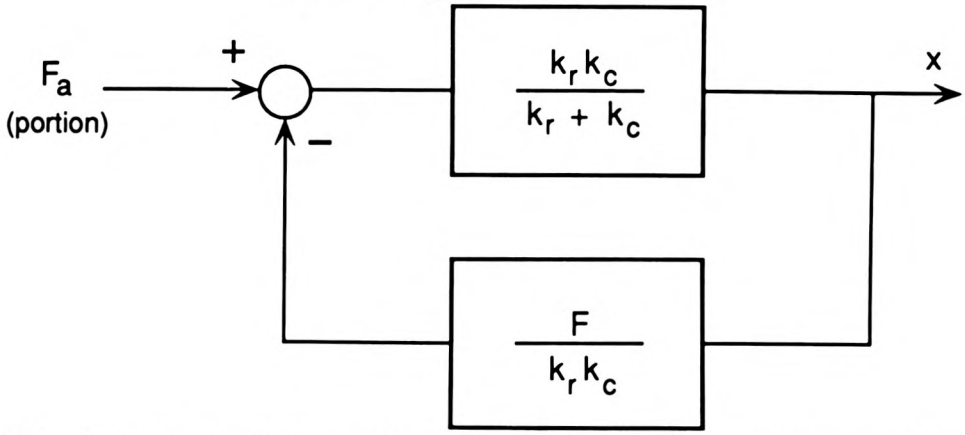

FIGURE 2 Block diagram illustrating the effective load of the cochlear superstructure as seen from the basilar membrane.

For these simulations, it was assumed that the time delay T is individually set for each OHC, according to its place along the cochlear partition. Specifically, it was assumed that T was equal to $n\pi/\omega_0$, where f_0 is the "characteristic" frequency (CF) of the basilar membrane at the location of that OHC. This assumption of individual OHC timing was inspired by the recent work of Zweig (1990), who showed that adding a properly timed delay term to the classical spring-mass-damper representation of the cochlear partition resulted in model output which matched physiological responses very well. In addition, Brundin et al. (1989) showed that at least some forms of motility are tuned to the CF of the individual OHC. For any one run of the model, the value of n was held constant for all sections of the model.

The cochlear-partition model used in these simulations has a spatial map patterned after that of the cat. The mass of each section was assumed fixed at .05 gm/cm^2 and k_b was set according to the resonance equation. For any one run of the model, the relative characteristics of the cochlear partition were kept constant throughout the length of the cochlea. That is, the values of k_r and k_c were made a constant fraction of k_b all along the partition, as was the value of $r\omega_0$. The force constant F_0 was also made a fixed multiple of k_b for any one run. 1400 sections were included in each simulation (700 was the minimum necessary for stable simulations). All simulations were run in the frequency domain (a possibility because of the model's linearity).

Model Output

Representative output of the model produced by a 5-kHz input is shown in Fig. 3, for various values of the force constant. When F_0 is set at zero (no OHC motility), the output (dot-dash line) is heavily damped and its amplitude shows no peak (Fig. 3A). As F_0 is increased, two major effects occur. A peak forms near the 12-mm place (the "characteristic" place) and a trough forms near the 8.5-mm place. The higher the value of F_0, the greater are these effects. At the highest value of F_0 used ($1.76k_b$), there is a tip-to-tail ratio of approximately 45 dB. Because of stability requirements at the 10-kHz place, the highest value of F_0 that can be used is $1.8k_b$, the value of (k_c+k_r) (see below).

The characteristics of some of the responses shown in Fig. 3 are very reminiscent of measured basilar-membrane vibration patterns. For the higher values of F_0, the output has a strong peak with relatively wide bandwidths (Q_{10}=6.6 for the highest value of F_0 used), very similar to the response shapes observed experimentally (e.g. Robles et al., 1986).

The time delay factor n used in all of the simulations of Fig. 3 was unity. Evaluation of $F(\omega)$ (Eq. 5) shows that for this delay the 5-kHz tone produced, at the 5-kHz place, a phase shift of the OHC's motile force that was exactly $-3\pi/2$ radians ($-\pi - \pi/2$). Thus the denominator of the bracketed term (which gives the effective load of the organ-of-Corti superstructure) in Eq. 4 became equal to [1 + j( )]. This in turn forced the whole superstructural term into the form of [1 - j( )]. Clearly, the negative sign of the imaginary portion of this term canceled, in part, the positive imaginary term ($j\omega r$) produced in Eq. 4 by the damping r.

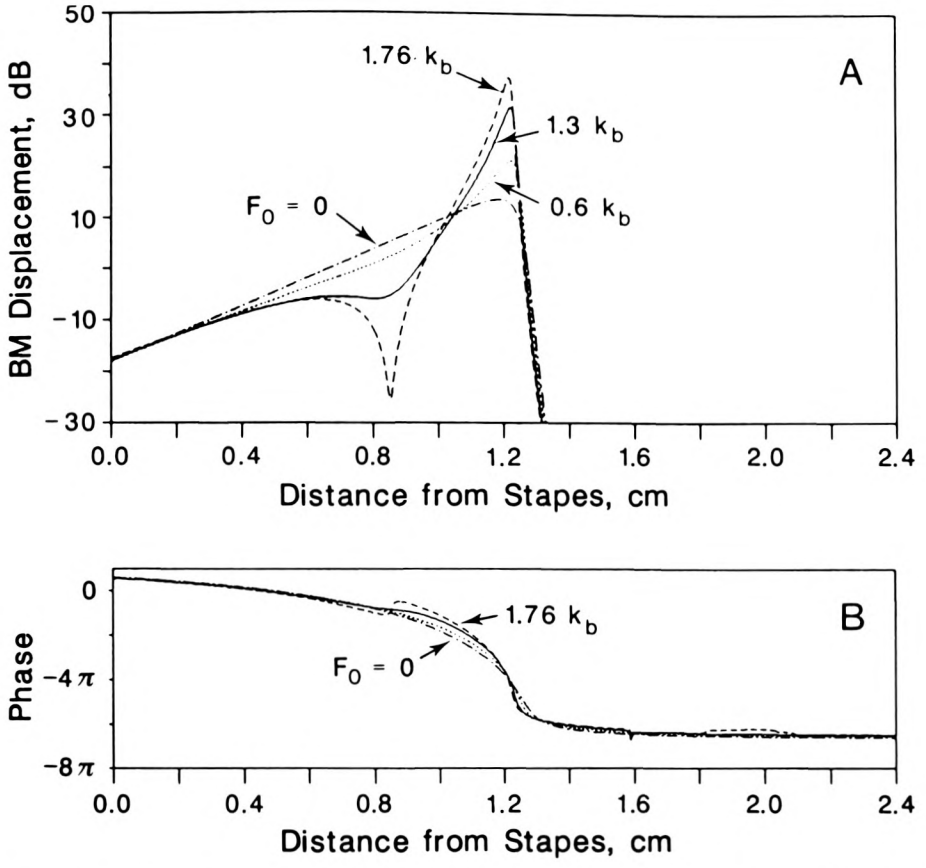

FIGURE 3 Responses of the model to a 5-kHz sinusoid for 4 different values of F_0 (0, $0.6k_b$, $1.3k_b$ and $1.76k_b$). (A) Amplitude, in dB re: stapes displacement. (B) Phase, in radians re: stapes displacement. For these and the following responses, $k_r = k_c = 0.9k_b$ and $r\omega_0 = 0.2k_b$.

An unexpected feature of the responses in Fig. 3A is the presence of troughs near the 8.5-mm place. Just such inverted troughs ("shoulders") are observed in the frequency threshold curves (FTCs) of some high-frequency auditory-nerve fibers (e.g. Liberman and Kiang, 1978). Analysis of Eq. 4 indicates that these troughs occur near the place where the denominator of the superstructural term has minimum magnitude (producing maximum impedance magnitude). Clearly, this denominator minimum occurs when the term $F/(k_r+k_c)$ is negative real, thus forcing the entire superstructural term to be purely real and positive. As such it behaves as a spring and so forms, in Eq. 4, an addition to the stiffness of the basilar membrane k_b. The depth of the trough is a reflection of the magnitude of this addition. Manipulation of the delay term shows that the denominator minimum occurs at the place where the characteristic frequency is twice that of the exciting frequency. It is encouraging therefore that, when observed, the shoulder observed in the FTC of an auditory-nerve fiber is at the corresponding frequency, approximately half of the fiber's CF (e.g Fig. 1 of Liberman and Kiang, 1978).

The phase characteristics of the responses, shown in Fig. 3B, are quite realistic. Each curve asymptotes near -6π radians, resulting in a total phase shift of about -7π radians, which is only slightly less than that observed experimentally in the chinchilla (Robles, et al., 1986). Notice that as the sharpness of the amplitude peak grows, the

phase shift near the characteristic place becomes more rapid. A corresponding trend was also observed experimentally in basilar-membrane vibrations (Geisler and Rhode, 1982).

For the damping used in Fig. 3 ($r\omega_0 = 0.2k_b$), it was judged that the optimum values for the spring and F_0 parameters for the 5-kHz response were $0.9k_b$ and $1.3k_b$, respectively, and that the best value for the delay factor n was unity. The data in Fig. 4 show that an appreciable range is allowed in that delay factor. When the delay was increased to $1.1\pi/\omega_0$, the peak became smaller but broader. By contrast, a delay of $0.9\pi/\omega_0$ produced a sharper, narrower peak. Not until the delay factor was reduced to 0.86 did instability result.

Figure 5 shows the responses produced at various exciting frequencies, with F_0 chosen at each frequency to produce the optimum response shape. The results are very realistic, with each response resembling very closely that inferred from the FTC of an auditory-nerve fiber innervating that particular characteristic place (cf. Liberman and Kiang, 1978). Note that increasingly larger values of F_0 were needed at increasingly higher frequencies. This trend implies that F_0 should not be a constant multiplier of k_b, as originally assumed, but rather should have decreasing value with increasing longitudinal position.

Based on "two-tone suppression" work originally presented at the preceding conference in this series (Yates et al., 1989), it was hypothesized that the OHC motile forces must make important contributions to membrane vibrations not only at the exciting tone's characteristic place, but also in the regions immediately basal to that place. To test that hypothesis, the model was run with F_0 set to zero at all points basal to the 10.2-mm place (the 7-kHz place, marked by an arrow head). The output of this "impaired" model to a 5-kHz tone is seen in Fig. 6, superimposed on the normal response. The two responses are dramatically different, supporting the claim that

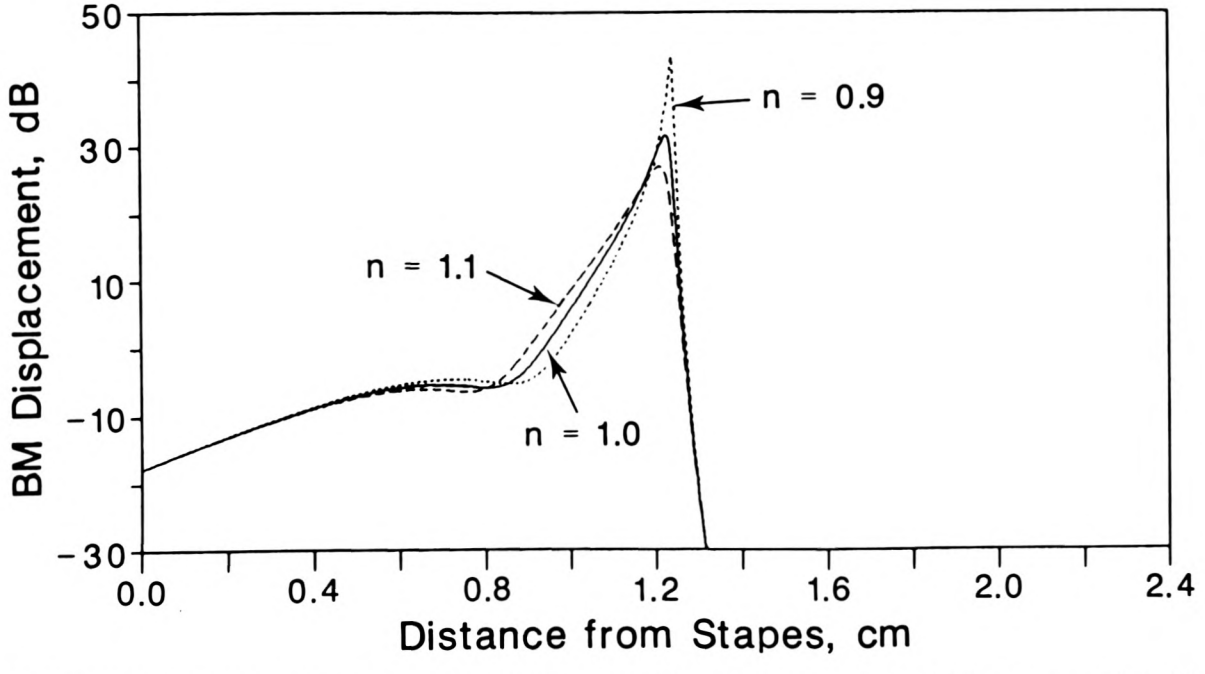

FIGURE 4 Responses of the model to a 5-kHz sinusoid for 3 different values of delay factor n (0.9, 1.0 and 1.1). $F_0 = 1.3k_b$.

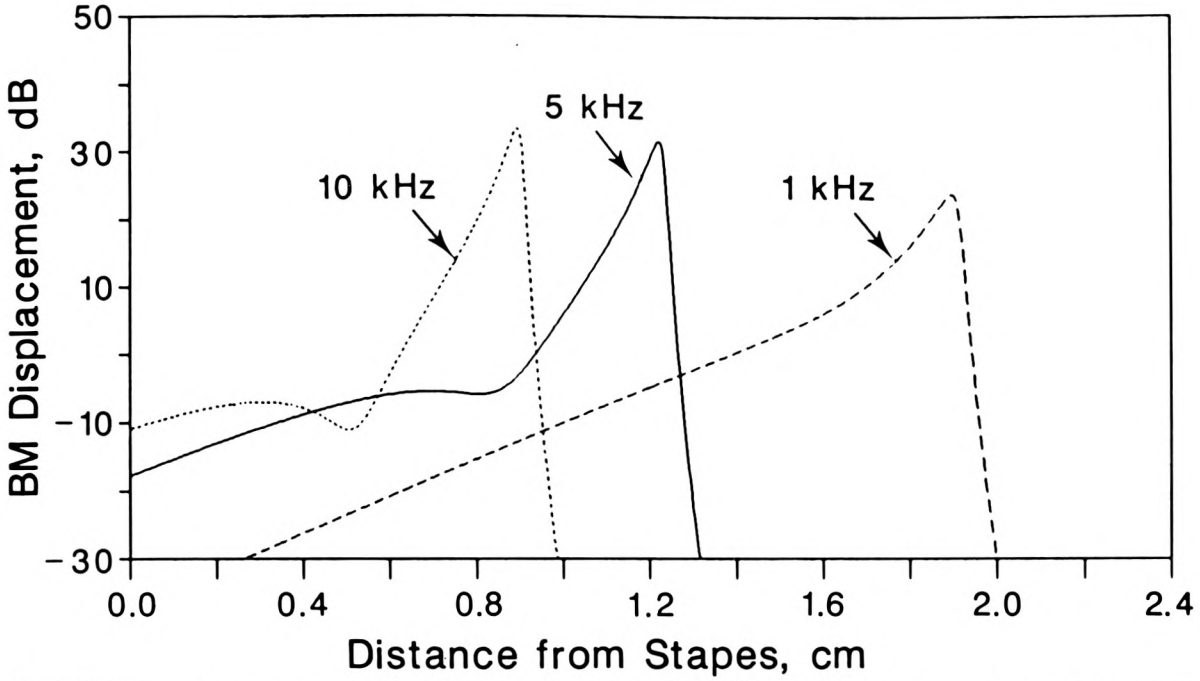

FIGURE 5 Responses of the model to sinusoids of 3 different frequencies (1, 5 and 10 kHz). F_0 = $1.0k_b$, $1.3k_b$, and $1.5k_b$, respectively.

active processes over an appreciable length of the cochlea are needed in order to produce normal responses to even a single tone. One unusual feature of the "impaired" response is that its magnitude, in regions basal to the characteristic place, is larger than normal. This hypersensitivity, probably caused by reflections, serves as a model for the low-frequency hypersensitivity sometimes observed in the responses of auditory-nerve fibers in damaged cochleas (cf. Liberman and Kiang, 1978).

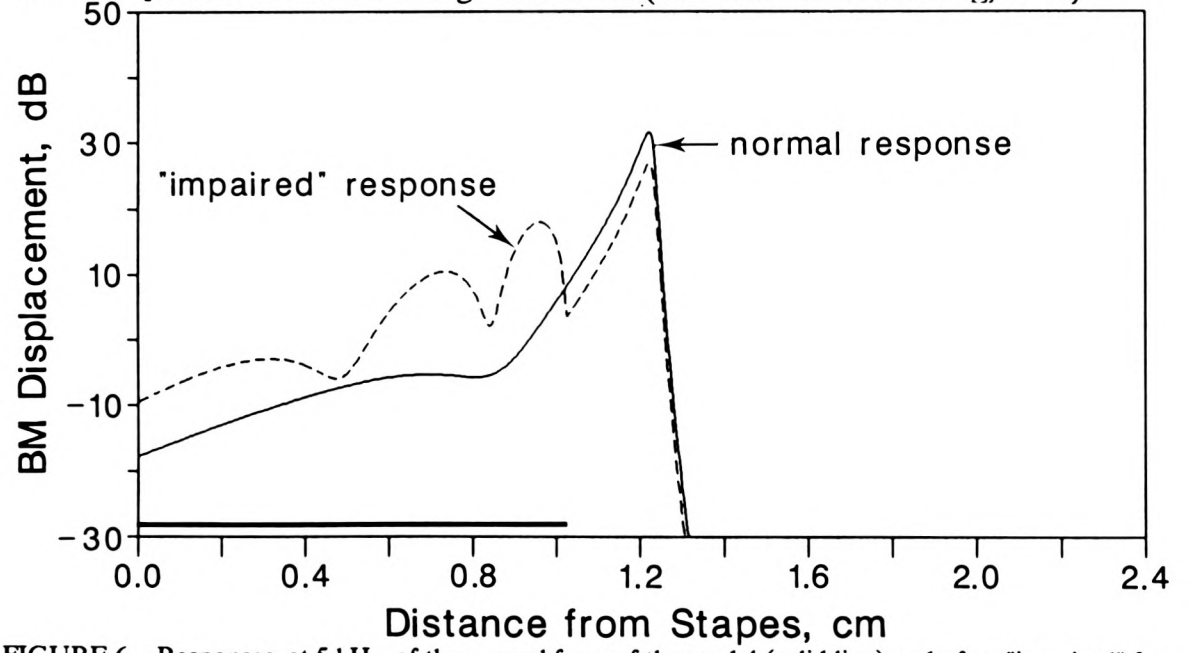

FIGURE 6 Responses, at 5 kHz, of the normal form of the model (solid line) and of an "impaired" form (dotted line). In the latter, F_0 was set to zero at all locations basal to the 10.2-mm place (marked by bar); otherwise F_0 = $1.3k_b$.

Discussion

The output of the model shares many attributes of observed cochlear responses. 1) Large tips (of 40 - 60 dB) are produced which have relatively wide bandwidths. 2) Troughs appear in these responses at the location where the CF is twice the driving frequency (corresponding to a trough at half the CF in the frequency response of a single location). 3) The phase properties, asymptoting at values near -6π, indicate that the responses are traveling waves whose velocities are functions of tip magnitude. 4) The OHC motility forces at locations basal to the characteristic place of an exciting tone have important roles to play in the overall response. This agreement between so many features of the model output and the observed responses, especially on points not deliberately programmed for (e.g. the phase asymptotes and the amplitude troughs), argues that our model provides a useful model of the physiological mechanisms at work.

It is important to note that our model, for the values of F_0 that we used, is stable. This stability, at any particular place, is formally established by excitation at CF/2. For it is at this frequency that the denominator of the superstructural term in our Eq. 4 becomes (with $n=1$) purely real. According to the Nyquist stability criterion, the "loop gain", $F/(k_c+k_r)$ in this case, must be more positive than -1.0 at this frequency. For our simulations, the loop gain at CF/2 (with $n=1$) is $-F_0/1.8k_b$ everywhere. Thus, since F_0 was always smaller than $1.8k_b$, all of our simulations were stable.

The form of our force function (Eq. 5) is similar to Ashmore's Eq. 2 for isolated OHCs (1987), except that we used a -j in place of his cascaded low-pass filters. This -j term, similar in form to the transfer function of a low-pass filter at $f>>f_{cutoff}$, suggests that a low-pass filter could also be used. Yet simulations, run with either one or two low-pass filters substituted for the -j in Eq. 5, proved to be unstable for values of parameters which produced realistic response shapes. Stable but unrealistic responses are produced with deletion of the -j term. Physically realizeable force functions, similar in effect to Eq. 5 (which is unrealizeable), are being sought.

The band-pass characteristics of the model's responses (large peaks with relatively wide band-widths) have been shared by few other cochlear-partition models. The first of these appears to have been the Neely-Kim model (1983). Both models share the characteristic that the parameters of *several* subsystems of each radial slice of the model are set according to position along the cochlear partition. The Neely-Kim model requires two interacting separately-tuned resonant circuits at each location along the partition, while our model requires only basilar-membrane tuning and a particular time delay. The simplicity of the latter model is attractive.

Zweig's model (1990), referred to earlier, also yields realistic responses. For the term which must be added to the classical cochlear-partition impedance function, he derived a pure time delay having a value, tuned to the cochlear place, of $3.5\pi/\omega_0$. For the model presented here, the optimum effective delay value was found to be about $1.5\pi/\omega_0$. The difference can be attributed to the fact that the added impedance term in the present model, while related to Zweig's, is not just a delay but also has a complex denominator (cf. Eq. 4).

Another model which demonstrates band-pass characteristics has been devised by Kolston and Smoorenburg (1990). They made no attempt to identify the elements in their model with particular physiological structures, so it is difficult to compare their model with ours. Nevertheless, the two models do share certain characteristics: in particular the OHC motile forces exert important effects upon the imaginary (spring and mass) component of the net cochlear-partition impedance as well as on the real (damping) component.

For the simulations presented here, the magnitudes of reticular-lamina movement relative to those of basilar-membrane movement (y/x) never reached large values at CF (≤ 3). These low values contrast sharply with the very large ratios recently measured in *in vitro* preparations of the apical cochlea by Khanna et al. (1989). More work will be needed before further conclusions can be drawn.

Acknowledgement

This work was supported by NIH Grant NIDCD-DC00116.

References

Ashmore, J.F. (1987) A fast motile response in guinea-pig outer hair cells: The cellular basis of the cochlear amplifier. J. Physiol. (London) 388, 323-347

Brundin, L., Flock, A. and Canlon, Barbara (1989) Tuned motile responses of isolated cochlear outer hair cells. Acta Otolaryngol. Suppl. 467, 229-234.

Geisler, C.D. (1976) Mathematical models of the mechanics of the inner ear. In: Handbook of Sensory Physiology, Vol. 5/3. (Eds. Keidel, W.D. and Neff, W.D.) Springer-Verlag, Berlin, pp. 391-415.

Geisler, C.D. and Rhode, W.S. (1982) The phases of basilar-membrane vibrations. J. Acoust. Soc. Am. 71, 1201-1203.

Geisler, C.D. (1986) A model of the effect of outer hair cell motility on cochlear vibrations. Hearing Res. 24, 125-131.

Khanna, S.M., Flock, A. and Ulfendahl, M. (1989) Comparison of the tuning of outer hair cells and the basilar membrane in the isolated cochlea. Acta Otolarnygol. Suppl. 467, 151-156.

Kolston, P.J. and Smoorenburg, G.F. (1990) Does the cochlear amplifier produce reactive or resistive forces? (this volume).

Liberman, M.C. and Kiang, N.Y.S. (1978) Acoustic trauma in cats: Cochlear pathology and auditory-nerve activity. Acta Oto-laryngol. Suppl. 358, 1-63.

Liberman, M.C. and Dodds, L.W. (1984) Single-neuron labeling and chronic cochlear pathology. III. Stereocilia damage and alterations of threshold tuning curves. Hearing Res. 16, 55-74.

Mountain, D.C., Hubbard, A.E. and McMullen, T.A. (1983) Electromechanical processes in the cochlea. In: Mechanics of Hearing (Eds: de Boer, E. and Viergever, M.A.) Delft University Press, Delft, pp. 119-126.

Neely, S.T. and Kim, D.O. (1983) An active cochlear model showing sharp tuning and high sensitivity. Hearing Res. 9, 123-130.

Robles, L., Ruggero, M.A. and Rich, N.C. (1986) Basilar membrane mechanics at the base of the chinchilla cochlea. I. Input-output functions, tuning curves, and response phases. J. Acoust. Soc. Am. 80, 1364-1374.

Yates, G.K., Geisler, C.D., Patuzzi, R.B. and Johnstone, B.M. (1989) Saturation of receptor currents accounts for two-tone suppression. In: Cochlear Mechanisms (Eds: Wilson, J.P. and Kemp, D.T.) Plenum Publishing Co., New York, pp. 177-188.

Zweig, G. (1990) The impedance of the organ of Corti (this volume).

Comments and discussion

KOLSTON

Your cochlear amplifier (CA) model is attractive in its simplicity: 3rd order rather than 4th order as in other models. However, it is possible that the model will require refinement before it can simulate a realistic mechanical response:

(1) In Fig. 3, the peak at CF produced by the CA is only 20 dB above the "dead" response. In Fig. 5, the BM versus stapes displacement has a peak of only 30 dB. Both of these observations suggest that, when exhibiting a reasonably broad peak, the sensitivity of the model is at least 30 dB too low at CF (Sellick, et al., 1982, 1983).

(2) Your values for the stiffness k_c and k_b are approximately equal. This does not agree with experimental measurements which indicate that the combined OHC stereocilia and tectorial membrane stiffness is more than an order of magnitude less than that of the BM (Strelioff and Flock, 1984; Zwislocki and Cefaratti, 1989).

GEISLER

For purposes of discussion, let us pick Fig. 15 from Sellick et al. (1982) as being representative of BM vibrations. Several isovelocity curves obtained from the same animal are depicted in that figure. The curve obtained at near normal conditions shows a sharply tuned response with a CF of about 17 kHz. Post mortem, the sensitivity of that same spot on the BM to 17-kHz stimulation had decreased by about 80 dB. However, the CF of that spot had dropped to about 12 kHz and the membrane's sensitivity to 12-kHz stimulation was unchanged (at 40 dB less than the original 16-kHz sensitivity). In short, an alive-to-dead ratio of about 40 dB was observed when only responses to CF frequencies are considered.

The comparable ratio for our model's response to 10 kHz is about 30 dB. Thus, we feel that the sensitivity of our model is at least of the right order of magnitude. What is not very realistic is the relatively stable longitudinal position of the model's response peak to a single tone as the amount of feedback is varied. As mentioned above, a point on the actual BM experiences a drop in CF of about half an octave as the animal dies. Yet in the model, a negligible change in characteristic place occurs as feedback is eliminated (cf. Fig. 3). We are seeking remedies for this weakness.

DE BOER

In your calculations you use values for k_c / k_b and k_r / k_b both of the order of unity. Can you provide arguments for this choice ? My own estimate for k_c / k_b is approximately 0.01 (or even smaller).

Comments and discussion

GEISLER

As you both observed, the ciliary stiffnesses used in the model seem unrealistically high. In our initial work with this model we assumed, for convenience that k_r and k_c were of equal strength. We have not yet run the model with a wide variety of parameters, so we really cannot say what the effects of reducing k_c to realistic values will be. On the surface, it appears that, were k_c to be reduced, keeping the crucial feedback factor ($k_c - k_r$) unchanged in magnitude, the effective strength of the feedback would be reduced (cf. Eq. 4). Yet perhaps increases in other parameters could offset this reduction in feedback strength. We plan to report on such parameter manipulations at a later date.

References

Sellick , P.M., Yates, C.K., and Patuzzi, R. (1982). Measurement of basilar membrane motion in the guinea pig using the Mössbauer technique. J. Acoust. Soc. Am., 72, 131-141.

Sellick, P.M., Yates, C.K., and Patuzzi, R. (1983). The influence of Mössbauer source size and position on phase and amplitude measurements of the guinea pig basilar membrane. Hear. Res., 10, 101-108.

Strelioff, D., and Flock, Å, (1984). Stiffness of sensory-hair bundles in the isolated guinea pig cochlea. Hear. Res., 15, 19-28.

Zwislocki, J.J., and Cefaratti, L.K. (1989). Tectorial membrane II: stiffness measurements in vivo. Hear. Res., 42, 211-227.

DOES THE COCHLEAR AMPLIFIER PRODUCE REACTIVE OR RESISTIVE FORCES?

Paul J. Kolston[1] and Guido F. Smoorenburg

Department of Otorhinolaryngology
University Hospital Utrecht, 3508 GA Utrecht, The Netherlands.
[1]Present address: *Department of Physiology*
University of Bristol, Bristol BS8 1TD, England.

Introduction

The response of the cochlea exhibits a peak that is very sensitive to its physiological state. It is virtually certain that this response peak is produced by mechanical force generators within the cochlea which alter the mechanics of the basilar membrane (BM) in a frequency and place specific manner. These extra, metabolically-sensitive processes have been given the name *cochlear amplifier* (Davis, 1983). In order to understand how the cochlear amplifier (CA) is coupled to BM mechanics, it is necessary to have a cochlear model which properly accounts for the three dimensional structure of the cochlear partition. Owing to the structural complexity of the organ of Corti no such model yet exists, and hence great care must be exercised when interpreting the results obtained from cochlear modelling studies (Kolston, 1990).

In all recent studies it has been found that a realistic response peak can only be simulated when the main effect of the CA is the injection of energy into the travelling wave (e.g. de Boer, 1983; Neely and Kim, 1983,1986; Diependaal *et al*, 1987; Geisler and Shan, 1990; Zweig, 1990). The underlying rationale behind these models is that the CA increases BM motion by increasing the stimulus to the BM where the response needs to be enhanced. This increases the pressure difference between the cochlear scalae and, with an appropiate choice of parameters, results in a response peak that is similar to that measured experimentally.

However, recently it has been found possible to simulate certain features of the BM response (selectivity and trauma changes) in a cochlear model without the injection of energy by the CA (the so-called OHCAP model - Kolston and Viergever, 1989). The main criticism of the OHCAP model, that it does not simulate cochlear sensitivity, is overcome in this paper by the description of a model in which relatively small amounts of energy are injected for frequencies *very* near the CF. This new model can simulate the recent experimental data of BM response to sinusoidal stimuli in a more efficient manner (in terms of the maximum CA force required) than other cochlear models. If the mechanisms of this model are correct, the manner in which the CA forces are coupled to the BM needs to be reassessed.

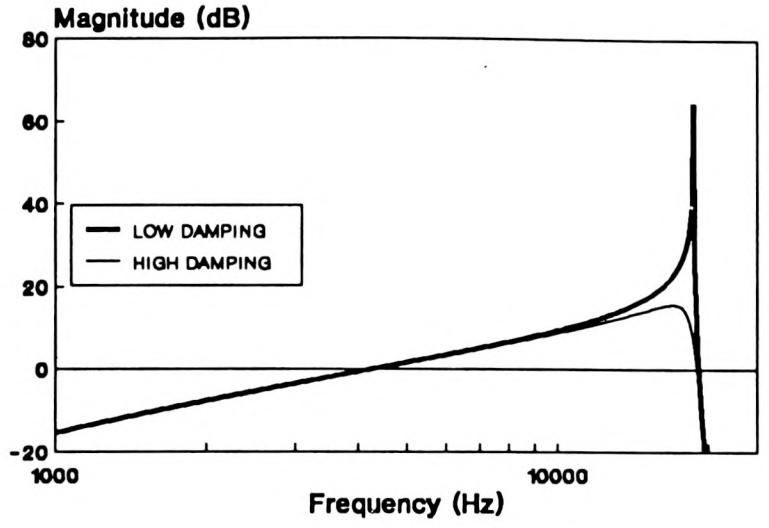

FIGURE 1 The response of a simple second-order cochlear model, shown as basilar membrane (BM) velocity versus stapes velocity, for two values of BM resistance (1 and 200 dyn.s.cm^{-3}). A small resistance value produces a large sensitivity at the characteristic frequency (CF), but at the expense of an unrealistically sharp peak.

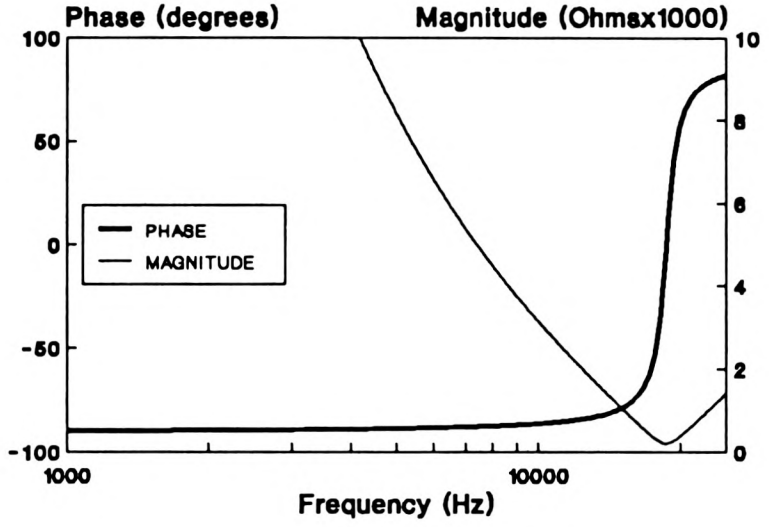

FIGURE 2 Magnitude and phase of the BM impedance in a second-order cochlear model, for large BM damping. A phase value of -90° indicates stiffness, 0° indicates (positive) damping, and 90° indicates mass. For all frequencies below the CF, the BM is stiffness dominated. It is only at the CF that the resistance dominates, indicating why a small value of BM resistance affects the response only at CF (as shown in Fig. 1).

Producing a response peak

In the recent cochlear models, a large response peak is produced by increasing the stimulus to the BM. On the other hand, a reduction in the net BM impedance (i.e. the impedance of the BM plus the CA) will also cause the response to increase. Figure 1 shows the response at one point of a cochlear model with a simple second-order series BM impedance, for two values of the BM resistance. Figure 2 shows the magnitude and phase of the BM impedance in the model, for the larger value of BM resistance (i.e. with greater damping). The magnitude of the BM impedance is equal to the vector addition of two (orthogonal) components: real (r_{bm}) and imaginary ($\iota\omega m_{bm} + k_{bm}/\iota\omega$). The phase of the

BM impedance indicates the dominant form of impedance. For all stimulus frequencies away from the CF, the BM impedance is large and is dominated by its imaginary component: for low frequencies the BM is stiffness dominated, and for high frequencies it is mass dominated. It is only immediately adjacent to the CF that the real component of BM impedance dominates. The sensitivity of the model at CF can be made arbitrarily large by making the BM resistance arbitrarily small. However, a small value of the BM resistance does not affect the dominating imaginary component away from the CF (as shown in Fig. 2), and hence results in a very sharp response peak. The recent experimental data suggest that this is not realistic.

Therefore, the phase of the force generated by the CA needs to be arranged so that its effective impedance, Z_{ca}, is predominantly imaginary and positive; the presence of the CA will then partially cancel the (negative) imaginary component of the BM impedance in the frequency region just below CF. The amount of impedance cancellation will be dependent on the magnitude of Z_{ca}. For frequencies much less than the CF, $|Z_{ca}|$ must be small compared to the BM stiffness so that the presence of the CA has little effect on the response. For stimulus frequencies in the rising peak region, $|Z_{ca}|$ should become comparable to the BM stiffness, resulting in a near cancellation of the imaginary component of the BM impedance. *Very* near the CF, the real component of the BM impedance dominates the overall impedance. With the imaginary component approximately equal to zero, the response sensitivity is still not high enough. Therefore, the CA needs to add energy for frequencies *very* near the CF.

The cochlear model

Models for the CA that involve a reduction of only the imaginary component of the BM impedance have been reported previously (Kolston, 1988, 1989; Kolston and Viergever, 1989; Kolston *et al.*, 1989). The basic principles of operation of one of those models (called the FOHC model - Kolston, 1989; Kolston and Viergever, 1989) and the model presented here are the same: the CA is a one-port device, in that it has, as its input, the motion of the BM and, as its output, a force that is assumed to act directly on the BM. This force produces an effective impedance (i.e. force divided by velocity) that adds to the BM impedance, thereby influencing BM mechanics and hence BM motion. The transfer function between the CA force and the BM motion is assumed to be controlled by internal filtering within the CA. The filtering action of the CA (which is also present in other cochlear models) could be a combination of mechanical, chemical and/or electrical processes - more experimental data on the CA is required before the actual processes can be determined.

FORMULATION

The usual macro-mechanical assumptions are made in the formulation of the model (e.g. Viergever, 1980; Neely, 1981). The model takes the form of a one-dimensional transmission line: ignoring multi-dimensional fluid motion has little effect on the response of cochlear models with a point-impedance representation for the BM (e.g. Diependaal, 1988).

One section of the transmission line model, in electrical network form, is shown in Fig. 3. The voltage sources in the CA model represent mechanical force generators, and are

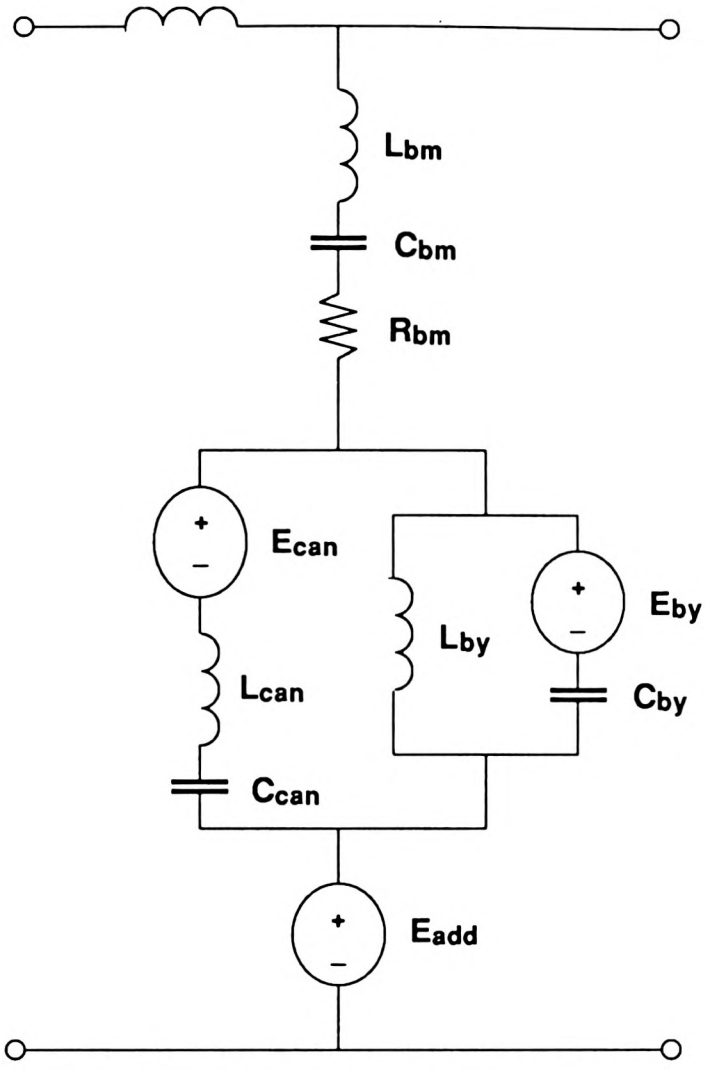

FIGURE 3 One section of the cochlear model, showing the model for the cochlear amplifier (CA), in electrical network form. The CA is assumed to exert forces directly on the BM and hence appears in series with the BM impedance. The voltage sources represent forces generated by the CA, and are described by: $E_{can} = -2V_{can}$, where V_{can} is the potential difference across C_{can} and L_{can}; $E_{by} = -R_{by} I_{by}$, where I_{by} is the current through the voltage source; and $E_{add} = -R_{add} I_{bm}$, where I_{bm} is the current through the CA model (which is analogous to the BM velocity).

described by: $E_{can} = -2V_{can}$, where V_{can} is the potential difference across C_{can} and L_{can}, $E_{by} = -R_{by} I_{by}$, where I_{by} is the current through the voltage source; and $E_{add} = -R_{add} I_{bm}$, where I_{bm} is the current through the CA model (which is analogous to the BM velocity).

The CA model shown in Fig. 3 was obtained by considering the easiest way by which to realize an impedance that would increase the motion of the BM in the required manner. Firstly, it is necessary to include in series with the BM an impedance that (partially) cancels that of the BM; the left branch of the CA model has an impedance equal and opposite to the imaginary component of the BM impedance. If the model included only this branch then the response would be increased over all frequencies. This is obviously not realistic, and so the right branch is added to ensure that the cancellation is frequency dependent. The amount of cancellation then depends on the relative magnitudes of the impedances of the two branches. The right branch is a parallel resonant circuit, and so for low stimulus frequencies has a relatively low impedance, thereby ensuring that the left branch has little effect on the overall BM impedance. Near the CF, however, the parallel circuit resonates, resulting in a large impedance in this branch. This means that the left branch remains to cancel the BM impedance, producing a small overall imaginary impedance. The real component of the BM

impedance is cancelled by the series voltage source, and hence a large response at CF is produced. It should be remembered, once again, that the peak is produced mainly by the reduction in the imaginary component; the reduction of the real component only has an affect very near the CF. The gain coefficients of the force generators are multiplied by a constant γ, whose value is assumed to be inversely related to the degree of trauma in the cochlea (see below).

Note that the circuit shown in Fig. 3 is not necessarily the most economical manifestation of the CA, nor does it correspond to a realistic arrangement of recognisable elements - the particular topology shown in Fig. 3 is merely used to illustrate the basic principles of the operation of the model. The identification of the components comprising the CA model has not been attempted, since the site of the CA is still not clear.

RESPONSE

The cochlear model was analyzed in the frequency domain using the method described in Kolston *et al.* (1990). The number of sections used was chosen such that a doubling of the number had no significant effect on the response. Causality and stability were checked (and confirmed) using the method outlined in Koshigoe and Tubis (1982). The middle ear model used in conjunction with the cochlear model was the same as that described in Kolston *et al.* (1990).

Figure 4 shows a comparison between the experimental data obtained by Robles *et al.* (1986), and the response of the model (for various values of γ) using the following parameters (x is distance from the stapes):

fluid density	$1.0\ g.cm^{-3}$	L_{bm}	$4.0 \times 10^{-2}\ g.cm^{-2}$
scala length	3.5 cm	C_{bm}	$1.0 \times 10^{-9}\ e^{3.7x}\ cm^3.dyn^{-1}$
scala height	0.1 cm	R_{bm}	$2.0 \times 10^{2}\ dyn.s.cm^{-3}$

L_{can}	$4.0 \times 10^{-2}\ g.cm^{-2}$
C_{can}	$1.0 \times 10^{-9}\ e^{3.7x}\ cm^3.dyn^{-1}$
L_{by}	$5.0 \times 10^{-1}\ g.cm^{-2}$
C_{by}	$5.0 \times 10^{-10}\ e^{3.7x}\ cm^3.dyn^{-1}$
R_{by}	$5.0 \times 10^{4}\ dyn.s.cm^{-3}$
R_{add}	$1.7 \times 10^{2}\ dyn.s.cm^{-3}$

If it is assumed that the model gain parameter γ is proportional to the amplitude of the OHC receptor current (i.e inversely related to the amount of trauma), then the reduction in model sensitivity at CF shown in Fig. 4 correlates very well with the experimental observations of Patuzzi *et al.* (1989). This correlation is at least as good as that between the model of Neely and Kim (1986) and the experimental data.

Figure 5 shows the magnitude and phase of the impedances in the model, for the normal response shown in Fig. 4. For all frequencies below CF, the phase of the CA impedance is approximately 100°, indicating that the main effect of the CA is to cancel the (negative) imaginary component of the BM impedance. Where the phase is approximately 180°, the magnitude of the CA force is very small and hence only a small amount of energy is injected by the CA.

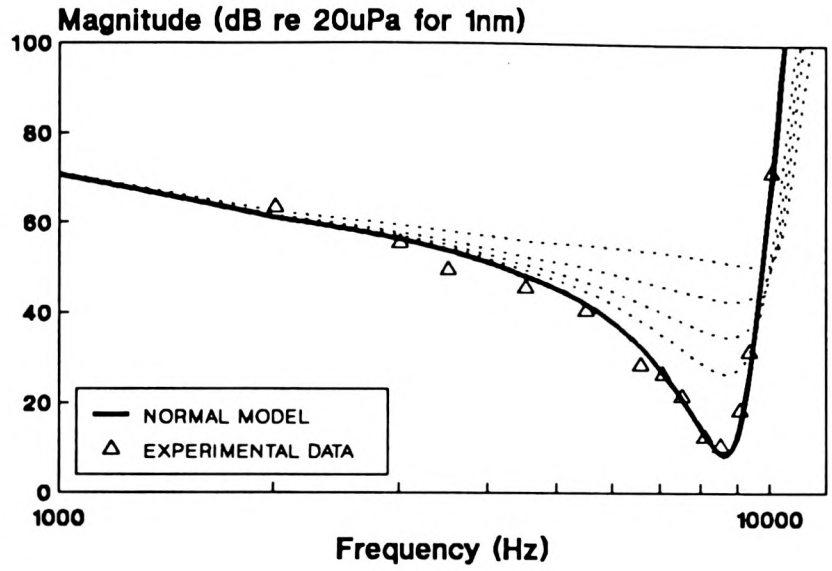

FIGURE 4 Response of the cochlear model, 4.5mm from the stapes, compared with the experimental data obtained in the chinchilla by Robles et al. (1986). The response shows the eardrum sound pressure level required to elicit a BM displacement of 1nm. The various curves show the response for various values of the CA gain parameter γ: 1.0, 0.95, 0.90, 0.80 and 0.50.

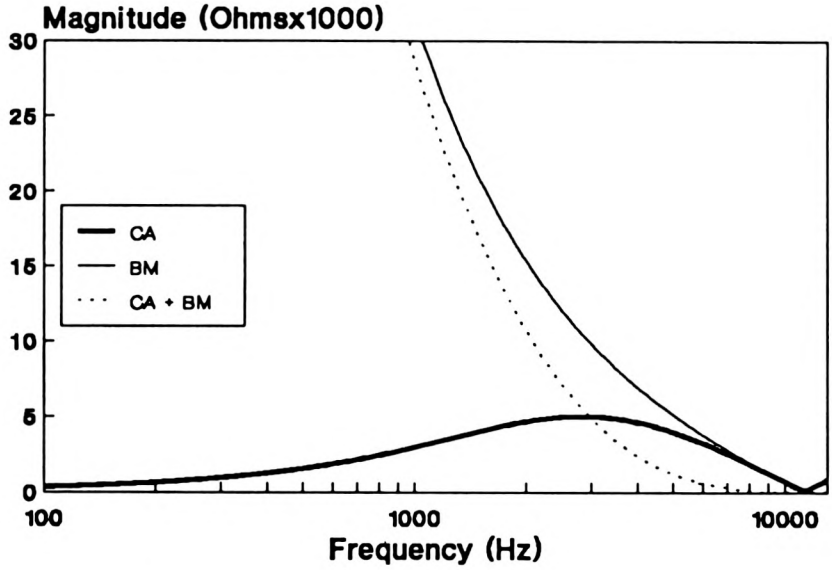

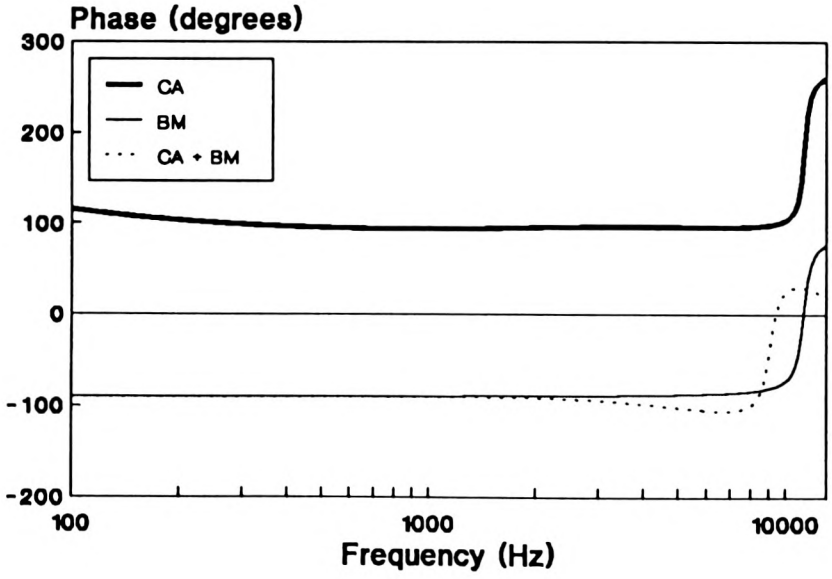

FIGURE 5 Magnitude and phase of the impedances in the cochlear model, for the response shown in Fig. 4 (with $\gamma = 1.0$). For all frequencies less than the CF, the phase of the CA impedance is approximately 100°, indicating that the main effect of the CA is to reduce the (negative) imaginary component of the BM impedance. This reduction in the magnitude of the net BM impedance causes the response peak shown in Fig. 4.

Discussion

The cochlear model presented in this paper produces a realistic response by including CA forces that are predominantly reactive, rather than resistive as in previous cochlear models. In order to simulate the sensitivity of the measured response *at* the CF, the CA must add energy. However, the maximum CA force required is much less than previously thought necessary - in Kolston *et al.* (1990) it is shown that when using predominantly reactive CA forces, the maximum force required to produce a given response is more than an order of magnitude less than when using predominantly resistive forces.

Perhaps the whole question of force generation in the cochlea needs to be clarified. In particular, when reference is made to active processes it must be remembered that these processes, whilst enhancing the response of the BM, are not necessarily adding energy to the cochlea. In particular, the misconception that force generation equals energy production needs to be exorcized - it is possible to have force generators in a mechanical system (or voltage sources in an electrical cicuit, as in Fig. 3) that do not affect the net amount of energy contained within a particular system. If, for example, a force compresses a spring, the force generator delivers potential energy to the system. However, this energy is returned to the force generator in the form of kinetic energy when the force is removed. Therefore, over one period of excitation the net energy produced is zero. A reactive force generator merely redistributes the energy already present in the system; in the case of the cochlea, a reactive CA force would convert potential energy stored in the BM stiffness into kinetic energy (i.e. it would increase BM motion).

Clearly, when using the term "active", a distinction needs to be made between activity in the physiological sense and activity in a modelling (or theoretical) sense. We suggest that processes which generate forces in the cochlea should be called "physiologically-active processes", and that the term "energetically-active processes" could be used when the generated forces are *predominantly* resistive and negative. Using these definitions, the model described in this paper uses physiologically-active processes to produce a realistic response; whereas other models use energetically-active processes.

In order to determine whether CA forces are resistive or reactive in the *real* cochlea, experimental investigations should consider not simply the magnitude of the force generated, but also its phase. That is, the complex impedance of the force should be measured; it can then be determined if this force can be effectively coupled to BM mechanics, once the structural parameters of the organ of Corti are known. If the "floppiness" of the OHC stereocilia is important to the operation of the CA (e.g. Zenner *et al.*, 1988; Kolston and Viergever, 1988), future experimental investigations should attempt to measure not only the stiffness component of stereocilia impedance. In future experiments into OHC body length changes, it is suggested that the fluid used in *in vitro* preparations should offer both a resistive and a reactive impedance to motion.

Acknowledgement

This work was financially supported by the Netherlands Organisation for Scientific Research.

References

de Boer, E. (1983). No sharpening? A challenge for cochlear mechanics. J. Acoust. Soc. Am., 73, 567-573.

Davis, H. (1983). An active process in cochlear mechanics. Hearing Research, 9, 79-90.

Diependaal, R.J. (1988). Nonlinear and active cochlear models: analysis and solution methods. Doctoral thesis, University of Technology, Delft, The Netherlands.

Diependaal, R.J., de Boer, E. and Viergever, M.A. (1987). Cochlear power flux as an indicator of mechanical activity. J. Acoust. Soc. Am., 82, 917-926.

Geisler, C.D. and Shan, X. (1990). A model for cochlear vibrations based on feedback from motile outer hair cells. (This volume).

Kolston, P.J. (1988). Sharp mechanical tuning in a micromechanical cochlear model. J. Acoust. Soc. of Am., 83, 1481-1486.

Kolston, P.J. (1989). Towards a better understanding of cochlear mechanics: A new cochlear model. Doctoral thesis, University of Canterbury, Christchurch, New Zealand.

Kolston, P.J. (1990). What do we really know about cochlear mechanics? Comments on Theoretical Biology, (In Press).

Kolston, P.J. and Viergever, M.A. (1988). How do the outer hair cells influence cochlear mechanics? Report WITA-MF88.06, Delft University of Technology, The Netherlands.

Kolston, P.J. and Viergever, M.A. (1989). Realistic basilar membrane tuning does not require active processes. In Cochlear Mechanisms - Structure, Function and Models, edited by J.P. Wilson and D.T. Kemp, (Plenum Press, London), pp 415-424.

Kolston, P.J., Viergever, M.A., de Boer, E., and Diependaal, R.J. (1989). Realistic mechanical tuning in a micromechanical cochlear model. J. Acoust. Soc. of Am., 86, 133-140.

Kolston, P.J., de Boer, E., Viergever, M.A., and Smoorenburg, G.F. (1990). What type of force does the cochlear amplifier produce? J. Acoust. Soc. of Am., 88, (In Press).

Koshigoe, S. and Tubis, A. (1982). Frequency-domain investigations of cochlear stability in the presence of active elements. J. Acoust. Soc. Am., 73, 1244-1248.

Neely, S.T. (1981). Fourth-order partition dynamics for a two-dimensional model of the cochlea. Doctoral thesis, Washington University, Missouri, USA.

Neely, S.T. and Kim, D.O. (1983). An active cochlear model showing sharp tuning and high sensitivity. Hearing Research, 9, 123-130.

Neely, S.T. and Kim, D.O. (1986). A model for active elements in cochlear biomechanics. J. Acoust. Soc. Am., 79, 1472-1480.

Patuzzi, R.B., Yates, G.K. and Johnstone, B.M. (1989). Outer hair cell receptor current and sensorineural hearing loss. Hearing Research, 42, 47-72.

Robles, L., Ruggero, M.A., and Rich, N.C. (1986). Basilar membrane mechanics at the base of the chinchilla cochlea. I. Input-output functions, tuning curves, and response phases. J. Acoust. Soc. Am., 80, 1364-1374.

Viergever, M.A. (1980). Mechanics of the inner ear. A mathematical approach. Doctoral thesis, University of Technology, Delft, The Netherlands.

Zenner, H.P., Reuter, G., Plinkert, P.K., Zimmermann, U., and Gitter, A. (1988). Outer hair cells possess acetylcholine receptors and produce motile responses in the organ of Corti. In Cochlear Mechanisms - Structure, Function and Models, edited by J.P. Wilson and D.T. Kemp, (Plenum Press, London), pp 93-98.

Zweig, G. (1990). The impedance of the organ of Corti. (This volume).

Comments and discussion

WATTS

In your paper, you conclude on the basis of minimization of force magnitude and energy efficiency in a long-wave model that the cochlear amplifier should effect a reactive (stiffness or mass) change rather than a resistive (damping) change. However, de Boer (No sharpening ? A challenge for cochlear mechanics, 1983) suggests that a negative damping should be the preferred mechanism in a short-wave model to allow the phase response to be independent of input level, as is observed experimentally (i.e., by Rhode, 1971, in the squirrel monkey). Can these arguments be reconciled ?

KOLSTON

I agree with your implication that a consideration of the differences in phase behavior in long-wave and short-wave models is important. However, it is not clear that de Boer's argument supporting energy-injecting models applies when *slight* changes in the phase response are allowed. Furthermore, the amount of change in phase accumulation with and without the cochlear amplifier in physically-realizable models (as opposed to de Boer's purely phenomenological model) is approximately the same (Kolston, et al., 1990).

DUIFHUIS

Some general comments on your analysis of reactivity vs resistivity, I feel, are in order. I agree that reactive forces probably play an important role in the cochlea. However, I dispute that your analysis provides an argument against the existence of active (I mean ' energy injecting') processes in the cochlea. Let me emphasize three relevant objections.

(1) If you want to base the argument on the shape of the tip of the tuning curve then 1-dimensional model analysis is insufficient. Three-dimensional analysis provides different (broader) peaks.

(2) The real cochlea is nonlinear down to very low levels. That is relevant if you analyze iso-response contours, although the effect very close to the tip may be small.

(3) Most severely, real active models have been in study with the purpose to describe spontaneous otoacoustic emissions. A reactive structure, as defined by yourself, cannot account for this phenomenon.

KOLSTON

We did not intend to imply that the impedance-reducing model provides proof against the existence of energy-injecting processes within the cochlea. All cochlear models that exhibit a realistic response include a cochlear amplifier (CA) that exerts both resistive and reactive forces on the BM: in previous models the resistive forces dominated; in our model the reactive forces dominate, with the corresponding advantage of a minimization of CA force magnitude.

Responding to your objections in order:

(1) If the BM is represented as a point-impedance, with one degree of freedom in the radial direction, the differences in the responses of 1-D, 2-D and 3-D models are trivial compared to the response changes caused by the presence of the CA (Diependaal, 1988). Furthermore, an accurate 3-D model would incorporate the complex structural geometry of the organ of Corti: no such model exists.

(2) We show model tuning curves compared with experimental data obtained very near BM threshold, and assume that the data is accurately reflecting the response of the cochlea. We consider that, in order to be considered an accurate representation of the real system, a cochlear model must simulate these data. Virtually all non-linear models do not do this: we believe that non-linear effects should be incorporated into a model only after it has accurately simulated the measured response of the cochlea to the most simple types of stimuli: pure tones producing very small displacements of the BM.

(3) As mentioned above, our model does include (low magnitude, negative) resistive forces, so we can see no reason why the model could not produce SOAEs. Since it is only the phase relationship between the CA force and the stimulus that determines the relative magnitudes of the resistive and reactive force components, we suggest that structural anomalies along the organ of Corti (e.g.: rotated OHC stereocilia, extra rows of OHCs, missing or displaced OHCs, Furness, et al, 1990) could later the effective phase of the CA force and hence result in extra amounts of energy being added to the cochlea, causing SOAEs

References

Kolston, P.J., de Boer, E., Viergever, M.A., Smoorenburg, A.F. (1990). What type of force does the cochlear amplifier produce ? J. Acoust. Soc. Am. (in press).

Diependaal, R.J. (1988). Nonlinear and active cochlear models: analysis and solution methods. Doctoral Thesis, Delft University of Technology , The Netherlands.

Furness, D.N., Hackney, C.M., and Hynd, A.N. (1990). Rotated stereociliary bundles and their relationship with the tectorial membrane in the guinea pig cochlea. Acta Otolaryngol.

THE BASILAR MEMBRANE NONLINEAR INPUT-OUTPUT FUNCTION

Graeme K. Yates

The Auditory Laboratory, Department of Physiology, The University of Western Australia, Nedlands, 6009, Western Australia.

Introduction

It is now clear that the mechanical behaviour of the basilar membrane (BM) is highly nonlinear and that this nonlinearity plays an important part in hearing. In particular, the nonlinear growth of the BM input-output (I/O) function (Sellick and Patuzzi, 1983; Robles et al., 1986; Yates et al. 1990) significantly extends the dynamic range of the cochlear response, and may well explain how the ear can respond to sounds which vary in loudness over more than 120 dB. Winter et al. (1990) recently demonstrated that the auditory nerve can code intensity-changes over a range in excess of 100 dB, thereby solving a problem which has existed for many years, and Yates et al. (1990) established that the BM nonlinear input-output function is almost certainly responsible for this (Sachs and Abbas, 1974).

Although an empirical description of the BM I/O function now exists and various theoretical and analogue models can reproduce much of the behaviour, there is little understanding of what factors determine this nonlinearity and of why it possesses its particular form. This paper addresses that shortcoming and examines some implications.

The Source of the Nonlinearity

Zwicker (1986) described a model of the cochlea in which a nonlinearity in the active-feedback gave rise to a range of nonlinear phenomena having striking parallels with cochlear physiology. In particular, his model produced nonlinear I/O functions, generated distortion-products and demonstrated nonlinear interactions between multi-component signals similar to two-tone suppression (2TS) in the cochlea. Zwicker did not, however, suggest a physiological mechanism for the nonlinearity. Patuzzi et al. (1989) did, and demonstrated a strong correlation between loss of cochlear-microphonic (CM) and elevation of auditory-nerve thresholds. They suggested that the nonlinearity in the outer hair cell (OHC) current-transduction process was responsible for many of the nonlinear effects. Subsequently, Geisler et al. (1990) showed a close correlation between thresholds for 2TS and the sound pressure level (SPL) at which the CM first showed evidence of nonlinearity. We now examine this relationship further and investigate some of the properties which it implies.

It is not the intention to provide a quantitative mathematical model which reproduces exactly the mechanics of the BM, but rather to examine the properties of a nonlin-

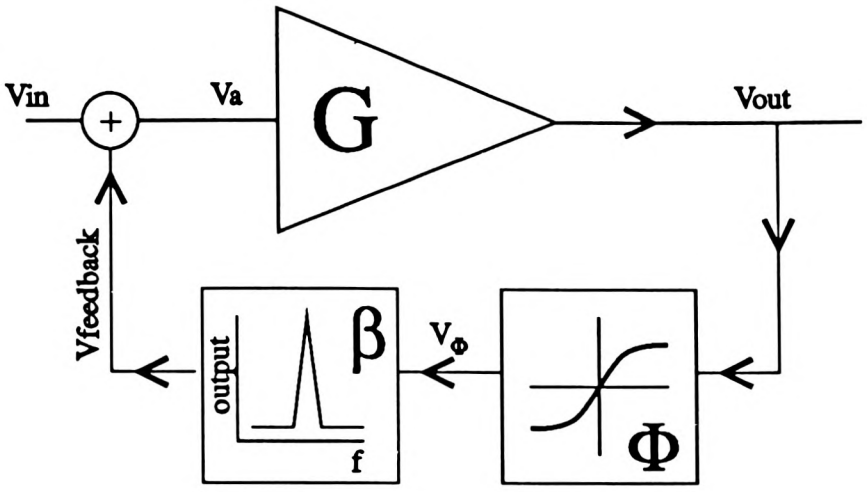

FIGURE 1 (A) Schematic of the electrical analogue considered in this paper. See text for explanation.

ear feedback systems which has some characteristics in common with the cochlea. The result will be an improved understanding of the processes which govern cochlear mechanics. We consider a simple model (Yates, 1990) which includes only the basics of the presumed cochlear nonlinear-feedback system: a source of input energy, an output of some sort, a nonlinear feedback path with a frequency-selective element, and a summing junction. The analogy is considered in electronic terms although it could take many other forms.

Figure 1 shows the analogue considered: it takes the form of a summing junction at the input to a buffer amplifier, and a nonlinear element and bandpass filter contained within a positive feedback loop. The input signal is analogous to the pressure input to the cochlea, the summing junction is analogous to the pressure fields existing in the fluids driving the basilar membrane and the amplifier is analogous to the basilar membrane and its mechanical motion. The feedback loop represents the active-process in the cochlea with the saturating CM of the outer hair cells being modelled by the nonlinearity Φ and the frequency-selective feedback (Neely and Kim, 1983, 1986) being contained within the feedback gain-setting parameter β. The shape of the nonlinearity Φ initially is chosen to be a simple Boltzmann function, in common with some previous suggestions (Holton and Hudspeth, 1983), but other forms considered gave qualitatively similar results.

It is assumed that changes in cochlear sensitivity are frequently the result of damage which reduces the *number* of displacement-sensitive channels at the top of the hair cells (Patuzzi et al. 1989), and we model that as a reduction in the value of β. Thus, manipulations which alter the feedback gain will reduce the amount of feedback without altering the shape of the nonlinear transfer function, the drive to the nonlinearity or the scaling between it and the output signal.

Results

Initially we consider as the nonlinear element the simple Boltzmann transfer function defined by

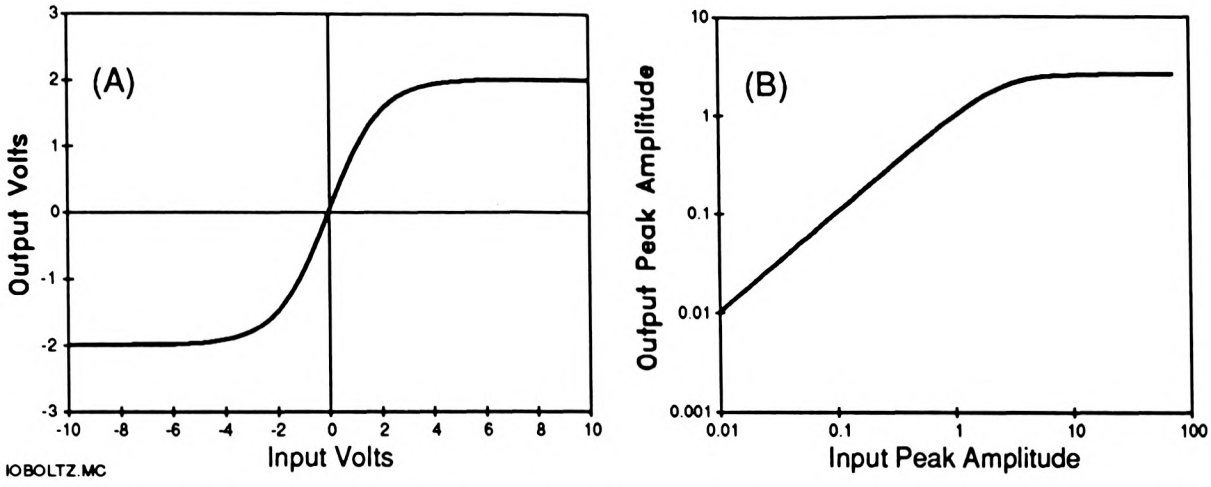

FIGURE 2 (A) Static transfer function for a simple Boltzmann function. (B) Sine-wave I/O function for the same static function. Note for future reference that the function does not saturate until an input voltage greater than 1 volt.

$$\Phi(v) = 4 \left\{ \frac{\exp(v)}{1 + \exp(v)} - 0.5 \right\} \qquad (1)$$

and plotted in figure 2A. This represents the static response to a static input, but to calculate the behaviour of the circuit we must consider the I/O function in response to a sinusoidal stimulus. This is plotted in figure 1B. Thus, (B) represents the peak-amplitude feedback voltage when the nonlinearity is driven by a sinusoidal output voltage. This feedback signal is then passed through a band-pass attenuation element with the transfer function

$$V_\Phi = \begin{cases} \beta(V_{out}) & f = CF \\ 0 & f <> CF \end{cases} \qquad (2)$$

and summed with the input signal. (CF is the pass-band frequency.) The summed signal then passes through the amplifier to become the output signal.

Calculation of the I/O function for the complete circuit is complicated by the nonlinearity, so a different technique is used to avoid solving a nonlinear equation. Since we do not require (indeed, it is usually not possible to obtain) an explicit function for the relationship between input and output, the order of the calculation is reversed and we compute the input amplitude necessary to produce a given output voltage. Thus, figure 3 is plotted by computing the input voltage for a range of output voltages in the following way.

$$V_{in} = V_a - V_{feedback} \qquad (3)$$

where

$$V_{feedback} = \beta.\Phi(V_{out}) \qquad (4)$$

The solid line of figure 3 shows the result. (The value of G is taken as 1 throughtout this paper.) The calculated I/O function shows three distinct regions: an initial segment at low intensities which is quite linear with intensity, a second segment at intermediate intensities which has a flatter slope, and a third, high-intensity, region which approaches

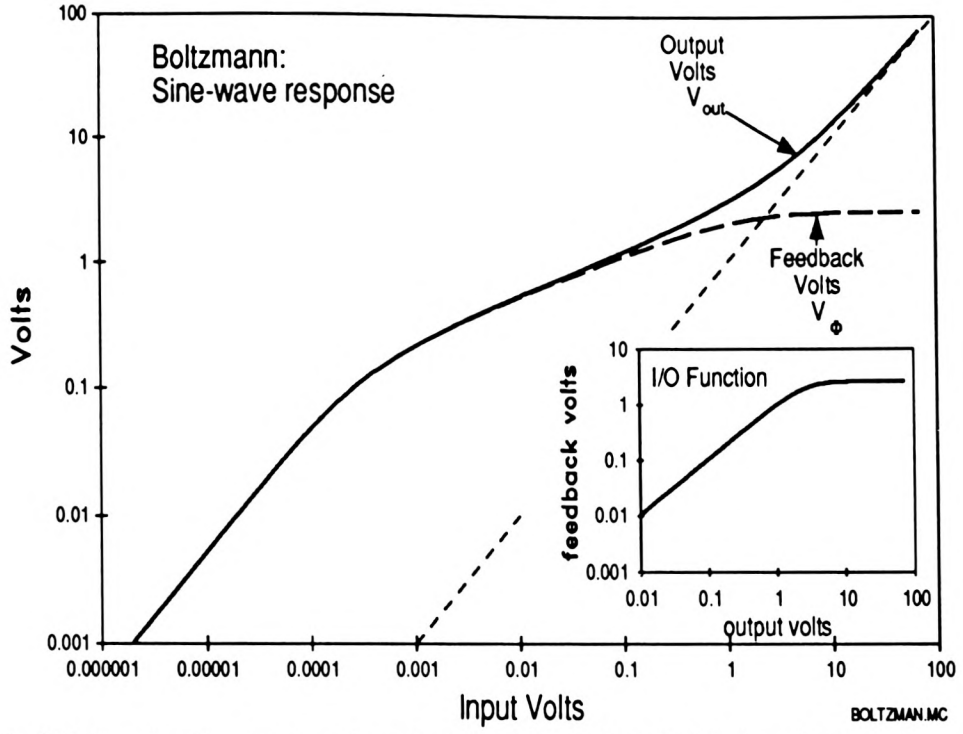

FIGURE 3 I/O function for the complete circuit of figure 1 with Φ being the Boltzmann function of figure 2. Solid line is the output voltage. Long dashes: output from the nonlinear element, before β. Short dashes: I/O function with feedback loop opened. Note that the output voltage becomes nonlinear well before obvious nonlinearity in Φ. β = 0.998, G = 1.0. The inset repeats figure 2B.

linearity again. The first two sections correlate well with similar segments seen in BM mechanical measurements (Sellick et al., 1982; Robles et al., 1986) while the third has been seen only in damaged preparations (Johnstone et al., 1986) but may well exist in the undamaged preparation. We now consider each section in turn.

THE LOW-INTENSITY SEGMENT

For CF input voltages less than 0.1 millivolts, the I/O function of figure 3 is straight and has a slope of unity, i.e., it is quite linear. The gain of the overall circuit is 54 dB, consistent with the feedback ratio β of 0.998. In this region the effect of Φ is negligible and the circuit acts as a simple positive-feedback circuit with closed-loop gain given by

$$V_{closed} = \frac{G.V_{in}}{1 - G.\beta.\Phi(V_{in}).} \qquad (5)$$

THE MID-INTENSITY SEGMENT

When the input voltage exceeds 0.5 millivolts the I/O function abruptly becomes nonlinear, falling behind the linear extrapolation from the initial segment. In the region between 0.001 and 1 volts the output voltage increases by only 0.36 dB for each 1 dB increase in input amplitude. Over this range the gain between input and output is falling rapidly with intensity. In terms of the output voltage, figure 3 shows that the circuit becomes nonlinear at an output voltage of about 0.2 volts.

It is important to note that the onset of nonlinearity in the output-voltage curve for the overall circuit does not correspond with any obvious feature in the feedback nonlinearity I/O function. In particular, the function Φ appears to be quite linear up to an out-

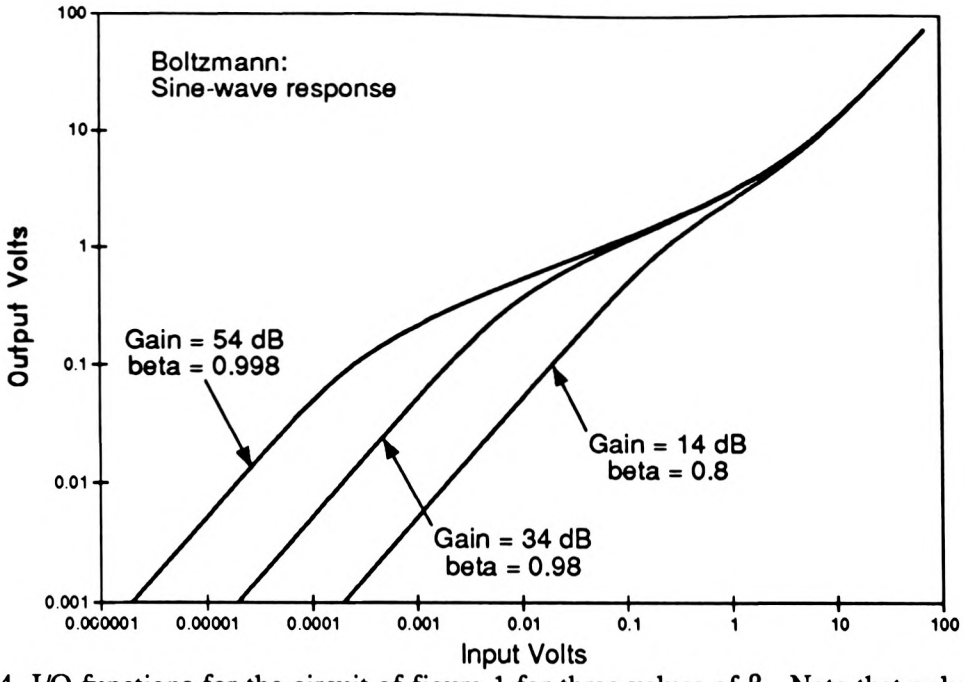

FIGURE 4 I/O functions for the circuit of figure 1 for three values of β. Note that only the low-intensity segments are affected, with the higher-intensity segment being almost unaffected.

put voltage of 1-2 volts, whereas the I/O function for the overall circuit becomes nonlinear at around 0.2 volts, a full 20 dB lower. The explanation for this lies in the extreme sensitivity of a positive-feedback circuit to small changes in loop parameters. The denominator of Eq.5 represents the difference between two nearly-equal numbers and, hence, is very sensitive to small changes in Φ or β. For small input voltages, if the insertion gain of $\Phi(V_{in})$ changes by as little as a factor of 0.001, the denominator will change by a factor of 2. Thus, the onset of obvious nonlinearity in the output voltage occurs when the nonlinearity in Φ is still very small.

THE HIGH-INTENSITY SEGMENT

At very high input levels the feedback nonlinearity Φ saturates almost completely, effectively opening the feedback loop and causing the circuit gain to fall to the open-loop case. The I/O curve then approaches asymptote with the open-loop I/O function.

Comparison with the cochlea

Relating the above back to the concepts of Patuzzi et al. (1989) suggests the following. The initial, linear, segment of the BM I/O function is limited to displacements of the BM for which the CM production by the outer hair cells is highly linear and within which the full drive of the active process acts on the BM. The intermediate segment results when small deviations from linearity in the production of OHC currents cause the closed-loop gain of the cochlea to fall as the stimulus intensity is increased. Effectively, the active process becomes less-and-less effective in assisting the displacement of the BM. In the high-intensity segment the active process is almost ineffective, and the mechanics reverts to the passive case.

COCHLEAR PATHOLOGIES

Insults to the cochlea appear to affect the number rather than the properties of the transduction channels active in the OHCs (Patuzzi et al., 1989). According to the analogy described here, this would result in a reduction of the low-intensity closed-loop gain

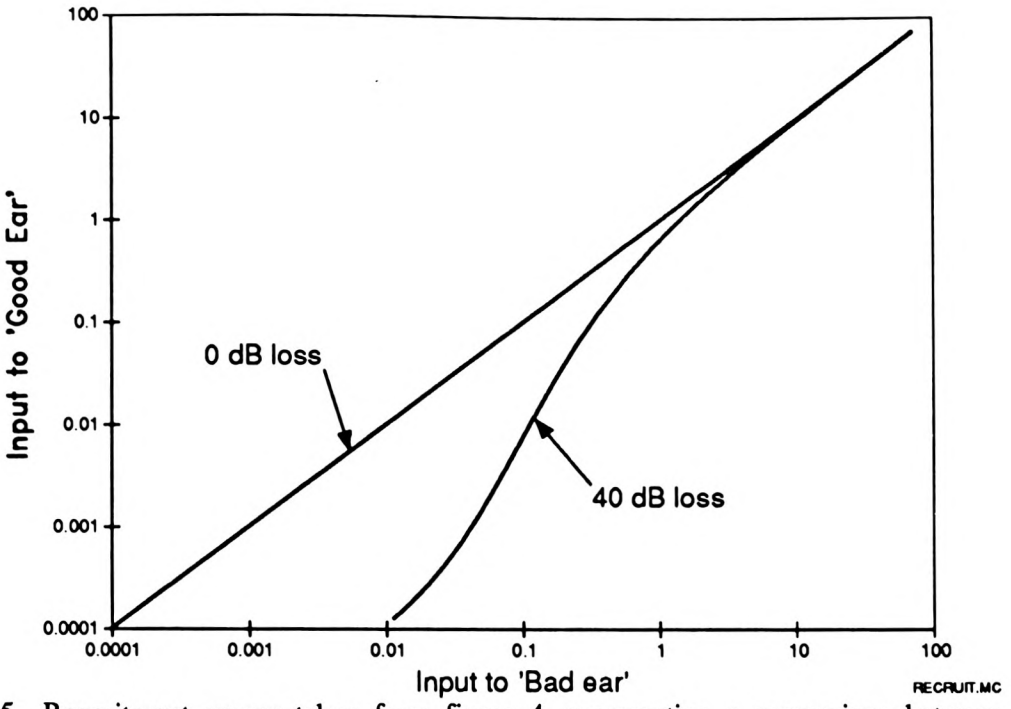

FIGURE 5 Recruitment curves taken from figure 4, representing a comparison between two circuits with different feedback gain β. The abscissa represents the input voltage necessary to produce a given output level for the lower-gain circuit. The ordinate represents the input voltage to the higher-gain circuit for the same output (β = 0.998). The straight line shows the expected value for β unchanged (at 0.998). The curved line is for β = 0.8.

(i.e., of β) and a consequent reduction in the sensitivity of the BM mechanics. The low-intensity segment of the BM I/O function would shift to the right (see Sellick et al., 1982; Robles et al., 1986). At higher stimulus levels, the reduction in the feedback loop-gain would be less important, and the effect on the I/O function would be reduced. Finally, at high stimulus intensities the effects of trauma would be negligible and the BM I/O curve would be unaffected. This is illustrated by figure 4 which shows the effect of a reduction in β from 0.998 to 0.98 and 0.8. Each change displaces the low input-level segment by 20 dB to the right, while the high intensity-level segment is virtually unaffected.

These effects are qualitatively just what is observed experimentally (Patuzzi et al., 1989). Small changes in the CM production (measured at low frequencies, for which the positive-feedback loop is ineffective) produce large changes in cochlear sensitivity at CF, but have little effect on the high-intensity responses at any frequency.

RECRUITMENT

Figure 4 also provides a clue as to the mechanisms involved in recruitment. The more-sensitive curve of that figure may be interpreted as the normal case, with the less-sensitive curves as the hearing-impaired cases. Comparison of the two enables the calculation of a 'recruitment' curve, in which is plotted the input-voltage required to produce a given output voltage for the 'normal' case against the input-voltage required for the same output in the case of the 'hearing impaired' circuit. Figure 5 shows such an analysis for the 54 dB and 14 dB cases in figure 4, a 'hearing loss' of 40 dB. The curve has a form similar to that published for recruitment in cases of hearing loss of the order of 40 dB. It shows the characteristic steeper slope of the impaired ear approaching the flatter slope of the normal ear at higher intensities. The rate of recruitment is, however, slower at low intensities (the bottom end of the recruitment curve is concave upwards), reflecting the steeper slope of the low-intensity normal hearing.

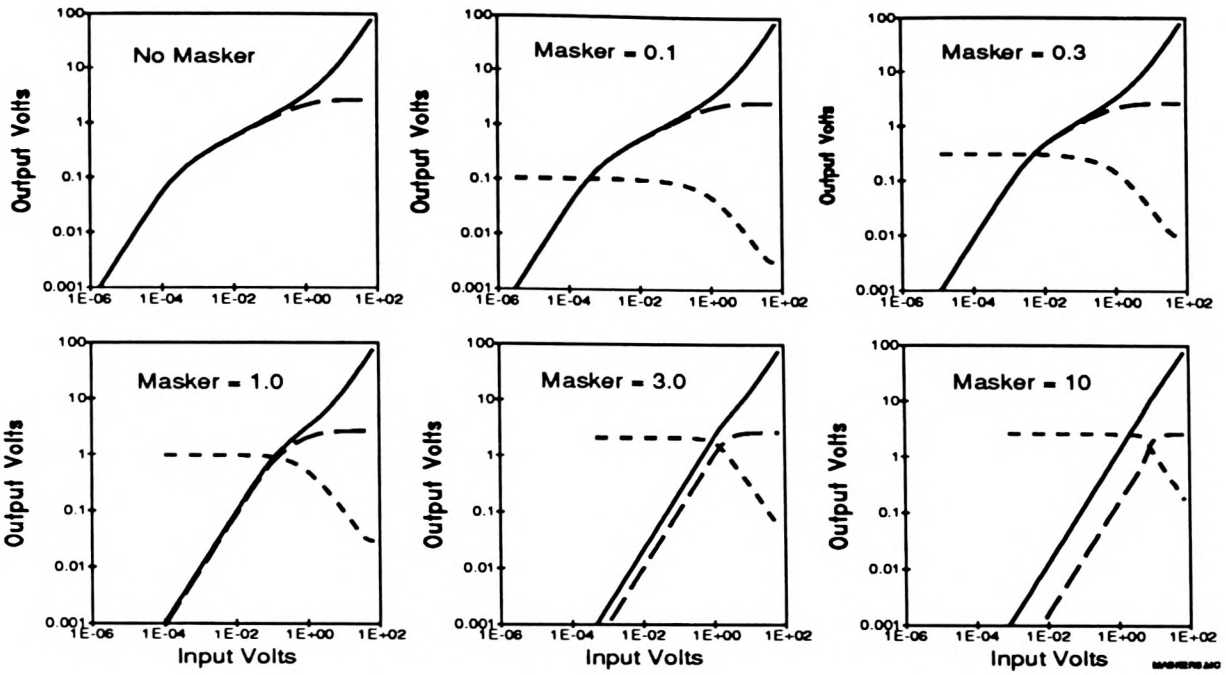

FIGURE 6 I/O functions at CF for six different amplitudes of a suppressor signal. Each graph shows the I/O function for a signal at CF, presented simultaneously with a suppressor tone at a different frequency. Increasing amplitudes of suppressor shift the low-intensity segment to the right while leaving the high-intensity segment virtually unchanged. The largest suppressor has almost completely removed any feedback gain. Solid line: output voltage. Long dashes: amplitude of suppressor component of output from the nonlinearity Φ. Short dashes: amplitude of CF component of output from nonlinearity Φ.

TWO-TONE SUPPRESSION

Finally, we investigate the phenomenon of 2TS, in which the response to an existing first tone is reduced by the addition of a second input tone (Arthur et al., 1971).

For the electronic analogue considered here, a suppressor tone may be modelled by applying a second input signal at a frequency other than CF. Such a signal will not activate the feedback loop since it will not be passed by the frequency-selective element β, but it will still drive the nonlinearity, Φ, thereby modulating the transmission of a probe signal at CF. The response to such a complex signal was calculated by assuming a given level of suppressor at the input and then calculating the level of the probe signal necessary to produce a given output signal, as for the simple case above. In this case, however, the analogy with the cochlea is not so accurate since the circuit of figure 1 is a single element whereas the cochlear travelling wave is a distributed process with a distributed nonlinearity. In spite of this, however, we may take the amplitude of the probe tone which is present at the output as a measure of the probe-tone response to the combined signals. Figure 6 shows the results for several levels of masker signal.

Each successive increase in the masker voltage reduces the low-intensity gain but does not change the response at higher intensities. This is because the larger suppressor signals effectively reduce the gain of the feedback loop by driving the nonlinearity Φ close to and into saturation, thereby reducing the loop gain for the CF tone. At the higher intensities the loop is ineffective anyway, so the suppressor has little influence.

A second consequence of increasing suppressor intensity is a shift of the (linear) low-intensity segment to the right. This effect is observable in auditory-nerve recordings as a shift to higher intensities of rate-intensity functions recorded in the presence of a

suppressor tone (Rhode et al., 1978). The corner intensity at which nonlinearity is first detectable also shifts to higher intensities, and upwards. A consequence of this should be the change in shape of sloping-saturation rate-intensity functions during suppression, which has been observed (Sokolowski et al., 1989).

Conclusion

Although most of the nonlinear phenomena described in this paper have previously been seen in analogue and computer models of the cochlea, it is clear that an understanding of the basic physics of these effects is easily obtained from much simpler considerations. A simple analogue circuit with a positive feedback loop containing a saturating nonlinearity exhibits many of the phenomena seen in these models and in the cochlea itself. The nonlinear growth of the basilar membrane I/O function, the change in shape of the I/O function with trauma, recruitment and 2TS all have parallels in such a model and are easily understood in such terms.

References

Arthur, R.M., Pfeiffer, R.R. and Suga, N. (1971). Properties of two-tone inhibition in primary auditory neurones. J.Physiol.(London). 212, 593-609.

Geisler, C.D., Yates, G.K., Patuzzi, R.B. and Johnstone, B.M. (1990). Saturation of outer hair cell receptor current causes two-tone suppression. Hear Res 44, 241-256.

Holton, T. and Hudspeth, A.J. (1983). A micromechanical contribution to cochlear tuning and tonotopic organization. Science 222, 508-510.

Johnstone, B.M., Patuzzi, R. and Yates, G.K. (1986). Basilar membrane measurements and the travelling wave. Hearing Res. 22, 147-153.

Neely, S.T. and Kim, D.O. (1983). An active cochlear model showing sharp tuning and high sensitivity. Hearing Res. 9, 123-130.

Neely, S.T. and Kim, D.O. (1986). A model for active elements in cochlear biomechanics. J.Acoust.Soc.Am. 79, 1472-1480.

Patuzzi, R.B., Yates, G.K. and Johnstone, B.M. (1989). Changes in cochlear microphonic and neural sensitivity produced by acoustic trauma. Hearing Res. 39, 189-202.

Rhode, W.S., Geisler, C.D. and Kennedy, D.T. (1978). Auditory nerve fiber responses to wideband noise and tone combinations. J. Neurophysiol. 41, 692-704.

Robles, L., Ruggero, M.A. and Rich, N.C. (1986). Basilar membrane mechanics at the base of the chinchilla cochlea. I. Input-output functions, tuning curves, and phase responses. J.Acoust.Soc.Am. 80, 1364-1374.

Sachs, M.B. and Abbas, P.J. (1974). Rate versus level functions for auditory-nerve fibres in cats: tone-burst stimuli. J.Acoust.Soc.Am. 56, 1835-1847.

Sellick, P.M., Patuzzi, R. and Johnstone, B.M. (1982). Measurement of basilar membrane motion in the guinea pig using the Mossbauer technique. J.Acoust.Soc.Am. 72, 131-141.

Sokolowski, B.H.A., Sachs, M.B. and Goldstein, J.L. (1989). Auditory nerve rate-level functions for two-tone stimuli: Possible relation to basilar membrane nonlinearity. Hear Res 41, 115-124.

Winter, I.H., Robertson, D. and Yates, G.K. (1990). Diversity of characteristic frequency rate-intensity functions in guinea pig auditory nerve fibres. Hear Res (in press).

Yates, G.K. (1990). Basilar membrane nonlinearity and its influence on auditory nerve rate-intensity functions. Hear Res (in press).

Yates, G.K., Winter, I.H. and Robertson, D. (1990). Basilar membrane nonlinearity determines auditory nerve rate-intensity functions and cochlear dynamic range. Hear Res (in press).

Yates, G.K., Geisler, C.D., Patuzzi, R.B. and Johnstone, B.M. (1989). Saturation of receptor currents accounts for two-tone suppression. In, Cochlear Mechanisms: Structure, Function and Models. J.P.Wilson and D.T.Kemp, Eds. Plenum Press., 177-184.

Zwicker, E. (1986). A hardware cochlear nonlinear preprocessing model with active feedback. J.Acoust.Soc.Am. 80, 146-153.

ACTIVE COCHLEAR FEEDBACK: REQUIRED STRUCTURE AND RESPONSE PHASE

J.J. Zwislocki

Institute for Sensory Research, Syracuse University, Syracuse, NY, 13244-5290, USA

Introduction

According to indirect experimental evidence, derived mainly from acoustic cochlear emissions (Kemp,1978), wave propagation in the cochlea is supported by metabolic energy. The motility of OHCs associated with an alternating electrical field (Brownell et al. 1985) is likely to be the mechanism for the energy delivery (e.g. Ashmore,1986). If the cells respond mechanically to the alternating electrical fields they themselves generate, conditions for an electromechanical feedback are provided. Several models of the feedback were proposed in the past (e.g. Kim et al., 1980; Mountainet al. 1983; Neely and Kim, 1986) but were not sufficiently explicit to establish the required structural and phase conditions. Analysis of these conditions and an experimental confirmation of its crucial results are the subject of this article.

Theoretical Considerations

The structures of the cochlear partition are schematized in Fig. 1, together with the vectors indicating their gross relative magnitudes and directions of motion. For simplicity of explanation, it is assumed that the part of the basilar membrane underlying the hair cells moves in cross section like a stiff beam rotating around the margin of the osseous spiral lamina. Recent measurements of Miller (1985) suggest that this is a reasonable approximation. Reissner's membrane has been omitted as having a negligible mechanical effect. The radius L_O connects the point of rotation with the reticular lamina at the location of the second row of OHCs. At that location, the reticular lamina moves at a right angle to the radius with the velocity V_B which has to be equal to the velocity of the basilar membrane at a distance L_O from the point of rotation. The velocity can be analyzed into two components, one perpendicular (V_T) and one parallel (V_R) to the basilar membrane. The former will be referred to as "transversal", the latter, as "radial" according to cochlear directions. Note that the reference point for the velocity components has been shifted to the undersurface of the tectorial membrane in order not to interfere with the schematized stereocilia bundles in the subtectorial space.

Associated with the velocities are forces which are related to them through appropriate impedances. The forces interact with each other through torques determined by the distances of the points of force application to the point of rotation. The resulting lever

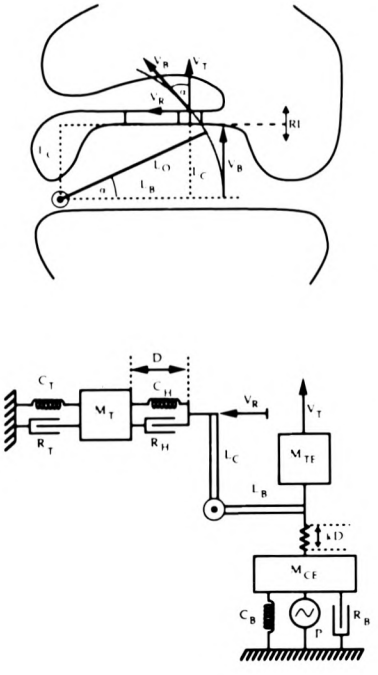

FIGURE 1 (Upper part) Schematic cross section of the organ of Corti with the indicated simplified modes of motion of its parts. Radius L_O connects the assumed point of rotation of the basilar membrane with the reticular lamina at the location of the OHCs. The vector V_B indicates the basilar-membrane displacement at the distance L_O from the point of rotation. V_T and V_R are the transversal and radial components of the reticular-lamina displacement at the location of the OHCs. L_B and L_C are the levers associated with these components. The vectors RL schematize the displacements of the reticular lamina relative to the basilar membrane resulting from OHC motility. See text for further explanations.

(Lower part) Mechanical network analog of the structures schematized above. Note the lever pair L_B and L_C coupling the transversal motion of the basilar membrane, V_T, to the radial motion component, V_R, of the reticular lamina. The springlike structure kD indicates a velocity source resulting from the OHC motility. The source output is assumed to be proportional to the deflection of the stereocilia, D, modelled by the deformation of the spring C_H. See text for further explanation.

associated with the velocity V_T is L_B, and that associated with the velocity V_R, L_C.

The lower part of the figure depicts the corresponding mechanical impedance network based on the structure of the cochlear partition. From the bottom right, the elements C_B and R_B stand for the compliance and resistance of the basilar membrane, respectively; its mass is included in the effective mass of the organ of Corti, M_{CE}. The source P indicates the force resulting from the sound-pressure difference across the cochlear partition. The spring-like structure designated as kD stands for a velocity source associated with the OHC motility. The source has to be a high-impedance, velocity, source because of the structural rigidity of the organ of Corti, necessary for effective vibration transmission from the basilar membrane to the reticular lamina that holds the apical parts of the OHCs. Because of the high impedance of the source, kD, the axial rigidity of the stereocilia bundles and the incompressible fluid separating the tectorial membrane from the reticular lamina, the effective mass of the tectorial membrane, M_{TE}, associated with the transversal velocity, V_T, is added to the effective mass of the organ of Corti, M_{CE}. The radial velocity, V_R, and its associated impedance network are coupled to the transversal velocity, V_T, and its associated impedance network through the levers L_B and L_C. The elements C_H and R_H correspond to the radial compliance and resistance of the stereocilia bundles, respectively. The elements M_T, C_T and R_T indicate, respectively, the mass of the tectorial membrane and its viscoelastic attachment to the spiral limbus. For orientation, it should be pointed out that compression of the spring C_H during counterclockwise (toward scala vestibuli and the modiolus) rotation of the

levers, L_B and L_C means the stereocilia deflection toward the spiral ligament (excitatory), its expansion, the stereocilia deflection toward the modiolus (inhibitory).

The source, kD, is assumed to act through expansion and contraction of the spring, C_H, in agreement with the observations of OHC motility (e.g. Brownell et al.,1985). Expansion increases the distance between the basilar-membrane and tectorial-membrane masses and produces a counterclockwise rotation of the levers L_B and L_C. Contraction brings the masses closer together and produces a clockwise rotation of the levers. Since, at most sound frequencies, the basilar-membrane complex has a higher impedance than the stereocilia and tectorial-membrane complex (Zwislocki and Cefaratti, 1989), the magnitude of the relative motion of the tectorial-membrane mass and of the lever tips is greater than that of the basilar-membrane mass.

At sufficiently low sound frequencies, the mass effect of the tectorial membrane is negligible, and the radial motion of the tectorial membrane in relation to the radial motion of the reticular lamina must be determined by the relation between the compliance of the stereocilia, C_H, and that of the tectorial membrane, C_T. Since, even for relatively large C_T, force is required to move the tectorial membrane, the reaction force must deflect the stereocilia outward, toward the spiral ligament, when the basilar membrane is displaced toward scala vestibuli, and inward, toward the modiolus, when it is displaced in the opposite direction. This is evident from Fig. 1 and is in agreement with the classical model of cochlear shear motion and hair-cell stimulation. It is well established that outward deflection of the stereocilia produces hair-cell depolarization.

Let us now investigate the relationship between OHC motility and this mode of relative motion between the tectorial membrane and the reticular lamina. Brownell et al. (1985) have demonstrated that OHC depolarization is associated with their shortening. As a consequence, the reticular-lamina surface must move toward the basilar membrane when the basilar membrane moves toward scala vestibuli and the tectorial membrane. This is indicated by the arrow RL pointing downward. Since, under these circumstances, the motion of the reticular lamina partially counteracts the effect of the basilar-membrane motion, the shear motion between the tectorial membrane and the reticular lamina is reduced and, with it, the deflection of the stereocilia and the hair-cell depolarization. This amounts to a *negative* feedback.

Obviously, to obtain a positive feedback, both the basilar membrane and the reticular lamina relative to it must move in the same transversal direction. For this to occur, OHCs have to be depolarized during basilar-membrane displacement toward scala tympani, not vestibuli, so that the stereocilia have to be deflected toward the spiral ligament, not the modiolus, during the same phase of basilar-membrane vibration. Such a deflection phase can occur only if the magnitude of the radial displacement of the tectorial membrane is greater than that of the reticular lamina. This is possible only through a parallel-resonance effect. A parallel resonance of the stereocilia loaded with the tectorial-membrane mass has been suggested for the mammalian cochlea more than 10 years ago (Zwislocki, 1980).

The kinematic relationships between the radial motions of the tectorial membrane and the reticular lamina and the resulting shear motion are illustrated more explicitly by the vector diagrams of Fig. 2. It is assumed that the stereocilia deflection of the OHCs is practically identical to the shear displacement. The coordinate system is based on the cochlear cross-sectional geometry. The spiral ligament is to the right, and the modiolus,

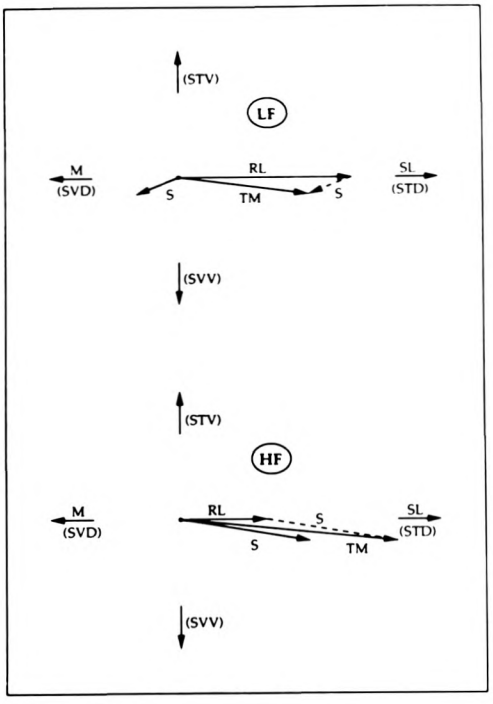

FIGURE 2 Vector diagrams schematizing the radial displacment relationships between the reticular lamina and the tectorial membrane, which produce the shear displacments between the two structures. RL and TM are the radial displacement vectors of the reticular lamina and the tectorial membrane, respectively, and S is the shear-diplacement vector. SL means the spiral-ligament direction, M, the modiolus direction. For the reticular lamina, the SL direction is always associated with basilar-membrane displacement toward scala tympani (STD), and the M direction, with its displacement toward scala vestibuli (SVD) (Compare with Fig. 1). In the upper diagram the TM vector is assumed to be smaller than the RL vector; in the lower diagram, the opposite is true. The first situation is assumed to prevail at low sound frequencies (LF), the second, at higher sound frequencies (HF) at low and medium SPLs. See text for further explanation.

to the left. The vertical coordinates indicate the velocities of motion toward the spiral ligament and the modiolus, respectively. For the reticular-lamina vector, RL, the displacement toward the spiral ligament is associated of necessity with basilar-membrane displacement toward scala tympani, the displacement toward the modiolus, with the basilar-membrane displacement toward scala vestibuli, as is evident in Fig. 1. Vector TM, representing the radial displacement of the tectorial membrane, lags somewhat that of the reticular-lamina vector, RL, because of a necessary effect of friction.

In the upper diagram, the TM vector is made somewhat smaller than the RL vector, a relationship that must prevail at sound frequencies sufficiently below the parallel-resonance frequency (LF), as was already mentioned. The shear-displacement vector, S, is equal to the vector difference between the TM and RL vectors. It points toward the modiolus, the hyperpolarizing direction for the OHCs. If the vectors were rotated by 180^{o}, and the RL vector pointed toward the modiolus, as this happens during basilar-membrane displacement toward scala vestibuli, the shear-displacement vector would point toward the spiral ligament, the depolarizing direction, in agreement with the classical model. This is evident in the upper part of Fig. 1.

In the lower diagram of Fig. 2, the TM vector is made larger than the RL vector, in agreement with the parallel-resonance effect at higher frequencies (HF). Here, the shear-displacement vector, S, points toward the spiral ligament, the *depolarizing* direction, during basilar-membrane displacement toward *scala tympani*. Comparing the upper and lower diagrams, we can conclude that the excitation phase of the OHCs should change from the displacement of the basilar membrane toward scala vestibuli at low sound frequencies to its displacement toward scala tympani around the best frequency.

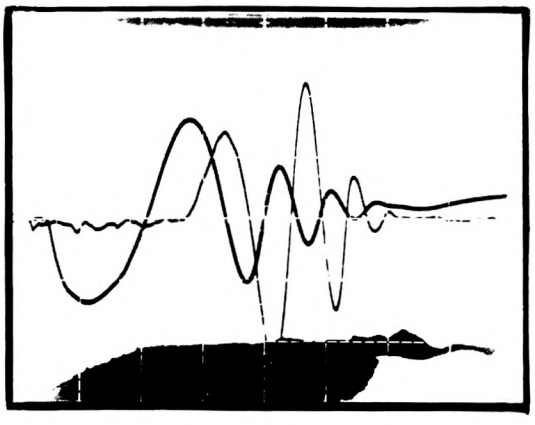

FIGURE 3 Recording of the alternating potential of a Hensen cell in terms of $y = Y \sin [\omega t + \phi(\omega)]$ as a function of $\log \omega = \log (2\pi f)$. The time delay, t, reflects wave travel time in the cochlea and is approximately constant; the phase, $\phi(\omega)$, is relative to the voltage at the earphone terminals. It includes phase contributions of the earphone and the middle ear, which are assumed to be independent of SPL and the state of the cochlea and to be small. The thin line refers to a SPL of 40 dB, the thick line to that of 90 dB (reduced amplification). See text for further explanation.

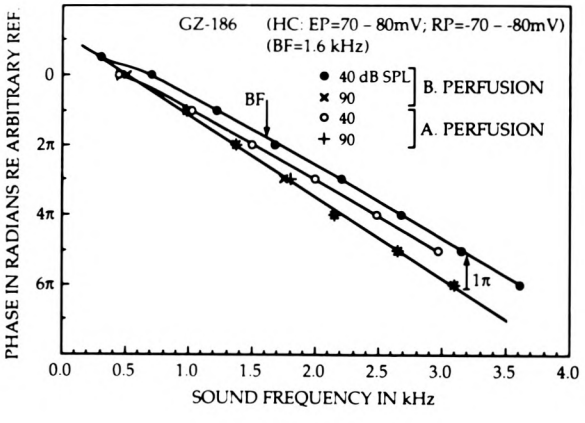

FIGURE 4 Hensen-cell response phase recorded on two cells, one before salicylate treatment, and one, after the treatment. The cells were at the same cochlear location and had practically the same resting potential. The endolymphatic potential was nearly the same also. Note the phase lag produced by the salicylate at 40 but not 90 dB. The 90-dB curves indicate an approximately 180^{o} shift relative to the pretreatment 40 dB curve. See text for further explanation.

Experimental Verification

It is likely that the parallel resonance of the stereocilia and tectorial-membrane system is supported by the electromechanical feedback provided by the OHCs. If this is true, reduction of the feedback should decrease the vibration amlitude of the tectorial membrane and, as a consequence, change the response phase of the OHCs. This would be reflected in the lower diagram of Fig. 2 by a clockwise rotation of the S vector from the spiral ligament, SL, toward the modiolus, M. According to indirect experiments on acoustic cochlear emissions, the feedback is ineffective at high SPLs (e.g. Kemp and Chum, 1980). By recording alternating receptor potentials of OHCs and their reflection in HCs and CM, we were able to show that, indeed, the response phase changes by about 180^{o} between low and high SPLs (Zwislocki,1988). The phenomenon is illustrated in Fig. 3, which shows alternating potentials of a Hensen cell (HC). The curves, plotted over log frequency, follow the function $y = Y \sin [\omega t + \phi(\omega)]$ with reference to the earphone input. The thin curve corresponds to 40 dB, and the thick one, to 90 dB SPL. Phase opposition between the two curves is unmistakable at the higher frequencies. According

to experiments on acoustic cochlear emissions (e.g. Long and Tubis, 1988) and direct experiments on the motility of isolated OHCs (Shehata et al. 1990), sodium salicylate suppresses the motility. It should be expected, therefore, that it suppresses the feedback.

Putting together the high SPL and salicylate effects, we can generate the following quadruple hypothesis resulting from our model of the cochlear feedback: 1) In a normally-functioning cochlea, at low and medium SPLs, the OHC depolarization phase should change from scala vestibuli at low sound frequencies to scala tympani at the higher frequencies (~180^{o}). 2) At high SPLs, the phase should coincide with basilar-membrane displacement toward scala vestibuli at all freqencies. 3) Injection of the salicylate into the perilymph should make the response phase rotate toward scala vestibuli at low and medium SPLs. 4) At high SPLs, where the feedback is ineffective, the salicylate should have no phase effect.

The corresponding experimental results are shown in Fig. 4. They refer to two SPLs, 40 and 90 dB, and to the two states, before and after salicylate treatment. At 40 dB, the closed circles indicate an approximately 180^{o} shift between the low and higher frequencies, and the open circles, a shift toward scala vestibuli, due to the salicylate effect. There is no salicylate effect at 90 dB, as indicated by the slanted and straight crosses, which practically overlap. Note that the 90-dB curve is shifted by about 180^{o} relative to the 40-dB curve at all but the lowest frequencies. Clearly, the results support the 4 hypotheses and, consequently, the model from which they were derived.

It should be pointed out that accumulating evidence for a tuned cochlear feedback (Brundin et al., 1990), does not change the relationships included in this article.

Acknowledgements

I thank L.K. Cefaratti for essential assistance in the experimental work, photography and manuscript formatting; Dr. N.B. Slepecky, for valuable suggestions; Dr. W.E. Shehata, for the specification of the Na-salicylate solution in artificial perilymph; R. Mitchell, for manufacture and maintenance of precision insruments; A. Wixson, for the maintenance of the electronic equipment; and D. Arpajian for computer graphics. Work supportet by NIDCD Javits Grant DC00074-28.

References

Ashmore, J.F. (1986) The cellular physiology of isolated outer hair cells: Implications for cochlear frequency selectivity. In: Auditory Frequency Selectivity (Eds: Moore, B.C.J. and Patterson, R.D.) Plenum Press, London, pp. 103-108.

Brownell, W.E., Bader, C.R., Bertrand, D. and Ribaupiere, Y. (1985) Evoked mechanical responses of isolated cochlear hair cells. Science 227, 194-196.

Brundin, L., Flock, A., and Canlon, B. (1990) Sound induced motility of cochlear outer hair cells shows tuning. ARO Abstracts 13, 227.

Kemp, D.T. (1978) Stimulated acoustic emissions from within the human auditory system. J. Acoust. Soc Am. 65, 1386-1391.

Kemp, D.T. and Chum, R. (1980) Properties of the generator of stimulated acoustic emissions. In: Nonlinear and Active Mechanical Processes in the Cochlea (Eds: Kemp, D.T. and Anderson, S.D.) Hearing Res. 2, 213-232.

Kim, D.O., Neely, S.T., Molnar, C.E. and Matthews, J.W. (1980) An active cochlear model with negative damping in the partition: Comparison with Rhode's ante- and post-mortem observations. In: Psychophysical, Physiological and Behavioral Studies in Hearing (Eds: Brink, G. v.d. and Bilsen, F.A.) Delft University Press, Delft, pp. 7-15.

Long, R.R. and Tubis, A. (1988) Modification of spontaneous and evoked otoacoustic emissions and associated psychoacoustic microstructure by aspirin consumption. J. Acoust. Soc. Am. 84, 1343-1353.

Miller, C.E. (1985) Structural implications of basilar membrane compliance measurements. J. Acoust. Soc. Am. 77, 1465-1474.

Mountain, D.C., Hubbard,A.E. and McMullen, T.A. (1983) Electromechanical processes in the cochlea. In: Mechanics of Hearing (Eds: de Boer, E. and Viergever, M.A.) Delft University Press, Delft, pp. 119-126.

Neely, S.T. and Kim, D.O. (1986) A model for active elements in cochlear biomechanics. J. Acoust. Soc. Am. 79, 1472-1480.

Shehata, W.E., Brownell, W.E., Cousillas, H. and Imredy, J.P. (1990) Salicylate alters membrane conductance of outer hair cells and diminishes rapid electromotile responses. ARO Abstracts 13, 252-253.

Zwislocki, J.J. (1980) Five decades of research on cochlear mechanics. J. Acoust. Soc. Am. 67, 1679-1685.

Zwislocki, J.J. (1988) Phase reversal of OHC response at high sound intensities. In: Cochlear Mechanisms: Structure, Function and Models (Eds: Wilson, J.P. and Kemp, D.T.) Plenum Press, London, pp. 163-168.

Zwislocki, J.J. and Cefaratti, L.K. (1989) Tectorial membrane II: Stiffness measurements *in vivo*. Hearing Res. 42, 211-228.

Section 4

Electrophysiology

SPONTANEOUS ACTIVITY OF AUDITORY AFFERENT NEURONES IN THE SPIRAL GANGLION OF THE PIGEON

Anthony W. Gummer

Developmental Neurobiology Group, The Australian National University, Research School of Biological Sciences, Canberra, ACT 2601, Australia

Introduction

In the avian (Manley, 1979; Manley and Gleich, 1984; Manley *et al.*, 1985; Temchin, 1988) and reptilian (Crawford and Fettiplace, 1980; Eatock *et al.*, 1981) auditory nerves there exists a population of afferent fibres which exhibit quasiperiodic spontaneous activity. The interval histogram of such activity shows decaying maxima, separated at approximately equal intervals, named the preferred interval by Manley (1979). These histograms contrast with those reported for other species (e.g. Kiang, 1965; Walsh *et al.*, 1972; Robertson and Manley, 1974), and with the balance of histograms from other fibres in birds and reptiles, where after an absolute refractory period the interval histogram decays exponentially from it's modal value, as if generated by a truncated, homogeneous Poisson process. However, for quasiperiodic spontaneous activity both the modal interval and the preferred interval are related to the characteristic frequency (CF) of the neurone. Earlier reports (Manley, 1979; Crawford and Fettiplace, 1980; Eatock *et al.*, 1981), as well as the one by Temchin(1988), report that the modal and preferred intervals are approximately equal to the CF-period, whereas the more recent papers from Manley and coworkers (Manley and Gleich, 1984; Manley *et al.*, 1985) maintain that these intervals are on average 15% longer than the CF-period. In these papers Manley estimated the preferred interval as the weighted average of the intervals of the second and higher maxima of the interval histogram, whereas Temchin(1988) calculated it from the number of minima in a specified time frame of the autocorrelation histogram.

The aim of the present work was to elucidate underlying mechanisms by using a more appropriate means of quantifying the temporal structure of spontaneous activity. This was achieved firstly with the aid of the Fourier transform of the histogram of successive intervals of single-unit activity, yielding the preferred frequency (the reciprocal of the preferred interval), the amount of "phase-locking" to the preferred frequency, and the harmonic content. Secondly, the interval histograms were statistically fitted with the interval probability density function (pdf) derived from a random walk model of the spike generator.

Methods

Single-unit activity was recorded from the spiral ganglion of the ketamine-xylazine (60 & 12 mg kg^{-1}) anaesthetized pigeon, in a sound attenuating chamber, using aluminosilicate glass micropipettes (Clark, SM100F-10) filled with 3M KCl. Data are from cochleae in good physiological condition, as judged by compound action potential frequency tuning curves. The appropriate methods are described extensively in Gummer *et al.* (1987). The single-unit characteristic frequency (CF) and CF-threshold were estimated from rastre plots of the response area (159-15000 Hz), with frequency- and SPL-steps of 1/16-1/8 oct, and 3-5 dB, respectively.

Theory

Fitting of the interval histograms with the interval pdf of a truncated, *homogeneous* Poisson process (Snyder, 1975), or in the case of detectable preferred intervals, a *nonhomogeneous* Poisson process, demonstrated a larger number of short intervals than expected from the estimated rate constant describing the asymptotic, exponential decay of the histogram. An explanation was sought in terms of a simplified version of the noisy integrate and fire model of Stein (1965). The Stein model postulates the existence of both excitatory and inhibitory postsynaptic potentials (epsp and ipsp), with Poisson distributed arrival times; the psps decay exponentially with time constant, τ, towards the resting membrane potential, summate linearly and produce a neuronal spike when a threshold potential is reached. Stein showed that the presence of τ allowed the threshold to be reached even when ipsps dominated. In such cases the interval pdf exhibits a sharp peak, after the absolute refractory period, "followed initially by a period of faster than exponential decay which gradually beca(o)mes more and more exponential at long times" (Stein, 1965).

Ipsps have been recorded intracellularly from hair cells in lateral line canal organs in response to efferent stimulation (Flock and Russell, 1976). In the present analysis, however, they are associated with hyperpolarization of the afferent dendrite, possibly by extracellular currents derived from excitation of neighbouring hair cells, as proposed by Hill *et al.* (1989) in the case of sound evoked neural activity.

A general closed form solution of Stein's random walk problem does not exist, and, as such, numerous approximation strategies have evolved. They may be divided in two categories, one where simplified random walk problems are solved (e.g. Wilbur and Rinzel, 1982), and the other where a random walk is approximated by a diffusion process (e.g. Johannesma, 1969). The latter approximation requires that the mean rates of incoming epsps and ipsps be "large" compared with the mean spike rate, and that their mean amplitudes be "small" compared with the difference between the threshold and resting potentials (Cox and Miller, 1968). The latter requirement is not satisfied by most neurones in the mammalian and avian auditory periphery, where the steep onset of the interval histogram implies that each epsp is capable of eliciting a spike. The other modelling approach usually results in series expansions for the interval pdf which are too cumbersome for our purposes. Since the complications primarily arise in the presence of the decay time constant, τ, the approach adopted here is to design a simplified Stein model with a closed form solution in the absence

of τ, which can be used to fit the experimental interval histogram data. It turns out that the proposed model produces a better fit, in the least mean square (lms) sense, than the still simpler one without inhibition. Beginning with these lms estimates, a simulation with τ included can be performed, and the resulting interval histogram statistically compared with the experimental histogram. With slight adjustment of the lms estimates (0-20%), and the appropriate choice of τ, the experimental and simulated interval histograms can be "well matched".

The original Stein model is simplified by assuming: i) the epsps and ipsps are pulses of equal and opposite strength; ii) both the potential, a, to which the membrane potential is reset after a constant absolute refractory period, t_o, following the preceding spike, and the threshold potential, $c>a$, are integer multiples of the psps, having normalized strength of unity; iii) all integer values of the membrane potential, v, up to $v=c$, are allowed. Stein (1965) gives an expression for the mean interval under similar restrictions, but where only nonnegative integers of v are implicitly assumed, his expression originating from a well-known result for a simple single-server queue with Poisson distributed arrivals and departures of constant rates (Bailey, 1964). The pdf of successive intervals under restrictions (i) - (iii) has not been found by the author in the literature, for neither time invariant nor time variant input rates. Space restrictions require that the result be only stated, with only a few of the steps outlined. However, the derivation does use familiar techniques for the statement and solution of the difference equations describing queuing processes (Bailey, 1964), so that the outline should be sufficient for the interested reader to confirm the result.

Let $\lambda(u)$ and $\mu(u)$ denote the instantaneous rates of the epsps and ipsps, respectively, and $F_v(u)$ denote the *conditional* probability of the membrane voltage being at level v at time u, given the reset potential, a, at time $u_{n-1}+t_o$, where u_{n-1} is the (n-1)-st spike time. Then F_v is defined by the forward set of Kolmogorov difference equations:

$$\frac{dF_v}{du} = \lambda F_{v-1} - (\mu + \lambda)F_v + \mu F_{v+1} \qquad v \le c-2 \tag{1a}$$

$$\frac{dF_{c-1}}{du} = \lambda F_{c-2} - (\mu + \lambda)F_{c-1} \tag{1b}$$

$$\frac{dF_c}{du} = \lambda F_{c-1} \tag{1c}$$

subject to the initial condition: $F_a(u_{n-1}+t_o)=1$. Since the function F_c appearing in Eq.(1c) is the conditional probability of the membrane potential being equal to the threshold value c, the function $F_c(u_n)$ represents the conditional probability of the n-th spike interval being $t=u_n-u_{n-1}$, given the reset potential, a, at time $u_{n-1}+t_o$. The corresponding conditional pdf, denoted by $f_c(u_n)$, is simply the derivative of $F_c(u_n)$.

In order to find a closed form expression for F_c it is assumed that the rates $\lambda(u)$ and $\mu(u)$ are proportional functions of time; that is, the rates differ only with respect to their mean values, λ_o and μ_o. This assumption is consistent with the extracellular current hypothesis for the generation of ipsps, provided the current is derived predominantly from excitation of hair cells in close proximity to the hair cell innervated by the afferent dendrite. With this simplification and after transforming the time variable by integration of $\lambda(u)$, or $\mu(u)$, from $u_{n-1}+t_o$ to u, the set of equations (1) transform to a set of temporally homogeneous equations, which are readily solved for the transformed F_c by the standard method of probability-generating functions. By extension of the results for simple queuing processes (Bailey, 1964), a stable solution for F_c exists when and only when $\lambda_o > \mu_o$. The solution is then transformed back to the original time coordinate in the usual manner, where it is required that the instantaneous rates be positive and nonzero in order that F_c be single-valued.

The pdf $f_c(u_{n-1}+t)$ is conditional on the deterministic reset potential, a, at time $u_{n-1}+t_o$, and therefore, conditional on a spike having been generated in the incremental time interval $[u_{n-1}, u_{n-1}+\Delta t)$, the probability of which is equal to $\lambda(u_{n-1})\Delta u_{n-1}$, the probability of an epsp arriving in this interval. (An ipsp can not elicit a spike when the time constant τ is infinite). Therefore, the (unconditional) pdf of successive intervals, denoted by p(t), is found by integrating the product $f_c(u_{n-1}+t).\lambda(u_{n-1})$ over all u_{n-1}, and dividing by λ_o to ensure that p(t) is a true pdf with unit area (Johnson, 1974). The evaluation of the integral is simplified if $\lambda(u)$ can be written as a Fourier series with fundamental frequency f_1:

$$\lambda(u) = \lambda_o \left[1 + 2\sum_{k=1}^{\infty} S_k \sin(2\pi f_k u + \phi_k)\right] \qquad (2)$$

in which all components satisfy the high-frequency condition:

$$\frac{2S_k\lambda_o}{\pi f_k} << 1 \qquad (3)$$

where S_k and ϕ_k are, respectively, the synchronization index and phase of the k-th harmonic component. Then p(t) is given by

$$p(t) = p_o(t-t_o)\left[1 + 2\sum_{k=1}^{\infty} S_k^2 \cos(2\pi f_k t)\right] \qquad (4)$$

where $p_o(t-t_o)$ is the interval pdf when the psps arrive at time invariant rates:

$$p_o(t-t_o) = \frac{2\lambda_o(\lambda_o/\mu_o)^{(\eta-1)/2}\, \eta\, I_\eta[2(\lambda_o\mu_o)^{1/2}(t-t_o)] \exp[-(\lambda_o+\mu_o)(t-t_o)]}{2(\lambda_o\mu_o)^{1/2}(t-t_o)} \qquad (5)$$

where $t>t_o$, $\eta = c-a$, and $I_\eta[]$ is the η-th order modified Bessel function of the first kind (Abramowitz and Stegun, 1965).

The result of Eq.(4) is well known in the absence of ipsps ($\mu_0 = 0$) and where only one epsp is required to reach threshold ($\eta = 1$); then, under the high-frequency condition (3), p(t) is the pdf of successive intervals of a truncated, nonhomogeneous Poisson process (Johnson, 1974; Bi et al., 1988). When $\mu_0 = 0$, but $\eta > 1$, p(t) becomes a truncated, nonhomogeneous gamma process of order η.

From the time multiplication property of Fourier transforms it is clear that the Fourier spectrum P(f) of p(t) consists of the Fourier spectrum $P_0(f)$ of $p_0(t-t_0)$, together with $P_0(f)$ centred at harmonics of $\pm f_1$, but attenuated by S_k^2 (Johnson, 1974), and phase shifted by $\pm 2\pi f_k t_0$. Then under the high-frequency condition (3), the preferred frequency (PF) of the spontaneous activity may be estimated as the frequency of the largest peak, excluding the one centred at zero frequency, of the amplitude spectrum of successive intervals. The estimate of the synchronization index, S_1, is the square root of the PF-spectral amplitude. Clearly, these estimates do not require *a priori* knowledge of $p_0(t-t_0)$. However, the parameter values t_0, λ_0, μ_0 and η were readily estimated by nonlinear, lms fitting (Wolberg, 1967) of the experimental interval histograms with the function p(t) of Eq.(4), with either fixed or variable S_k and f_k, derived initially from the Fourier spectrum. The pdf $p_0(t-t_0)$ has mode located at t_0 only when $\eta = 1$. Furthermore, the onset of the experimental histograms after this dead time, t_0, was usually steep, so that η was fixed at unity in these cases.

Results and Discussion

Examples of the histograms of successive intervals of spontaneous activity are shown in Fig.1 for four neurones with similar CF and CF-thresholds, arranged in descending order of synchronization indices. Neurones in (a-c) exhibited quasiperiodic discharge with PF approximately equal to CF. Periodicity was not detected for the neurone in d. The noise floor for the synchronization index was 0.15-0.2, with total number of intervals, N = 8279.

The synchronization index S_1 at the PF tended to increase with decreasing PF, as shown in Fig.2. Of the 105 auditory neurones characterized (in 10 pigeons), 49 exhibited quasiperiodicity, independent of CF-threshold. Eight of these neurones exhibited a significant second harmonic component (not illustrated), accountable in half the cases by the exponential nonlinearity often associated with the spike generator (Johnson, 1974; Siebert, 1970).

The PF was equal to either CF or CF/2, as indicated in Fig.3 by the regression lines of slope 1 and 0.5, respectively. Before fitting, the data were divided in two groups according to the rule PF/CF > -0.5 oct, and PF/CF ≤ -0.5 oct. If the data were presented as one population then one would conclude that the preferred interval was 19% longer than the CF-period, consistent with observations in the starling (Manley and Gleich, 1984; Manley *et al.*, 1985). However, when presented as in Fig.3, the data suggest that spontaneous activity is generated by noise passing through a filter tuned to CF; in most cases (70%) the discharge was synchronized to CF, but in others the neurone fired to every second cycle of the filtered signal.

Although the asymptotic decay of the interval histograms was exponential, there were more short intervals than expected of a truncated, Poisson process, whether

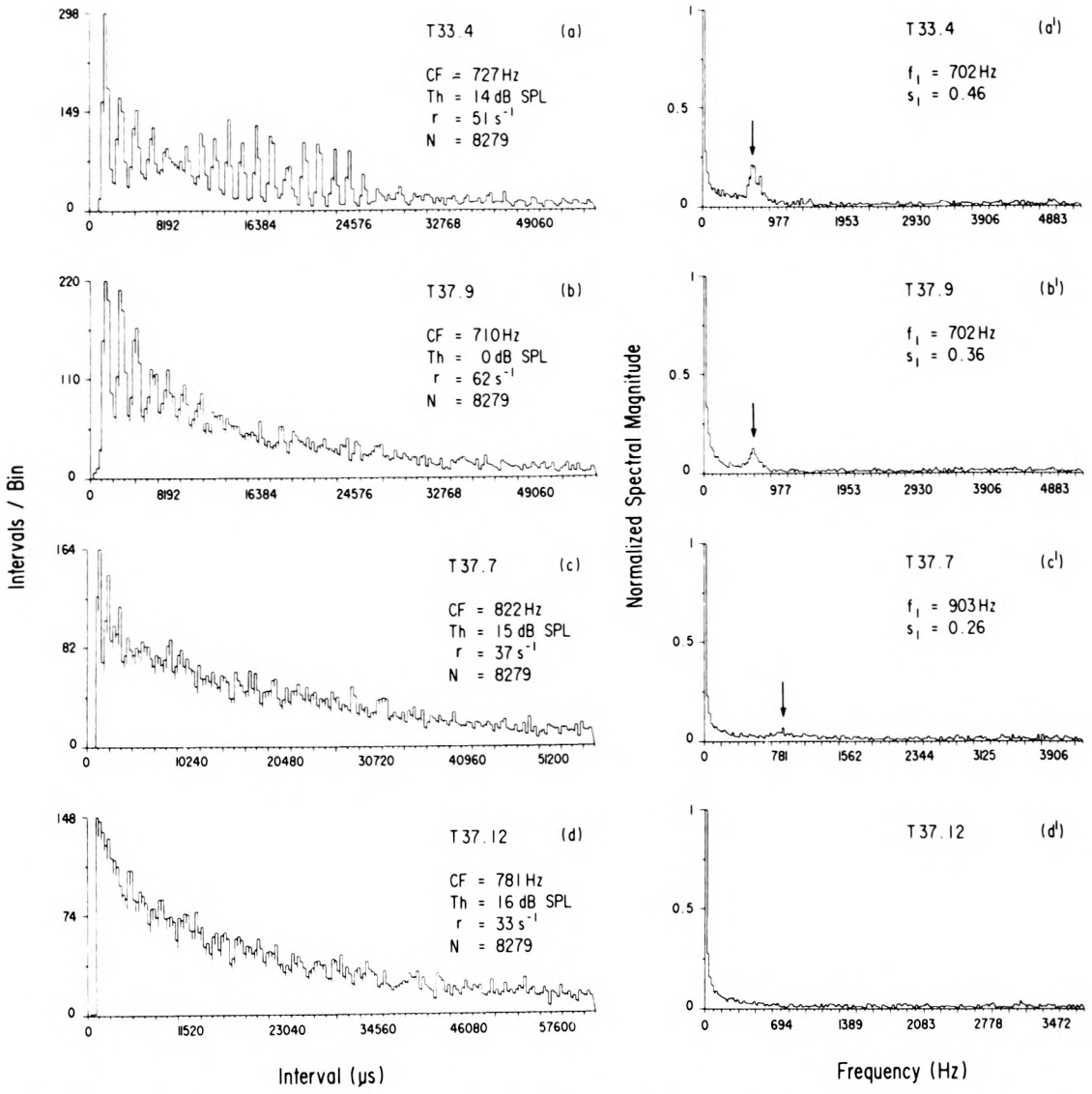

FIGURE 1 Histograms of successive intervals (a-d), and their Fourier amplitude spectra (a'-d'), of spontaneous activity recorded from four neurones with similar characteristic frequency (CF) and CF-threshold (Th). r: mean firing rate; N: total number of intervals; f_1: preferred frequency (arrow); S_1: synchronization index at f_1.

homogeneous or nonhomogeneous. The same phenomenon is evident in the published data of Manley and Temchin. In the example depicted in Fig.4 there are 40% more modal intervals than expected which, according to the purely excitatory model, could not have been generated by a small amplitude oscillation of the instantaneous epsp rate: a synchronization index of 0.45 (Eq.2) would have been required to produce the 40% excess, which, for the number of intervals recorded, is at least 6 dB greater than the detection threshold of synchronization index achieved by the Fourier spectral method. This conclusion presumes that the high-frequency condition (3) is satisfied; for a mean firing rate of 33 s^{-1}, a frequency of the order 20 Hz would have been required to violate the condition, which is not only much less than the CF of 781 Hz, but should be detected in the interval histogram as a low-frequency oscillation, of the kind observed for the neurone in Fig.1a. The excitation-inhibition model (Theory) was developed to account for the short-interval excess.

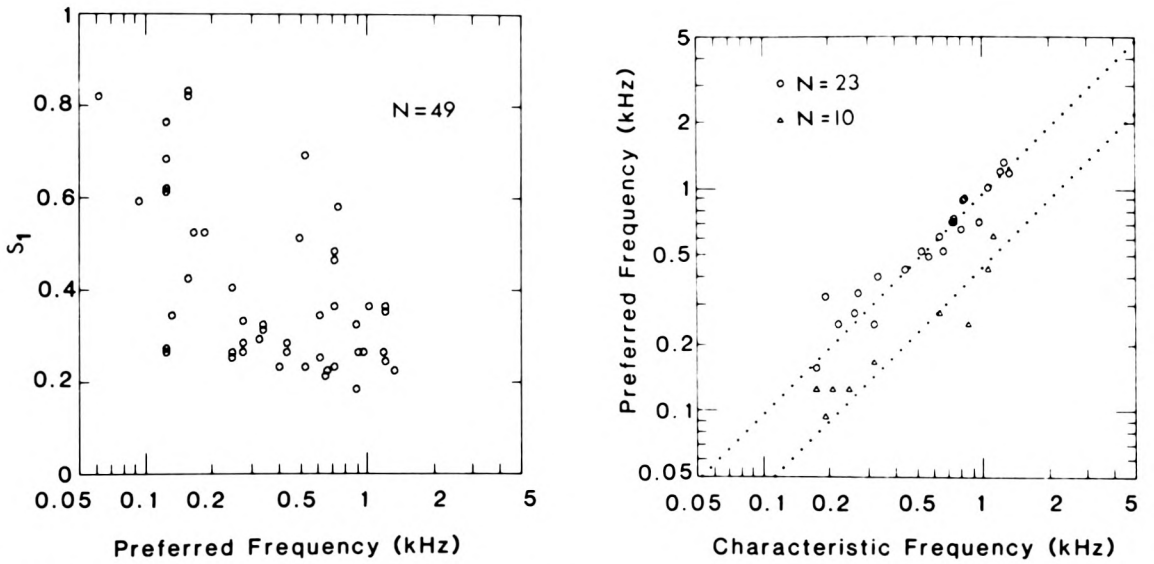

FIGURE 2 Synchronization index, S_1, of the first harmonic component versus preferred frequency of spontaneous discharge.

FIGURE 3 Preferred frequency of spontaneous discharge versus characteristic frequency of tone-pip evoked activity, divided in two groups according to the rule: PF/CF > -0.5 oct (N=23), and PF/CF ≤ -0.5 oct (N=10). Dotted lines: regression lines with slopes of 0.96±0.02 (N=23), and 0.45±0.03 (N=10), which are not statistically different (t-test at 95% level) to 1 or 0.5, respectively.

The unlabelled curve in Fig.4 is a lms fit to the interval histogram, using the homogeneous interval pdf of Eq(5). The estimated ratio of ipsp-rate to epsp-rate, μ_o/λ_o, is 0.33±0.04, yielding a root mean square error half that for the fit with the classical excitation model. Although improved, the model still underestimates the

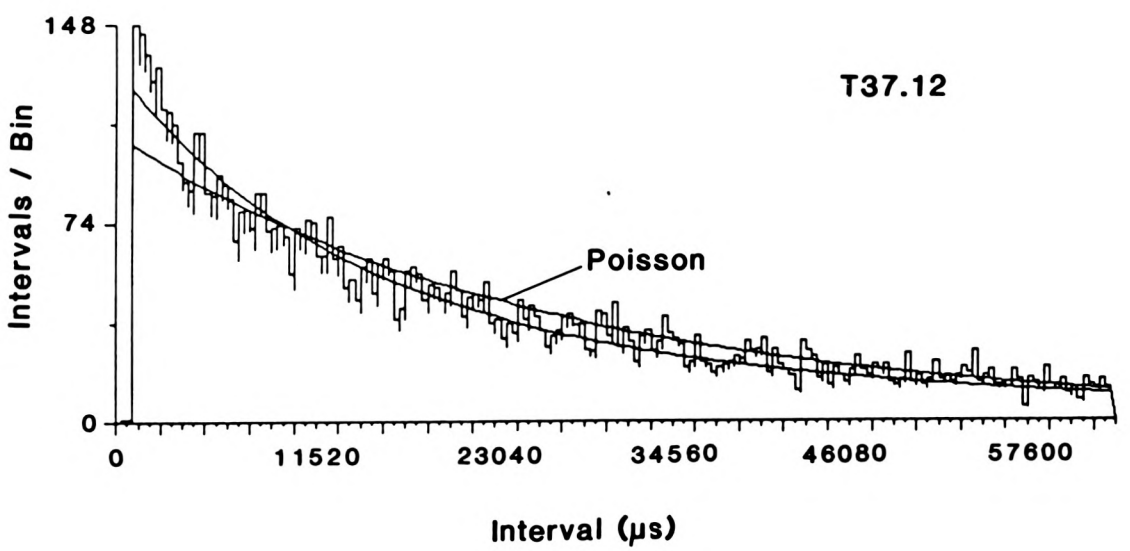

FIGURE 4 Comparison of the interval histogram of spontaneous discharge of neurone T37.12 (see Fig.1d) with the theoretical curves of the classical excitation model (labelled Poisson) and of the excitation-inhibition model (not labelled), with lms estimates: $\lambda_o = 41.8 \pm 0.7\ s^{-1}$, $\mu_o/\lambda_o = 0.33 \pm 0.04$, and rms error=2; a statistically significant harmonic component was not found (Wolberg, 1967).

number of modal intervals (20%). Simulation showed that this discrepancy is removed when an appropriate time constant, τ, for psp decay is included ($\tau = 0.6$ ms, with μ_0/λ_0 changed from 0.33 to 0.35). Similar observations were made with interval histograms of quasiperiodic spontaneous discharge. Fifty percent of interval histograms were fitted by the excitation-inhibition model, and 40% by the classical excitation model.

Conclusion

The quasiperiodic spontaneous activity of auditory afferent neurones appeared to be generated by noise passing through a filter tuned to the CF of the neurone. A random walk model of spike generation, possessing both epsps and ipsps at the afferent dendrite, statistically described the histogram of successive intervals.

References

Abramowitz, M. and Stegun, I.A. (1965) Handbook of Mathematical Functions. Dover, New York.

Bailey, N.T.J. (1967) The elements of Stochastic Processes. J. Wiley, New York.

Bi, Q., Brown, J.L. Jr. and Lachs, G. (1988) Statistical expectation of the interval histograms from marginal time statistics of the Poisson process. J. Acoust. Soc. Am. 83, 1186-1189.

Cox, D.R. and Miller, H.D. (1968) The Theory of Stochastic Processes. Methuen, London.

Crawford, A.C. and Fettiplace, R. (1980) The frequency selectivity of auditory nerve fibres and hair cells in the cochlea of the turtle. J. Physiol. 306, 79-125.

Eatock, R.A., Manley, G.A. and Pawson, L. (1981) Auditory nerve fibre activity in the Tokay Gecko. I. Implications for cochlear processing. J. Comp. Physiol. 142, 203-218.

Flock, A and Russell, I. (1976) Inhibition by efferent nerve fibres: Action on hair cells and afferent synaptic transmission in the lateral line canal organ of the burbot *Lota lota*. J. Physiol. 257, 45-62.

Gummer, A.W., Smolders, J.W.T. and Klinke, R. (1987) Basilar membrane motion in the pigeon measured with the Moessbauer technique. Hear. Res. 29, 63-92.

Hill, K.G., Stange, G., Gummer, A.W. and Mo, J. (1989) A model proposing synaptic and extra-synaptic influences on the responses of cochlear nerve fibres. Hear. Res. 39, 75-90.

Johannesma, P.I.M. (1969) Diffusion models for the stochastic activity of neurons. In: Neural Networks (Ed: Caianiello, E.R.) Springer-Verlag, Berlin, Heidelberg, New York, pp. 116-144.

Johnson, D.H. (1974) The Response of Single Auditory-Nerve Fibers in the Cat to Single Tones: Synchrony and Average Discharge Rate. Ph.D. thesis, Massachusetts Institute of Technology, Cambridge, Massachusetts.

Kiang, N.Y.-S. (1965) Discharge Patterns of single fibers in the cat's auditory nerve. M.I.T. Press, Cambridge, Massachusetts.

Manley, G.A. (1979) Preferred intervals in the spontaneous activity of primary auditory neurons. Naturwissen. 66, 582-584.

Manley, G.A. and Gleich, O. (1984) Avian primary auditory neurons. Naturwissen. 71, 592-594.

Manley, G.A., Gleich, O., Leppelsack, H.-J. and Oeckinghaus, H. (1985) Activity patterns of cochlear ganglion neurones in the starling. J. Comp. Physiol. A 157, 161-181.

Robertson, D. and Manley, G.A. (1974) Manipulation of frequency analysis in the cochlear ganglion of the guinea pig. J. Comp. Physiol. 91, 363-375.

Siebert, W.M. (1970) Frequency discrimination in the auditory system: place or periodicity mechanisms? Proc. IEEE 58, 723-730.

Stein, R.B. (1965) A theoretical analysis of neuronal variability. Biophys. J. 5, 173-194.

Synder, D.L. (1975). Random Point Processes. J. Wiley, New York.

Temchin, A.N. (1988) Unusual discharge patterns of single fibers in the pigeon's auditory nerve. J. Comp. Physiol. A 163, 99-115.

Walsh, B.T., Miller, J.B., Gacek, R.R. and Kiang, N.Y.-S. (1972) Spontaneous activity in the eighth cranial nerve of the cat. Intern. J. Neurosci. 3, 221-236.

Wilbur, W.J. and Rinzel, J. (1982) An analysis of Stein's model for stochastic neuronal excitation. Biol. Cybern. 45, 107-114.

Wolberg, J.R. (1967) Prediction Analysis. D. van Nostrand, New Jersey.

Comments and discussion

MANLEY

Gummer implies that in the papers of Manley and Gleich (1984) and Manley, et al. (1985), only when "presented as one population," was the "preferred interval" significantly longer than the CF period. In fact, the value of 15-20% longer intervals than the CF period as given in those papers refers not to an average of pooled data. A perusal of Fig. 1c and d of Manley and Gleich (1984) and 11d and e of Manley, et al. (1985) shows clearly that the value of 15-20% refers to the "peak of the distribution" or mode of the frequency histograms of a) the product of the mode of the interval histograms and the CF of the cell and b) the product of the "basic interval" of the interval histogram (as defined in those papers) and the CF. Had we really presented the data of a) as "one population," then the average would be 1.6 (60% longer than the CF period) and not 15-20% longer. Thus there appears to be a real discrepancy between the pigeon and the starling data.

It is important to note that in an analysis of the residual phase derived from near-threshold phase roll-off measurements for starling primary fibers, Gleich (1988) demonstrated that the "CF" derived from the phase data was also about 15% lower than the acoustic CF.

GUMMER

The question refers to three parameters which must be addressed separately: i) the preferred (or basic) interval of the interval histogram (IH) of spontaneous activity (SA); ii) the modal interval of the IH of SA; iii) the *CF* as derived from phase data of sound evoked activity.

i) In the two papers referred to by Manley (Manley and Gleich, 1984; Manley *et al.*, 1985) it is categorically stated that: "The spacing of the peak intervals was, on average, 15% greater than the CF-period interval of the respective units (Fig. 11)." (Manley *et al.*, 1985). This is also substantiated by Fig. 1d in Manley and Gleich (1984) and by Fig. 11e in Manley *et al.* (1985), where it is clear that the average is from one population. (Although "mode" was probably meant by "average", it is irrelevant for this parameter because the data appear to be approximately normally distributed). I would have arrived at a similar conclusion (but replacing 15% by 19%) were I to have considered a single population. However, by partitioning the data (Fig. 3), it becomes clear that preferred intervals of SA are generated by noise passing through a filter tuned to CF.

ii) A similar statement was made by Manley for the modal interval as for the preferred interval: "In TIH [*time-interval histogram*] of lower-frequency cells without preferred intervals, the modal interval was also on average about 15% longer than the CF-period interval (Fig. 11)." (Manley *et al.*, 1985). As Manley emphasized, there is greater scatter in the histogram of the product of the CF and the mode of the IH (his Fig. 11d), partly because units with long modes from a "shoulder"-type of IH were included. However, it is clear that Manley's so-called "average" value of 15% is actually the "mode" of the population, thus excluding this type of "shoulder" IH. It should also be stressed, as it was by Manley, that modal intervals from units which did not exhibit a detectable preferred interval were included in his population. Again, I would also arrive at a similar conclusion were the modal-interval data not partitioned

as described in the text for the preferred-interval data. The modal interval is, of course, dependent on the relationship between the absolute refractory period, t_o, and the CF; one can show both experimentally and theoretically that: the modal interval is a multiple of 1/CF, where for positive non-zero t_o, the appropriate multiple, n, is determined by t_o according to the rule:

$$n = 1 + \text{int}(CF.t_o)$$

where int() denotes the integer-value function.

iii) Without measurement of cochlear microphonics or columella-footplate motion it is not possible to reliably derive the residual phase from near-threshold measurements of the preferred firing phase of period histograms. Perhaps the best that one can do, at present, is to refer to the dependence of preferred phase on SPL reported by Narins and Gleich (1986) for the starling. There it is shown that there exists a "crossover-frequency" at which the phase response is independent of intensity; this frequency occurred consistently *above* CF for cells with CF's above 0.3 kHz. This is consistent, after some teleological argument, with classical linear filter theory where the natural frequency, which should be derived from the phase response, is above the frequency of maximum amplitude response (the CF). It is, however, inconsistent with that derived from the near-threshold measurements by Gleich (1988). How all this relates to the temporal properties of spontaneous activity is yet to be carefully investigated.

In conclusion, there is no discrepancy between the pigeon and starling data. Any apparent discrepancy is one of interpretation of similar data: by appropriate analysis the present paper has shown that the spontaneous activity of avian auditory afferent neurones is generated by noise passing through a filter tuned to the CF of the neurone.

References

Gleich, O. (1988). Doctoral Thesis, Department of Zoology, Technical University, Munich.

Narins, P.M., Gleich, O. (1986). Phase response of low-frequency cochlear ganglion cells in the starling. In: Auditory Frequency Selectivity (Ed: Moore, B.C.J., and Patterson, R.D.) Plenum Pub. Co., pp. 209-216.

TWO-TONE RATE SUPPRESSION IN AUDITORY NERVE FIBRES: TIME COURSE OF SUPPRESSION AND EXCITATION IN PERI-STIMULUS TIME HISTOGRAMS.

K.G. Hill[1] and A.R. Palmer[2].

[1]*Research School of Biological Sciences, Australian National University, Canberra ACT 2601, Australia.*

[2]*MRC Institute of Hearing Research, University of Nottingham, Nottingham NG7 2RD, England.*

Introduction

An explanation for two tone rate suppression of responses in cochlear nerve fibres is central to understanding the cochlear mechanisms that determine sensory coding in the ear. Recently, it has been proposed that the origin of the suppression lies in the fundamental concept of cochlear gain, i.e. active electro-mechanical feedback to the displacement response of the basilar membrane (BM), which determines the level of synaptic drive from inner hair cells (IHCs) to afferent nerve fibres (Geisler et al., 1990). In this "saturation feedback model", the amplitude of the electrical response of outer hair cells (OHCs) determines the amount of high gain feedback, which is applied to a restricted longitudinal extent of the BM. This conception conforms with a saturating nonlinearity (receptor current of OHCs) and narrow band pass- filtered feedback. In response to appropriate stimuli, the saturating non-linearity provides suppression of individual frequency components (interference - Engebretson and Eldridge, 1968) and a relative attenuation of the displacement response at that BM location, specific to the attenuated frequency component. In this paper, we consider the time course of suppression and excitation of neural rate driven by characteristic frequency (CF), that results from the superposition of a test tone (suppressor) on a continuous probe tone at CF. The data suggest that factors other than suppressive effects at the IHC are involved in rate suppression.

Methods

Rate responses were measured in single cochlear nerve fibres in the anaesthetized guinea pig. Stimuli consisted of single tone bursts and continuous tones at fibre characteristic frequency (CF), on which a gated test tone (suppressor) was superimposed. Gated tones were of 50 ms overall duration with 5 ms rise and fall times, repeated at approximately 5 Hz. Spike times relative to the cycle trigger were pooled into 1 ms bins for construction of peristimulus time histograms (PSTH). Each histogram was produced from 256 tone presentations

Results

For test tones set about one octave below the CF, the two tone rate function (response rate relative to test tone level) generally is a non monotonic function, in which the CF-driven rate first is reduced (two tone rate suppression - 2TRS) and then increased (net excitation in the two tone response). At the transition between 2TRS and two tone excitation, discharge rate during the test tone matches that driven by the CF tone alone. The rate function displays a suppression threshold T, a suppression maximum M and a balance point B (Figure 1). Two tone peristimulus response time histograms obtained for test tones above the suppression threshold show maximum 2TRS to produce a period of generally flat, suppressed spike rate for the duration of the test tone. As test tone level was increased above suppression maximum, the onset of 2TRS preceded excitation by the test tone, causing an onset notch to occur in the PSTH. The shorter latency of suppression with respect to excitation by the test tone may be attributed to the ramp onset of the test tone, i.e. test tone amplitude passes through the suppressing range of level before causing excitation. Similar considerations could contribute to the offset notch also observed in two tone PSTHs above maximum suppression level. Consistent with this interpretation, the onset notch persists in strong excitation two tone responses. In addition, however, post- excitation suppression, attributable to adaptation at the hair cell-nerve fibre synapse, causes a more sustained rate depression, following termination of the test tone (Figure 2).

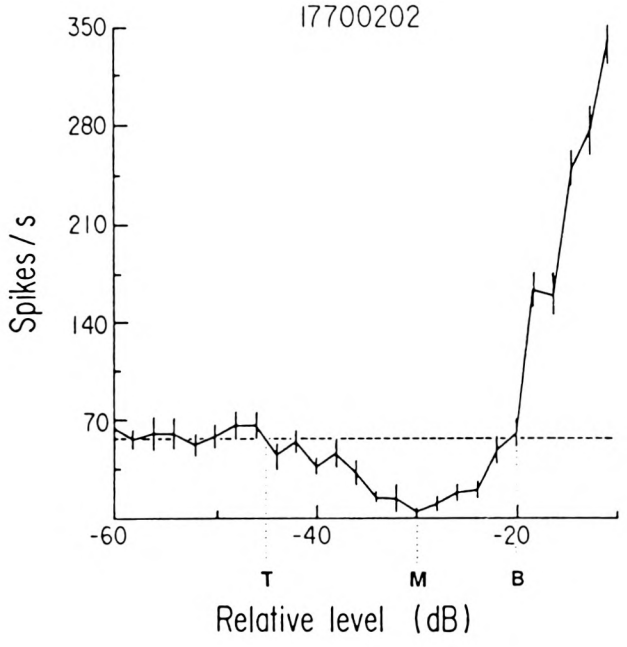

FIGURE 1 Typical, nonmonotonic two tone rate- intensity function. Spike rate during the gated suppressor tone is plotted against level of the suppressor tone, the probe tone at CF being continuous. At point T, suppressor tone reaches suppression threshold, at M suppression is at maximum, at B suppressor tone reaches the balance point.

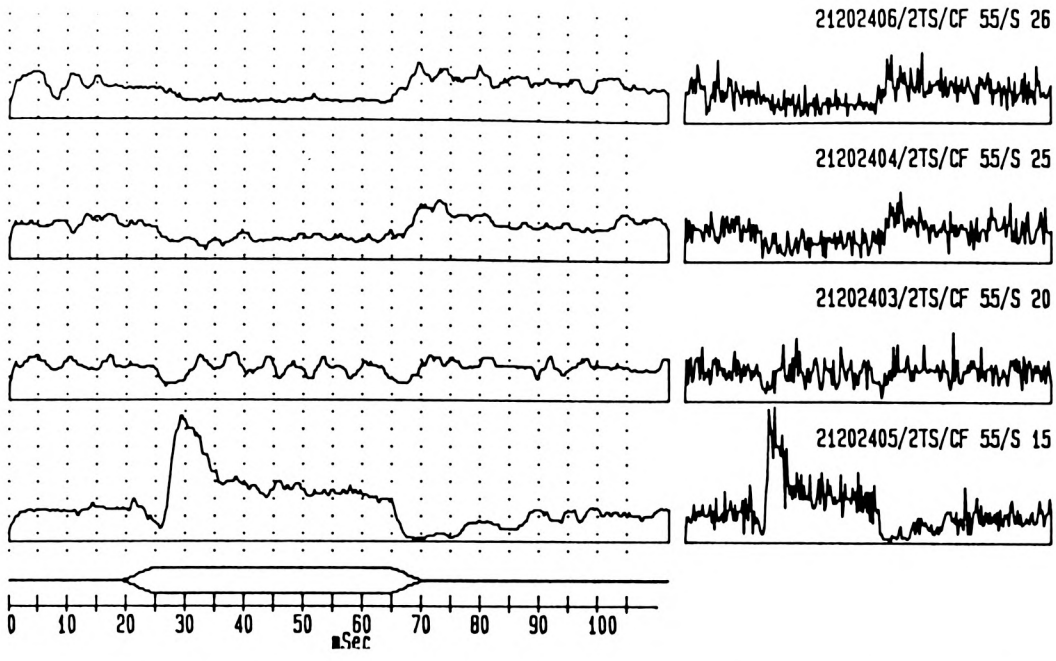

FIGURE 2 Two tone post stimulus time histograms (PSTHs) obtained from one fibre for several levels of a suppressor tone, while the probe tone was presented continuously. Right column shows raw data, left column shows expanded and smoothed PSTHs and gated suppressor (test) tone envelope with time scale. With increased level of the test tone, rate suppression intensifies then reverts to excitation. Note: overshooting rebound following maximum suppression (top and second from top); onset and offset notches (third from top); persistence of onset notch and post tone rate depression in the excitatory response (bottom).

The attribution of the onset notch in two tone PSTHs to transient 2TRS during the ramp of the test tone envelope is not the only possibility, however, for similar onset notches occasionally are observed in PSTHs for single tones. Such short latency, transient suppression in single tone responses may occur for both CF or suppressor frequency tones (Figures 3,4).

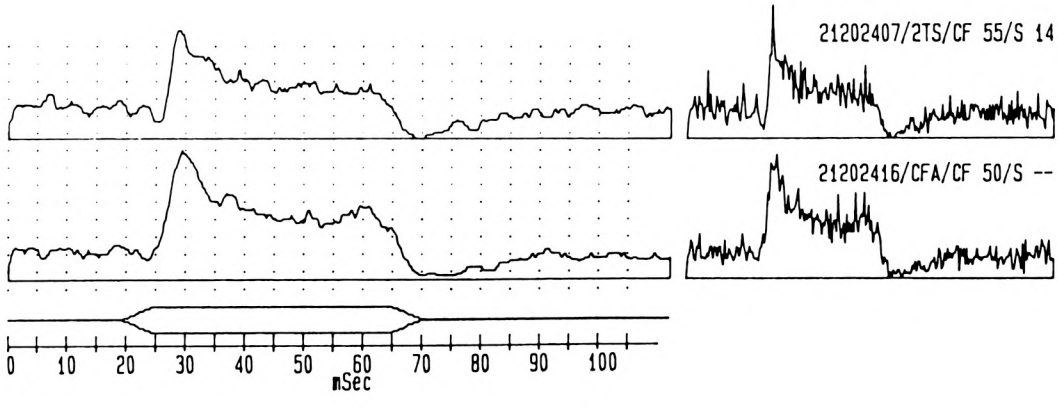

FIGURE 3 PSTHs for one fibre for two tone (top) and CF tone alone (bottom). A prominent onset notch occurs in the two tone response, a less-pronounced onset notch occurs in the single tone response.

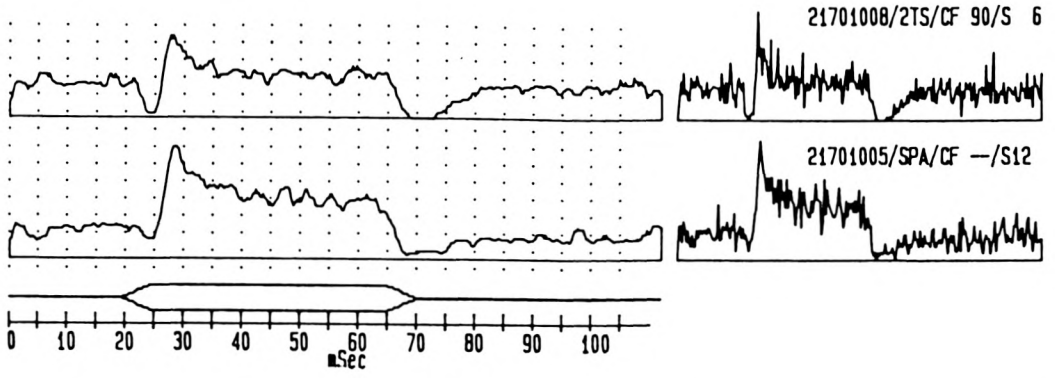

FIGURE 4 As for Figure 3 - Comparison is between two tone response and response to test tone alone.

As the level of the test tone is raised above threshold, its excitatory effect reverses the trend of 2TRS. In the paradigm we have used, the continuous probe tone adapts the hair cell- nerve fibre synapse, so that rate increase in response to the test tone, when superimposed on the probe, is slower than when the test tone is presented alone (Figure 5).

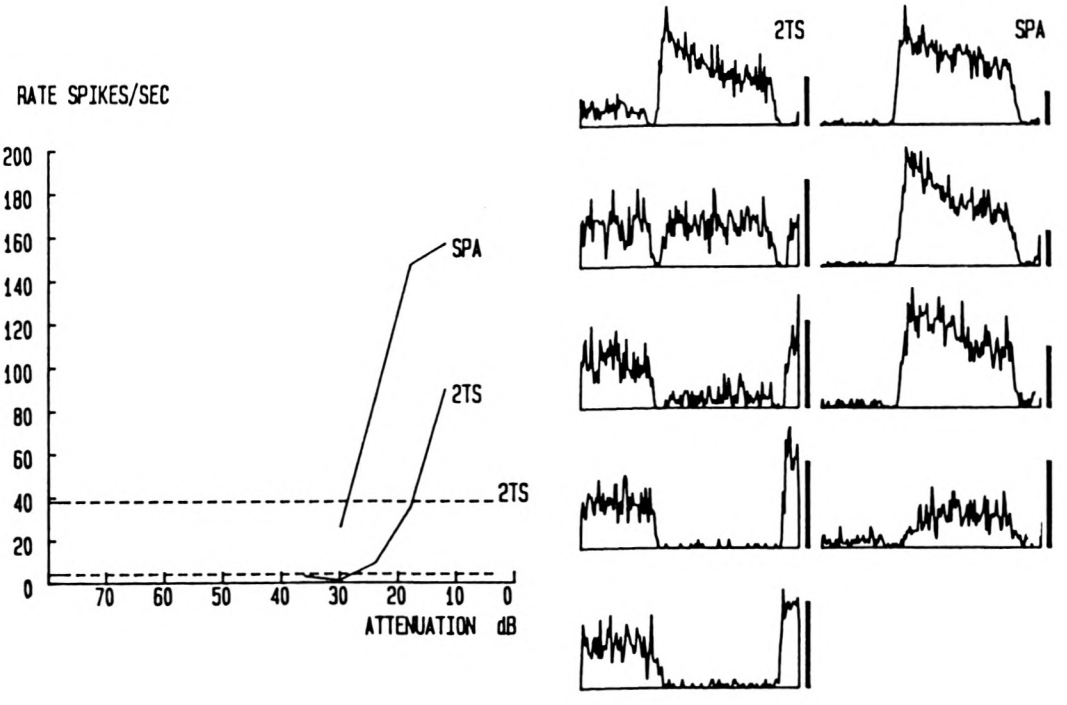

Figure 5. Rate functions (left) and PSTHs (right) for response to two tone and suppressor tone alone stimuli. In rate functions, dashed lines show spontaneous rate (lower) and probe driven rate (upper). In PSTHs, test tone level is the same for two tone and suppressor alone stimuli in each row and increases towards top in steps of 6 dB. Vertical bars to right of each PSTH represent 20 spikes per bin.

The state of adaptation of the synapse due to depolarization of the IHC is not expected to discriminate between equal amplitude IHC potentials produced by probe or suppressor tone. If neural firing rate is presumed to reflect synaptic drive and, therefore, IHC receptor potential, then the balance point in the rate function implies equal IHC receptor potential before, during and following the test tone.

At test tone levels above the suppression maximum, for which excitation is due to the test tone itself, notches in PSTHs could be attributed to transient 2TRS occurring during the tone envelope ramps, notwithstanding such notches in responses to single tones. However, intensity dependent growth of the offset notch, in the absence of sustained 2TRS during presentation of the test tone at lower levels, is not consistent with this interpretation. The notch clearly occurs post-test tone and appears conformal with post-excitation adaptation (Figure 6). Even when clear 2TRS occurs below the balance point level, the offset notch sometimes appears extended and even deeper than maximum 2TRS (Figure 7).

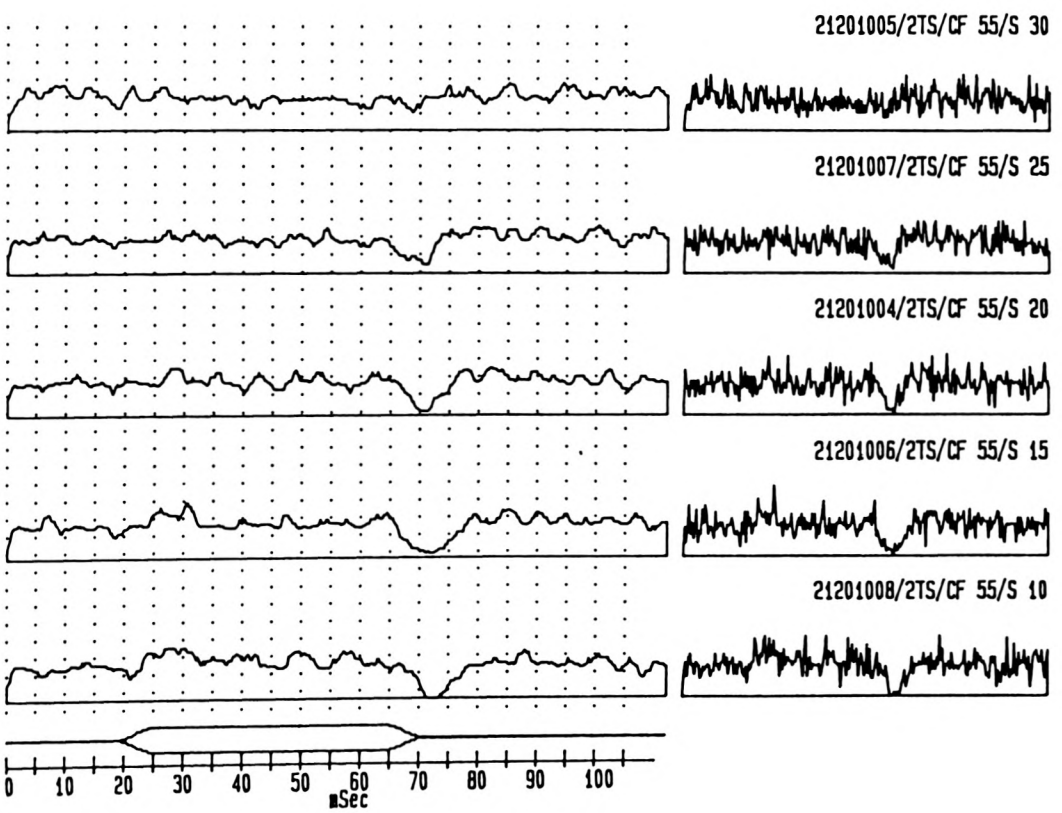

FIGURE 6 As for Figure 3. The offset notch develops with increased level of the test tone without overt 2TRS and becomes pronounced without strong excitation of rate.

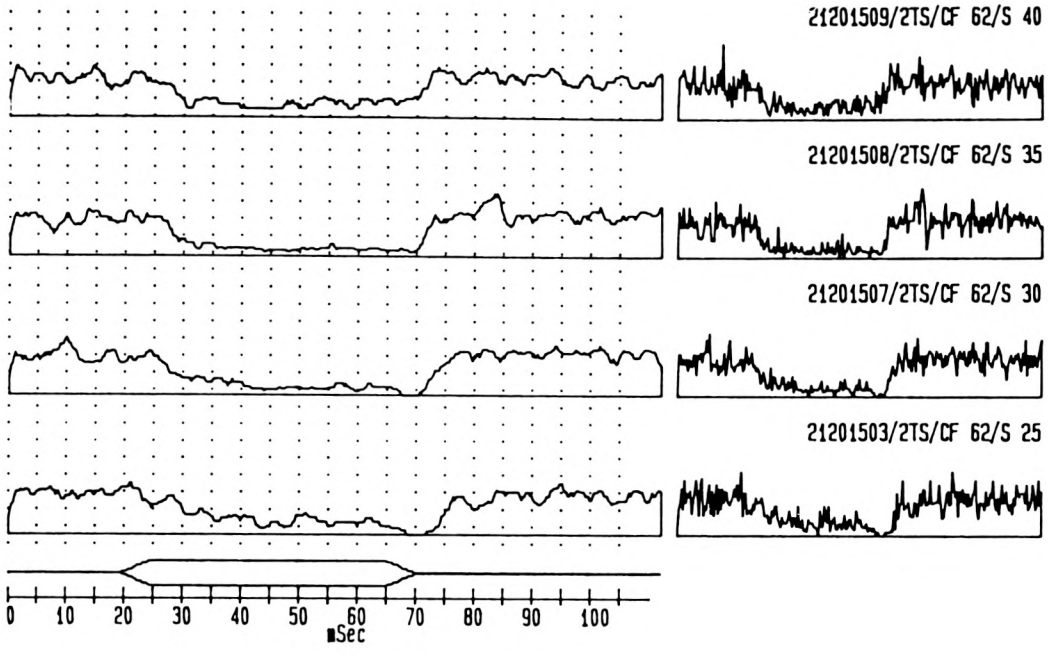

Figure 7. The offset notch develops with increased level of the test tone after the termination of the period of pronounced 2TRS; and is even deeper than maximum 2TRS.

Discussion

Conventionally, post tone depression of rate is attributed to the adaptation mechanism at the synapse and, therefore, post tone depression signals excitation of the hair cell-nerve fibre synapse. How could such indications of hair cell excitation occur, without consequent excitation of rate? If the post tone depression is the result of excitation at the hair cell- nerve fibre synapse, then during the tone, suppression of rate must have occurred in the fibre, proximal to the synapse.

Two forms of rate depression are described that are not consistent with contemporary hypotheses that suppression of IHC receptor potential is the basis of 2TRS. The short latency onset notch is not limited to conditions of transient 2TRS during envelope ramps. It also could be interpreted as a subtle response to an excitatory tone that is potentiated in the two tone situation. The post-test tone depression of rate in the two tone case, suggests that IHC excitation has occurred without consequent rate excitation.

These observations are not predicted by the hypothesis that rate suppression in nerve fibres occurs solely as a result of attenuation of mechanical stimulation of inner hair cells. A model previously has been proposed in which suppression acts directly on fibres proximal to the synapse (Hill et al., 1989), with which these observations would be consistent.

References

Engebretson, A.M. and Eldredge, D.H. (1968) Model for the nonlinear characteristics of cochlear potentials. J.A.S.A. 434(2), 548- 554.

Geisler, C.D., Yates, G.K., Patuzzi, R.B. and Johnstone, R.M. (1990) Saturation of outer hair cell receptor currents causes two tone suppression. Hearing Research 44, 241-256.

Hill, K.G., Stange, G., Gummer, A.W. and Mo, J. (1989) A model proposing synaptic and extrasynaptic influences on the responses of cochlear nerve fibres. Hearing Research 39, 75-90.

FURTHER EVIDENCE FOR TUNING MECHANISMS OF HIGH DYNAMIC ORDER IN LOWER VERTEBRATES

Edwin R. Lewis, Michael G. Sneary, Xiaolong Yu

Department of Electrical Engineering and Computer Science, University of California, Berkeley, California 94720

Introduction and Summary

In recent years, data from individual hair cells have suggested that frequency selectivity in lower vertebrates is accomplished by the amplitude tuning peaks of underdamped electrical resonances (Crawford and Fettiplace, 1981; Lewis and Hudspeth, 1983; Pitchford and Ashmore, 1987). In the present study we have used the reverse-correlation (REVCOR) method (Evans, 1989; Eggermont et al, 1983; de Boer and Kuyper, 1968; de Boer and de Jongh, 1977) to study linear tuning responses from primary afferent axons of the three inner-ear organs in which these resonances were first reported -- the turtle basilar papilla and the frog sacculus and amphibian papilla. The characteristic signature of a single (underdamped) resonance comprises the following features: (1) impulse response in the form of a sinusoid with exponentially declining amplitude, (2) sinusoidal steady-state phase shift limited to one-half cycle, (3) convexity of the gain (amplitude) tuning curve limited to the highest three decibels (where the tuning curve is plotted on the conventional log-log coordinates), and (4) absolute values of the limiting slopes of the gain tuning curve which sum to two (decades per decade). If the outputs of resonances were added (not subtracted) in parallel, producing a tuning structure of high dynamic order, the characteristic signature of that structure would comprise features (2) and (4) from the previous list, plus (5) global concavity of the gain tuning curve (convexity only within approximately 3 dB of the tuning peaks). Among 155 axons included in this study, all displayed the following properties: (1) impulse responses that are more complex than exponentially decaying sinusoids, (2) sinusoidal steady-state phase shifts ranging over one or more cycles, (3) gain tuning curves exhibiting global convexity (with occasional, local concavity) and, (4) limiting gain-tuning-curve slopes whose absolute values sum to numbers considerably greater than two. We conclude that frequency selectivity in these axons is not accomplished by underdamped resonance peaks acting alone or in parallel combination (through positive addition), but rather by the asymptotic slopes of amplitude tuning curves, made steep by high dynamic order.

Methods

The turtle preparation was essentially the same as that of Fettiplace and Crawford (1978). Two frog preparations were used, one involving a ventral approach to the eighth nerve with the frog mounted upside down (adapted from Capranica and Moffat, 1975), and one involving a dorsal approach with the frog rightside up (adapted from Frishkopf and Goldstein, 1963). Frogs were anesthetized with a combination of Ketamine and Nembutal. Individual axons were penetrated with glass micropipettes and identified by their responses to stimulus bursts. Each animal preparation was placed within an acoustic isolation chamber in which ambient sound and seismic signals were attenuated to levels at least 20 dB below the lowest stimuli used in our experiments.

Seismic stimuli for saccular axons were generated by an electromagnetic driver attached to a thick platform on which the animal rested. Auditory stimuli were presented through a closed-field system coupled to the tympanum. Stimulus waveforms (as monitored by a calibrated microphone or accelerometer) and nerve fiber spikes from the microelectrode were recorded on tape and also sent directly to an IBM PC AT computer equipped with a lab-built REVCOR board (with 1024-bin resolution) for on-line analysis. The stimulus was Gaussian distributed, band-limited noise (+/- 3 dB rms amplitude from 40 to 1500 Hz for turtle and bullfrog auditory units and from 5 to 1000 Hz for bullfrog saccular units) presented continuously while data was accumulated. Impulse responses were estimated directly from REVCOR analysis, and amplitude and phase tuning curves were generated by Fourier transform of those estimates. Because the noise was band-limited, each estimated impulse response was accompanied by an anticausal component that masked part of the true time delay (latency) in the response. For the 40 to 1500 Hz stimulus, the duration of this component was less than 0.5 ms; for the 5 to 1000 Hz stimulus it was less than 1.0 ms.

Results and Discussion

REVCOR analysis was performed on responses from 31 afferent axons from the turtle basilar papilla, 61 afferent axons from the bullfrog saccule and 63 afferent axons from the bullfrog amphibian papilla. The shapes of the impulse responses and tuning curves estimated from this analysis for individual axons showed no obvious variations as the stimulus noise amplitude was varied over several tens of dB. For the turtle basilar papilla and frog amphibian papilla, REVCOR derived impulse responses from low-frequency axons displayed nearly monotonically decaying envelopes, similar to those expected from second order resonances. Unlike the impulse responses of second order resonances, however, these consistently displayed a conspicuous increase in the period of the oscillation as the envelope decayed (Figs. 1A, 2A). In the higher frequency axons of both receptors, envelopes of impulse responses were conspicuously nonmonotonic, with the maximum occurring at the peak of the third or fourth half cycle of oscillation (Figs. 1B, 2B). Again the period of oscillation increased from the beginning to the end of the impulse response--- a common property of high-order band-pass filters. For the frog sacculus, the impulse responses typically were either essentially biphasic (Fig. 3A) or displayed many cycles of ringing (Fig. 3B). Once again, the period of oscillation increased from the beginning to the end of the response.

In REVCOR-derived impulse responses from the turtle basilar papilla, Crawford and

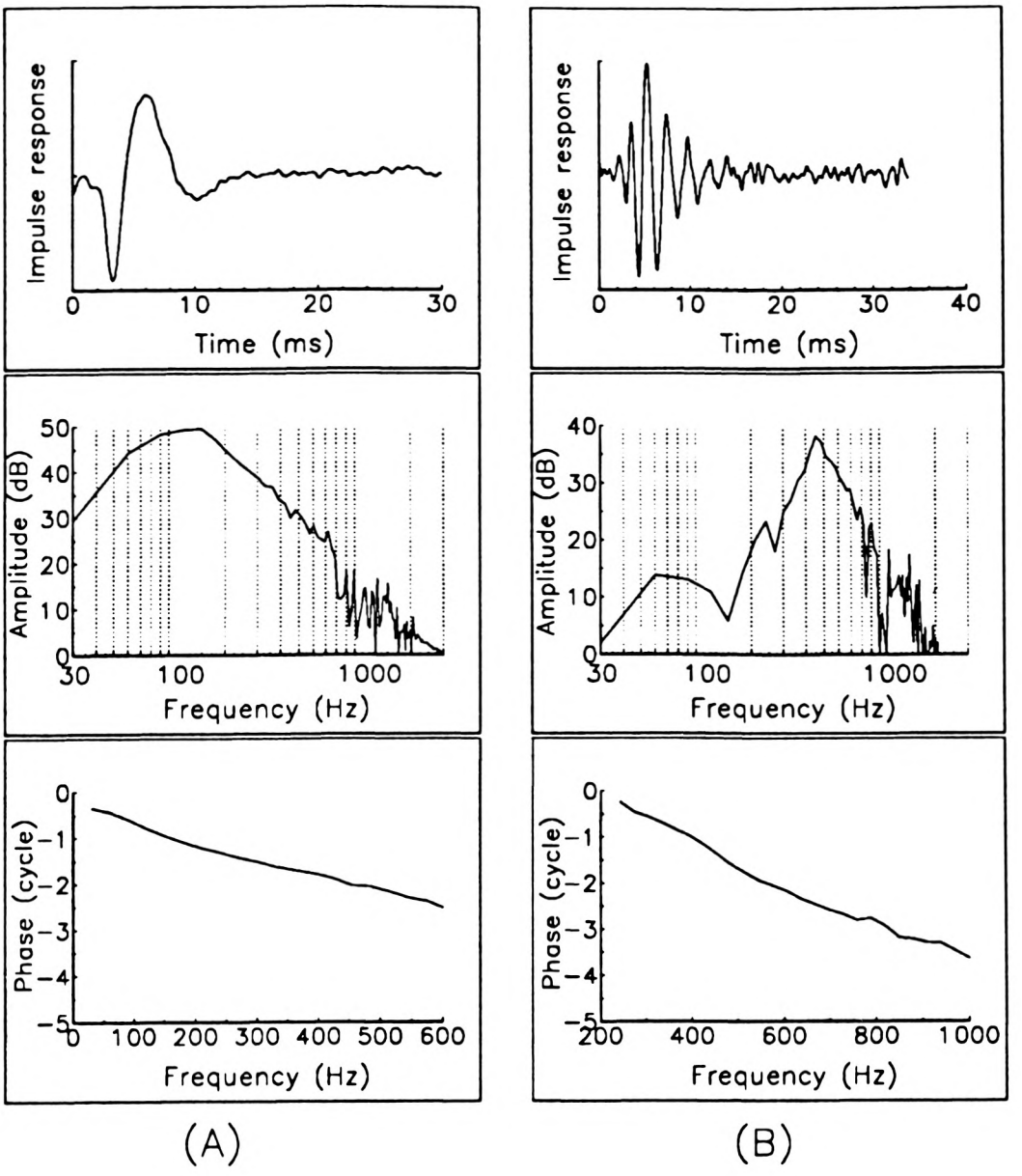

FIGURE 1 REVCOR-derived impulse responses and amplitude and phase tuning curves for two primary afferent axons of the red-eared turtle basilar papilla. In both cases the REVCOR time window was 33 ms (32.2 us per bin). (A) The stimulus noise level was 82 dB SPL (over the entire 40-1500 Hz band); REVCOR analysis was based on 9,286 spikes. (B) The stimulus noise level was 72 dB SPL; REVCOR analysis was based on 8182 spikes.

Fettiplace (1980) observed this same effect-- period increasing from beginning of impulse response to end. One might attribute this to the voltage-dependence of the resonance frequency in the hair cell's electrical resonance. Under this argument, positive

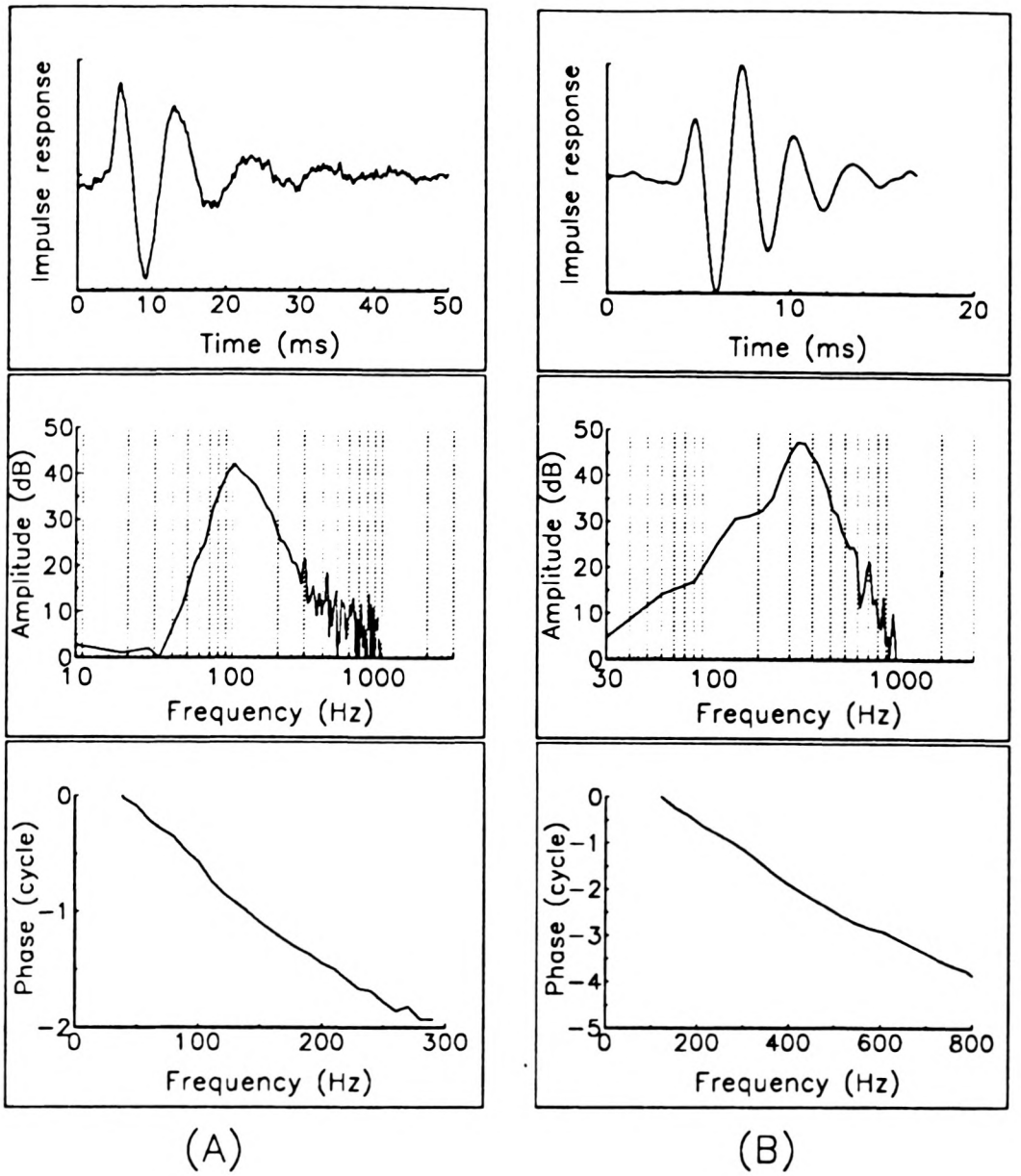

FIGURE 2 REVCOR-derived impulse responses and tuning curves for primary afferent axons from the amphibian papilla of the American bullfrog. (A) The stimulus noise level was 72 dB SPL; REVCOR analysis was based on 4,884 spikes; the REVCOR time window was 100 ms. (B) The stimulus noise level was 72 dB SPL; REVCOR analysis was based on 3,864 spikes; the REVCOR time window was 33 ms.

swings of the stimulus waveform would lead to resonances of shorter period, negative swings to resonances of longer period (Art and Fettiplace, 1987). The Revcor-derived impulse response, however, is the time-inverted mean of the noise waveforms

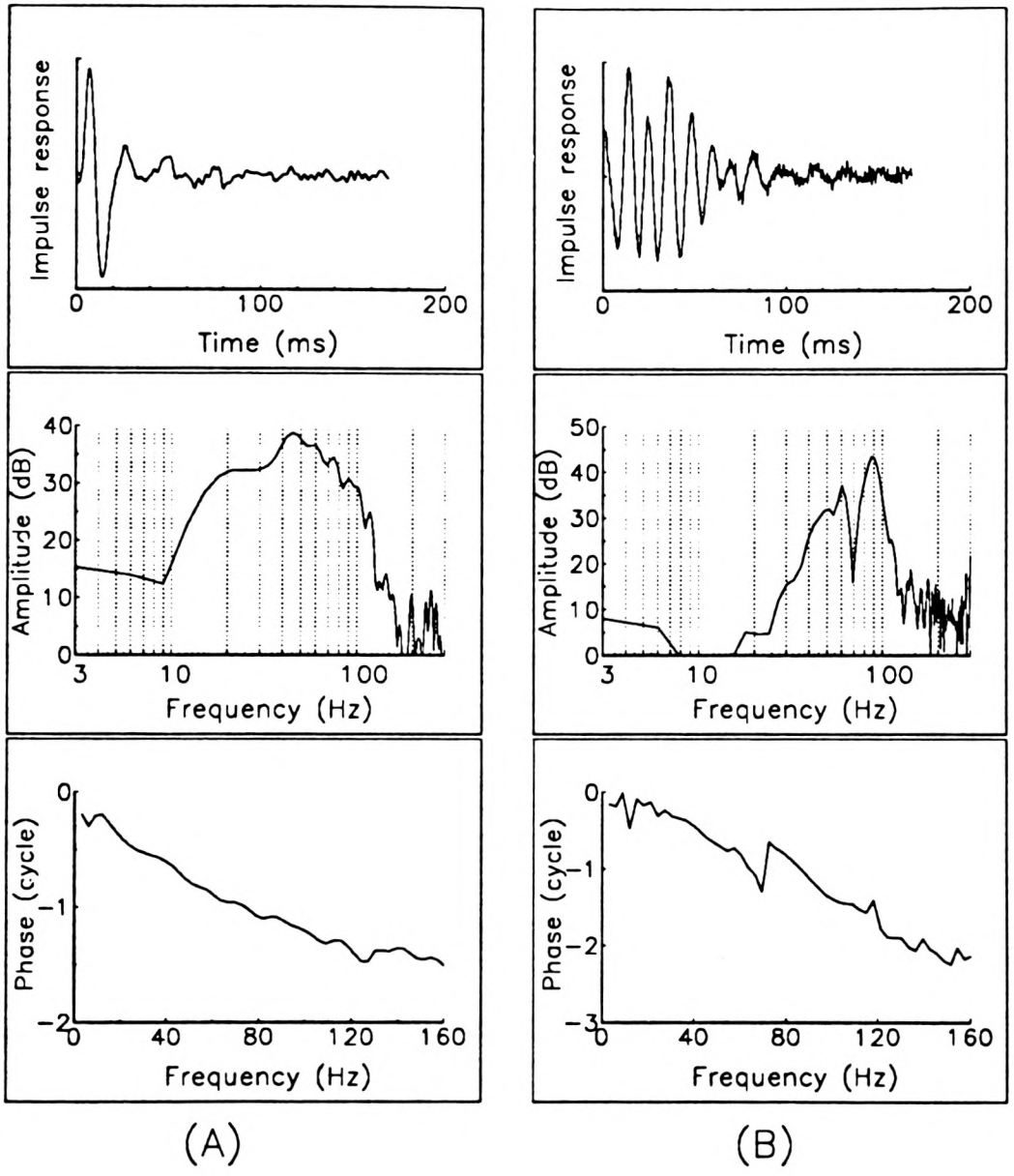

FIGURE 3 REVCOR-derived impulse responses and tuning curves for primary afferent axons from the sacculus of the American bullfrog. The REVCOR time window was 330 ms. (A) The stimulus noise level was 0.00063 cm/s^2 for 1-Hz bandwidth; REVCOR analysis was based on 9,528 spikes. (B) The stimulus noise level was 0.00063 cm/s^2 rms for 1-Hz bandwidth; REVCOR analysis was based on 31,494 spikes.

occuring immediately before spikes. Thus, in Fig. 1B, the mean stimulus waveform was both positive and negative when it was long. Furthermore, short and long periods occurred at places of comparable amplitude in the same REVCOR response. We believe

this rules out the proposition that the change of period is a consequence of changing states of the resonance. A much simpler explanation is the presence of higher-order dynamics (e.g., order five as proposed by Crawford and Fettiplace, 1981) in the peripheral tuning.

As expected, amplitude tuning curves derived from essentially biphasic impulse responses of saccular axons usually were broad and lacked sharp peaks (Fig. 3A). Some of these curves were especially broad and flat, with pass bands extending over more than two octaves and bounded by band edges whose (log-log) slopes summed to more than ten- - implying dynamic order greater than ten. All tuning curves derived from the ringing form of the saccular impulse response (Fig. 3B) exhibited deep notches. In single subjects, it often happened that one axon would exhibit a notched tuning curve and a neighboring axon would not. The peaks of the notches occurred at frequencies ranging approximately from 30 to 70 Hz: and the frequencies of the peaks varied from axon to axon in single subjects. In the corresponding phase tuning curve, each notch was accompanied by a positive jump of approximately one half cycle--- as expected from a high Q, second order antiresonance. Often, a notch was immediately adjacent to a sharp peak accompanied by a negative phase jump of one-half cycle-- as expected from a high-Q resonance. In those cases, the notch itself still was accompanied by a positive half-cycle phase jump. Antiresonances are characteristic of, among other things, tuning structures in which resonances are located in feedback loops. Antiresonances appearing without adjacent resonances are characteristic of tuning structures in which resonances occur in feedback loops but not directly in the path of the signal.

Most of the amplitude tuning curves of turtle basilar-papillar axons and all 63 amplitude tuning curves from the bullfrog amphibian papilla exhibited either rounded peaks (Fig. 1A) with completely convex flanks or pointed peaks, with abrupt transition from upslope to downslope and nearly flat flanks (Figs. 1B, 2A). Occasionally, for turtle axons, the peak was sharp and exhibited some local concavity in one or both flanks, suggestive of a resonance. All 155 amplitude tuning curves (from all three endorgans) displayed global convexity. The sum of the amplitudes of the limiting slopes of the (log-log) amplitude tuning curves (estimated above the noise floor from the REVCOR process) was four to seven for the turtle axons-- implying tuning structure dynamics of order four to seven. For frog amphibian papillar and saccular axons, the limiting slopes usually implied even higher dynamic order, typically in the neighborhood of eight to ten, occasionally as high as sixteen.

Similar dynamic order was implied by the phase tuning curves, after correction for the apparent absolute latency in the estimated impulse response with anticausal component removed. van Dijk et al. (1990) demonstrated concomitant temperature dependence of the phase and amplitude tuning curves from a bullfrog amphibian-papillar axon, with the net phase shift at the tuning peak remaining nearly constant-- both curves shifting approximately 0.5 octave with a temperature shift of 7 deg. C. The shifting phase tuning curve spanned more than two cycles of phase shift, implying that a large component of the phase shift is associated with the dynamics of the tuning structure rather than with extraneous time delays.

In a number of previous papers, phase tuning curves similar to those shown here have been interpreted to imply time delays; and the delays often have been estimated as the average slope of phase vs. time (cycles of phase shift per Hz). A true time delay, strictly speaking, requires dynamics of infinite order. True time-delay is evident at the beginning

of each REVCOR-derived impulse response (e.g., approximately 4 ms in Fig. 2B); but the slopes of the phase vs. frequency curves are always greater than the values predicted from those delays. In fact, the best predictor of the average phase slope is the time to the maximum of the impulse response envelope. As it is in Fig. 1B, this time often is much greater than the time delay at the beginning of the impulse response. Thus, much of the average phase slope is contributed by the finite-order tuning dynamics rather than by true (infinite-order) time delays.

Conclusions

The results presented here imply that tuning in the red-eared turtle basilar papilla and the bullfrog amphibian papilla and sacculus is accomplished by structures of high dynamic order. For the turtle basilar papilla, Crawford and Fettiplace (1981) already have suggested a structure of order five, of which order two is provided by the middle ear, order two by the hair-cell resonance, and order one by some other element. Our results generally are consistant with this picture, but in higher-frequency axons suggest slightly higher dynamic order. This could be explained by the low-pass filter properties of the signal path from the transducer in the hair cell to the spike initiator site in the primary afferent axon (Weiss and Rose, 1988). The general convexity of the log-log amplitude tuning curves and lack of abrupt phase shifts in the phase tuning curves, however, suggest that frequency selectivity in these axons is achieved by the asymptotic amplitude slopes at high and low frequencies rather than by the peaks of underdamped resonances. The same thing appears to be true in the bullfrog amphibian papilla, but the dynamic order is somewhat higher, leading to steeper band edges in the amplitude tuning curves. Although a few saccular axons exhibit sharp antiresonances (sometimes accompanied by neighboring resonances), frequency selectivity again seems to be accomplished largely by the asymptotic slopes.

Acknowledgements

The original research reported here was supported by Grant DC 00112 from the National Institute on Deafness and Other Communication Disorders. We thank Mr. David Feld for construction of the REVCOR hardware used in this project.

References

Art, J.J. and R.F. Fettiplace (1987) Variation of membrane properties in hair cells isolated from the turtle cochlea. J. Physiol. 385: 207-242.

Capranica, R.R. and Moffat, A.J.M. (1975) Selectivity of the peripheral auditory system of spadefoot toads (Scaphiopus couchi) for sounds of biological significance. J. Comp. Physiol. 100: 231-249.

Crawford, A.C. and Fettiplace, R.F. (1980) The frequncy selectivity of auditory nerve fibres and hair cells in the cochlea of the turtle. J. Physiol. 306:79-125.

Crawford, A.C. and Fettiplace, R.F. (1981) An electrical tuning mechanism in turtle cochlear hair cells. J. Physiol. 312: 377-412.

de Boer, E. and de Jongh, H.R. (1977) On cochlear encoding: potentialities and limitations of the reverse-correlation technique. J. Acoust. Soc. Am. 63(1), 115-135.

de Boer, E. and Kuyper, P. (1968) Triggered correlation. IEEE Trans Biomed. Engrg. 15:169-179.

Eggermont, J.J., Johannesma, P.I.M. and Aertsen, A.M.H.J. (1983) Reverse-correlation method in auditory research. Quart Rev. Biophys. 16(3): 341-414.

Evans, E.F. (1989) Cochlear filtering: a view seen through the temporal discharge patterns of single cochlear nerve fibres. In: Cochlear Mechanisms (Eds: Wilson, J.P and Kemp, D.T.) Plenum, New York, pp. 241-250.

Fettiplace, R.F. and Crawford, A.C. (1978) The coding of sound pressure and frequency in cochlear hair cells of the terrapin. Proc. Roy. Soc. Lond. B. 203: 209-218.

Frishkopf, L.S. and Goldstein, M.H. (1963) Responses to acoustic stimuli from single units in the eighth nerve of the bullfrog. J. Acoust. Soc. Am. 35: 1219-1228.

Lewis, R.S. and Hudspeth, A.J. (1983) Frequency tuning and ionic conductance in hair cells of the bullfrog sacculus. In: Hearing--Physiological Bases and Psychophysics. pp 17-24. (Eds: R. Klinke and Hartmann, R.) Springer-Verlag, Berlin.

Pitchford, S. and Ashmore, J.F. (1987) An electrical resonance in hair cells of the amphibian papilla of the frog, Rana temporaria. Hearing Research 27, 75-84.

van Dijk, P., Lewis, E.R. and Wit, H.P. (1990) Temperature effects on auditory nerve fiber response in the American bullfrog. Hear. Res. 44: 231-240.

Weiss, T.F., Rose, C. (1988) A comparison of synchronization filters in different auditory receptor organs. Hearing Res. 33:175-180.

OBSERVATIONS ON STRUCTURE AND FUNCTION OF THE OLIVOCOCHLEAR PROJECTIONS IN CAT

M. Charles Liberman

Departments of Otolaryngology and Physiology, Harvard Medical School; and Eaton-Peabody Laboratory, Massachusetts Eye and Ear Infirmary, 243 Charles St., Boston, MA 02114

Introduction

The efferent projections to the inner ear are composed of two fundamentally different fiber types [Warr and Guinan, '79]: a system of relatively large myelinated fibers whose major peripheral target is the bases of outer hair cells (OHCs) [Kimura and Wersall, '62] and a system of smaller, unmyelinated fibers which project mainly to the dendrites of afferent fibers in the region under the inner hair cells (IHCs) [Smith, '61], as schematized in Figure 1. In addition, to these "classic" terminals of the olivocochlear bundle (OCB), there are a number of reports in the literature of other vesiculated terminals within the organ of Corti which may also be derived from the OCB [Ginzberg and Morest, '84; Hashimoto et al., '90; Bredberg, '77]. In most previous studies of OC projections, electron microscopic (EM) analysis has been used to distinguish afferent from efferent terminals. Due to the inherent sampling limitations of EM studies, the cochlear distribution of the various vesiculated terminals has never been systematically described.

Given the present state of ignorance about the functional significance of the OC system, especially the so-called "lateral" OC system, which projects mainly to the IHC area, a systematic study of the distribution of efferent terminal types within the organ of Corti was initiated in hopes of generating new insights into OC function. To this end, several cat cochleas were prepared for light-microscopic (LM) examination after immunohistochemical treatment designed to label all vesiculated terminals. The LM data was supplemented by serial-section EM analysis of selected cochlear regions. In the present report, some of the results from these analyses are discussed in the context of ongoing functional studies of the OC system. A more detailed report can be found elsewhere [Liberman et al., '90].

Methods

Cochleas from four cats were prepared for light-microscopic analysis as plastic-

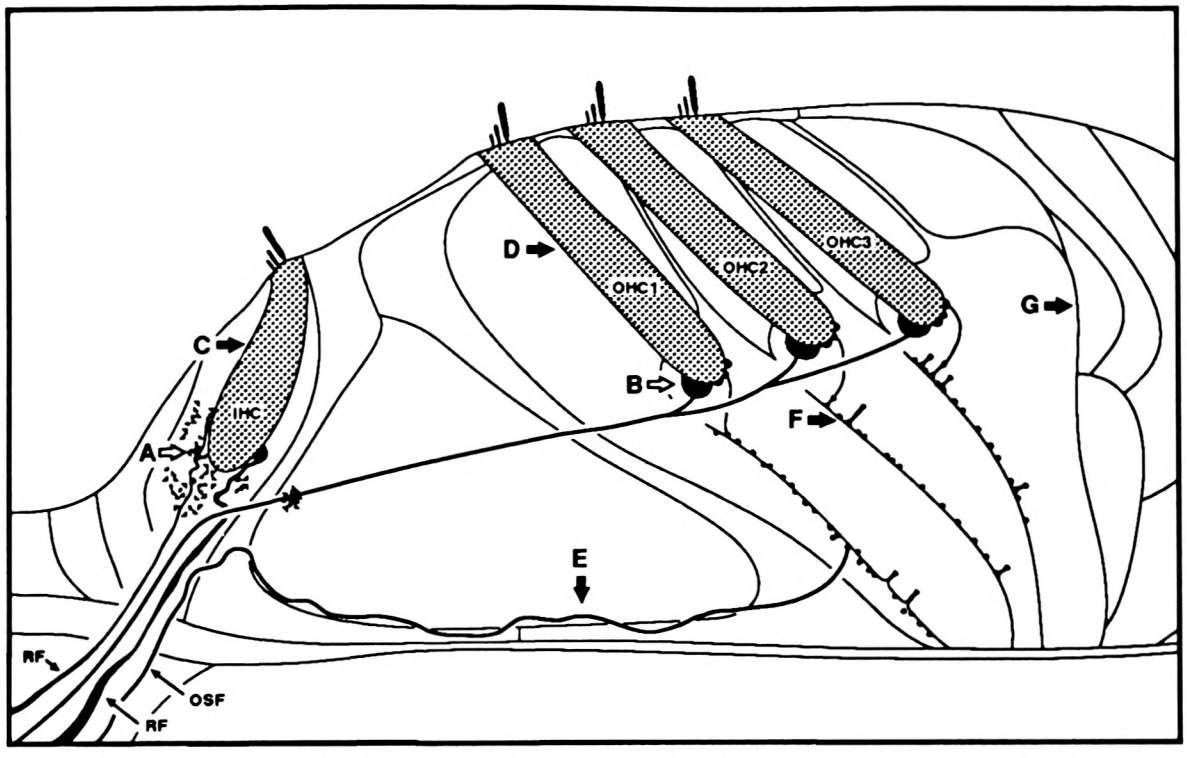

FIGURE 1 Schematic of the organ of Corti illustrating the locations of "classic" OC terminals (open arrows A and B) and "non-classic" terminals (filled arrows) on the supranuclear portions of inner and outer hair cells (C and D), on the floor of the tunnel (E), in the outer spiral bundles (F) and among the OHC supporting cells (G).

embedded surface preparations. The techniques have been described in detail elsewhere [Liberman et al., '90], In brief, each cochlea was fixed by intravascular perfusion and incubated in antibody to synaptophysin, a protein thought to be universally associated with clear synaptic vesicles throughout the nervous system [Navonne et al., '86]. The location of the antibody within the tissue was visualized by subsequent reaction with a biotinylated antibody against the anti-synaptophysin, which in turn was complexed with avidin-biotin-horseradish-peroxidase.

The light-microscopic analysis was complemented by electron-microscopic studies on one additional cochlea. Serial sections through the sensory epithelium were analyzed at 8 cochlear locations, evenly spaced from base to apex. The cochlea chosen for EM study was from a four-month old animal which had been born and raised in a low-noise environment [Liberman, '78] and for which the thresholds of auditory-nerve fibers were known to be exceptionally good.

Results and Discussion

The overall appearance of the synaptophysin-treated cochleas suggested that all of

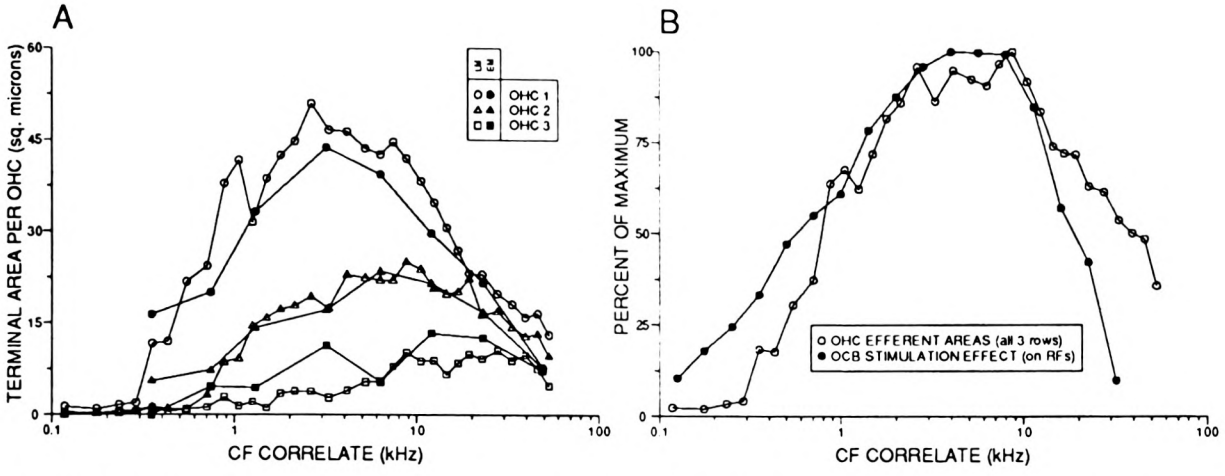

FIGURE 2 Panel A - Distribution of classic subnuclear efferent terminals on OHCs as a function of OHC row and cochlear location, from LM analysis of one synaptophysin-treated cochlea (open symbols) and from EM analysis of another normal ear. Panel B- Comparison of the cochlear distribution of OHC subnuclear efferent terminals (summed across all three OHC rows from LM data in panel A) with the distribution of average threshold shift seen in auditory nerve fibers when OCB activity is evoked by shocks (from data of Guinan and Gifford, '88).

the vesiculated terminals were labeled. Large terminals were seen on the bases of most OHCs, and a complex meshwork of beaded fibers under the IHCs was also clearly visible throughout the cochlea. In addition to these classic terminals of the MOC and LOC systems, respectively, labeled swellings were seen contacting the IHCs and the supranuclear portions of the OHCs. Swellings were also seen on the floor of the tunnel and among the OHC support cells.

Classic terminals at the OHC base

In two cochleas, attempts were made to estimate the total volume of labeled terminals contacting the OHC bases as a function OHC row and cochlear location. The silhouette areas of all labeled terminals under each OHC were measured and the average terminal area per OHC computed (open symbols in Figure 2A): for each row of OHCs there is more terminal area in the base than in the apex, and at any cochlear location the first-row OHCs is much more richly innervated than than the second or third-row cells.

These values for terminal distribution obtained from light-microscopic (LM) analysis of synaptophysin-treated ears are in good quantitative agreement with EM measurements of the total cross-sectional area of vesicle-filled terminals contacting OHC bases obtained in a different study (filled circles in Figure 2A). The excellent agreement between the LM and EM data provide strong evidence that the anti-synaptophysin treatment is actually staining all of the vesicle-filled terminals, thus increasing our confidence that the technique provides a good way to survey the entire complement of OCB terminals within the inner ear.

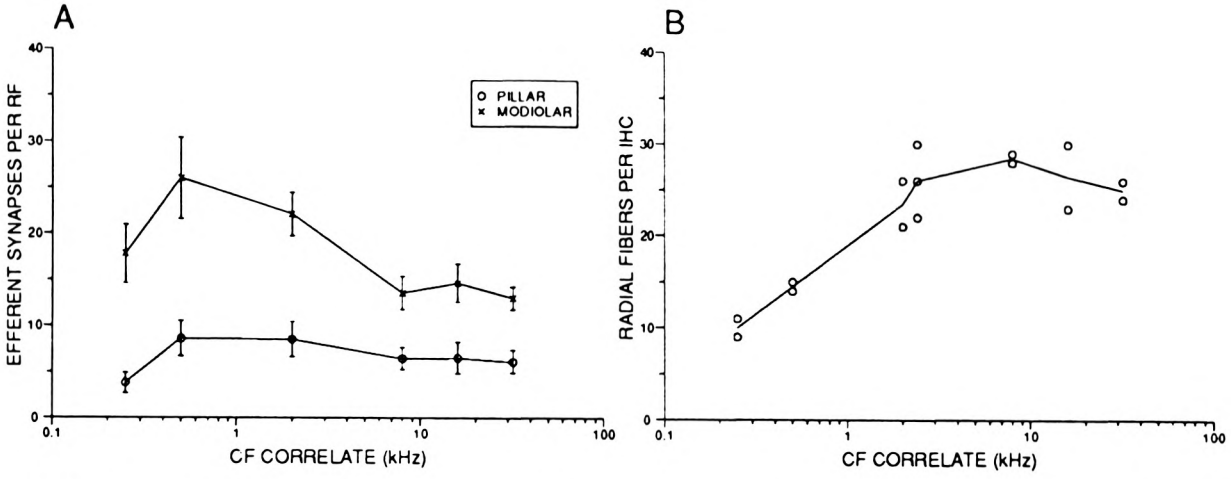

FIGURE 3 Panel A - Number of efferent synapses per radial afferent fiber seen in serial electron micrographs through a pair of IHCs at six cochlear locations. Afferent fibers are classified as "pillar" or "modiolar" on the basis of the location of the terminal swelling on the IHC (See Liberman, '82). Panel B - number of radial afferent fibers per IHC, as counted from the same database used for the analysis shown in panel A.

The cochlear distribution of classic OCB terminals on OHCs is very similar to the frequency distribution of classic OCB effects on auditory-nerve thresholds. In Figure 2B, the average terminal areas from all three OHC rows are summed at each cochlear location, normalized and compared to the average threshold shifts seen in single auditory-nerve fibers of different characteristic frequency (CF) when the OCB is shocked at the floor of the fourth ventricle [Guinan and Gifford, '88]. The cochlear region of maximal efferent innervation (6 to 10 kHz) corresponds very closely to the CF region in which the maximal effects of OCB electrical stimulation are seen.

The maximal effects of *sound-evoked* OCB activity, at least in anesthetized cats, is shifted somewhat towards lower frequencies. Warren and Liberman ['89] found that contralateral broad-band noise raised thresholds for auditory-nerve fibers to ipsilateral tones, with a maximal effect for fibers with CF between 1 and 3 kHz. This discrepancy between shock-evoked and sound-evoked effects presumably arises because single efferent neurons with CFs between 1 and 3 kHz respond to sound much more vigorously than those tuned between 6 and 10 kHz [Liberman, '88].

Classic terminals in the IHC area

Although the inner spiral bundles were clearly visible in the synaptophysin-treated ears, quantification was extremely difficult, because the density of terminals was high, and their sizes and shapes were highly variable. Thus, we chose to quantify the innervation in this region at the EM level only. At each of six cochlear locations, serial sections through a pair of IHCs and associated afferent innervation were reconstructed and the number of efferent synapses per afferent fiber was determined. Two important features of the results are illustrated in Figure 3A. First, it is clear that there

are significant differences at all cochlear location between those afferent fibers originating from pillar vs. modiolar faces of the IHCs. From previous studies, we know that pillar-side afferents are almost exclusively those with high spontaneous-discharge rates (SRs) and low thresholds, while low- and medium-SR afferents (with relatively high thresholds) are found almost exclusively on the modiolar face of the IHC [Liberman, '82]. The data in Figure 3A suggest that low and medium-SR afferent are much more richly innervated than high-SR afferents. The data also suggest that, if there is any longitudinal gradient in efferent innervation of radial afferents, innervation density (expressed as synapses per afferent fiber) is greater in the apex than in the base. However, since there are more afferents per IHC in the base than in the apex (Figure 3B), the total number of efferent synapses per mm of cochlear length is probably more uniform along the spiral.

The observations summarized in Figure 3A suggested the hypothesis that the LOC innervation of radial fibers might play some role in establishing or maintaining the differentiation of afferent fibers into SR groups, i.e. that the massive LOC innervation of modiolar afferents was responsible for their low SRs and high thresholds. To test this hypothesis a series of cats was chronically de-efferented. Histological tests confirmed that, in three animals, virtually all efferent terminals from both LOC and MOC systems were eliminated. However, even six months after complete de-efferentation, the differentiation of auditory-nerve afferents into three SR groups, and the relative proportions of each group, were basically unchanged from control ears [Liberman, '90].

In the de-efferented group, the overall rates of SR were significantly lower than in control ears, suggesting a net excitatory influence of the efferents to the IHC area. However, as discussed elsewhere [Liberman, '90], it is possible that the SR abnormalities could be ascribed to other effects of the brainstem surgery used to cut the OCB. The most striking result of the chronic de-efferentation study was how few of the fundamental response properties of auditory nerve fibers (to tones in quiet) were affected.

Non-classic efferent terminals

In addition to the well-known terminal-types described above, synaptophysin-treated cochleas also showed labeled terminals of several other types. All these non-classic terminals were small, i.e. closer in size to those seen in the inner spiral bundle than to those seen at the bases of the OHCs. We attempted to classify these terminals based on the post-synaptic targets, as well as could be determined at the LM level. These targets (illustrated schematically in Figure 1) include a) the supranuclear portions of IHCs and OHCs, b) the OHC afferent fibers, either at the floor of the tunnel where they cross or within the spiralling bundles under the OHCs, and c) supporting cells, either the third-row Deiters cells or Hensen cells. As illustrated in Figure 4, all these non-classic terminal types are common in the apical half of the cochlea and virtually absent in the base.

The synaptophysin immunolabeling suggests that these non-classic terminals

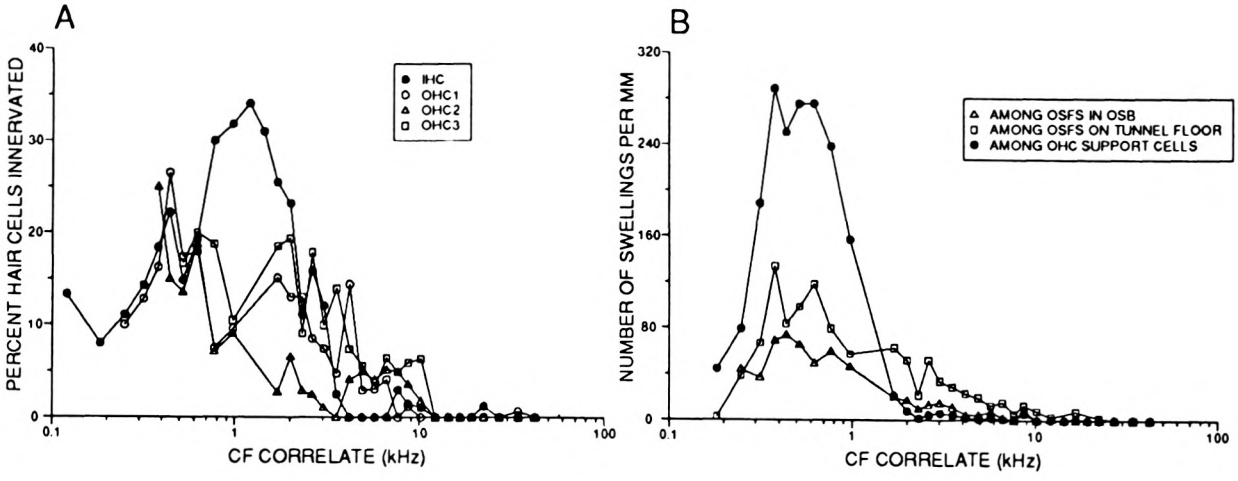

FIGURE 4 Distribution of various non-classic terminal types as a function of cochlear location as seen in one synaptophysin-treated cochlea. Terminals in panel A are supranuclear swellings on IHCs or OHCs (as indicated at X and Y in Figure 1). In panel B, terminal types represented by triangles, squares and filled circles are those located at positions indicated by X, Y, and Z in Figure 1.

contain clear vesicles, however EM data are required to prove that they are synaptic in nature. EM studies in both cat and guinea pig have shown vesiculated terminals making synaptic contact with the IHCs [Liberman et al., '90; Hashimoto et al., '89], and studies of supranuclear terminals on OHCs also suggest they make synaptic contact [Bredberg, '77]. Synapses between vesiculated terminals and OHC afferents have been noted on the floor of the tunnel and in the outer spiral bundles [Ginzberg and Morest, '84]. Thus, the only non-classic terminal not yet studied at the EM level are those in the Hensen/Deiters cell area.

The brainstem origins of these non-classic terminal types are unclear. The size and morphology of the terminals is more like those LOC terminals in the inner spiral bundles than the MOC terminals under the OHCs. However, the location in the OHC region might suggest an MOC origin.

Regardless of the origin of these terminals, the data suggest fundamental longitudinal differences in the morphological organization of the OC system. Such differences are intriguing in light of physiological studies of the responses of single MOC neurons to sound. These physiological studies also suggest important functional differences between those efferents with low CFs and those with high CFs, with respect to such characteristics as binaurality, shape of rate-level functions and degree of spontaneous activity [Liberman, '88]. It may be that the function of efferent feedback differs significantly in cochlear apex vs the cochlear base.

References

Bredberg, G. (1977) Ultrastructural features of the small nerve endings high up on the outer hair

cells. In: Psychophysics and Physiology of Hearing (Eds. Evans, E.F. and Wilson, J.P.) Academic Press, London, pp.12-13.

Ginzberg, R.D. and Morest, D.K. (1984) Fine structure of cochlear innervation in the cat. Hearing Res. 14, 109-127.

Guinan, J.J. and Gifford, M.L. (1988) Effects of electrical stimulation of efferent olivocochlear neurons in cat auditory nerve fibers.III.Tuning curves and thresholds at CF. Hearing Res. 37, 29-46.

Hashimoto, S., Kimura, R.S. and Takasaka, T. (1990) Computer-aided three-dimensional reconstruction of the inner hair cells and their nerve endings in the guinea pig cochlea. Acta Otolaryngol (in press).

Kimura, R.S. and Wersall, J. (1962) Termination of the olivocochlear bundle in relation to the outer hair cells of the organ of Corti in guinea pig. Acta Otolaryngol. 55, 11-32.

Liberman, M.C. (1978) Auditory nerve response from cats raised in a low-noise environment. J. Acoust. Soc. Amer. 63, 442-455.

Liberman, M.C. (1982) Single-neuron labeling in the cat auditory nerve. Science 216, 1239-1241.

Liberman, M.C. (1988) Response properties of cochlear efferent neurons: monaural vs. binaural stimulation and the effects of noise. J. Neurophysiol. 5, 1779-1798.

Liberman, M.C. (1990) Effects of chronic cochlear de-efferentation on auditory nerve response. Hearing Res. (in press).

Liberman, M.C., Dodds, L.W. and Pierce, S. (1990) Afferent and efferent innervation of the cat cochlea; quantitative analysis using light and electron microscopy. J. Comp. Neurol (in press).

Navonne, F., Jahn, R., DiGioia, G., Stukenbok, H., Greengard, P., and De Camilli, P. (1986) Protein p38: An integral membrane protein specific for small vesicles of neurons and neuroendocrine cells. J. Cell. Bio. 103, 2511-2519.

Smith, C.A. (1961) Innervation patterns of the cochlea. The internal hair cell. Ann Otol. Rhinol. Laryngol. 70, 504-527.

Warr, W.B. and Guinan, J.J. (1979) Efferent innervation of the organ of Corti: two separate systems. Brain Res. 173: 152-155.

Warren, E.H. and Liberman, M.C. (1989) Effects of contralateral sound on auditory nerve responses.I.Contributions of cochlear efferents. Hearing Res. 37, 89-104.

THE STING IS IN THE TAIL

Vera F. Prijs, Jan Keijzer, Ruurd Schoonhoven and Huib Versnel

Ear, Nose and Throat Department, Leiden University Hospital, PO Box 9600, 2300 RC Leiden, The Netherlands

Introduction

In the normal cochlea only fibers that are tuned to low frequencies show phase-following responses due to the low-pass filter mechanisms situated at the level of inner hair cell and synapse. As a result, in fibers with low characteristic frequency (CF) click-evoked post-stimulus time histograms (PSTHs) show a periodicity associated with CF (Kiang et al., 1965), while in high-CF fibers the PSTH reflects only the envelope of the filter's impulse response. For high click intensities, the symmetry of PSTHs to rarefaction clicks and condensation clicks (RC and CC) in high-CF fibers can be lost (Antoli-Candela and Kiang, 1978). There, a phase-following-like character seems to emerge at click intensities for which the spectral level of the click reaches above the low-frequency tail of the frequency threshold curve (FTC). Such phenomena must be expected to be even more prominent in cases of cochlear pathology where the sensitivity of the tail of the FTC has increased (Liberman and Dodds, 1984; Harrison and Prijs, 1984; Versnel et al., 1989).

In this contribution we study the influence of the tail of the FTC on temporal discharge patterns in responses to clicks of both polarities. Experimental data in normal and noise-damaged guinea pigs are combined with model simulations in order to hypothesize a mechanism underlying the modified temporal discharge behavior.

Methods

A. ANIMAL RESEARCH

Terminal experiments were performed in normal (12) and abnormal (7) hearing guinea pigs. In the latter group noise trauma had been induced under general anesthesia 3-4 weeks before the experiment by a 2 hour presentation of a 6 kHz pure tone at 122 dB SPL (Versnel et al., 1989).

Single auditory nerve fiber responses were recorded using standard techniques. Medication, surgery and equipment used for sound stimulation and physiological recordings were extensively described by Prijs (1986) and Versnel et al. (1990). Probe stimuli were 100 μs clicks presented at an inter-stimulus interval of 128 ms.

For each fiber the following data were obtained: a frequency threshold curve (FTC), the spontaneous firing rate (SR), and PSTHs to clicks of both polarities at different intensities. From the PSTHs combined figures were made, rarefaction click (RC) responses being plotted downward and condensation click (CC) responses upward.

B. THE COMPUTATIONAL MODEL

The simulation model reflects a functional description of the different stages of cochlear processing.

The outer and middle ear are represented by a single first order bandpass filter with center frequency at 4 kHz.

The basilar membrane section is modeled as a set of parallel frequency channels. The impulse responses of the filter contained in each channel is taken to be a sinusoid modulated with a gamma distribution function (cf de Boer, 1975; van Stokkum, 1989):

$$h(t)= c\ ((t-\alpha)/ß)^{\gamma-1} \exp-((t-\alpha)/ß) \cos(2\pi f_0 t+\phi_0). \quad (1)$$

The parameter α basically represents a travelling wave delay. The parameter c controls the sensitivity of the filter, and f_0 and ϕ_0 are the center frequency and phase of the filter. The combination of ß and γ determines the shape of the envelope, i.e. the tuning quality.

In order to study separately the influence of the tail of the FTC on temporal response properties we model tip and tail area as two separate gamma-envelope filters acting in parallel. This implies that a single basilar membrane channel is then characterized by a linear combination of two impulse responses as given in (1) at different center frequencies, reflecting tip and tail of the tuning curve, respectively.

Each basilar membrane channel is followed by an inner hair cell section modeled according to Shamma et al. (1985). A first-order low-pass filter with cut-off frequency of 2 kHz is added to achieve the correct phase-lock characteristics of neural discharges (Palmer and Russel, 1986; Versnel et al., 1990).

Finally, the probabilitity of spike generation is assumed to depend linearly on the synaptic output, with a conversion factor to control the maximum driven rate, and is modified by a refractory mechanism according to Lütkenhöner et al. (1980).

A number of model parameters was especially adapted to guinea pig data. For convenience, the parameter α was used to include both travelling wave, synaptic and neural conduction delays. It was taken to be 1 ms as estimated from click PSTHs from normal-hearing animals (Versnel et al., 1990). The tuning parameters ß and γ applying for the normal cochlea were derived from the same data. To simulate the deteriorated cochlea these parameters were also adapted to tuning characteristics found in noise-damaged animals. Parameters concerning refractoriness were derived from our spontaneous activity data following Lütkenhöner et al. (1980).

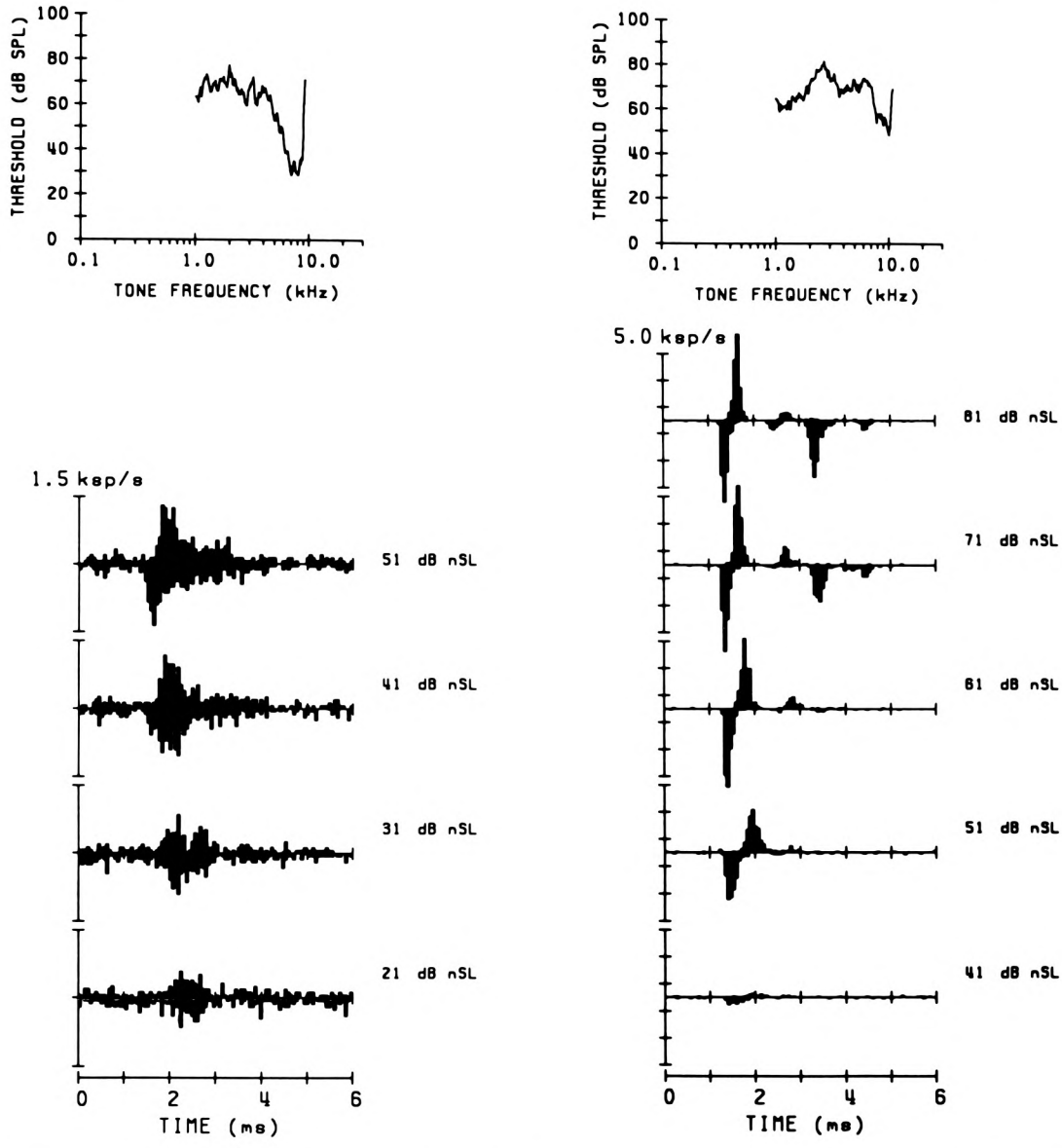

FIGURE 1 Frequency threshold curves (FTC) and click-evoked PSTHs at different click intensities. The condensation click response is plotted upward, the rarefaction click response downward. (a, left) Normal fiber with CF=8.1 kHz, SR=110 sp/s. (b, right) Pathological fiber from noise damaged cochlea with CF=10 kHz, SR=6 sp/s.

Results

The click levels presented in this paper, denoted as dB nSL, are given with respect to the average threshold of the click-evoked compound action potential in a group of normal hearing guinea pigs. In the latter group it appears that for CFs below 10 kHz a single fiber's click threshold (in dB nSL) is, on average, 10 dB lower than the pure-tone threshold at CF (in dB SPL).

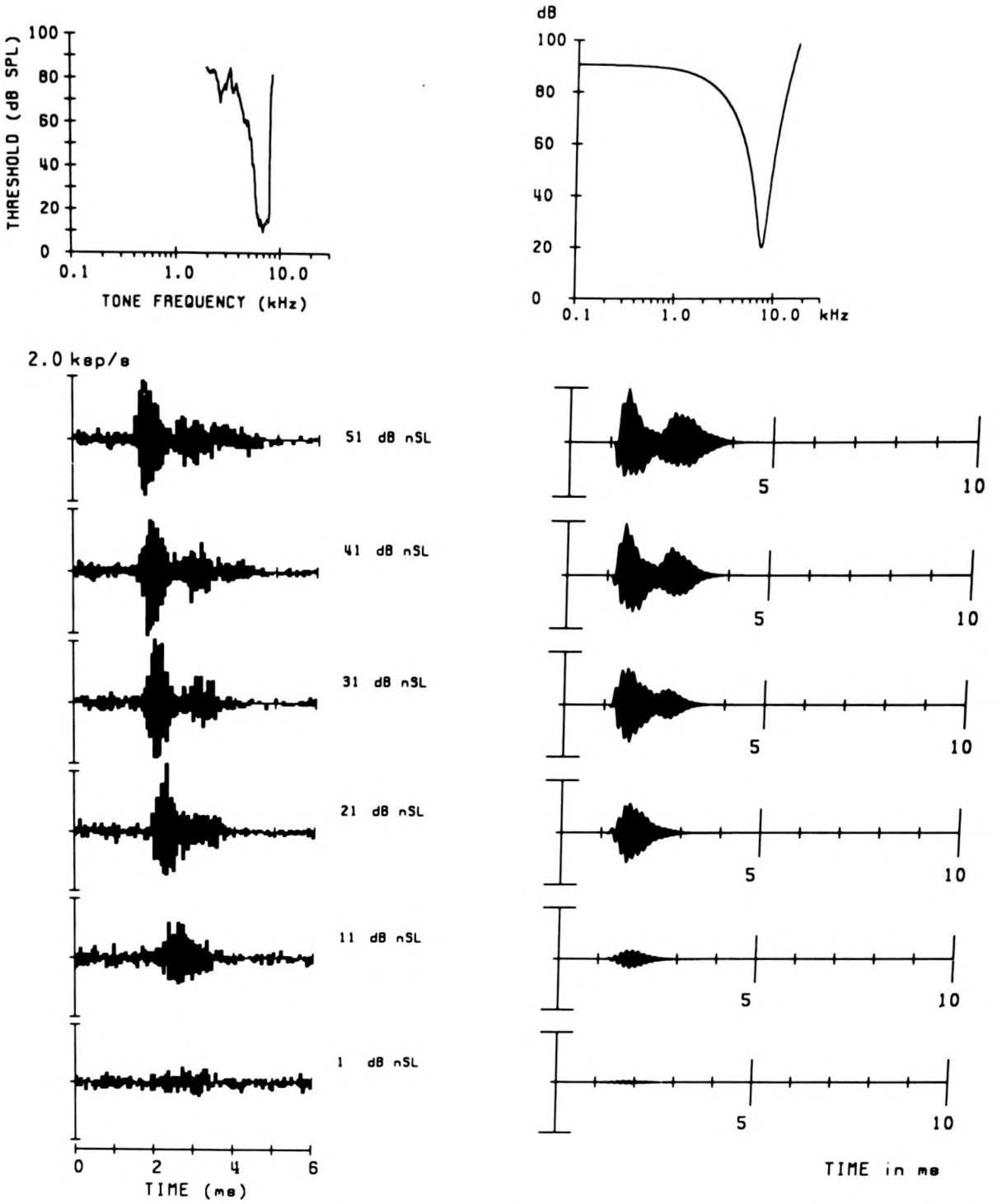

FIGURE 2 FTCs and associated PSTHs at different click intensities in a normal high-frequency fiber. The condensation click response is plotted upward, the rarefaction click response downward. (a, left) Experimental data, CF=6.9 kHz, SR=131 sp/s. (b, right) Corresponding model simulations for a fiber with similar tuning characteristics.

In Fig. 1a combined CC and RC PSTHs for different intensities are given for a normal high-CF fiber. The CC and RC responses are symmetrical up to about 50 dB above threshold, i.e. up to the level where the (approximately flat) spectrum of the click reaches the low-frequency tail of the FTC. This pattern can change dramatically when the cochlea is damaged and an abnormal FTC is measured. Fig. 1b shows an abnormal FTC at similar CF and the corresponding click PSTHs. Responses are asymmetrical at all levels.

In order to further investigate the phenomena shown in Fig. 1 model simulations were performed, first for normal, then for abnormal fibers. In Fig. 2a we show experimental data for a normal fiber with a CF of 7 kHz, and in Fig. 2b corresponding responses predicted by the model with similar, simulated tuning characteristics (single filter with f_0=7 kHz, ϕ_0=0, ß=0.2 ms and γ=4). Both the experimental and the simulation results reflect the non-phase-following character of a high-frequency fiber. The second peak at high intensities due to repetitive firing is reproduced properly. The intensity dependent latency shift is only partly reproduced in the simulations.

Figs 3a and b represent the experimental and simulated data for a low-frequency fiber with CF of 0.5 kHz. In the simulation a single filter with f_0=0.5 kHz, ϕ_0=π, ß=0.7 ms and γ=4 was used. The phase-following character of the response is evident. In both experimental and simulated data the peaks become skew at high intensities due to refractory effects.

In Fig. 4a, the experimental data of an abnormal fiber in a noise-damaged cochlea are shown. The fiber's CF is about the same as that of the high-frequency fiber in Fig. 2. Comparison of Figs 2a and 4a clearly shows the changes in FTC and the corresponding temporal behavior. At low intensities, the response is dominated by the early, narrow peak associated with the high-frequency tip. At increasing intensities the low-frequency tail is activated as well, leading to phase-locked low-frequency peaks in the PSTH. The phase-following character - caused by the hypersensitive tail - resembles that of a low-frequency fiber as shown in Fig. 3a, while the latency of the high-CF fiber's response is much shorter than that of the low-CF fiber of Fig. 3a. For the simulation of this pathological fiber two parallel filters of slightly different sensitivity were assumed, one representing the tip (f_0=7 kHz, ϕ_0=0, ß=0.1 ms and γ=3), the other representing the tail (f_0=0.5 kHz, ϕ_0=0, ß=0.5 ms and γ=3). Their combined tuning properties and the model-predicted PSTHs are shown in Fig. 4b. The low-frequency phase-following is qualitatively well reproduced by the model. Its simulated frequency of 0.5 kHz, a value derived from the most sensitive area of the FTC tail, is too high as compared to the experimental PSTH data.

Discussion

Our experimental data show that, apart from a change in a fiber's sensitivity, its temporal response pattern can be changed considerably in pathology. In that respect they differ from data presented by Salvi et al. (1983) who only found threshold increases.

We have hypothesized that part of these findings is associated with the tail of the tuning curve, which in pathology may become more sensitive either in an absolute sense or relatively to the tip when the latter becomes less sensitive. We therefore formulated a description of basilar membrane frequency selectivity in terms of a set of parallel filters, representing the tip and tail aspects of the tuning curve. Simulations of click PSTH data in the normal cochlea yield satisfactory reconstructions of experimental data.

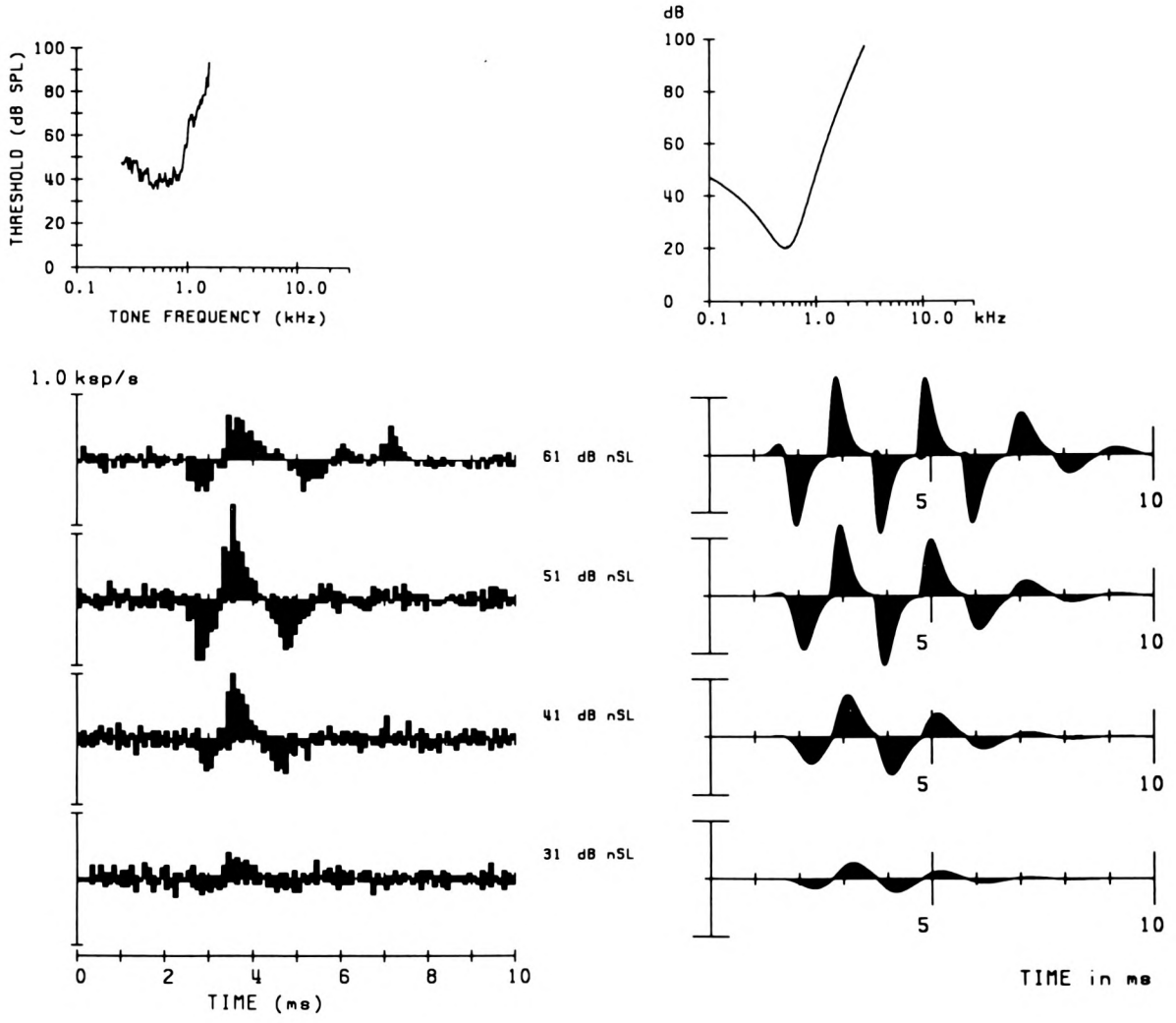

FIGURE 3 FTCs and associated PSTHs at different click intensities in a normal low frequency-fiber. The condensation click response is plotted upward, the rarefaction click response downward. (a, left) Experimental data, CF=0.54 kHz, SR=74 sp/s. (b, right) Corresponding model simulations for a fiber with similar tuning characteristics.

The simulated PSTHs show a realistic frequency following in low-CF fibers and correctly predict a second peak in high-CF fibers at high intensities. The latter is due to repetitive firing after the absolute refractory period has ended, as is clearly seen by comparing the computed synaptic output to the PSTH generated including the refractory mechanism (not shown here). Intensity dependent latency shifts are evidently not fully reproduced by the present linear filter model, since α, ß and γ are taken independent of stimulus level.

Simulations of pathological fibers show that with the double-filter model the experimentally observed temporal discharge patterns can qualitatively well be reproduced. Improvements in the model concept can be made by including an intensity dependent gain and tuning of the FTC-

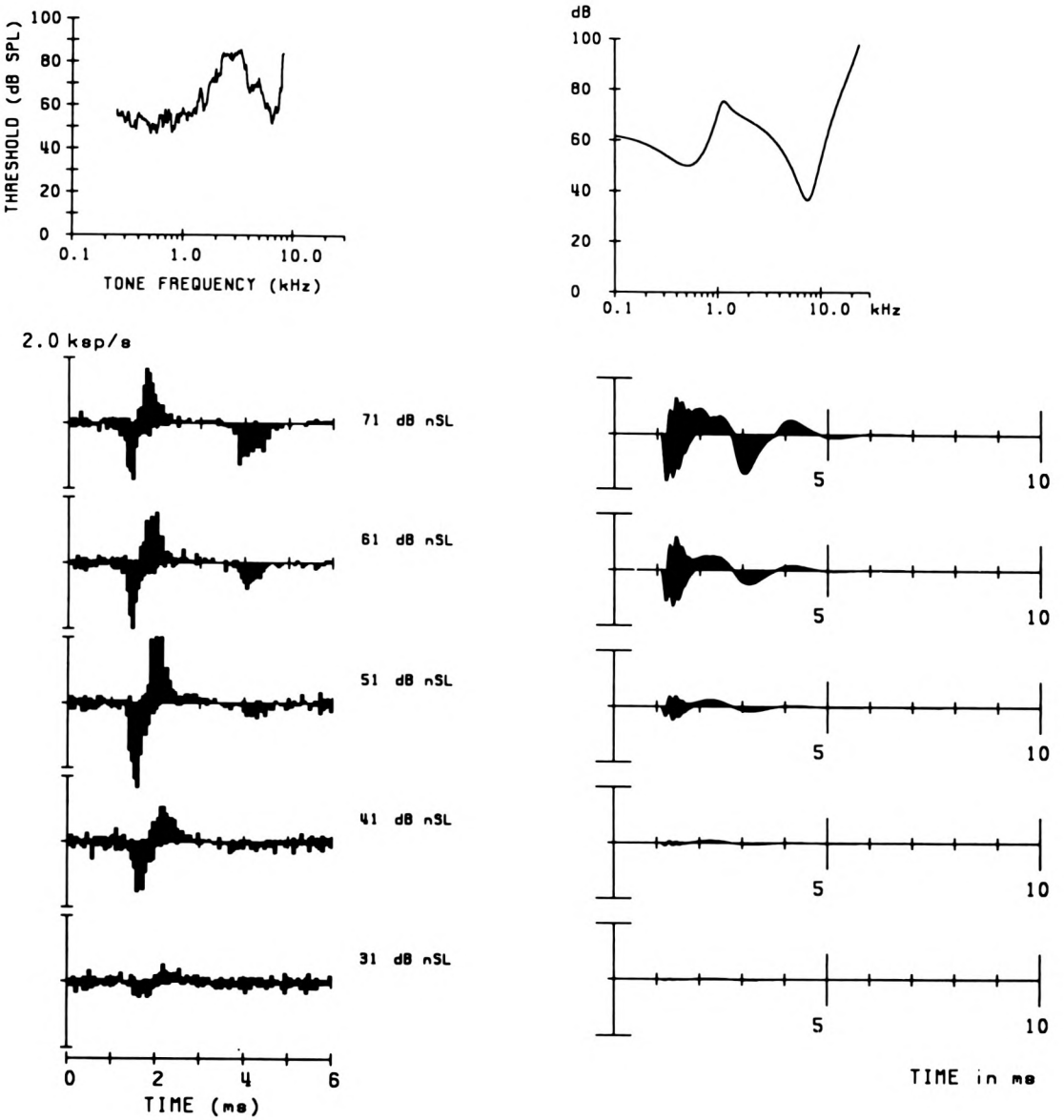

FIGURE 4 FTCs and associated PSTHs at different click intensities in a pathological fiber from a noise-damaged cochlea. The condensation click response is plotted upward, the rarefacion click response downward. (a, left) Experimentel data, CF=6.5 kHz, SR=126 sp/s. (b, right) Corresponding model simulations for a fiber with similar tuning characteristics.

tip filter and, especially for the damaged cochlea, a less sharply tuned tail section. The relative sensitivity of tip and tail also show some discrepancies (Fig. 4). Apart from the basilar membrane mechanics here also a further refinement of the middle ear and inner hair cell/synapse section may be required.

We conclude that temporal discharge patterns of high-CF auditory-nerve fibers can considerably be influenced by the tail of the tuning curve, in particular in the pathological cochlea. Global characteristics of click-evoked responses are correctly reproduced by a simple model of cochlear

frequency selectivity based on a broad filter representing the tail of the tuning curve in parallel to a sharp filter representing the tip.

Acknowledgements

This study was supported by the Netherlands Organization for Scientific Research (NWO) and by the Heinsuius Houbolt Fund.

References

Antoli-Candela, F., and Kiang, N.Y.S. (1978) Unit activity underlying the N_1 potential. In: Evoked electrical activity in the auditory nervous system (Eds: Naunton, R.F., Fernandez, C.) Academic Press, New York, pp 165-189.

Boer, E. de (1975) Synthetic whole-nerve action potentials for the cat. J. Acoust. Soc. Am., 58, 1030-1045.

Harrison, R.V., Prijs, V.F. (1984) Single cochlear fibre responses in guinea pigs with long-term endolymphatic hydrops. Hear. Res. 14, 79-84.

Kiang, N.Y.S., Watanabe, T., Thomas, E.C., Clark, L.F. (1965) Discharge patterns of single fibers in the cat's auditory nerve. MIT Res. Monograph 35, Cambridge (Mass), MIT Press.

Liberman, M.C., Dodds, L.W. (1984) Single-neuron labeling and chronic cochlear pathology. III. Stereocilia damage and alterations of threshold tuning curves. Hear. Res. 16, 55-74.

Lütkenhöner, B., Hoke, M., Bappert, E. (1980) Effect of recovery properties on the discharge pattern of auditory nerve fibres. In: Cochlear and Brainstem Evoked Response Audiometry and Electrical Stimulation of the VIIIth Nerve (Eds: Hoke, M., Kauffmann, G., Bappert, E.) Scand. Audiol. Suppl. 11, 25-43.

Palmer, A.R., Russell, I.J. (1986) Phase-locking in the cochlear nerve of the guinea pig and its relation to the receptor potential of inner haircells. Hear. Res. 24, 1-15.

Prijs, V.F. (1986) Single unit response at the round window of the guinea pig. Hear. Res. 21, 127-133.

Salvi, R.J., Hamernik, R.P., Henderson, P. (1983) Response patterns of auditory nerve fibers during temporary threshold shift. Hear. Res. 10, 37-67.

Shamma, S.A., Chadwick, R.S., Wilbur, W.J., Morris, K.A., Rinzel, J. (1985) A biophysical model of cochlear processing: Intensity dependence of pure-tone responses. J. Acoust. Soc. Am. 80, 133-145.

Stokkum, I.H.M. van, Gielen, C.C.A.M. (1989) A model for the peripheral auditory nervous system of the grassfrog. Hear. Res. 41, 72-85.

Versnel, H., Prijs, V.F., Schoonhoven, R. (1989) Single-fibre and whole-nerve responses to acoustic click stimuli in noise-damaged cochleas, presented at XXVIth Workshop on Inner Ear Biology, Paris, abstr. P 76.

Versnel, H., Prijs, V.F., Schoonhoven, R. (1990) Single-fibre responses to clicks in relationship to the compound action potential in the guinea pig. Hear. Res. 46, 147-160.

Section 5

Emissions

Can basilar membrane tuning be inferred from distortion measurement?

A.M. Brown and S.A. Gaskill

Laboratory of Experimental Psychology
University of Sussex, Falmer, Brighton, BN1 9QG, UK

Introduction

As the frequency of two tones progressively converge, an increasing number of distortion sidebands of the family $(n+1)f1-nf2$ (where n is a positive integer) can be detected in cochlear electrical and mechanical responses. If the distortion is measured in the ear canal sound pressure when the stimulus levels are low, each distortion component follows a simple pattern of a rise to a maximum in magnitude, followed by a decline, often to the noise floor, as the f1 and f2 frequencies approximate (Wilson, 1980; Brown & Kemp, 1985; Harris *et al.*,1988). Distortion has its origin at the stimulus frequency place for the higher frequency stimulus (f2) in the cochlea (Hall, 1980; Kim *et al.*,1980), so it is somewhat surprising that distortion level decreases as its own frequency approaches that of f2. The aim of this work was to see whether the distortion-generating mechanism itself is being suppressed as the stimuli are approximated in frequency or whether the distortion is being subjected to some secondary filtering.

Methods

The distortion was measured in the ear canal using specially designed probes containing two loudspeakers (Knowles 1712) and a microphone (Knowles 1842). The microphone response was amplified (60 dB) and fed to a Hewlett Packard 3561A spectrum analyser. The measurement of human and rodent emissions has been described elsewhere (Brown,1987;Gaskill & Brown,1990) and differed in the two species only in the use of different sized probes and the administration of anaesthetic to immobilise the rodents.

Nine normal hearing human subjects (10 ears) and seven pigmented guinea pigs were used in this study. Each subject was tested to see whether distortion fell within normal limits by measuring 2f1-f2 distortion at $^1/_3$ rd octave intervals across the stimulus frequency range 500 to 9800 Hz for humans and 2 to 19.8 kHz for guinea pigs (distortion 'audiograms'). The stimulus frequency separation was set according to the f2/f1 ratio of 1.225 and stimulus levels were 50/55 dB SPL for L1 and 35/40 dB SPL for L2 (Gaskill & Brown,1990; Brown & Gaskill,1990).

In order to study the effect of stimulus frequency separation on distortion level, the frequency of f2 was fixed and the frequency of f1 was determined by f2/R, where R=1.01 to 1.4 in steps of 0.01. The frequency of f2 was chosen from those frequencies which gave relatively high levels of 2f1-f2 in the distortion 'audiogram' and ranged from 1587 to 6349 Hz in humans and 6349 to 10080 Hz in guinea pigs.

The highest levels of distortion are generated when L1 is greater than L2, and this is particularly true at low stimulus levels (Gaskill & Brown, 1990). Therefore, to maximise distortion levels, stimulus levels were set with L1 32 to 0 dB higher than L2 on a graded scale (*e.g.*, for L2=10 dB SPL, L1 =42 dB SPL and for L2 = 65 to 70 dB SPL, L1=L2). For each stimulus frequency ratio, the level of each distortion component was computed using an effective analysis bandwidth of 0.25 or 0.125 Hz.

Sound levels are in dB re 20 μPa.

Results

With an f2 stimulus level of 35-40 dB SPL, f1 set 15-18 dB higher in level, and an f2/f1 ratio of 1.1, it is possible to detect up to three lower sidebands above the noise floor. If the separation of the two tones is varied, each distortion component can be seen to peak at different f2/f1 ratios. Figure 1 shows examples from a guinea pig and a human ear of the changing level of two distortion components, 2f1-f2 and 3f1-2f2, as a function of stimulus frequency separation, with f2 fixed in frequency and f1 varying. The human example shows a clear peak, but it is not always so clear owing to peaks and troughs in distortion level which tend to obscure the overall trend, particularly when f2 was low in frequency.

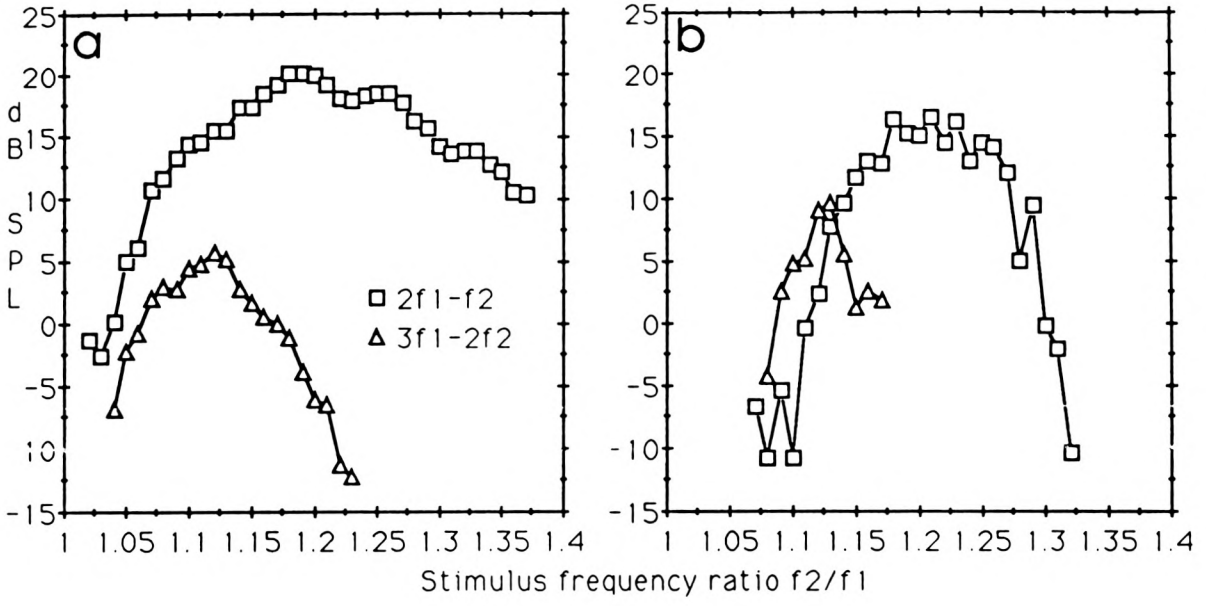

FIGURE 1 Distortion magnitude as a function of stimulus frequency ratio f2/f1
a) guinea pig f2=8000 Hz; L2=40 dB SPL; L1=55 dB SPL
b) human f2=5039 Hz; L2=40 dB SPL; L1=55 dB SPL

If the data is replotted to show the distortion level as a function of its own frequency (see figure 2), it is clear that both components have magnitude maxima at a common frequency. This frequency is approximately half an octave below f2.

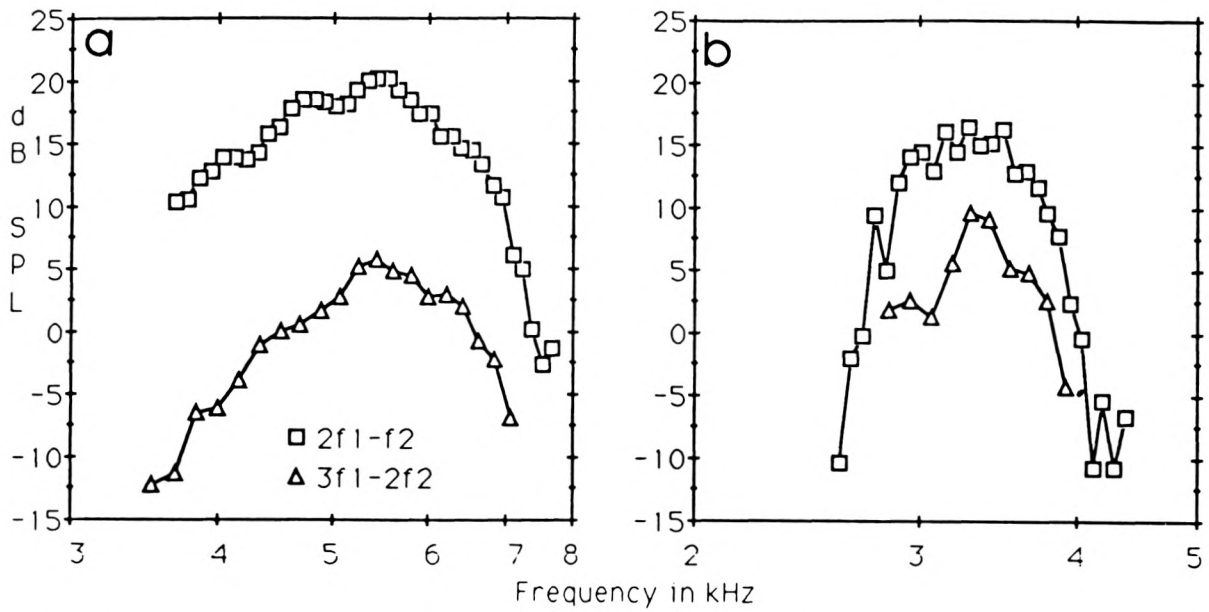

FIGURE 2 Distortion magnitude as a function of frequency. Data as in figure 1.

The half octave relationship holds for all distortion components measured at all f2 frequencies studied in both guinea pig and human ears, provided the level of f2 does not exceed 40 dB SPL (in some guinea pigs the relationship was lost for L2 above 35 dB SPL). If all data was grouped regardless of component order (2f1-f2, 3f1-2f2 *etc*) and frequency of the f2 stimulus (L2 at or below 40 dB SPL), the components peaked at a frequency 0.552 (sd 0.08) of an octave below f2 for the 34 human measurements made, and 0.567 (sd 0.14) of an octave below f2 for the 12 guinea pig measurements. By implication (and from previous experiments where f1 was fixed), there is no relationship between the f1 frequency and the frequency at which distortion components collectively reach their maximum level.

The peak in distortion is fairly broadly tuned with asymmetric slopes; the high-pass being more gradual than the low-pass. If all components at all frequencies are considered together, the Q_{10} for the human data (34 measurements) gave an average of 2.64 (sd 0.18), with low pass slope at the 3 dB down point of 100 dB/octave (sd 5.7) and high pass at the 3dB down point of 72 dB/octave (sd 4.1). The equivalent calculations for the 12 guinea pig measurements gave a Q_{10} of 1.5 (sd 0.16), low pass slope of 83 dB/octave (sd 11.29) and high pass of 46 dB/octave (sd 6.1). The rate of decline in level of 2f1-f2 (from its peak to about 10 dB down) as the stimuli converge is apparently independent of the level of either of the stimuli, provided that the level of f2 does not exceed 40 dB SPL. This is shown for both guinea pig and human ears in Figure 3. At the higher levels (but still below 40 dB SPL for f2), the decline at higher frequencies becomes steeper and the peak becomes progressively broader towards low frequencies (see open circles figure 3a).

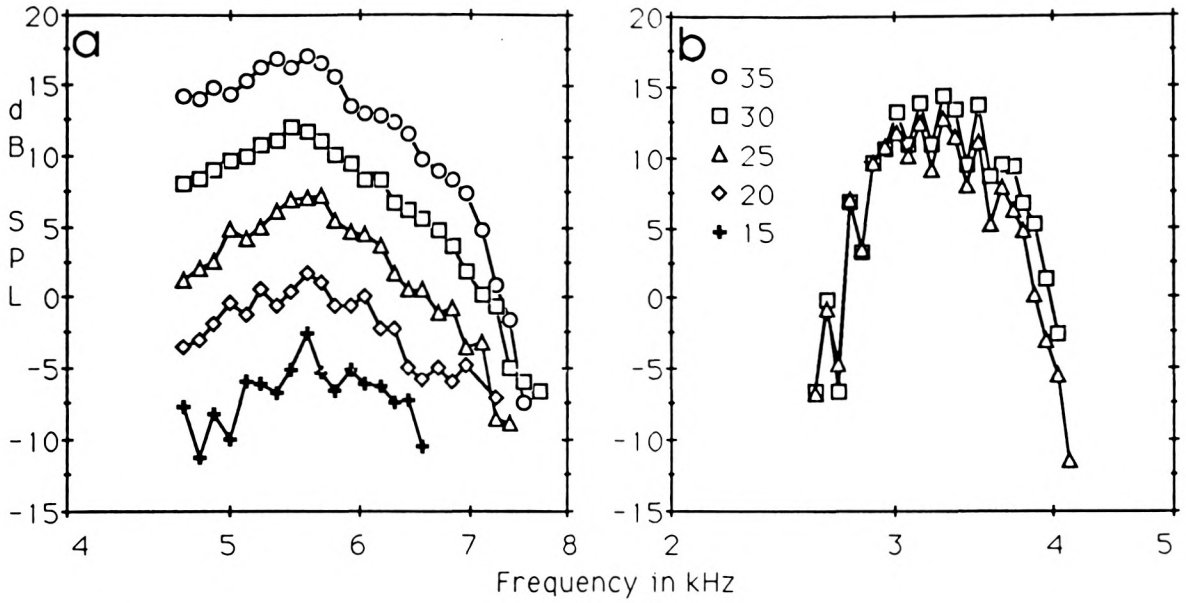

FIGURE 3 2f1-f2 level plotted as a function of its frequency for varying L2.
a) Guinea pig. L2=15 to 35 dB SPL, as shown on graph. Level difference in dB between L1 and L2 decreasing from 33 to 18 in 3 dB decrements. b) Human L2=25 and 30 dB SPL.
Note the fine structure in the human response which is repeated at both stimulus levels.

The levels of four lower sidebands are shown in figure 4 for both guinea pig and human ears when a relatively high level (60 dB SPL) f2 is used. For f2 levels above 40 dB SPL (sometimes 35 dB for guinea pigs), the frequency relationship between the distortion components is lost: the 2f1-f2 peak tends to shift down in frequency, and at the same time relatively more 2f1-f2 and 3f1-2f2 are measurable when the stimuli are close in frequency.

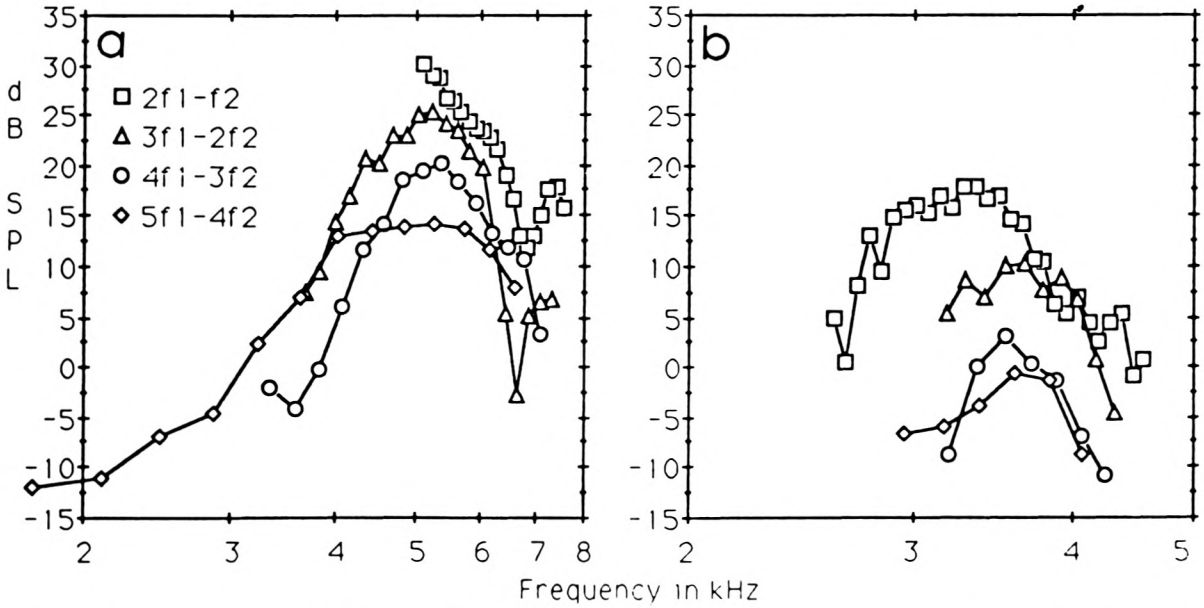

FIGURE 4 Four distortion components as a function of frequency using high level stimulation: L2=60 dB SPL; L1=62 dB SPL. a) guinea pig; f2=8000Hz. b) human; f2=5039 Hz

Discussion

The distortion we measure using low levels of sound stimulation (L2 ≤ 40 dB SPL) reaches its maximum level when the distortion frequency, regardless of component or f2 frequency, falls just over half an octave below the high frequency stimulus. Distortion level declines at a common frequency as the stimuli diverge, indicating that a high pass filter is in operation. This conclusion was also drawn some time ago by Smoorenburg (1972) as a result of his psychoacoustic studies on intermodulation distortion. The fact that the distortion also declines in level as the stimuli *converge* only came to light when 2f1-f2 distortion was measured as an oto-acoustic emission (Wilson, 1980). We have been able to show that all distortion components decline similarly as a function of their frequency. This suggests low pass filtering of the distortion components rather than the distortion-generating process being inactivated or suppressed by the proximity in frequency of the stimuli, since each component maximum (2f1-f2, 3f1-2f2 *etc*) occurs for a different stimulus frequency separation.

What is the relationship on the cochlear partition between f2 and the frequency half an octave below? Experiments using traumatic levels of sound (*eg*. Cody & Johnstone, 1981) have led us to believe that the region of enhanced mechanical vibration in the cochlea is half an octave below (in frequency) or apical (along the cochlear partition) to the peak of passive BM response to the same frequency. The enhanced vibration for a frequency of 8kHz is, therefore, also the region of a passive travelling wave peak for a frequency one half octave below this (5.6 kHz). The source of the relatively 'low - Q' filter, the presence of which which we have inferred from distortion magnitude data, may therefore be the passive mechanics of the BM at the f2 place which is 'tuned' to the lower frequency. An alternative explanation, and one which would accord with Allen's nonlinear model (see Allen, J.B., in this volume) is that the tectorial membrane is responsible for this filtering as the TM (according to the model) will have a low impedance at a frequency half an octave below f2 and will transmit substantial vibration to the cochlear fluids at this frequency. The loss of a clear band-pass characteristic at higher stimulus levels may be associated with the broadening of the vibration pattern in a basalward direction and the consequent increase in the spatial distribution of distortion generation. The distortion generated by low-level stimuli probably has a relatively discrete origin on the cochlear partition and shows the filter characteristic clearly. As the stimulus levels are increased and the number of distortion generating sites with varying phase relations increase, cancellation of out-of-phase components obscures the band-pass filtering so clearly demonstrated at low stimulus levels.

In summary, our findings suggest *either* that the basilar membrane is filtering the response at the f2 place due to its 'passive' properties *or* that there is some other structure, most likely the tectorial membrane, which is responsible for filtering the distortion before it reaches the ear canal.

Acknowledgement

This work was supported by the Medical Research Council

References

Brown, A.M. (1987) Acoustic distortion from rodent ears: a comparison of responses from rats, guinea pigs and gerbils. Hear.Res. 31,25-39.

Brown, A.M. & Gaskill,S.A. (1990) Measurement of acoustic distortion reveals underlying similarities between human and rodent mechanical responses. J.Acoust.Soc.Am.,88 (July)

Brown, A.M. & Kemp, D.T. (1985) Intermodulation distortion in the cochlea: Could basal vibration be the major cause of round window CM distortion? Hear.Res.,19,191-198.

Cody, A.R. & Johnstone, B.M. (1981) Acoustic trauma: Single neuron basis for the 'Half-Octave' shift. J.Acoust.Soc.Am.,70,707-711.

Gaskill, S.A. & Brown, A.M. (1990) The behaviour of the acoustic distortion product, 2f1-f2, from the human ear and its relation to auditory sensitivity. J.Acoust.Soc.Am.,88 (July)

Harris, F.P., Lonsbury-Martin, B.L..,Stagner, B.B.,Coats, A.C. & Martin, G.K. (1989) Acoustic distortion products in humans: Systematic changes in amplitude as a function of f2/f1 ratio. J.Acoust.Soc.Am.85,220-229.

Hall, J.L. (1980) Cochlear models; evidence in suport of mechanical nonlinearity and a second filter. Hear.Res. 2,455-464.

Kim, D.O. ,Molnar, C.E. & Matthews, J.W. (1980) Cochlear mechanics: nonlinear behaviour in two-tone responses as reflected in cochlear-nerve-fibre responses and in ear canal sound pressure. J.Acoust.Soc.Am. 67,1704-1721.

Smoorenburg, G.F. (1972) Audibility region of combination tones. J.Acoust.Soc.Am., 52,603-614.

Wilson, J.P. (1980) The combination tone, 2f1-f2, in psychophysics and ear canal recording. In 'Psychophysical, Physiological and Behavioural Studies in Hearing. eds. G. van den Brink & F.A. Bilsen. Delft Univ. Press, Delft, the Netherlands. pp 43-50.

CHANGES IN STIMULUS FREQUENCY OTOACOUSTIC EMISSIONS PRODUCED BY TWO-TONE SUPPRESSION AND EFFERENT STIMULATION IN CATS

John J. Guinan Jr.

Dept. of Elec. Eng. & Comp. Sci., and Research Lab of Elec., Mass. Inst. of Tech.
Eaton-Peabody Lab, Mass. Eye & Ear Infirmary, 243 Charles St., Boston MA 02114.

Summary

Efferent activity and two-tone suppression might affect the cochlear amplifier at different sites but produce similar effects. Their effects on stimulus-frequency otoacoustic emissions (SFEs) were compared in cats by measuring the vector change in ear-canal sound pressure. The results indicate that contributions to the SFE originate along a large fraction of the length of the cochlea, and that SFEs may provide a 'window' into the action of the cochlear amplifier.

Introduction

Considerable evidence indicates that the high sensitivity and frequency selectivity of the mammalian cochlea is produced by active mechanical processes in outer hair cells (OHCs). Mountain et al (1983) have hypothesized that this 'cochlear amplifier' consists of a feedback system formed by a mechanic-to-electric (ME) transducer, centered around the OHC stereocilia, coupled to an electric-to-mechanic (EM) transducer, perhaps in the OHC cell body. Such cochlear amplifiers are located all along the basilar membrane and are coupled by the fluid and by passive cochlear mechanics. With this hypothesis, cochlear emissions are due to the outputs of the EM transducers.

This hypothesis suggests that two-tone suppression and inhibition by medial olivocochlear efferents might be due, in part, to similar mechanisms. Two-tone suppression might be due to the suppressor tone driving the ME transducer into partial saturation thereby reducing its gain (Geisler et al, 1990), and efferent inhibition might be due to a reduction of the gain of the EM transducer. Since both agents might produce similar reductions in the overall gain of the cochlear amplifier, they might both produce similar reductions in cochlear emissions. These ideas led us to compare the effects of two-tone suppression and efferent stimulation on cochlear emissions.

We examined changes in stimulus frequency otoacoustic emissions (SFEs). Unlike distortion products, SFEs do not require a nonlinearity for their production and may be generated by linear processes, e.g. by the array of EM transducers in response to the traveling wave. We already have data on the effects of stimulation of medial olivocochlear efferents on SFEs in cats (Guinan 1986, 1990). Data on the effects of two-tone suppression on SFEs are available for man (Kemp and Chum, 1980), but not for

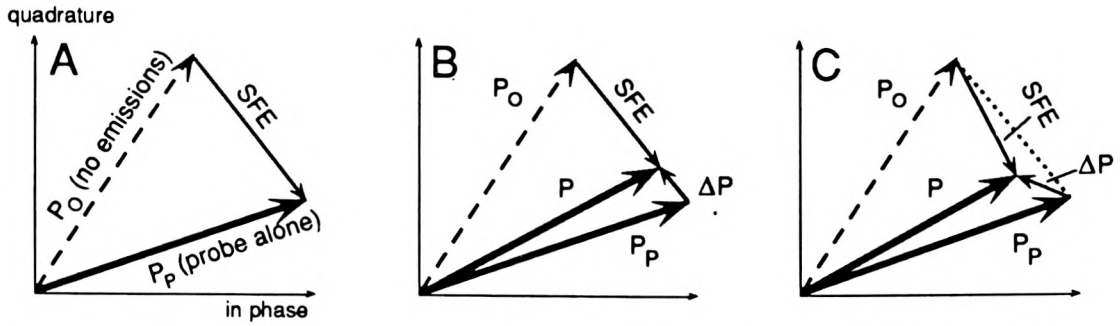

FIGURE 1 Vector diagrams showing the relationship of ΔP to the SFE. In each panel, the sound pressure, P, is the sum of the pressure with no emissions, Po, and the SFE. **A**: P = Pp = the pressure with the probe tone alone, SFE = the baseline SFE, **B,C**: the SFE is altered by two-tone suppression or efferent activity. ΔP = P - Pp. In B, the altered SFE has the same phase as the baseline SFE.

cats. We present here preliminary data on basic properties of SFEs in cats, and on the interactions of efferent stimulation and two-tone suppression.

Methods

Our methods were similar to those of Guinan (1986). Briefly, we anesthetized cats with Dial in urethane and stimulated medial efferents with an electrode at the floor of the fourth ventricle. On cats with efferent stimulation, the middle-ear muscles were cut. We used an acoustic system sealed into the ear canal with probe and suppressor tones generated by separate transducers (B&K 4136 and DT 48). Sound pressure was measured with a B&K 4179 and corrected to obtain the sound pressure near the tympanic membrane.

Sound pressures were analyzed by a lockin amplifier into in-phase and quadrature components which were sampled and averaged by a computer. As shown in Fig. 1A, the probe-tone sound pressure, Pp, is assumed to be the sum of a pressure generated by the source if there were no emissions, Po, plus the SFE (Kemp & Chum, 1980). Kemp and Chum assumed that Po is a scaled version of the pressure measured at a high sound level (at which emissions are presumed to be negligible). We avoided using Po and expressed evoked changes in sound pressure as ΔP, the vector change in ear-canal sound pressure relative to the pressure with the probe tone alone (Fig. 1 B,C). As a first approximation, ΔP can be thought to result from the removal of part of the SFE which is normally present with the probe tone (see Fig. 1). We have mostly studied ΔP's using probe tones at 40 dB SPL. Spot checks with probes at 20-50 dB SPL produced similar results.

Results

Changes in ear-canal sound pressure produced by two-tone suppression, ΔPtt, or by stimulation of olivocochlear efferents, ΔPoc, could be measured over a very wide range of probe frequencies (0.2-30 kHz). Suppressor tone bursts produced ΔPtt's with fast rise and fall times (a few ms or less) whereas efferent stimulation produced ΔPoc's with much slower rise and fall times (tens of ms) (Fig. 2). We have never seen a ΔPoc, or a component of ΔPoc, with a rise time of a few ms. Sometimes, high-sound-level suppressors produced ΔPtt's with long, low amplitude "tails" which may be due to the

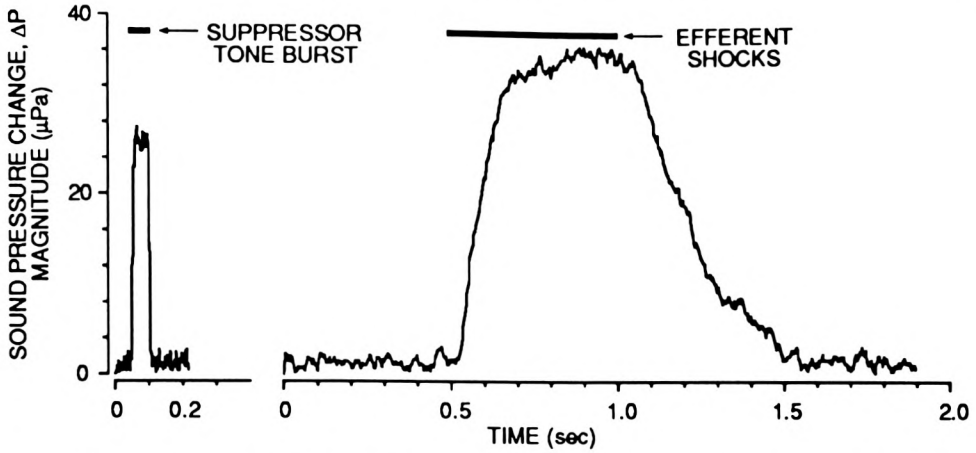

FIGURE 2 Time courses of ΔP's at 8 kHz produced by suppressor tone bursts (left) or efferent shocks (right). Suppressor tone bursts were 11 kHz, 40 dB SPL, 50 ms duration, 4/s (512 responses averaged). Efferent shocks were 200/s for 500 ms, every 2.05 sec (64 responses averaged). The continuous probe tone was 8 kHz, 40 dB SPL. Cat 36.

suppressor tone evoking efferent activity and a ΔPoc. To minimize efferent activity evoked by the suppressor, we used short, low-duty-cycle suppressors (usually 50 ms every 251 ms).

Suppressor tones had different effects depending on their frequency and level (Fig. 3). For suppressor frequencies near and below the probe frequency (Fig. 3A), ΔP magnitude usually increased monotonically as the suppressor level was increased and ΔP phase stayed within about one quadrant for different suppressor levels and frequencies. These data are consistent with the idea that increasing the level of the suppressor removed increasing parts of the SFE produced by the probe tone.

For suppressor frequencies well above the probe frequency (Fig. 3 B,C), the relationship of ΔP to suppressor level and frequency was complex. For low-level suppressors, the phase of ΔP varied across frequency throughout all quadrants. For high-level suppressors, the phases were again within about one quadrant. Thus, the pattern of ΔP appears to be different for low-level and high-level suppressors. The transition from low-level to high-level regions was shown in some suppressor level functions by a dip and sometimes by an abrupt phase change. In some ways, the pattern of ΔP's from high-frequency, high-level suppressors was similar to the ΔP's from low-frequency suppressors. However, more data are needed for this relationship to be fully understood.

Insight into the relationship of ΔP and suppressor frequency is provided by Fig. 4. This figure shows that for suppressor frequencies near and below the probe frequency, ΔP phase was relatively constant, and ΔP magnitude was low. For higher frequencies, ΔP phase increased monotonically with suppressor frequency, and ΔP magnitude peaked each time ΔP phase was the same as the phase from low-frequency suppressors. Our data suggest that the phase pattern in Fig. 4 is representative for most combinations of low to moderate sound-level probes and suppressors. We need more data to determine whether the magnitude pattern in Fig. 4 is representative. Our interpretation of these data is that the ΔP from a low-level, high-frequency suppressor is the suppression, or removal, of SFE components which originate from the cochlear region tuned to the suppressor tone. With this interpretation, the data in Fig. 4 indicate that substantial contributions to the SFE arise from wide areas along the length of the cochlea and that the phase of these contribution varies greatly along the length of the cochlea.

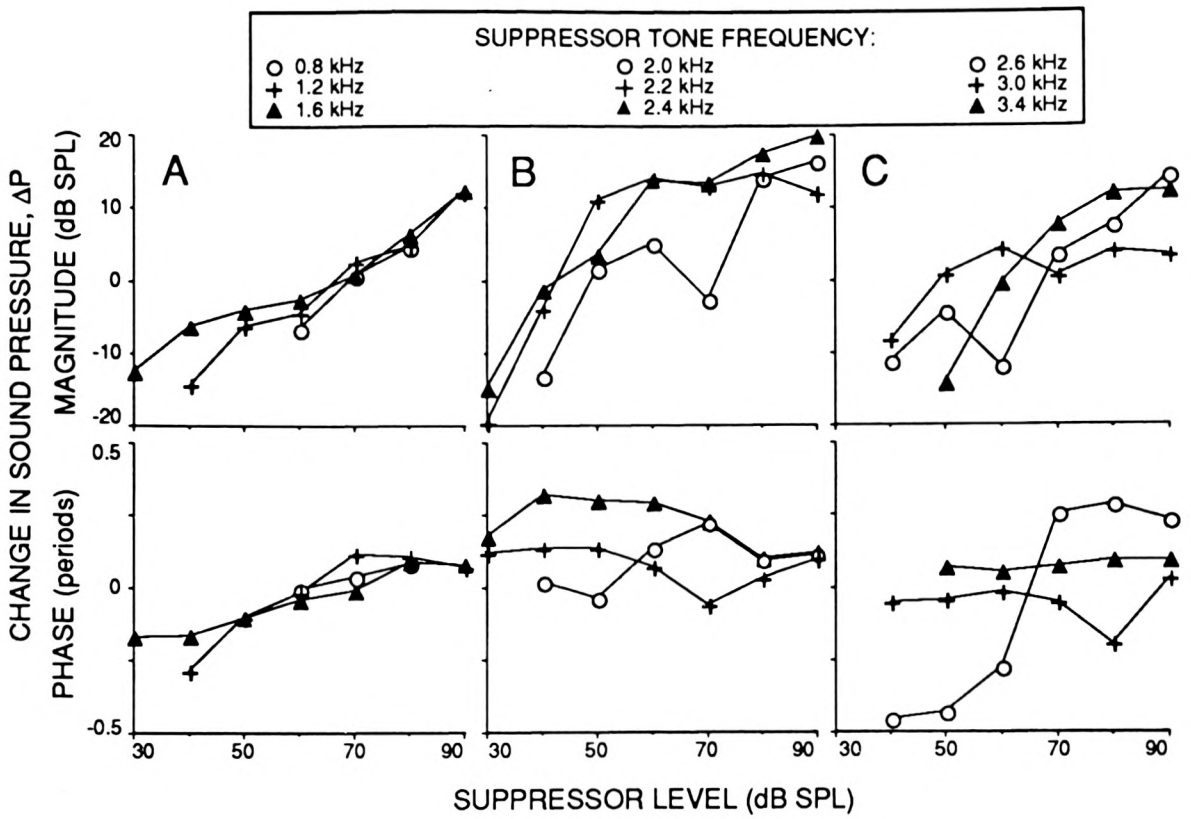

FIGURE 3 ΔP's at 1.8 kHz produced by suppressor tones of various frequencies and levels. Suppressor tone bursts were 50 ms duration, 4/s. Each point is an average from 128 or more responses in a 30 ms window beginning 20 ms after the suppressor onset. The continuous probe tone was 1.8 kHz, 39 dB SPL. Cat 39.

Changes in sound pressure produced by efferent stimulation were relatively simple. Usually, as the magnitude of ΔPoc increased, the phase of ΔPoc was constant (Fig. 5). At low probe-tone levels, ΔPoc magnitude from strong efferent stimulation was normally just a few dB below the SFE magnitude, and ΔPoc phase was approximately opposite to the SFE phase (Guinan, 1990). This indicates that ΔPoc results from the removal of a large fraction of the SFE. In other words, efferent activity suppresses SFEs.

We have preliminary data comparing ΔP's produced by efferent stimulation and suppressor tones on the same cat and with the same probe tone (e.g. Fig. 6). In the three cases in which the suppressor frequency was near or below the probe frequency, the phase of ΔPoc was similar (i.e. in approximately the same quadrant) to the phase of ΔPtt (e.g. Fig. 6 bottom-left). When efferent and suppressor stimuli were presented simultaneously, the resulting pressure change (ΔPoc+tt in Fig. 6) also had a similar phase. In contrast, with high-frequency, low-level suppressors, the phase of ΔPtt was sometimes very different from the phase of ΔPoc, and the ΔPoc+tt resulting from simultaneous presentation of the stimuli was almost a vector addition of the separate ΔPoc and ΔPtt (Fig. 6 bottom- right).

Discussion

Let us consider in more detail ΔP as a function of suppressor frequency (Fig. 4); it provides the key to understanding the origin of SFEs. First, note that the ΔP's in Fig. 4

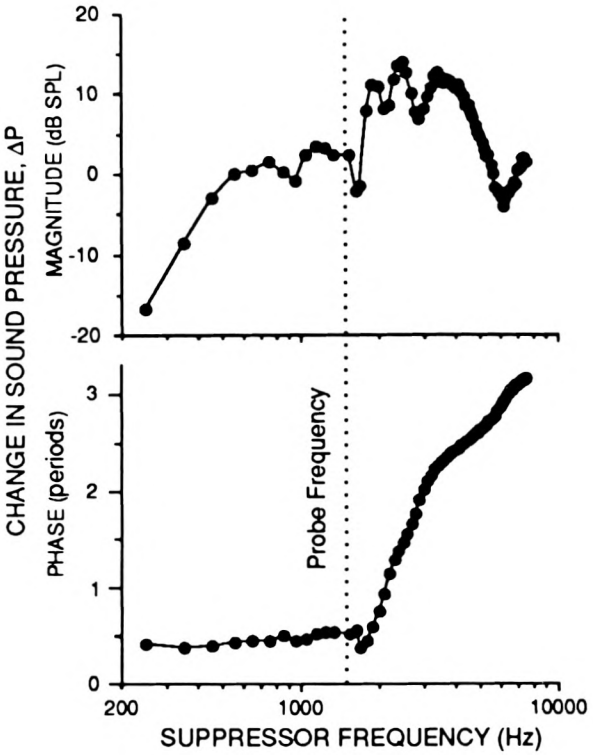

FIGURE 4 ΔP's at 1.5 kHz produced by suppressor tones of various frequencies. Suppressor tone bursts were 50 ms duration, 4/s at 60 dB SPL. Each point is an average from 64 responses in a 30 ms window beginning 20 ms after the suppressor onset. The continuous probe tone was 1.5 kHz, 41 dB SPL. Cat 40.

are changes in the ear-canal sound at the *probe* frequency, 1.5 kHz. When a suppressor tone is added, say at 8 kHz, basilar membrane motion in response to the suppressor is large at the 8 kHz place and drives the ME transducer into partial saturation. This saturation decreases the response of the ME transducer to the *probe* tone and thus decreases the mechanical output from the EM transducer at the *probe* frequency. The result is a decrease in the contribution to the probe-tone SFE from the 8 kHz place, the cochlear region tuned to the suppressor tone. This decrease of locally generated SFE is probably the major factor which produces the ΔP for the 8 kHz suppressor in Fig. 4.

At the cochlear place tuned to the suppressor tone, the 8 kHz place in our example, the reduced mechanical output from OHCs may reduce the amplitude of the probe-tone forward traveling wave. How much it does this will depend on how much amplification of the probe-tone 1.5 kHz response was provided by the 8 kHz cochlear place which, in turn, is dependent on many factors including the phase of the OHC mechanical output relative to the motion of the basilar membrane. If the suppressor reduces the forward traveling wave at 1.5 kHz, then the suppressor will also reduce 1.5 kHz SFE contributions from sources apical to the 8 kHz place. However, for very low-level suppressors at which the change in the forward traveling wave is minimal, the suppressor phase pattern must be similar to that shown in Fig. 4, because for low suppressor levels, the phase is constant for a given suppressor frequency (Fig. 3 B,C). Considering this, we think that the ΔP pattern in Fig. 4 is due largely to local effects at the cochlear place tuned to the suppressor. As suppressor level increases, suppression of the forward traveling wave might become an increasing fraction of the total effect and cause the change from the ΔP pattern for low-level suppressors in Fig. 3 B,C to the ΔP pattern for high-level suppressors.

For suppressor frequencies well below the probe frequency, suppression must occur in a different way. Considerably apical to the cochlear place tuned to the 1.5 kHz probe tone, there is almost no motion at the probe frequency. Thus, for very low frequency suppressors, the suppression probably occurs near the 1.5 kHz cochlear place, where the

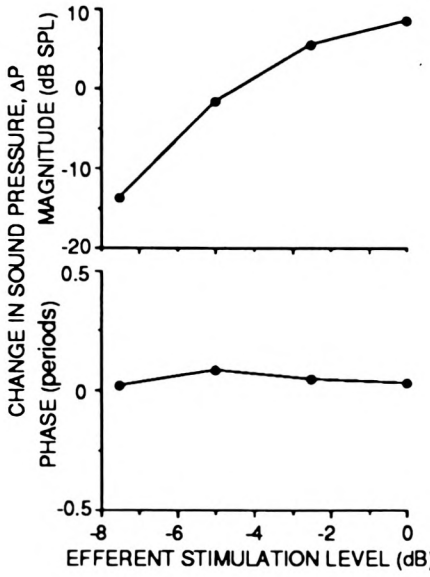

FIGURE 5 ΔP's at 8 kHz produced by efferent stimulation. Efferent shocks were 200/s for 1 sec, every 3 sec. Each point is an average from 64 responses in a 300 ms window beginning 250 ms after the shock onset. The continuous probe tone was 8 kHz, 40 dB SPL. Cat 35.

probe tone, by itself, drives the ME transducer into partial saturation. There, because of the shape of the ME transducer nonlinearity, the addition of the suppressor tone will produce a small net increase in the saturation of the ME transducer, and a reduction of the mechanical output at the probe frequency.

Note that the largest ΔP's were found for suppressor frequencies above the probe frequency, and not, for instance, at the probe frequency (Fig. 4). This correlates with a variety of data which indicate that the active region at which the cochlear amplifier has significant effect is basal to the peak of the traveling wave. Since, according to the Mountain et al. (1983) model, a change in the SFE indicates that the output of the cochlear amplifier was changed, the suppressor tone data are, in a sense, showing where the active region is for the 1.5 kHz probe tone.

Studies of basilar membrane motion indicate that the response of the basilar membrane to a probe tone is close to linear except near the cochlear place tuned to the probe tone. Thus, except in this region, contributions to the SFE may be generated by linear processes, and may grow linearly with probe-tone level. The measured overall growth of SFEs is usually only slightly less than linear, which is consistent with our conclusion that a significant fraction of the SFE originates from cochlear regions distant from the place tuned to the probe tone.

Considering all of these ideas, we propose the following hypothesis to account for the origin of SFEs in cats. SFEs originate from a wide area basal to the cochlear place tuned to the probe tone. The contributions from different places vary greatly in phase, but since larger magnitudes are found for certain phases, SFE components from along the cochlea add to produce a net SFE. Shock-evoked efferent activity produces effects which are greatest in the central part of the cochlea, but which extend throughout the length of the cochlea. Thus, it is likely that efferent activity depresses SFE contributions which originate all along the length of the cochlea. This is consistent with our data which show that shock-evoked efferent activity can remove most of the SFE. Finally, the additivity of ΔP's produced by efferent activity and two-tone suppression depends on a variety of factors including: the extent to which these agents act at the same place in the cochlea, the degree of nonlinearity in the generators of SFEs, and on how much efferent activity reduces the basilar membrane response to the suppressor tone alone.

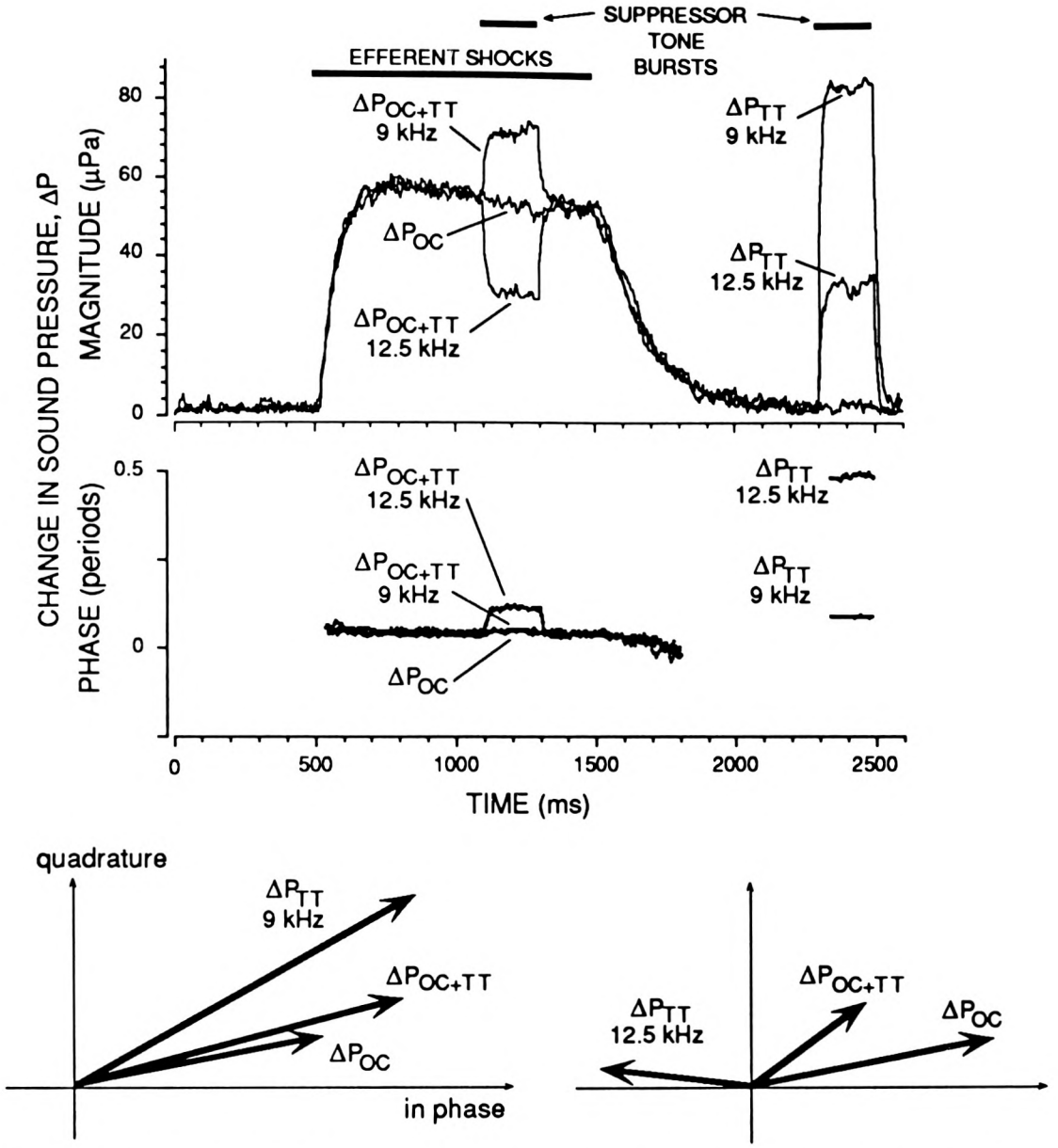

FIGURE 6 ΔP's produced by efferent stimulation and two-tone suppression. TOP and MIDDLE: Magnitudes and phases of three average responses to bursts of efferent shocks at 200/s every 3 sec. One average response had no suppressor tones, one had pairs of suppressor tone bursts at 9 kHz, 60 dB SPL, and one had pairs of suppressor tone bursts at 12.5 kHz, 35 dB SPL. The first suppressor burst was during the efferent shocks and the second was after the efferent effects had died away. Phase is shown only when it was well defined, i.e. for ΔP > 10 μPa. BOTTOM: Vector diagrams of the above data. Each vector is an average from 64 responses in 175 ms windows which began 25 ms after the suppressor onset time and ended with the suppressor tones. The continuous probe tone was 8 kHz, 40 dB SPL. Cat 35.

It seems worth commenting on the fact that our results appear to differ from Kemp and Chum's (1980) description of the effects of suppressor tones on SFEs in man. Kemp and Chum found that suppressor tones reduced the magnitude of the SFE, but had little effect on the angle of the SFE (Fig. 1B). Kemp and Chum also found that an intense suppressor at a frequency close to the probe frequency removed essentially all of the SFE. In this case, ΔP would be the same amplitude as the unsuppressed SFE and of opposite

phase. We expected to obtain similar results in cats, and to be able to use the maximal ΔP from a suppressor tone as a measure of the SFE. This is one reason why in the suppressor-tone experiments we didn't measure the SFE by the scaling method of Kemp and Chum. We did not, however, find the largest ΔP's for suppressor frequencies near the probe frequency. Furthermore, for high-level suppressors at different frequencies, ΔP phases converged, but only to within a quadrant. We now plan to measure, in the same animals, ΔP from two-tone suppression and SFEs by the scaling method, and to compare the results.

Thus, there appear to be some real differences between our results and those of Kemp and Chum. One source of this difference may be species, cat vs. man. Another is methodological. We used tone bursts as suppressors and anesthetized animals, whereas Kemp and Chum used continuous tones and awake subjects. Continuous tones in awake subjects might elicit significant efferent activity, so that Kemp and Chum may have been measuring a combination of suppressive and efferent effects.

On the other hand, for low-level suppressors, much of the apparent difference between the two sets of data is probably due to the different methods used to analyze the data. We expressed our results as ΔP whereas Kemp and Chum used the SFE vector. If the phase of the suppressed SFE is constant for all suppressors, as in Fig. 1B, then the phase of ΔP is constant and there is little difference between the two methods. However, if ΔP can have any phase angle, as in Fig. 1C, then large phase variations in a small ΔP, will produce very little change in the phase of the suppressed SFE. Thus, our data showing large phase changes in ΔP may be consistent with Kemp and Chum's data for man, and there may be a high-frequency suppression region in man similar to the region in cat in which ΔP phase varies strongly with suppressor frequency.

Acknowledgements

We thank the many members of the Eaton-Peabody Laboratory who provided help throughout this work, particularly Drs. John Rosowski, Bertrand Delgutte, and Nelson Kiang for helpful comments. This work was supported by NIH grants R01 NS20269 and R01 DC00235.

References

Geisler, C.D. Yates, G.K. Patuzzi, R.B. and Johnstone, B.M. (1990) Saturation of outer hair cell receptor currents causes two-tone suppression. Hearing Res. 44,241-256.

Guinan, J.J., Jr. (1986) Effect of efferent neural activity on cochlear mechanics. Scand. Audiol. Suppl. 25,53-62.

Guinan, J.J., Jr. (1990) Inhibition of stimulus frequency emissions by medial olivocochlear efferent neurons in cats. (in prep)

Kemp, D.T. and Chum, R.A. (1980) Observations on the generator mechanism of stimulus frequency acoustic emissions - two tone suppression. In: Psychophysical, Physiological and Behavioral Studies in Hearing. (Eds: van den Brink, G. and Bilsen, F.A.) Delft Univ. Press. pp. 34-41.

Mountain, D.C. Hubbard, A.E. and McMullen, T.A. (1983) Electromechanical processes in the cochlea. In: Mechanics of Hearing. (Eds: deBoer, E. and Viergever, M.A.) Delft Univ. Press, pp 119-126.

GROWTH FUNCTIONS OF TONE BURST EVOKED AND DISTORTION-PRODUCT OTOACOUSTIC EMISSIONS IN HUMANS

F.P. Harris and R. Probst

HNO-Universitätsklinik
Kantonsspital, CH-4031 Basel, Switzerland

Introduction

Transiently evoked and distortion-product otoacoustic emissions (TEOAEs, DPOAEs) are both low-level acoustic phenomena that are measured in the human ear canal coincident with acoustic stimulation. Short-duration signals such as clicks or tonebursts stimulate TEOAEs. Two continuous signals that are closely spaced in frequency produce DPOAEs. There are similarities and differences in the characteristics of the two forms of emissions. Therefore, the extent to which they are being generated by the same mechanisms has not been determined.

It is known that both emissions are generated within the cochlea, are nonlinear, and probably involve an active component related to outer hair cells (e.g., Davis, 1983; Kemp, 1978; Zwicker & Lumer, 1985). Both are reduced in amplitude or are eliminated by processes that disrupt normal cochlear function (e.g., Harris, 1989; Kemp, 1979; Probst et al., 1990). External signals presented either ipsilaterally or contralaterally influence the level of both emissions (e.g., Kemp, 1979; Puel & Rebillard, 1990; Zwicker, 1983). The input-output or growth functions of TEOAEs and DPOAEs exhibit saturation with increases in stimulus levels (e.g., Kemp, 1979; Lonsbury-Martin et al., 1990). However, other properties of the growth functions and additional characteristics of the two emissions are not equivalent. Transiently evoked otoacoustic emissions may be produced by low-level stimuli and their levels are large relative to stimulus levels. In humans, TEOAEs exhibit unique spectral and temporal patterns when they are produced by broadband stimuli. In nonmammalian species, they are small and are difficult to detect (Kemp & Brown, 1983). In contrast, DPOAEs measured from humans are typically 50 to 60 dB below the stimulus levels. In nonhuman species, DPOAE levels range from 30 to 40 dB below the primary-tone levels (Kemp & Brown, 1984; Lonsbury-Martin et al., 1987). The input-output functions of DPOAEs depend strongly upon stimulus parameters and are characterized by irregularities (Gaskill & Brown, 1989; Harris et al., 1989; Lonsbury-Martin et al., 1990; Probst & Hauser, 1990). The relation of TEOAEs and DPOAEs is not fully understood.

In this study, the input-output or growth functions of both emissions were compared at the same frequency region in individual ears. Our purpose was to determine if the functions are subject to the same influences when they are generated by frequency-specific stimuli at comparable "presumed" generation sites within the cochlea.

Methods

SUBJECTS

Eight men and two women, ranging in age from 18 to 29 years (M = 23 years), were paid to participate as subjects. Subject selection criteria included good general health by history, hearing thresholds <15 dB HL from .25 to 8 kHz (including .75, 1.5, 3, and 6 kHz), normal immittance results, normal otoscopic check, and no spontaneous otoacoustic emissions (SOAEs) in the test ear. Distortion-product otoacoustic emissions and TEOAEs were measured in one ear of each subject. The sample consisted of three right and seven left ears. Click-evoked otoacoustic emissions obtained from all test ears had a broad frequency range.

STIMULI AND PROCEDURES

Emissions were elicited in the frequency regions of 1, 2, and 4 kHz using the stimuli that are described in Table 1. For DPOAEs, either the geometric mean of f1 and f2 (GM condition) or the f1 frequency (F1 condition) was at one of the three frequencies. A frequency separation ratio of f2/f1 = 1.22 was selected as being optimal for the generation of 2f1-f2 across frequency based upon the parametric studies of Harris et al. (1989) and Gaskill and Brown (1989). Stimulus levels varied by condition. In the GM condition, stimuli were equal in level and in the F1 condition, L2 was 15 dB below the level of L1. This difference in level was selected based upon results of parametric studies by Probst and Hauser (1990) and by Gaskill and Brown (1989) indicating that maximal distortion levels are measured with L1>L2. In both conditions, stimuli were decreased in 5 dB steps from 65 to 25 dB SPL (or until no response was observed in the spectrum above the system's noise floor). For TEOAEs, cosine-windowed tonebursts presented at a 20-ms rate were used as stimuli. They ranged in level from approximately 36 to 84 dB average peak intensity level in the ear canal and were presented in increasing 6-dB steps. For DPOAE measures, subjects were seated in a sound-treated enclosure and a probe, consisting of an ER-10 microphone and two ER-2 earphones, was placed securely in the outer ear canal using a foam eartip. Stimuli at f1 and f2 were generated by separate channels of an HP3326A frequency synthesizer, were delivered separately to each of the two earphones, and were mixed acoustically in the ear canal. The ear canal sound pressure

Table 1. Stimuli for eliciting transiently evoked and distortion-product otoacoustic emissions

Emission Type	Stimulus Region (kHz)		
TEOAE (tonebursts)	**1**	**2**	**4**
frequencies (kHz)	1	2	4
duration (ms)	3	3	2.5
DPOAE (2 pure tones)			
GM (kHz)	**1**	**2**	**4**
f1	0.905	1.81	3.621
f2	1.104	2.209	4.418
2f1-f2	0.706	1.411	2.824
F1 (kHz)	**1**	**2**	**4**
f2	1.22	2.44	4.88
2f1-f2	0.78	1.56	3.12
GM	1.104	2.209	4.418

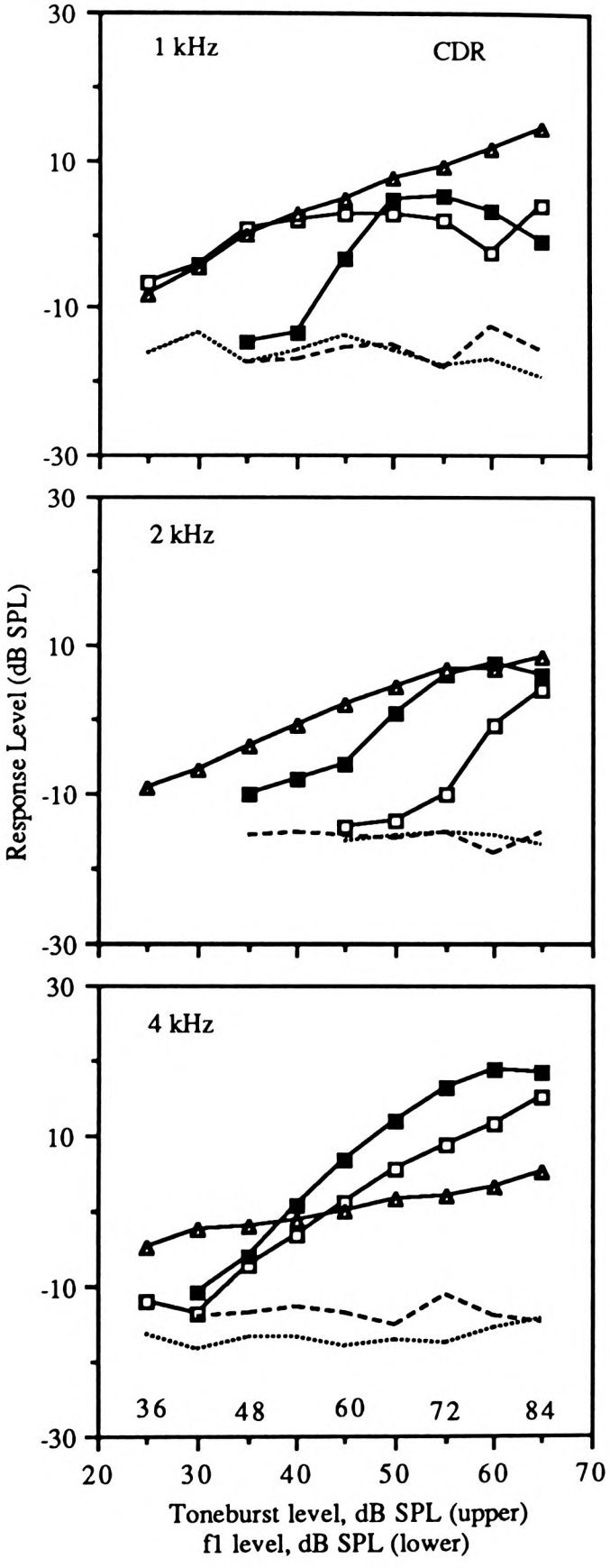

FIGURE 1 TEOAE and DPOAE growth functions for subject CD (TEOAE, triangles; DPOAE GM, open squares; F1, filled squares. Dotted and dashed lines represent the levels of the noise floor for the DPOAE conditions)

was detected by the microphone, and the output was led to an ER-72 preamplifier followed by a custom-built low-noise amplifier filter with a cutoff frequency of 400 Hz that provided 20 dB of amplification. Following amplification, 8 fast Fourier transforms of the output were sampled by an HP3561A signal analyzer. Frequency windows of 400 Hz for the 1 kHz condition and of 500 Hz for the 2 and 4 kHz conditions resulted in analysis bandwidths of 1.5 and 1.875 Hz respectively using a Hanning weighting function. The level of 2f1-f2 and of the noise floor at a representative adjacent frequency were recorded manually. Order of presentation of stimulus frequencies was counterbalanced across subjects.

All testing for TEOAEs was performed with an ILO88 Otodynamic Analyser (Otodynamics Ltd, 1988) controlled by a Compaq Portable III computer. Subjects were seated in a quiet laboratory environment for testing. A probe consisting of a loudspeaker and a microphone was sealed securely in the subject's ear canal using a foam earplug. One of the three tonebursts was presented at a gain setting on the instrument of -30 dB (approximately 36 dB SPL) and 256 samples of the ear canal sound pressure were averaged in the 20 ms poststimulus time. Averaged responses were bandpass filtered and stored for later analysis. The selected stimulus then was increased in consecutive 6-dB steps until averaged responses were obtained for nine levels. This procedure was repeated for the two remaining frequencies.

Results were analyzed using a repeated-measures analysis of variance type model with SAS on a VAX 8830 computer and with Statview II on a Macintosh IIX computer.

Results

Slopes of the growth functions for both TEOAEs and DPOAEs were calculated on their linear portions using a least-squares regression technique. Growth functions were compared both within and across stimulus conditions.

The structure of the growth functions for DPOAEs and for TEOAEs varied by stimulus condition. Distortion-product otoacoustic emission functions were characterized by saturation, rollovers, and irregularities as listed in Table 2. Saturation and rollover occurred when L1 was above 50 dB SPL and were more common in the F1 than in the GM condition. Rollovers and irregularities were present only with stimuli in the 1 and 2 kHz regions. Growth functions of TEOAEs did not exhibit the dips and rollovers that were characteristic of the DPOAE functions. For the range of stimulus levels used, functions were predominantly linear. This finding is illustrated in Figure 1 where the results for one subject are displayed. The DPOAE functions became more linear as frequency increased.

Mean slopes (+/- 1*SD*) for both TEOAEs and DPOAEs are illustrated in Figure 2. For both the GM and F1 DPOAE conditions, slopes increased as the stimulus-frequency region increased. Mean slopes ranged from .66 to .95 for the GM condition and from .90 to 1.04 for the F1 condition. Within a frequency region, GM and F1 slopes were not significantly different from each other. In contrast to the DPOAE functions, TEOAE slopes decreased as frequency increased (M = .54, .45, .28 for the three frequencies respectively). Because of the large differences in variance between the DPOAE and TEOAE slopes (see Figure 2), data were transformed logarithmically for general statistical analysis. Overall analysis of the DPOAE and TEOAE results revealed a significant difference [F (53,34) = 5.81, p<.0001]. Only at 4 kHz were both GM and F1 DPOAE slopes significantly different from the TEOAE slopes (p<.0001). At 2 kHz, the F1

Table 2. Categories of DPOAE growth functions

Stimulus region (kHz)	LIN	SAT	ROLL	IRR	NR
1 GM	6	1	0	3	-
1 F1	1	3	6	-	-
2 GM	7	-	-	2	1
2 F1	4	1	3	1	1
4 GM	10	-	-	-	-
4 F1	3	7	-	-	-

Changes in DPOAE level with L1, L2

LIN (Linear): >2 dB increase with increasing 5-dB steps
SAT (Saturation): <2 dB change with L1>50 dB SPL
ROLL (Rollover): >2 dB decrease with L1>50 dB SPL
IRR (Irregular): flat, low level response, dips
NR (No response): <6 dB above noise floor

slopes differed from the TEOAE slopes (p=.0285), and at 1 kHz none of the slopes were significantly different from each other.

Individual emission levels were compared for DPOAEs obtained with L1 from 50 to 65 dB SPL and TEOAEs obtained with stimuli at 66 dB SPL at each frequency region. Maximum DPOAE levels were measured for all ears for this range of stimulus levels in either condition. Results for the three conditions are illustrated in the scatterplots in Figure 3. The 4 kHz results were not combined with the 1 and 2 kHz results because of the significant differences in their characteristics. Levels of DPOAEs and comparable TEOAEs were correlated (r=.83; r=.89; r=.61 for the 1, 2, and 4 kHz regions respectively). In two ears, DPOAEs were absent or were below 1*SD* of the mean levels obtained with stimuli in the 2 kHz region. Levels of toneburst-evoked emissions at 2 kHz for these ears also were smaller in comparison to response levels at 1 and 4 kHz.

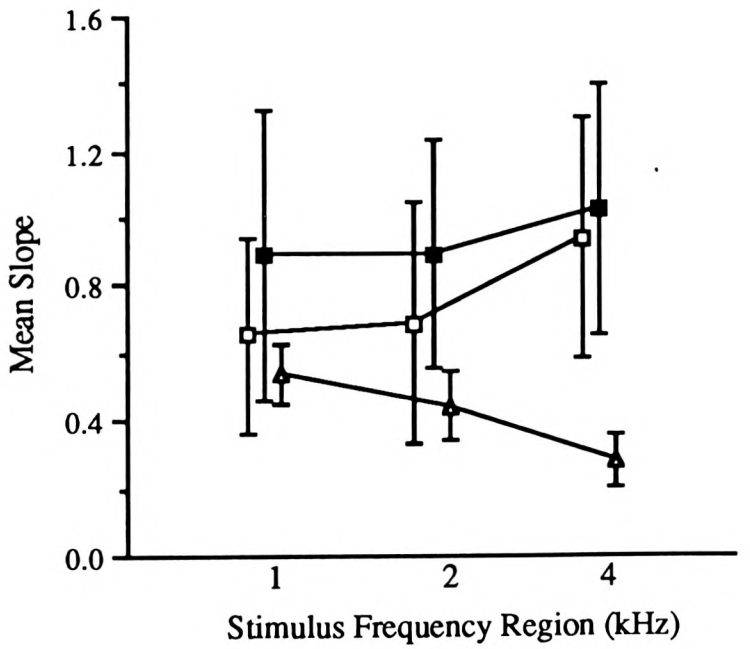

FIGURE 2 Mean (±1 *SD*) TEOAE and DPOAE slopes. (TEOAE, triangles; DPOAE GM, open squares; F1, filled squares)

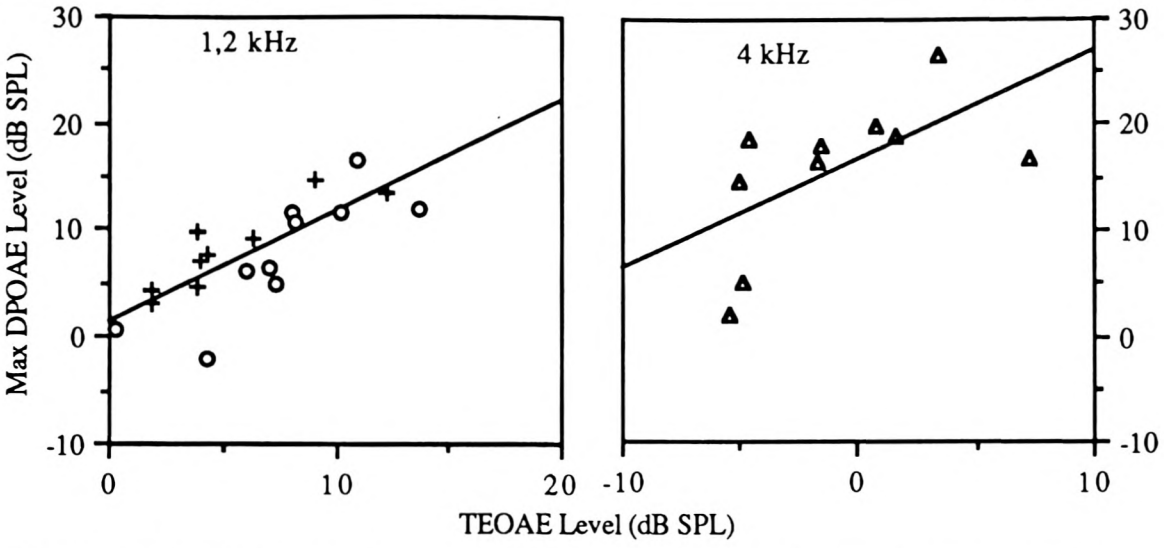

FIGURE 3 Correlation of maximum DPOAE and TEOAE levels by stimulus frequency region. (Left panel: 1 kHz, circles; 2 kHz, crosses)

Discussion

The purpose of this study was to evaluate the correspondence of TEOAEs and DPOAEs in the same ear at comparable frequency regions by measuring their growth functions to frequency-specific stimuli. Results indicated that growth functions of the two emissions varied in shape and slope as a function of stimulus condition. Factors both extrinsic and intrinsic to the presumed generation site within the cochlea may account for these variations.

At 1 and 2 kHz, the slopes of TEOAE and DPOAE growth functions were comparable, and the levels of the responses were correlated. Differences between the two emissions were primarily in the patterns of their growth functions. There were irregularities in DPOAE growth functions that were not present in the functions of TEOAEs. These features diminished, and the DPOAE growth functions became more linear as the frequency region of the primary-tone stimuli increased. Several factors may have contributed to this trend. When TEOAEs are elicited with tonebursts, both the stimuli and the dominant energy in the response are within the same frequency span. Whereas for DPOAE generation, two pure tones are interacting not only with each other in both the forward and reverse directions, but also with multiple combination tones generated within the cochlea coincident with two-tone stimulation. These complex interactions would be expected to result in nonmonotonic patterns of growth for DPOAEs. Similar findings were reported by Lonsbury-Martin et al. (1990) for DPOAEs generated with stimuli corresponding to the GM condition. Zwicker and Harris (1990) also described irregularities in the growth functions of DPOAEs generated in the 1 to 2 kHz range that were always associated with abrupt phase shifts. Phase was not measured in this study and cannot be eliminated as a factor contributing to the patterns in the DPOAE results.

Transiently evoked otoacoustic emissions from human ears are often dominated by specific idiosyncratic frequencies, especially at lower stimulus levels. Such strongly emitting frequency regions are known to influence the growth functions of TEOAEs (Probst et al., 1986; Zwicker, 1983), and probably contribute to the irregularities in the growth functions of DPOAEs (Lonsbury-Martin et al., 1990; Zwicker and Harris, 1990).

In this study, an attempt was made to control for such strongly dominant influences by including only ears with broad spectrum TEOAEs and no SOAEs. However, all ears had relatively dominant frequency regions that were apparent in their click-evoked responses. It is conceivable that these areas probably influenced the generation and transmission of both emissions unpredictably.

At 2 kHz, the levels of both emissions were reduced in the ears of two subjects. Other investigations of both DPOAEs and TEOAEs in normally hearing subjects also have reported similar decreases in this frequency range (Lonsbury-Martin et al., 1990; Ryan & Kemp, 1989). The reasons for the irregularities in responses generated with stimuli in this region have not been specifically delineated.

At 4 kHz, TEOAEs and DPOAEs were significantly different in the slopes and shapes of the growth functions, and the levels of the responses did not correspond as closely as at 1 and 2 kHz. Growth functions of TEOAEs were more compressive than either the DPOAE functions in this region or the TEOAE functions generated in other frequency regions. The toneburst and the emission at 4 kHz may have been interacting significantly because of the short latencies of the transiently evoked response. Furthermore, the frequency-dependent effects of the middle ear on both the forward and the reverse transmission of energy may have been a factor influencing the emissions differently in the higher frequencies. Both of these possiblities were proposed by Wit and Ritsma (1980) who observed reduced amplitude of evoked emissions stimulated with 4.2 kHz tonebursts. The steep growth in level with saturation at 4 kHz for the DPOAE functions appears to be characteristic of functions obtained with similar stimuli (Lonsbury-Martin et al., 1990). These features may result not only from a reduction of the influences contributing to the findings in the 1 and 2 kHz regions, but also from contributions by undetermined cochlear factors responsible for the sharper tuning present in the high frequency regions.

Both TEOAEs and DPOAEs represent a noninvasive means of evaluating cochlear function. Despite the differences in their growth functions, there were similarities in the level patterns of the responses across frequency within individual ears. This implies that each emission is being generated by elements of a mechanism that they both have in common. Comparison of other characteristics of TEOAEs and DPOAEs, such as the influence of suppression, contralateral stimulation and cochlear damage may further clarify the exact relationship between these two different kinds of emissions.

Acknowledgements

This work was supported by Swiss National Foundation Project Nr. 32-25514.88. The authors gratefully acknowledge the valuable assistance of Peter Schumacher for consultation with statistical analyses.

References

Davis, H. (1983). An active process in cochlear mechanics, Hear. Res. 9, 79-90.

Gaskill, S.A. and Brown, A.M. (November,1989). The relationship between acoustic distortion (2f1-f2) and threshold sensitivity. Paper presented at the meeting of the Brit. Soc. of Audiol., Nottingham, England.

Harris, F.P. (1989). Distortion-product emissions and pure-tone behavioral thresholds. Paper presented at the 2nd Int'l. Symp. on Cochlear Mechanics and Otoacoustic Emissions, Rome, Italy.

Harris, F.P., Lonsbury-Martin, B.L., Stagner, B. B., Coats, A.C. and Martin, G.K. (1989). Acoustic distortion products in humans: Systematic changes in amplitude as a function of f2/f1 ratio. J. Acoust. Soc. Am. 85, 220-229.

Kemp, D.T. (1978). Stimulated acoustic emissions from within the human auditory system, J. Acoust. Soc. Am. 64, 1386-1391.

Kemp, D.T. (1979). Evidence of mechanical nonlinearity and frequency selective wave amplification in the cochlea, Arch. Otorhinolaryngol. 224, 37-45.

Kemp, D.T. and Brown, A.M. (1983). A comparison of mechanical nonlinearities in the cochleae of man and gerbil from ear canal measurements, in *Hearing--Physiological Bases and Psychophysics*, edited by R. Klinke and R. Hartmann (Springer, Berlin), pp. 82-88.

Kemp, D.T. and Brown, A.M. (1984). Ear canal acoustic and round window electrical correlates of 2f1-f2 distortion generated in the cochlea, Hear. Res. 13, 39-46.

Lonsbury-Martin, B.L., Harris, F.P., Stagner, B.B., Hawkins, M.D., and Martin, G.K. (1990). Distortion-product emissions in humans: I. Basic properties in normally hearing subjects, Ann. Otol. Rhinol & Laryngol. Supp. 147, 3-14.

Lonsbury-Martin, B.L., Martin, G.K., Probst, R., and Coats, A.C. (1987). Acoustic distortion products in rabbit ear canal. I. Basic features and physiological vulnerability, Hear. Res. 28, 173-189.

Probst, R., Antonelli, C. and Pieren, C. (1990). Methods and preliminary results of distortion product otoacoustic emissions in normal and pathologic ears. Adv. Audiol. (in press).

Probst, R. Coats, A.C. Martin, G.K., and Lonsbury-Martin, B.L. (1986). Spontaneous, click- and toneburst-evoked otoacoustic emissions from normal ears, Hear. Res. 21, 261-275.

Probst, R. and Hauser, R. (1990). Dependency of the otoacoustic distortion product emission 2f1-f2 on primary-tone level variation L2-L1 in normal human ears. Poster presented at the midwinter meeting of the Assoc. for Research in Otolaryngol.

Puel , J.-L. and Rebillard, G. (1990). Effect of contralateral sound stimulation on the distortion product 2f1-f2: Evidence that the medial efferent system is involved. J. Acoust. Soc. Am., 87, 1630-1635.

Ryan, S. and Kemp, D. (1989). Otoacoustic emissions. What should we measure? Paper presented at the meeting of the British Soc. of Audiol., Nottingham, England.

Wit, H.P. and Ritsma, R.J. (1980). Evoked acoustical responses from the human ear: Some experimental results, Hear. Res. 2, 253-261.

Zwicker, E. (1983). Delayed evoked oto-acoustic emissions and their suppression by Gaussian-shaped pressure impulses, Hear. Res. 11, 359-371.

Zwicker, E. and Harris, F.P. (1990). Psychoacoustical and ear canal cancellation of the (2f1-f2)-distortion product. J. Acoust. Soc. Am., 87, 2583-2591.

Zwicker, E. and Lumer, G. (1985). Evaluating traveling wave characteristics in man by an active nonlinear cochlear preprocessing model. In: Peripheral Auditory Mechanisms. (Eds: Allen, J.B. et al.) Springer, Berlin, pp. 250-257.

SOUND INDUCED CHANGES IN ELECTRICALLY EVOKED COCHLEAR EMISSIONS

A.E. Hubbard[1], H.H.Nakajima[2], E.S.Olson[3] and D.C.Mountain[4]

[1]Dept. of Electrical, Computer, and Systems Engineering, [1,4]Dept. of Otolaryngology, and [1,2,3,4]Dept. of Biomedical Engineering, Boston University, Boston, MA 02215.

Introduction

We have previously proposed that the outer hair cells (OHC) interact with the hydromechanical elements of the cochlea to form a series of active filters which provide the high sensitivity and frequency selectivity observed in the responses of inner hair cells (IHC) and auditory nerve fibers (Mountain et al, 1983). The active filtering is the result of a feedback loop consisting of the mechanical-to-electrical (forward) transduction process driving an electrical-to-mechanical (reverse) transduction process located in the OHC. The reverse transduction response may be due to haircell length changes or stereociliary motion, both of which have been demonstrated in vitro using injected current (Brownell et al.,1985; Ashmore,1987; Crawford and Fettiplace, 1985). For acoustic frequencies well below the characteristic frequency of a given cochlear location the feedback is negative. This negative feedback serves to increase the apparent stiffness of the basilar membrane for low frequency stimuli. Support for this active-stiffness hypothesis has come from experiments in which we have injected sinusoidal current into scala media and measured acoustic response (emissions) in the ear canal of experimental animals (Mountain et al, 1983; Hubbard and Mountain, 1983; Mountain and Hubbard, 1989; Hubbard and Mountain, 1990).

A conceptual model of our active-stiffness hypothesis is illustrated in Figure 1. The basilar membrane is displaced by the acoustic stimulus and in turn excites both the OHC and the IHC hair bundles. Displacement of the OHC hair bundle opens the forward transduction channels resulting in an OHC receptor current. The OHC receptor current produces an extracellular potential, the cochlear microphonic (CM) (Dallos et al.,1982; Russell et al., 1986). The OHC receptor current regulates force production via the reverse transduction process. At high acoustic frequencies a phase shift in the feedback loop changes the feedback from negative to positive. This shift to positive feedback results in a significant increase in the IHC and auditory nerve sensitivity.

OHC reverse transduction can be excited directly by injecting current into the cochlea. The resulting mechanical disturbance results in electrically-evoked acoustic emissions which can be measured at the tympanic membrane. The magnitude of the emissions can be increased by the simultaneous presence of acoustic stimuli which are intense enough

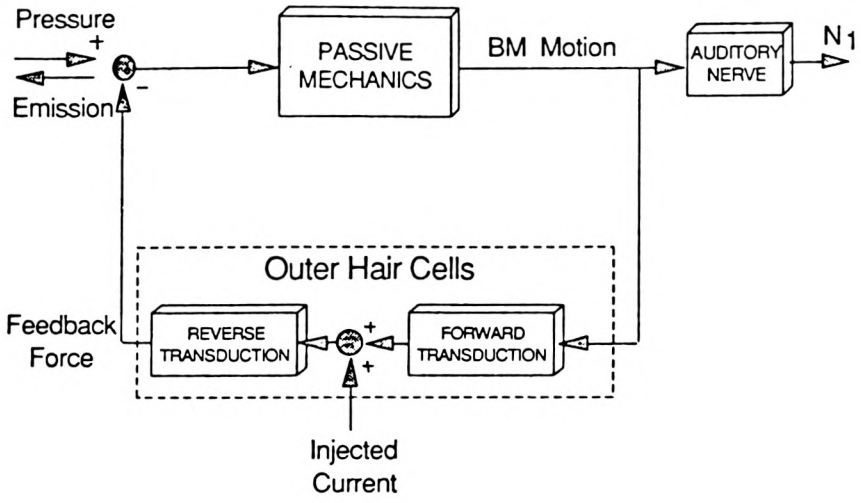

FIGURE 1 Schematic diagram of cochlear feedback system.

to saturate the forward transduction process (Mountain and Hubbard, 1989). This enhancement effect is graded with the level of the acoustic stimulus and the enhancement saturates at high sound pressure levels, similar to the way in which CM saturates. The enhancement can also be produced using intravenous furosemide, which lowers the electromotive force driving the transduction current, thereby reducing the gain of forward transduction (Hubbard and Mountain, 1990).

To further explore the characteristics of cochlear forward and reverse transduction, we used loud sounds which altered auditory nerve thresholds. Before and after the loud sounds were delivered, a measure of forward transduction (the CM) and a measure of reverse transduction (electrically-evoked emissions) were recorded. The whole-nerve action potential (N_1) was used as an indicator of auditory threshold.

We found that N_1-threshold became poorer and CM decreased following traumatizing tonal stimulation. By contrast, we found that the electrically-evoked emission usually increased following loud-tone delivery. To understand the relationship of the data to specific mechanisms, we considered the active stiffness model. Interpreted in such a context, present results indicate that several elements in the system can be damaged separately by loud tone stimuli.

Experimental Method

Experiments were carried out using deeply anesthetized gerbils using protocols previously described (Mountain and Hubbard, 1989). We first collected baseline data for all experimental variables which were to be measured following traumatizing tone delivery. We produced threshold shifts 29 times by exposing gerbils to pure tones (100-110 dB SPL for 3-10 minutes) with damage-tone frequencies (4500 Hz, 1800 Hz, 800 Hz) corresponding to first, second, and third turn cochlear best-frequency regions. Electrically-evoked emissions and the whole-nerve action potential were monitored before and after traumatizing sounds were delivered.

When measuring the acoustic enhancement effect, we simultaneously delivered both electrical and tonal stimuli, at 800 Hz and 1200 Hz respectively. The current level for

the electrical stimulus was 15 uA p-p. Concurrent tonal stimuli were increased from levels of 10 to 80 dB SPL. These stimulus parameters have been found to produce large emissions and strong enhancements using an electrode placed in the second cochlear turn. The maximum enhancement effect was computed as the difference between the emission at the lowest and highest sound levels of the enhancing tone.

Using a different data collection paradigm, the frequency dimension was explored. We elicited emissions without an enhancing tone present, at seven electrical stimulus frequencies. We obtained a CM response area using five different sound levels and sweeping the acoustic stimulus frequency. N_1 response areas were also obtained by averaging the N_1 response to tone pips. Fourteen frequencies were used. The tone pips were systematically increased in sound level. N_1 threshold was taken as the sound level required to cross a 10 uV criterion level.

Results

Figure 2 shows typical changes in N_1 threshold which occur following each of three damaging-tone presentations. Figure 3 shows the emission changes which were measured in the same animal. Notice that even when changes in the N_1 in the region of the electrode are small, changes begin to show up in the emissions. The acoustic frequency used to elicit N_1 can be related to cochlear place, using a place-frequency map. We have included an arrow in Figure 2 indicating the 'place' of the second turn electrode, as translated into the frequency domain. Comparing Figure 2 and Figure 3, we see that the largest changes in the emissions occur when large N_1 threshold shifts occur at a frequency which corresponds to a basilar-membrane region which is approximately centered on the current-delivery electrode. By the time the N_1 damage pattern completely surrounds the electrode region, there are large and wideband changes in the emissions. Little additional change occurs with subsequent damaging tone delivery.

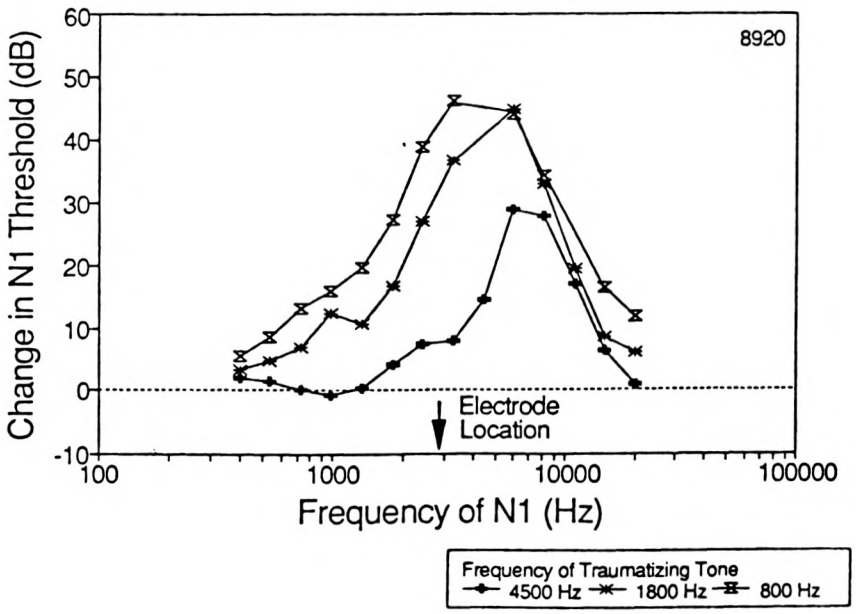

FIGURE 2 Changes in N_1 threshold produced by traumatizing tones.

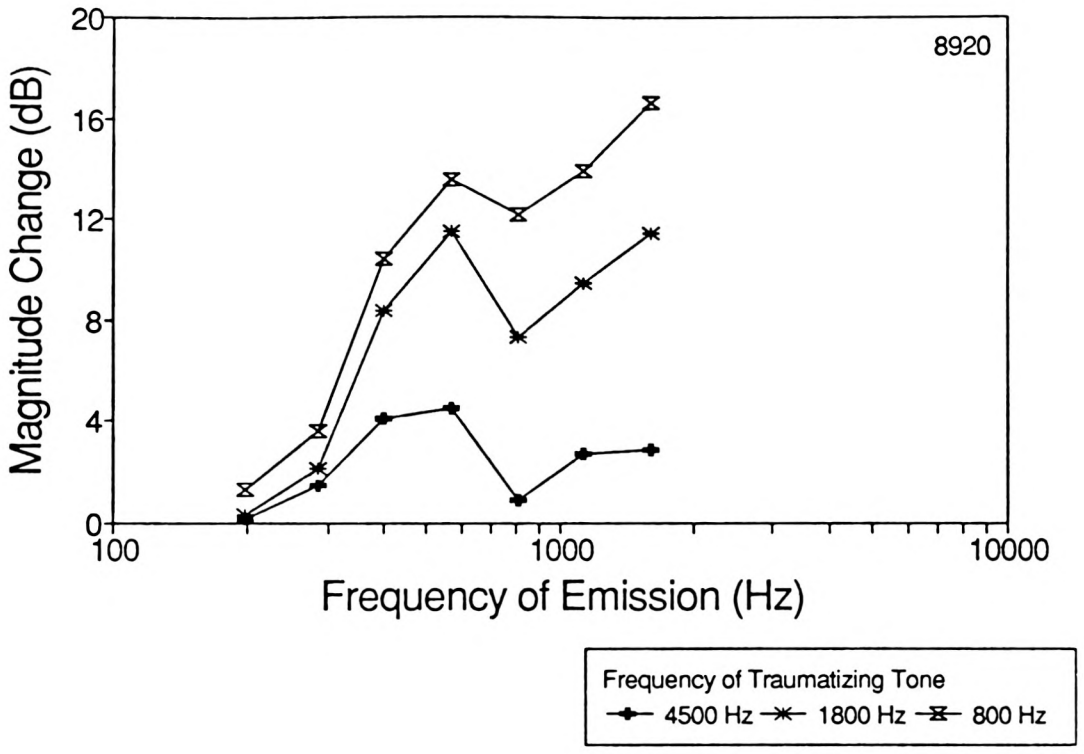

FIGURE 3 Changes in emissions produced by traumatizing tones.

The enhancement effect diminished in all presentations of acoustic overstimulation. Figure 4 shows two curves plotting emission values versus SPL. The lower curve is a control data set. The upper curve was obtained following delivery of a traumatizing tone. The curves demonstrate the typical increase in the emissions at lower sound levels of the acoustic stimulus. The increase usually continues for successive traumatizing tone presentations. The maximally-enhanced emission usually stayed constant as damage progressed with successive damaging-tone delivery, but it decreases following what we believe to be severe damage. In a few cases, the whole emission versus sound-level curve is displaced upwards, possibly due to a change in the fraction of the injected current passing through the haircells.

Figure 5 shows that N_1 threshold changes at 2500 Hz due to loud sounds are strongly correlated with changes in the maximum enhancement effect measured at 800 Hz. The straight line is the linear regression line. The correlation coefficient was -.943 for the two animals shown. Figure 6 shows the corresponding CM-damage data from the same two animals. While the data shown in Figure 5 are well fit using a straight line in log-log coordinates, the CM data are plotted in the coordinate system originally used by Patuzzi et al., (1989) and fit with a quadratic regression line (solid curve) with a correlation coefficient of -0.884. A similar quadratic fit to the data of Patuzzi et al., (1989) (dashed curve) is provided for comparison.

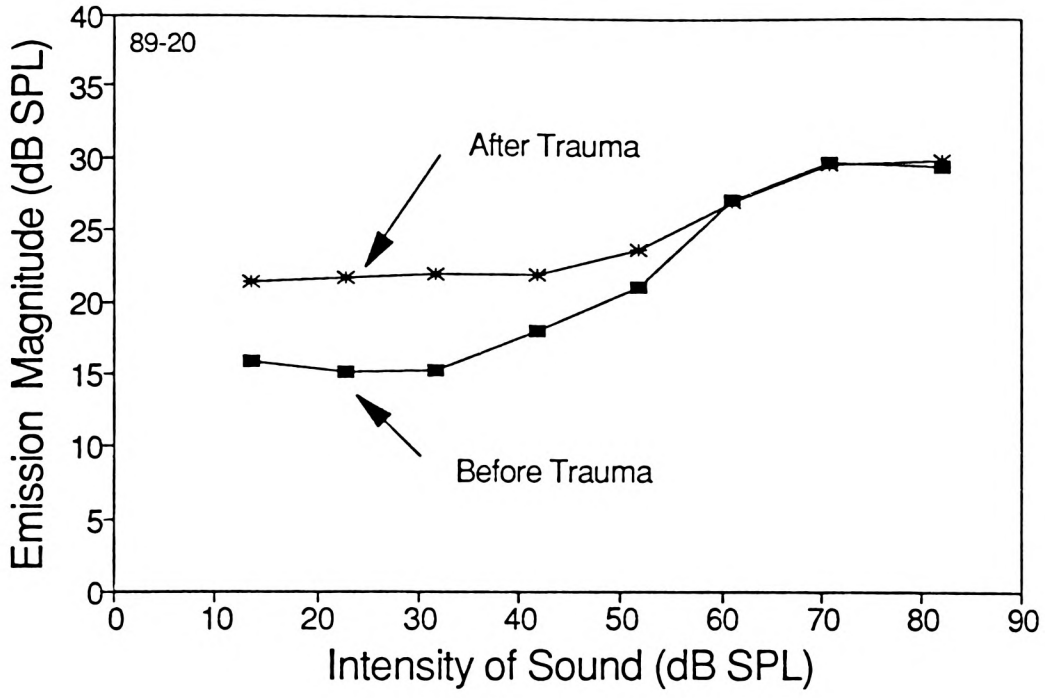

FIGURE 4 Changes in acoustic enhancement produced by traumatizing tones.

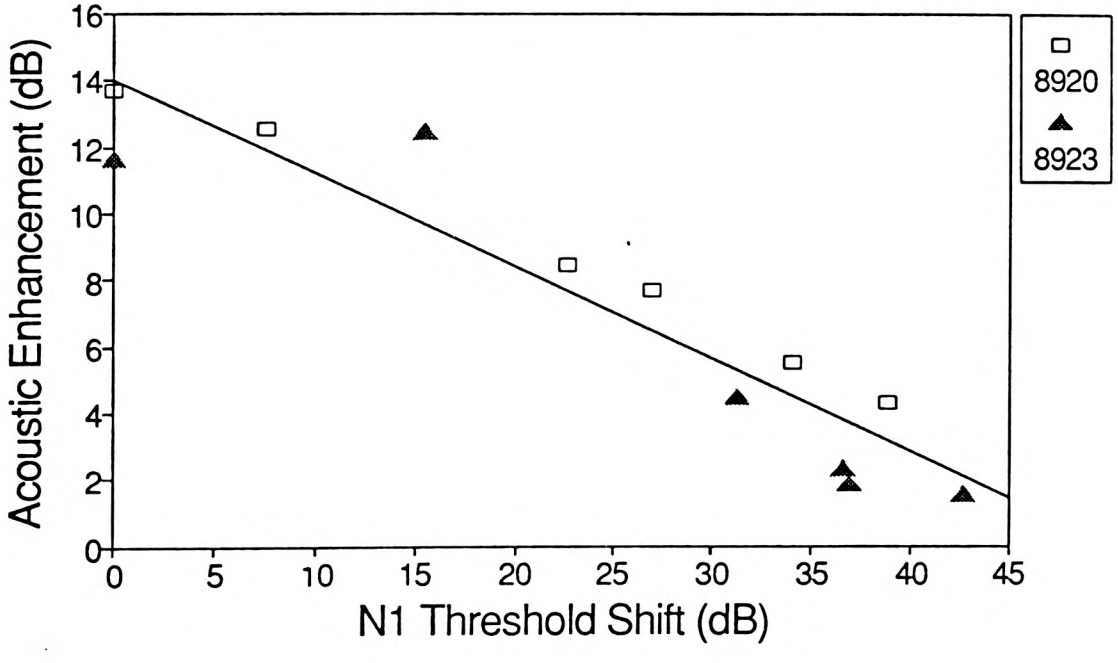

FIGURE 5. The changes in the acoustic enhancement effect produced by traumatizing tones are related to N_1 threshold shifts.

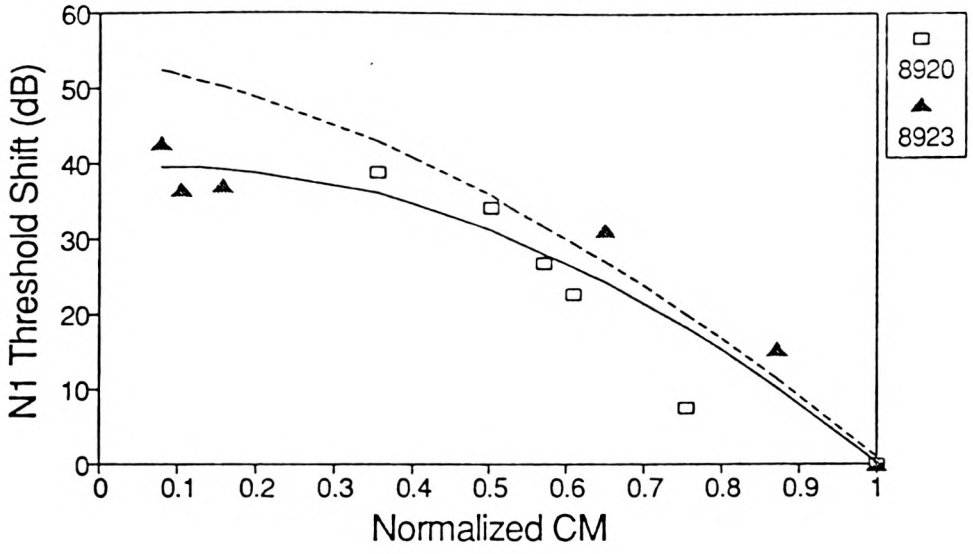

FIGURE 6 The changes in CM are related to changes in N_1 threshold shift following traumatizing tone delivery. The dashed line is the equation, N_1 Threshold Shift = $54.26 - 20.67x - 32.60x^2$. The solid line is the equation, N_1 Threshold Shift = $39.36 + 6.56x - 45.67x^2$. x is the normalized CM.

Discussion

To interpret the experimental results, we separated the negative feedback system attributes into those which dominate at low frequency and those which are significant at high frequency. This is required since the emissions are a low-frequency phenomenon (Mountain and Hubbard, 1989) and the N_1 is a high-frequency phenomenon. To explore the first case, suppose the stimulus frequency is low, as in the case of the emissions, and the loop gain is reduced. If the gain reduction is substantial, then the feedback is effectively eliminated. Since at low frequency, the function of the loop is to increase the effective stiffness of the basilar membrane, opening the loop decreases the effective stiffness. Therefore, force produced by the electrical excitation (reverse transduction) will produce relatively greater basilar-membrane motion with the loop open. Thus the emission will be increased. In the presence of enhancing acoustic stimuli, the rate of emission increase is greater at low acoustic stimulus levels than at high levels. This is because at high SPL the loop is already opened to some extent due to saturation of forward transduction. If the change in the emission magnitude due to acoustic trauma differs at low SPL from the change at high SPL, the result is a change in the maximum enhancement effect. Next, consider the feedback system as an amplifier whose mission is to optimally increase the response to high-frequency tones. If it is a feedback amplifier which produces positive feedback at high frequencies, then decreasing the loop gain will decrease the positive feedback. Therefore the amplifier performance at the characteristic frequency is degraded with reduction in loop gain, which increases N_1 threshold.

It appears that the loud sounds which we used always altered forward transduction and only occasionally altered reverse transduction. We believe this, because not only in the fixed-frequency enhancement experiment but also in the frequency-domain experiments, the trend is for the unenhanced emission to increase with tonal overstimulation. We

interpret the increase in the unenhanced emission to mean that loop gain decreased. Since the CM response to low-level tonal stimuli decreased following traumatizing tones, we attribute loop gain reduction to diminished forward transduction gain.

The fitting equation used by Patuzzi et al. (1989) seems to suit our data, c.f. Figure 6. Perhaps the most notable difference is that we were not able to produce as large an N_1 shift as they did. This is likely because they were working in a cochlear region tuned to higher frequencies, where the tip-to-tail ratio is initially greater.

We found that the entire CM versus sound level curve was not always modified by traumatizing tones in a way which could be summarized as only a shift in the ordinate values (Patuzzi et al.,1989). Such a situation would imply that the number of active transduction channels was reduced by the traumatizing tone. In several experiments, the maximum obtainable CM response had not been decreased, even though at lower sound stimulus levels the CM was diminished. This suggests that the effect of the traumatizing loud sound was to alter the operating point of the forward transduction channels. In general, our data are summarized by shifts both in the abscissa and the ordinate of the CM versus sound level input-output curve.

Following sufficient acoustic overstimulation, both the enhanced and unenhanced emission can decrease markedly. This may be due to a failure of the reverse-transduction mechanism, possibly even total haircell disruption. When the gain of reverse transduction decreases, the model predicts that the emission should drop also. This is because reverse transduction gain is a feed-forward component in the system transfer function for the emissions. In other words, if there is no reverse transduction, there are no emissions.

References

Ashmore, J.F.(1987) A fast response in guinea-pig outer hair cells. The cellular basis of the cochlear amplifier. Physiol. 388,323-347.

Brownell, W.E., Bader, C.R., Bertrand, D., and de Ribaupierre, Y. (1985) Evoked mechanical responses of isolated cochlear outer hair cells. Science 227, 194-196.

Crawford, A.C. and Fettiplace, R. (1985) The mechanical properties of ciliary bundles of turtle cochlear hair cells. J. Physiol. 364, 359-379.

Dallos, P., Santos-Sacchi, J., and Flock, A. (1982) Intracellular recordings from cochlear outer hair cells. Science 217, 582-584.

Hubbard, A.E. and Mountain, D.C (1983) Alternating current delivered into the scala media alters sound pressure at the eardrum. Science 222, 510-512.

Hubbard, A.E. and Mountain, D.C. (1990) Forward and reverse transduction: Differential suppression and enhancement. Hear. Res. 43, 269-272.

Jack, J.J.B., Noble, D. and Tsien, R.W. (1983) Electric Current Flow in Excitable Cells. Clarendon Press, Oxford, pp. 25-82.

Misrahy, G.A., Hildreth, K.M., Shinabarger, E.W., and Gannon, W.J. (1958) Electrical properties of the wall of endolymphatic space of the cochlea (Guinea Pig). Amer. J. Physiol. 194, 396-402.

Mountain D.C. and Hubbard, A.E. (1989) Rapid force production in the cochlea. Hear. Res. 42, 195-1112.

Mountain, D.C., Hubbard, A.E., and McMullen, T.A. (1983) Electro-mechanical processes in the cochlea. In: Mechanics of Hearing, Delft Univ. Press, pp. 119-1111.

Patuzzi, R.B., Yates, G.K., and Johnstone, B.M. (1989) Changes in cochlear microphonic and neural sensitivity produced by acoustic trauma. Hear. Res. 39, 189-202.

Russell, I.J., Cody, A.R., and Richardson, G.P. (1986) The responses of inner and outer hair cells in the basal turn of the guinea-pig cochlea and in the mouse cochlea grown in vitro. Hear. Res. 22, 199-216.

Acknowledgement: This work was supported by the Deafness Research Foundation.

Comments and discussion

WIT

Would you consider an alternative explanation for the observations that you have presented ? If alternating current is injected into a conducting fluid, it may create mechanical vibration in the fluid. So your electric current might create an acoustical stimulus right at the site of the injecting electrode. This signal might come out into the ear canal through the middle ear ("electrophonic" signal).

At the same time the signal might create a "stimulus frequency otoacoustic emission"; and this emission might also come out. So what you then measure is the sum of two signals with the same frequency; and the phase relation may be such that the amplitude of the sum signal is smaller than the amplitude of the "electrophonic" signal.

If the process that creates the otoacoustic emission signal is disturbed, this may result in a signal with a larger amplitude coming out of the ear canal. (The electrophonic component is expected to be very robust; while the otoacoustic emission component will be very vulnerable.)

HUBBARD

We have previously looked for evidence which addresses the effect you propose. We followed the emission postmortem, and the signal fell into the noise level over the frequency range of approximately 100 Hz to 2000 Hz. The noise level is on the order of 40-50 dB down from the normal level of the electrically elicited emission. The post-mortem result may be adversely influenced by general changes in tissue characteristics, and thus we do not feel this evidence is unequivocal. To sidestep the complications of the post-mortem experiment, we used furosemide with kanamycin to kill haircells while the animal was still alive. After drug administration, the emission is enhanced and CM falls. CM increases as soon as the EP begins to increase. About one hour following drug administration, with EP high and still recovering, CM falls. At this time, the electrically elicited emission falls approximately 20 dB. In summary, potentially-relevant data fail to reveal a second "robust" source of acoustic energy which couples from the electrode into the fluid and radiates out through the middle ear, skipping the haircells altogether.

CHAOTIC DYNAMICS OF OTOACOUSTIC EMISSIONS

Douglas H. Keefe[1], Edward M. Burns[2], Robert Ling[2] and Bernice Laden[1]

[1] *School of Music, DN-10*
University of Washington, Seattle, WA 98195, USA
[2] *Department of Speech and Hearing Sciences, JG-15*
University of Washington, Seattle, WA 98195, USA

Introduction

The discovery of otoacoustic emissions (OAE) has encouraged a re-assessment of active mechanisms in hearing. Nonlinear oscillators are attractive candidates for understanding active processes in hearing, and otoacoustic emissions in particular. Even the simplest nonlinear oscillators used in current theories show limit cycle behavior, but they are also capable of more complex, chaotic, behavior. For example, the forced, van der Pol oscillator utilized in models of hearing (Duifhuis et al., 1986; Tubis et al., 1988) is also known to exhibit chaotic behavior. It is unknown whether OAEs actually exhibit chaotic behavior.

The most common routes to chaos observed (Swinney, 1986) include period doubling (periodic→period doubling→chaos), quasi-periodicity (periodic→quasi-periodic→chaos), and intermittency (synchronized→intermittent chaos→chaos). Chaotic systems can also be sub-divided into endogenous chaos, in which the system behavior unfolds without external interaction, and forced chaos, in which the system is driven by a external stimulus, for example, a sinusoidal signal. Due in part to the wide varieties of chaotic systems, different analysis methods are used. One of the most important and direct methods is the use of power spectral analysis for identifying period-doubling, quasi-periodicities, and broad-band spectra. Additional methods discussed below can distinguish deterministic from stochastic broad-band spectra.

The statistical properties of spontaneous otoacoustic emissions (SOAE) provide evidence that emissions are produced by an active nonlinear system, rather than narrow-band filtered noise (Bialek and Wit, 1984). While different SOAE components present in the same ear may represent different dynamical processes, interactions between SOAE components have been observed in some measurements, including so-called intermodulation distortion products, mutual suppression, and non-contiguous, dynamically linked SOAEs (Burns et al., 1984). The connection

between intermodulation distortion products, particularly cubic difference tones (CDT), and SOAEs describes an assumed active mechanism using the terminology of a passive nonlinearity, but alternative explanations are possible using nonlinear dynamics.

The quasi-periodic route involves the generation of two sinusoids whose frequencies need not be simply related. In fluid mechanical experiments on Couette flow, the two components occur at moderate control parameter values, and quadratic and cubic difference tone components are generated as the nonlinear control parameter is increased, until a broad-band chaotic regime is entered (Fenstermacher et al., 1979). In some circumstances, the spectral components are phase-locked, *i.e.*, each of the two components is a harmonic of an underlying fundamental. Such quasi-periodic spectra have been observed for aggregates of heart cells, in which the two periodicities represent active sources beating at two rates in physically distinct locations (Glass et al., 1986), and in woodwind musical instrument multiphonic tones, in which the input impedance has strong peaks at inharmonically related frequencies (Keefe and Laden, 1990). Thus, quasi-periodic spectra may be indications of multiple active sites, or multiple reflection sites feeding back to a single active site. The strong similarity of the linked, non-contiguous emissions to quasi-periodic spectra reported in other systems motivated this investigation.

Methods

Pressure measurements were made using an Etymotic ER-10B microphone inserted snugly into the ear canal using a plastic tip, with the subject seated in a sound-attenuated booth. The spectral components of the microphone signal were monitored using a spectrum analyzer, and the signal was amplified and digitally recorded (typically at a sample rate of 22 kHz) using a computer. In experiments utilizing an external tone, a sinusoidal signal was amplified and delivered by a Etymotic ER-3 transducer coupled to the ear canal via a plastic tube.

CORRELATION DIMENSION

One method of determining whether a system is chaotic is to compute the correlation dimension of the measured time series, when embedded in a higher dimensional reconstructed phase space (Grassberger and Procaccia, 1983). Based upon an ear canal pressure measurement, the single time series $\{x(t)\}$ is embedded in an M-dimensional phase space using a delay time τ to form the vector $X_n = \{x(t_n), x(t_n + \tau), x(t_n + 2\tau), \ldots, x(t_n + [M-1]\tau)\}, n = 1, \ldots, N - M + 1$. Here, X_n represents the n-th vector (of dimension M), and N is the number of samples in the time series. The optimal choice of time delay is that for which the mutual information between $x(t)$ and $x(t+\tau)$ across all sampled data is a minimum. This mutual information is the number of bits, on average, which can be predicted of the state $x(t+\tau)$, given that the state $x(t)$ is known. An efficient algorithm exists for computing mutual information (Fraser and Swinney, 1986).

The correlation dimension is widely used to describe chaotic behavior due to the following properties: (1) its value is 1 for a limit cycle independent of the embedding dimension M, (2) its value exceeds 1 and is fractional for a chaotic

attractor independent of M, (3) its value grows with increasing M for a stochastic signal, and (4) it is a lower bound for the fractal dimension and much simpler to calculate. It is calculated by counting the number $C(R)$ of vectors (of dimension M) which are within a ball of radius R in the M-dimensional phase space, relative to a particular reference vector. The correlation sum $C(R)$ is calculated over a range of radii and embedding dimensions, averaged over multiple reference vectors. The key property which differentiates deterministic from stochastic signals is whether a scaling region exists, that is, whether $slope = d\log C/d\log R$ plot approaches a constant independent of M. If a scaling region exists, this slope is an estimate of the correlation dimension. Our figures show *slope* versus $\log C$, because the resulting plots overlap if a scaling region exists. The implementation of the mutual information and correlation dimension calculations is described elsewhere (Keefe and Laden, 1990).

ACAUSAL FILTERING

If the intent is to extract the correlation dimension of a chaotic signal in the presence of noise, causal filters cannot be used to improve the signal to noise ratio, since the calculated correlation dimension is biased. This means that narrow band filtering such as used in a lock-in amplifier cannot be used. Acausal lowpass filtering does not bias the correlation dimension, and can be used to improve signal to noise (Mitschke, 1990). The result is that a scaling region can be more easily found when working with noisy signals. Unfortunately, the ear canal spectrum is most noisy at low frequencies, mainly due to unrelated physiological noise.

We have investigated the use of acausal bandpass filtering to improve estimates of correlation dimension (Keefe and Ling, 1990), specifically using acausal Butterworth filter designs with roll-offs of -12 or -24 dB/octave. To test whether acausal bandpass filtering is acceptable, we added varying degrees of noise to the Lorenz attractor, whose spectra is broad-band and heavily weighted to low frequencies, and found that acausal bandpass filtering biased the correlation dimension whereas acausal lowpass filtering did not. We added varying levels of noise to a saxophone multiphonic tone, whose spectra is quasi-periodic, and found that acausal bandpass filtering was acceptable as long as the cut-on frequency was sufficiently low to include the first few spectral components. Acausal bandpass filtering may be useful as long as the chaotic spectral energy lies within the passband.

Results and Discussion

We began by re-analyzing the data on Subject 9 from Table I of Burns et al. (1984), which showed three sets of dynamically linked, CDT SOAEs for the same ear. In a biperiodic spectrum each line spectral component f_{mn} can be expressed as a multiple of two basis frequencies f_1 and $f_2 > f_1$ by $f_{mn} = mf_1 + nf_2$, for non-negative integers m and n. If the basis frequencies are phase-locked, then there exist non-negative integers r and s such that $f_1 = rf_0$, and $f_2 = sf_0$, and all components of the spectra may be expressed in terms of an integer multiple J of the fundamental f_0 by $J = f_{mn}/f_0 = mr + ns$. The results are shown as Subject A in Table 1, where the fundamental f_0 was selected using a least mean

squares (LMS) fit of the frequencies to a harmonic series. The corresponding LMS

TABLE 1 Periodicities in linked non-contiguous emissions

A	f	1065.8	1120.1	1225.3	1330.6	1410	1488.9	1595.6	1701.8
	J f_0	1064.4	1117.6	1224.1	1330.5	1410.3	1490.2	1596.6	1703.0
	J	40	42	46	50	53	56	60	64
B	f	1408.1	1524.1	1731.2	1915.6	2053.9	–	–	–
	J f_0	1407.9	1523.3	1731.0	1915.6	2054.1	–	–	–
	J	61	66	75	83	89	–	–	–

error function is illustrated in Figure 1a as a function of possible f_0, and the sharp dip at $f_0 = 26.61$ Hz is evident. In terms of the harmonic number J, the alternate

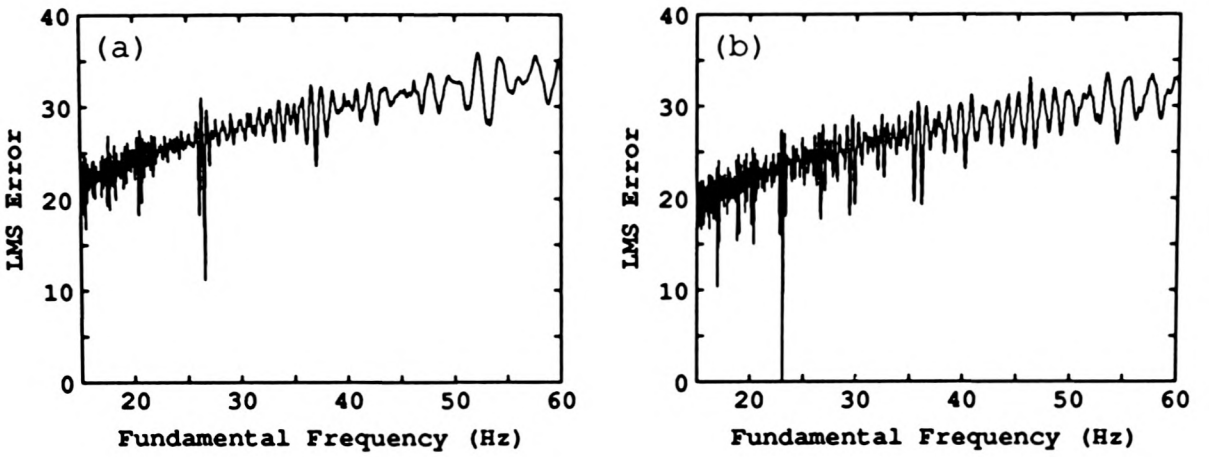

FIGURE 1 (a) LMS error vs. f_0 for Subject A; (b) LMS error vs. f_0 for Subject B

dynamical states discussed by Burns et al. (1984) were $\{46, 50, 60\}$ and $\{46, 53, 64\}$. A similar analysis for a second subject (Female, 12 yrs.) with linked non-contiguous emissions showed a similar periodic structure (Subj. B in Table 1 and Figure 1b), and the underlying fundamental was $f_0 = 23.08$ Hz. The alternate states were $\{66, 75, 83, 89\}$ and $\{61, 75, 89\}$. The frequencies of the pair of strongest emissions formed a ratio of 6:5 for subject A, and 89:75 for subject B (compare, 6/5=90/75). These implicate a low phase-locking frequency of approximately 25 Hz, but they do not predict spectral energy at this frequency. Spectral components tend to cluster around the two strongest components, but noise and the reverse middle ear tranfer function limit detection of components below approximately 500 Hz, even if present. This description of linked non-contiguous SOAE suggests either linked active sources, or mechanical wave reflections on the basilar membrane coupled to a single active site. Jones et al. (1986) have formulated a theory of interacting van der Pol oscillators which accounts for a single set of CDT SOAEs, whereas the description of the spectra as a quasi-periodic spectrum couples the frequencies of sets of CDTs.

ENDOGENOUS CHAOS IN A SOAE

An ear canal pressure time series was recorded (22 kHz sample rate) in a subject (adult female) with fairly strong SOAEs between 400 and 2100 Hz and large amplitude modulation. The time series was acausally bandpass filtered (-24 dB/octave fall-off) from 400-2100 Hz, and Figure 2 illustrates the two-dimensional phase portrait of the filtered time series plotted against a delayed version of itself by τ=1,5,7, and 21 samples. Too small a delay ($\tau = 1$) produced a poor reconstruction of the phase space since trajectories remained close to the diagonal line of identity, whereas too large a delay ($\tau = 21$) also produced a poor reconstruction since there was additional folding of the trajectories. Intermediate values of τ gave acceptable reconstructions.

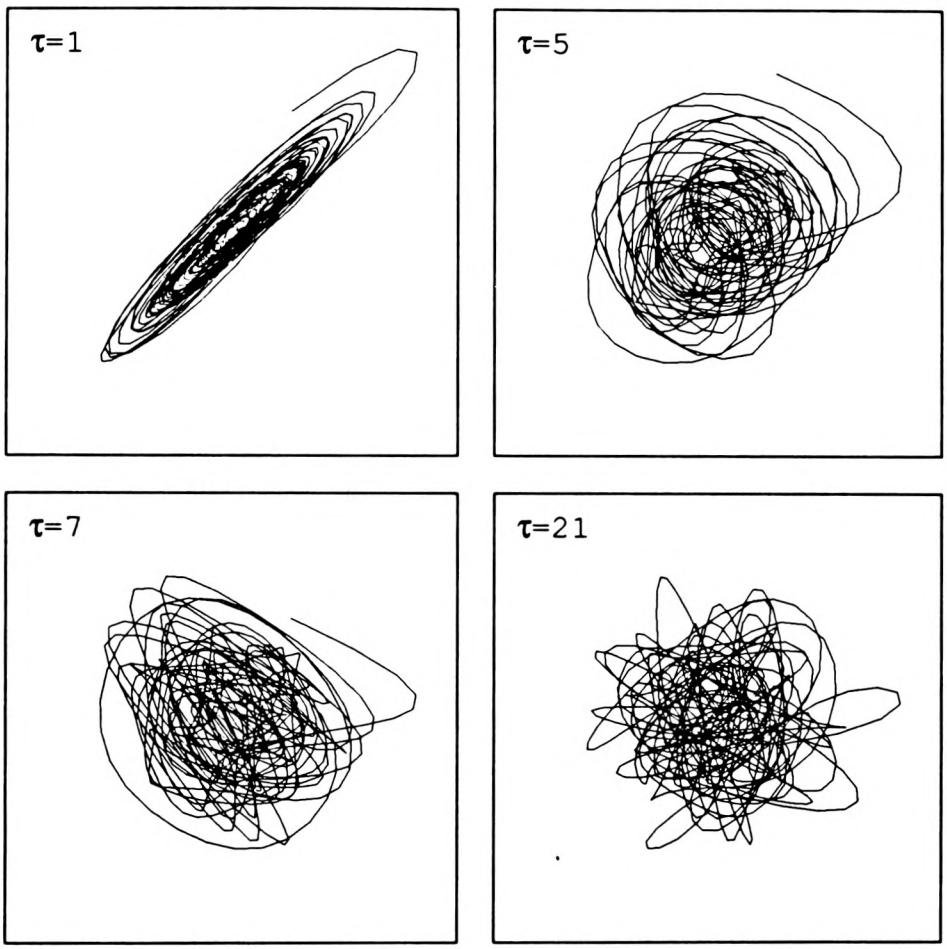

FIGURE 2 Two-dimensional phase portraits $x(t + \tau)$ versus $x(t)$ for delays of 1,5,7 and 21 samples.

The calculated mutual information had its first dip at a delay of 7 samples, and was quite near its dip at 5 samples. These delays were used for the phase space reconstructions, and correlation dimension runs used 65,536 samples, 600 reference vectors, and embedding dimensions of 10 to 200 in steps of 10. Figure 3 shows *slope* as a function of $\log C$ for $\tau = 5$ and 7 samples. The maximum value of slope increased

with increasing embedding dimension in the lower range of $\log C$ values, and this increase in slope with increasing M is characteristic of a stochastically dominated signal. A scaling region was observed for both delays at $\log C$ values between 15.0 and 15.5 at very high embedding dimensions, the latter tending to extract the deterministic component of the signal relative to lower embedding dimensions. The correlation dimension of the acausally filtered SOAE was approximately 3.4, which signifies that the dynamics of this spontaneous emission was chaotic.

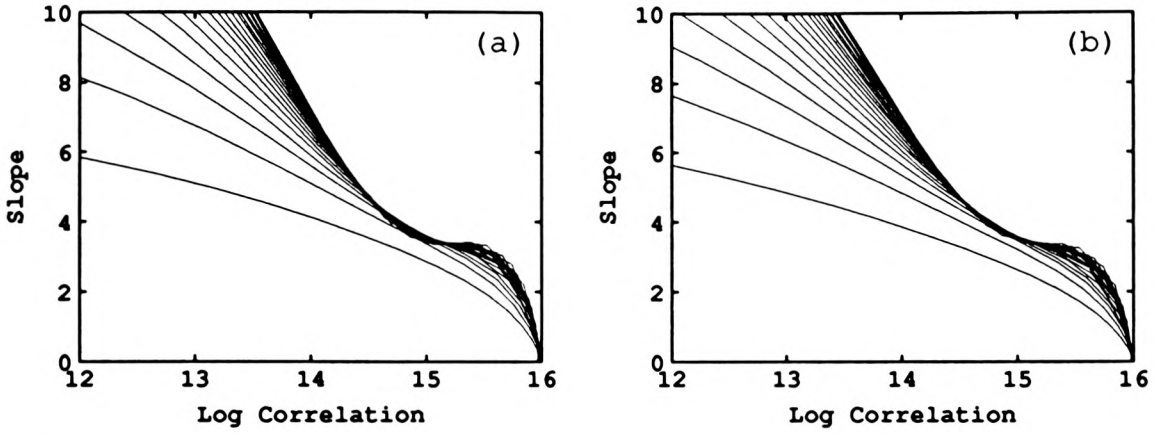

FIGURE 3 Slope ($\Delta \log C(R)/\Delta \log R$) versus $\log C(R)$, for embedding dimensions M=10, 20, 30, ..., 200 : (a) τ=5 samples, (b) τ=7 samples.

CHAOS IN A SINUSOIDALLY FORCED SOAE

An external sinusoidal tone at 4560 Hz was introduced into the ear canal of a subject with a strong emission near 4600 Hz. The level of the external tone was varied from 34 to 26 dB SPL in 1 dB steps. Entrainment of the emission to the external tone was observed only at the highest level, as is evident in the power spectra (see Figure 4). All time series were acausally bandpassed filtered from 4000-5300 Hz, using a -24 dB/octave rolloff, the mutual information was measured to determine optimal delay, and the correlation dimension was measured. In all cases, a 1 sample delay was optimal. Typical correlation dimension runs used 32,768 samples, 300 reference vectors, and embedding dimensions of 8 to 18. When the emission was entrained, a broad scaling region was found and the correlation dimension was 1.06, as compared to the theoretical prediction of 1.00 for a limit cycle oscillator (Figure 5a). This discrepancy was most likely due to background noise. A scaling

TABLE 2 Dependence of Correlation Dimension upon External Tone Level

Stimulus SPL (dB)	34	33	32	31	30	29	28	27	26
Correlation Dimension	1.06	1.17	1.25	1.42	1.42	1.75	1.74	1.77	1.78

region was found for all other external tone levels, and the correlation dimension was 1.25 for a level of 32 dB SPL, thus indicating a chaotic response (Figure 5b). The correlation dimension increased with decreasing external tone level, and dis-

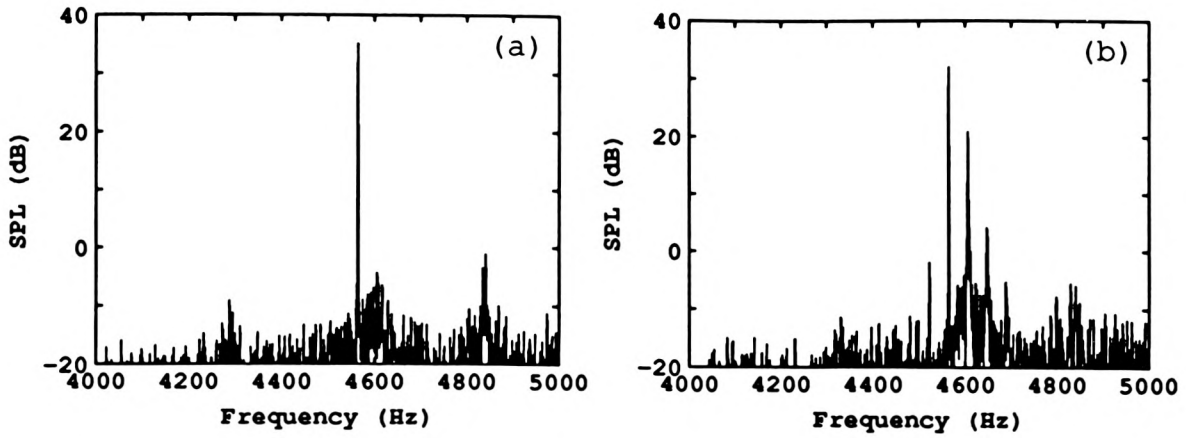

FIGURE 4 Ear canal pressure spectra versus frequency for two external tone levels: (a) 34 dB SPL; (b) 32 dB SPL

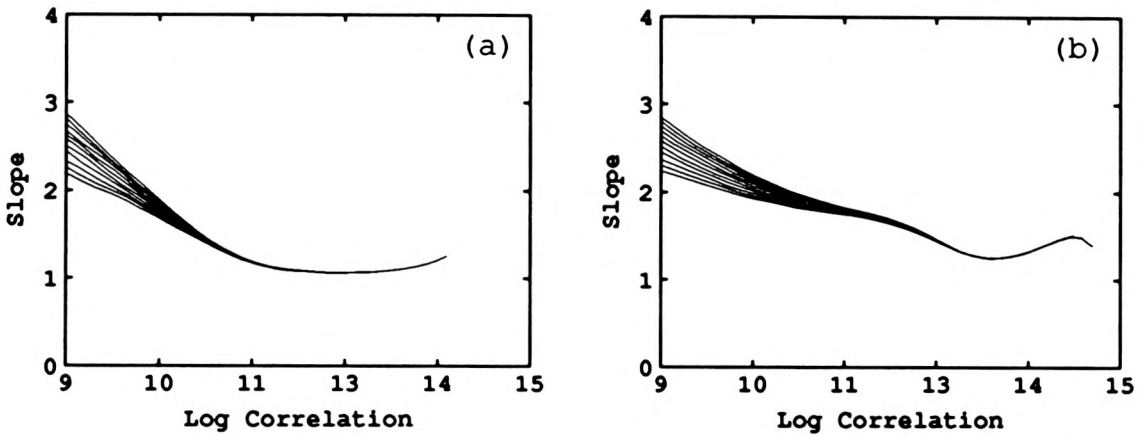

FIGURE 5 Slope ($\Delta \log C(R)/\Delta \log R$) versus $\log C(R)$ for embedding dimensions M=8, 8, 10, ..., 18, for external tone levels of: (a) 34 dB SPL; (b) 32 dB SPL

crete steps in the correlation dimension from 1.4 to 1.7-1.8 are apparent (Table 2). To summarize, the complexity of the chaotic attractor increased as the external tone level decreased.

For a particular range of control parameters, the forced van der Pol oscillator goes into chaos via period doubling, and its correlation dimension varies from 1.15 to 1.29 (Rajasekar and Lakshmanan, 1988). If one accepts the van der Pol oscillator as a plausible active source model, the added reflection delays in the cochlear system may be responsible for the quasi-periodic route to chaos suggested by the side-bands of the forced emission (Figure 4b).

Conclusions

Our main results were that endogenous chaos was observed for an acausally filtered SOAE, and sinusoidal forcing in the vicinity of a SOAE produced a chaotic response. The spectral structure of dynamically linked, non-contiguous SOAEs

can be explained as a quasi-periodic spectrum, with an underlying phase-locking frequency below 30 Hz. The presence of chaos in OAEs and the quasi-periodic spectrum of linked, non-contiguous SOAEs are consistent with the view that OAEs in humans are produced by mechanically coupled, nonlinear active processes.

Acknowledgment

Work supported by NIH.

References

Bialek, W.S. and Wit, H.P. (1984) Quantum limits to oscillator stability: theory and experiments on acoustic emissions from the human ear. Phys. Lett. A 104, 173-178.

Burns, E.M., Stickland, E.A., Tubis, A., and Jones, K.L. (1984) Interactions among spontaneous otoacoustic emissions. I. Distortion products and linked emissions. Hearing Res. 16, 271-278.

Duifhuis, H.M, Hoogstraten, H.W., van Netten, S.M., Diependaal, R.J., and Bialek, W. (1986) Modelling the cochlear partition with coupled van der Pol oscillators. In: Peripheral Auditory Mechanisms (Eds. Allen, J.B., Hall, J.L., Hubbard, A., Neely, S.T., and Tubis, A.) Springer-Verlag, Berlin, pp. 290-297.

Fenstermacher, P.R., Swinney, H., and Gollub, J.P. (1979) Dynamical instabilities and the transition to chaotic Taylor vortex flow. J. Fluid Mech. 94, 103-128.

Fraser, A.M. and Swinney, H. L. (1986) Independent coordinates for strange attractors from mutual information. Phys. Rev. A 33, 1134-1140.

Glass, L., Shrier, A., and Belair, J. (1986). Chaotic cardiac rhythms. In: Chaos (Ed. Holden, A.V.) Princeton, Princeton, pp. 237-256.

Grassberger, P. and Procaccia, I. (1983) Measuring the strangeness of strange attractors. Physica 9D, 189-208.

Jones, K. J., Tubis, A., Long, G.R., Burns, E.M., and Strickland, E.A. (1986) Interactions among multiple spontaneous otoacoustic emissions. In: Peripheral Auditory Mechanisms (Eds. Allen, J.B., Hall, J.L., Hubbard, A., Neely, S.T., and Tubis, A.) Springer-Verlag, Berlin, pp. 266-273.

Keefe, D.H. and Laden, B. (1990) Chaotic dynamics of woodwind instrument multiphonics. Submitted to J. Acoust. Soc. Am.

Keefe, D.H. and Ling, R. (1990) Acausal bandpass filtering of noisy, chaotic signals. Manuscript in preparation.

Mitschke, F. (1990) Acausal filters for chaotic signals. Phys. Rev. A 41, 1169-1171.

Rajasekar, S. and Lakshmanan, M. (1988) Period-doubling bifurcations, chaos, phase-locking and devil's staircase in a Bonhoeffer-van der Pol oscillator. Physica D 32, 146-152.

Swinney, H.L. (1986) Experimental observations of order and chaos. In: Nonlinear Dynamics and Chaos (Thompson, J.M.T. and Stewart, H.B.) Wiley, Chichester, pp. 332-349.

Tubis, A., Long, G. R., Sivaramakrishnan, S., and Jones, K.L. (1988) Tracking and interpretative models of the active-nonlinear cochlear response during reversible changes induced by aspirin consumption. In: Cochlear Mechanisms, Structure, Function, and Models (Ed. Wilson, J.P. and Kemp, D.T.) Plenum, New York, pp. 323-330.

OBSERVATIONS ON SIMULTANEOUS SFOAE AND DPOAE GENERATION AND SUPPRESSION

David T. Kemp, David N. Brass and Mark Souter

Institute of Laryngology and Otology, UCMSM,
330 Gray's Inn Rd London WC1X 8EE

Introduction

Two-tone otoacoustic distortion product measurements are usually made without reference to the stimulus frequency emissions being generated at the same time. Similarly the suppression of a stimulus frequency emission by a second tone is usual reported without reference to distortion product generation. However in general both stimulus and distortion product components result when two tones pass through a nonlinear transmission path. Data on both are needed to test models of the underlying mechanism.

Figure 1 describes the relationships between stimulus frequency and distortion product outputs for a simple saturating nonlinearity. OAE observations of course do not constitute observations of transmission through the single nonlinear pathway, but through a field of spacially distributed transmission paths and sources along the cochlea partition. The contribution of each elemental nonlinear component (ie each OHC) might be modelled as a simple saturating system but thousands of these contributions summate to produce OAEs Calculation of the outcome would need knowledge of the spacial distribution and characteristics of the 'sources' of OAEs integrated with a realistic nonlinear active cochlear model. There are so many unkowns with respect to the cochlea in general and OAEs in particular that it would be difficult to have confidence in the outcome of such an analysis. Some further insights into the behaviour of OAEs would be of use. We can explore the characteristics of OAE generation experimentally by changing the frequencies, and the relative and absolute levels of two tonal stimuli. The resulting input-output functions,growth curves, suppression curves and tuning curves can then be used to test hypothesese of OAE generation and summation. In this study we have tried to gain a qualitative understanding of what is observed in two tone OAE experiments in terms of the broadest description of the spacial distribution of the activity contributing to OAEs, and to the hearing process.

To observe both the amplitude and latency of both SFOEAs and DPOAEs generated during two tone stimulation, we used the 'nonlinear balance' method of Kemp and Souter (1988), as further developed by Brass and Kemp 1991. The method is illustrated in figure 2. Essentially a pulsed tone (f1 or f2) is employed to suppress the OAE evoked by a continuous tone , and in addition it generates DPs. The suppression can be partial, giving mutual suppression data or, with large and near-frequency pulsed tone, it can be 100%, giving the absolute OAE level for the continuous tone. The time reference of the pulsed tone allows latency to be measured for each component.

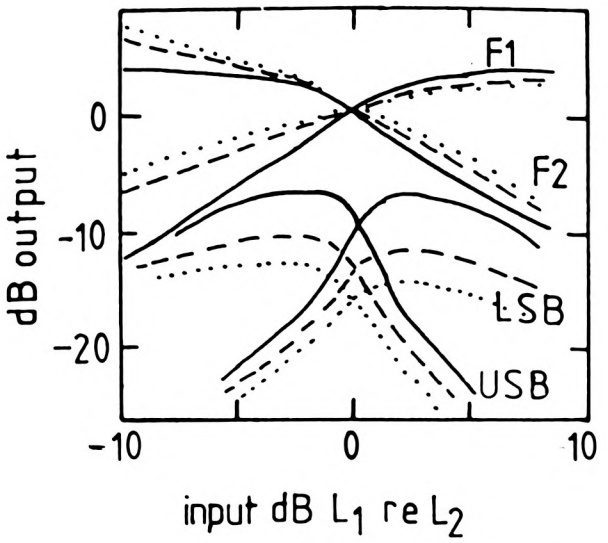

FIGURE 1 Transmission through a nonlinear system: If two sinusoidal signals are applied to any simple nonlinear transmission path then in general what emerges is a mixture of the input signal frequencies f1 and f2, intermodulation distortion products (2f1-f2,2f2-f2 etc) , and harmonics, and all the cross intermodulation frequencies. This figure illustrates how the proportions of f1,f2, 2f1-f2, 2f2-f1, depend on the relative amplitudes of f1 and f2, and the severity of the nonlinearity.

Output levels are computed for a nonlinear system receiving two tones f1 and f2 at levels L1 and L2. LSB is the lower sideband or 2f1-f2. L1 is fixed, while L2 decreases along x, giving higher values of L1dB re L2.. The solid line is for a 100% saturated input-output function (square step). The dashed line is for a cube root transfer, and the dotted for a square root transfer function. Note how the increasing level of f2, towards the left, decreases (suppresses) the output of f1, even though L1 is held constant. The output of f1 begins to decrease rapidly when L2 > L1. There is always some mutual suppression between f1 and f2 but the strongest of the two has the 'advantage' in passing through the nonlinear system and partially suppresses the output of the other. Note also that the intermodulation components are maximum when the amplitudes of f1 and f2 are similar, but not identical. The lower side band (2f1-f2) is greatest when F1 is al little stronger than F2, and the reverse for 2f2-f1.

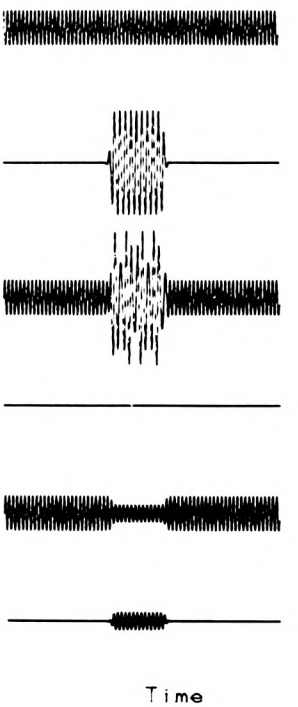

FIGURE 2 The method used to observe two tone interactions and SF and DP OAEs. One of two tones is continuously present, the other was pulsed on for 16ms at controlled times and phases. Stimulus generation and ear canal sound pressure digitisation is synchronised in time segments of 40ms. The continuous tone frequency is selected such that its phase alternated in consecutive sections. By digital addition and subtration of interleaved time segments, some with and some without the pulsed tone, in a stimulus cancelling paradigm the DIFFERENCE caused to the ear canal sound field by the presense of the pulsed tone, (exclusive of the pulsed tone itself) was obtained. We call this the (nonlinear) residual. The top two traces show the continuous and the pulsed stimulus respectively. Next down is the combined stimulus. In a block of 4 stimulus sections, the first two sections contained only the continuous tone, the following two sections contained pulsed tones, of the same polarity and phase, thus meeting the continuous stimulus in opposite phases. Subtraction of the two pulsed sections and the two non pulsed sections respectively, then the subtraction of the two results, results in zero, except for nonlinear interaction products- called the residual. In the figure and below the line, is shown the notional OAEs to the continuous tone, with a depressed portion during the pulsed tone. Finally, bottom, the waveform manipulations extract the 'missing' OAE during the pulsed tone- the residual.
The residual level is a function of both stimuli. Its relation to the OAE requires explanation. If the pulse tone was so strong as to suppress any otoacoustic response to the continuous tone, then the difference, or 'summation residual' would consist of the OAE that was produced in response to the continuous tone alone and which was not produced during the continuous and pulsed tone combined. In the general case, with the pulsed tone comparable in size and not too different in frequency to the continuous tone, the residual would comprise that **part** of the continuous tone OAE that had been suppressed by the pulsed tone. Hence a growth of residual with increasing pulsed tone, is actually a suppression of the SFOAE. (reverse logic). There is also the distortion product present , however this is generated only **during** the pulsed tone (ie when both f1 and f2 are present) , and it represents the actual DPOAE. Because of the need to cancel the pulsed tone , components phased locked to it are not registered. Two experiment are needed. When f1 is pulsed, the f2 residual and 2f1-f2 can be measured,.With f1 pulsed, f2 residual and 2f2-f1 can be recorded. Being produced apical to its frequency place in the cochlea, 2f2-f1 is normal heavily attenuated

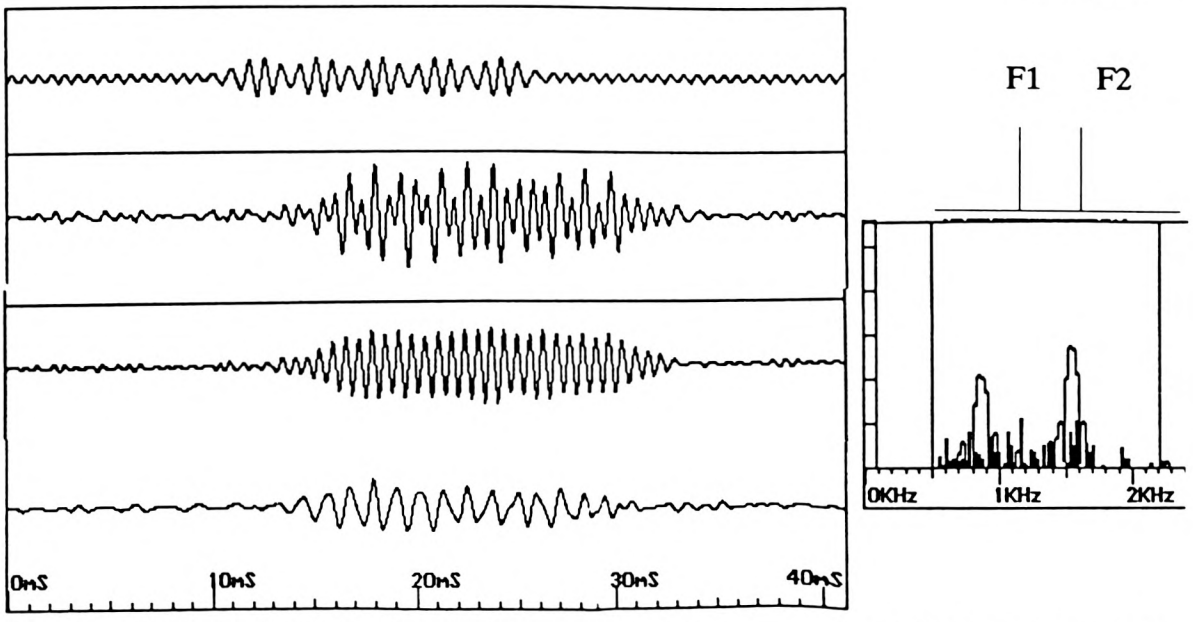

Figure 3. Experimental data showing stimulus frequency and distortion product OAEs in a human ear. Top: The stimulus during a section containing both the continuous and the pulsed tone. In this case f2 is a continuous tone of 1550Hz at 60dBspl, and f1 1200Hz, 70dB, pulsed on for 16ms. Second down: the residual due to the nonlinear interaction between the two tones. It clearly is complex, and contains different components to the stimulus about (ie the beats are different) Frequency analysis (right) reveals two components, at f2(1550Hz) and 2f1-f2 (850Hz). Time domain filtering reveals the envelope of the two component (lower two). Note the latencies of the DP and F2 OAEs. of about 5ms and the rise and fall times.These are not the result of the band limiting applied (500-2200Hz) The SFOAE (residual) commences synchronously with the DP. The DP is small than the SFOAE. This is common but can be reversed for certain stimulus combinations Note: The OAE output at F1, is not show. It is cancelled in this experiment, and requires the alternative experiment where F2 is pulsed.

RESULTS

Two tone observation were made on 3 normal adult subjects. Figure 3 shows an example of data obtained. Stimulus frequency emissions and distortion frequency emissions can both be seen in the time domain. The absolute and relative levels of each component depends strongly on the stimuli. Figure 4 shows levels of DP and F1 and F2 residuals as a function of the intensity of F2. It demonstrates a trade-off between f1 and f2 OAE residuals levels, and the broad 'off-center' peak in 2f1-f2 generation, which are characteristics of saturating nonlinear systems as described in figure 1.

SUPPRESSION RATE

The rates of suppression of the output of one tone with increasing level of the other is an important characteristic of nonlinear systems. In figure 1 this approaches unity (1dB/dB). The actual frequencies of f1 and f2 are unimportant in a memory-less model nonlinearity. In the ear, suppression rate depends on the stimulus-suppressor frequency ratio. Figure 5 shows OAE suppression rate data obtained using a swept suppressor intensity method.. The rate of suppression is about 1dB/dB for lower frequency suppressors, but is as little as 0.3dB/dB for higher frequency suppressors- unlike the model. We might suppose each nonlinear element along the basilar membrane (eg the OHC stereocilial bundle) did behave like the model as far as the mutual suppression of f1 by f2 and f2 by f1, and for the DP generation. In this case the most distortion product generation (LSB + USB etc) at be each element would then be when L1 = L2

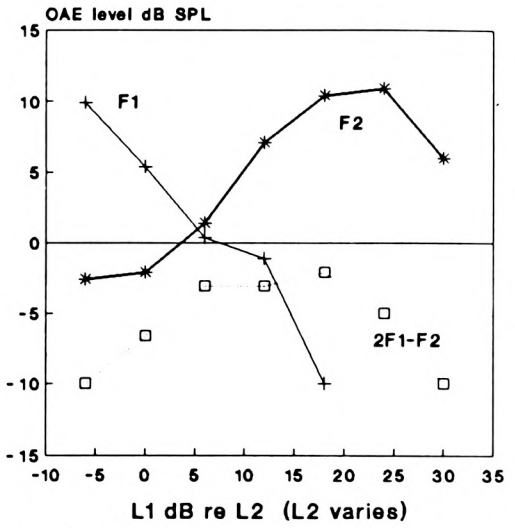

Figure 4 Experimental data for one human ear showing the behaviour of OAE response components during two tone stimulation, as a function of the level of F2. The method used to obtain this data is described in figures 2 and 3. F1 was fixed at 1247Hz 60dB . F2 was 1624Hz (F2/F1 = 1:1.3) The level of F2 (L2) decreases along the x axis, leading to an increase in L1/L2dB, marked on the axis. As in the computed example in figure 1, OAE levels of F1 and F2 behave in a complementary manner relative to the point of equal F1 and F2 output. The DP output is broadly peaked with the maximum DP is obtained with L1 > L2. Note however that in this figure F1 and F2 OAEs are residuals and represent suppression of an existing OAE. Caution is required making comparisons with figure 1. When L1 > L2, the F2 OAE2 residual is seen to be strong even though L2 is decreasing. This means that the actual OAE at F2 is being progressively more suppressed by the F1 . The same behaviour is found in the model.

locally at the nonlinearity. But for the cochlea as a whole the proportions of f1 and f2 vary with place along the BM making the net OAE dependent on a complex summation. The place of maximum DP generation would change with f1,f2, L1 and L2. For example if f2 > f1, then for the amplitudes of f1 and f2 can only be equal at the f2 place when L1 > L2 eternally. If L1 = L2 externally, then the place receiving equal stimulation will be basal to the f2 peak. From figure 4 we observe that f1 and f2 , (1:1.3) react equally when L1 > L2 by 5dB. We interpret this as a wave envelope effect, a linearity property.

OAE iso-suppression tuning curves can be constructed from suppression rate data such as in figure 5. Figure 6 shows a set of tuning curves from Kemp and Chum for different degrees of suppression. There is a shift of the tuning curve minimum to the high frequency side of the test stimulus of about 0.2 octave (1:1.2) when *lower* suppression criteria are used. This is direct consequence of the frequency dependent suppression slope. It can be seen from figure 5 that there is no detectable suppression from any *lower* frequency tones of levels more than 20dB below the stimulus level. In contrast ALL the HF suppressors give some suppression even when smaller than 20dB below the stimulus level. So OAEs are more easily suppressed by weak higher frequency suppressors, than by weak lower frequency suppressor. This is contrary to

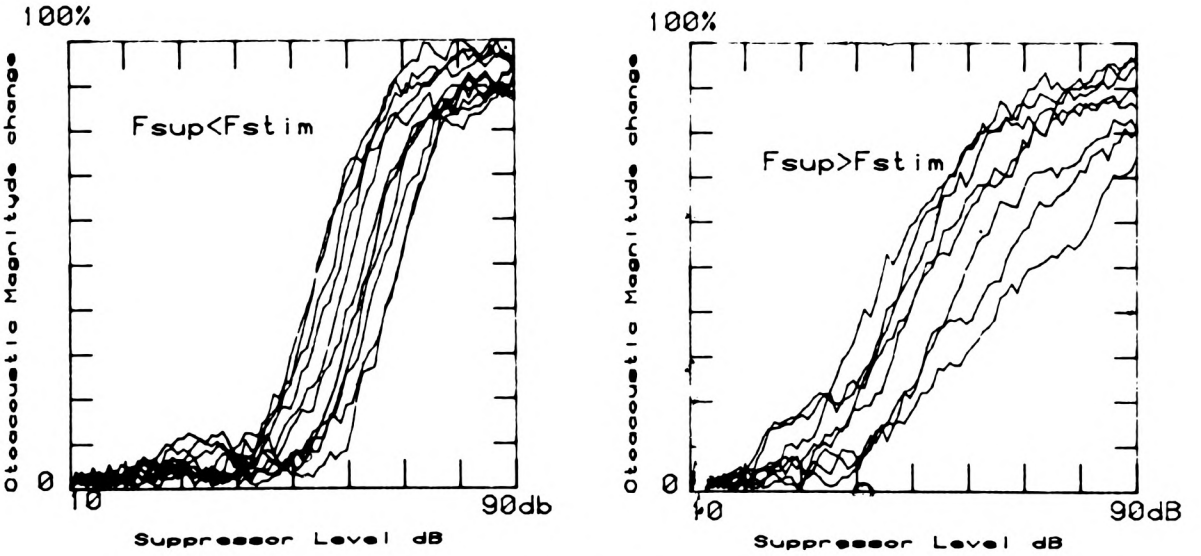

FIGURE 5: Changes in the OAE in response to a continuous 60dBspl 1256 Hz tone caused by a suppressor tone (left) at various lower frequencies , down to 900Hz, and (right) to various higher frequencies up to 1725Hz, as the level of suppressor was slowly swept from 0 to 90dBspl.(Kemp Chum method)

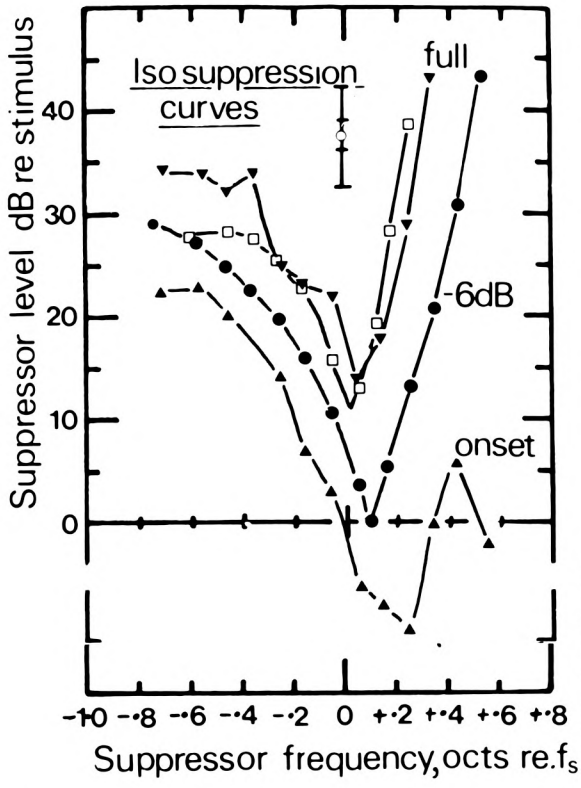

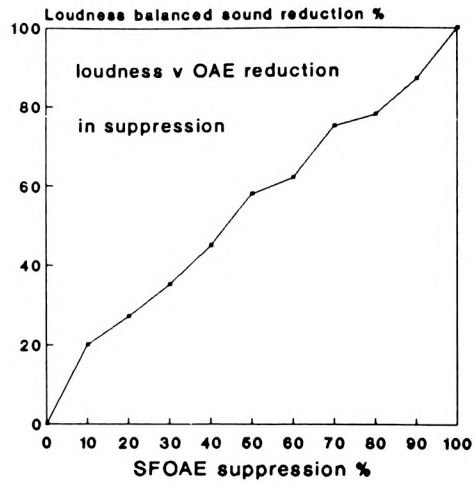

Figure 6 left: from Kemp and Chum isosuppression tuning curves derived from data such as in figure 5 by plotting the suppressor level needed to achieve specific suppression percentage criteria. Note how a lower suppression criterion shifted the centre of the curve to higher frequencies with evidence for very poor tuning on the high frequency side for minimal suppression criteria. Kemp and Chum noted that the stimulus remained audible until suppression was full. Right: we explored the relation between OAE suppression and loudness. Left, the OAE to 1600Hz is progressively suppressed by a 1700Hz tone. Loudness of the 1600Hz continuous tone was assessed by binaural loudness balancing. The percentage loudness balancing sound reduction required during partial OAE suppression follows closely the percentage reduction in OAE sound pressure level.

'intuitive' thinking on auditory tuning curves which are characterised by steep high frequency slopes. Using the residual method we explored OAE suppression in more detail in three subjects. Figure 7. shows suppression rates for higher and lower frequency suppressors and figure 8, iso-suppression contours. The contours show well the shift of suppression 'tuning' towards higher frequencies. There is a dramatic change from the expected "sharp tuning" obtained with high suppression criteria, to broader

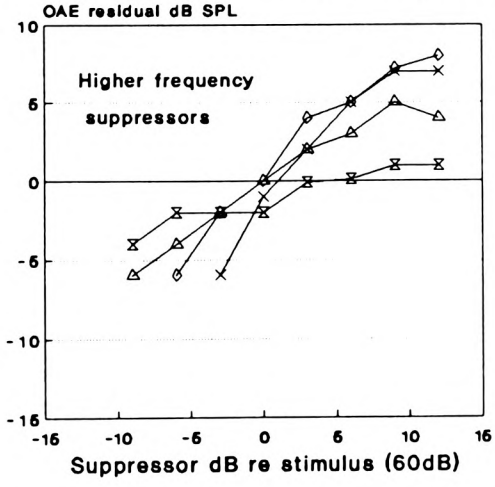

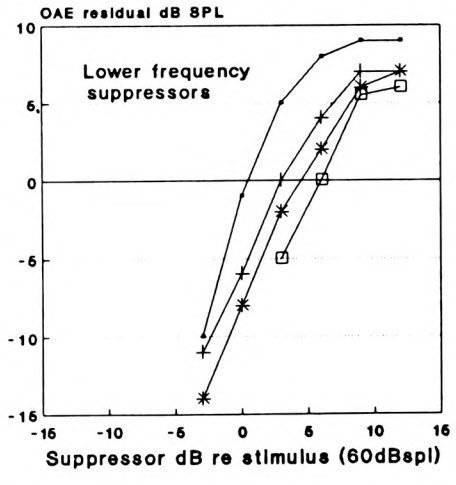

FIGURE 7 Experimental data showing the OAE residual due to suppression , as a function of suppressor tone level. The continuous test tone was at F = 1599Hz, 60dBspl. Left Suppressor frequencies above F, reading down through the data points at the right, suppressor frequencies were 1.1,1.2,1.3,1.5 times F stim respectively. Right data for lower frequency suppressors, reading down, Fstim, F,F/1.1, F/1.3, F/1.5. Data from three individuals showed the greater slope for lower frequency suppressors re high frequency suppressors . Note that for suppressors 10dB below the stimulus, higher frequencies caused substantial suppression whilst lower frequencies did not.

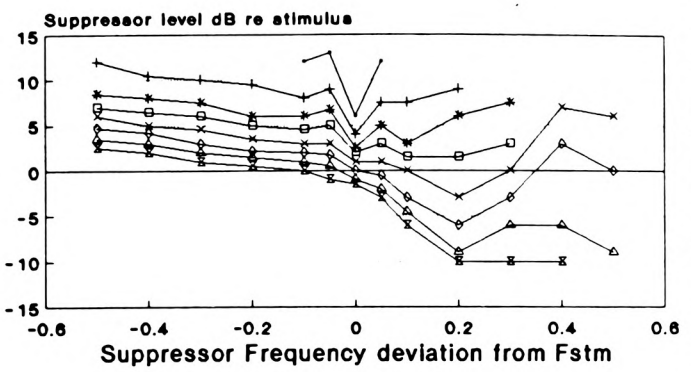

Figure 8 Iso suppression tuning curves were constructed from data sampled in figure 7, Actually they are iso-residual level curves. Taking the residual level obtained with the highers level suppressors as the full OAE, we can express the residual levels a %suppression of the OAE. List the curces from top to bottom the OAE is: 90%, 70%,60%,40%,30%,25%,15% and 10% suppressed. As the method/instrumentation employs was intolerant to high levels of suppressor (transducer nonlinearity becomes important) the 'norm al' sharp aspect of tuning was not full observed. The method was sensitive to small suppression residuals.

higher frequency tuning, for low suppression criteria. Phase was also measured. OAE residuals obtained using lower frequency suppressors showed a greater phase changes with increasing suppressor levels, (eg 40degrees) than did high frequency derived OAEs (less than 20 degrees). Suppressors near 1.3f, produced the least phase change.

MODEL OF THE HF MINIMUM-SUPPRESSION OAE TUNING ANOMALY

The envelope of the cochlear travelling wave for a tonal stimulus is highly asymetrical. Moving away from the base, the wave amplitude increases at first gradually until near to the place, it rises sharply, then falls precipitously on the apical side . This assymetry has interesting consequences for suppression. See figure 9a. Suppression can result mechanically in the cochlea if a second stimulus dominates and takes control of a saturating nonlinearity mechanism which is contributing to the excitation. Refering back to figure 1, we noted that at each non linear element, the suppressor had little effect unless its amplitude was nearly equal or larger than the stimulus level at the place of the nonlinearity. (termed 'dominance').How could this translate into OAE suppression curves? In figure 9b we derive a function simply related to the amount of basilar membrane where the suppressor dominates any vibration due to the stimulus. Iso suppression tuning curves constructed from this data show the tuning curve spreading to higher frequencies as lower suppression criteria are employed- just as in experimental OAE data. (figure 9c).

Discussion and Conclusions

We have reviewed several interesting aspects of two tone OAE generation and suppression well away from threshold levels. Elementary considerations of the properties of saturating nonlinearities and of the assymetry of the cochlear travelling wave seem useful in gaining an intuitive understanding of the behaviour of OAEs. In two tone experiments the relative amplitudes of simultaneously generated OAEs at f1,f2 and 2f1-f2, follow the general pattern expected from a saturating nonlinearity. The L1/L2 offset of the pattern may be accounted for by the spacial displacements of f1 and f2 peaks in the cochlea. Very poor suppression tuning is shown by stimulus frequency OAEs when a minimal suppression criteria is selected. Allowing for the implications of travelling wave assymetry, this behaviour is highly consistent with the f_{stim} OAE energy being dependent on a region of nonlinear elements, which extends basally from beyond the f_{stim} peak to at least the $1.3f_{stim}$ place on the basilar membrane. This result

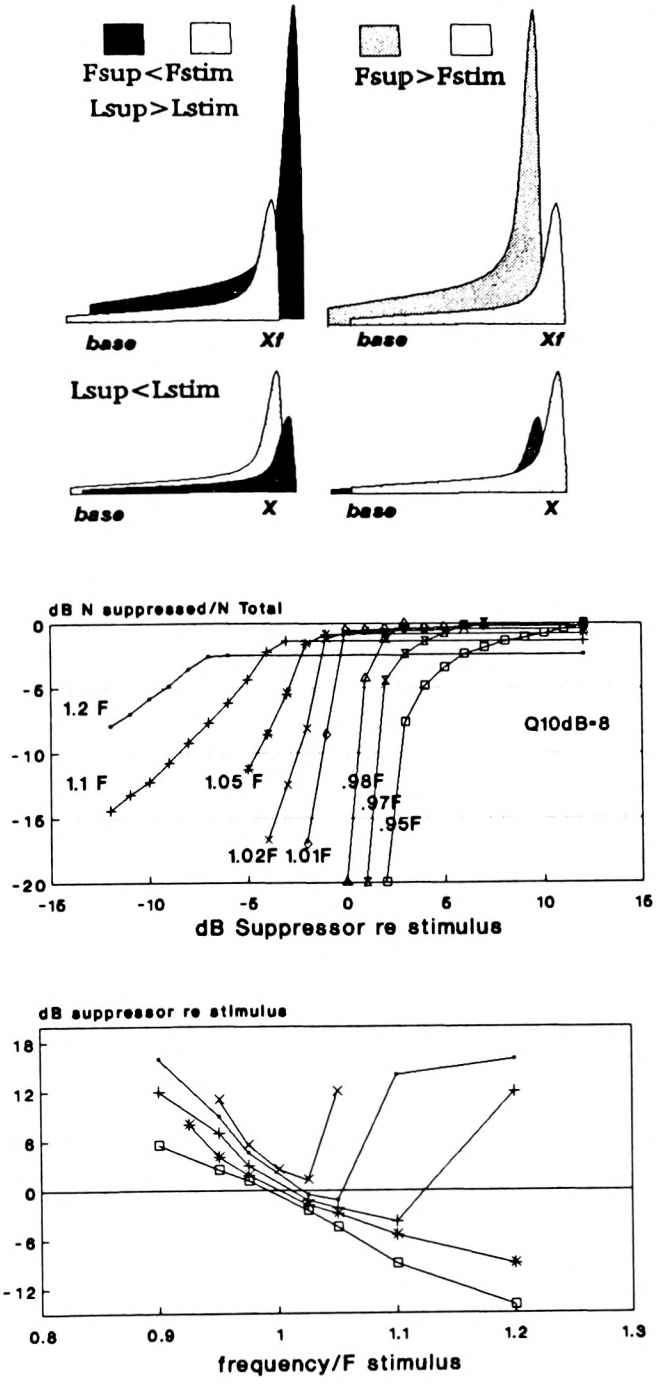

FIGURE 9 An examination of the way the kind of spacial assymetry found in the cochlear travelling wave (TW) envelope could give rise to the anomalous 'suppression tuning' curves from in OAE studies. a) The top panel represents TW envelopes. The vertical scale represents vibration amplitude A. The 'stimulus' is fixed in intensity (Lstim) and frequency Fstim, and is shown lightly shaded. The place of maximum vibration is at Xf. A suppressor with F < Fstim and L > Lstim, can achieve dominance (ie A > Astim) over every part of the BM stimulated by the stimulus. The suppressor vibration 'controls' any saturating nonlinearity. In contrast a higher frequency suppressor can dominate only a part of the basal side of the stimulus TW even when L > > Lstim. This conforms to the 'normal' feature of suppression tuning. Now consider a small suppressor (eg L = -10dB re stim). Being placed more basally it can still dominate over a significant region. In contrast a lower frequency suppressor can dominated any nonlinearity only over a very short region of the BM at the apical cut off.
b) The center panel. Given a profile of the travelling wave, and assuming quasi linearity discussed in the text) we can compute the length of BM over which the suppressor dominates for each suppressor level and frequency. We can then construct a 'suppression' graph similar to the OAE data (figure 8). The panel shows the result for a simple model $A = a(XF-X)/(1-b(XF-X)^3)$, $X <= XF$ The exact form is not critical . Higher frequency suppressors accummulate dominated length slowly but reach a lower final value. Lower frequency suppressors have no affect until a threshold is reached, then rapidly accummulate dominated length. Taking this data we constructed iso-length tuning curves,. These are shown in the lower panel (c) There is a remarkable similarity with experimental data in that the 'iso suppression' (dominated length) curves spill over into the high frequency areas when lower suppression criteria are used. The absolute values in the model used are of little relevance. It is just a computational illustration of the properties of superimposition, assymetrical spacial distributions. The models works qualitatively as well with a wide range of TW shapes and a wide range of formulas for integrating the suppressor dominated region. eg area under the curve. .

parallels current thinking on the optimal location for the cochlear amplifier. However a greater susceptability of f_{stim} OAE's to weak high frequency suppressors (eg 1.3 f_{stim},) does not in itself require that f*stim* OAEs be transmitted *from* a region basal to the f_{stim} peak, or that f_{stim} OAEs are especially dependent on this region. Frequencies below f_{stim} suppress OAEs in a manner which suggests they act on nonlinear elements at and apical to the peak. The substantial latency of OAEs and the suppression-residual phase changes typical of low frequency suppressors supports the involvement of the peak, where phase gradients are strong.

The minimal-suppression OAE tuning anomaly is a direct product of the low suppression slopes obtained with higher frequency suppressors. This characteristic is not confined to OAEs. Many other tone-on-tone suppression data, including neural, haircell, data etc shows similar characteristics, ie greater susceptability to *weak higher* frequency than to *weak lower* frequency tones. We think the significance of this has not been fully explored. The same characteristic is observed psychophysically. In partial masking, loudness is reduced more rapidly by a rising intensity lower frequency masker, than by a higher frequency suppressor. The latter commences at a lower masker level, just as for OAEs.

We propose that changes in $_{fstim}$ OAE amplitude (eg in partial suppression) can correspond directly and quantatively with changes in the excitation resulting in sensation which may or may not be exactly equivalent to the travelling wave amplitude. When we compared loudness reduction in partial masking with OAE reduction (Figure 6b) we found a one-to -one quantitative correspondance between OAE suppression, and the loudness balanced tones sound pressure reduction. We continue to believe that the absolute level of the unsuppressed fstim OAEs has little significance(other than indicating relatively normal function), and that it can be attributed to those spurious (anatomical) factors leading to the escape of OAE energy. We think SFOAE transmitting sources are most effective when stimulated by the peak of a travelling wave. However changes in the the OAE which is transmitted seem to provide an accurate linear readout of changes to an important internal excitory parameter, which accummulates over a more basal region. If so our observations on the spacially extended contributions to OAE energy are correct, it means that the level of excitation leading to loudness also depends substantially on mechanically active nonlinear elements extending well basal to the peak. These elements (OHCs) could well be saturated (as required by our nonlinear 'dominance' arguement) at the intermediate levels used here (around 60dB) over much of the region base to place. If each OHC released a similar but limited pulse of mechanical energy per deflection, each contributing to the magnitude of the forward wave, then this would explain the good correlation between the dominated-length function in the model, and the suppression properties observed. At moderate stimulus levels the magnitude of the nonlinear interactions would be limited to the low saturation level of the active mechanism at each point, not the entire wave amplitude, justifying the quasi linear assumption made in the model.

Acknowledgements

Supported by Hearing Research Trust and the Medical Research Council

References

Kemp D.T. and Chum 1980 Observations on the generator mechanism of stimulus frequency acoustic emissions- two tone suppression. In: Psychophysical, Physiological and Behavioural Studies in Hearing. (Eds:van den Brink, G. and Bilsen F.A.) Delft Univ. Press.

Kemp D.T. and Souter M 1988 The dynamics of cochlear perturbations following brief acoustic and efferent stimulation- otoacoustic and CM data. In Basic Issues in Hearing Es Duifuis, Horst and Wit, Academic Press pp 116-123

Brass D and Kemp D.T. ... Measurement of steady tone evoked otoacoustic emissions and comparison with click evoked emissions. . Submitted to JASA August 1990.

COMPONENTS OF THE $2f_1$-f_2 DISTORTION PRODUCT IN THE EAR CANAL OF THE BOBTAIL LIZARD

Geoffrey A. Manley[1], Christine Köppl[1] and Brian M. Johnstone[2]

[1]*Institut für Zoologie, Technical University, Munich, FRG*
[2]*Dept. of Physiology, University of W. Australia, Perth, Australia*

Introduction

Cubic distortion products (DP) in the sound field of the external auditory meatus have been measured at several levels in a variety of species (e.g., Brown, 1987; Kemp and Brown, 1983, 1984, 1986; Kim et al., 1980; Lonsbury-Martin et al., 1987; Martin et al., 1987; Rosowski et al., 1984; Schmiedt and Adams, 1981; Schmiedt and Addy, 1982; Wilson, 1980; Zurek et al., 1982). The hearing organ processes acoustic stimuli which can differ enormously with reference to their sound pressure. As the ear is made up of a number of structures with different degrees of inherent nonlinearity, it is not surprising to find that the amount of distortion measurable is not only level dependent, but originates from a variety of sources (e.g., Brown, 1987; Kim et al., 1981; Rosowski et al., 1984; Whitehead et al., 1990). The distortion output in the ear canal resulting from these different sources depends in a complex way on the frequency, frequency ratio, level, and phase of the primary tones fed to the ear.

In recent years, the development of more sensitive measuring equipment and of fast spectrum analyzers has made it easier to measure DPs in the sound field of the external meatus. This facility has suggested the use of DPs arising from the normal operation of the organ of Corti as objective and non-invasive measures of the performance of the hearing organ in a clinical context. Thus it has become more important to understand the principles underlying their generation and the factors that lead to reduced output.

As in the study of other features of hearing systems, the comparison of data from nonmammalian species can help in delineating those response characteristics which are fundamental to vertebrate hearing organs and those which result from structural and physiological arrangements unique to mammals. Responses common to all terrestrial vertebrate ears can often be more easily studied in more robust nonmammalian ears.

The present study was undertaken for two reasons. Firstly, Rosowski et al (1984) found a component of the cubic DPs in the alligator lizard which appeared at very low sound pressure (their component 3), but which they were unable to study in detail, as it only slightly exceeded their noise level. These authors attributed a component appearing

at somewhat higher SPL (component 2) to nonlinearities in the macromechanical stage of stimulus processing in the inner ear. However, the alligator lizard has a very small papilla, in which most of the hair cells are not connected by a tectorial structure, suggesting that it would be very difficult to pick up emitted hair-cell activity. We wished to examine this question in the bobtail lizard, a species which has a much larger number of hair cells, all covered with tectorial structures.

The second reason for this study was to help elucidate those characteristics of DPs that are useful for the assessment of the integrity of specific cochlear regions; i.e., those components which originate in a frequency-specific fashion from the hearing organ.

The inner ear of the bobtail lizard is well developed, containing almost 2000 hair cells in its 2mm length (Köppl, 1988). Two groups of afferent nerve fibres have been defined, which differ in a number of aspects of their discharge characteristics. There are low-CF fibres (up to about CF 0.8 kHz) which innervate an apical hair-cell area and high-CF fibres (CF 0.85 to 4.5 kHz) innervating the hair-cell area in the longer basal papillar segment (Köppl and Manley, 1990a,b; Manley et al., 1990a,b). We have previously presented evidence that the tectorial system of the basal, high-CF papillar segment (a chain of sallets) subdivides this segment into about 80 functional units. The frequency tuning and selectivity of each unit is most likely determined by the stiffness of all hair-cell bundles connected to the tectorial sallet and by the mass of the sallet (Manley et al., 1988, 1989).

The present paper is a preliminary report on the characteristics of the cubic DP $2f_1$-f_2 in the bobtail lizard's ear canal.

Material and Methods

This study was carried out using 20 bobtail lizards, *Tiliqua rugosa*, captured wild under licence in Western Australia and kept in outside cages. They were maintained in captivity for periods of between 4 and 24 weeks before being used in the present study, (most animals being used several times), and fed ad lib on a diet of fruit, vegetables, meat and eggs, with a multi-vitamin supplement. Following the experimental series, most animals were returned to their natural environment. To enable DP measurements, they were anaesthetized with diazepam (Valium, 2 mg/kg initial dose, i.p.) and Nembutal (25 mg/kg, i.p.) and maintained lightly anaesthetized on smaller supplementary doses. The animals did not need to be respirated and they recovered following the experiment. In the few cases in which studies of anoxia were carried out, animals were more deeply anaesthetized and paralysed with alcuronium chloride (Alloferin, a single dose of 0.5 mg/kg, i.m.). They were then respirated using a small animal air pump running at a speed of about 12 RPM, which approximates the rate of breathing of resting animals. In three cases, DPs were measured before and after the death of the animal, death being induced by a nembutal overdose followed by turning off the respiratory pump.

Continuous pure tones were generated and attenuated by HP 3325A frequency synthesizers under computer control and fed separately via additional manual attenuators to two Beyer DT 770 headphones. The headphones were enclosed in custom-built metal cases connected by 7cm plastic tubes containing acoustic damping material to just behind the tip of the cone-shaped cover of a B & K 0.5" microphone. The cone's tip was sealed

with petroleum jelly into the lizard's external ear canal. Individual sound calibrations were carried out, which were also used to assess the goodness of the ear-canal seal. The microphone output was amplified 20 dB via a B & K low-noise preamplifier and fed directly to the input of an HP 3561 dynamic signal analyzer (DSA).

In general, data collection was fully automated, using a PC with an IEEE 488-bus system to control the frequency synthesizers and the DSA. We chose a series of standard primary tones (f1), and studied the presence and magnitude of the DP $2f_1$-f_2 in the sound field of the external ear canal by presenting varying frequencies of f_2 (mostly 16 ratios of f_1:f_2 between 1.03 and 1.63). The SPLs of both primaries were kept equal to within +/- 5 dB and raised in 5 dB steps, mostly beginning around 20 and ending near 70 dB SPL. The level of f_2 was adjusted by the computer according to the individual calibration table, to maintain the primaries at the same level.

The level of the DP was read automatically from the DSA after 5 or 10 averages of RMS FFT spectra, using a Hanning window and a bandwidth of 3.75 or 1.875 Hz. In addition, noise values at +10 Hz and -10 Hz from the DP were read off and averaged, enabling the assessment of DP levels with reference to the noise in that frequency band. The computer stored the result of the presentation of the entire matrix of frequency combinations and levels. Data were then analyzed off-line using a program that calculated iso-output response contours, threshold contours for various DP output levels and I/O functions for each ratio, all with or without reference to the stored noise levels. Thresholds of DP-production were defined as the primary SPL at which the DP amplitude reached a level 2 standard deviations above the noise level around the DP frequency, as averaged over the measurements at all primary levels up to 70 dB SPL. These threshold values were only accepted if the DP output at the next higher primary level also met the same criterion. The DP was studied for its dependence on f_1, the primary ratio and level, and for the changes ensuing during anoxia and death. The DPs produced directly by the acoustic driver system were assessed both in the dead animal and by measuring them in a closed "dummy" ear canal, consisting of a plastic tube of the dimensions typical of the ear canal and closed at the "eardrum" end by a loosely-stretched sheet of "Parafilm" laboratory plastic film.

Results

Within the range of SPLs normally used, the DPs produced directly by the acoustic driver system were below the noise level in the animal (0 to <-10 dB SPL). The lowest primary levels at which DPs produced directly by the earphones in a (quieter) dummy system were measurable was generally greater than 80 dB SPL. They thus have little influence on the data reported here.

The ear of the bobtail lizard produces DPs which, at the lowest detectable levels, can be as large as 28 dB below the primary tones, but are typically between 30 and 40 dB below. The values depend on the frequency, level and ratio of the primaries. The lowest levels at which DPs were measurable are frequency dependent in a way resembling the neural audiogram, being most sensitive between 1 and 2 kHz, for primaries of levels below 10-20 dB SPL (Fig. 1).

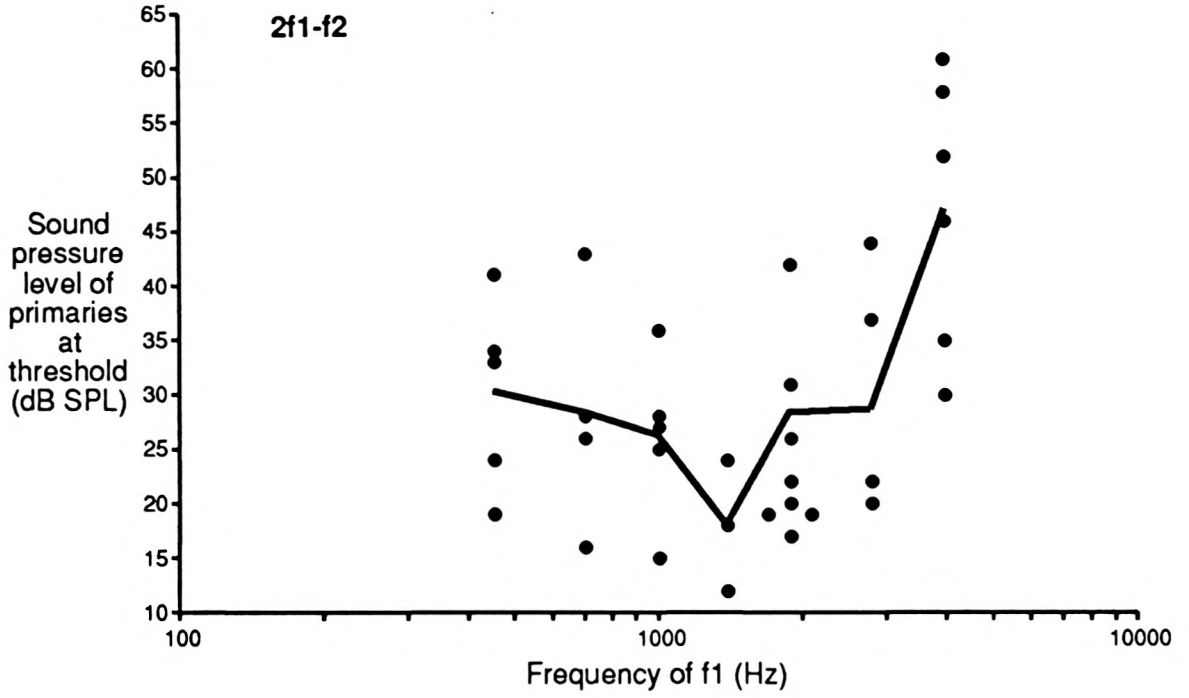

FIGURE 1 The lowest primary levels producing criterion "threshold" DP output at any ratio of primaries. f_1 normally = 0.455, 0.705, 1.005, 1.4, 1.9, 2.8 and 4.0 kHz. The continuous line joins the average threshold values for the standard f_1 frequencies.

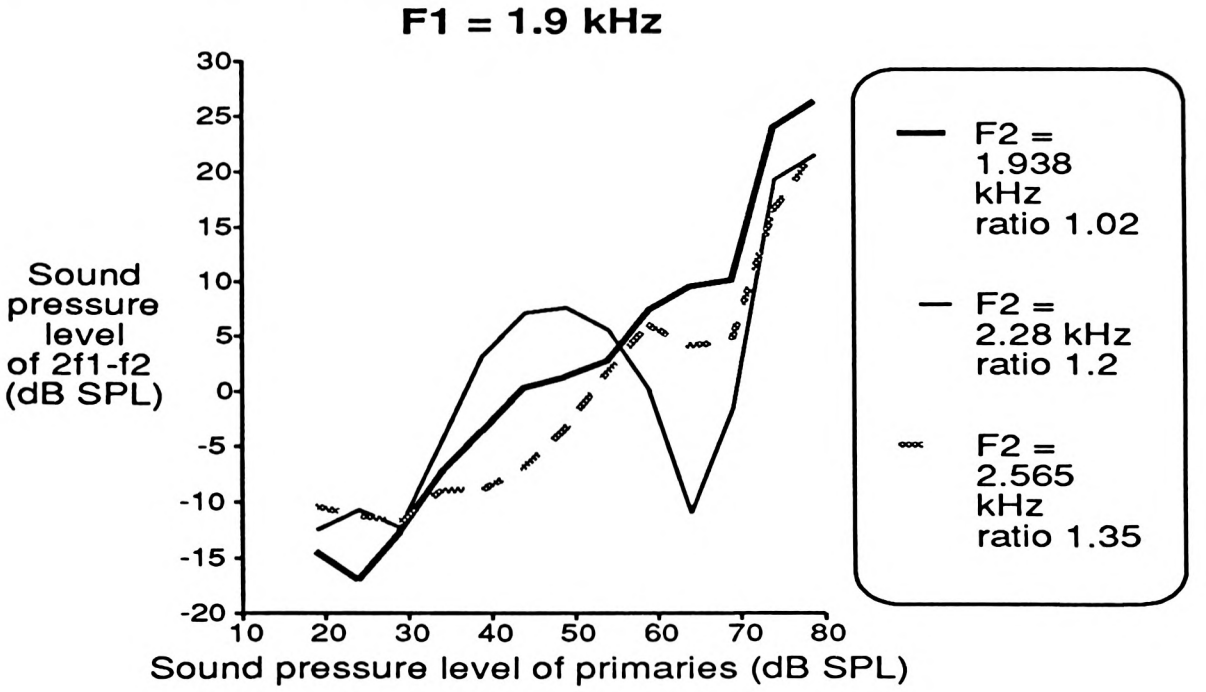

FIGURE 2 Level of the DP $2f_1$-f_2 in the ear canal of the bobtail lizard as a function of the level of the primary tones in one animal. Parameter is the ratio of the primary tones. f_1 = 1.9 kHz.

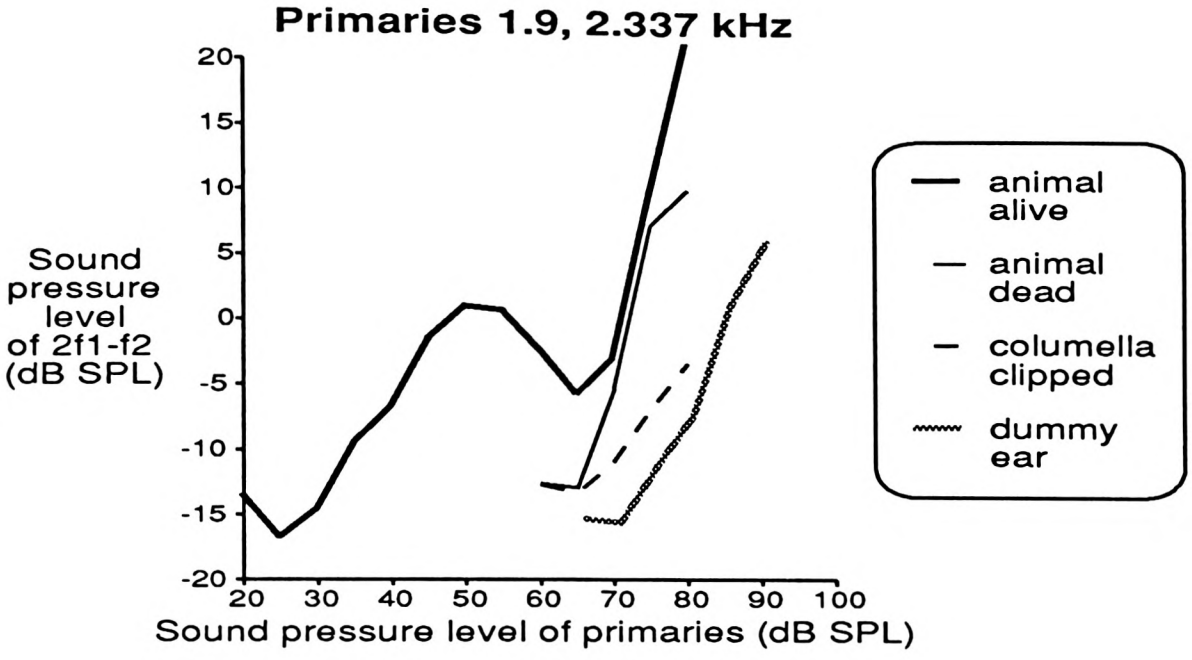

FIGURE 3 Level of the DP $2f_1$-f_2 in the ear canal of the bobtail lizard as a function of the level of the primary tones under different conditions. f_1 = 1.9 kHz. "Animal dead" represents a measurement about three hours after turning off the respirator.

DPs grow with intensity within 20 dB of their threshold at a maximal rate of about 1 dB/dB increase in primary levels. Growth rates are frequently slower and/or show sharp notches at particular primary ratios and levels. At levels above 55-65 dB SPL, depending on the primary frequency and the ratio of the primaries, additional sources of DPs become obvious, which have faster growth rates and normally show interference with DPs already present at lower levels. This is frequently indicated by a notch in the I/O function preceding a prominent change in slope (Fig. 2).

The optimal primary-tone ratio of higher-frequency primaries for producing $2f_1$-f_2 often changes with the level of the primaries. The DP produced in response to low primary levels, disappears rapidly following anoxia or death (Fig. 3). The higher-level components, however, do not and can only be strongly reduced by severing the ear ossicle (Fig. 3). Thus, in addition to the low-level DPs, which we suggest originate from active hair cells (comparable to component 3 in the alligator lizard), there seems to be at least one other, higher-level, component.

Discussion

When comparing the bobtail lizard to most mammals, it appears as if in the bobtail, the relative level of DPs produced for a given primary level is quite large (see, e.g., Lonsbury-Martin et al., 1987; Wilson, 1980; Zurek et al., 1982). They are, however, comparable to those of the gerbil (Brown, 1987). This may be due to a number of factors, including the absence of substantial basilar-membrane movement in the inner-ear (Manley et al., 1988) as an absorber of DP energy and to the very small size and great thickness of the "round window" in this species. Our experimental system made it

possible to measure in detail in the bobtail the equivalent of component 3 of the alligator lizard (Rosowski et al., 1984). Of course, the DP output in our species may also be greater than in the alligator lizard, due to the bobtail's larger number of hair cells, all of which are covered by tectorial material.

Brown (1987), Zurek et al. (1982) and Lonsbury-Martin et al. (1987) show that in the chinchilla, gerbil, guinea pig, rabbit and rat, the threshold and magnitude of DPs vary in a way consistent with the behavioural audiogram of these species. Similarly, in the bobtail lizard, the threshold for generation of $2f_1$-f_2 varies in parallel with the middle-ear transfer function (Fig. 1; Manley et al., 1988). The fact that the absolute primary levels eliciting threshold DPs correspond remarkably well to the best neural thresholds (Manley et al., 1990a) implies that these low-level DPs originate from hair cells that show significant cubic distortion at their lowest operating levels.

In the alligator lizard, Rosowski et al. (1984) suggested that most of the DPs they measured using primaries of levels above about 50 dB SPL arose from nonlinearities of the cochlear partition itself. These components had a high slope of growth (near 3) with primary level. The amount of DP output in the bobtail at high primary levels is very much lower than reported for the alligator lizard, where 80 dB SPL stimuli produced 60 dB SPL DPs. As we did not use a very high-impedance measuring system, however, this difference is difficult to evaluate. Data collected under anoxia and after death indicate that in the bobtail lizard, DPs measured using primaries below about 50 dB SPL originate predominantly from highly physiologically-vulnerable inner-ear components. Data collected at higher levels is much less or not vulnerable to anoxia. At optimal ratios and using primaries near the most sensitive frequencies for the bobtail's auditory papilla, there is thus a "window" of primary levels up to 40 dB wide between threshold and 50 dB SPL, within which the DPs seem to originate from hair cells. When other primary frequencies or suboptimal ratios (which necessitate using higher primary levels) are used, this window can be much narrower. As the slope of growth with level for the higher-level components is much more rapid than that of low-level components (slope up to 3 dB/dB increase in primary level, rather than 1 dB/dB), the lower-level DP components become very rapidly obscured by a small additional increase in primary levels. The critical level is about 50-60 dB SPL, depending on f_1 and on the ratio of the primaries. These data are relevant to the continuing discussion on the site of origin of cubic DPs and on their usefulness as assessors of the integrity of specific cochlear regions.

Ear-canal DPs in the gerbil elicited by 70 dB SPL primaries were not particularly vulnerable to anoxia, suggesting to Schmiedt and Adams (1981) that $2f_1$-f_2 is not a sensitive indicator of hair-cell activity. In contrast, Kemp and Brown (1984), using levels of 60 dB SPL in the same species, came to the opposite conclusion. Schmiedt and Addy (1982) found in the gerbil and cat that DPs generated by 70 dB SPL primaries reflected the recovery of the whole-nerve response following temporary threshold shift better than did DPs from 80 dB SPL primaries. Similarly, in the guinea pig, Brown et al. (1989) found that DPs generated by primary levels of 60 dB SPL or below revealed functional evidence of gentamicin poisoning of outer hair cells, but DPs produced by higher primary levels did not. These studies and others on animals (e.g., Wiederhold et al., 1986) and on humans (Smurzynski et al., 1990) have resulted in quite different conclusions about the "usefulness" of DPs as indicators of cochlear integrity. Both Kemp

and Brown (1984) and Lonsbury-Martin et al., (1987) have suggested that one possible origin of the differences seen may be the use of different primary levels. In the rabbit, Lonsbury-Martin et al. (1987) found that DPs generated by 65 dB primary tones decline after death, whereas those resulting from 75 dB tones did not. If there are several sources of DPs, each with its own level dependence, then clearly the results of suppression-tuning and anoxia experiments will be dependent on the primary levels (e.g., Brown, 1987; Kim et al., 1981; Rosowski et al., 1984; Whitehead et al., 1990). In a related study (Manley and Köppl, in preparation)), we measured the suppressive effect of a third tone of varying frequency and level on ear-canal DPs in the bobtail lizard using DPs generated by primary tones of different SPLs, At primary-tone levels below about 55 dB SPL, iso-suppression tuning curves for 2f1-f2 were sharply tuned and most sensitive near the frequencies of the primaries. In contrast, tuning curves for DPs produced at higher levels were most sensitive about 0.5 octaves below the primary frequencies.

Rosowski et al. (1984) concluded that since their components 1 and 2, measurable at primary levels of 55 dB and above, were not associated with hair-cell processes, they are not particularly useful indicators of cochlear health. The low-level DPs of the bobtail lizard are, however, very vulnerable to anoxia and thus behave quite differently from the data described at higher levels in the alligator lizard and, indeed, high-level DPs in the bobtail lizard. Thus it is clear that, as in mammals, the value of DPs for assessing the state of the hearing organ in lizards depends strongly on the level of the primaries used for measurement. The suppression tuning curve data from the bobtail lizard suggest that only DPs produced by primary tones of levels below about 55 dB SPL originate in that species primarily in the region activated at low levels by the primary tones. If mammals also show a level of primaries above which DPs may predominantly originate from more distributed hair-cell or even from other sources and show strong level dependence, then the difference in primary levels of 10 dB between the studies of Kemp and Brown (1984) on the one hand and Schmiedt and Adams (1981) on the other could be explained. Thus, if as in human data, DP levels lie well below those of the primaries (> 40 to 50 dB), the permissible "window" for studying DPs generated by active hair cells may be quite narrow and will be species- and frequency-specific. In applying DPs in a clinical context, therefore, it is critically important to establish the lowest level for optimal primary ratios in human ears and to measure using only primary levels well below those generating fast growth rates.

Acknowledgements

The computer programs used in these experiments were written in Garching by Martin Baumann. Supported by an Akademie-Zusatzstipendium to GAM from the VW-Stiftung and a program grant to BMJ from the Australian NH&MRC.

References

Brown, A.M. (1987) Acoustic distortion from rodent ears: a comparison of responses from rats, guinea pigs and gerbils. Hearing Res. 31, 25-38.

Brown, A.M., McDowell, B. and Forge, A. (1989) Acoustic distortion products can be used to monitor the effects of chronic gentamicin treatment. Hearing Res. 42, 143-156

Kemp, D.T. and Brown, A.M. (1983): A comparison of mechanical nonlinearities in the cochleae of man and gerbil from ear canal measurements. In: Hearing - physiological bases and psychophysics, pp. 82-87. Editors: R. Klinke and R. Hartman. Springer Verlag, Berlin, Heidelberg.

Kemp, D.T. and Brown, A.M. (1984): Ear canal acoustic and round window electrical correlates of $2f_1$-f_2 distortion generated in the cochlea. Hearing Res. 13, 39-46.

Kemp, D.T. and Brown, A.M. (1986): Wideband analysis of otoacoustic intermodulation. In: Peripheral auditory mechanisms, pp. 306-313. Editors: J.B. Allen, J.L. Hall, A. Hubbard, S.T. Neely and A. Tubis. Springer Verlag, Heidelberg, New York.

Kim, D.O., Molnar, C.E. and Matthews, J.W. (1980): Cochlear mechanics: Nonlinear behavior in two-tone responses as reflected in cochlear-nerve-fiber responses and in ear-canal sound pressure. J. Acoust. Soc. Am. 67, 1704-1721.

Kim, D.O., Zurek, P.M. and Clark, W.W. (1981) Ear-canal acoustic distortion products ($2f_1$-f_2) and ($2f_2$-f_1) can be suppressed or enhanced by a third tone. J. Acoust. Soc. Amer. 69. S51

Köppl C (1988) Morphology of the basilar papilla of the bobtail skink Tiliqua rugosa. Hearing Res. 35:209-228

Köppl C, Manley GA (1990a) Peripheral auditory processing in the bobtail lizard Tiliqua rugosa. II: Tonotopic organization and innervation pattern of the basilar papilla. J Comp Physiol A 167:101-112

Köppl C, Manley GA (1990b) Peripheral auditory processing in the bobtail lizard Tiliqua rugosa. III. Patterns of spontaneous and tone-evoked nerve-fibre activity. J Comp Physiol A 167:113-127

Lonsbury-Martin, B.L., Martin, G.K., Probst, R. and Coats, A.C. (1987): Acoustic distortion products in rabbit ear canal. I. Basic features and physiological vulnerability. Hearing Res. 28, 173-189.

Manley G A, Yates G, Köppl C (1988) Auditory peripheral tuning: evidence for a simple resonance phenomenon in the lizard Tiliqua. Hearing Res 33:181-190

Manley GA, Köppl C, Yates GK (1989) Micromechanical basis of high-frequency tuning in the bobtail lizard. In: Wilson JP, Kemp D (eds) Cochlear Mechanisms - Structure, Function and Models. Plenum Press, N.Y. pp. 143-150

Manley GA, Köppl C, Johnstone BM (1990a) Peripheral auditory processing in the bobtail lizard Tiliqua rugosa. I: Frequency tuning of auditory-nerve fibres. J Comp Physiol A 167:89-99

Manley GA, Yates GK, Köppl C, Johnstone BM (1990b) Peripheral auditory processing in the bobtail lizard Tiliqua rugosa. IV: Phase-locking of auditory-nerve fibres. J Comp Physiol A 167:129-138

Martin, G.K., Lonsbury-Martin, B.L., Probst, R. , Scheinin, S.A. and Coats, A.C. (1987): Acoustic distortion products in rabbit ear canal. II. Sites of origin revealed by suppression contours and pure-tone exposures. Hearing Res. 28, 191-208.

Rosowski, J.J., Peake, W.T. and White, J.R. (1984): Cochlear nonlinearities inferred from two-tone distortion products in the ear canal of the alligator lizard. Hearing Res. 13, 141-158.

Schmiedt, R.A. and Adams, J.C. (1981): Stimulated acoustic emissions in the ear canal of the gerbil. Hearing Res. 5, 295-305.

Schmiedt, R.A. and Addy, C.L. (1982): Ear-canal acoustic emissions as frequency-specific indicators of cochlear function. J. Acoust. Soc. Am. 72, S6.

Smurzynski, J., Leonard, G., and Kim, D.O. (1990) Distortion product otoacoustic emissions: basis for an objective assessment of cochlear functional state. Abstracts 13th Midwinter Mtg. Assoc Res in Otolaryngol. p. 239

Whitehead M.L., Lonsbury-Martin B.L. and Martin, G.K. (1990) Parametric features of otoacoustic distortion generation in the rabbit. Abstracts 13th Midwinter Mtg. Assoc Res in Otolaryngol. 240-241.

Wiederhold, M.L., Mahoney, J.W. and Kellog, D.L. (1986): Acoustic overstimulation reduces $2f_1$-f_2 cochlear emissions at all levels in the cat. In: Peripheral auditory mechanisms, pp. 322-329. Editors: J.B. Allen, J.L. Hall, A. Hubbard, S.T. Neely and A. Tubis. Springer Verlag, Heidelberg, New York.

Wilson, J.P. (1980): The combination tone, $2f_1$-f_2, in psychophysics and ear-canal recording. In: Psychophysical, physiological and behavioural studies in hearing, pp. 43-50. Editors: G. van den Brink and F.A. Bilson. Delft Univ. Press, Delft.

Zurek, P.M., Clark, W.W. and Kim D.O. (1982): The behavior of acoustic distortion products in the ear canals of chinchillas with normal or damaged ears. J. Acoust. Soc. Am. 72, 774-780.

Comments and discussion

WHITEHEAD

You demonstrated, in your poster at this meeting that the bobtail lizard has strong spontaneous otoacoustic emissions over the frequency range in which you have measured distortion-product otoacoustic emissions. In humans, the spontaneous emission generator appears to be at least partially separate from the distortion-product emission generator, and there is much evidence that the two emission types interact (e.g., Furst et al., 1988; Wier et al., 1988). Is it possible that the apparent difference between the observed distortion-product emissions at low and high stimulus levels in the bobtail lizard are not due to different distortion-product emission generators, as you suggest, and as seems to be the case in small mammals (e.g., Norton and Rubel, 1990; Whitehead, et al., 1990), but are due to interactions between the spontaneous and distortion-product emissions at low but not at high primary-tone levels ?

MANLEY

(1) The spontaneous otoacoustic emissions of the bobtail lizard are not remarkably strong. The peak amplitude at a bandwidth of 15 kHz is -3dB SPL (mode of distribution). They are, however, remarkably frequent, each ear having an average of 10 emissions.

(2) The correspondence of the frequency ranges of the spontaneous- and DP- emissions is due to their likely origin in the basal segment of the basilar papilla, which is tuned from about 0.8 to 4.5 kHz (Köppl and Manley, 1990a). In contrast to human data, both emission types are detectable up to the highest-frequency limit of frequency mapping in the bobtail lizard.

(3) There are no consistent differences in the behavior of the DP emissions in animals with and those without spontaneous emissions (in preparation), suggesting no significant interactions between the two. The presence of a spontaneous emission may or may not be manifested in small perturbations in the output level of the DP emissions. The interactions we see are small and occur at levels well below the approximate 55 dB SPL level which marks the transition from the DP behavior of low-level primaries to that at higher levels.

(4) The shape of the primary-fibre neural tuning curves (Manley et al., 1990a) would suggest that above 55 dB SPL, the excitation pattern on the basilar papilla rapidly becomes much larger. This factor will undoubtedly have an important influence on the behavior of the DP emissions and may obviate the necessity of postulating different DP generators.

References

Furst, M., Rabinowitz, W.M., and Zurek, P.M. (1988). Ear canal acoustic distortion at $2f_1$-f_2 from human ears: Relationship to other emissions and perceived combination tones. J. Acoust. Soc. Am., 84, 215-221.

Norton, S.J., and Rubel, E.W. (1990). This volume.

Whitehead, M.L., Lonsbury-Martin, B.L. and Martin, G.K. (1990). This volume.

Wier, C.G., Pasanen, E.G. and McFadden, D. (1988). Partial dissociation of spontaneous otoacoustic emissions and distortion products during aspirin use in humans. J. Acoust. Soc. Am., 84, 230-237.

ACTIVE AND PASSIVE ADP COMPONENTS IN MAMMALIAN AND AVIAN EARS

Susan J.Norton[1] and Edwin W Rubel[2]

[1] *Department of Hearing and Speech*
University of Kansas Medical Center
Kansas City, KS 66103
[2] *Hearing Development Laboratories*
University of Washington
Seattle, WA 98195

Introduction

In recent years, a number of investigators have suggested that the mammalian cochlea consists of two systems: one sharply tuned and physiologically vulnerable, and the other broadly tuned and relatively invulnerable. Davis (1983) suggested these two systems were active and passive, respectively. The majority of data supporting this hypothesis come from animal studies including Mossbauer measurements of basilar membrane displacement (e.g. Sellick, Patuzzi and Johnstone, 1982; Johnstone, Patuzzi and Sellick, 1984; Johnstone, Patuzzi and Yates, 1986) and recordings from single 8th nerve fibers (e.g. Sellick, Patuzzi and Johnstone, 1982; and see Kiang et al., 1986 for a review).

Figure 1 is a schematic representation of basilar membrane displacement at characteristic frequency (CF) as a function of stimulus level after Johnstone et al. (1984). Data from normal healthy cochleae and from damaged or post-mortem cochleae are represented by the solid and dotted lines, respectively. The function could just as easily represent AP (e.g.Pujol and Uziel, 1989) growth functions. One interpretation of the hyperbolic functions seen in the healthy ear is that responses to stimuli below 40-60 d SPL represent a mechanical resonance requiring metabolically active feedback processes (e.g. Neely and Kim, 1983, 1986; Davis, 1983). These active feedback forces are frequently associated with the outer hair cells (OHCs). The active processes have a limited dynamic range. At high stimulus levels the basilar membrane activity is dominated by large passive displacements. Post-mortem data or responses in the absence of functional OHCs reflect these passive components of basilar membrane displacement.

In this paper, we present acoustic distortion product (ADP) data from mammalian and avian ears during maturation. Our results support the hypotheses that: (1) there are basically two non-linear processes, one active and one passive, operating within both species; and (2) that ADPs are a non-invasive reflection of these processes. Data from normal developing gerbils and data from chickens following gentamicin administration are presented. Gerbils are altricial with respect to hearing. Responses to auditory stimuli develop primarily during the first post-natal month. Chickens, on the other hand, are precocial with respect to hearing. However, following destruction of hair cells by noise or ototoxic drugs shortly after birth, chicken have the ability to regenerate hair cells. The regeneration process follows the same anatom-

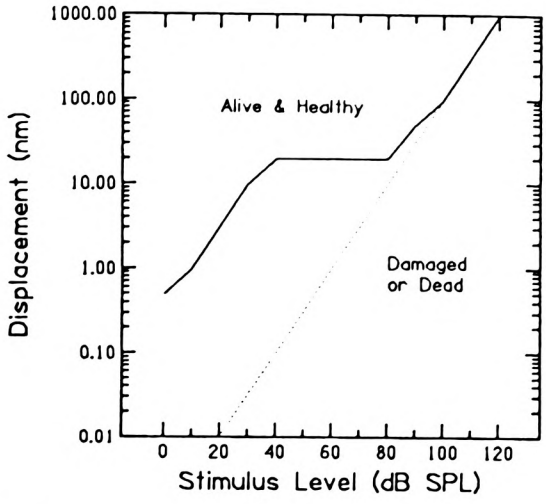

FIGURE 1. Schematic representation of basilar membrane displacement as a function of stimulus level. Solid line represents the response of a mature, normal cochlea, while the dotted line represents the response in a cochlea with damaged or non-functioning OHCs or from a recently dead animal.

ical sequence as hair cells in normal developing embryonic chicks (Cotanche, 1987a,b). Thus, the development of acoustic distortion product emissions accompanying hair cell maturation could be studied *in vivo* post-natally in both a mammalian and an avian ear.

Methods

ANIMALS

Mammals. Gerbils (*Meriones unguiculates*) ranged in age from postnatal day (P) 13 to 102. Gerbils P60 or greater were classified as adults. Animals were given a single injection of atropine sulfate (.05-0.1 mg, i.m.), followed by pre-anesthetic tranquilizer, ketamine hydrochloride (20 mg/kg, i.m.), then anesthetized with sodium pentobarital (40 mg./kg, i.p.) or chloral hydrate (400 mg/kg, i.p.). Supplemental doses of both the tranquilizer and anesthetic were administered as needed during the experiment to eliminate nociceptive responses. The pinna and outer third of the gerbil's external ear canal were surgically removed to facilitate probe placement.

Avians. Chickens (*Gallus gallus (domesticus)*) ranged in age from 11 to 164 days post-hatch (P). Chickens received a single dose of atropine sulfate, followed (.01 mg/kg, i.m.) by a pre-anesthetic tranquilizer, Vetalar (0.8 mL/kg, i.m.), then anesthetized with Equithesin (1.5 mL/kg, i.p.). Supplemental doses of both the tranquilizer and anesthetic were administered as needed during the experiment. Only the external ear covering was removed prior to probe placement. Experimental chickens received a 10-day course of gentamicin (50 mg/kg) beginning at P1. ADPs were measured either one day, or 2,6,8,10,12,14,18 or 22 weeks post-gentamicin. Age matched control birds were also studied.

PROCEDURES

Animals were placed in a double-walled IAC booth and secured to custom-designed head holders. Rectal temperature was maintained at 37 degrees C by an automatically regulated heating pad placed underneath the animal. An ER-10B microphone probe, used to measure the ear canal sound pressure levels, was fit in the ear canal using custom designed probe tips. Stimuli were presented through two ER-2 (gerbils) or two ER-3A (chickens) earphones connected to separate sound delivery tubes of the ER-10B probe assembly. Two sinusoidal stimuli, F1 and F2, F1 < F2, were presented simultaneously through separate channels. The sound pressure level outputted by each earphone at the probe tip was calibrated

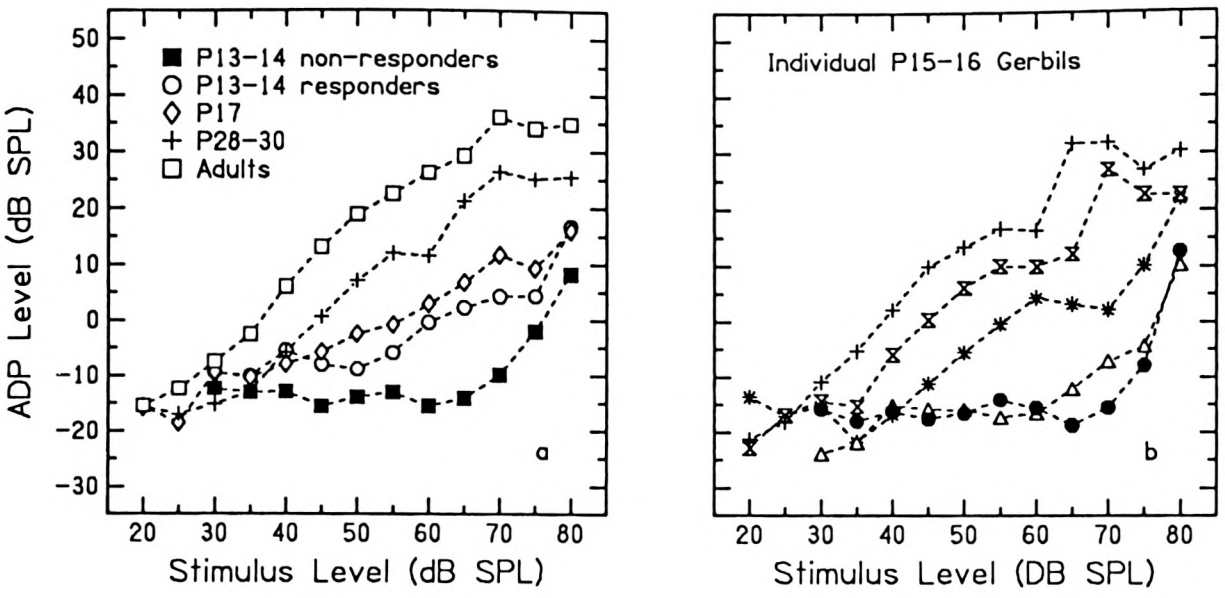

Figure 2. ADP level as a function of stimulus level for F2=2.6 kHz. (a) Mean data for gerbils as a function of age. (b) Data are for individual gerbils in the P15-16 age group.

from 0.2 to 15.0 kHz using the ER-10B microphone and a Hewlett Packard 3561A Signal Analyzer. Ear canal sound pressure level at the frequency of the acoustic distortion product 2F1-F2, the cubic difference tone or CDT, was measured using the ER-10B and the spectrum analyzer. For measurement of ADPs, the spectrum analyzer was center at the CDT frequency with a span of 0.2 kHz, yielding a resolution of .25 Hz. The ratio F2/F1 was 1.3. F2 ranged from 1.3 to 13.0 kHz for the gerbils and 0.5 to 5.0 kHz for the chickens. L1 equaled L2 and levels ranged from 10 to 80 dB SPL in 5-dB steps. Measurements were made on normal healthy animals, dead animals and animals treated with gentamicin.

Results

Our primary interest in this paper is the ADP amplitude input-output function, and it's relationship to cochlear status. Figure 2a shows mean ADP levels as a function of stimulus level for F1 = 2.0 kHz and F2 = 2.6 kHz from gerbils as a function of postnatal age in days. ADPs from the gerbil cochlea appear first in response to middle and high-frequency stimuli (F2=3.9 to 13.0 kHz) and appear last for low frequencies (F2=1.3 to 2.6 kHz). Mature appearing responses are found first for F2 frequencies from 5.2 to 13.0 kHz (Norton, Bargones and Rubel, 1990). These results are consistent with anatomical changes which occur during maturation of the cochlea and the timing of maturation of physiological responses to mid and high frequencies (e.g. Retzuis, 1884; Rubel, 1978; Pujol et al., 1980; Arjmand et al. 1988; Echteler et al., 1989; Sanes et al, 1989). In Figure 2a immature P13-14 animals (filled squares) show responses only at stimulus levels above 70 dB SPL. More mature P13-14 animals (open circles) showed typical two part I/O functions, except that thresholds were elevated and emission amplitudes were low. For P17 animals, the emis-

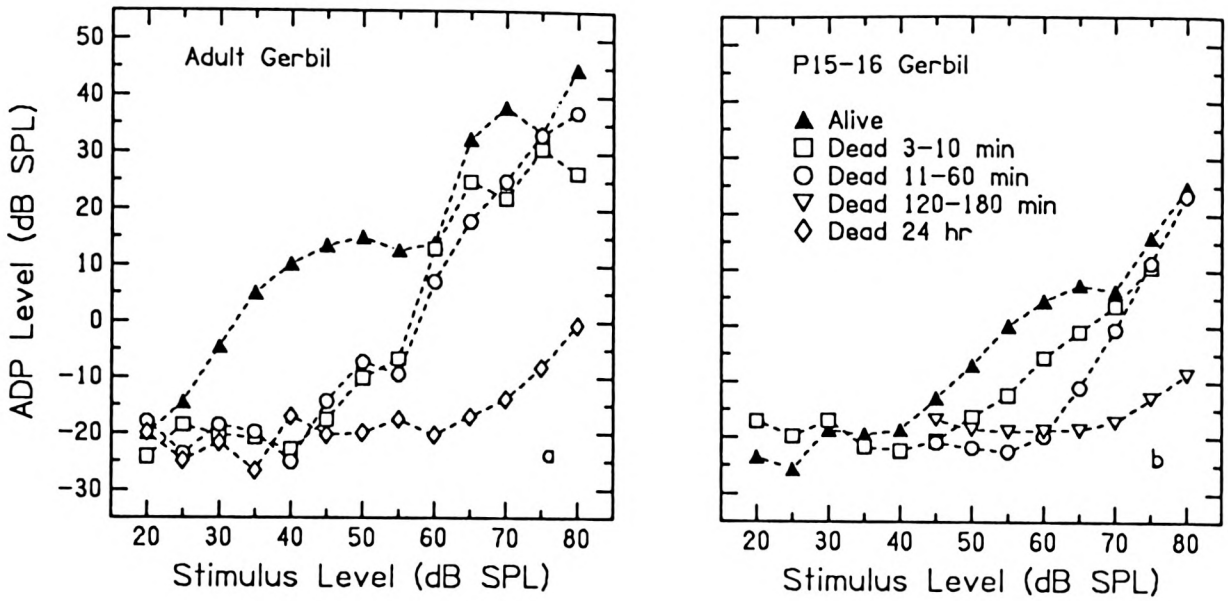

Figure 3. Same as Figure 2, except the parameter within each panel is animal state; alive and healthy versus various times after death by Nembutal overdose. Data for an adult animal are shown in a and data for a P15-16 gerbil are shown in b.

sion threshold decreased and its amplitude increased for stimuli below 80 dB SPL. This trend continued for older animals, with the threshold as well as the level at which saturation began decreasing and overall amplitude increasing. Averaging the data across animals tended to obscure non-monotonicities in the I/O functions. Figure 2b shows data for typical individual P15-16 gerbils. Considerable variability was typical of the younger age groups, but almost non-existent for P20-21 and P28-30 animals. Again responses in our youngest animals (filled circles) occur only to high level stimuli, and the growth function is steep and monotonic. As illustrated by the open triangles, initial responses to stimuli below 70-75 dB SPL have much slower growth functions which appear to be saturating. As the animals matures both parts of the function move to the left and the dynamic range increases, but the two components are still distinct. As this migration continues, the upper part of the function becomes non-monotonic. One interpretation of these data is that as the active process matures, it exerts increasing influence on basilar membrane responses and on the passive non-linearity.

Although we do not claim that death recapitulates development in reverse, we think it provides a time-lapsed snap shot of the interplay between active and passive processes within the cochlea. Figure 3 shows I/O functions for two gerbils as a function of time after death. Within 3 to 10 minutes after injection of a lethal dose of Nembutal, the lower part of the function drops significantly for both animals. However, while the function rapidly becomes monotonic for the younger animal (b), for the adult (a) residual non-monotonicities persist for a couple of hours. The upper part of the function persisted unchanged for up to an hour post-mortem, but within 2 to 3 hours after death responses were non-existent. Our interpretation of these age differences in post-mortem responses is that the active process is weaker and contributes less to the overall function in the young animals than in the adults.

In another experiment, we employed ADP emissions and brain evoked potentials to measure the functional recovery of regenerating hair cells in chickens following a 10-day course of gentamicin (50 mg/kg per day) beginning one day after birth (Norton, Tucci and Rubel, 1990). This gentamicin treatment initially destroys almost all hair cells in the basal 25% of the cochlea. Over the 4-5 weeks the drug treat

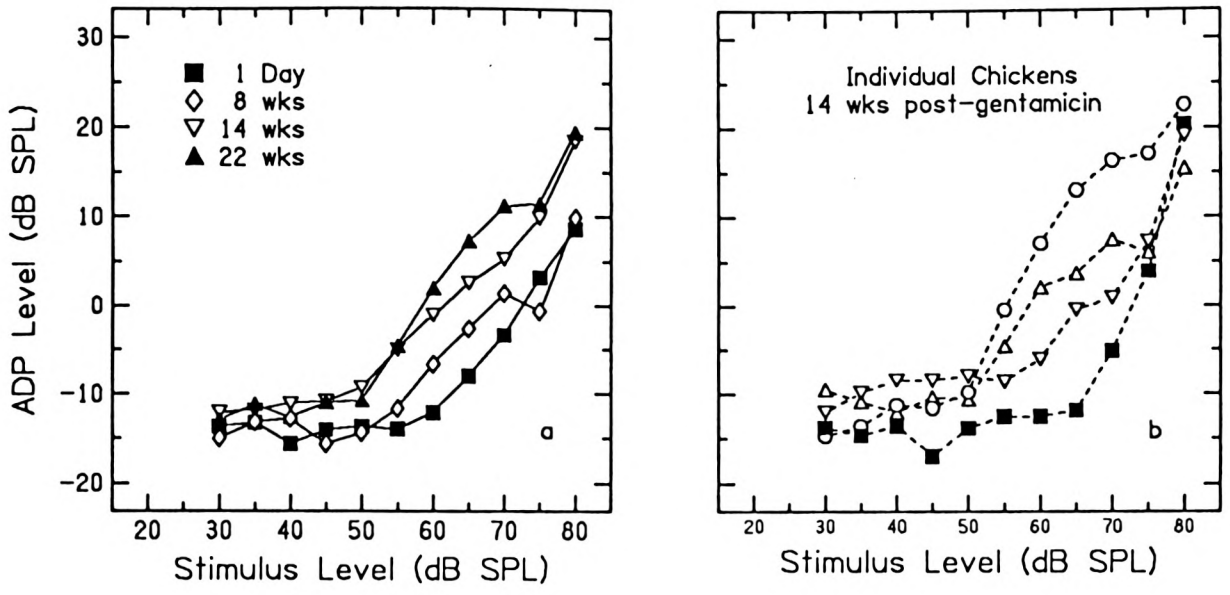

Figure 4. Same as Figure 2, except that data are for chickens who received a 10-day course of gentamicin beginning one day after birth. The parameter in panel a is time post-treatment. Data represent means across birds. Data in b are for individual birds within the 14-week post-treatment group. F2=2.0 kHz.

ment the lesion spreads apically. During and following the period of aminoglycoside treatment hair cells begin to regenerate in the avian cochlea (Cruz et al., 1987). By 22 weeks the cochlea has returned to a nearly normal status anatomically and evoked potential thresholds have returned to near normal levels (Tucci and Rubel, 1990; Duckert and Rubel, 1990). We were interested in the functional status of regenerated hair cells. Data in Figure 4 are for F2=2000 Hz, which is normally coded in the basal 30% of the chicken basilar papilla. One day post-gentamicin, the mean chick ADP I/O function as seen in the lefthand panel (filled squares) is steeply rising and monotonic with a threshold of about 65 dB SPL. By 8 weeks post-treatment, the I/O function has two distinct parts; above threshold (55 dB SPL) the function rises steadily, saturates at 65-70 dB SPL, then increases dramatically at 80 dB SPL. As recovery proceeds the function moves to the left and the dynamic range increases, just as in the maturing gerbil. 22 weeks post-treatment experimental chickens were indistinguishable from control birds at F2=3.0 kHz and below. Figure 4b shows data for individual birds at 14 weeks post-treatment. Again the variability across animals within an age cohort resembles the changes seen across age groups. Preliminary anatomical data (SEM and TEM) show small regenerating hair cells throughout the inferior one-half of the papilla in the short hair cell region at 6 weeks post-treatment. The regenerated hair cells often exhibit microvilli on their surface next to stereocilia bundles. In the 6 week specimens, stereocilia bundles are often disoriented. By 22 weeks hair cells had a normal appearance and stereocilia orientation was relatively uniform. Thus, normal ADP functions appear to be associated with normal stereocilia on short hair cells. However, more detailed anatomical data are needed in order to discern the relationship between hair cell status and ADP emissions.

Discussion

We have attempted to summarize evidence that ADP emissions can be dissociated into at least two components; an "active" component which is sensitive, rapidly saturates and is metabolically vulnerable, and a "passive" component which is seen at higher stimulus levels, increases rapidly (i.e. with a slope > 1) with stimulus intensity and is relatively robust. These two components can be dissociated by comparing ADP I/O functions before and after euthanasia, and by comparing immature and mature systems. The terms "active" and "passive" are relatively controversial. Some investigators prefer less mechanistic, more descriptive terms such as "low level" versus "high level", or "vulnerable" versus "invulnerable or less vulnerable". We have used the term "active processes" in reference to the most sensitive emissions, i.e. the saturating part of the I/O function seen at the lowest stimulus levels in mature animals with a normally functioning cochlea. We have used this term in concurrence with it usual *biological* meaning. That is, in biologically systems an "active process" usually refers to its dependence on ATP hydrolysis. Dependence on ATP is usually indicated by rapid changes as a function of hypoxia or hypothermia and suspectibility to metabolic poisons such as oubain or cyanide. In the case of emissions, the cellular sources of energy are unknown at this time but it is reasonable to hypothesize that ATP is involved, possibly through its role in maintaining the active transport systems in outer hair cells. During anoxia or after death the rapid decay of active transport systems due to the loss of oxygen and glucose is coincident with rapid loss of the most sensitive portion of the ADP I/O function, i.e. responses to stimuli below about 65 dB SPL. The slower decay of emissions evoked by higher level stimuli, seen between three minutes and two hours after death, is not likely due to an active biological mechanism (as defined here). We suggest that a more likely explanation of these later changes lies in alterations of the mechanical properties resulting from tissue degradation (i.e. proteolysis).

The general form of the ADP amplitude I/O functions from mature, healthy gerbils and chickens is strikingly similar to Mossbauer measurements of basilar membrane displacement in healthy mammals. This could be a coincidence, or an indication that ADP generation and basic properties as a function of stimulus level are governed by the same mechanisms which govern basilar membrane displacement. The similarities as well as the difference in the ADP functions in the two species in various cochlear states suggest that it is the latter. Yates (1990) reports very similar input-output functions from a simple analog model of a presumed cochlear non-linear feedback system designed to mimic BM displacement. As the gain term, related to OHC receptor current in his model, is decreased the I/O functions become monotonic. His functions are very similar to those shown by our immature gerbils and chickens with immature regenerating hair cells.

Although the basic shape of the I/O functions is the same for the two species, ADP thresholds differed by approximately 20 dB in the frequency region discussed. That is, ADP thresholds for F2=2.0 to 3.0 kHz were 25-30 dB SPL for the adult gerbils and 45 to 50 dB SPL for the healthy chickens. In addition, maximum ADP level differed by about 20 dB in the two species. It should be noted that behavioral thresholds in this frequency region also differ in the two species: 26 dB SPL at 1.0 kHz, 24 dB SPL at 2.0 kHz and 37 dB SPL for the chicken (Gray and Rubel, 1985) versus 6 dB SPL at 1.0 kHz, 3.4 dB SPL at 2.0 kHz and 2.7 dB SPL at 4.0 kHz for the gerbil (Ryan, 1976). These differences may reflect differences in middle ear structure - chickens have a single columella while gerbils have three ossicles - and/or differences in cochlear structure and function.

Gerbils have a coiled cochlea with 3 1/4 turns and an Organ of Corti, while chickens have a flat, tubular cochlea and a basilar papilla. The basilar membrane is 11-15 mm long in the gerbil and 3 to 5 mm in the chicken. Gerbils have four distinct rows of hair cells, one row of inners and three rows of outers, while the chicken basilar papilla is covered by a continuous distribution of hair cells which range from "tall" on the superior edge to "short" on the inferior edge. The tall hair cells sit on a fibro-cartilaginous

plate, while the short hair cells are found on the basilar membrane. Tall hair cells, like inner hair cells receive primarily afferent innervation while short hair cells, like outer hair cells receive primarily efferent innervation (Takasaka and Smith, 1971; Rebillard and Pujol. 1983). In both species there is a basilar membrane traveling wave. Our data from developing gerbils and chickens with regenerating hair cells suggests that ADP generation at low to moderate stimulus levels is mediated by active processes intrinsically related to normal outer hair cell maturity and possibly to short hair cells, respectively. In the absence of functional outer or short hair cells ADP growth functions are monotonic and most likely due to a passive mechanical basilar membrane nonlinearity. This passive nonlinearity is not dependent upon the endocochlear potential (EP) since the EP is full strength, at least in the gerbil significantly before ADPs begin to mature. Furthermore, preliminary anatomical data indicate that in the chickens, normal ADP behavior is correlated with the presence of a normal complement of normal short hair cells in a given frequency region. As outer and short hair cells mature in their respective species ADPs increase in a similar manner. Initially their behavior suggests the presence of a high threshold, low-output (low-gain?) saturating nonlinearity easily distinguished from the passive nonlinearity. Gradually the sensitivity and output of the active nonlinearity increase until it can "mask" the contribution of the passive nonlinearity in some cases.

References

Arjmand, E., Harris, D. and Dallos, P. (1988) Developmental changes in frequency mapping of the gerbil cochlea: comparisons of two cochlear locations. Hrg. Res. 32, 93-96.

Cotanche, D.A. (1987a) Regeneration of hair cell stereociliary bundles in the chick following severe acoustic trauma. Hrg. Res. 30, 181-196.

Cotanche, D.A. (1987b) Regeneration of the tectorial membrane in the chick cochlea following severe acoustic trauma. Hrg. Res. 30, 197-206.

Corwin, J.T. and Cotanche, D.A. (1988) Regeneration of sensory hair cells after acoustic trauma. Sci. 240, 1772-174.

Cruz, R.M., Lambert, P.R. and Rubel, E.W (1987) Light microscopic evidence of hair cell regeneration after gentamicin toxicity in chick cochlea. Arc. Otolaryngol. 113, 1058-1062.

Davis, H. (1983) An active process in cochlear mechanics. Hrg. Res. 9, 79-90.

Duckert, L.G. and Rubel, E.W (1990) Ultrastructural observations on regenerating hair cells in the chick basilar papilla. Hrg. Res. In Press.

Echteler, S.M., Arjamand, E. and Dallos, P. (1989) Developmental alterations in the frequency map of the cochlea. Nature 341, 147-149.

Gray, L. and Rubel, E.W (1985) The development of absolute thresholds in chickens. J. Acoust. Soc. Am. 77, 1162-1172.

Johnstone, B.M., Patuzzzi, R. and Yates, G.K. (1986) Basilar membrane measurements and the traveling wave. Hrg. Res. 22, 147-153.

Kiang, N.Y.S., Liberman, M.C., Sewell, W.F. and Guinan, J.J. (1986) Single unit clues to cochlear mechanisms. Hrg. Res. 22, 171-182.

Neely, S.T. and Kim, D.O. (1983) An active cochlear model showing sharp tuning and high sensitivity. Hrg. Res. 9, 123-130.

Neely, S.T. and Kim, D.O. (1986) A model for active elements in cochlear biomechanics. J. Acoust. Soc. Am. 79, 1472-1480.

Norton, S. J., Bargones, J.Y. and Rubel, E.W (1990) Development of otoacoustic emissions in gerbil: evidence for micromechanical changes underlying development of the place code. Submitted to Hrg. Res.

Norton, S.J., Tucci, D.L. and Rubel, E.W (1990) Comparison of acoustic and neural responses from avian ears following gentamicin. Paper presented at the ARO Midwinter Meeting.

Patuzzi, R., Johnstone, B.M. and Sellick, P.M. (1984) The alteration of the vibration of the basilar membrane produced by loud sound. Hrg. Res. 13, 99-100.

Pujol, R., Carlier, E. and Lenoir, M. (1980) Ontogenetic approach to inner and outer hair cell functions. Hrg. Res. 2, 423-430.

Pujol, R. and Uziel, A. (1989) Auditory development: peripheral aspects. In: Handbook of Human Growth and Developmental Biology Vol. I. Part B (Eds.: Meisami, E. and Timiras, P.S.) CRC Press, Boca Raton, pp.109-130.

Rebillard, M. and Pujol, R. (1983) Innervation of the chicken basilar papilla during its development. Acta Otolaryngol. 96, 379-388.

Retzius, G. (1884) Das Gehororgan der Wirbeltiere. II. Das Gehorogan der Reptilien, der Vogel und Saugetiere. Samson and Wallin, Stockholm.

Rubel, E.W. (1978) Ontogeny of structure and function in the vertebrate auditory system. In: Handbook of Sensory Physiology, Volume 9, Development of Sensory Systems (Ed: Jacobsen, M.) Springer-Verlag, New York, pp. 135-237.

Ryals, B.M. and Rubel, E.W (1988) Hair cell regeneration after acoustic trauma in adult *coturnix* quail. Sci. 240, 1774-1776.

Ryan, A. (1976) Hearing sensitivity in the mongolian gerbil, *Meriones unguiculatus*. J. Acoust. Soc. Am. 59, 1222-1226.

Sanes, D.H., Merickel, M. and Rubel, E.W (1989) Evidence for an alteration of the tonotopic map in the gerbil cochlea during development. J. Comp. Neuro. 279, 436-444.

Sellick, P.M., Patuzzi, R. and Johnstone, B.M. (1982) Measurements of basilar membrane motion in the guinea pig using the Mossbauer technique. J. Acoust. Soc. Am. 72, 131-141.

Takasaka, T. and Smith, C.A. (1971). The structure and innervation of the pigeon's basilar papilla. Ultrastruct. Res. 35, 20-65.

Tucci, D. and Rubel, E.W (1990) Physiological status of regenerated hair cells in avian ear following aminoglycoside ototoxicity. Submitted to Otolaryngol. Head Neck Surg.

Yates, G. (1990) The basilar membrane nonlinear input-output function. This Volume.

A GENERALIZED VAN DER POL-OSCILLATOR COCHLEA MODEL

M.P.M.G. van den Raadt and H. Duifhuis

Biophysics Department, Rijksuniversiteit Groningen, the Netherlands

Introduction

Over the last decade it has become clear that active and nonlinear behavior of the cochlea is to a certain extent similar to that of a Van der Pol-oscillator. This was first proposed by Johannesma (1980). It was worked out in more detail by several groups (*e.g.*, van Netten and Duifhuis, 1983, Duifhuis *et al.*, 1985, Jones *et al.*, 1986, Diependaal *et al.*, 1987, van Dijk and Wit, 1988). We have been working on a cochlea model with many active components, i.e. self-sustained oscillators. Initially this was set up with spatial parameters that varied smoothly. The classical parabolic damping profile was used. Our major emphasis, however, shifted toward potentially more realistic biophysical models. For the damping term we now use a function in which two parts can be discerned. First, a passive (positive) part with exponential "tails", which provides response behavior with a log-like characteristic for external stimuli. Secondly, there is an active (negative) part that, if sufficiently strong, produces net active (negative damping = energy production) behavior. In order to model spontaneous emissions, we also introduced spatial discontinuities in the damping parameters.

Model

We briefly repeat basic properties of the 1-dimensional, active cochlea model. They have been discussed in more detail in Duifhuis *et al.* (1985). Active, oscillatory behavior of adjacent points in a cochlea is only meaningful on a discrete grid, because the points can have opposite amplitudes, which is impossible for arbitrarily close points. The physiological structure yields a grid size of about 10 μm. Our computational grid is still one order of magnitude coarser. Thus, we cannot yet take all fine structure properties into account. Our primary aim is to investigate the effect of the shape of the damping term in the generalized Van der Pol-oscillator. For the time being we have restricted ourselves to a further analysis of the 1-dimensional cochlea model.

A mathematical formulation of a coupled Van der Pol-oscillator model is:

$$(my_{tt} + dy_t + sy)_{xx} - \frac{2\rho}{h} y_{tt} = 0 \tag{1}$$

where m, d, and $s = s_0 \exp(-\lambda x)$ represent basilar membrane[1] (BM) mass, damping and stiffness per unit area. ρ is the fluid density, h the scala height, and y the BM-deflection. The cochlea is modelled with 400 equally spaced elements that follow from Eq. 1. One element is added to act as a simple middle ear, thus giving a physical coupling with the air environment. The helicotrema point misses one neighbor, but sees a fluid environment.

The physical equation is transformed to a dimensionless version:

$$(y_{tt} + Dy_t + Sy)_{xx} - a^2 y_{tt} = 0 \tag{2}$$

Scale values are: $x_0 = 35$ mm, $y_0 = 1$ nm, and $t_0 = 1$ ms. With the parameter values $m = 0.5$ kg/m^2, $s_0 = 10^{10}$ Pa/m, $\lambda = 300$ m^{-1}, this yields $a = 70$, and $S = 2.10^4 \exp(-10.5x)$. The complete form that we use for D is:

$$D(x, y_t) = D_0(x) \left(\frac{\chi \sinh(\alpha y_t)}{\alpha y_t} - \frac{2\gamma}{\cosh(\beta y_t)} \right) \tag{3}$$

where the positive part provides the log-like behavior and the negative part accounts for the active properties. The velocity independent factor $D_0(x) = 5\sqrt{2} \exp(-5.25x)$ scales the dependent part of D to the order 1.

In this study we consider effects of the parameters β and γ, which represent the width and the depth of the active part of the damping term. In principle, both affect the total energy balance. The effects have been analyzed on a single oscillator. The results can be summarized as follows: Both increment of width and of depth increase the limit cycle amplitude. Increasing the depth, however, yields a limit cycle behavior similar to that of the parabolic Van der Pol-oscillator with an increasing value of the classical damping parameter ϵ. This means that the nonlinear behavior becomes more obvious. Increment of width, on the other hand, yields a smooth oscillation with an increasing onset part, similar to the response of a filter with increasing selectivity (decreasing bandwidth).

Smoothly varying damping parameters

So far we have primarily analyzed the behavior of a model with smoothly varying parameters. Level effects for single tone stimuli, using the given model parameters, have been reported (Duifhuis, 1988). Those results clearly show that the chosen nonlinearity can describe a large dynamic range, something the parabolic damping term can not. For single tone responses the differences between nonlinear active and nonlinear passive models are limited

[1] In fact these parameters represent the entire cochlear partition.

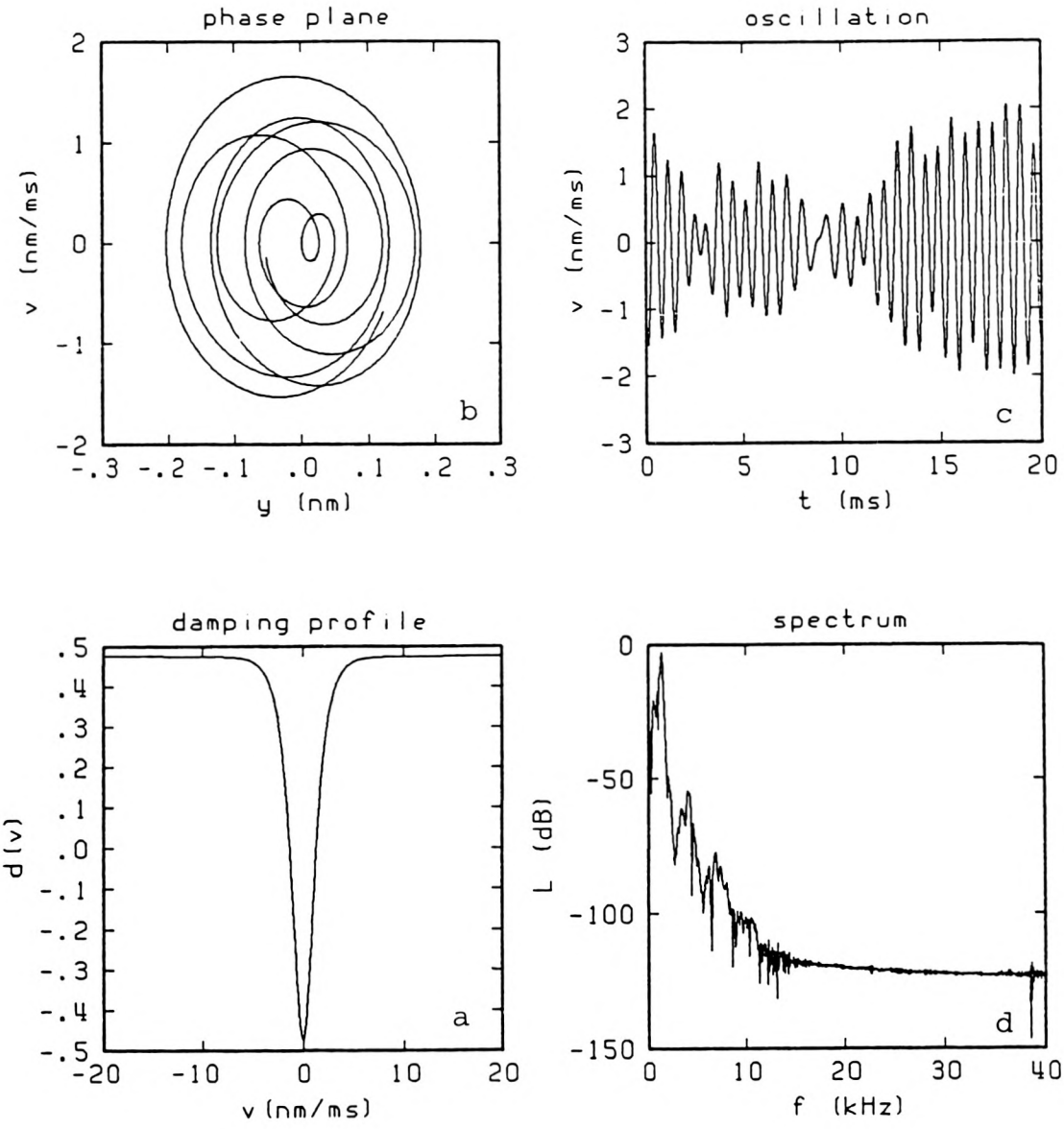

FIGURE 1 Typical behavior of one oscillator element in the model with spatially smoothly varying damping and stiffness parameters. Cochlear location: $x = 18$ mm, corresponding to a resonance frequency of approx. 1.5 kHz. Damping parameters: $\alpha = 0.01$, $\beta = \gamma = \chi = 1$. Panel *a* shows the local damping function for 'small' v, displaying the active part in particular. Panel *b* displays the phase plane solution (velocity against deflection) over a 5 ms trajectory, starting at $y_0 = 0.12$ nm and $v_0 = -0.68$ nm/ms. Panel *c* gives the velocity over a period of 20 ms, also starting at (y_0, v_0). Panel *d* presents the spectrum of v, in dB *re* 1 nm/ms.

to the 40 dB-range above threshold (*re* 1 nm/ms). In the active model the responses are enhanced. This effect decreases with increasing stimulus level.

Here we present additional results for the undriven model. Figure 1 shows typical response profiles at $x = 18$ mm from the stapes. The damping parameter values are $\alpha = 0.01$, $\beta = 1$, $\gamma = 1$, and $\chi = 1$. The time increment used in the numerical analysis is 2.5 μs. Panel *a* shows the 'active part' of the damping profile. Panel *b* gives a phase plane picture which shows the irregular behavior of the solution. (A single oscillator would produce a simple closed orbit.) This is due to the interaction with neighboring oscillators. The irregularities are also clearly observable in the corresponding temporal response (Panel *c*), and finally it is present in the frequency spectrum of this response in Panel *d*, in particular in the shape of the peaks (*cf.* also Fig. 3).

The observed irregularity is still under study.

Locally deviating damping parameters

Of course, one of the primary aims to study active rather than passive cochlea models is to understand the biophysics of spontaneous otoacoustic emissions (SOAE). Although an active cochlea with smoothly varying parameters, as described in the previous section, emits sound, it does so in a very broad spectrum.

In order to obtain a significant spectral component in the evoked activity it is necessary to have a significantly protruding source. The simplest case is the passive model with a single strongly active oscillator. Another case is that, where against a background as described in the previous section, the same strong oscillator is significantly more active than its environment. In this section we describe results of the analysis of these two cases.

A single strongly active element is located at $x = 18$ mm. It is obtained by broadening the negative part of the damping function, or, in terms of Eq. 3, by decreasing β considerably. In this example we used $\beta = 0.001$ compared to $\beta = 1$ for the background (as in the previous section). For the one-oscillator version $\gamma = 0$ except at $x = 18$ mm where $\gamma = 1$. In the case with the active background $\gamma = 1$ for all x. In both cases $\alpha = 0.01$ and $\chi = 1$ for all x.

Figure 2 shows the obtained velocity profiles across the BM. The profiles are very similar around the location of the source. The responses are also similar to responses evoked by external stimuli of appropriate strength. A sufficiently strong external stimulus has been shown to entrain part of the irregular response around the point of resonance (Duifhuis *et al.*, 1985). Obviously, a relatively strong oscillator also entrains its active environment.

Finally, Fig. 3 shows spectra for these two cases. The lefthand panel, *a* - *c* presents results for the situation without background, the righthand panel, *d* - *f* displays the corresponding spectra for the case with background activity. The spectra are given at three locations: upper row, at the location of the dominant oscillator ($x = 18$ mm); middle row, basalward, at $x = 16.1$ mm; bottom row, at the ear canal.

The top row figures, 3*a* and 3*d*, are very similar, although not identical. They are largely determined by the local source. The active background

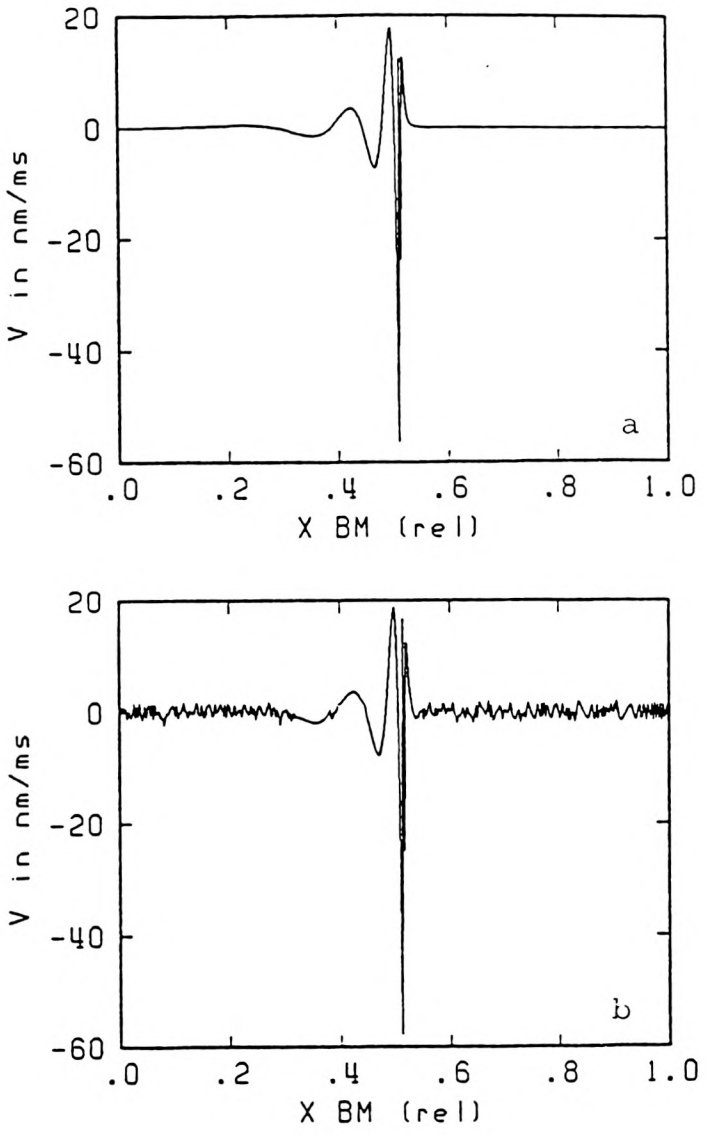

FIGURE 2 Velocity profiles (snap shot) across BM with a strongly active oscillator at $x = 18$ mm. At this point $\beta = 0.001$ and $\gamma = 1$. In Panel *a* the rest of the cochlea is passive ($\gamma = 0$), parameters as in Fig. 1. Panel *b* presents the response for the situation where there is a background activity with $\beta = 1$ and $\gamma = 1$. Other parameters for all x: $\alpha = 0.01$ and $\chi = 1$.

is primarily apparent between DC and $f = 1.5$ kHz. It is clear that the spectra contain only odd harmonics of the fundamental, a result that we use as a check for the behavior of the assumed odd nonlinearity (even damping function).

The middle row shows marked differences between the passive and active background conditions, but in both the prominent peaks occur at odd harmonics of the source frequency. The fundamentals are still virtually equal in Figs. 3*b* and 3*e*, but they have dropped approx. 30 dB with respect to the top row. The higher harmonics are significantly stronger in 3*e*, although they are still more than 50 dB below the level of the fundamental.

The bottom line shows the spectra at the ear canal, using the same reference level. In Fig. 3*c* only the fundamental remains. Figure 3*f* shows the spectrum of the smoothly active cochlea with a peak of approximately 30 dB due to the source at 18 mm. The background level is representative

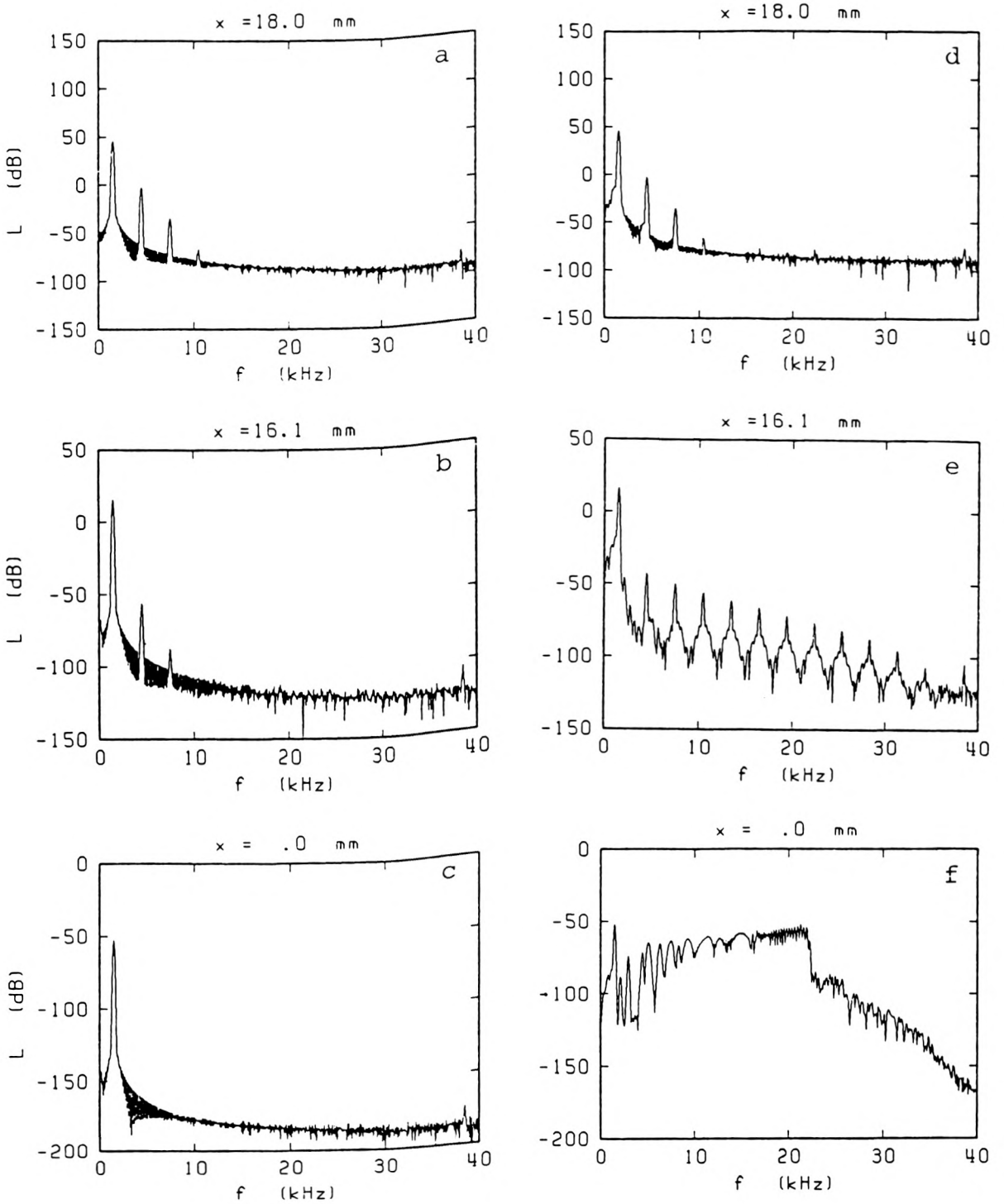

FIGURE 3 Spectra of velocity responses at three locations in cochlea and middle ear. Top row: at the site of the single strong oscillator. Middle row: 1.9 mm basalward of this site. Bottom row: near the ear drum. Left hand panels *a* - *c* present results for the case without background activity, and *d* - *f* for the situation with background activity. Parameters as in Fig. 2.

for the behavior of this type of model, that is to say, its envelope is. Peak height at 1.5 kHz is almost equal in $3c$ and $3f$. The fine-structure in $3f$ is irregular.

Summary

In this study we report preliminary results of a generalized coupled Van der Pol-oscillator cochlea model with one strong oscillator. The single dominant oscillator affects the response profile basalward from its location. This is shown clearly in the velocity profiles. These profiles are similar to responses evoked by external stimuli of appropriate strength.

Two points are of interest with regard to the spectra. First, in both cases the source frequency is clearly observable in the ear canal. This suggests that a dominant oscillator on the macromechanical level can produce SOAE's. Secondly, in the cochlea weak spectral components can, at least locally, be enhanced considerably by the presence of other self-sustained oscillators.

We are beginning to analyse the occurence of interference effects.

Finally, it should be understood that proper numerical evaluation of the coupled oscillator model requires considerable computation time. Proper initial conditions cannot be predicted, but have to be evaluated. Any restart with modified model parameters necessitates an onset run of the order of at least 100 ms.

Acknowledgement

This project has been supported by the Netherlands Organization for Scientific Research, N. W. O., through the Foundation for Biophysics. We also acknowledge fruitful discussions with E. de Boer, H. W. Hoogstraten and S. M. van Netten.

References

Diependaal, R. J., Duifhuis, H., Hoogstraten, H. W., and Viergever, M. A. (**1987**). "Numerical methods for solving one-dimensional cochlear models in the time domain", J. Acoust. Soc. Am. **82**, 1655–1666.

van Dijk, P., and Wit, H. P. (**1988**). "Phase-lock of spontaneous oto-acoustic emissions to a cubic difference tone", in *Basic Issues in Hearing*, edited by H. Duifhuis, J. W. Horst, and H. P. Wit (Academic, London), pp. 101–105.

Duifhuis, H. (**1988**). "Cochlear macromechanics", in *Auditory Function. Neurobiological basis of hearing*, edited by G. M. Edelman, W. E. Gall, and W. M. Cowan, chapter 6, pp. 189–211 (A Neurosciences Institute Publication, Wiley, New York).

Duifhuis, H., Hoogstraten, H. W., van Netten, S. M., Diependaal, R. J., and Bialek, W. (**1985**). "Modelling the cochlear partition with coupled Van der Pol oscillators", in *Peripheral Auditory Mechanisms*, edited by J. B. Allen, J. L. Hall, A. E. Hubbard, S. T. Neely, and A. Tubis (Springer, New York), pp. 290–297.

Johannesma, P. I. M. (**1980**). "Narrow band filters and active resonators. Comments on papers by D. T. Kemp & R. A. Chum, and H. P. Wit & R. J. Ritsma", in *Psychophysical, physiological, and behavioural studies in hearing*, edited by G. van den Brink and F. A. Bilsen (Delft University Press, Delft), pp. 62–63.

Jones, K., Tubis, A., Long, G. R., Burns, E. M., and Strickland, E. A. (**1986**). "Interactions among multiple spontaneous otoacoustic emissions", in *Peripheral Auditory Mechanisms*, edited by J. B. Allen, J. L. Hall, A. Hubbard, S. T. Neely, and A. Tubis (Springer-Verlag, Berlin), pp. 266–273.

van Netten, S. M., and Duifhuis, H. (**1983**). "Modelling an active, nonlinear cochlea", in *Mechanics of Hearing*, edited by E. de Boer and M. A. Viergever (Nijhoff/Delft Univ. Press, Netherlands), pp. 143–151.

Quantitative Evaluation of Limit-Cycle Oscillator Models of Spontaneous Otoacoustic Emissions

Carrick L. Talmadge,[1] Glenis R. Long,[2] William J. Murphy,[1] and Arnold Tubis[1]

[1] *Department of Physics; Purdue University, West Lafayette, IN 47907*
[2] *Department of Audiology and Speech Sciences; Purdue University, West Lafayette, IN 47907*

Introduction

Single limit-cycle-oscillator models of spontaneous otoacoustic emissions (SOAE's) are based on the assumption that the pattern of interactions between spontaneous emissions and external tones in the ear canal may be partially described by the gross compaction of a full cochlear model to a single nonlinear differential equation such as that of a free (or driven) Van der Pol oscillator. Such an equation incorporates, in a highly idealized way, the type of nonlinear-active damping which, if assumed to be present over certain portions of the cochlear partition, would produce stabilized cochlear self-oscillations and lead to measurable spontaneous emissions in the ear-canal. These models have been used successfully by our group and by Wit and collaborators to account for a number of features of the emission data including: a) statistical properties of emissions (e.g. Bialek and Wit, 1984; Wit, 1986; van Dijk, 1990); b) suppression of emissions (Long and Tubis, 1990) and synchronization (phase locking) of emissions by external tones (e.g., van Dijk, 1990; Long, *et al.*, 1990); and c) reduction of the level of emissions by aspirin consumption (e.g., Long and Tubis, 1988a,b).

In this paper, we describe several studies which are designed to probe the validity of these models. In particular we obtain two independent estimates of the active damping parameter of a Van der Pol model of an SOAE from: 1) data on the dynamical interactions of SOAE's with external tones during suppression and the release from suppressions (Schloth and Zwicker, 1983; Dallmayr, 1983, 1985); and 2) the details of the frequency-locking or synchronization tuning curves of these SOAE's.

Theoretical Results

The single Van der Pol oscillator model of a spontaneous emission, in isolation or in interaction with an external tone, is described by the differential equation,

$$\ddot{y} + (-r_1 + r_2 y^2)\dot{y} + \omega_0^2 y = E\cos\omega t, \qquad (1)$$

where y is interpreted as the incremental pressure in the ear canal, the approximate limit cycle frequency ω_0 is associated with the angular frequency of a spontaneous emission, r_1 and r_2 are respectively the active and nonlinear damping components, t is time, ω is the angular frequency of the external tone and E is proportional to the external tone transducer voltage. In order to have a limit-cycle solution of Eq. (1), both r_1 and r_2 must be positive, in which case the approximate solution in the absence of external driving ($E = 0$) is (Nayfeh, 1973, pp. 245-248)

$$y = a_0 \cos(\omega_0 t + \phi_0), \tag{2}$$

where ϕ_0 is a constant phase and the amplitude a_0 is given by

$$a_0 = 2\sqrt{\frac{r_1}{r_2}}. \tag{3}$$

To the extent that Eq. (1) is a reasonable descriptor of an SOAE, it provides several independent means for obtaining estimates of the active parameter r_1. One of these is based on the observation of the temporal behavior of the emission's level during external-tone suppression and following release from suppression (Zurek and Clark, 1981; Schloth and Zwicker, 1983). The other is based on an analysis of the frequency locking tuning curves (Zwicker and Schloth, 1984; Long and Tubis, 1988a; 1990).

Relaxation Dynamics of the Van der Pol Oscillator

In order to study the relaxation dynamics of the Van der Pol oscillator, we consider the application of a square-wave modulated external tone with frequency ω sufficiently far away from ω_0 and with a duty cycle sufficiently long for fully developed suppression and recovery from suppression to occur. By applying the Krylov-Bogoliubov method of averaging (c.f., Nayfeh and Mook, 1979; Hanggi and Riseborough, 1983) to Eq (1), we obtain the approximate results,

$$y(t) = a(t) \cos(\omega_0 t + \phi), \tag{4}$$

$$\dot{a}(t) = \frac{1}{2} r_1 a(t) \left[1 - 2\frac{\Lambda^2}{a_0^2} - \frac{a(t)^2}{a_0^2}\right], \tag{5}$$

$$\Lambda = \frac{E}{\omega_0^2 - \omega^2}, \tag{6}$$

where ϕ is a constant.

We consider first the case of suppression of an emission by an external tone [$a(0) = a_0$, and $a(t \to \infty) = \kappa a_0$], for which the solution of Eq. (5) is

$$a(t) = \frac{\kappa a_0}{\sqrt{1 + (\kappa^2 - 1)\exp(-r_1 \kappa^2 t)}}, \tag{7}$$

$$\kappa^2 = 1 - 2\Lambda^2/a_0^2. \tag{8}$$

For recovery from suppression by the external tone of the emission [$a(0) = \kappa a_0$, $a(t \to \infty) = a_0$], we have

$$a(t) = \frac{a_0}{\sqrt{1 + (1/\kappa^2 - 1)\exp(-r_1 t)}}. \tag{9}$$

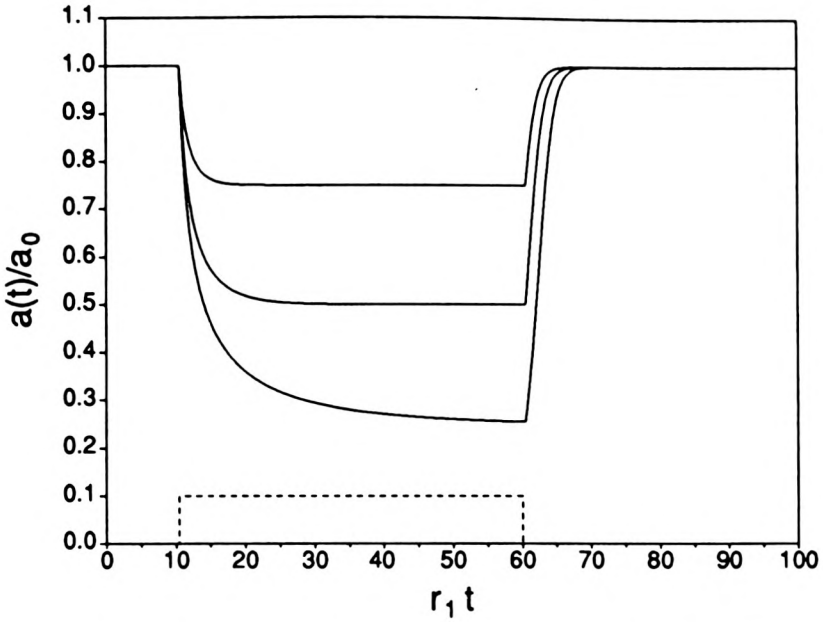

FIGURE 1 Level of the Van der Pol oscillator during one modulation cycle (dashed line) of the suppressing tone for various levels of the external tone.

The behaviors given by Eqs. (7) and (9) are plotted in Fig. 1. It can be shown that the exponential factor r_1 in the recovery behavior of Eq. (9) is unchanged if the dynamical model of SOAE's given by Eq. (5) is replaced by

$$\ddot{y} + (-r_1 + r_2|y|^p)\dot{y} + \omega_0^2 y = E\cos\omega t, \tag{10}$$

with $p > 0$. On the other hand, the exponential factor $\kappa^2 r_1$ in the suppression behavior of Eq. (7) depends directly on the form of the nonlinear component of the damping. We conclude that fits to data on the recovery from suppression are insensitive to the specific form of the nonlinear damping of the underlying limit-cycle oscillator model, in contrast to the case of fits to onset-of-suppression data.

So far we have only considered models which incorporate linear stiffness. We relax this assumption by modeling SOAE's with the differential equation,

$$\ddot{y} + (-r_1 + r_2 y^2)\dot{y} + \omega_0^2(y + \varepsilon y^3) = E\cos\omega t. \tag{11}$$

Applying the Krylov-Bogoliubov method, we find

$$y(t) = a(t)\cos(\omega_0 t + \phi(t)), \tag{12}$$

$$\dot{a}(t) = \frac{1}{2} r_1 a(t)\left[1 - 2\frac{\Lambda^2}{a_0^2} - \frac{a(t)^2}{a_0^2}\right], \tag{13}$$

$$\dot{\phi}(t) = \frac{3\varepsilon a_0^2 \omega_0}{8}\left[2\frac{\Lambda^2}{a_0^2} + \frac{a(t)^2}{a_0^2}\right]. \tag{14}$$

We see from Eq. (13) that nonlinear stiffness does not affect the amplitude relaxation process to first order. There is, however, a transient effect on phase during the process of suppression or relaxation of the oscillator. The solution of Eq. (14), when a suppressing tone is turned on at $t = 0$ and $\phi(0) = \phi_0$ is given by

$$\phi(t) = \frac{3}{8}\varepsilon a_0^2 \omega_0\left[(1-\kappa^2)t + \frac{1}{r_1}\log\left(\frac{e^{\kappa^2 r_1 t} + \kappa^2 - 1}{\kappa^2}\right)\right] + \phi_0. \tag{15}$$

Finally, the solution during relaxation, when the suppressor is turned off at $t = 0$ and again $\phi(0) = \phi_0$, is

$$\phi(t) = \frac{3}{8}\frac{\varepsilon a_0^2 \omega_0}{r_1} \log\left(\kappa^2 e^{r_1 t} + 1 - \kappa^2\right) + \phi_0. \tag{16}$$

Frequency Locking Tuning Curves

We consider frequency locking tuning curves which are obtained from the response of the SOAE to the application of an external tone, which is swept slowly in frequency through a region containing the frequency of the emission. The frequency at which the locking(unlocking) occurs for a Van der Pol oscillator is given by the approximate expression (Nayfeh, 1973, pp. 250-253; Hanggi and Riseborough, 1983),

$$(\omega - \omega_0)^2 + \frac{r_1^2}{16} = \frac{E^2}{2\omega_0^2 a_0^2}, \tag{17}$$

for $|\omega - \omega_0| \gtrsim 0.28864 r_1$ and by

$$\left(\frac{12(\omega-\omega_0)^2}{r_1^2} + 1 - \sqrt{1 - \frac{12(\omega-\omega_0)^2}{r_1^2}}\right) \times \left(2 - \sqrt{1 - \frac{12(\omega-\omega_0)^2}{r_1^2}}\right) = \frac{27E^2}{2r_1^2\omega_0^2 a_0^2}, \tag{18}$$

for $|\omega - \omega_0| \lesssim 0.28864 r_1$.

In Eqs. (17) and (18), E is interpreted as the force on the SOAE oscillator due to the external tone. Unfortunately, E is *not* a directly measurable quantity, but instead is a function of P_e, the instantaneous pressure in the ear canal. For this preliminary study, we assume linearity of $E(P_e)$, so that we can rewrite Eq. (17), for example, as

$$(\omega - \omega_0)^2 + \frac{r_1^2}{16} = kP_e^2, \tag{19}$$

where $\sqrt{k}$ is the assumed constant of proportionality. Eq. (19) and the analogous equation to Eq. (18) can be fit to the tuning curve data for the parameters ω_0, r_1 and k.

Methods

The levels of spontaneous otoacoustic emissions and external tones in the ear canal were detected by an Etymotic Research ER-10 microphone and evaluated by a Wavetek 5820A Spectrum Analyzer. An Etymotic Research ER-2 tubephone attached to the ER 10 assembly was used to transduce the external tones. In order to model the suppression and recovery of a spontaneous otoacoustic emission, the transient behavior of an SOAE was measured in response to a pulsed (168.34 msec on/off - 2 msec rise/fall) sinusoid generated by a Hewlett Packard 3325A function generator. The ear canal signal was amplified and bandpassed filtered ($Q = 1$) by an Ithaco 3961 Lock-in amplifier centered at the frequency of the emission before being

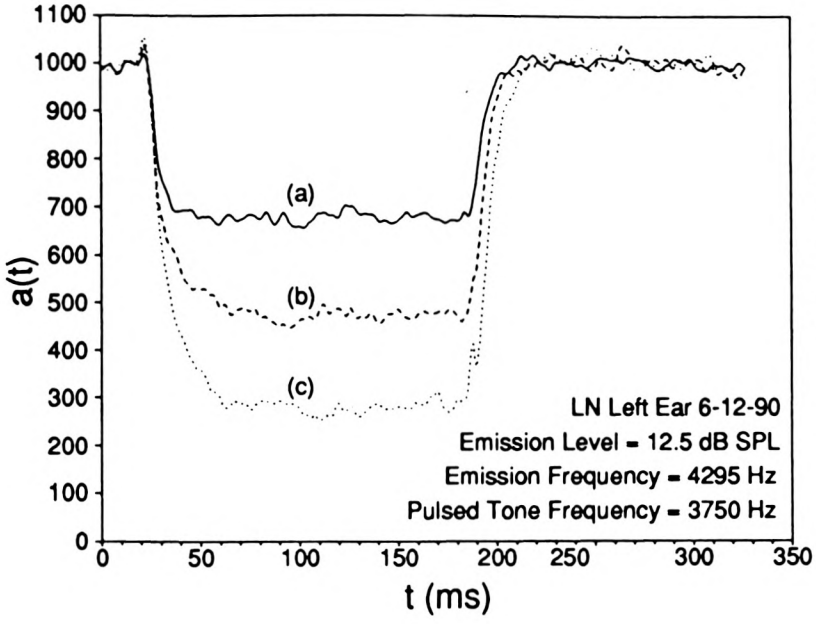

FIGURE 2 Effect of a pulsed external tone on the level of an SOAE for subject LN. Here (a), (b), and (c) were obtained with different levels of the external tone [see Table 1].

TABLE 1 Results for fitting the experimentally measured response of the level of an SOAE for subject LN to a pulsed external tone, as described in the text.

Data Set	Level of Suppressor	dB Suppression	$1/r_1$ (suppression)	$1/r_1$ (recovery)
(a)	37 dB SPL	−3.2 dB	3.12 ms	5.39 ms
(b)	38	−6.4	2.48	5.41
(c)	39	−11.2	1.28	4.87
—	—	—	(2.29 ± 0.54) ms	(5.22 ± 0.18) ms

sampled at 100 kHz by a Data Translation DT2827 16 bit A/D board installed in a Zenith 386/16 PC compatible computer. Each data set was analyzed on a NeXT computer by digital filtering using a time domain finite response band pass filter centered at the emission frequency and averaged over 62 repetitions.

The level and frequency of an external tone needed to synchronize a spontaneous emission was determined by recording the RMS level of the sound pressure in the ear canal in the presence of a sweeping external tone generated by a Hewlett Packard 3325A function generator. The frequency range of the sweep was chosen to be 30 Hz, and the time of sweep was 50 seconds. The ear canal signal was filtered and analyzed by a Bruel and Kjaer 2010 heterodyne analyzer. A DC voltage proportional to the log RMS level within a filter (31.6 Hz) centered around the frequency of the sweeping stimulus was stored on a Tektronix 2230 digital storage oscilloscope and transferred to the Zenith 386 computer and the NeXT computer for further analysis. The frequencies of the sweeping tone at which the RMS level changed from regular beating to stability and back to regular beating were determined for each level of the external tone.

The results presented here were obtained from two human subjects. The emis-

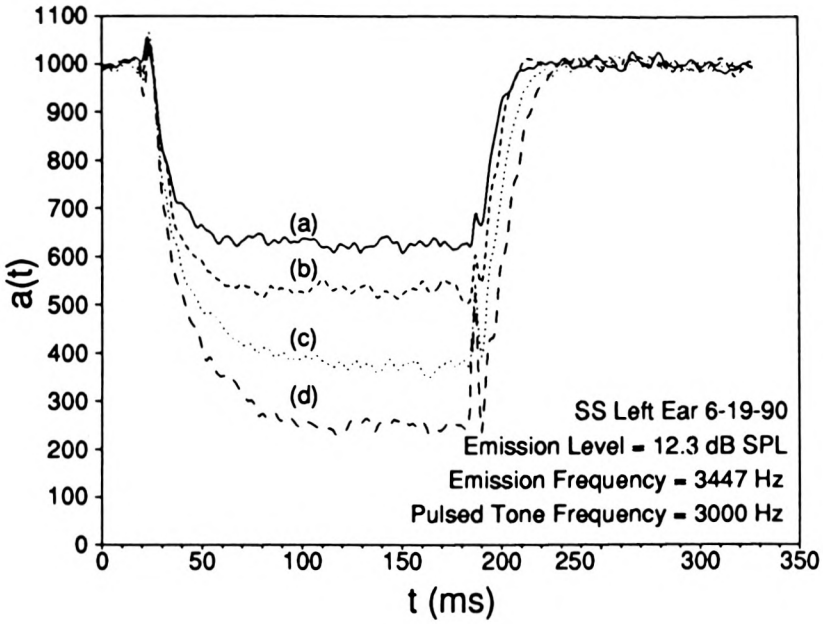

FIGURE 3 Effect of a pulsed external tone on the level of an SOAE for subject SS. Here (a), (b), (c), and (d) were obtained with different levels of the external tone [see Table 2].

TABLE 2 Results for fitting the experimentally measured response of the level of an SOAE for subject SS to a pulsed external tone, as described in the text.

Data Set	Level of Suppressor	dB Suppression	$1/r_1$ (suppression)	$1/r_1$ (recovery)
(a)	39 dB SPL	−4.0 dB	3.21 ms	5.66 ms
(b)	40	−5.5	2.66	5.32
(c)	41	−9.0	2.99	6.06
(d)	42	−11.5	2.08	6.31
—	—	—	(2.74 ± 0.25) ms	(5.84 ± 0.22) ms

sion studied from subject LN's left ear had a typical frequency of 4285-4310 Hz, and an amplitude of 13-15 dB SPL. The emission studied from subject SS's left ear had a typical frequency of 3445-3465 Hz and an amplitude of 11-14 dB SPL.

Results

Fig. 2 shows the suppression and relaxation behavior of an SOAE for one subject (LN) for 3 different levels of a pulsed external tone. We observe that the qualitative behavior of these curves is similar to those for an isolated Van der Pol [see Fig. 1]. These data were fit to Eq. (7) during suppression and Eq. (9) during recovery from suppression, and the results of these fits are presented in Table 1. We also show the results for another subject (SS) in Fig. 3 and Table 2.

In a preliminary analysis, an independent estimate of r_1 determined by fitting Eqs. (17) and (18) to the frequency locking tuning curve shown in Fig. 4. We obtained the average value of $1/r_1 = (9.8 \pm 2.7)$ ms using only the lowest three levels

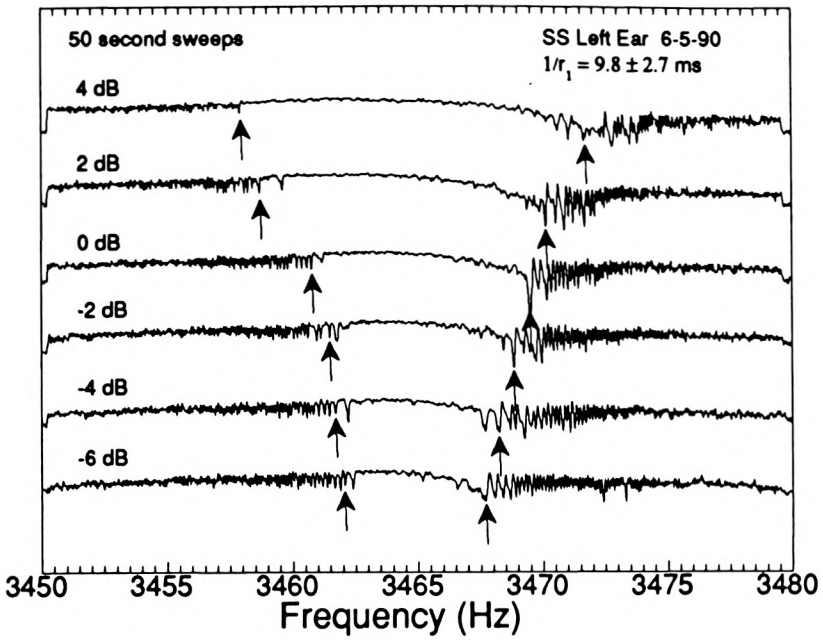

FIGURE 4 Frequency locking tuning curve obtained from a sweeping external tone. Here the arrows show the values chosen for the point of entrainment or loss of entrainment.

shown. There was a marked systematic increase with level of the external tone (if all values were used, a values of $1/r_1 \cong 40.3$ ms was obtained). This systematic increase may be due, in part, to the inadequacy of the first-order theory for high levels of the external tone (as has been demonstrated in numerical simulations). We are currently studying this along with the effects of noise on the frequency locking tuning curve.

Discussion

In this paper we have shown that the frequency locking tuning curve and the dynamics of the recovery from suppression of an SOAE are correlated in the way implied by a simple Van der Pol model of the emission. In particular, we find that the relaxation parameter r_1 determined from the preliminary analysis of the frequency locking tuning curve data using Eq. (17) is in agreement with that obtained from the recovery function given by Eq. (9). Additionally, using Eq. (9) and the SOAE relaxation data of Schloth and Zwicker (1983), we find $1/r_1 \cong 6.8$ ms, which is also in agreement with these two estimates.

However, the value of r_1 extracted from the onset-of-suppression data using Eq. (7) appears to be in disagreement with the values obtained from the frequency locking and relaxation from suppression data. Using Eq. (7) and the Schloth and Zwicker SOAE suppression data, in which the emission was suppressed by -6.4 dB, we find $1/r_1 \cong 4.4$ ms, which is also characteristically lower than the value obtained from their recovery-from-suppression data. As was mentioned in Theoretical Results, the discrepancy between the value of r_1 measured in the suppression data and the value obtained from the recovery-from-suppression data may be evidence that the nonlinear component of damping of the underlying dynamical model is different from that of the Van der Pol oscillator.

It is, of course, expected that otoacoustic emissions recorded from a human ear canal may not be fully modeled by a single limit-cycle oscillator. Even in the case of a nonlinear active damping of the Van der Pol type highly localized in the cochlear partition, there are several effects which are not accounted for by a simple oscillator model of an SOAE. First, there will be a time delay in the response of the emission, which reflects the time for the traveling wave to arrive at the site of the emission in the cochlea. Secondly, there may be filtering of both the external tone and of the emission from both the cochlea and the middle ear. The results of studies of these effects in the context of full cochlear model simulations will be reported elsewhere.

Acknowledgements

We would like to thank Hero Wit and Savithri Sivaramakrishnan for helpful discussions. This work was supported in part by NIH grant NIDCD-DC00307.

References

Bialek, W.S., and Wit, H.P. (1984) Quantum limits to oscillator stability: Theory and experiments on acoustic emissions from the human ear. Phys. Lett. 104A, 1973-1978.

Dallmayr, C. (1985) Spontane oto-akustische Emissionen: Statistik und Reaktion auf akustische Störtöne. Acustica 59, 67-75.

Dallmayr, C. (1987) Stationary and dynamical properties of simultaneous evoked otoacoustic emissions (SEOAE). Acustica 63, 243-255.

Hanggi, P. and Riseborough, P. (1983) Dynamics of nonlinear dissipative oscillators. Am. J. Physics 51, 347-351.

Long, G. R. and Tubis, A. (1988a) Investigations into the nature of the association between threshold microstructure and otoacoustic emissions. Hear. Res. 36, 125-138.

Long, G. R. and Tubis, A. (1988b) Modification of spontaneous and evoked otoacoustic emissions and associated psychoacoustic microstructure by aspirin consumption. J. Acoust. Soc. Am. 84, 1343-1353.

Long, G. R., Tubis, A., and Jones, K. L. (1990) Changes in synchronization and suppression tuning curves of spontaneous oto-acoustic emissions when the levels of the emissions are modified by aspirin consumption. Submitted to J. Acoust. Soc. Am.

Nayfeh, A. H. Perturbation Methods. John Wiley, New York (1973)

Nayfeh, A. H. and D. T. Mook, D. T. Nonlinear Oscillations. John Wiley, New York, (1979).

Schloth, E. and Zwicker, E. (1983) Mechanical and acoustical influences on spontaneous oto-acoustic emissions. Hear. Res. 11, 285-293.

Van Dijk, P. (1990) Characteristics and Mechanisms of Spontaneous Otoacoustic Emissions. Thesis, University of Groningen, The Netherlands.

Wit, H.P. (1986) Statistical properties of a strong spontaneous otoacoustic emission. In: Peripheral Auditory Mechanics (Eds: by J.B. Allen, J.L. Hall, A.E. Hubbard, S.T. Neely, and A. Tubis) Springer Verlag, Berlin, pp. 221-228.

Zurek, P. M. and Clark, W. W. (1981) Narrow-band acoustic signals emitted by chinchilla ears after noise exposure. J. Acoust. Soc. Am. 70, 446-450.

Zwicker, E. and Schloth, E. (1984) Interrelation of different oto-acoustics emissions. J. Acoust. Soc. Am. 75, 1184-1154.

ACTIVELY AND PASSIVELY GENERATED ACOUSTIC DISTORTION AT $2f_1$-f_2 IN RABBITS

M.L. Whitehead, B.L. Lonsbury-Martin, and G.K. Martin

Dept. of Otorhinolaryngology and Communicative Sciences,
Baylor College of Medicine, Houston, TX 77030, U.S.A.

Introduction

Upon stimulation of the mammalian ear by two tones of frequencies f_1 and f_2, distortion-product otoacoustic emissions (DPOAEs) can be measured at $2f_1$-f_2 in the ear canal. These DPOAEs are vulnerable to cochlear insult; in small mammals $2f_1$-f_2 DPOAEs below stimulus levels of 60-70 dB SPL disappear more rapidly post mortem, and are considerably more vulnerable to traumas such as asphyxia and aminoglycoside poisoning, than those above this level (Schmiedt & Adams, 1981; Kemp & Brown, 1984; Schmiedt, 1986; Lonsbury-Martin et al., 1987; Brown et al., 1989).

This differential vulnerability suggests that DPOAEs at low and high stimulus levels are generated by different mechanisms (Brown, 1987). The great physiological vulnerability of the low-level DPOAE generator, and its inferred "saturation" at around 60-70 dB SPL, has led to its association with the active, micromechanical process, thought to involve outer hair cell (OHC) motility, that appears to enhance basilar membrane motion at low stimulus levels. The relative resistance to trauma of the higher level mechanism has led to its association with the passive, macromechanical properties of the cochlear partition (Brown, 1987).

Nonmonotonicities are often seen in the growth of $2f_1$-f_2 DPOAE amplitude in small mammals (Kim, 1980; Fahey & Allen, 1986; Wiederhold et al., 1986; Brown, 1987; Lonsbury-Martin et al., 1987). The sharpness and depth of some of the reported notches suggests a phase-cancellation between two sources of similar magnitude (Wiederhold et al., 1986; Brown, 1987). Such notches are typically found at 60-70 dB SPL or higher, but not lower, consistent with the hypothesis of different low- and high-level DPOAE generators producing approximately equal outputs at these stimulus levels.

The nonmonotonicities of DPOAE growth appear to vary with stimulus parameters, i.e., frequency, frequency separation of the primaries (Fahey & Allen, 1986, 1988), the level difference of the primaries (Wiederhold et al., 1986; Brown, 1987), and whether DPOAE growth is measured as a function of the level of one or both primary tones (Fahey & Allen, 1986, 1988; Brown, 1987).

To study the contribution of the low-level DPOAE generator to the measured ear-canal distortion, we have made detailed measurements of the dependence of $2f_1$-f_2 DPOAE amplitude on stimulus parameters in the rabbit ear canal. The observed dependence of nonmonotonicities in $2f_1$-f_2 DPOAE growth on stimulus parameters provides evidence in support of the hypothesis of different DPOAE generators below and above 60-70 dB SPL.

Methods

Awake pigmented and albino New Zealand strain rabbits were placed in a standard plastic restrainer. The head was stabilized by a head brace surgically implanted several days previously. All experiments were carried out in a sound-proofed booth.

The two primary tone signals were produced by a dual-channel synthesizer and attenuated under computer control by matched attenuators, transduced by two dynamic earspeakers (Beyer, DT-48), acoustically mixed, and delivered to the sealed ear canal via a speculum incorporating a probe tube attached to a 1/2"-condenser microphone. The amplitude of the $2f_1$-f_2 DPOAE, and the noise floor, at 50 Hz above DPOAE frequency, were measured automatically from spectra (n=4) collected with a dynamic-signal analyzer.

Primary levels were maximally 75 dB SPL, as the acoustic middle-ear reflex may be activated in the awake rabbit at and above this level, at some of the frequencies used, causing decreases in DPOAE amplitude in the ear canal (Whitehead et al., 1990).

To determine the effect of varying primary frequency and level on DPOAE amplitude, equilevel primaries (i.e., $L_1=L_2$) at a frequency separation of $f_2/f_1=1.25$ were used. "Audiograms" were collected from 24 ears of 12 rabbits by measuring DPOAEs at 1-10 kHz, in 0.2-kHz steps, at three primary levels; $L_1=L_2=45$, 60 and 75 dB SPL. Additionally, in some ears, growth functions were collected by measuring DPOAEs, at 50-Hz steps of DPOAE frequency over a limited frequency range, while decreasing $L_1=L_2$, from 75 dB SPL, in 2-dB steps, until the emission was undetectable.

To determine the effect of varying primary frequency separation, f_2/f_1 "ratio functions" were collected from 12 ears of six rabbits. The DPOAEs were measured at 2, 4, and 5.656 kHz, for $f_2/f_1=0.59$-1.77, 0.49-1.61, and 0.39-1.49, respectively, in 0.02 steps, at three primary levels; $L_1=L_2=45$, 60 and 75 dB SPL. Additionally, in 12 ears of six rabbits, growth functions were collected, by decreasing $L_1=L_2$, from 75 dB SPL, in 5-dB steps, until the emission was undetectable, for DPOAEs at 2, 4, and 5.656 kHz, at $f_2/f_1=1.01$-1.57, 1.01-1.53, and 1.01-1.49, respectively, in 0.04 steps.

The DPOAE growth as a function of individual primary level was determined in 12 ears of six rabbits. The DPOAEs were measured at 2, 4, and 5.656 kHz, for $f_2/f_1=1.25$, while decreasing the level of one stimulus from 75 to -15 dB SPL, in 5-dB steps, while holding the other stimulus fixed, at levels ranging from 75 to -15 dB SPL, in 10-dB steps.

Results

In Fig. 1A, mean (n=23 ears) DPOAE "audiograms" are plotted for primaries at $L_1=L_2=45$, 60 and 75 dB SPL. Note that two frequency scales are given; DPOAE frequency and the geometric-mean frequency of the primaries. The DPOAE amplitude increased with frequency up to DPOAE=10 kHz. In Fig. 1B, the mean 45-dB "audiogram" is replotted to indicate its variability (±1 SD). These SDs are typical of rabbit DPOAE measurements, thus SDs are excluded from later plots.

From these plots, a clear fine-structure of DPOAE amplitude variation with frequency can be seen, which was consistent between ears, and was approximately parallel at 45 and 75 dB SPL. The 60-dB "audiogram," however, varied relative to the 45- and 75-dB "audiograms," implying that DPOAE growth varies systematically with frequency over this level range, in a similar way in all normal, young rabbit ears.

The nature of this variation is illustrated, for one ear, in Fig. 2, which plots growth functions ($f_2/f_1=1.25$, $L_1=L_2$), in 2-dB steps, obtained at 50-Hz intervals, from 3.8-4.8 kHz; a frequency region over which the mean 60-dB "audiogram" approached and then moved away from the 45-dB "audiogram" (Fig. 1A). This demonstrates that the variation of 60-dB "audiograms," relative to the 45- and 75-dB "audiograms," was due to notches in the growth functions around 60 dB SPL. At the frequencies where notches occurred, they

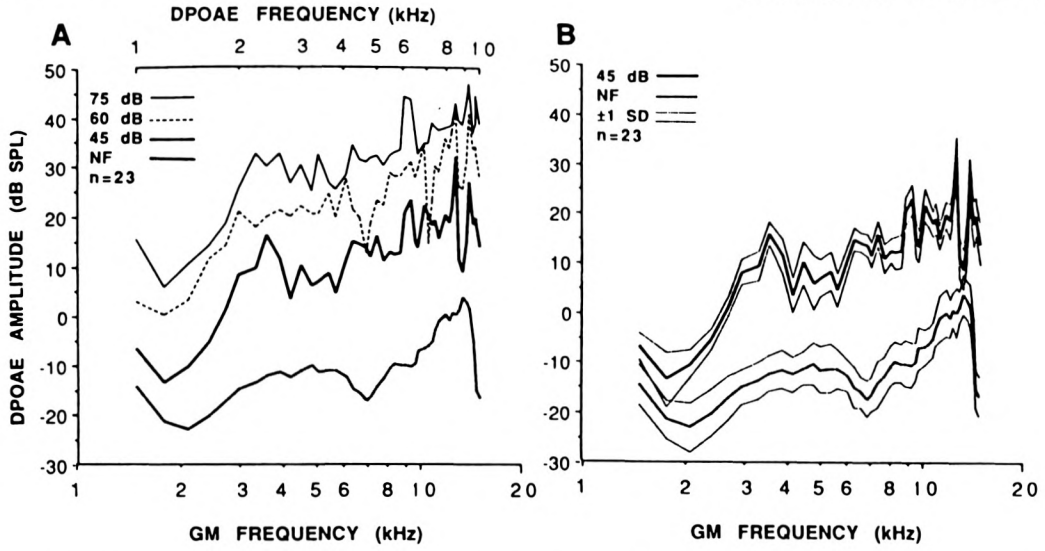

FIGURE 1 A: Mean (n=23 ears) DPOAE "audiograms" obtained at $L_1=L_2=45$, 60 and 75 dB SPL, $f_2/f_1=1.25$. Note the two frequency scales. GM frequency = geometric-mean frequency of the primaries, i.e., $(f_1 x f_2)^{0.5}$. B: The 45-dB "audiogram," and the noise floor, replotted ±1 SD, to demonstrate the small interanimal variability of DPOAE measures in rabbits.

were seen only around 60-70 dB SPL, and at any one frequency there was never more than one notch below 75 dB SPL (e.g., Fig. 2). It is clear that for a given primary frequency separation ($f_2/f_1=1.25$) and primary level difference ($L_1-L_2=0$ dB), nonmonotonicities in the growth functions at around 60 dB SPL were systematically dependent on frequency.

The DPOAE growth at low stimulus levels in Fig. 2 was close to 1 dB/dB, and varied little with frequency. In Fig. 3A, the slopes of the straight, low-level part of mean (n=23 ears) DPOAE growth functions are plotted against frequency. Clearly, at low stimulus levels, DPOAE growth varies little over a wide range of frequencies. The threshold of DPOAE detection was close to primary levels of 25 dB SPL, except at the lowest frequencies. Note that only four RMS averages were used and, with a greater number of time-locked averages, these thresholds could be considerably reduced. Above about 70 dB SPL, there was compressive nonlinearity, as can be seen in Fig. 2.

In Fig. 4A, mean (n=12 ears) primary frequency separation (f_2/f_1 ratios) functions, obtained at $L_1=L_2=45$, 60 and 75 dB SPL, are plotted for the 4-kHz DPOAE. The curves show an increase of DPOAE amplitude to a maximum at an f_2/f_1 ratio of around 1.3, and a decrease above this ratio. The optimum ratio was lower at 60 than at 45 and 75 dB (i.e., the optimum ratio was nonmonotonically dependent on stimulus level), and decreased with increasing frequency. There was a change of shape of the ratio function with increasing stimulus level, in that below the optimum f_2/f_1 it was steeper at low levels, whereas above the optimum f_2/f_1 it was steeper at high levels. Thus, although both the 45- and 75-dB curves demonstrate similar optimum ratios, at 75 dB, DPOAEs were large at small f_2/f_1 ratios, but small at the highest f_2/f_1 ratios, whereas at 45 dB, DPOAEs were present at large f_2/f_1 ratios, but absent at small f_2/f_1 ratios. These findings suggest different constraints on DPOAE generation at high and low stimulus levels, consistent with the hypothesis of different DPOAE generators at high and low stimulus levels. Similar trends were observed for DPOAEs at 2 and 5.656 kHz.

In Fig. 4B, the lower level ratio functions have been subtracted from the higher level ratio functions, and the differences plotted as a function of f_2/f_1 ratio, for the 4-kHz DPOAE. It can be seen that DPOAE growth varies systematically with f_2/f_1 ratio.

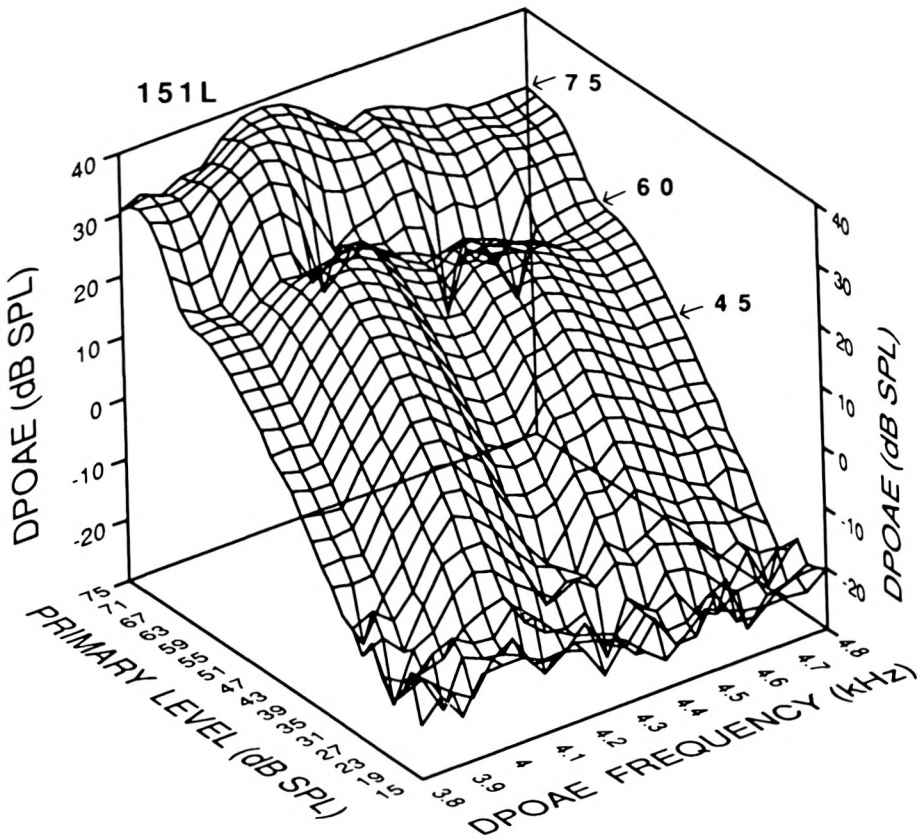

FIGURE 2 Growth functions for DPOAEs from 3.8-4.8 kHz, in 50-Hz steps, for ear 151L. $L_1=L_2$, $f_2/f_1=1.25$. There are frequency-dependent notches around 60 dB SPL between 4.0-4.7 kHz, i.e., where the 60-dB "audiogram" approaches the 45-dB "audiogram" (Fig. 1A).

From 60-75 dB, $2f_2-f_1$ growth (i.e., $f_2/f_1<1$) was expansively nonlinear (around 1.5 dB/dB). There was a peak of growth close to $f_2/f_1=1$, but as f_2/f_1 increased above 1, growth decreased to near 0 dB/dB, rapidly recovered to greater than 1 dB/dB near the mean optimum ratio (triangle on *x*-axis), then rapidly decreased to below 0 dB/dB before showing a final recovery. Growth from 45-60 dB was inversely correlated with that from 60-75 dB above $f_2/f_1=1.1$ ($r=-0.64$, $p<0.001$), with no growth between 45-60 dB at the peak of growth between 60-75 dB. These difference curves were similar at all three frequencies, and imply that $2f_1-f_2$ DPOAE growth varies systematically with primary frequency separation over the 45-75 dB level range.

The variations of the 60-dB ratio functions relative to the 45- and 75-dB curves (Fig. 4A), imply the presence of nonmonotonicities in DPOAE growth functions around 60 dB SPL at certain f_2/f_1 ratios. This has also been observed at higher stimulus levels in the cat (Fahey & Allen, 1986). Mean (n=12 ears) 4-kHz DPOAE growth functions at 0.04 steps of f_2/f_1 ratio over regions encompassing notches are plotted in "3D" in Fig. 5, clearly demonstrating the existence of notches at stimulus levels of around 60 dB that, for an arbitrarily fixed DPOAE frequency (2, 4 or 5.656 kHz) and primary level difference ($L_1-L_2=0$ dB), were systematically dependent on f_2/f_1 ratio, i.e., frequency separation, or frequency of the primaries. Around the optimum f_2/f_1 ratio, thresholds were low, and notches occurred around 60 dB SPL. At the lowest f_2/f_1 ratios, both growth slope and threshold increased, and growth was monotonic. At high f_2/f_1 ratios, thresholds increased only slightly, and saturation occurred at stimulus levels of around 60 dB SPL.

In Fig. 3B, the slopes of the straight, low-level parts of the growth functions are plotted against f_2/f_1 ratio. It can be seen that DPOAE growth was close to 1 dB/dB at

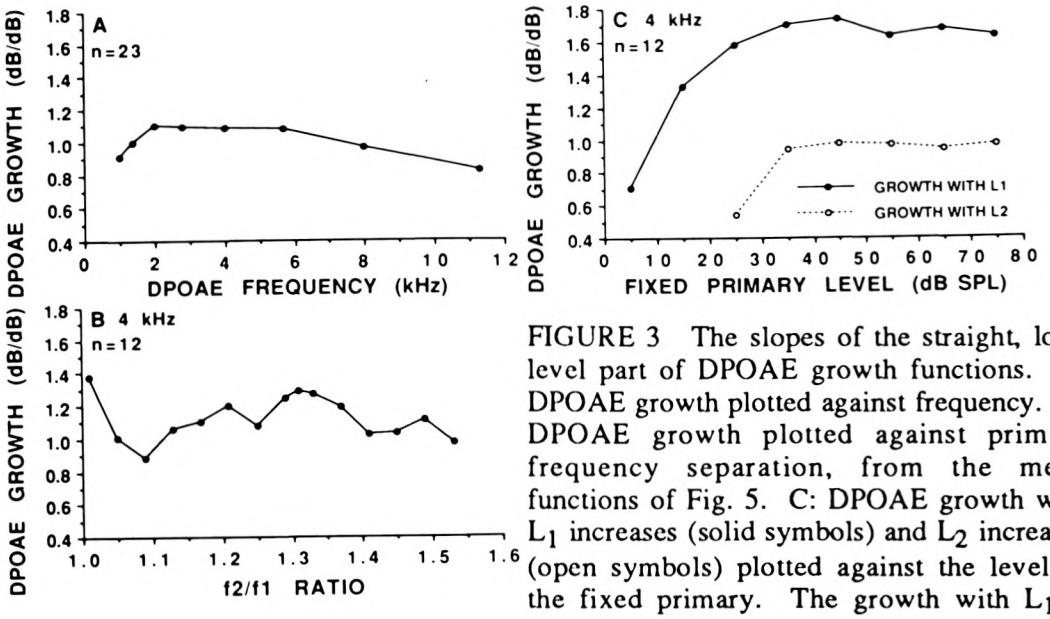

FIGURE 3 The slopes of the straight, low-level part of DPOAE growth functions. A: DPOAE growth plotted against frequency. B: DPOAE growth plotted against primary frequency separation, from the mean functions of Fig. 5. C: DPOAE growth with L_1 increases (solid symbols) and L_2 increases (open symbols) plotted against the level of the fixed primary. The growth with L_1 is from the mean functions of Fig. 6.

low stimulus levels, and varied little with f_2/f_1 ratio, although it tended to increase as f_2/f_1 approached 1. Similar results were obtained for DPOAEs at 2 and 5.656 kHz.

In Fig. 6, the mean (n=12 ears) growth of the 4-kHz $2f_1$-f_2 DPOAE is plotted as a function of L_1 (varying in 5-dB steps) at 10-dB increments of L_2. Similar plots were obtained for DPOAEs at 2 and 5.656 kHz. Moving to the left across this plot illustrates growth as a function of L_1, and moving to the right illustrates growth as a function of L_2. It is clear that notches systematically occurred in DPOAE growth as a function of L_1, for L_1 close to 65 dB SPL, when L_2<55-60 dB SPL. Shallow notches were also present in DPOAE growth as a function of L_2, for L_2 close to 55 dB SPL, when L_1<65 dB SPL, although these notches were obscured in Fig. 6 by averaging and by the 10 dB resolution of L_2. The "3D" plots give the impression of a low-level "hump"

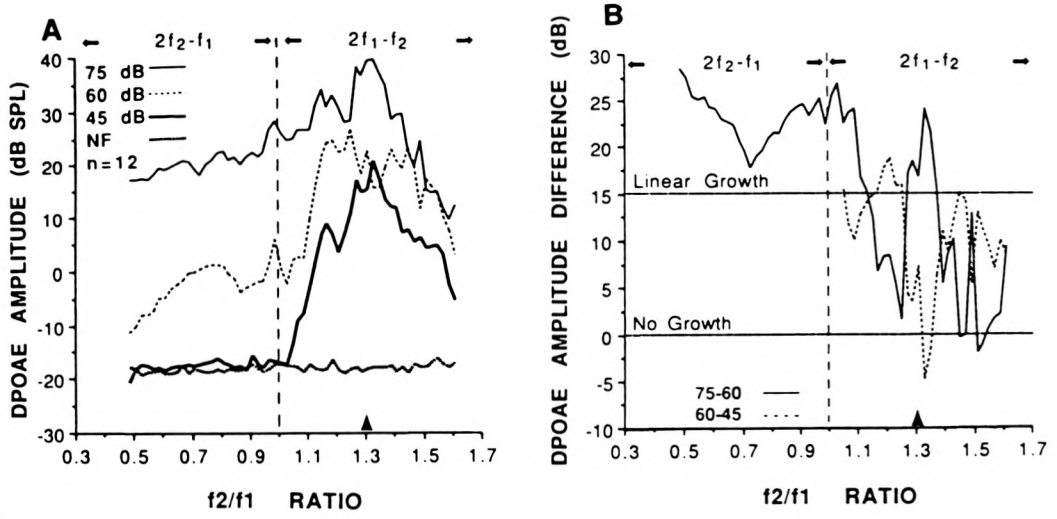

FIGURE 4 A: Mean (n=12 ears) primary frequency separation functions, for the 4-kHz DPOAE, obtained at L_1=L_2=45, 60 and 75 dB SPL. Note that when f_2/f_1<1, the DPOAE measured is $2f_2$-f_1. B: The differences between the higher- and lower-level ratio functions, plotted against f_2/f_1 ratio. The triangles on the x-axes represent the mean optimum ratio for the 4-kHz DPOAE.

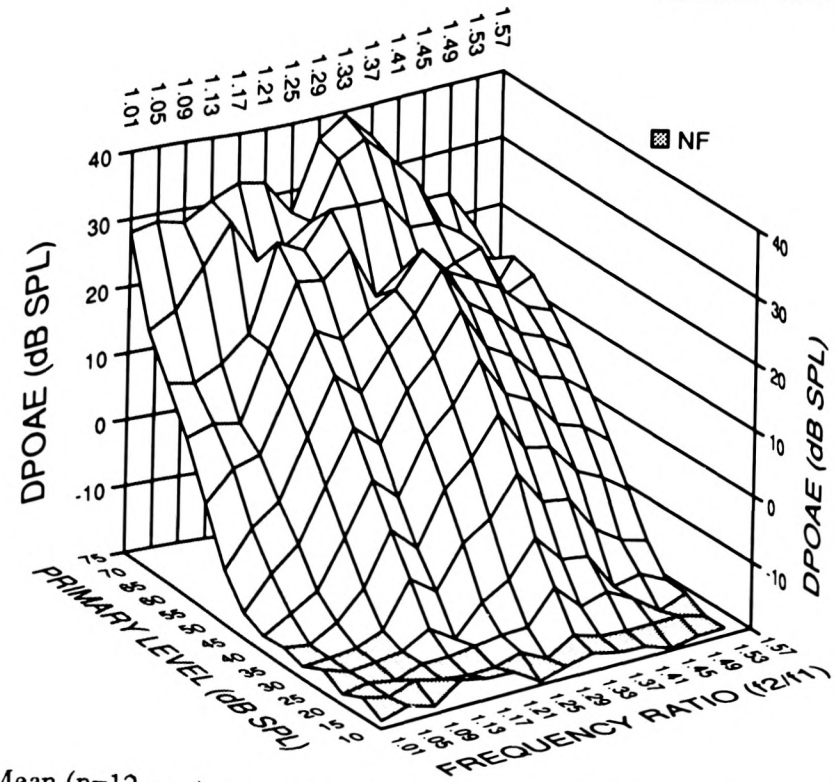

FIGURE 5 Mean (n=12 ears) growth functions, for the 4-kHz DPOAE, obtained at f_2/f_1 ratios from 1.01-1.53, in 0.04 steps, $L_1=L_2$. Shaded regions represent no DPOAE detectable above the noise floor.

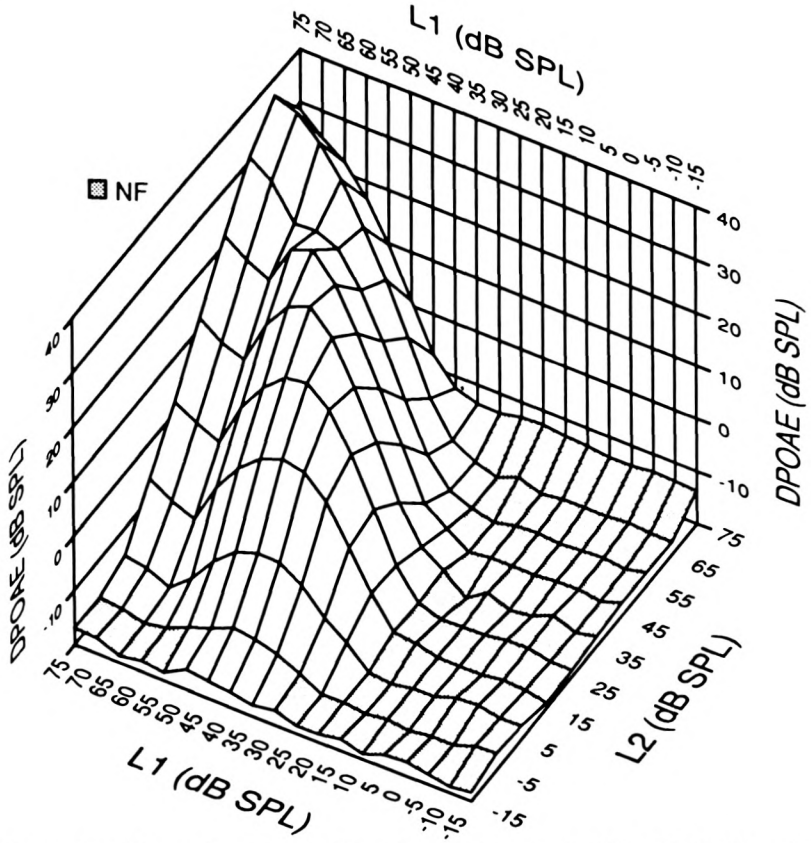

FIGURE 6 Mean (n=12 ears) growth functions, for the 4-kHz DPOAE, obtained with L_1 varying in 5-dB steps, at 10-dB increments of L_2. Shaded regions represent no DPOAE detectable above the noise floor.

superimposed on a higher-level background, consistent with the hypothesis of separate low- and high-level DPOAE generators.

The slopes of the low-level, straight parts of the 4-kHz DPOAE growth functions are plotted in Fig. 3C for both L_1 increases (solid circles) and L_2 increases (open circles), in each case as a function of the level of the fixed primary. The DPOAE growth as a function of L_1 increased with L_2 level to around 1.6 dB/dB. Growth as a function of L_2 also increased with the level of the fixed primary, to slightly less than 1 dB/dB.

It is clear from Fig. 6 that DPOAEs are detectable for much lower levels of L_2 than L_1, and that the level of L_2 producing the maximum-amplitude DPOAE is highly dependent on the fixed L_1 level, whereas the level of L_1 producing the maximum-amplitude DPOAE is only slightly dependent on the fixed L_2 level. The primary level difference, L_1-L_2, producing the greatest DPOAE amplitude is positive, and increases with decreasing L_2. Detailed inspection of Fig. 6 further reveals that, when both primaries are varied, increasing L_1-L_2 above 0 will result in greater notches in the growth functions, as observed in the cat (Wiederhold et al., 1986) and gerbil (Brown, 1987).

Discussion

The results demonstrated that notches in $2f_1$-f_2 DPOAE growth functions are common at stimulus levels of around 60-70 dB SPL, and absent below this level, in the rabbit. This is consistent with the hypothesis of two DPOAE generators having similar outputs at this stimulus level. These notches are systematically dependent on primary tone frequency (Figs. 1, 2), frequency separation (Figs. 4, 5), individual primary level, and primary level difference (Fig. 6). If the notches are indeed due to the interaction of two generators, then the relative phases and/or amplitudes of the two outputs must systematically change with these stimulus parameters.

These nonmonotonicities may represent the boundaries between the low- and high-level DPOAE generators. This suggestion is supported by the occurrence of the notches at around 60-70 dB SPL; the stimulus level that appears to divide the vulnerable from the less vulnerable DPOAEs. Recent measurements in our laboratory of post-mortem changes of rabbit DPOAEs further support this distinction.

If these notches do delimit the outputs of separate low-level and high-level mechanisms, we can make some definite statements about the behavior of the low-level ("active," "micromechanical"?) generator. Firstly, the output of the low-level generator varies similarly with frequency to that of the high-level generator. This can be seen in Fig. 1A, where the 45- and 75-dB DPOAE "audiograms," apparently produced by the low-level and high-level generators, respectively, parallel each other closely. Secondly, the output of the low-level generator varies with primary frequency separation differentially to that of the high-level generator. Whereas the two have maximum output at similar f_2/f_1 ratios (Fig. 4A), the low-level generator is favored at high f_2/f_1 ratios (i.e., the 45-dB ratio function demonstrates a shallower high-ratio cut-off), and the high-level generator is favored at the low f_2/f_1 ratios (i.e., the 75-dB ratio function demonstrates a shallower low-ratio cut-off). Perhaps variation of the f_2/f_1 ratio may provide a means for independent study of the two mechanisms (Brown, 1987). The maximum interaction between the two generators appears to occur at around the optimum ratio.

The growth of the low-level DPOAEs suggests that the generator behaves more as expected from an "essential," rather than a cubic, nonlinearity. Whereas DPOAE growth with only L_2 increasing was close to 1 dB/dB, growth with only L_1 increasing did not reach the 2 dB/dB expected from a cubic nonlinearity (Fig. 3C). For L_1=L_2, DPOAE

growth was close to 1 dB/dB over a wide range of frequencies and f_2/f_1 ratios (Figs 3A, 3B). From a cubic nonlinearity, slopes of 3 dB/dB would be expected. Close to $f_2/f_1=1$, DPOAE growth with $L_1=L_2$ tended to increase slightly, but here detection thresholds were also high, i.e., the high-level generator may be dominant at these small ratios (see above, and also Brown, 1987). The same high-level generator may be solely responsible for the generation of the $2f_2-f_1$ DPOAE, which has a high threshold, steep growth, and does not demonstrate the notches indicative of the interaction of two generators (Fig. 4A, and Lonsbury-Martin et al., 1987). In support of this suggestion, the ratio functions of Fig. 4A do not demonstrate any clear discontinuity around $f_2/f_1=1$ at 75 dB SPL.

The observed DPOAE growth agrees with that reported for similar primary-tone levels in the guinea pig and gerbil (Brown, 1987), but is different to the apparently power-law behavior of $2f_1-f_2$ in the cat reported by Fahey and Allen (1986, 1988). However, the majority of Fahey and Allen's stimuli were above the maximum level used in the present study, and they may have been studying the high-level DPOAE generator.

The presence of two different DPOAE generators has clear implications for models of cochlear nonlinearity, and for the design and interpretation of experiments and clinical tests utilizing DPOAEs as monitors of cochlear condition.

Acknowledgements: Research supported in part by funds from the Public Health Service (DC00313, DC00613, ES03500) and the Deafness Research Foundation to Baylor College of Medicine.

References

Brown, A.M. (1987) Acoustic distortion from rodent ears: A comparison of responses from rats, guinea pigs and gerbils. Hear. Res. 31, 25-38.

Brown, A.M., McDowell, B. and Forge, A. (1989) Acoustic distortion products can be used to monitor the effects of chronic gentamicin treatment. Hear. Res. 42, 143-156.

Fahey, P.F. and Allen, J.B. (1986) Characterization of cubic intermodulation distortion products in the cat external auditory meatus. In: Peripheral Auditory Mechanisms (Eds: Allen, J.B., Hall, J.L., Hubbard, A.E., Neely, S.T. and Tubis, A.) Springer-Verlag, New York, pp. 314-321.

Fahey, P.F. and Allen, J.B. (1988) Power law features of acoustic distortion product emissions. In: Basic Issues in Hearing (Eds: Duifhuis, H., Horst, J.W. and Wit, H.P.) Academic Press, London, pp. 124-134.

Kemp, D. T. and Brown, A.M. (1984) Ear canal acoustic and round window correlates of $2f_1-f_2$ distortion generated in the cochlea. Hear. Res. 13, 39-46.

Kim, D.O. (1980) Cochlear mechanics: Implications of electrophysiological and acoustical observations. Hear. Res. 2, 297-317.

Lonsbury-Martin, B.L., Probst, R., Coats, A.C. and Martin, G.K. (1987) Acoustic distortion products in rabbits. I. Basic features and physiological vulnerability. Hear. Res. 28, 173-189.

Schmiedt, R.A. (1986) Effects of asphyxia on levels of ear canal emissions in gerbil. Assoc. Res. Otolaryngol. Abst. 9, 140, 112-113.

Schmiedt, R.A. and Adams, J.C. (1981) Stimulated acoustic emissions in the ear canal of the gerbil. Hear. Res. 5, 295-305.

Whitehead, M.L., Lonsbury-Martin, B.L. and Martin, G.K. (1990) The effects of the crossed acoustic reflex on distortion-product otoacoustic emissions in rabbits. In Submission, Hear. Res.

Wiederhold, M.L., Mahoney, J.W. and Kellogg, D.L. (1986) Acoustic overstimulation reduces $2f_1-f_2$ cochlear emissions at all levels in the cat. In: Peripheral Auditory Mechanisms (Eds: Allen, J.B., Hall, J.L., Hubbard, A.E., Neely, S.T. and Tubis, A.) Springer-Verlag, New York, pp. 322-329.

EFFECTS OF TYMPANIC MEMBRANE MODIFICATION ON DISTORTION PRODUCT OTOACOUSTIC EMISSIONS IN THE CAT EAR CANAL

Michael L. Wiederhold

Department of Otolaryngology, the University of Texas Health Science Center at San Antonio and Audie L. Murphy Veterans Hospital, San Antonio, TX 78284-7777, USA

Introduction

Acoustic distortion-product (DP) signals recorded in the external ear canal reflect nonlinearities in cochlear mechanics. The level of DP signals is reduced by processes known to damage the organ of Corti, including noise exposure (Kim et al., 1980, Zurek et al., 1982, Siegel et al., 1982, Rosowski et al., 1984, Dolan and Abbas, 1985, Schmiedt, 1986, Wiederhold et al., 1986, Martin et al., 1987). Thus, DP measurement has been suggested as a diagnostic tool to assess the physiologic state of the organ of Corti (Probst, 1990). Changes in middle-ear stiffness have been shown to alter otoacoustic emissions (e.g., Kemp, 1981). We have noted large variation in the level and threshold for detection of ear-canal DP's in humans with normal or near-normal hearing. We see less variability in cats selected for normal-appearing tympanic membranes (TM), whereas cats with scarred or thickened TM's have lower DP's which require high primary-tone levels to become detectable. This suggests that an important component of DP variability is related to TM or middle-ear pathology. Here we report results of studies in which the TM was modified, either by adding mass or by causing a leak with a small perforation. The aim was to assess the effects of these modifications on forward and reverse transmission through the middle ear and to determine if such modifications might have disproportionate effects on ear-canal DP signals.

Methods

All measurements were obtained from cats anesthetized with dial in urethane (90 mg/kg). Acoustic stimuli were delivered through a closed acoustic system with a 1-inch condenser microphone (Bruel & Kjear 4144) as the sound source. DP and primary-tone levels were measured through a probe tube with a B & K 4134 1/2-inch microphone and analyzed with a Nicolet 660B dual-channel spectrum analyzer with resolution of 0.2 Hz. With this system, the noise floor at 2.8 kHz was approximately -15 dB SPL. In Figures 1, 2 and 4-7, data plotted at -20 dB SPL are the first points in a series at which a signal could not be differentiated from noise. Primary tones were presented either at equal level ($L_2 = L_1$) or with the higher-frequency tone (f_2) 10 dB lower than L_1. Primary levels were increased from DP detection threshold to L_1 = 80 dB SPL, in 1 to 3 dB increments. If, after TM modification, no DP could be detected at 80 dB SPL, L_1 was increased to 90 or 95 dB SPL.

The TM was modified either by gluing a piece of platinum foil over the umbo with super glue or by making a 1.2 mm perforation with a sharp needle. The pieces of foil were 7 or 14 mg and were folded to 2 x 2 mm surface area. Transmission differences were assessed using narrow-band filtered clicks formed by passing a square pulse of duration $1/2f_o$ through a band-pass filter with slopes of 48 dB/octave above and below f_o. Auditory-nerve (N_1) responses were recorded with a wire electrode near the round window.

Results

For this study, DP's were generated by presenting primary-tone stimuli at 4.0 and 5.2 kHz (f_2/f_1 = 1.3) and the $2f_1 - f_2$ cubic DP at 2.8 kHz was recorded in the sealed external ear canal. Figure 1 shows ear-canal DP growth functions both for equal-level primaries and for $L_2 = L_1 - 10$ dB for a typical animal. The 10 dB offset produces a lower threshold for detection of the DP signal and maximizes DP level for moderate-level primaries. A similar conclusion by Schloth is reported by Probst (1990). Brown (1990) finds optimal DP's in humans with L_2 15 dB below L_1. The pronounced dip at L_1 = 67 dB SPL for equal levels and at 73 dB for the 10 dB offset are probably due to cancellation of out-of-phase components (see Zwicker, 1980). DP's produced with primaries below the dip are more sensitive to noise damage (Wiederhold et al., 1986; Rosowski et al., 1984) so the 10 dB offset stimuli are preferable for assessing cochlear pathology.

To produce a DP signal in the ear canal, the primary tones must be transmitted through the middle ear to the cochlea and the DP signal must be transmitted retrogradely through the middle ear. A reduced DP level could thus be due to impaired forward or reverse transmission through the middle ear, or to changes at the DP generation site in the cochlea. The TM modifications performed here are not expected to damage the cochlea, so changes in DP levels are likely due to changes in middle-ear transmission.

Figure 2 illustrates DP growth before and after gluing a 7 mg weight to the TM. Note that, after applying the weight, DP signals for primaries below the dip (73 dB

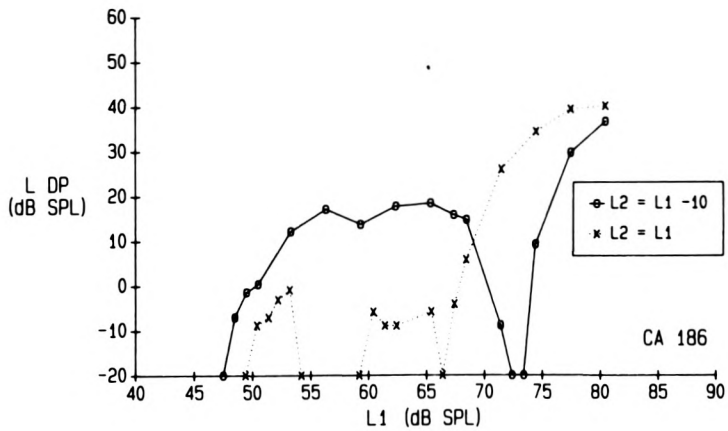

FIGURE 1 Growth of $2f_1 - f_2$ distortion-product (DP) signal in cat ear canal produced by primary tones at 4.0 and 5.2 kHz (as for all other figures). Solid line and circles: L_2 maintained 10 dB lower than L_1. Dotted line: primary tones at equal levels. In both cases the ordinate is L_1. Cat 186.

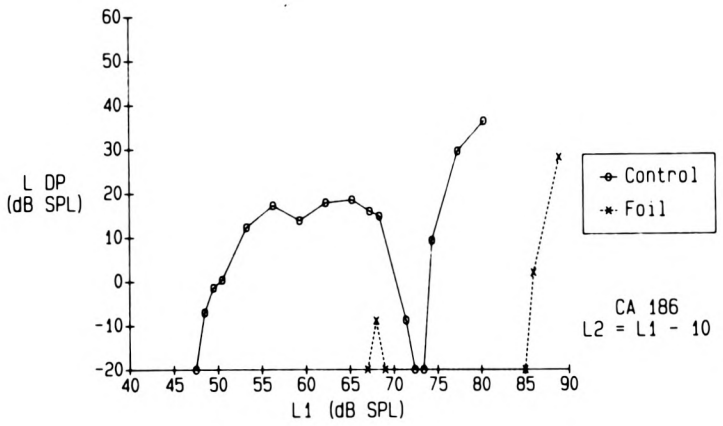

FIGURE 2 Growth of DP in control condition (solid line with circles), as in Figure 1, and after gluing a 7 mg piece of platinum foil to the tympanic membrane with gel-type super glue (dashed line with x's). Cat 186.

SPL) are greatly reduced and that the high-level portion of the growth function is shifted higher by the weight.

The change in forward transmission was tested by observing changes in N_1 responses to narrow-band transient stimuli with spectra centered at the primary frequencies. Orthograde transmission at the primary frequencies was assessed with a 5.0 kHz filtered click. Figure 3 shows N_1 amplitude- and latency-v-level functions before and after placing the 7 mg weight. At low and moderate levels, both functions appear to be shifted horizontally a constant amount by the weight, consistent with a purely conductive hearing loss. The average shift of 11 dB was determined by averag-

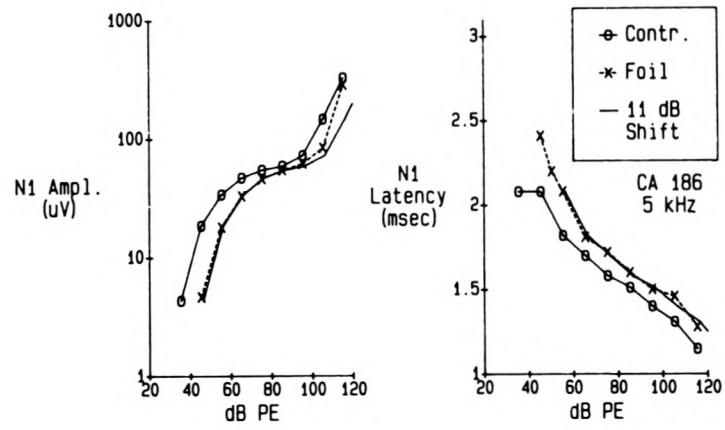

FIGURE 3 Plots of amplitude (left) and latency (right) of N_1 responses recorded near the round window in response to 5 kHz filtered clicks, formed by passing a 100 usec square pulse through a band-pass filter with roll-offs of 48 dB/octave above and below 5 kHz. Stimulus level presented in dB Peak Equivalent, re 20 aPascal. Solid lines with circles: control measurements. Dashed lines with x's: Measurements after gluing 7 mg weight to TM. Solid lines with no symbols: control plots shifted 11 dB to higher levels.

Table 1 Orthograde Transmission Losses (dB)

	7 mg Foil				14 mg Foil		
Cat#	2.8kH	5kHz	10kHz	Cat#	2.8kHz	5kHz	10kHz
180	5	03	04	182	9	11	15
181	4	02	02	183	5	08	10
186	8	11	10	184	0	11	08
Avg.	5.7	5.3	5.3		4.7	10.0	11.0
	Perforation						
198	6.5	4.1	nm				

ing horizontal distance between the two plots at each data point. At the highest levels (100 - 120 dB SPL PE), the amplitude function deviates from a parallel shift.

The cochlear electrode had to be removed and later replaced to allow fixation of the weight to the TM. This procedure can affect N_1 amplitude if the electrode is not replaced at the same point, with the same contact resistance but small changes in electrode placement do not change response latency (Montandon et al, 1975). Thus, we have used the shift in the N_1 latency function as a measure of transmission loss. Table 1 lists shifts observed with filtered clicks centered at 2.8, 5.0 and 10.0 kHz for three animals each with 7 and 14 mg weights and one animal with a TM perforation. At the higher frequencies (5 and 10 kHz) the 14 mg weight caused approximately a 5 dB greater transmission loss than did the 7 mg weight. We used the same technique to measure transmission changes at 2.8 kHz, the frequency of the $2f - f_2$ DP. These shifts averaged 5.7 dB for 7 mg weights and 4.7 dB for 14 mg weights.

If the effects of the weights on transmission through the middle ear were equal for signals travelling in either direction, the changes in DP growth should be predictable

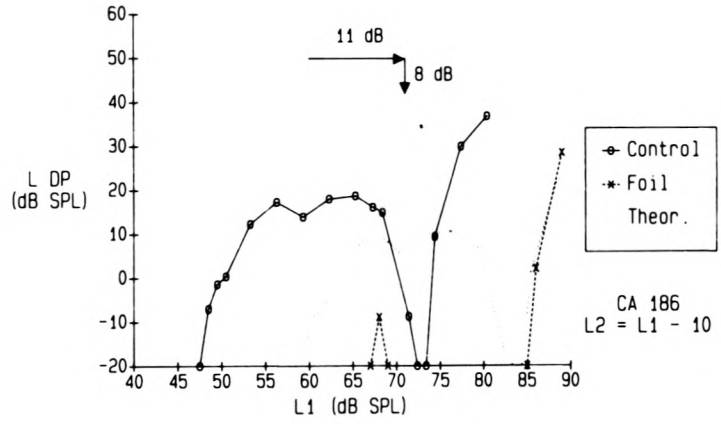

FIGURE 4 DP growth, as in Figure 2, before and after placing 7 mg weight on TM (solid and dashed lines, respectively). Dotted line without symbols: control growth function shifted to right by 11 dB (the change in transmission at 5.0 kHz) and downward by 8 dB (the change in transmission at 2.8 kHz--the DP frequency). Note that observed DP with weight for L_1 = 68 dB SPL is 25 dB below the theoretical prediction. Cat 186.

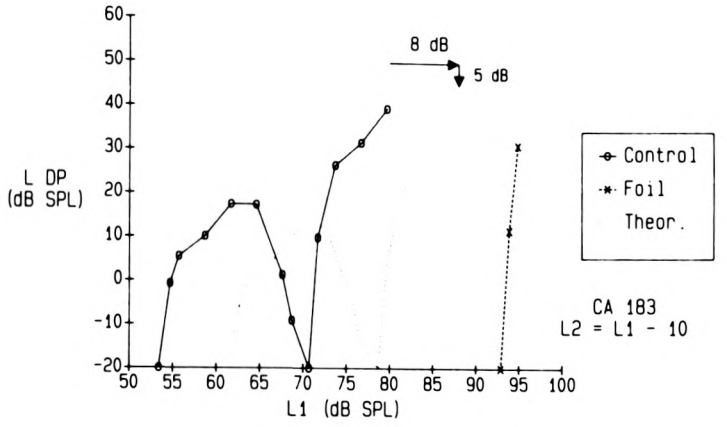

FIGURE 5 Comparison of control DP growth, that observed with a 14 mg weight and the growth predicted from transmission losses observed at 2.8 and 5 kHz, 5 and 8 dB, respectively. Cat 183.

from the transmission measurements at 5.0 and 2.8 kHz: assuming that measurements at 5 kHz adequately assess inward transmission at 4.0 and 5.2 kHz, the primary stimuli reaching the organ of Corti should be reduced by the shift measured with the 5.0 kHz filtered click, D_5. If the primary-tone stimuli were both raised by D_5 dB, the stimulus at the organ of Corti should be restored to its control amplitude, as would the locally generated DP. The DP signal generated by the higher-level primaries would then propagate toward the base of the cochlea and suffer a transmission loss equal to $D_{2.8}$ in reaching the external ear canal. This would shift the ear-canal DP growth function downward by $D_{2.8}$. Figure 4 illustrates this predicted change in DP growth for the case illustrated in Figure 2. The "theoretical" curve is the control DP growth function shifted to the right by D_5 (11 dB) and downward by $D_{2.8}$ (8 dB). Note that, below the dip, the observed ear-canal DP levels are at least 25 dB below those predicted for equal losses in either direction. Similar cases of observed and predicted changes in DP growth with 14 mg weights are illustrated in Figures 5 and 6. In both of these cases,

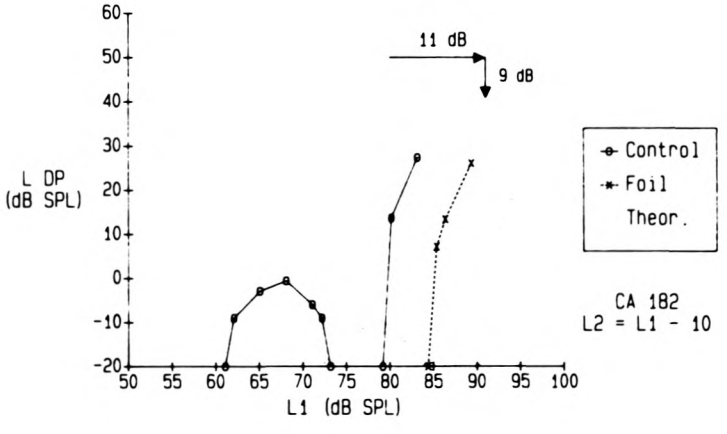

FIGURE 6 Control, weighted and predicted DP growth, as in Figure 5, with 14 mg weight. Cat 182.

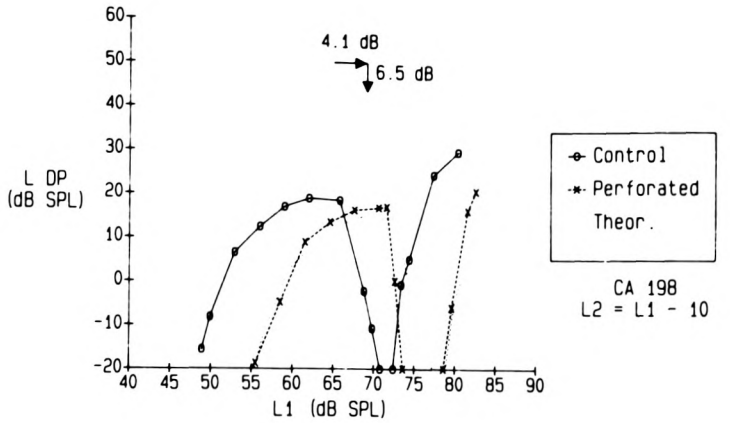

FIGURE 7 Control, modified and predicted DP growth functions, as in Figures 4-6, with a 1.2 mm perforation in the TM. No weights were applied. Note that in this case the transmission losses observed at 2.8 and 5.0 kHz (6.5 and 4.1 dB, respectively) do satisfactorily predict DP growth at most levels. Cat 198.

after the weight was placed, no DP could be recorded with primaries below the level of the dip. Predicted and observed effects of TM loading on DP growth above the dip are quite similar with the 7 mg weight, as illustrated in Figure 4. With the 14 mg weights, in Figure 5 the observed DP above the dip required primaries nearly 15 dB greater than those predicted from the shifts at 2.8 and 5 kHz. However, in the case illustrated in Figure 6, at high levels the observed DP's are produced by primaries 5 dB lower than predicted from the N_1 latency shifts.

Figure 7 illustrates changes in the DP growth after a 1.2 mm perforation is made in the TM, causing transmission losses of 6.5 and 4.1 dB at 2.8 and 5.0 kHz, respectively. In this case, the predicted change in DP growth is quite similar to what is observed. In contrast to the findings with weights applied to the TM, a small TM perforation does appear to reduce transmission equally in either direction.

Conclusions

The pieces of platinum foil glued to the TM clearly add mass to the middle-ear system. Although the folded foil had a contact area of only 4 mm^2, the gel-type super glue adherent to the foil would also increase the stiffness of this portion of the TM. The weights of 7 and 14 mg were chosen to be close to, but somewhat higher than the 4 mg calculated by Lynch, et al. (1982) as the combined mass loading of the stapes and cochlea. It is apparent that adding the weights reduces DP level in the ear canal to a greater extent than predicted by changes in forward transmission, as assessed by changes in filtered-click N_1 latency-v-level series.

The added mass apparently loads the middle ear, looking toward the external ear canal. The mechanical signal flowing in this direction normally faces a low-impedance air-filled space, and the addition of a 7 to 14 mg mass has a substantial effect on outward transmission. An acoustic signal travelling into the middle ear normally encounters an increased impedance, and the weights affect transmission in this direction to a smaller degree than they do reverse transmission. The effects of

impedance mismatches at the stapes or ear canal on transmission of otoacoustic emissions has been treated in an analytic model by Matthews (1983) and an analog model by Zwislocki (1986) and are qualitatively consistent with our findings.

It is not possible to determine from our data how much more than the 2.8 kHz forward transmission loss the DP signal is attenuated in traversing the middle ear to the external ear canal after weight is added to the TM. From the data in Figure 4, the only DP above the noise floor with primaries below 85 dB SPL was 25 dB below the predicted DP level for the corresponding primary level (L_1 = 68 dB SPL). With 7 mg weights in other animals, isolated points were 15 to 40 dB below the predicted curves. One cat (#181) showed only small shifts with a 7 mg weight and its DP growth was within 5 dB of prediction at most levels. With 14 mg weights, as in Figures 5 and 6, DP's produced by primary tones below 80 dB SPL never exceeded the noise floor. For 14 mg weights, reverse transmission is attenuated by at least 25 dB more than the reduction in orthograde transmission at 2.8 kHz, whereas 7 mg weights cause excess DP transmission losses of 5 to 25 dB. In the case illustrated in Figure 5, the 14 mg weight reduced the DP at L_1 = 85 dB SPL by more than 50 dB, whereas inward transmission at the DP frequency (2.8 kHz) is reduced by only 5 dB.

TM scars add both mass and stiffness to the TM, as do the weights glued to the TM. Changes in reverse transmission could explain the reduced levels of DP's seen in cats with obvious signs of TM scarring. Since many human subjects have a history of recurrent middle-ear disease, they may have residual TM changes. Tympanometry, usually performed with a probe tone at 220 Hz, does not adequately assess middle-ear function at 2.8 to 5.6 kHz, which are the frequencies of interest for the DP signals we have studied here. Care must be exercised in interpreting DP recordings used for diagnostic purposes; although DP level is decreased by noise-induced hearing loss, the results presented here indicate that DP level can also be reduced by TM and middle-ear pathology, with a normal cochlea. The 14 mg weights we applied completely abolished detectable DP signals produced by moderate-level primaries but caused only minor reductions in orthograde transmission, from 0 to 9 dB. Threshold increases this small would be considered normal audiologically, but a 50 dB DP reduction would usually be considered significant. Our results indicate that such a reduction might not indicate any cochlear abnormality.

Acknowledgements

Troy Carter's assistance in preparing this manuscript is gratefully acknowledged. Supported by Veterans Administration Medical Research Funds.

References

Brown, A.M., Gaskill, S.A. (1990) Can basilar membrane tuning be inferred from distortion measurement? In: Mechanics and Biophysics of Hearing (This volume).

Dolan, T.G. (1985) Changes in the $2f_1 - f_2$ acoustic emission and whole nerve response following sound exposure: Long-term effects. J. Acoust. Soc. Am. 77,1475-1483.

Kemp, D.T. (1981) Physiologically active cochlear micromechanics-one source of tinnitus. In: Tinnitus, Ciba Found. Symp. (Eds: Evered, D. and Lawrenson, G.) Pitman, London. pp. 54-81.

Kim, D.O. (1980) Cochlear mechanics: Nonlinear behavior in two-tone responses as reflected in cochlear-nerve-fiber responses and in ear-canal sound pressure. J. Acoust. Soc. Am. 67,1704-1721.

Lynch, III, T.J., Nedzelnitsky, V., Peake, W.T. (1982) Input impedance of the cochlea in cat. J. Acoust. Soc. Am. 72,108-130.

Martin, G.K., Lonsbury-Martin, B.L., Probst, R., Coats, A.C. (1987) Acoustic distortion products in rabbit ear canal. II. Sites of origin revealed by suppression contours and pure-tone exposures. Hear. Res. 28,191-108.

Matthews, J.M. (1983) Modeling reverse middle ear transmission of acoustic distortion signals. In: Mechanics of Hearing (Eds: de Boer, E. and Viergever, M.A.) Delft Univ. Press, Delft, The Netherlands, pp 11-18.

Montandon, P.B., Megill, N.D., Kahn, A.B., Peake, W.T., Kiang, N.Y.S. (1975) Recording auditory-nerve potentials as an office procedure. Ann. Otol. Rhinol. Laryngol. 84,2-10.

Probst, R. (1990) Otoacoustic emissions: An overview, Adv. Oto Rhino Laryngol. 44, 1-91.

Rosowski, J.J., Peake, W.T., White, J.R. (1984) Cochlear nonlinearities inferred from two-tone distortion products in the ear canal of the alligator lizard. Hear. Res. 13,141-158.

Schmiedt, R.A. (1986) Acoustic distortion in the ear canal. I. Cubic difference tones: Effects of acute noise injury. J. Acoust. Soc. Am. 79,1481-1490.

Siegel, J.H., Kim, D.O., Molnar, C.E. (1982) Effects of altering organ of Corti on cochlear distortion products $f_2 - f_1$ and $2f_1 - f_2$. J. Neurophysiol. 47,303-328.

Wiederhold, M.L., Mahoney, J.W., Kellogg, D.L. (1986) Acoustic overstimulation enduces $2f_1 - f_2$ cochlear emissions at all levels in the cat, In: Peripheral auditory mechanisms (Eds: Allen, J.B., Hall, J.L., Hubbard, A. Neely, S.T., Tubis, A.) Springer, Berlin, pp. 322-329.

Zurek, P.M., Clark, W.W., Kim, D.O. (1982) The behavior of acoustic distortion products in the ear canals of chinchillas with normal or damaged ears. J. Acoust. Soc. Am. 72,774-780.

Zwicker, E. (1980) Nonmonotonic behavior of $(2f_1 - f_2)$ explained by saturation-feedback model. Hear. Res. 2,513-518.

Zwislocki, J.J. (1986) Forward and backward cochlear waves. In: Proceedings of Second International Congress on Acoustics. Toronto, Canada, pp B7-6.

SPONTANEOUS OTOACOUSTIC EMISSION GENERATORS BEHAVE LIKE COUPLED OSCILLATORS

Hero P. Wit

Institute of Audiology
University Hospital, Groningen, The Netherlands

Introduction

Properties of spontaneous otoacoustic emissions (SOAE's) are such that SOAE generators can best be described by self-sustaining oscillators (Bialek and Wit, 1984). These oscillators are thought to reside in the inner ear, and to be closely related to the hair cell transduction process. In this view this process makes use of positive feedback to enhance frequency selectivity, and SOAE's are merely a (non-disturbing) by-product, caused by too strong feedback in some of the inner ear active filters.

A model that incorporates this view (both implemented in hardware and in software) has been developed in the past decade by Zwicker and collaborators (Zwicker 1979; Zwicker and Peisl, 1990). A realistic, but more simple, model to describe the properties of a single SOAE is given by Tubis et al. (1989).

If the inner ear is made up of an array of active filters (oscillators), it can be expected that the array elements will interact: behaviour like it is known for coupled oscillators might be observed. In a first attempt to model such behaviour Duifhuis et al. (1986) made a model of coupled Van der Pol oscillators for the cochlear partition. And experimental observation of behaviour of SOAE spectra, indicative of the presence of coupled oscillators in the inner ear, has been reported by several authors (Burns et al., 1984; Jones et al., 1986; Frick and Matthies, 1988).

In this paper we describe the behaviour of adjacent peaks (frequency distance smaller than 100 Hz) in SOAE spectra. And we show that this behaviour can be described satisfactorily by a model of two coupled Van der Pol oscillators. The idea to study two coupled Van der Pol oscillators, to obtain insight in properties of SOAE spectra, is not entirely new (Murphy et al., 1989). But in this earlier study it was used to investigate so-called alternate states in multiple spectra.

Methods

SOAE's were recorded with a sensitive microphone and stored on

videotape (Van Dijk and Wit, 1990), to be analysed afterwards.

Spectra of successive time samples were obtained with a Unigon 4512 FFT analyser, connected to a Datalab 4000 signal averager for storage of the spectra. By appropriate triggering a selected part of a spectrum (64 datapoints) was stored. This process was repeated every 265 milliseconds. In this way 64 consecutive spectra were recorded (spanning 17 seconds of SOAE recording).

This study focusses on the behaviour of spectral peaks in SOAE recordings lying closely together (frequency distance smaller than 100 Hz). For such a pair of peaks it was observed in one subject that they were alternately present. To study whether these alternations were abrupt or gradually, instantaneous frequency was determined. This was done by separately narrow band filtering of the peaks with a B & K 1623 tracking filter (6% bandwidth) and a B & K 2120 filter (3% bandwidth). Then the output signals of the filters were added and time between consecutive positive-going zero-crossings was measured with a timer (HP 5326A), and plotted as a function of time after DA conversion.

Correlation between amplitudes of two spectral peaks was measured by bandpass filtering the peaks as described above. After filtering the signals were rectified and low pass filtered (cut-off frequency 40 Hz). In this way the envelope signals for two SOAE's were obtained. Cross-correlation between these two envelopes was measured with an Advantest R9211A dual channel spectrum analyzer.

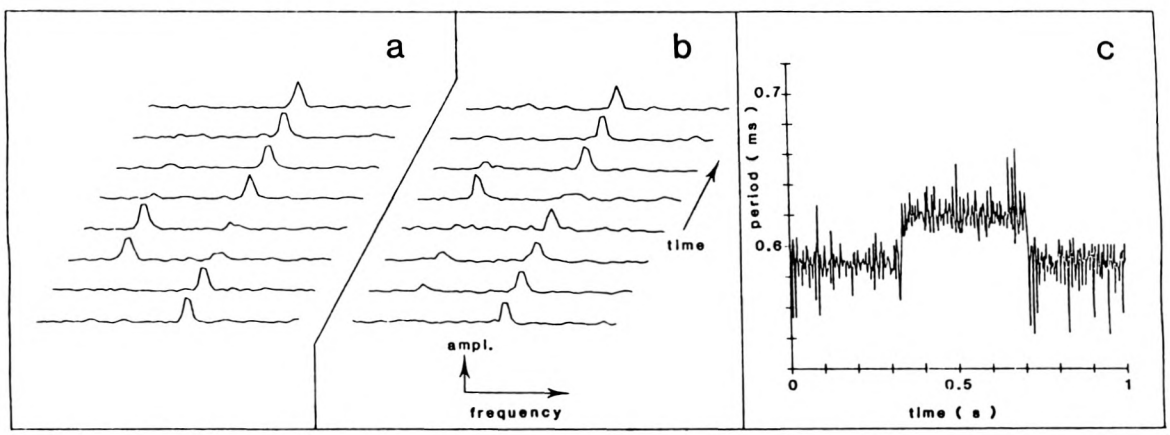

FIGURE 1 **a and b: Successive spectra of SOAE's from subject CS. Time between spectra: 265 ms. Spectral peaks are present at 1612 Hz and at 1700 Hz.**

c: Instantaneous period of the signal for which spectra are shown in a. Note the sudden jumps from 1.700^{-1} = 0.59 ms. to 1.612^{-1} = 0.62 ms. and back.

Results

Figure 1a gives 8 consecutive spectra (out of 64 recorded spectra) for subject CS. Alternation of the two spectral peaks is clearly visible. The situation shown in figure 1b occured for the same subject approximately 3 seconds later. Figure 1c gives instantaneous period (the reciprocal of instantaneous frequency) as a function of time. The jumps shown in this figure correspond to the spectral change that can be seen in figure 1a.

Figure 2a gives 8 consecutive spectra for two other spectral peaks of an SOAE recording of the same subject (from the same ear). No sudden spectral changes can be seen. But amplitude fluctuations are present. An average cross-correlation function (256 averages) for amplitudes of these two peaks is shown in figure 2b. Negative correlation around t = 0 is present. This means that amplitude increase for one spectral peak is accompanied by amplitude decrease for the other peak.

A few pilot studies on recordings with peaks with substantially larger frequency separation revealed no measurable correlation.

Figure 2c gives the cross-correlation function for two peaks from another subject (WK).

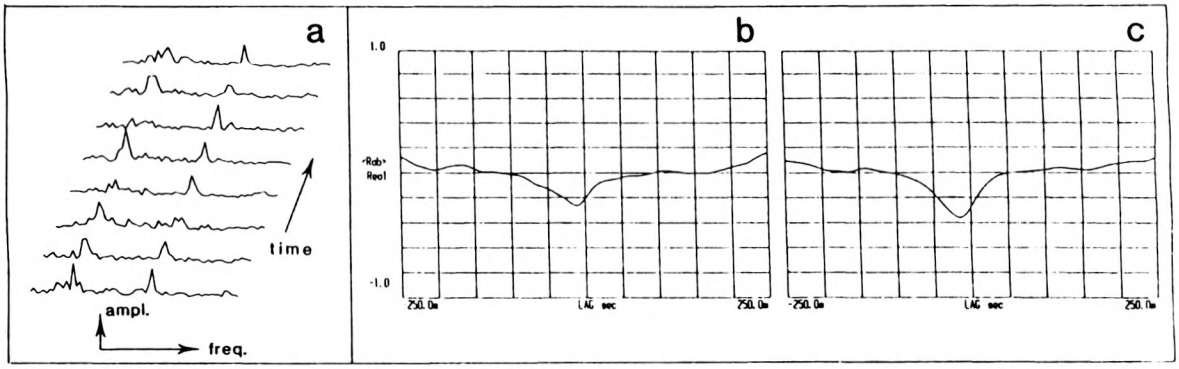

FIGURE 2 a: Successive spectra of SOAE's from subject CS. Time between spectra: 265 ms. Spectral peaks are present at 1300 Hz and at 1396 Hz (same ear as in figs. 1a en b).
b: Average cross-correlation function for amplitudes of peaks as shown in a.
c: Average cross-correlation function for amplitudes of 2 SOAE's (at 1040 Hz and at 1128 Hz) from subject WK.

Computermodel

We considered two mutually coupled Van der Pol oscillators described by the differential equations:

$$\ddot{x}_1 + \varepsilon (x_1^2 - a_1^2)\, \dot{x}_1 + \omega_1^2 x_1 = k x_2$$
$$\ddot{x}_2 + \varepsilon (x_2^2 - a_2^2)\, \dot{x}_2 + \omega_2^2 x_2 = k x_1 \qquad [1]$$

(A dot denotes differentiation with respect to time)
For $k = 0$ the oscillators are uncoupled, and their amplitudes and frequencies are $2a_1;\omega_1/2\pi$ and $2a_2;\omega_2/2\pi$ respectively.

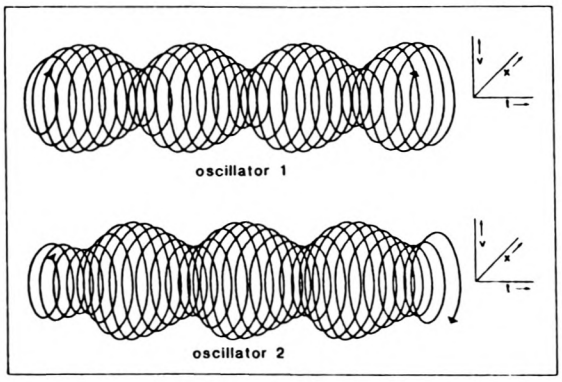

FIGURE 3 "Three-dimensional" plots showing continuous changing of (calculated) limit cycles of two weakly coupled Van der Pol oscillators. Parameter values were:
$\varepsilon = 0.2$, $a_1 = 1$, $a_2 = 1$, $\omega_1 = 1.0$, $\omega_2 = 1.1$, $k = 0.1$

Each equation in [1] can be replaced by a set of first order differential equations:

$$\dot{x}_1 = v_1$$
$$\dot{v}_1 = -\varepsilon(x_1^2 - a_1^2)v_1 - \omega_1^2 x_1 + kx_2 \qquad [2]$$

; and a similar set for $(\dot{x}_2, \dot{v}_2)$
With these two sets of equations subsequent values of x_1, v_1, x_2 and v_2 were calculated with a personal computer, using the relations $x_{t+\Delta t} = x_t + \dot{x}_t.\Delta t$ and $v_{t+\Delta t} = v_t + \dot{v}_t.\Delta t$ (The value for Δt was 0.1 in these calculations). In other words: x_1, v_1, x_2 and v_2 were calculated as a function of time, for a given set of parameters k, ε, a_1, a_2, ω_1 and ω_2, and some chosen initial values.
For large enough coupling constant k (and/or small enough frequency difference) the oscillators synchronize, and a stable limit-cycle (closed trajectory in the x,v plane) is reached for both oscillators.

For weaker coupling, however, no stable situation is reached by the oscillators. The trajectory in the x,v plane keeps changing, as is shown in figure 3. It turns out that two frequencies are strongly present in the output signal x(t) of both oscillators; the strongest one of these being approximately equal to the frequency of the oscillator in the uncoupled case k = 0. (see figure 4).

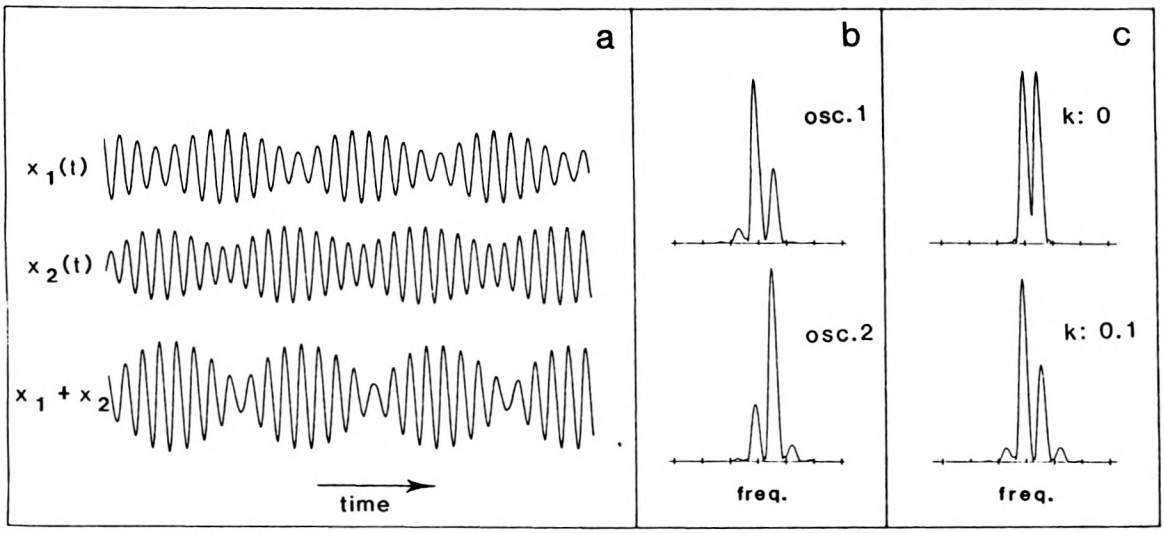

FIGURE 4 a: Calculated output signals x_1 (t) and x_2 (t) of two weakly coupled Van der Pol oscillators, and the sum of these two signals. Parameter values: ε = 0.1, a_1 = 1, a_2 = 1, ω_1 = 1.0, ω_2 = 1.1, k = 0.1
b: Amplitude spectra of x_1 (t) and x_2 (t)
c: Lower panel: amplitude spectrum of x_1 (t) + x_2 (t).
Upper panel: amplitude spectrum of x_1 + x_2 (for comparison), in the situation that the oscillators are not coupled.

When the two output signals of both oscillators are added, the phase-relations between the components of $x_1(t)$ and $x_2(t)$ are such that the spectrum of $x_1(t)$ + $x_2(t)$ has two strong components of unequal magnitude (for the given set of parameters), as is shown in figure 4c.

The magnitude of these components is stable in time. But a different situation occurs if the parameters a_1 and (or) a_2 fluctuate. (These parameters are proportional to the amplitude of the oscillators in the uncoupled case). To simulate such a fluctuation the calculation was repeated for different values of a_2, while a_1 was kept constant. (We have assumed that the time scale for fluctuations is much larger than the period of an oscillation, what means that amplitude fluctuations occur slowly). The result is shown in figure 5a.

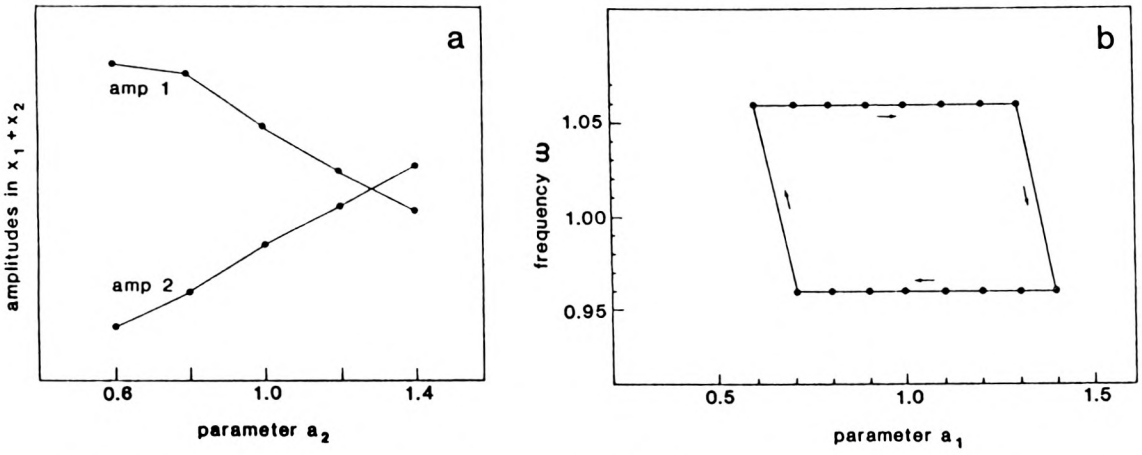

FIGURE 5 a: Amplitude of the two spectral components as shown in figure 4c (lower panel), for different values of parameter a_2. Parameter a_1 was kept at 1.0 in the calculations. Other parameters were the same as in figure 4.

b: Frequency of synchronized oscillation of two coupled Van der Pol oscillators. Parameter values: $\varepsilon = 0.1$, $a_2 = 1$, $\omega_1 = 1.00$, $\omega_2 = 1.03$, $k = 0.1$
Parameter a_2 was kept at a fixed value until calculation results showed a stable situation; then it was increased (or decreased) by 0.1 etc.

Some feeling for the behaviour of two weakly coupled Van der Pol oscillators can be obtained from the study of one oscillator driven by a sinusoidal signal with a frequency different from that of the undriven oscillator. For a small enough frequency difference and a strong enough driving force phase-lock or entrainment occurs: the oscillator is forced to oscillate with the frequency of the driving signal. Phase-lock or entrainment is a well-documented phenomenon for otoacoustic emissions (Long et al., 1988; Tubis et al., 1989; Van Dijk and Wit, 1990). For a weaker driving force or a larger frequency difference the oscillator keeps oscillating at approximately it own frequency f_1 while a weaker component with approximately the frequency f_2 of the driving force is also present in the oscillator motion. When in this situation the magnitude of the component at the oscillator frequency f_1 is changed (by changing a parameter of the oscillator), the magnitude of the weaker component at f_2 is not affected. And when the strength of the external force is increased, the magnitude of the f_2 component increases, while at the same time the magnitude of the f_1 component decreases (Stoker, 1950). The situations shown in figures 3 and 4 were obtained for $\omega_1 = 1$ and $\omega_2 = 1.1$. For smaller frequency difference (leaving the coupling constant k and the damping parameter ε unchanged) a quite different situation occurs: Two stable situations are possible, in which both oscillators are synchronized. Which of the two situations occurs depends on the amplitudes of the uncoupled oscillators and their history.

This is shown in figure 5b. To obtain this figure a_2 was kept fixed at 1, while calculations were made for different values of a_1. If a_1 was increased from 1.3 to 1.4 (and both oscillators were in the stable "high" frequency situation with $\omega = 1.06$), the system changed to the stable state with "low" frequency $\omega = 0.96$. When a_1 was then lowered again, the system jumped back to the high frequency state below $a_1 = 0.7$, etc. Note that the frequency difference between the two states ($\omega = 1.06$ and $\omega = 0.96$) is larger than that between the frequencies of both oscillators in the uncoupled state ($\omega_1 = 1$ and $\omega_2 = 1.03$).

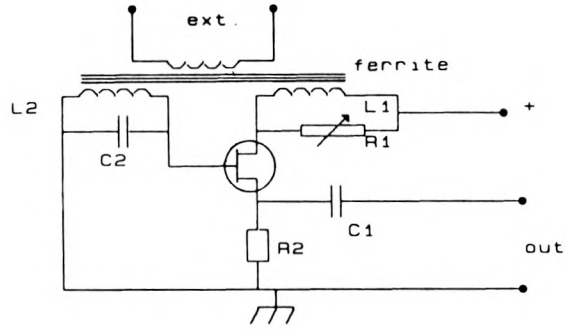

FIGURE 6 Circuit of simple FET-oscillator. Two of these oscillators were coupled in order to study the behaviour of noise-driven coupled oscillators. Narrow band noise (see text) was applied to the "ext." input.

Electronic model

In order to study the influence of slow random amplitude fluctuations in weakly coupled oscillators, two FET-oscillators were constructed. The circuit is given in figure 6. These oscillators were coupled by placing the ferrite rods at a short distance from each other along the same axis. The output signals of both oscillators were electronically added, and the sum signal was used as a model for an otoacoustic emission signal with two spectral components (with frequencies 3.6 and 4.0 kHz respectively). Signals resembled those given in figure 4 closely. Amplitude fluctuations were generated by applying narrow band noise with center frequency equal to the oscillator frequency to the external input. (see figure 6) of the oscillator. This was done for both oscillators.

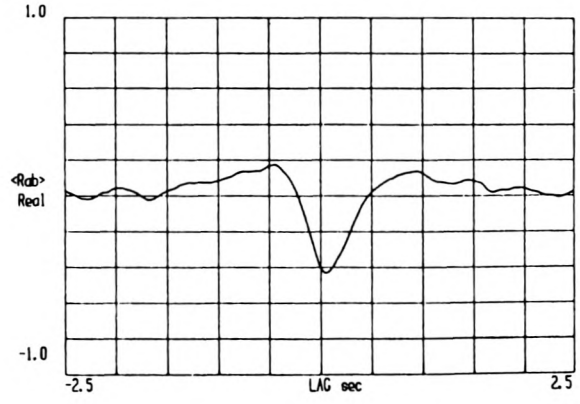

FIGURE 7 Average cross-correlation function for the amplitudes of the two components present in output signal of two coupled FET-oscillators (as shown in figure 6). This output signal was obtained by adding the outputs of the individual oscillators. Both oscillators were driven by (independent) narrow band noise.

The sum signal with two spectral components with (slowly) fluctuating amplitudes was analyzed in the same way as described for real otoacoustic emission signals in the "experimental results" section of this paper. A typical example of the outcome of this analysis is given in figure 7. The cross-correlation function shown in this figure closely resembles the results for real otoacoustic emissions given in figure 2.

Discussion

The computer model shows that the amplitudes of the two components in the output signal $x_1(t) + x_2(t)$ of two not too strongly coupled oscillators with a small frequency difference are related: if one amplitude increases the other decreases and vice versa. So for two (slowly) fluctuating amplitudes we expect a negative correlation. This is observed for adjacent SOAE's (figure 2). Possible sources for amplitude fluctuation of SOAE's are random noise forces inside the inner ear (Bialek and Wit, 1984), or fluctuation of oscillator parameters. Fluctuation of the feedback force for instance corresponds with fluctuation of parameter a in equation [1]. Consider a "free-running" Van der Pol oscillator:

$$\ddot{x} + \varepsilon(x^2 - a^2 - \alpha_1)\dot{x} + \omega^2 x = 0,$$

in which α_1 is fluctuating. This equation can be rewritten as:

$$\ddot{x} + \varepsilon(x^2 - a^2)\dot{x} + \omega^2 x = \varepsilon\alpha_1\dot{x}.$$

For small ε the oscillation x(t) will be almost sinusoidal. So the last equation is that of a Van der Pol oscillator driven with a force of its own frequency with fluctuating magnitude. This means that driving an oscillator with narrow band noise centered around the oscillator frequency is a good model for an oscillator with fluctuating feedback force. Therefore the oscillators in the electronic model were driven with narrow band noise.

The computermodel also shows (figure 5) that parameters for two coupled oscillators can be changed in such a way that alternation between two stable states occurs. If we assume that two coupled oscillators in this situation have fluctuating amplitudes (for the same reasons as described above), these fluctuations have to exceed a certain value in order to change state, because of the hysteresis-effect shown in figure 5b. So we expect that the oscillators remain in one state for a while before they jump to the other state, and this is exactly what is observed for SOAE's (figure 1). A somewhat different, but closely related, situation has been described by Shirai et al. (1977). These authors treat jumps between two states with different amplitudes, instead of different frequencies.

Conclusion

The phenomena described in this paper again give evidence for the fact that the inner ear employs active filtering. (At least if we believe that SOAE's are strongly related to the haircell transduction process).
So it seems that the era of passive cochlear models is over.

References

Bialek, W.S. and Wit, H.P. (1984) Quantum limits to oscillator stability: theory and experiments on acoustic emissions from the human ear. Phys. Lett. 104A, 173-178.

Burns, E.M., Strickland, E.A., Tubis, A. and Jones, K. (1984) Interactions among spontaneous otoacoustic emissions.
I. Distortion products and linked emissions. Hearing Res. 16, 271-277.

Duifhuis, H., Hoogstraten, H.W., Van Netten, S.M., Diependaal, R.J. and Bialek, W. (1986). Modelling the cochlear partition with coupled van der Pol oscillators. In: Peripheral Auditory Mechanisms (Eds: Allen, J.B., Hall, J.L., Hubbard, A., Neely, S.T. and Tubis, A.) Springer, Berlin, pp. 290-297.

Frick, L.F. and Matthies, M.L. (1988). Effects of external stimuli on spontaneous otoacoustic emissions. Ear and Hearing 9, 190-197.

Jones, K.L., Tubis, A., Long, G.R., Burns, E.M. and Strickland, E.A. (1986) Interactions among multiple spontaneous otoacoustic emissions. In: Peripheral Auditory Mechanisms (Eds: Allen, J.B., Hall, J.L., Hubbard, A., Neely, S.T. and Tubis, A.) Springer, Berlin, pp. 266-273)

Long, G.R., Tubis, A., Jones, K.L. and Sivaramakrishnan, S. (1988) Modification of the external-tone synchronization and statistical properties of spontaneous otoacoustic emissions by aspirin consumption. In: Basic Issues in Hearing (Eds: Duifhuis, H., Horst, J.W. and Wit, H.P.) Academic Press, London, pp. 93-100.

Murphy, W.J. et al. (1989) private communication, and paper presented at Association for Research in Otolaryngology (ARO) Meeting (feb. 1989).

Shirai, K., Akizuki, K. and Yamada, T. (1977) Behaviour of bistable oscillatory system with random external force. Bull. JSME 20, 548-553.

Stoker, J.J. (1950) Nonlinear vibrations, John Wiley, New York, pp. 169-170.

Tubis, A., Long, G.R., Sivaramakrishnan, S. and Jones, L.J. (1989) Tracking and interpretive models of the active-nonlinear cochlear response during reversible changes induced by aspirin consumption. In: Cochlear Mechanisms; Structure, Function and Models (Eds: Kemp, D.T. and Wilson, J.P.) Plenum Press, New York, pp. 323-330.

Van Dijk, P. and Wit, H.P. (1990) Synchronization of spontaneous otoacoustic emissions to a $2f_1 - f_2$ distortion product. J. Acoust. Soc. Am., accepted.

Zwicker,E. (1979) A model describing nonlinearities in hearing by active processes with saturation at 40 dB. Biol. Cybernetics 35, 243 - 250.

Zwicker, E. and Peisl, W. (1990) Cochlear preprocessing in analog models, in digital models and in the human inner ear. Hearing Res. 44, 209-216.

Comments and discussion

DE BOER

In passive linear cochlear models of the transmission-line type, the primary wave undergoes a substantial power loss before it reaches its destination. In a conventional model this loss is on the order of 15 dB (de Boer, 1980). In the case of a click-evoked OA emission Kemp (1978) estimates that the reflected energy at the ear drum is of the same order of magnitude as the incident energy. On this basis he formulated a transmission-line model in which the once-reflected wave undergoes a further reflection at the tympanic membrane, and so on and so on. A spontaneous OA emission would, in this view, arise when the doubly-reflected wave would enhance the wave at the reflecting site so that an oscillation arises. Now we have a dilemma here: how should we model SOAEs ? Should we consider a basically passive model in which one or more oscillators are imbedded ? Or should we first try to develop a better model, one that overcomes the signal loss, for instance by making a more efficient model (Kolston and Smoorenburg, this volume) by developing a system that amplifies the wave as it propagates, or both ? It is difficult to decide.

I hope that the following remarks provide a clearer perspective of this issue. Let us consider the latter case. The resulting model can turn out to be stable or unstable at the zero point (in this case it goes into spontaneous oscillation everywhere). In the former case the elaborations of Wit are probably equally relevant as in the purely passive case. The reason is that the impedances of the structures surrounding the oscillators will not be too much different from what they are in a passive structure. After all, signal amplification in an active model should be a gradual process.

However, this might, at first sight, not be true when the active model turns out to be unstable. Such a model, with one source of enhanced oscillation, is described by Van den Raadt and Duifhuis (this volume). In such a model the interaction between two prominent oscillators may well turn out to have different properties. As is shown in the cited paper an oscillator entrains the surrounding oscillators over a certain length of the cochlea and the interaction between two prominent oscillators really becomes a multi-oscillator problem. Let us hope that the study of such complicated situations provides the necessary insight.

LYON

The notion of an oscillator is closely related to the lightly-damped mass-spring resonance model of the basilar membrane. Steele and others have argued that unrealistically large masses are needed for such models to make sense. Can you recast your analysis in terms of coupled modes of an active wave propagation model, in which energy supplied to the traveling wave results in a pseudoresonance, with a possibility of oscillation when reflections are caused by irregularities ?

Comments and discussion

WHITEHEAD

I have studied quite a few ears possessing "quasi-stable" or "state-switching" spontaneous otoacoustic emissions. The frequency distance between adjacent "switching" components increases with frequency, as does the mean spacing between adjacent stable (i.e., non-switching) spontaneous emission components. While the frequency spacing between adjacent switching components increases with frequency, however, it remains quite constant on the Bark scale; for 14 pairs of adjacent state-switching components, the mean spacing was 0.35±0.05 Bark, with a range of 0.27-0.42 Bark (Whitehead, 1988). Note that the clearly quasi-stable components shown in Fig. 1 of Dr. Wit's paper are separated by approximately 0.33 Bark. (Barks calculated using eqn. 3 of Zwicker and Terhardt, 1980). Interestingly, this spacing approximately corresponds to the minimum spacing observed between adjacent stable spontaneous otoacoustic emission components in any one ear. Thus, it appears that components separated by more than 0.4 Bark are stable, but as the spacing decreases below 0.4 Bark the components tend to become quasi-stable, and that components spaced by much less than 0.3 Bark do not occur in the same ear. If a Bark is estimated to correspond to about 1 mm along the cochlea, over the frequency range in which spontaneous emissions are observed in humans, this suggests that the minimum spacing of spontaneous emission components in any one ear is approximately 0.35 mm, and that at these close spacings, the individual components tend to be quasi-stable.

References

de Boer, E. (1980). Auditory Physics. Physical principles in auditory theory I, Physics Reports.

Kemp, D.T. (1978). Stimulated acoustic emissions from within the human auditory system. J. Acoust. Soc. Am., 64, 1386-1391.

Whitehead, M.L. (1988). The interactions and instability of spontaneous otoacoustic emissions (SOAEs): Clues to the nature of the emission generator. Brit. J. Audiol., 23, 172.

Zwicker, E. and Terhardt,, E. (1980). Analytical expressions for critical-band rate and critical bandwidth as a function of frequency. J. Acoust. Soc. Am., 68, 1523-1524.

Section 6

Macromechanical Measurements

MEASUREMENT OF THE MIDDLE EAR TRANSFER FUNCTION IN CAT, CHINCHILLA AND GUINEA PIG

Laurent Décory, Rodolphe B. Franke, and Armand L. Dancer

French-German Research Institut, BP34, 68301 Saint-Louis Cédex, France

Introduction

As part of a study aimed at determining the origin(s) of the interspecific differencies in susceptibility to noise (Décory, 1989), we have measured the transfer function of the middle ear (TFME) in the cat, the chinchilla and the guinea pig. For a given stimulus applied in front of the tympanic membrane (TM), the sound pressure at the base of the scala vestibuli (SV) has been recorded from 100 to 20000 Hz. Using these experimental data in relation to the measurements of the displacement of the umbo or the stapes performed by various authors we have calculated the acoustic power (W_c) entering the cochlea and the acoustic imput impedance of the cochlea (Z_c) in these three species.

These measurements are completed by some results obtained previously in the guinea pig in the very low frequency range.

Methods

In order to determine the TFME, it is necessary to measure simultaneously the sound pressure in front of the TM and at the base of the SV. The acoustic stimulation is produced in closed system. Using a calibrated probe microphone, the sound pressure (amplitude and phase) is measured in front of the TM (≈1mm). The stimulation levels ranged from 70 to 120 dB SPL. The intracochlear sound pressure measurements were performed using a miniature piezoresistive transducer (Kulite) equipped with a probe filled with silicon fluid (Franke et al., 1982). The acoustic input impedance of the probe (≈10^{14} $N{\cdot}s{\cdot}m^{-5}$ at 1 kHz) is much higher than that of the guinea pig's cochlea (≈10^{11} $N.s.m^{-5}$; Dancer and Franke, 1980). The calibration was performed in a closed coupler filled with the same fluid and driven by a quartz disc. Thus we obtained the frequency response (amplitude and phase) of the probe in the 20-20000 Hz range with good accuracy. All animals were deeply anaesthetized; then the bulla was opened widely (the septum being left intact in cat). A hole (ϕ≈0.25 mm) was drilled into the SV of the basal turn. This drilling was done at the most accessible part of the basal turn, i. e. in cat, guinea pig and chinchilla at 8, 7.2 and 5.5 mm respectively from the base. Then, the probe was put into place; its conical shape allows a good seal. The animal was then exposed to a swept frequency (100-20000 Hz) pure tone. The signal to noise ratio was improved by means of

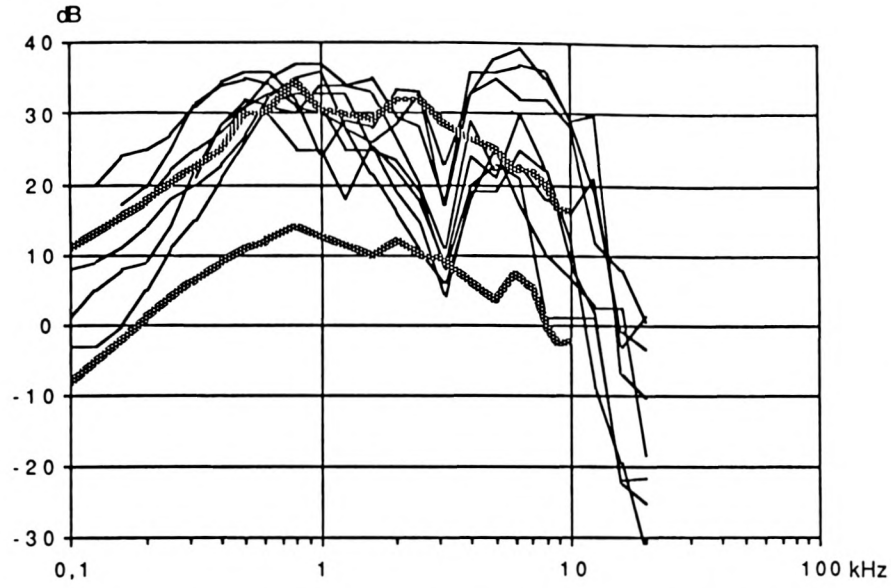

FIGURE 1
Amplitude of the sound pressure in SV in cat (N=8) (solid lines) (compared to the extreme values measured by Nedzelnitsky (1980) (wide grey lines). In both cases, the reference is the sound pressure at the TM.

a narrow band tracking filter. All the following data correspond to the amplitude and the phase of the intracochlear sound pressure referenced to the amplitude and the phase of the sound pressure in front of the TM. Whatever species is considered, the intracochlear sound pressure is linear in the whole stimulation range (70 - 120 dB SPL).

Results

The sound pressure was measured in the SV of the first turn of the cochlea, in cats (N=8), in chinchillas (N=9) and in guinea pigs (N=11) for a given sound pressure level in front of the TM. As mentioned above, this measure was feasible only at a certain distance from the oval window. In order to determine the frequency range within which the measurements correspond to the real TFME, we also measured the sound pressure in the scala tympani (ST) of the first turn of the cochlea (at the same distances from the base than previously) in cats (N=6), chinchillas (N=4) and guinea pigs (N=5).

As a preliminary guidance, figures 1 and 2 represent all the results obtained in cat (in

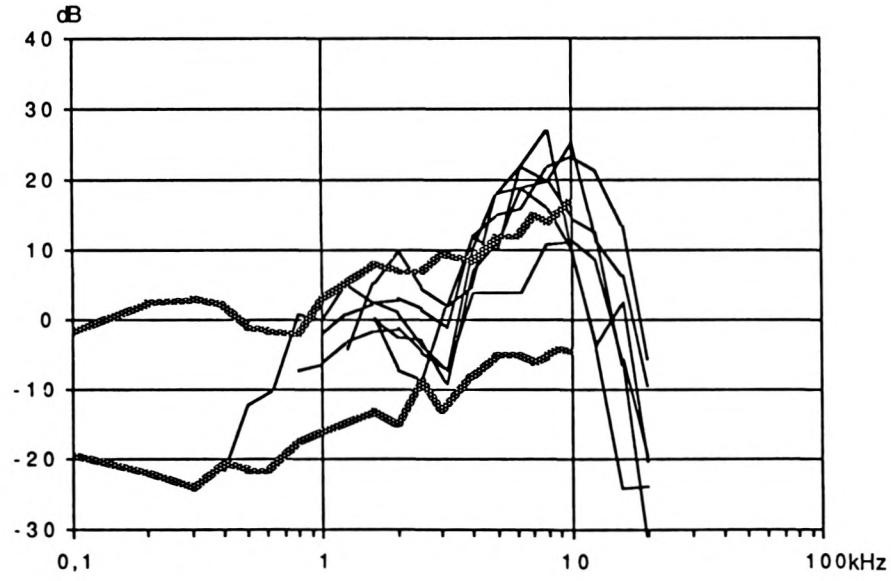

FIGURE 2
Amplitude of the sound pressure in ST in cat (N=6) (solid lines) (compared to the extreme values measured by Nedzelnitsky (1980) (wide grey lines). In both cases, the reference is the sound pressure at the TM.

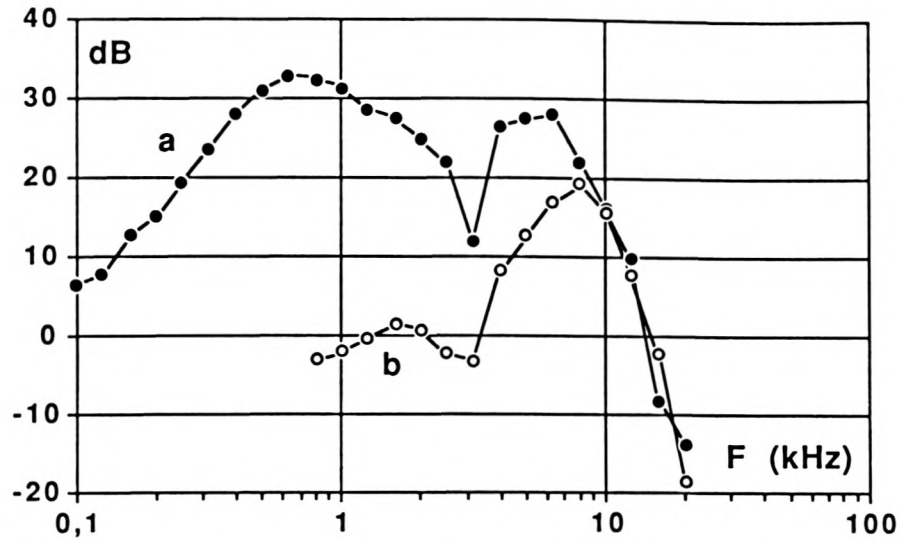

FIGURE 3
Average amplitude of the sound pressure in the first turn of SV (a) and ST (b) in cat. (Ref.: sound pressure at the TM).

SV and in ST respectively) compared to the Nedzelnitsky's extreme data (1980) (our results correspond to open bulla and intact septum and thus show an antiresonance at about 3 kHz, whereas Nedzelnitsky's data were obtained with open bulla and removed septum). It is noticeable that in SV as well as in ST our results are rather close to the maximum values recorded by Nedzelnitsky.

Figure 3, representing our average data in cat, shows that the sound pressure in ST is low up to 3 kHz; it then increases sharply to attain at about 9 kHz, the same magnitude as in SV (the distance to the base is equal to 8 mm which corresponds to a caracteristic frequency of 9 kHz). Thus, the value of the TFME is valid only at frequencies lower than 9 kHz since beyond this frequency, the sound pressure measured in SV no longer corresponds exactly to that existing close to the oval window (Dancer and Franke, 1982).

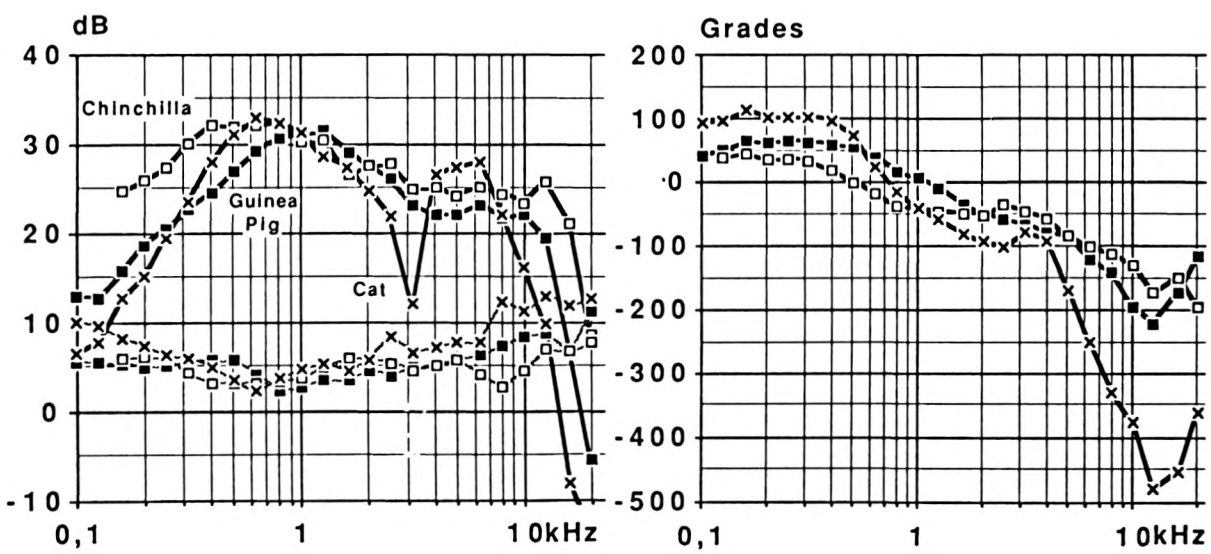

FIGURE 4 Average amplitude and phase of the sound pressure in the first turn of SV (ref.: sound pressure at the TM) in the three species (continuous lines). Standard errors are presented in dotted lines.

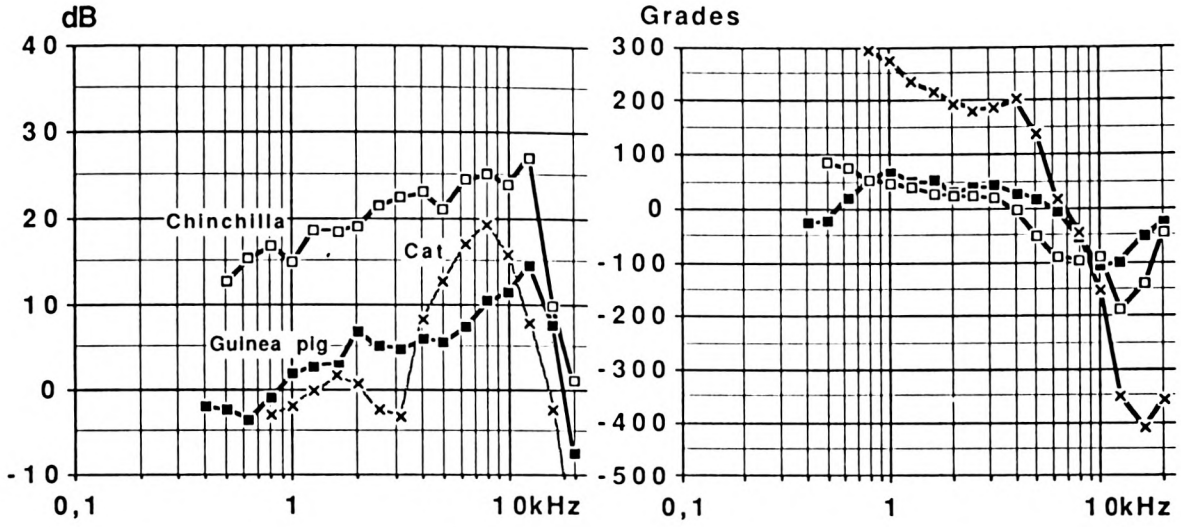

FIGURE 5 Average amplitude and phase of the sound pressure in the first turn of ST (ref.: sound pressure at the TM) in the three species (phase in cat may be wrong by π).

Interspecific comparison of the transfer functions

Figure 4 presents the average amplitude and phase of the sound pressure measured in the first turn of SV in cat, chinchilla and guinea pig (re. sound pressure at the TM). Between 500 and 10000 Hz the amplitudes are similar in the three species: the observed differencies are within one standard deviation (<10 dB). The main difference concerns the negative peak appearing at 3 kHz in cat; it is due to the secondary cavity of the bulla (measurements on animals with removed septum have given results comparable to those of Guinan and Peake, 1967 and Nedzelnitsky, 1980 in that frequency range).

Figure 5 presents the average sound pressure recorded in ST in the three species (re. sound pressure at the TM). The interspecific differencies are probably attribuable to the location of the probe which is peculiar to each species. Thus, in chinchilla (probe at 5.5 mm from the basal end and CF $\approx$ 5 kHz) the sound pressure in ST is much higher even at low frequencies than in cat (8 mm and 9 kHz) and in guinea pig (7.2 mm and 11 kHz).

Therefore, the curves of the fig. 4 represent strictly the TFME only at frequencies below 9 kHz in cat, 5 kHz in chinchilla and 11 kHz in guinea pig. Taking into account these restrictions, we can observe that the transmission differencies in the three species are very small, at least for frequencies higher than 800 Hz.

In these experimental conditions, the amplitude of TFME is maximum (31 to 33 dB) at 600 Hz in cat and chinchilla and at 1200 Hz in guinea pig. Below these frequencies, the amplitude decreases progressively. In the low frequency range, the slope of the amplitude of TFME is equal to about 6 dB/oct. in the chinchilla and guinea pig and 12 dB/oct. in the cat.

Acoustic power entering the inner ear

At the input to the cochlea when driven by pure tone, the active acoustic power is given by: $W_c=P_c \cdot U_c \cdot \cos\varphi$ (where P_c is the rms sound pressure at the input of the cochlea, U_c the rms volume velocity of the stapes and φ the phase lag of U_c versus P_c).

According to several authors (Tonndorf et al., 1966; Khanna and Tonndorf, 1971; Dancer et al., 1980; Lynch et al., 1982) in a passive cochlea, the acoustic input impedance is purely resistive in the frequency range considered ($\cos\varphi=1$). Thus $W_c \approx P_c \cdot U_c$. Having measured P_c it remains to determine U_c in order to calculate W_c.

Stapes displacement can be used to calculate its volume velocity: $U_c=2\pi f \cdot A_s \cdot X_s$ (where A_s is the area of the stapes footplate, X_s its displacement and f the driving frequency). In order to determine X_s we can use: in the cat, the results of Guinan and Peake (1967) obtained with open bulla and intact septum; in the chinchilla, those of Ruggero et al. (1990) and in the guinea pig, the results of Wilson and Johnson (1975), Manley and Johnstone (1974) and Dancer et al. (1979). For a sound pressure of 1 Pa (94 dB SPL) in front of the TM, and for three given frequencies: 2, 4 and 8 kHz, we obtain the following stapes volume velocities ($Uc=2\pi f \cdot As \cdot Xs$ in $m^3 \cdot Pa^{-1} \cdot s^{-1}$):

	2 kHz	4kHz	8 kHz
Cat	$1.9 \cdot 10^{-10}$	$3.3 \cdot 10^{-10}$	$2.0 \cdot 10^{-10}$
Chinchilla	$3.5 \cdot 10^{-10}$	$3.5 \cdot 10^{-10}$	$2.1 \cdot 10^{-10}$
Guinea pig	2.2 to $5.5 \cdot 10^{-10}$	0.87 to $2.5 \cdot 10^{-10}$	0.84 to $2.0 \cdot 10^{-10}$

It is notable that in these experimental conditions these values are very close from one species to another and from one frequency to another.

From the curves given in fig. 4, we can calculate the acoustic power which enters the cochlea for a sound pressure of 1 Pa in front of the tympanum ($W_c=U_c \cdot P_c$ in W/Pa):

	2 kHz	4 kHz	8 kHz
Cat	$3.3 \cdot 10^{-9}$	$7.0 \cdot 10^{-9}$	$2.5 \cdot 10^{-9}$
Chinchilla	$8.4 \cdot 10^{-9}$	$6.3 \cdot 10^{-9}$	$3.5 \cdot 10^{-9}$ (*)
Guinea pig	5.1 to 12.8 $\cdot 10^{-9}$	1.1 to $3.2 \cdot 10^{-9}$	0.96 to $2.4 \cdot 10^{-9}$

Taking into account the uncertainties which affect the numerous measures involved in the determination of the acoustic power, these results show that in our experimental conditions and for a given sound pressure level at the TM, the acoustic power entering the cochlea is very similar in these three species.

Acoustic input impedance of the cochlea

From the previous data it is possible to derive the acoustic input impedance of the cochlea in these three species: $Z_c=P_c/U_c$. According to Nedzelnitsky (1980), Lynch et al. (1982) and Dancer and Franke (1980), Z_c is purely resistive in the frequency range considered. Therefore, we can calculate $R_c \approx Z_c=P_c/U_c$ (in $N \cdot s \cdot m^{-5}$) :

	2 KHz	4 kHz	8 kHz
Cat	$9.2 \cdot 10^{10}$	$6.4 \cdot 10^{10}$	$6.3 \cdot 10^{10}$
Chinchilla	$6.9 \cdot 10^{10}$	$5.2 \cdot 10^{10}$	$7.9 \cdot 10^{10}$ (*)
Guinea pig	4.2 to $11.0 \cdot 10^{10}$	5.0 to $14.0 \cdot 10^{10}$	6.1 to $14.5 \cdot 10^{10}$

*) Subject to the restriction made in § 3

We can note that Z_c is practically constant from one species to another, in this frequency range. The litterature gives following approximate values for Z_c (in $N \cdot s \cdot m^{-5}$):

- in the cat: $35 \cdot 10^{10}$ at 2 and 4 kHz according to Tonndorf et al (1966), adapted by Lynch et al., (1982); $5 \cdot 10^{10}$ at 2, 4 and 8 kHz according to Nedzelnitsky (1980) and $12 \cdot 10^{10}$ at 2 and 4 kHz according to Lynch at al. (1982),
- in the chinchilla: about $6.7 \cdot 10^{10}$ at 2, 4 and 8 kHz according to Ruggero (1990),

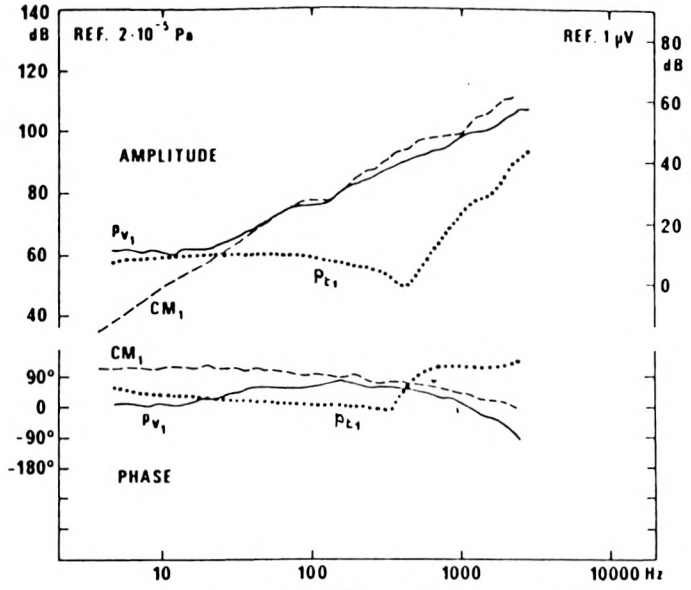

FIGURE 6
Amplitude and phase of CM_1, p_{v1} and p_{t1} versus frequency (N≥5; ref.: constant volume displacement at the input of the ear).

- in the guinea pig: $4.5 \cdot 10^{10}$ at 2, 4 and 8 kHz according to Dancer et al. (1979).

Measurement at low frequencies in the guinea pig

Given the importance of the mechanical behaviour of the cochlear structures at very low frequencies (Patuzzi et al., 1989; Ruggero et al., 1986), we wanted to recall some important results obtained previously (Franke et al.,1982) from acoustic pressure measurements performed in guinea pig.

This study was performed under the same experimental conditions (see § 2) except that a more sensitive transducer was used. Additionally, the differential microphonic potential (CM_1) was measured in the basal part of the cochlea.

Fig. 6 shows the amplitude and phase of CM_1 and of the sound pressure in SV (p_{v1}) and ST (p_{t1}) of the first turn as a function of frequency.

Below 30 Hz, the amplitudes of p_{v1} and p_{t1} are identical and in phase with the stimulus but the amplitude of CM_1 decreases at 6 dB/oct. with a 90° phase lead. Above 30 Hz, in ST, the acoustic pressure remains constant and in phase with the acoustic stimulus up to at least 200 Hz and beyond 400 Hz, it increases rapidly by about 15 db/oct. with a corresponding phase lead. Above 30 Hz, the amplitude curves of p_{v1} and CM_1 have many common characteristics: the slope of about 6 dB/oct. is broken only at about 100 Hz by a small plateau previously described by Dallos (1970).

These results can be easily explained by considering the simplified electric analog

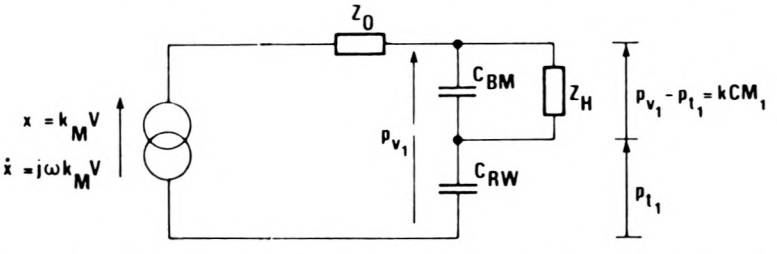

FIGURE 7 Low frequency electric analog. (V: voltage applied to the emitting microphone; k_M, k: constant factors; Z_o: acoustic impedance of the ossicles including the oval window; x: volume displacement at the entrance to the ear).

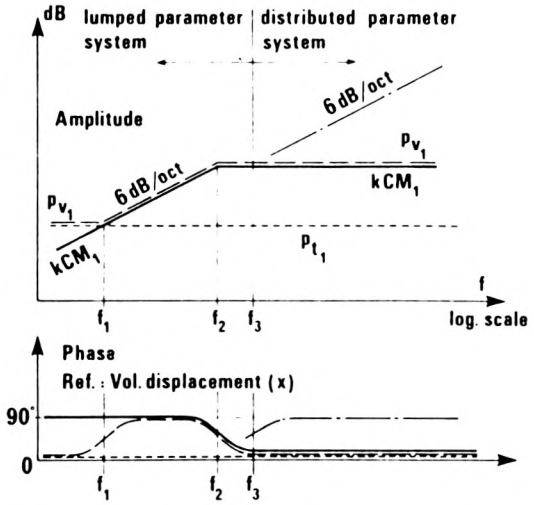

FIGURE 8
Schematic diagram resulting from the electric analog of figure 7.

presented on fig. 7, which depicts the auditory receptor driven by a constant volume displacement source (Franke et al. 1982).

If we consider that the CM_1 is proportional to the displacements of the basilar membrane and that the displacements of this membrane are proportional to the differential pressure (p_{v1}-p_{t1}), we obtain the results shown in fig. 8. The volume displacement of the oval window being constant for all frequencies, p_{t1} is also constant because the round window can be regarded as a pure compliance. CM_1, which is proportional to the differential pressure, is also constant in the frequency range over which the compliance of the basilar membrane predominantes ($f > f_2$), but it decreases proportional to the frequency when the leakage resistances of the helicotrema (R_H) and of the associated parts of the scalae are predominant ($f < f_2$). p_{v1} has the same behaviour as CM_1, except at very low frequencies ($f<f_1$), at which it cannot be smaller than p_{t1}. This is valid at frequencies low enough to disregard propagation phenomena (the basilar membrane vibrating like a plate). If this is not the case ($f>f_3$), the cochlea cannot be considered to consist of lumped parameters, but as its input impedance is nearly resistive at medium frequencies (see §6), p_{v1} as well as CM_1 will increase proportionally to frequency. If the input resistance of the cochlea is lower than the impedance of the helicotrema, which is in fact purely resistive for low frequencies in guinea pig, an amplitude shift will occur between the two straight parts of the curves having 6 dB/oct. slopes, and this shift thus coincides with a plateau ($f_2<f<f_3$) (fig. 8). Comparing the curves of fig. 8 to the amplitude and phase recordings of CM_1, p_{t1} and p_{v1} (fig. 6), we can observe a good agreement.

With the help of these measurements and some direct biophysical measurements, the following values for the guinea pig cochlea could be determined:

- the compliance of the round window: $C_{RW} = 1.4 \cdot 10^{-13}\ m^5N^{-1}$
- the compliance of the whole basilar membrane: $C_{MB} = 0.9 \cdot 10^{-13}\ m^5N^{-1}$
- the acoustic resistance of the helicotrema (including that of the scalae which is probably significative in the upper turns): $R_H = 5.2 \cdot 10^{10}\ Nsm^{-5}$

Conclusion

In our experimental conditions (closed circuit and open bulla), the measurement of the

TFME in cat, chinchilla and guinea pig showed that above 800 Hz, interspecific variations of amplitude are not important. From these measurements and from data available in the literature, the acoustic power entering the cochlea and its acoustic input impedance have been calculated. The acoustic imput impedance is practically identical in the three species.

Results obtained previously in the guinea pig in the very low frequency range led to the development of a simple electrical model of the cochlea and allowed us to explain the mechanical behaviour of the cochlea at very low frequencies.

References

Dancer, A., Franke, R., Buck, K. et Evrard, G. (1979) Etude de la transmission du stimulus acoustique au niveau du récepteur auditif chez le cobaye. ISL - R 113/79.

Dancer, A. and Franke, R. (1980) Intracochlear sound pressure measurements in guinea pigs. Hearing Res., 2, 191-205.

Dallos, P. (1970) Low-frequency auditory characteristics: species dependance. J. Acoust. Soc. Am. 48, 490.

Dancer, A. et Franke, R.(1982) Pression acoustique intracochléaire: mesures directes et modèles. Acustica, 51, 18-28.

Décory, L. (1989) Origines des differences interspécifiques de susceptibilité au bruit. Thèse Doct. Univ. Bordeaux II, France.

Franke, R., Dancer, A., Lenoir, M., Evrard, G. et Buck, K. (1982) : Etude des phénomènes hydromécaniques cochléaires aux basses et très basses fréquences chez le cobaye. ISL-R 121/82.

Guinan, J. and Peake, W.T. (1967) Middle ear characteristics of anesthetized cats. J. Acoust. Soc. Am., 41, 1237-1261.

Lynch, T.J., Nedzelnitsky, V. and Peake, W.T. (1982) Input impedance of the cochlea in cat. J.Acoust. Soc.Am.,72, 108-130.

Manley, G.A. and Johnstone, B.M. (1974) Middle ear function in the guinea pig. J. Acoust. Soc. Am., 56, 571-576.

Nedzelnitsky, V. (1980) Sound pressures in the basal turn of the cat cochlea. J. Acoust. Soc. Am., 68, 1676-1689.

Patuzzi, R.B., Yates, G.K. and Johnstone, B.M. (1989) The origin of the low-frequency microphonic in the first cochlear turn in guinea-pig. Hear. Res. 39, 177-188.

Ruggero, M.A., Robles, Rich., N.C. and Costalupes, J.A. (1986) Basilar membrane mechanics at the base of the chinchilla cochlea. II. Responses to low-frequency tones and relationship to microphonics and spike initiation in the VIII nerve. J. Acoust. Soc. Am. 80, 1375-1393.

Ruggero, M.A., Rich, N.C., Robles, L. and Shivapuja, B.G. (1990) Middle ear response in the chinchilla and its relationship to mechanics at the base of the cochlea. J. Acoust. Soc. Am., 87, 1612-1629.

Tonndorf, J., Khanna, S.M. and Fingerhood, B.J. (1966) The input impedance of the inner ear in cat. Ann. Otol. Rhinol. Laryngol., 75, 752-763.

Wilson, J.P. and Johnstone, J.R. (1975) Basilar membrane and middle-ear vibration in guinea pig measured by capacitive probe. J. Acoust. Soc. Am., 57, 705-723.

HELMHOLTZ REVISITED: DIRECT MECHANICAL DATA SUGGEST A PHYSICAL MODEL FOR DYNAMIC CONTROL OF MAPPING FREQUENCY TO PLACE ALONG THE COCHLEAR PARTITION[1]

Eric L. LePage

Hearing Conservation Unit, National Acoustic Laboratories,
126 Greville Street, Chatswood, N.S.W. 2067, AUSTRALIA.

Introduction

There exists two and possibly three kinds of motility of the outer hair cells (OHC). The form of the motility first documented by in vitro measurement was evidence of length changes with electric stimulation and modification of the medium (Brownell *et al.*, 1985; Zenner *et al.*, 1985; Flock *et al.*, 1986; Zenner, 1986; Slepecky *et al.*, 1988; Canlon *et al.*, 1988; Brundin *et al.*, 1989). The origin of this slow motility is not clear but may be due to some form of excitation-contraction coupling (Zenner *et al.*, 1985; Flock *et al.*, 1986; Zenner, 1986b). Isolated OHC have been demonstrated to exhibit fast motility under *in vitro* conditions with electric current stimulation (Brownell *et al.*,, 1985; Zenner *et al.*, 1985; Ashmore, 1987). Electro-osmosis (Kachar *et al.*, 1986) has been speculated to account for fast mechanical events. The OHCs are turgid, and osmotic modulation of their turgidity has been implicated in the slow changes in cell shape (Brownell, 1984; 1989; Flock, 1986; Dulon *et al.*, 1988). Although the slow motility has now been demonstrated in several species, its utility has yet to be incorporated into any comprehensive model. Changes in efferent activity have been shown to result in changes in the mechanics by direct measurement (LePage, 1989) suggesting the involvement of tonic activity of the OHC. Changes in the activity of the efferent neurone would likely lead to concurrent changes in the tonus in the targeted OHC. It seems likely therefore, that the slow motility has at least one role associated with the medial efferent system (Liberman, 1988). The group of twenty to fifty OHC which are contacted by a single medial efferent neurone can be classed as a "motor unit" by analogy with the bundle of skeletal muscle fibers contacted by a single motoneurone from the spinal cord. It is possible that central control of the tonic firing rate of individual efferent neurones may include electromechanical comb-filtering prior to IHC detection (LePage, 1989). OHC tonus may be the basis for central control of selective attention at the auditory periphery. Using otoacoustic emissions Puel *et al.*, (1988) have provided some supportive evidence for the hypothesis.

The modulation of OHC tonus clearly performs some important control function in

---

[1] Part of this work was presented at the 13th midwinter research meeting of the Association for Research in Otolaryngology, St. Petersburg Beach, Florida, February 4--8, 1990.

the cochlea. This paper examines the tonic load distribution on the various structural members of the organ of Corti, the tectorial membrane and basilar membrane and discusses a second major implication for auditory theory if this tonic force is significant in normal hearing sensitivity. There are several puzzling features of efferent involvement. For example, some measures of tuning appear unaffected by sectioning the crossed olivocochlear bundle (Rajan *et al.*, 1990). The model offers a potential resolution in terms of dynamic allocation of frequency to place (LePage, 1987c, 1988) and proposes a mechanism whereby such allocation is controlled by OHC tonus.

Methods

The data reported here were obtained either with a capacitive probe (LePage, 1987a) or fiber optic lever (LePage, 1989). Both techniques sense displacement and have sensitivities of 1nm/$\sqrt{Hz}$ or better with signal averaging.

Results

Modulation of that tonic force by stimulation of the hair cells produces changes in the basilar membrane position *in vivo* (LePage, 1987b; 1989) while they are responsible for changes in the mean position of the tectorial membrane in a cochlear explant *in vitro* (LePage *et al.*, 1989). These OHC length changes are visible through a phase-contrast microscope and have been recorded on videotape and using a fiber optic lever reproduced here in Fig. 1. For this purpose a small gold mirror is applied to the tectorial membrane to increase reflectivity and a sinusoidal electric field of 0 to 16 mV/μm applied to the preparation. The tectorial membrane responds to this stimulus

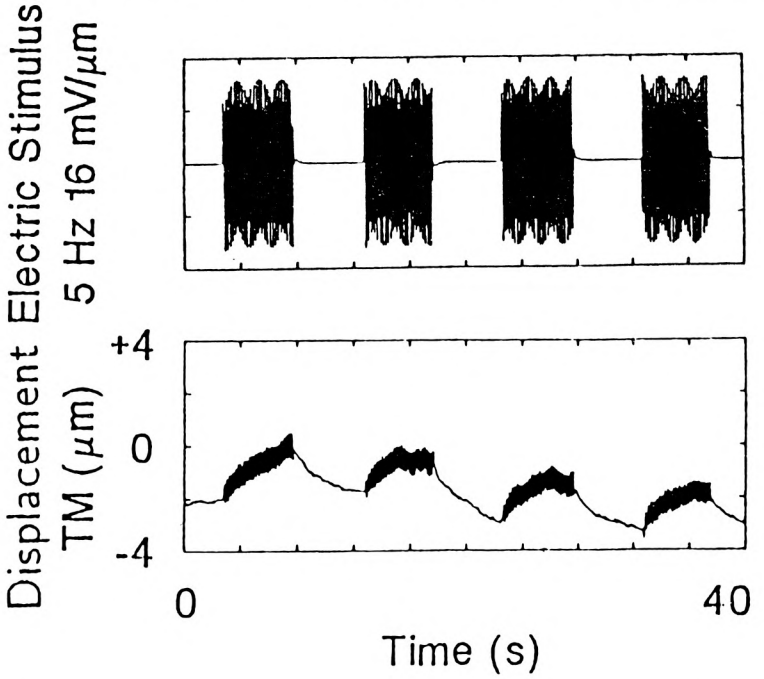

FIGURE 1 Fiber optic probe recording of the displacement of the tectorial membrane *in vitro* in a explanted surface preparation from guinea pig organ of Corti, stimulated by a sinusoidal electric field at 5 Hz (top trace, undersampled). The motion is a vibratory component driven by the electric field, plus a a steady summating displacement change indicating movement toward the probe tip which decays after the stimulus ceases. At the same time the motions may be viewed through a phase contrast microscope. These cease after about an hour when only passive electroconstrictive effects may be viewed at much higher stimulus levels.

with vibratory plus summating components of the motion which subsequently decay.

The summating shifts recorded in most cases are positive-going while the electric stimulus is applied and this is indicative of the mirror to optic probe tip decreasing. In turn this is consistent with elongation of the outer hair cells. Since these hair cells were taken from the apical turns the result is generally consistent with the elongation of apical guinea pig hair cells recorded by Canlon *et al.* (1988).

The full extent of the efferent influence may not just include modification of the stiffness and/or damping characteristics of the basilar membrane. A clue as to another effect is shown in Figure 2. It is a series of three displacement recordings of the vibratory response of the basilar membrane using a capacitive probe (LePage, 1987a),

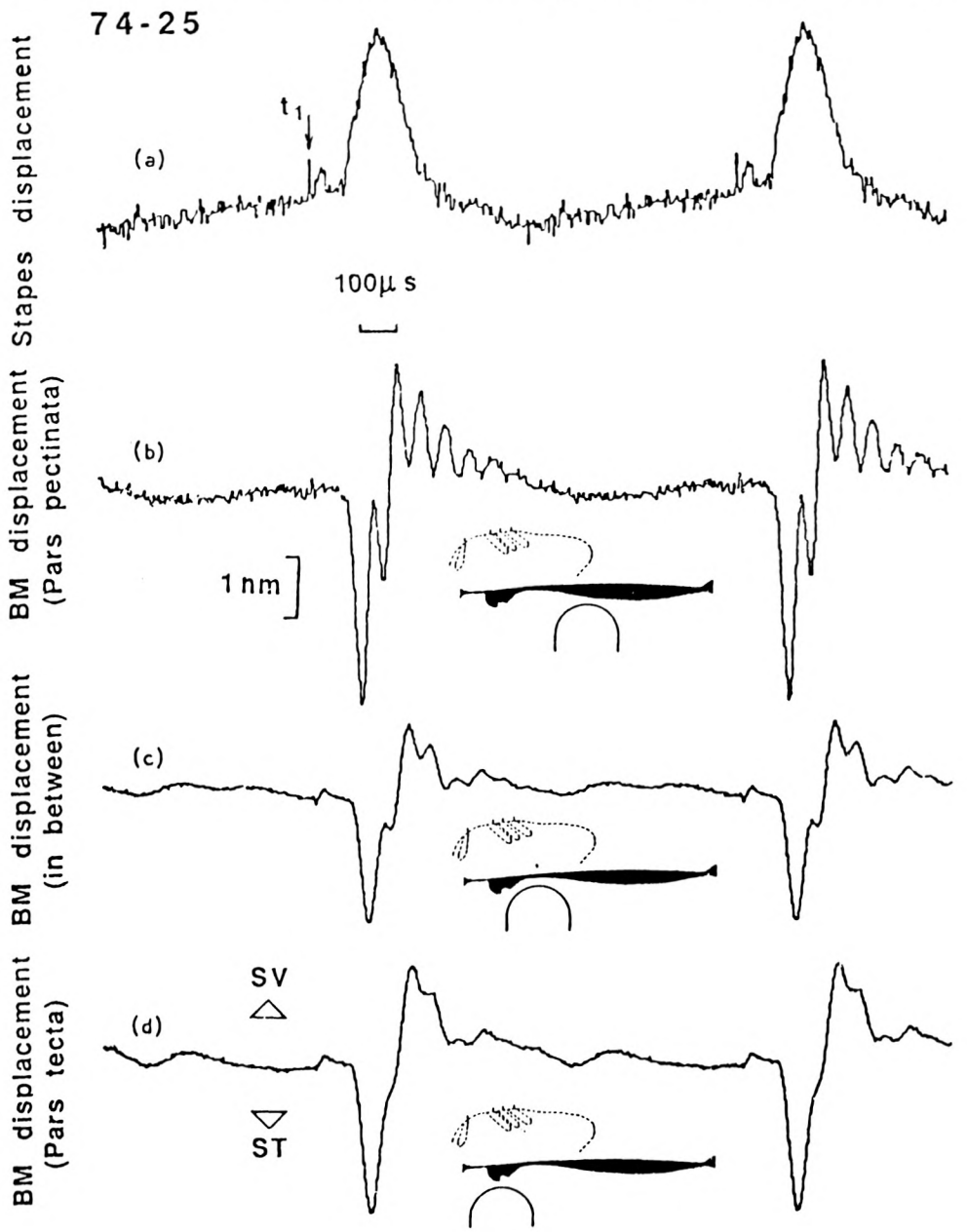

FIGURE 2 Recordings of the vibration of the long arm of the incus (a) plus three traces of showing radial dependence of the radial of the basilar membrane in response to repetitive clicks presented at time t_1. Trace (b) represents a lightly-damped response of the pectinate region (inset derived from Lim), trace (d) suggests that a motor driven transient of the arctuate region actually influences the pectinate zone and a point in between (c).

high pass filtered at 40 Hz, to repetitive clicks (T=1250 us) plus a single trace of the long arm of the incus (a) to the same stimulus. In each case the 10 μs electric pulse is delivered to the earphone at time t_1 and the data record is repeated for continuity. The basilar membrane recordings were all taken within a 30 minute period. The parameter being varied is the radial position of the tip of the probe. In trace (b), the tip is located at the middle of the basilar membrane adjacent to the pectinate zone (see inset). In (c) the tip has been moved toward the modiolus and will be in the neighborhood of the junction between the outer pectinate region and the inner arctuate region. Trace (d) is with the probe tip immediately adjacent to the bony spiral lamina and therefore the probe will be registering the motion of the arctuate region of the basilar membrane. The feature of interest is the change in the shape of the impulse response with radial position across the basilar membrane. The records indicate a variation in the vibration pattern as one moves from the pectinate zone to the arctuate zone. The pectinate zone would appear free to undergo a damped oscillation following the progress of the click wavefront, while the arctuate zone does not appear to vibrate in the same way, if at all. On the other hand it undergoes a significant biphasic transient in response to the click which is superimposed on the pectinate region as well.

The phenomenon requires more detailed examination with a technique with higher spatial resolution. However, these data suggest an important functional possibility of the efferent system which has not so far been considered. It is that the whole radial width of the basilar membrane does not vibrate. Instead, perhaps the pectinate zone is the only radial segment of the basilar membrane which actually vibrates when sound enters the cochlea. The arctuate region appears to be dominated by the influence of the motor activity of the OHC. The traces therefore suggest that the OHC twitch in response to the click wavefront.

The modified Helmholtz model

If the OHC length changes are responsible for the summating movements of the tectorial membrane, Fig. 1 indicates tonic force generation by the OHC. If these forces act upon the organ of Corti in the manner indicated by Fig. 2, then this suggests that the OHC *generate shear* between the reticular membrane and the tectorial membrane. Such a scheme has been formalised in a physical scale model (2000x) which is represented in Fig. 3a. The OHC apply a couple to the ends of the stereocilia. In turn, the force acting at the base of the OHC stereocilia constitutes a turning moment about the base of the inner pillar cell, the point at which the arches are hinged. So, the OHC act to cause rotation of the rigid arch. Since each radial fiber bundle of the pectinate zone is attached to the base of the outer pillar cell, a resolved part $\mathbf{T_R}$ of the tonic force exerted by the OHC on the arch will appear *in the plane* of the basilar membrane. The model requires that the lever and string system is under static tension maintained by the spiral ligament. The tectorial membrane will also be under radial tension. Modulating OHC tonus varies the shear, changing the radial tension both in the tectorial membrane and in the *pars pectinata*, resulting in small variations of the angle of the arch, and in turn, the position of the tectorial membrane and the deflection of the inner hair cell stereocilia. It follows that the ability of the OHC to generate force and also the static force in the spiral ligament become important parameters for frequency analysis. In this scheme the morphological configuration of the OHC stereocilia acquires new meaning in terms of a coupling system which can transmit considerable leverage, yet remain flexible to transverse vibration.

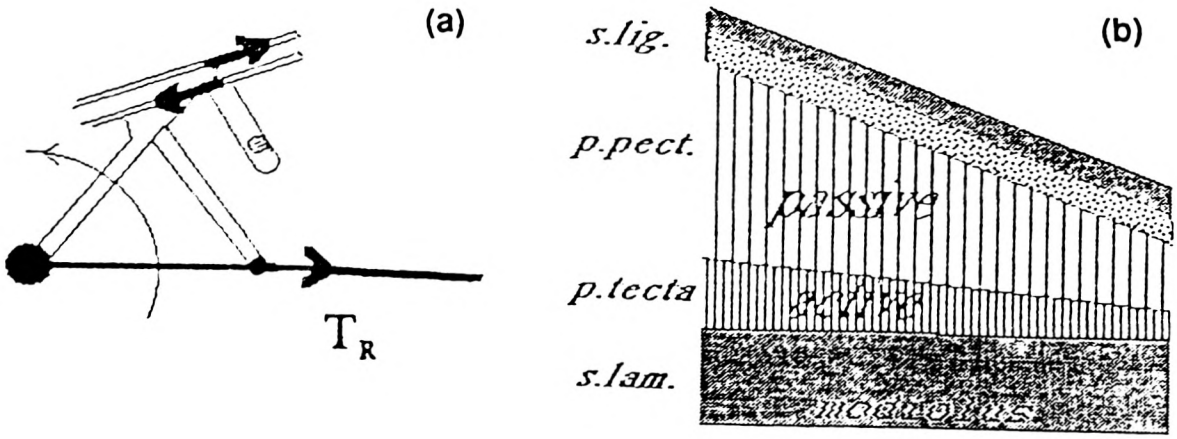

FIGURE 3 (a) Structural representation of the cross-section of the organ of Corti. The essential feature is that length changes of the outer hair cells produce the observed movements in the position of the tectorial membrane by generating shear between the reticular and tectorial membranes. Variations in the tonic force generated by the OHC result in a turning moment of the arch about its pivot at the edge of the bony spiral lamina. A resolved part of this force acts in the in the plane of the basilar membrane, varying the tension in the radial fiber bundles of the *pars pectinata*. (b) Efferent modulation of the tonus of individual OHC motor units varies the passive tuning properties of the basilar membrane amounting to the harp of Helmholtz plus active tuning.

The model therefore represents a revisitation of the resonant string model of Helmholtz (1885:1954). However, to this we have now added activity in the form of OHC tonus which modulates the tension of the strings (see Fig. 3(b)). The musical analogy which appealed to Helmholtz can be carried still further likening the action of the arch of the organ of Corti to the so-called *tremolo bar* of an electric guitar. Yet instead of changing the tension of all strings simultaneously, control of individual OHC motor units provides *independent* variation in the natural resonance properties of the pectinate zone, much like the action of the pedals of an orchestral harp which produce key changes by changing the tension in selected arrays of individual strings.

The resonance frequency of a stretched string in air is given by the first of Mersenne's laws, $f = (1/2l)\sqrt{(T/m)}$, in which f is the resonant frequency (Hz), l is the length of the vibrating portion of the string between two adjacent nodes, T is the tension and m is the mass per unit length. According to Helmholtz's theory, the radial tension will be highest in the first turn. For an estimate of the undamped vibration, let f = 20 kHz, l = 100 um, and mass of the string 100 pg, ($m = 10^{-8}$ kgm^{-1}). The required tension computes to 0.16 unt. If the turgor of the OHC is due to electro-osmosis the possibility of large osmotic forces exists and the ability of a motor unit to deliver forces of this order seems not unrealistic. Such a scheme could work equally well at 100 kHz. If the OHC cannot maintain a 25-fold increase in tension, the length of the strings can be reduced by a factor 5, or the mass by a factor of 25.

The implication of the model is that quite small variations in OHC tonus (much less than an order of magnitude) can result in substantial local changes in the gradient of the frequency-place map. For example a doubling of the radial tension of the bundles of *pars pectinata* will produce a half-octave shift in characteristic frequency.

Loss of OHC should therefore result in a change in the tonotopic organisation. In guinea pigs treated with kanamycin sulphate Robertson and Johnstone (1979) found that the characteristic frequencies of spiral ganglion cells did not rise above above 16 kHz. Indeed the normal gradient of 2.5 mm/oct for guinea pig was halved. A direct mechanical measurement study was carried out using capacitive probe (LePage,

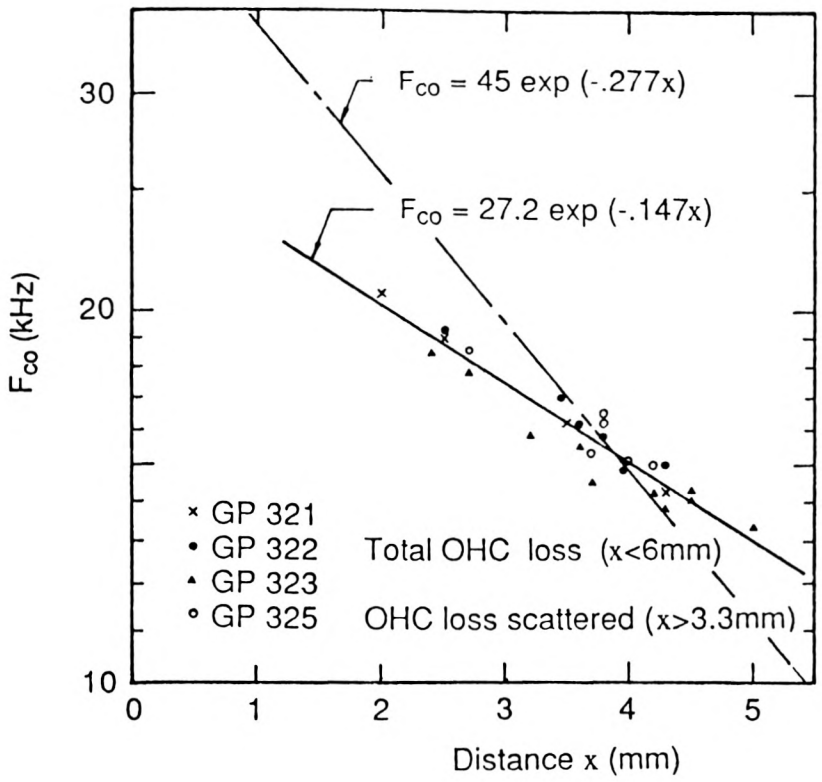

FIGURE 4 Lowpass cutoff frequencies versus place of direct mechanical measurement in kanamycin-treated guinea pigs. Instead of obeying the regular tonotopic gradient (dashed line), these animals do not show cutoff frequencies above 20 kHz while the gradient is halved.

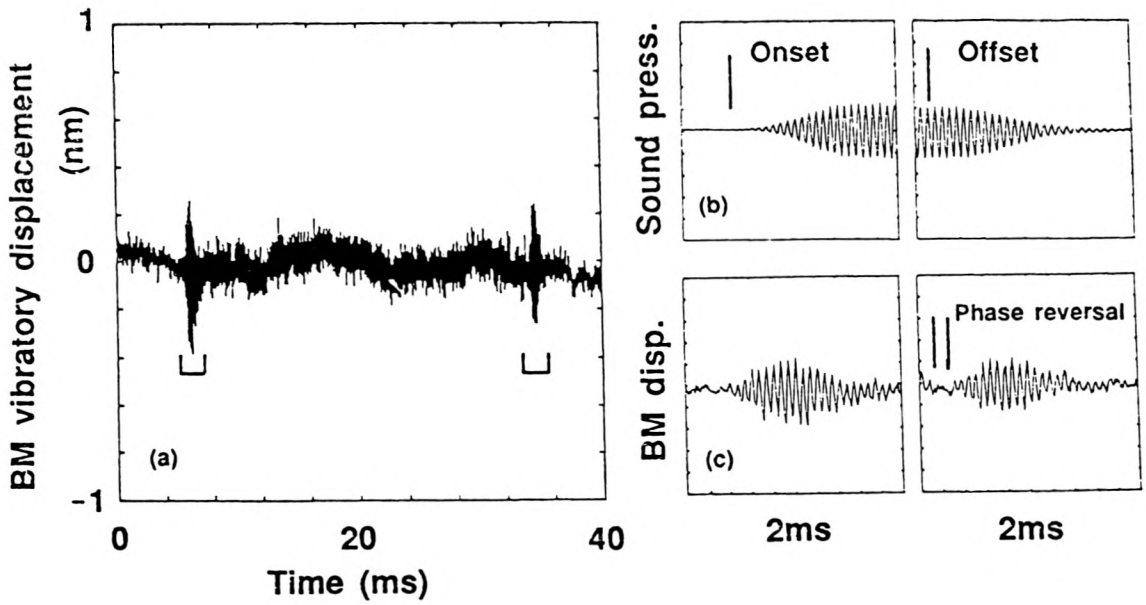

FIGURE 5. (a) Direct mechanical recording of basilar membrane *ac* displacement using a capacitive probe to a 15 kHz, 30 ms, 75dB SPL pure tone burst (1 ms rise/fall times) at the "14 kHz place" of the guinea pig cochlea. The right hand panels show two 2 ms segments of (b) the 1 mm probe tube pressure, in (c) the details of the vibratory transients, particularly the phase reversal during the fall time. The result suggests the existence of two processes of opposite phase effecting rapid frequency-alignment as the OHC maintain a balance condition.

1981) in which cutoff frequencies were determined in a series of kanamycin-treated guinea pigs over a 3 mm length of the basilar membrane in the basal turn. The results are presented in Fig. 4. The conclusion is the same. The basal turn no longer tunes to the highest frequencies and the observed gradient is, by co-incidence, halved.

Figure 5 shows a direct mechanical recording of the basilar membrane in the first turn of a fresh guinea pig preparation, in response to a 30 ms tone burst. The transient behavior in the amplitude with onset and offset of the tone burst was often seen in the series of experiments (LePage, 1987b). When it occurred, it was for frequencies above the expected characteristic frequency, where the high frequency notch occurs. This notch has been observed to change frequency systematically with level (expressed reciprocally as 330 dB/oct) and co-incides with the high-frequency transition in the triphasic bias pattern (LePage, 1989). Moreover, the finding is consistent with the hypothesis that the frequency-place map varies dynamically with the response of the OHC to the presence of the signal. At some stage during the stimulus risetime, the characteristic frequency of the place being measured is maximally aligned with the stimulus frequency with a brief period of resonance in the vibratory response.

Conclusions

The modified Helmholtz model possesses a number of inherent advantages. Firstly, it offers a much easier theoretical approach to explaining the very high slopes of the tuning curves; the high frequency cutoff merely shifts in place with level (LePage, 1987c). Secondly, it makes a great deal of sense of the highly-specialised morphology of the mammalian cochlea. Thirdly, the development of tension represents a significant evolutionary step from the lower vertebrates and imparts new understanding of the rise in frequency of a particular place with ontogenetic maturation (Rubel *et al.*, 1984). Fourth, a twitch response of the OHC to clicks may constitute the origin of click-evoked otoacoustic emissions (Kemp, 1978). Fifth, the model naturally accounts for presbycusis in terms of a progressive loss of turgor of the OHC resulting in loss of radial tension of the basilar membrane which will affect high frequency regions first. Sixth, localised changes in OHC tonus over a confined spatial region could result in distortions of the tonotopy. Modulation of OHC tonus can therefore effectively vary the density of neural projections to the central nervous system for any given frequency band. Seventh, reverse propagation of the travelling wave may even be possible. Fluctuations of force generation could result in instabilities due to local alternating forward and retrograde travelling waves leading to spontaneous emissions whose frequency can be pulled by the presence of tone. Finally, the model may account for the puzzling variability in acoustic overexposure. Many studies have shown a poor correlation between the extent of noise exposure and degradation of audiometric sensitivity. It would seem that the mammalian ear has the ability to absorb repeated acoustic insults without suffering a real loss of hearing sensitivity. A salient feature of cochlear morphology is the apparent redundancy in the numbers of OHC. The possibility exists that an important function of the OHC system is to dynamically smear the frequency representation so as to minimise the effects of aging and scattered OHC loss.

Acknowledgements

The author is grateful to H.P. Zenner and G. Reuter for assistance in collecting the data in Fig. 1; B.M. Johnstone for Fig. 4, and D.O. Kim and C.E. Molnar for Fig. 5.

References

Ashmore, J.F. (1987). A fast motile response in guinea pig outer hair cells: the cellular basis of the cochlear amplifier. J. Physiol. 338, 323--347.

Brownell, W.E., (1989). Slow electrically and chemically evoked volume changes in guinea pig outer hair cells. In "Biomechanics of Active Movement and Deformation of Cells", Springer-Verlag, N. Akas (Ed.), 493--498.

Brownell, W.E., Bader, C.R., Bertrand, D., and de Ribaupierre, Y. (1985). Evoked mechanical responses of isolated cochlear outer hair cells. Science, 227, 194--196, (1985).

Brundin, L., Flock, A. and Canlon, B. (1989). Sound-induced motility of isolated cochlear outer hair cells is frequency-specific. Nature, 342, 814--816.

Canlon, B., Brundin, L. and Flock, A. (1988). Acoustic stimulation causes tonotopic alterations in the length of isolated outer hair cells from guinea pig hearing organ. Proc. Natl. Acad. Sci. USA, 85, 7033--7035.

Dulon, D., Aran, J.M. and Schacht, J. (1988). Potassium-depolarization induces motility in isolated outer hair cells by an osmotic mechanism. Hearing Res. 32, 123--130.

Flock, A, Flock, B., and Ulfendahl, M. (1986). Mechanisms of movement in outer hair cells and a possible structural basis. Arch. Otorhinolaryngol. 243, 83--90.

Helmholtz, H. (1885:1954). On the sensations of tone. Dover Publications, New York.

Kachar, B., Brownell, W.E., Altschuler, R. and Fex, J. (1986). Electrokinetic shape changes of cochlear outer hair cells. Nature, 322, 365--368.

Kemp, D.T. (1978). Stimulated acoustic emissions from within the human auditory system. J.Acoust.Soc.Am., 64, 1386--1391.

LePage, E.L. (1981). Ph.D. Thesis. The role of nonlinear mechanical processes in mammalian hearing. The University of Western Australia.

LePage, E.L. (1987a). The application of a capacitive probe technique for direct observation of electromechanical processes in the guinea pig cochlea. J.Acoust.Soc.Am., 82, 126--138.

LePage, E.L. (1987b). Frequency-dependent self-induced bias of the basilar membrane and its potential for controlling sensitivity and tuning in the mammalian cochlea. J.Acoust.Soc.Am., 82, 139--154.

LePage, E.L. (1987c). A spatial template for the shape of tuning curves in the mammalian cochlea. J.Acoust.Soc.Am., 82, 155--164.

LePage, E.L. (1988). Motility of the outer hair cells and tuning in the mammalian cochlea. Abstracts of the eleventh midwinter meeting of the Association for Research in Otolaryngology, Clearwater Beach, Florida, p.29.

LePage, E.L. (1989). Functional role of the olivocochlear bundle: A motor unit control system in the mammalian cochlea. Hearing Res., 38, 177--198.

Liberman, M.C. (1988). Physiology of cochlear efferent and afferent neurons: Direct comparisons in the same animal. Hearing Res., 34, 179--192.

Patuzzi, R., Sellick, P.M. and Johnstone, B.M. (1984). The modulation of the sensitivity of the mammalian cochlea by low frequency tones. I. Primary afferent activity. Hearing Res., 13, 1--9.

Puel, J.-L., Bonfils, P. and Pujol, R. (1988). Selective attention modifies the active micromechanical properties of the cochlea. Brain Res., 447, 380--383.

Rajan, R., Robertson, D. and Johnstone, B.M. (1990). Absence of tonic activity of the crossed olivocochlear bundle in determining compound action potential thresholds, amplitudes and masking phenomena in anaesthetised guinea pigs with normal hearing sensitivities. Hearing Res., 44, 195--208.

Robertson, D. and Johnstone, B.M. (1979). Aberrant tonotopic organization in the inner ear damaged by kanamycin. J. Acoust. Soc. Am., 66, 466--469.

Rubel, E.W., Lippe, W.R. and Ryals, B.M. (1984). Development of the place principle. Ann. Otol.Rhinol.Laryngol., 93, 609--615.

Slepecky, N., Ulfendahl, M. and Flock, A. (1988). Shortening and elongation of isolated outer hair cells in response to application of potassium gluconate, acetylcholine and cationized ferritin. Hearing Res., 34, 119--126.

Zenner, H.P. (1980). Cytoskeletal and muscle like elements in cochlear hair cells. Arch. Otorhinolaryngol. 230, 82--92.

Zenner, H.P. (1986a). K^+-induced motility and depolarization of cochlear hair cells --- direct evidence for new pathophysiological steps in Meniere's disease. Arch. Otorhinolaryngol. 243, 108--111.

Zenner, H.P. (1986b). Molecular structure of hair cells. In Neurobiology of Hearing: The Cochlea, edited R.A. Alschuler, D.W. Hoffman and R.P. Bobbin. Raven Press, New York.

Zenner, H.P. (1986c). Motile responses in outer hair cells. Hearing Res. 22, 83--90.

Zenner, H.P. (1988). Motility of outer hair cells as an active, actin-mediated process. Acta Otolaryngol., 105, 39--44.

Zenner, H.P., Zimmermann, U. and Schmitt, U. (1985). Reversible contraction of isolated mammalian cochlear hair cells. Hearing Res. 18, 127--133.

Zenner, H.P., Arnold, W. and Gitter, A.H. (1988). Outer hair cells as fast and slow cochlear amplifiers with a bidirectional transduction cycle. Acta Otolaryngol. 105, 457--42.

Comments and discussion

MANLEY

I have two comments on the conclusions in this paper. Firstly, the reference to "a significant evolutionary step from the lower vertebrates" is obscure. Considering the fact that there are more similarities than differences between data from non-mammals and mammals and that we know relatively little about the so-called lower vertebrate inner ear, this statement is at best premature.

Secondly, I would like to point out that more recent data on the development of hearing in the chick obtained by single-fibre staining at different developmental ages (Manley et al., 1987) show that after hatching, the tonotopic map of the chick cochlea *does not change*. Thus, at least for tall hair cells, which receive the bulk of the afferent innervation in the avian basilar papilla (for refs. see Manley et al., 1989) there is no "rise in frequency of a particular place with ontogenetic maturation."

LEPAGE

It is necessary to reiterate a major point of my model intended for the mammal but which may have more general applicability. It is that the *location* of the excitation pattern or "travelling wave envelope" is *not fixed* in the manner which has been traditionally assumed. It depends not just upon the frequency of the stimulus but also on the state of the outer hair cell. It therefore depends upon the *time* since onset of the stimulus. That is, the map is being dynamically distorted by the *presence* of a pure tone. So, the *excitation pattern slides longitudinally with a change in the tonic state of the outer hair cell.* One of the major determinants of this state is sound pressure level. Another will be the availability of biological energy.

The notion of a fixed, one-to-one frequency place map constitutes a remnant of early passive models of the cochlea. The sharp tuning seen in the threshold response of various parameters is therefore not a true reflection of the shape of the excitation pattern at higher stimulus levels. This is because frequency response measurements generally *take more time to carry out than the outer hair cell does to change state.*

In terms of my model there is no major conflict between Rubel's and Manley's experiments. Each experiment in the chick tested quite different aspects of mapping the frequency to place. At low sound levels (Manley's experiment) there will be essentially no distortion of the map, whereas at damaging sound levels (Rubel's experiment) the distortion of the map is maximal. In my opinion the latter experiment still reflects a progressive maturation of the organ to withstand acoustic insult through maturation of control of dispersion of the acoustic energy. Moreover, the equivalent results for mammal (Harris and Dallos, 1984) are not directly addressed by the chick data.

Comments and discussion

It appears that the frog ear does not possess force generating elements to extend its dynamic range, but instead employs an adaptation mechanism contained within the detector cell (Jaramillo et al. this volume). Lack of demonstrated force generation is certainly true of still more primitive hearing organs, e.g. the lateral line. I thank Dr. Manley for the implicit suggestion that birds and reptiles have probably developed alternative mechanisms to extend the dynamic range (and protect against insult) probably also through force generation in some analogous manner. In mammals the outer hair cells appear to be the control elements yielding some form of automatic gain control (LePage, 1989; Lyon, this volume) which utilizes the creation of a spatial misalignment of the excitation pattern and the most sensitive place for any stimulus frequency (LePage, 1987c).

Reference

Harris, D.M. and Dallos, P. (1984). Ontogenetic changes in frequency mapping of a mammalian ear. Science, 225, 741-743.

MEASUREMENTS OF BASILAR MEMBRANE TUNING AND DISTORTION WITH LASER DOPPLER VELOCIMETRY

A.L. Nuttall, D.F. Dolan and G. Avinash

University of Michigan Medical School
Kresge Hearing Research Institute
1301 E. Ann St.
Ann Arbor, MI 48109-0506 USA

Abstract

A method is described for the measurement of basilar membrane (BM) vibration. It makes use of commercially made laser Doppler velocimetry (LDV) instrumentation which is adapted to a compound microscope. This allows visualization reflective objects placed on the BM and the focusing of the laser beam onto the reflective object (a glass microbead). We show examples of frequency tuning curves and displacement input/output intensity functions obtained with the technique and demonstrate that cubic distortion of both the local and propagated kind are present in mechanical responses of the membrane.

Introduction

The laser Doppler velocimeter or vibrometer (LDV) is a new commercially made instrument useful for cochlear physiological studies. Although certain laser based methods have already been used to study basilar membrane motion, including speckle detection (Kohlloffel 1972a,b), homodyne interferometry (Khanna 1986; Khanna et al 1986; Khanna and Leonard, 1982), and heterodyne interferometry (Willemin et al, 1988). LDV offers important advantages over some of these and other methods. For example, it does not require lowering the perilymph level as is necessary for the capacitive probe (Wilson, 1973; Wilson and Johnstone, 1975; Le Page, 1987) nor does it require a gamma radiation source, with attendant toxicity and mass loading problems associated with the Mössbauer technique (Sellick et al, 1983a; Klianga and Khanna, 1983; Rhode 1971). Perhaps the most important advantages of LDV are its linearity (1%), dynamic range (>160 dB), bandwidth (0.1 Hz to 1 MHz), and its ability to make almost arbitrarily small (in diameter) point measurements.

Using an implementation of LDV we have obtained measurements of basilar membrane

*Presented in part at the midwinter meeting Association for Research in Otolaryngology, 1990, St. Petersburg Beach, FL and Society for Neuroscience Meeting 1989, Phoenix, AZ.

Using an implementation of LDV we have obtained measurements of basilar membrane motion input/output intensity functions. They show compressive nonlinear growth for the topographic best frequency and the frequency tuning curves (isodisplacement functions) had sharply tuned tip regions. When the cochlea was stimulated by two pure tones, which are higher in frequency than the location being measured, propagated type "cubic" distortion was observed. A similar amount of cubic distortion was also seen in the local activity of the two primary tones.

Materials and Methods

To accomplish Doppler vibrometry of the BM, the laser beam of the LDV (Polytec Corp.) is directed through the objective lens of a compound microscope. The system uses a beam splitter which serves to direct the beam into the image pathway.

The microscope contains two focusing elements, the objective lens (L_1) and a lens (L_2) near the laser light source. The choice of an infinity corrected microscope objective lens simplifies the remaining optical design considerably. Laser light is delivered to the microscope through an optical fiber (light guide). An image of the fiber (diameter) is transferred to the object plane, reduced in size by the ratio of the focal length of L_1 to the collimating lens, L_2. Since the diameter of the Polytec Corp. LDV light guide is 5 μm, it is easy to achieve a diffraction limited spot size (i.e. determined by the numerical aperture of the objective lens).

ANIMAL PREPARATION

Pigmented guinea pigs were pre-anesthetized with nembutal (15 mg/kg, IP) and anesthetized with Innovar-Vet (0.4 ml/kg, IM). Supplemental doses of Innovar-Vet were given hourly to maintain an acceptable surgical anesthesia level (0.2 ml/kg IM). The general physiological condition of the animal was monitored by recording the heart rate and the body temperature. A tracheotomy and tracheal canulation maintained the airway although artificial ventilation was not used. The head was fastened into a heated head holder (Brown et al, 1983; Shore and Nuttall 1985) and a ventral and postauricular surgical dissection exposed the bulla which was carefully opened over a wide area. Although the tympanic membrane and ossicles were preserved, the tensor tympani muscle tendon was transected.

The cochlea was opened by carefully thinning the bony wall over the scala tympani of the first (basal) turn. This was accomplished using a narrow scalpel blade in a technique fully described by Brown and Nuttall (1984). The opening in the cochlea was about 0.5 mm in diameter and only the amount of perilymph necessary to clear and control bleeding was removed. The perilymph level returned to fill the cochlea by natural flow of cerebrospinal fluid. The head was oriented so that the basilar membrane was approximately horizontal in the region directly adjacent to the opening. Thus the microscope which views the basilar membrane was in the vertical position.

A 1/2 inch Bruel and Kjaer condenser microphone in an ear speculum fitted into the external meatus delivered sound in a closed field manner. Sound levels were calibrated using a probe microphone system (1mm probe tube B&K 1/2 condenser microphone) placed within 2mm of the tympanic membrane. A silver wire electrode was fixed into position on the round window membrane to record the cochlear compound action potentials (CAP). The reference electrode was a chlorided silver wire placed in the neck musculature.

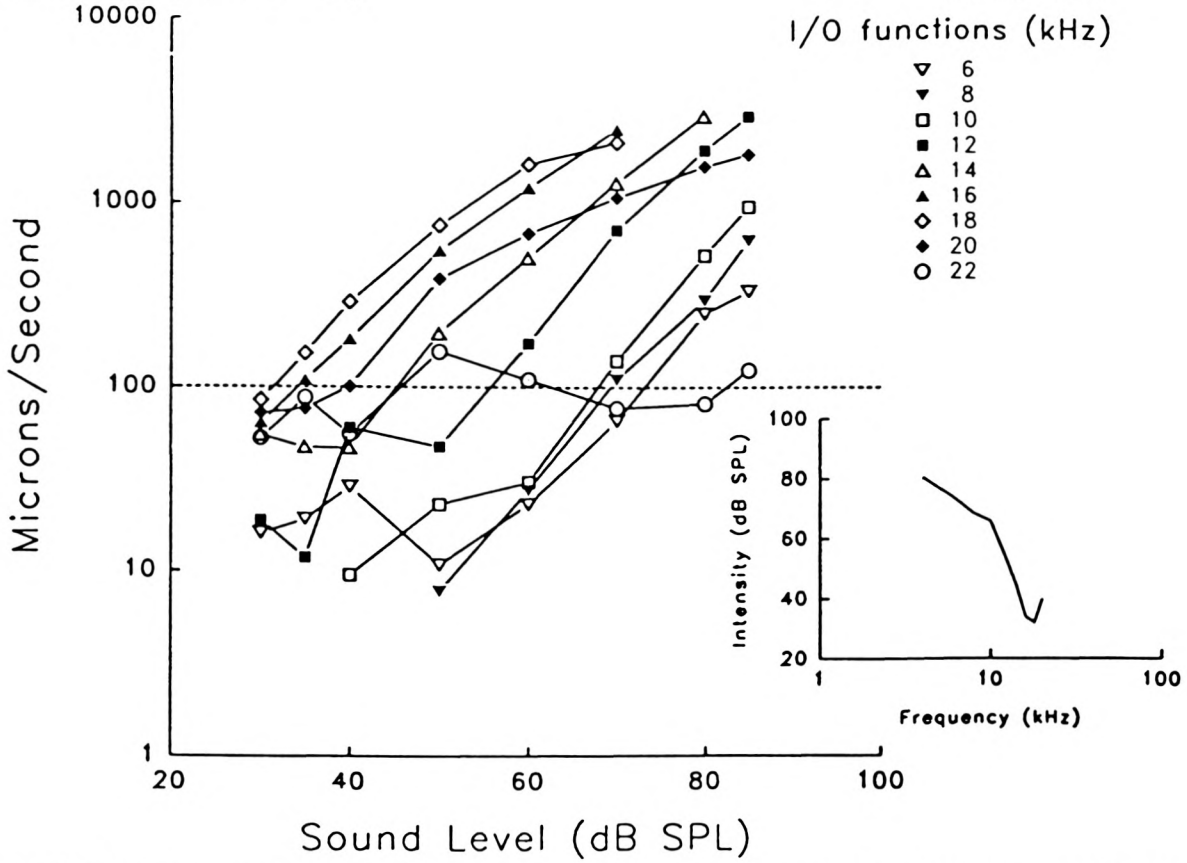

FIGURE 1. Intensity (input/output) functions obtained from a microbead located on the basilar membrane of the guinea pig. The characteristic frequency (CF) of the location was about 18.0 kHz. Intensity functions near the CF exhibit nonlinear (compressive) growth. The frequency tuning curve (insert) was derived from the input/output functions for a criterion of 100 microns/second.

Tone bursts (1 ms rise/fall time, 10 ms duration) given 10/s at frequencies between 1 and 40 kHz served to derive a CAP audiogram monitoring the condition of the cochlea.

Signals from the LDV were typically too small to be seen without some signal processing. While the time waveforms can be readily derived by signal averaging, this study used a lock-in amplifier (Stanford model SR530) to obtain the magnitude and phase of BM motion for signals consisting of one or two tones.

Sounds were delivered to the ear from a voltage controlled oscillator, with the aid of computer controlled attenuators and tone switches. A PC-AT type microcomputer was used to control the experiment and store the digitized data.

It is possible to obtain sufficiently strong reflections from opaque objects, however biological tissues have relatively low reflectance and do not normally provide reflections suitable for measurement (Khanna et al, 1989). Therefore, in practice, useable signals cannot be obtained from the BM or the osseous spiral lamina. Glass microbeads provided sufficient reflected signal to give full scale readings in the signal strength meter of the LDV. Solid glass microbeads (Mo-Sci Corp., Rolla, MO) of approximately 15-25 micron diameter with refractive index 2.1 were either coated with poly-L-lysine to enhance their adhesion to the BM or left uncoated. The microbeads were placed in saline and taken by

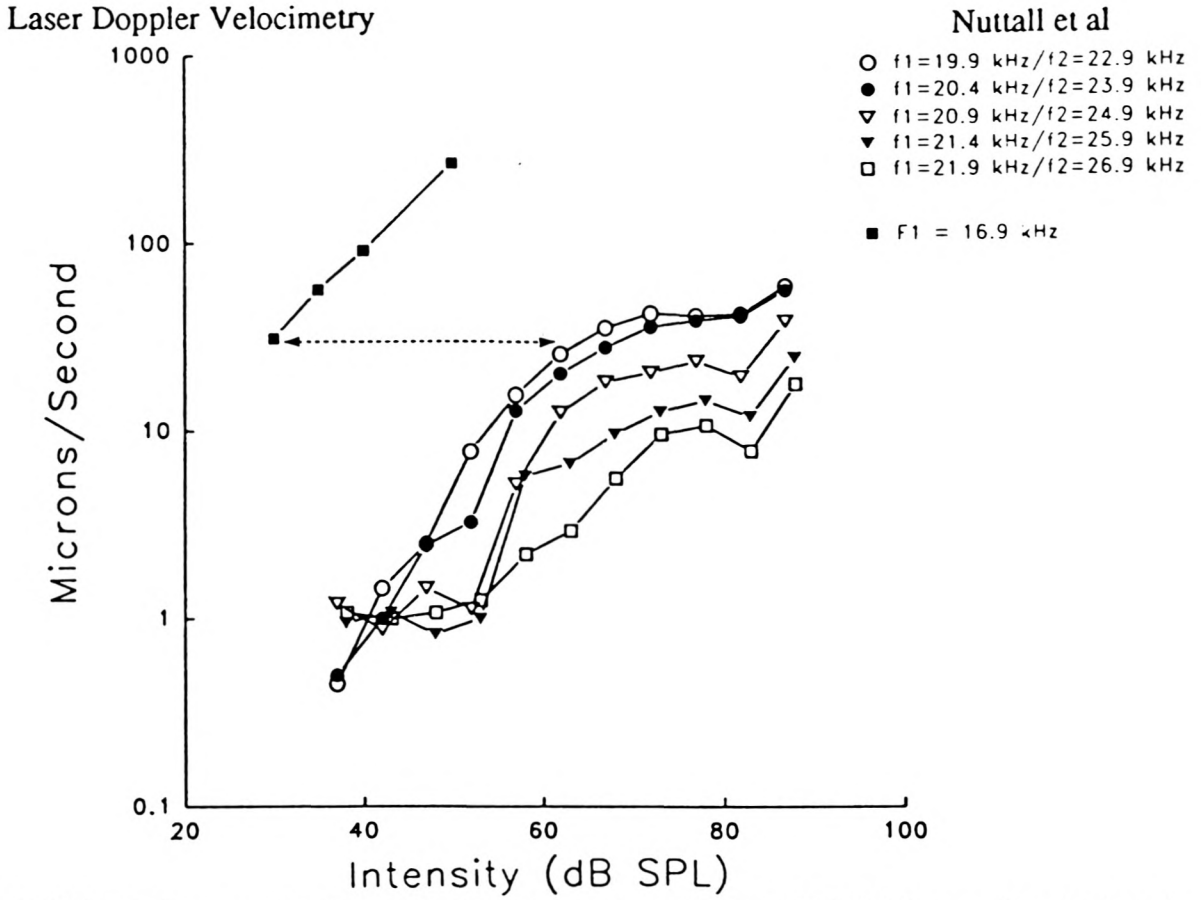

FIGURE 2. The growth of the cubic distortion product ($2f_1$-f_2 = 16.9 kHz) for equal level primaries raised from 30dB to 90dB SPL for a microbead with CF = 16.9 kHz. A portion of the input/output function at CF is shown in the upper left hand corner. The horizontal dashed line indicates approximately 30dB difference in level required to produce the same amount of velocity for the tone at CF.

suction into a micropipette. The pipette was held by a micromanipulator and positioned through the opening in the cochlea. Beads were dispensed into the cochlea by gently forcing them from the pipette. They fell by gravity onto the BM.

Results

Figure 1 shows a series of displacement intensity functions from 6kHz to 22kHz obtained from a microbead located over the tunnel of Corti. Some of the basilar membrane displacement functions show compressive nonlinear behavior. Tonal stimuli near the "best frequency" for this microbead (18kHz) show saturation at lower sound pressure levels. Frequencies below the best frequency demonstrate more linear growth with increasing sound pressure level. Similar characteristics have been observed in hair cell receptor potentials (Russell and Sellick, 1978; Goodman et al, 1982; Brown et al, 1986; And Dallos, 1985), rate-level functions from auditory nerve fibers, (Kiang et al, 1965; Geisler et al, 1974; Sachs and Abbas, 1974; and Evans, 1979), and the relatively linear growth functions for frequencies below CF has also been reported from other studies of BM motion (Rhode, 1971; and Sellick et al, 1982). The frequency threshold curve (insert) is derived from the input output functions using a criterion of 100 microns/second. The best frequency is 18kHz at approximately 30dB SPL and a tip to tail difference of approximately 40 dB.

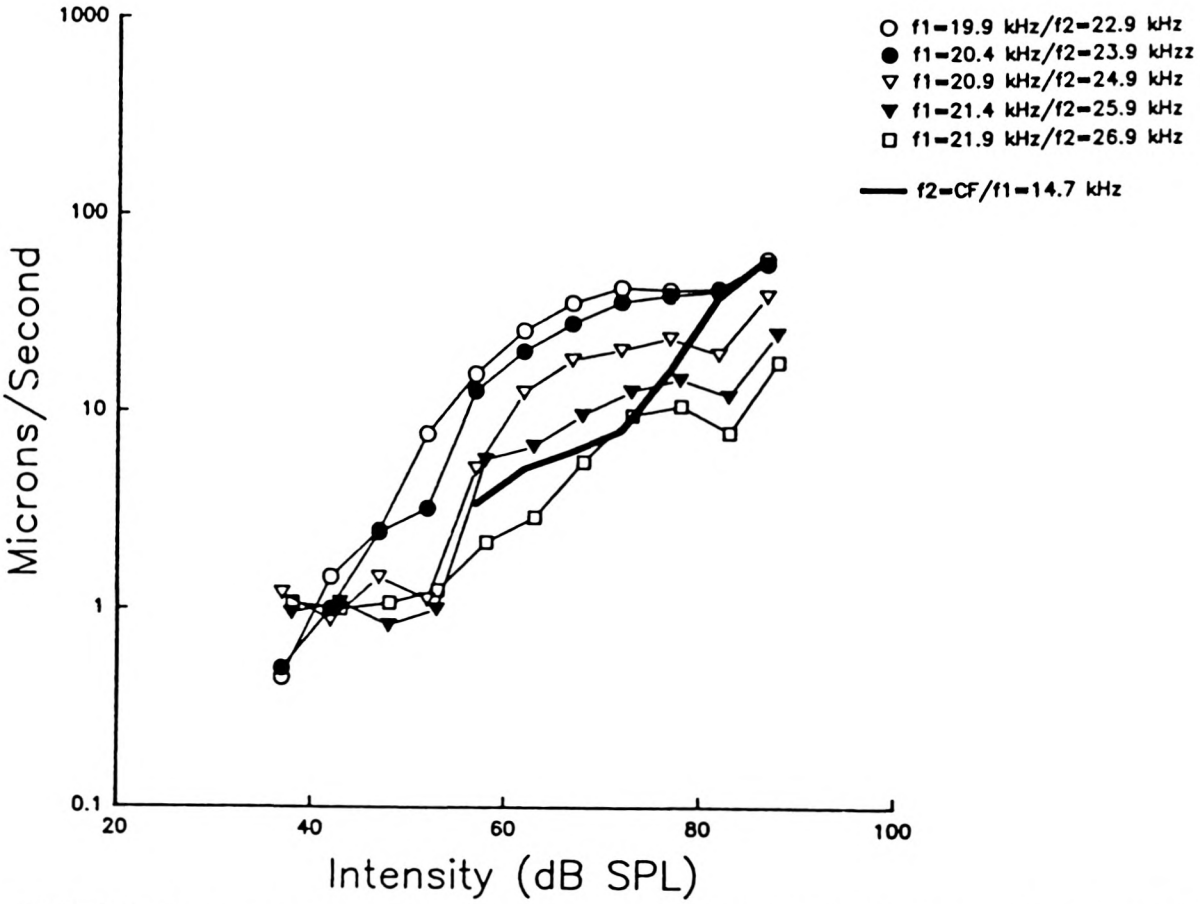

FIGURE 3. The growth of the cubic difference tone ($2f_1$-f_2 = 16.9 kHz) is compared to the growth of the "local" (solid black line) cubic difference tone (f_2 = CF and f_1 = 14.7 kHz).

Figure 2 shows, in a different guinea pig, the growth of the cubic distortion product ($2f_1$-f_2) for equal level primaries raised from approximately 30 dB SPL to 90 dB SPL. The upper left hand curve shows a portion of the input output function for a best frequency tone given alone at CF (16.9 kHz). For each curve, the primaries were adjusted so that the cubic distortion product was centered at the tonotopic best frequency for the microbead that was being measured. These chosen primaries (> 19 kHz) produce minimal or no vibration of the microbead. The energy of the cubic distortion product presumably is propagating to the location being measured. The horizontal dashed line indicates approximately 30dB difference in sound level to produce a comparable amount of velocity for a tone at CF and the cubic distortion product. These data are consistent with those reported in the psychophysical literature for the perceptual difference between the primary and the cubic distortion product. It is also consistent with our observations in a similar experiment measuring the dc receptor potential of inner hair cells. The spacing between the input/output functions for the cubic distortion products are similar, as well, to our observations from the inner hair cell. The cubic distortion product declines with a rate of about 100-200 dB/octave separation of the primaries.

In Figure 3 The local (thick solid black line) cubic distortion intensity function is compared with propagated cubic distortion product growth functions. The propagated functions are the same as those shown in Figure 2. The local cubic distortion was obtained

by placing f_2 at best frequency and f_1 at 14.7 kHz where $2f_1-f_2= 12.5$ kHz. To a first approximation, the local distortion product has a similar growth function shape and is on the same order of magnitude as the propagated distortion products.

Discussion

The LDV is a relatively new commercial instrument that measures the vector component of velocity directed along the axis of the laser beam. Related instrumentation uses multiple beams to determine the velocity of objects crossing the beams (laser anemometers). The velocity recorded is an instantaneous time measurement and is directionally sensitive. This is accomplished by heterodyne techniques and frequency demodulation electronics.

At present, with our limited experience with the laser Doppler vibrometer, we feel that this instrument is easily adapted for studies in peripheral auditory physiology. We have demonstrated here that the mechanical responses of the basilar membrane are finely tuned and show local and propagated intermodulation distortion.

Acknowledgements

This work was supported by NIH research grant NS 15107. The authors thank the Polytec Corp. (Redwood, CA) for the two week loan of the OVF-1000 during which time this study was accomplished and Mo-Sci Corp. for the gift of glass microbeads.

Literature Cited:

Bekesy G von. (1960): Experiments in Hearing. (McGraw Hill, NY).

Brown MC, Nuttall AL, Masta RI. (1983b): Intracellular recordings from cochlear inner hair cells: Effects of stimulation of the crossed olivocochlear efferents. Science 222:69-72.

Brown MC, Smith DI, Nuttall AL. (1983a): Anesthesia and surgical trauma: Their influence on the guinea pig compound action potential. Hearing Res. 10:345-358.

Brown, MC and Nuttall, AL. (1984): Efferent control of cochlear inner hair cell responses in the guinea pig. J. Physiol. 354:625-646.

Dallos P. (1985): Response characteristics of mammalian cochlear hair cells. J Neurosci 5: 1591-1608.

Durrani TS and Greated CA. (1977): Laser Systems in Flow Measurement, Plenum Press, New York.

Evans EF. (1979): Single unit studies of the mammalian auditory nerves. In: Auditory Investigations: The Scientific and Technological Basis. Ed. H.A. Beagley, Oxford Univ. Press.

Geisler CD, Rhode WS, Kennedy DT. (1974): Responses to tonal stimuli of single auditory nerve fibers and their relation to basilar membrane motion in the squirrel monkey. J Neurophysiol 37:1156-1172.

Goodman DA, Smith RL, Chamberlain SC. (1982): Intracellular and extracellular responses in the organ of Corti of the gerbil. Hearing Res. 7: 161-179.

Johnstone BM, Boyle AJF. (1967): Basilar membrane vibration examined with the Mössbauer technique. Science 158:389-390.

Khanna SM and Koester CJ. (1989): Optical sectioning characteristics of the heterodyne interferometer. Acta Otolaryngol (Stockh) Suppl 467:61-68.

Khanna SM, Johnson GW, Jacobs J. (1986): Homodyne interferometer for basilar membrane measurements. II. Hardware and techniques. Hearing Res. 23: 27-36.

Khanna SM, Leonard DGB. (1982): Basilar membrane tuning in the cat cochlea. Science 215: 305-306.

Khanna SM, Willemin JF, and Ulfendahl M. (1989): Measurements of optical reflectivity in cells of the inner ear. Acta Otolaryngol (Stockh) Suppl 467:69-75.

Khanna SM. (1986): Homodyne interferometer for basilar membrane measurements. Hearing Res 23: 9-26.

Kiang NYS, Watanabe T, Thomas EC, Clark LF. (1965): Discharge patterns of single fibers in the cat's auditory nerve. Research Monograph #35 (MIT, Cambridge).

Kliauga P, Khanna SM. (1983): Dose rate to the inner ear during Mössbauer experiments. Phys Med Bio. 28:359-366.

Kohlloffel LUE. (1972a): A study of basilar membrane vibrations. I. Fuzziness-detection: A new method for the analysis of microvibrations with laser light. Acustica 27:49-65.

Kohlloffel LUE. (1972b): A study of basilar membrane vibrations.II. The vibratory amplitude and phase pattern along the basilar membrane (post-mortem). Acustica 27, 66-81.

Kohlloffel LUE. (1972c): A study of basilar membrane vibrations. III. The basilar membrane frequency response curve in the living guinea pig. Acustica 27: 82-89.

LePage EL. (1987): The application of a capacitative probe technique for direct observation of electromechanical processes in the guinea pig cochlea. J Acoust Soc Am 82:126-138.

LePage EL. (1988): Fiber optic lever reveals sound-produced contractile component of basilar membrane motion. Abstracts Association for Research in Otolaryngology, Clearwater Beach, FL.

Nuttall AL, Dolan DF, Gopal A. (1989): Laser Doppler vibrometer measurements of basilar membrane motion in the guinea pig. Society for Neuroscience meeting, Phoenix, AZ.

Patuzzi RB, Sellick P. (1983): A comparison between basilar membrane and inner hair cells receptor potential input-output functions in the guinea pig cochlea. J Acoust Soc Am 74:1731-1741.

Rhode WS, Robles L. (1974): Evidence from Mössbauer experiments for nonlinear vibrations in the cochlea. J Acoust Soc Am 55:588-596.

Rhode WS. (1971): Observations of the vibration of the basilar membrane in squirrel monkeys using the Mössbauer technique. J Acoust Soc Am 49: 1218.

Russell IJ, Sellick PM. (1978): Intracellular studies of hair cells in the mammalian cochlea. J Physiol 284: 261-290.

Russell UJ, Sellick PM. (1977): Tuning properties of cochlear hair cells. Nature 267:858-860.

Sachs MB, Abbas PJ. (1974): Rate versus level functions for auditory-nerve fibers in cats: Tone burst stimuli. J Acoust Soc Am 56:1835-1847.

Sellick PM, Patuzzi R, Johnstone BM. (1982): Measurement of basilar membrane motion in the guinea pig using the Mössbauer technique. J Acoust Soc Am 72: 131-141.

Sellick PM, Patuzzi R, Johnstone BM. (1983b): Comparison between the tuning properties of inner hair cells and basilar membrane motion. Hearing Res. 10: 93-100.

Sellick PM, Yates GK, Patuzzi R. (1983a): The influence of Mössbauer source size and position on phase and amplitude measurements of the guinea pig basilar membrane. Hearing Res. 10:101-108.

Shore, SE and Nuttall, AL.: (1985): The effects of cochlear hypothermia on compound action potential tuning. J. Acoust. Soc. Am. 77:590-598.

Willemin J-F, Dändliker R, Khanna SM. (1988): Heterodyne interferometer for submicroscopic vibration measurements in the inner ear. J Acoust Soc Am 83: 787-795.

Wilson JP, Johnstone JR. (1975): Basilar membrane and middle-ear vibration in guinea pig measured by capacitive probe. J Acoust Soc Am 57: 705-723.

Wilson JP. (1973): A sub-miniature capacitative probe for vibration measurements of the basilar membrane. J Sound Vib 30: 483-493.

IN VIVO MEASUREMENT OF BASILAR MEMBRANE STIFFNESS

Elizabeth S. Olson and David C. Mountain

Dept. of Biomedical Engineering
Boston University, Boston, MA 02215, USA

Introduction

The basilar membrane is the underlying support of the cochlear partition. Its shape is that of a narrow, flat strip, tapering from the apex to the base of the cochlea. In ultrastructural observations in guinea pig the basilar membrane was found to be composed of three layers (Iurato, 1962). A layer of tympanic cells borders scala tympani. A 20 nm basement membrane borders the organ of Corti. In between is a noncellular layer, composed of protein filaments in a cottony ground substance. The filaments run transversely between the osseous spiral lamina and the spiral ligament. Voldrich (1978) observed that when the basilar membrane was deflected with a needle, the form of the deflection was a thin radial depression. This observation and the transverse anatomy suggest that the filaments behave structurally as a set of transverse beams with little longitudinal coupling.

The value of the stiffness of the basilar membrane is important to the understanding of the motion of the cochlear partition. The basilar membrane plus organ of Corti stiffness, coupled to the inertia of the fluid in the scalas, produces traveling wave motion in the cochela. The ratio of partition stiffness to mass, a value that decreases from base to apex, determines how far along the basilar membrane the traveling wave will go before it is rapidly attenuated.

Gummer et al (1981) and Miller (1985) measured basilar membrane stiffness in freshly excised cochleas of guinea pig. However, it has recently been shown that the workings of the cochlea deteriorate almost immediately following death of an experimental animal. This finding motivated the in vivo measurements of basilar membrane stiffness reported here.

Our basilar membrane stiffness measurements were done in the base of the gerbil cochlea. Basilar membrane stiffness was determined by contacting the basilar membrane with a stainless steel needle (tip diameter 25 μm) attached to a force transducer, putting the needle/transducer structure through a sinusoidal excursion with amplitude 5 or 25 nm, and measuring the dynamic return force exerted on the needle by the basilar membrane. Stiffness is calculated as amplitude of return force divided by amplitude of excursion. In other words, stiffness is equal to the slope of the force-vs-displacement curve. The dynamic stiffness was measured over a 24 μm range of static displacements and is presented as stiffness-vs-static displacement.

Methods

Gerbils of the species meriones unguicilatus (Mongolian gerbils) were used. The gerbil is given a subdermal injection of the analgesic tranquilizer acepromazine (dose 1

mg/kg) followed an hour later by an injection of the anesthetic sodium pentobarbital (initial dose 60 mg/kg). Supplemental 10 mg/kg doses of sodium pentobarbital are given when required. The temperature of the gerbil is maintained at 38° F. The gerbil is on its back with its head secured in a stereotaxic head holder. The left bulla is exposed and the bone of the bulla is partially removed. The cochlear bone surrounding the round window opening is scraped back approximately 100 μm with a small knife. The round window membrane is removed with a fine insect pin. A tiny bit of dye (fast green FCF no. F-7252 Sigma) is put on the round window before its removal, to help visualize the membrane.

After a swath of the round window membrane has been removed there is clear, approximately perpendicular, but limited access to the basilar membrane in the region where the basilar membrane is entering the first turn. The measurement position is approximately 1.3 to 1.4 mm from the very basal end of the basilar membrane.

The force probe consists of two parts: a voltage-to-motion transducer to produce the dynamic and static displacements of the transducer/needle structure, and a force-to-voltage transducer to detect forces on the needle. The needle, which is glued onto the force transducer, is 1.8 cm long and has a flattened tip with a diameter of 25 μm. The probe stiffness is approximately 3500 N/m. This is much greater than the basilar membrane stiffness, so the motion is not significantly diminished when the probe needle is loaded by the basilar membrane. The force probe is clamped onto a hydraulic microdrive which is mounted onto a micromanipular. The probe is manually positioned with the micromanipulator so that the end of the probe needle is inside the round window opening, and is pointed at, but roughly 70 μm up from, the basilar membrane. Further positioning of the probe is done remotely from outside the sound chamber. The needle is aimed at the center of the basilar membrane widthwise (170 to 180 μm wide here), but due to limited visibility, the true position of the needle is estimated as being centered to within half of the width.

To make contact between the needle and the basilar membrane the needle/transducer structure is put through a 35 nm peak sinusoidal excursion and advanced towards the basilar membrane in 1 μm steps with the hydraulic microdrive until contact is detected. As soon as a stable peak emerges from the noise viewed on the spectrum analyzer, contact is assumed. The minimum detectable peak (with no averaging) corresponds to a force of approximately 10 nN peak. The needle/transducer structure is then stepped in 1 μm steps to a maximum static displacement of 20 μm. It is then withdrawn in 1 μm steps to a -4 μm position. At each static position the transducer is put through 30 presentations each of a 5 nm peak sinusoidal excursion and a 25 nm peak sinusoidal excursion. Each presentation is 0.9 sec long. Most experimental runs were done at 80 Hz. In some runs the order of the static positions was pseudo-random.

During each excursion presentation the amplified transducer voltage is sampled 1500 times and the last 1024 samples are averaged over the 30 presentation. The averaged waveforms are stored in a PDP-11 computer and are Fourier analyzed for the magnitude and phase of the return force.

Mechanical noise, the dominant noise source, is attenuated by doing the experiments on a vibration isolation table in a sound chamber. The general noise level in the 20-200 Hz frequency range that is monitored during experiments is at a voltage level corresponding to a force of approximately 3.6 nN(RMS)/$\sqrt{Hz}$. The background noise level in the spectra of computer analyzed averaged data is at a level of 0.6 nN(RMS)/$\sqrt{Hz}$.

As a monitor of cochlear health, the compound action potential (CAP) response to tone bursts spanning the frequencies from 2 to 20 kHz at levels of 50, 60 and 70 dB SPL is measured. The CAP is measured via a silver wire electrode positioned just outside the

round window opening. The response is measured before the bone of the round window opening is cleared and the round window membrane removed, again just after round window membrane removal, and at interim periods during the experiment. The sound level is set with a half inch Bruel and Kjaer microphone attached to the left earbar, which is hollow. Tones are delivered through an earphone which is inserted into the end of the earbar.

Results

Basilar membrane stiffness measurements were performed in 18 gerbils. We emphasize the results from the last 12 gerbils because they were done with the same paradigm (described above). From the 12 gerbils we present results from 39 stiffness runs. In all but a few cases the probe was repositioned slightly between runs on the same animal. The last one or two runs of an experiment were sometimes done after the animal was sacrificed with an overdose of sodium pentobarbital.

Damage sometimes occurred during removal of the round window membrane. This caused severe reduction in the CAP response. Of the 12 cochleas, 2 were damaged during round window removal and 1 sustained localized damage to the basilar membrane before any measurements were made. In all but one experiment the CAP was severely reduced following the first stiffness measurement. In the one outstanding animal the measured stiffness was similar to but slightly larger than the stiffness measured in the other animals. In all animals which started with a healthy CAP response, the loss of the CAP following the first stiffness measurement was not correlated with a significant change in subsequent stiffness measurements. In one experiment an electrode was inserted into scala media, and the endocochlear potential was monitored throughout the course of a stiffness measurement. The endocochlear potential, which was stable prior to the stiffness measurement, was reduced by 21% of its original value during the course of the run. The reduction suggests that the stiffness measurement breaks tight junctions responsible for the electrical seal between scala media and scala tympani. Following the run the CAP response was substantially reduced. The reduced endocochlear potential would certainly contribute to the reduction in CAP.

In general the force exerted on the probe by the basilar membrane was close to 180° out of phase with the excursion. For example, the phases measured in the experimental run plotted in Fig 1 had a mean of -176°, and a standard deviation from the mean of 3°. 180° is the phase of a pure stiffness. A combination of drag and stiffness will result in a phase that lies between -90° and -180°. When the force is close to 180° out of phase with the excursion the data are presented as stiffness-vs-displacement curves, where stiffness, k, is the magnitude |dF|/|dx|.

TYPICAL FEATURES OF STIFFNESS

In measurements on cochleas that were not damaged during round window removal the stiffness-vs-displacement curves displayed a consistent shape. This shape is characterized by the features identified in Fig 1 and listed below.

1. Initial Plateau. 21 runs out of 39 had an initial plateau. The plateau varied in length between 2 and 12 μm, with a mean length of 4.6 μm, and had a stiffness that ranged from 0.2 to 1.2 N/m with a mean stiffness of 0.6 N/m. The length of the initial plateau is influenced by background noise, which is often dominated by animal noise and varies between experiments. In noisy experiments the basilar membrane is probably not detected until it has been deflected a relatively large distance. The initial plateau was

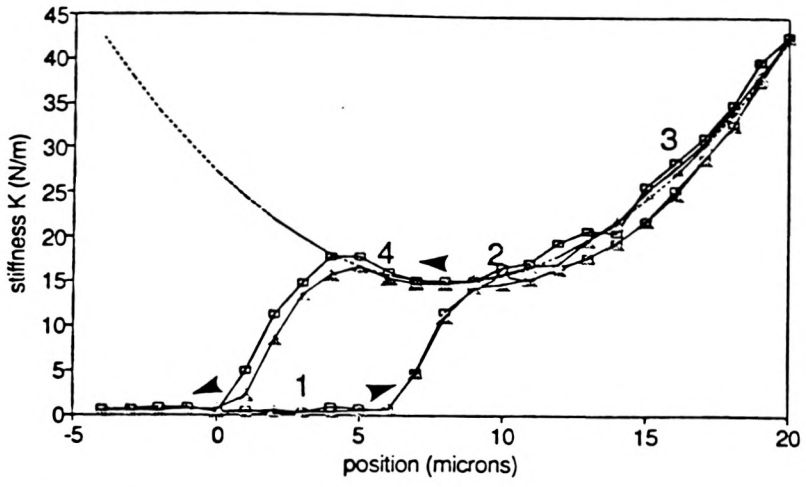

FIGURE 1 Basilar membrane stiffness measurement. Data from one stiffness run is plotted. Animal 016 run 1. Empty squares: 5 nm excursion. Filled triangles: 25 nm excursion. Dashed line: beam theory fit. The quadratic fit to the curve is $k = 15\ N/m + 0.19\ N/m \cdot \mu m^{-2}\ (x - 8.0)^2$. Arrows differentiate data taken as probe was advancing from data taken as probe was retracting. Features that were common to most measurements are identified with numbers. (1) Initial plateau. (2) Second plateau. (3) Final quadratic growth in stiffness. (4) Extension of second plateau as probe is retracted.

relatively short and sometimes absent in noisy experiments.

2. Second plateau. 33 out of 39 runs had a second plateau. In measurements in which the static position of the probe was advanced in order a rise lasting from 2 to 6 μm usually occurred beyond the initial plateau, ending in a region with reduced or even reversed slope. The stiffness of this second plateau region ranged from 1.4 to 20 N/m, but in 17 of the 33 detections of the plateau the stiffness was between 6 and 9 N/m. The mean was 9.1 N/m. 4 of the largest plateau stiffnesses, with values of 15, 16, 17 and 20 N/m were found in animal 016, in which the CAP was still healthy following the first and second stiffness runs.

One explanation for the rise to the second plateau is that the probe is becoming fully coupled to the basilar membrane over the rise region. To test this hypothesis a variation of the standard run was done in which the order of the static positions was randomized. Results from two consecutive measurements made at the same location are shown in Fig 2. The first run, Fig 2a, was done with randomly ordered static positions. In this case, following the 0 μm position the needle was advanced to the 8 μm position. The second run, Fig 2b, was done with ordered static positions. The two stiffness measurements are similar. However, the rise to the second plateau that occurs between the contact point and the 6 μm position in b is absent in a. These data support the explanation that the rise to the second plateau found in ordered measurements is due to probe coupling, and that the rise is absent in the random measurement because the initial 8 μm displacement fully coupled the probe to the basilar membrane.

3. Final growth. Stiffness grows out of the second plateau with a form that can be fitted with the quadratic function

$$k = k_p + A(x-x_p)^2.$$

This is the theoretical stiffness-vs-displacement relationship of a beam, where k_p is the beam's linear stiffness and x_p is the undeflected position of the beam. Both k_p and A, the coefficient of the quadratic term, depend on the dimensions, boundary conditions, and material of the beam. In Figs 1 and 2 fits of the quadratic function to the data are shown.

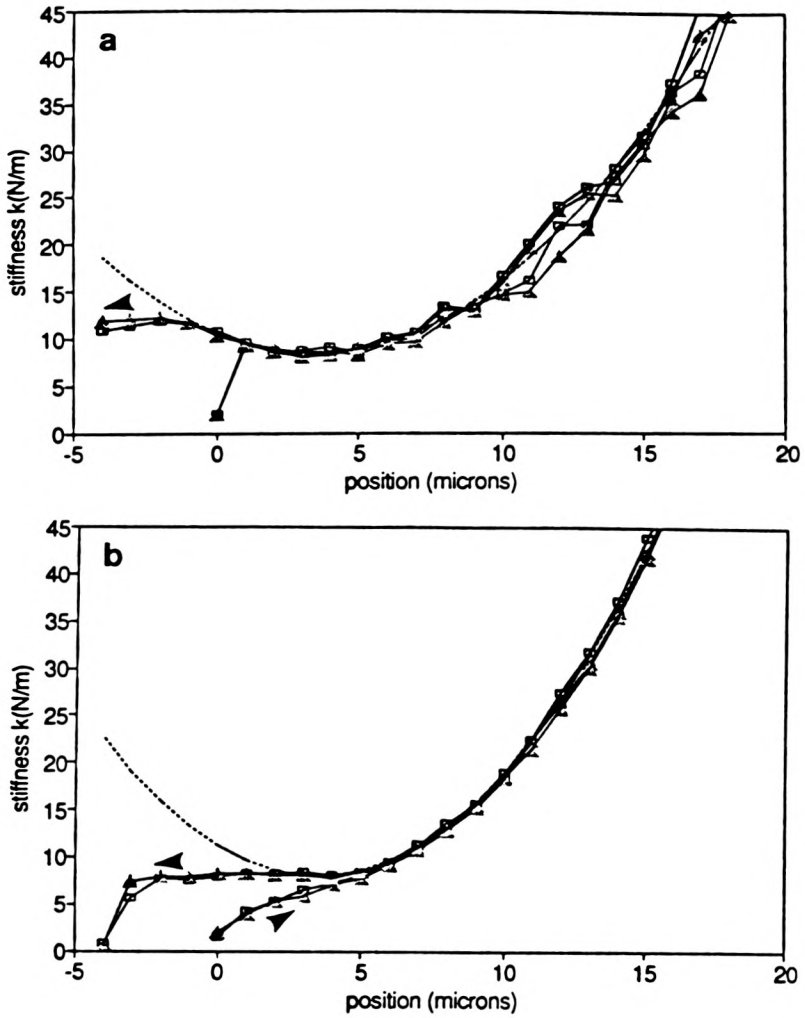

FIGURE 2 Stiffness measurements made with randomized and ordered static positions. Animal D11 runs 1 and 2. Empty squares: 5 nm excursion. Filled triangles: 25 nm excursion. Dashed line: beam theory fit. The quadratic fits to the curves are (a) $k = 8.5$ N/m + 0.18 N/m $\cdot$ μm^{-2} $(x - 3.5)^2$, (b) $k = 8.0$ N/m + 0.26 N/m $\cdot$ μm^{-2} $(x - 3.5)^2$. In the randomized run (a) the static positions were ordered as follows: 0,8,19,4,17,2,11,13, 10,6,12,20,3,7,16,14,1,18,9, 15,5, then reversed (5,15,...), and finally -1,-2,-3,-4.

4. Extension of the second plateau as the probe is retracted. In many cases the second plateau was extended to smaller static positions as the probe was retracted. In 17 runs the plateau was extended to the point that the stiffness increased.

These features were also present in measurements made within 2 hours post-mortem. In cochleas that were damaged during round window removal the stiffness was often smaller than in undamaged cochleas and the second plateau was reduced or absent.

NEGATIVE STIFFNESS

In 5 of the 18 gerbils in at least one run, only pre-mortem, the force on the needle was in phase with the excursion over some range of static postions. The magnitude was as large as 8 N/m, which is too large to attribute the in-phase force to inertial or surface tension forces. Possible sources for this "negative stiffness" are discussed below.

Discussion

COMPARISON WITH PREVIOUS MEASUREMENTS

One of the reasons for doing in vivo experiments was to look for differences in stiffness pre- and post-mortem. Our own observations of pre- versus post-mortem stiffness showed that the typical features of stiffness did not depend on the animal being alive. Therefore, we might expect the stiffness we measure to be similar to the stiffness

measured in excised cochleas. A relevant anatomical difference between gerbils and guinea pigs should be noted: most gerbil species have a relatively thick basilar membrane due to relatively large volume of acellular tissue, probably an increase in the cottony ground substance (Lay, 1972). However, the ground substance probably does not contribute to the basilar membrane point stiffness as much as other components, for example, the transverse protein filaments and possibly the organ of Corti.

Both Gummer et al and Miller reported a stiffness plateau upon contacting the basilar membrane that usually persisted over the first 2 to 3 μm of static displacement. Gummer et al's values of early plateau stiffness varied between 0.28 and 0.82 N/m. Miller's values of early plateau stiffness varied between 0.4 and 2.0 N/m. (Miller made measurements with a probe needle of diameter 10 μm. In a beam model of the basilar membrane, stiffness scales with probe diameter, so for the comparison with our data we multiply the stiffnesses she reports by 2.5. Miller made measurements across the width of the basilar membrane. We only include her measurements that were centered to within half of the basilar membrane width in this comparison.) Our initial plateau stiffness ranged from 0.2 to 1.2 N/m and had a mean length of 4.6 N/m. The magnitude of the initial stiffness plateau is similar in all three studies, and the length is slightly greater in our study.

Miller reported that the stiffness-vs-displacement relationship (which she measured over 10 μm) had three plateaus. The third plateau had a stiffness of approximately 1.4 to 12.5 N/m and persisted over roughly 3 μm. Our second plateau stiffness, which ranged from 1.4 to 20 N/m, with a mean of 9.1 N/m, is comparable to Miller's third plateau. Gummer et al did not report a plateau beyond the initial plateau, but did observe a "saturation " in stiffness increase. However, the saturation occurred at a stiffness of approximately 2 N/m, significantly smaller than the plateaus Miller and we measured.

INTERPRETATION OF DIFFERENT REGIONS OF STIFFNESS

A schematic of a cross section of the organ of Corti (Fig 3) illustrates a tentative interpretation of the different stiffness regions. The initial plateau is interpreted as the stiffness of shearable, but possible incompressible structures of the basilar membrane: underlying cells and cottony ground substance. This interpretation of the initial plateau was put forth by Miller (1985). The greater length of the initial plateau in our measurements relative to measurements in guinea pig probably reflects the greater thickness of the basilar membrane in gerbil.

The structures that produce the second plateau are not known. It is possible that the second plateau is the linear stiffness region of the beam-like transverse protein fibers of the basilar membrane. However, we cannot rule out a significant contribution to the stiffness from the organ of Corti. Miller's measurements indicated that the arches of Corti contributed to the stiffness. From light microscopic studies of an excised cochlea 4 hours post-mortem Miller reported that hair cells and Deiters' and Claudius' cells were no longer intact. In one of our experiments, which exhibited typical stiffness values, the CAP response to high frequency tones was not greatly reduced following two stiffness runs. This suggests that the hair and supporting cells are probably relatively intact in our experiments. Therefore, in Fig 3b,c and d we speculatively include a contribution to the second plateau stiffness from hair cells, specifically from the stereocilia/tectorial membrane interface. This inclusion can be justified by a rough calculation based on measurements of hair bundle stiffness made by Howard and Hudspeth (1988). They measured the stiffness of stereocilia bundles of bullfrog saccular hair cells by deflecting the bundle perpendicular to its axis with a glass fiber attached to the kinociliary bulb at the bundle's tip. Their measurements indicated that the stiffness due to the stereociliary pivots of a bundle was approximately 0.44 mN/m. To compare this stiffness with the

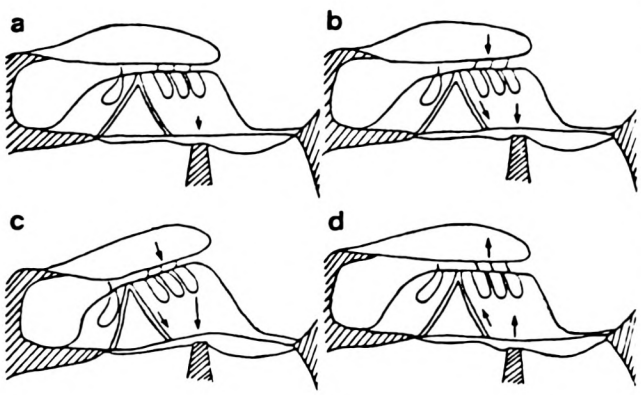

FIGURE 3 Speculative anatomical basis for different regions of stiffness. Arrows designate return forces. (a) Initial plateau. Return force is due to soft structures of the basilar membrane. (b) Second plateau. Probe is fully coupled to the basilar membrane. Return force is due to structural elements (transverse filaments) of the basilar membrane with probable contributions from organ of Corti structures. (c) Final quadratic growth. The return force is dominated by the beam-like transverse filaments of the basilar membrane, distorted beyond their range of constant stiffness. (d) Extension of second plateau as probe is retracted. Probe is stuck to the basilar membrane and pulling on structures that contribute to the second plateau.

stiffness we measure methodological as well as anatomical differences must be taken into account. To begin with methodological differences: we deflect the basilar membrane, not the stereociliary bundles. However, a given displacement of the basilar membrane is expected to produce a similarly sized shearing motion between the hair cells and the tectorial membrane so to a first approximation this difference requires no correction. A second difference in method is that our 25 μm diameter needle would contact an area containing at least three columns of outer hair cells, each containing three rows. This increases the expected bundle stiffness by approximately a factor of 10. Anatomical differences introduce larger corrections. The bundle height in the saccular hair cells was reported as 6.7 μm. In comparison the height of a basal outer hair cell's bundle is expected to be only 0.5 μm. (Lim, 1980). The bundle stiffness (measured as force per displacement of bundle tip), if it is due to a pivotal stiffness at the bundle's base, decreases as the bundle length squared. Therefore, the shorter outer hair cell bundle length produces a bundle stiffness that is greater than the saccular hair cell bundle stiffness by a factor of 100. These methodological and anatomical factors multiply to give a predicted factor of 1000 increase in stiffness in our measurements relative to the saccular hair cell measurements. Thus, we might expect to measure a stereociliary contribution to stiffness of at least 0.44 N/m. A second anatomical difference is also expected to increase the relative stiffness of the outer hair cell bundle. This is the "W" shape of the bundle, which would increase its resistance to shear. If the effect of the "W" formation increases the stiffness by a factor of 10, the stiffness of the stereocilia/tectorial membrane interface is 4.4 N/m, large enough to provide a significant contribution to our second plateau stiffness. Similar arguments applied to Strelioff and Flock's (1984) measurements of the stiffness of the stereocilia of cochlear hair cells also predict a stereociliary contribution to stiffness of this magnitude.

The quadratic growth in stiffness beyond the second plateau is the stiffness growth predicted for a beam-like structure. Because of the beam-like structure of the transverse protein filaments, this region is interpreted as the stiffness of the filaments deflected beyond their region of constant stiffness.

The extension of the second plateau as the probe is retracted, and the frequent increase in stiffness beyond a certain retracted position, is likely due to the probe being stuck to the basilar membrane.

A negative stiffness is expected to be measured at any static position at which the slope of the force-vs-displacement curve is negative. A negatively sloped region of the curve could arise from a stiff element that is attached to a gate: at some degree of displacement the gate opens, and the return force, instead of increasing with increasing displacement, decreases. A gated stiffness was hypothesized to exist in the stereociliary bundle of bullfrog saccular hair cells by Howard and Hudspeth (1988). The estimation of outer hair cell stereocilia stiffness given above supports this possibility. Negative stiffness might also be produced by voltage dependent length changes in outer hair cells (Brownell et al, 1985) or by pressure induced length changes in outer hair cells (Brundlin et al, 1990). However, the stiffness of outer hair cells, which Holly and Ashmore (1988) measured as 0.5 mN/m, makes these less reasonable candidates for the relatively large negative stiffnesses we have measured.

Summary

Our measurements, made in the base of the gerbil cochlea, indicate that structural components of the basilar membrane and organ of Corti have a point stiffness, represented in the second stiffness plateau, of approximately 9 N/m. The extent and magnitude of the initial stiffness plateau suggest that this plateau is due to soft structures of the basilar membrane that are shearable, but might be incompressible under pressure loading. Then the second plateau is the relevant stiffness for cochlear mechanics. We did not find differences in the stiffness pre-mortem vs early post-mortem, and the initial and second stiffness plateaus we found were similar to plateaus Miller found in measurements on excised cochlea of guinea pig. The only feature that was never found post-mortem was the occasional measurement of what might be a negative stiffness.

References

Brownell, W.E., Bader, C.R., Bertrand, D. and de Ribaupierre, Y. (1985) "Evoked mechanical responses of cochlear outer hair cells." Science 227: 194-196.

Brundlin, L., Flock, A. and Canlon, B. (1990) "Sound induced motility of cochlear outer hair cells shows tuning." Abstracts of the 13th Midwinter Research Meeting of the Association for Research in Otolaryngology. No. 260. (Ed. Lim, D.J.)

Gummer, A.W., Johnstone, B.M. and Armstrong, N.J. (1981) "Direct measurements of basilar membrane stiffness in the guinea pig." J. Acoust. Soc. Am. 70(5): 1298-1309.

Holly, M.C. amd Ashmore, J.F. (1988) "A cytoskeletal spring in cochlear outer hair cells." Nature 335: 635-637.

Howard, J. and Hudspeth, A.J. (1988) "Compliance of the hair bundle associated with gating of the mechanoelectric transduction channels in the bullfrog's saccular hair cell." Neuron 1: 189-199.

Iurato, S. (1962) "Functional implications of the nature and submicroscopic structure of the tectorial and basilar membranes." J. Acoust. Soc. Am. 34: 1386-1395.

Lay, D.M. (1972) "The anatomy, physiology, functional significance and evolution of specialized hearing organs of gerbilline rodents." J. Morph. 138: 41-120.

Lim, D.J. (1980) "Cochlear anatomy related to cochlear micromechanics. A review." J. Acoust. Soc. Am. 67(5): 1686-1695.

Miller, C.E. (1983) "Structural implications of basilar membrane compliance measurments." J. Acoust. Soc. Am. 77(4): 1465-1474.

Plassman, W., Peetz, W. and Schmidt, M. (1987) "The cochlea in gerbilline rodents." Brain Behav. Evol. 30: 82-102.

Strelioff, D. and Flock, A. (1984) "Stiffness of sensory-cell hair bundles in the isolated guinea pig cochlea." Hear. Res. 15:19-28.

Voldrich, L. (1978) "Mechanical properties of the basilar membrane." Acta Oto-Laryngol. 86: 331-335.

TWO-TONE DISTORTION PRODUCTS IN THE BASILAR MEMBRANE OF THE CHINCHILLA COCHLEA

Luis Robles*, Mario A. Ruggero and Nola C. Rich

Department of Otolaryngology,
University of Minnesota, Research East,
Minneapolis, MN 55414, U.S.A.
**on leave from Departamento de Fisiología y Biofísica,*
Facultad de Medicina, Universidad de Chile,
Santiago, Chile

Introduction

It has been known since the early 18th. century that distortion products (DPs) exist in the auditory sensation evoked by pairs of tones [Jones, 1935]. Such DPs, also known as combination tones, can be heard at frequencies that are combinations of the primary frequencies, such as f_2-f_1, $(n+1)f_1$-nf_2 and $(n+1)f_2$-nf_1, where f_1 and f_2 are the primary frequencies ($f_2 > f_1$, n = 1,2,3...). The most prominent and the best studied DPs are those with frequencies lower than those of the primary tones, particularly the "cubic difference tone" with frequency equal to $2f_1$-f_2 [Zwicker, 1955; Goldstein, 1967; Smoorenburg, 1972], but DPs at frequencies greater than those of the primary tones (i.e., at $2f_2$-f_1 and f_2+f_1) have also been reported [Zurek and Sachs, 1979]. Psychophysical studies on the frequency dependence of the $2f_1$-f_2 distortion component suggested that this DP is generated in a mechanical nonlinearity located at the basilar membrane (BM) or in a structure closely coupled to it [Goldstein, 1967; Smoorenburg, 1972]. This was supported by recordings of cochlear microphonics [Gibian and Kim, 1982] and of responses of auditory-nerve fibers [Goldstein and Kiang, 1968; Buunen and Rhode, 1978; Kim et al., 1980; Siegel et al., 1982], cochlear-nucleus neurons [Smoorenburg et al., 1976] and inner hair cells [Nuttall and Dolan, 1990], showing DPs at levels consistent with psychophysical data. Since the middle ear responds linearly to sound [Guinan and Peake, 1967; Ruggero et al., 1990] and since neural responses to DPs can be abolished by hair cell damage at cochlear sites preferentially tuned to the frequencies of the primary tones [Siegel et al., 1982], it was concluded that DPs are generated at these sites and propagate mechanically along the cochlea to the basilar membrane location tuned to the DP frequency [Kim et al., 1980; Siegel et al., 1982]. Additional support for this notion came from the discovery of the presence of DP otoacoustic emissions at the external auditory meatus of animals and humans upon stimulation of the ear with tone pairs [Kemp, 1979; Kim et al., 1980;

Mountain, 1980]. However, in spite of so much indirect evidence that DPs must be present in the mechanical response of the cochlear partition, and in spite of the demonstration that other strong nonlinearities do exist in the mechanical response of the basilar membrane even at moderate stimulus intensities [Rhode, 1971; Robles et al., 1976; Sellick et al., 1982; Patuzzi et al., 1984; Robles et al., 1986 a and b and 1989], until now efforts to find DPs in BM motion have failed [Wilson and Johnstone, 1973; Rhode, 1977], but for a single apparent exception [Nuttall et al., 1989]. We report here results obtained with a new laser-velocimetry technique [Nuttall et al., 1989 and 1990; Ruggero and Rich, 1990a] showing that two-tone DPs are indeed present in BM motion at low and moderate levels of stimulation.

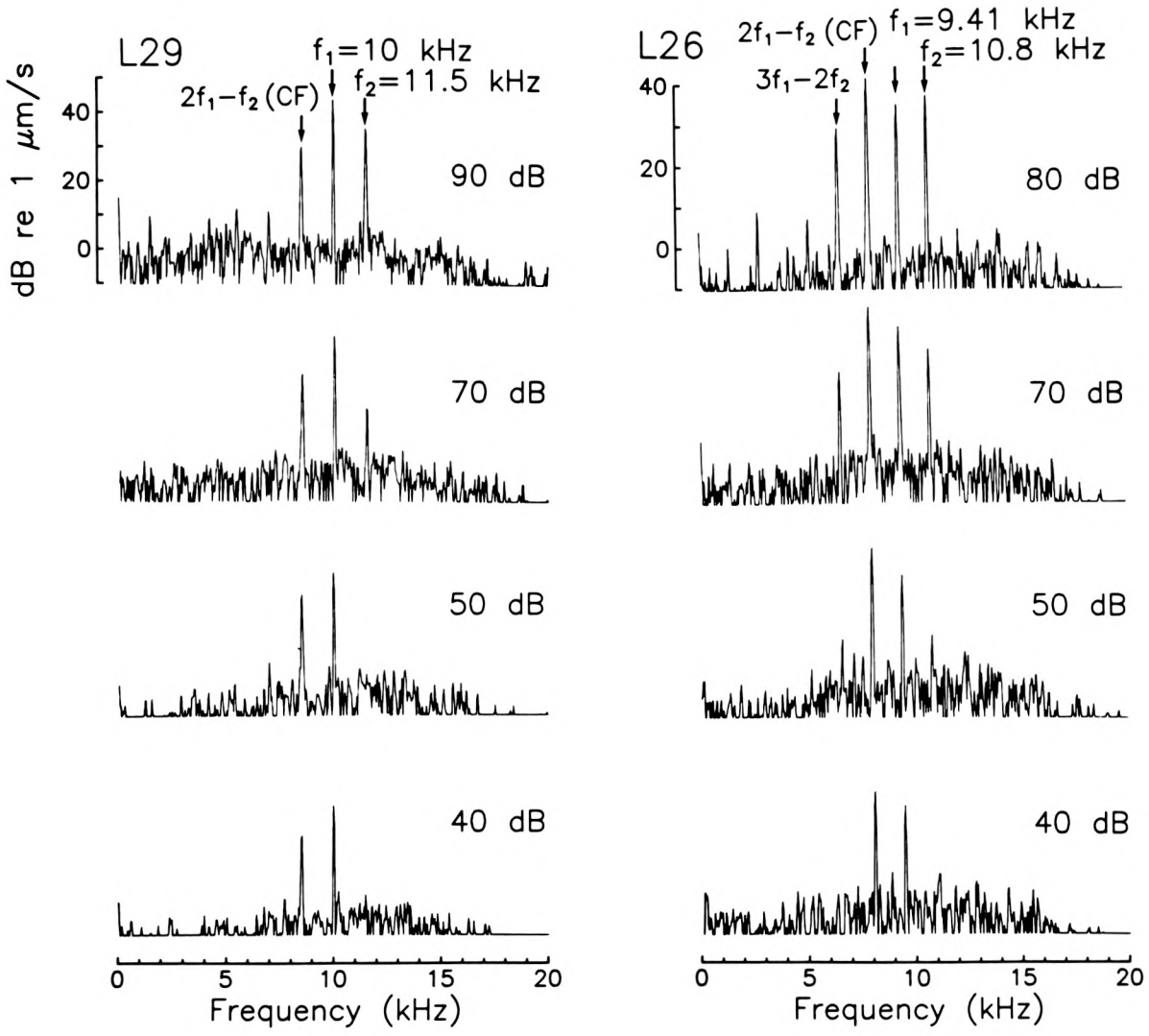

FIGURE 1 Frequency spectra of responses of basilar membranes L29 (left) and L26 (right) to two-tone stimuli, measured using laser velocimetry at the basal turn of the cochlea. Spectra were obtained by Fourier transformation of responses to equal-level tones (40-90 dB SPL) with frequencies chosen such that $2f_1$-f_2 corresponded to the characteristic frequency (8.5 kHz in L29 and 8 kHz in L26) of the basilar membrane location under measurement. The spectra show, in addition to peaks at the primary frequencies (f_1 and f_2), a prominent distortion peak at $2f_1$-f_2 in both animals, as well as at $3f_1$-$2f_2$ in L26. Note the disappearance of the response at frequency f_2 at the lowest stimulus levels.

Methods

Experiments were performed in chinchillas anesthetized with sodium pentobarbital. The velocity of the BM was determined by means of a laser velocimeter coupled to a compound microscope (Ruggero and Rich, 1990a): velocity was derived from the Doppler frequency shift of light reflected from glass microbeads (10-30 um diameter) previously dropped on the basal BM. Stimuli were presented through acoustically-coupled Beyer DT-48 earphones. The voltage output of the laser velocimeter was frequency filtered with a pass band of 2-15000 Hz before analog-to-digital conversion under computer control. Velocity responses were averaged over 1024 stimulus repetitions and Fourier transformed to obtain frequency spectra.

Results

Figure 1 displays frequency spectra computed by Fourier transformation of averaged responses of two BMs (L29, left, and L26, right) to two equal-level tones

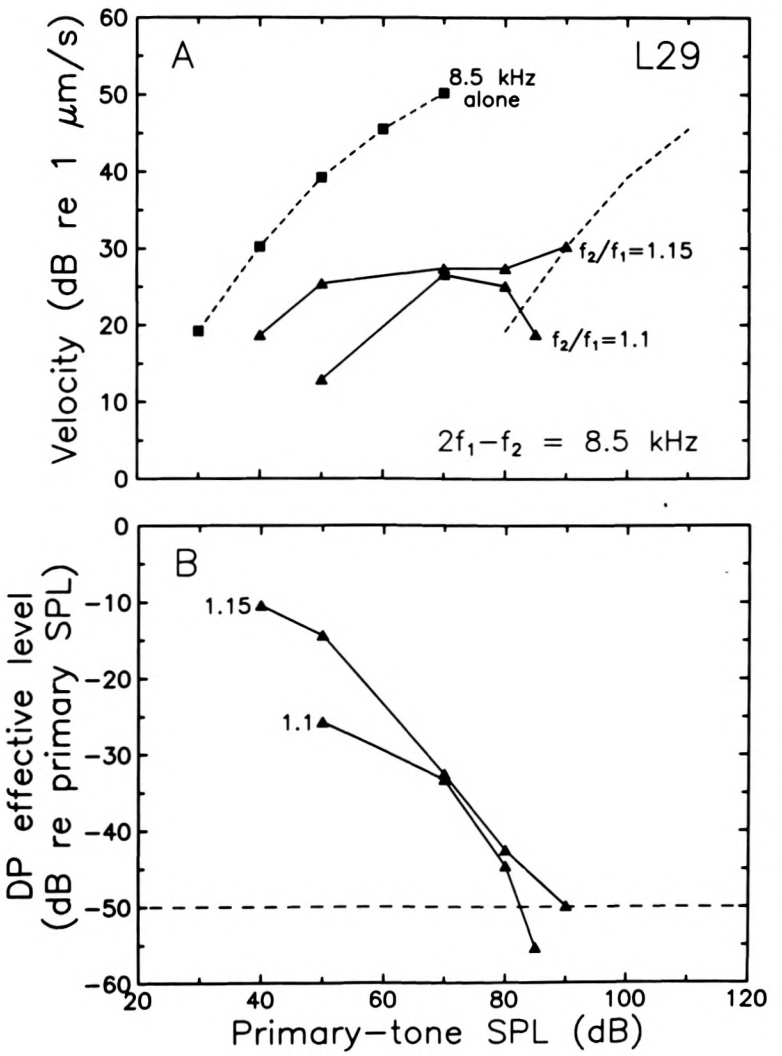

FIGURE 2 Velocity magnitude of the $2f_1$-f_2 distortion product (DP) as a function of primary-tone SPL (solid lines), measured in chinchilla L29. The primary-tone frequencies were chosen such that $2f_1$-f_2 coincided with CF (8.5 kHz). Data for the DP evoked by primary tones with a frequency ratio (f_2/f_1) of 1.15 are from the spectra in Fig. 1 (left). A) Squares represent the input-output velocity curve for a single tone at the DP frequency. The dashed line indicates the maximal levels of artifactual distortion products in the acoustical and measuring systems. B) DP data plotted as effective levels: i.e., as intensities of a single tone at the DP frequency required to evoke responses of the same magnitude as the DPs produced by the two-tone stimuli. Effective levels are expressed in dB relative to stimulus SPL.

presented at 40-90 dB SPL. The frequencies of the primary tones were chosen such that $2f_1$-f_2 equaled characteristic frequency (CF: the most sensitive frequency) for the cochlear location under measurement, as determined from responses to single tones. The spectra in Fig. 1 show, in addition to peaks at the primary-tone frequencies (f_1 and f_2), a large distortion peak at $2f_1$-f_2. The magnitude of this DP changed nonlinearly as a function of stimulus level: in L29 its peak level grew by only 12 dB for a 50 dB increase in the level of the primaries, while in L26 the growth was 9 dB for a 40 dB stimulus increase. In contrast, the responses to the higher-frequency primary tone (f_2) changed linearly with stimulus level in both animals; for primary tones at 40 and 50 dB SPL in L29 and 40 dB SPL in L26, the response to f_2 disappeared below the noise floor of the measuring system, while the $2f_1$-f_2 DP still exceeded the noise floor by more than 20 dB. Note that in L26 the responses at $2f_1$-f_2 were larger than the responses to either primary tone at all stimulus levels and, in addition, there was a prominent spectral peak at $3f_1$-$2f_2$.

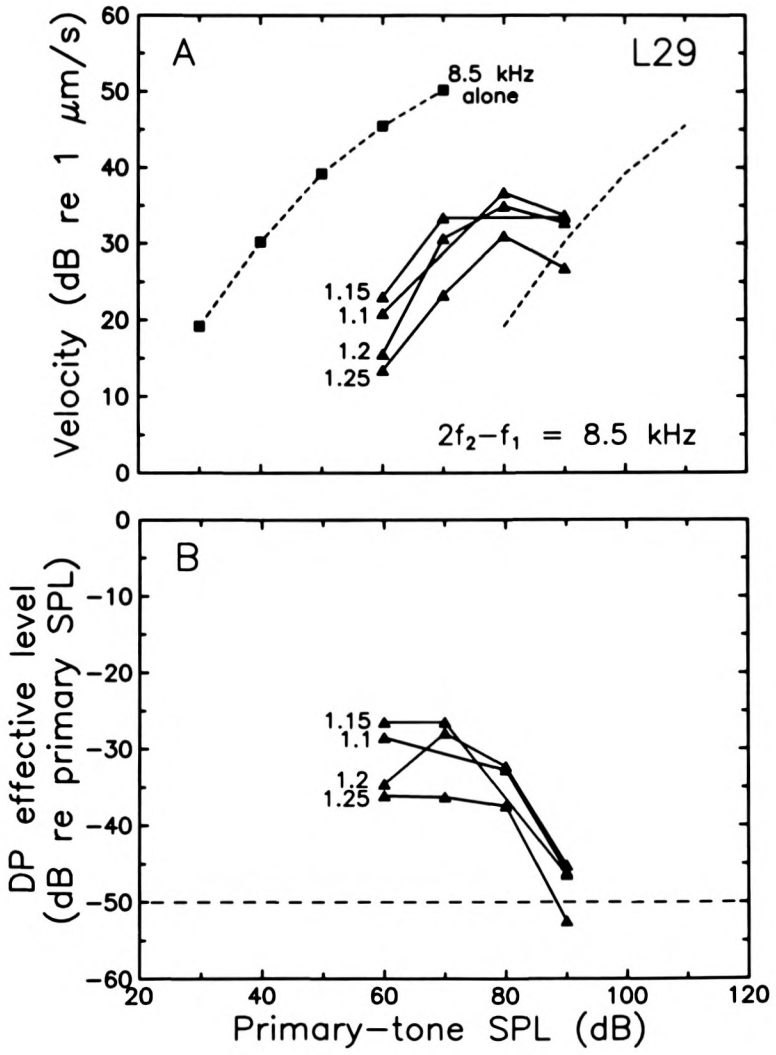

FIGURE 3 Velocity magnitude and effective level of the $2f_2$-f_1 distortion product as a function of primary-tone intensity. Same basilar membrane (L29) as in Figs. 1 and 2. All conventions as in Fig. 2.

Figures 2(A) and 3(A) illustrate the velocity magnitude (solid lines) of $2f_1$-f_2 and $2f_2$-f_1 DPs, respectively, measured in chinchilla L29 as a function of level of the primary tones. The primary-tone frequencies were chosen such that $2f_1$-f_2 (Fig. 2) or $2f_2$-f_1 (Fig. 3) corresponded to CF (8.5 kHz). The top panels also show the level dependence of responses to a single tone at the DP frequency (CF). Using this curve, "effective levels" of the DPs were computed as the intensities of single tones at the DP frequency required to elicit responses of the same magnitude as the DPs produced by two-tone stimuli. Effective levels of these DPs are plotted in Fig. 2(B) and 3(B) as dB relative to primary-tone SPL. Velocity amplitudes for the $2f_1$-f_2 DP [Fig. 2(A)] and the $2f_2$-f_1 DP [Fig. 3(A)] in most cases grew with primary-tone level up to 70-80 dB SPL, reaching a plateau or decreasing in magnitude with further increases in stimulus levels. The DP effective levels (relative to primary-tone SPLs) were largest at moderately low stimulus levels [Figs. 2(B) and 3(B)] and decreased monotonically as stimulus level increased.

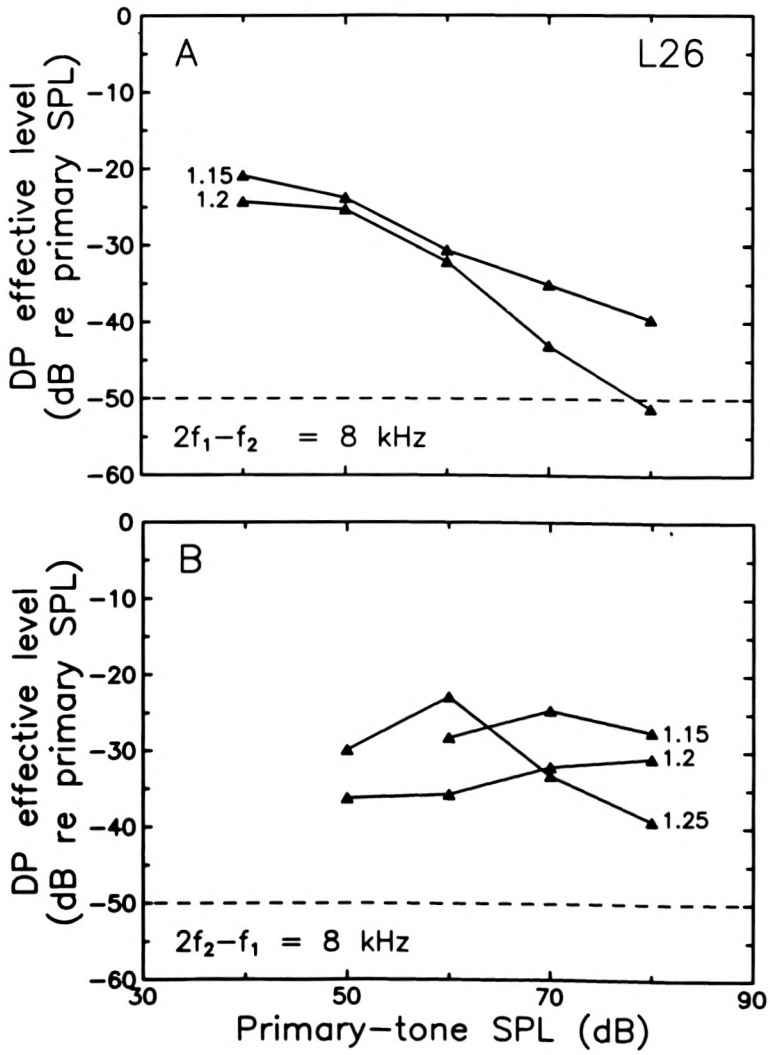

FIGURE 4 Effective level of the $2f_1$-f_2 (A) and $2f_2$-f_1 (B) distortion products in chinchilla L26 (expressed as dB re stimulus level), plotted as a function of primary-tone intensity. Data for the $2f_1$-f_2 DP evoked by primary tones with a frequency ratio (f_2/f_1) of 1.15 are from the spectra in Fig. 1 (right).

Effective levels of the $2f_1$-f_2 and $2f_2$-f_1 DPs in chinchilla L26 are shown in Fig. 4, expressed in dB relative to stimulus SPL. While the results for the $2f_1$-f_2 DP in L26 were similar to those from L29 (Fig. 2), the $2f_2$-f_1 DPs in L26 [Fig. 4(b)] were exceptional in that their effective levels did not diminish systematically as a function of increasing stimulus level. In six cochleae, DP effective levels (re primary-tone SPL) were as large as -11 dB for $2f_1$-f_2 and -24 dB for $2f_2$-f_1 at low and moderate stimulus levels. As stimulus level increased, the DP effective level usually decreased monotonically, the decrease being steepest for stimulus levels above 70-80 dB SPL. In most cases, at about 90 dB SPL the DP level became so low that it could be attributed to distortion generated in the stimulus or measuring systems (dashed lines, no symbols, Figs. 2-4).

Discussion

The prominent DPs that we have measured in the chinchilla BM undoubtedly originated in the cochlea: careful controls showed the DPs generated in the acoustical and measuring systems to be at least 50 dB below the level of the primary tones (see Figs. 2-4) and the response of the middle ear is linear even at stimulus levels higher than used here [Guinan and Peake, 1967; Ruggero et al., 1990]. In general, the characteristics of the $2f_1$-f_2 and $2f_2$-f_1 BM DPs were quite similar. The highest DP effective levels were almost always produced at the lowest stimulus intensities, and there usually was a decrease in DP level with increasing stimulus intensity. At low primary-tone intensities, $2f_1$-f_2 DPs often reached higher effective levels than $2f_2$-f_1 DPs. The levels of these $2f_1$-f_2 DPs in the BM are comparable to those found in responses of the cat's auditory nerve [Goldstein and Kiang, 1968; Buunen and Rhode, 1978] and cochlear nucleus [Smoorenburg et al., 1976], and in psychoacoustical studies in humans [Zwicker, 1955; Goldstein, 1967; Smoorenburg, 1972].

Our results are not conclusive in determining whether DPs are generated in the BM at cochlear locations with CFs equal to the primary-tone frequencies and subsequently propagate to the cochlear region with CF equal to the DP frequency. Nevertheless, the results of Fig. 1 support this idea: robust $2f_1$-f_2 DPs existed even when responses to the higher primary tone (f_2) were undetectable. Moreover, while the DP responses grew nonlinearly, the responses to the f_2 primary tone were quite linear. Since two-tone DPs are likely to be generated at BM locations where responses to the primary tones are highly nonlinear (i.e., at sites with CFs approximately equal to the primary frequencies), these results strongly suggest that the $2f_1$-f_2 DPs originated at a BM site basal to the place of measurement and subsequently propagated apically in the cochlea.

That DPs are present in the BM mechanical response to tone pairs, as shown here, is consistent with the existence of other BM nonlinearities, including the compressive growth of responses to tones and clicks [Rhode, 1971; Robles et al., 1976; Sellick et al., 1982; Robles et al., 1986 a and b; Ruggero and Rich, 1990a] and two-tone suppression [Patuzzi et al., 1984; Robles et al., 1986b and 1989]. The fact that two-tone DPs could not be previously demonstrated in BM responses is probably due to inadequate measuring methodology. In particular, the Mössbauer technique, which

has provided almost the entire experimental body of evidence on BM mechanical nonlinearities, is not well suited to the measurement of responses to complex stimuli, due to its own nonlinear characteristics. Thus, it is mainly as a result of the development of an essentially linear technique (laser velocimetry applied to cochlear measurements; Nuttall et al., 1989 and 1990; Ruggero and Rich, 1990a) that we have finally demonstrated that some of the most prominent two-tone DPs reported in psychophysical studies arise in the BM. In fact, these results - together with recent data on BM mechanical correlates of other two-tone interactions [Patuzzi et al., 1984; Robles et al., 1986b and 1989] - suggest that all strongly frequency-dependent nonlinear auditory phenomena originate in the mechanical response of the BM. Such nonlinearities may be produced by a mechanical action of the outer hair cells upon the BM [Patuzzi et al., 1989; Hubbard and Mountain, 1990; Ruggero and Rich, 1990b].

Acknowledgments

This work was supported by NIH (NIDCD) grants DC-00110 and DC-00419 and by smaller grants from the Minnesota Medical Foundation and the Lions 5M Hearing Research Endowment.

References

Buunen, T.J.F. and Rhode, W.S. (1978) Responses of fibers in the cat's auditory nerve to the cubic difference tone. J. Acoust Soc. Am. 64, 772-781.

Gibian, G.L. and Kim, D.O. (1982) Cochlear microphonic evidence for mechanical propagation of distortion products (f_2-f_1) and ($2f_1$-f_2). Hear. Res. 6, 35-59.

Goldstein, J.L. (1967) Auditory nonlinearity. J. Acoust. Soc. Am. 41, 676-689.

Goldstein, J.L. and Kiang, N.Y.S. (1968) Neural correlates of the aural combination tone $2f_1$-f_2. Proc. IEEE 56, 981-992.

Guinan, J.J., Jr. and Peake, W.T. (1967) Middle-ear characteristics of anesthetized cats. J. Acoust. Soc. Am. 41,1237-1261.

Hubbard, A.E. and Mountain, D.C. (1990) Haircell forward and reverse transduction: Differential suppression and enhancement. Hear. Res. 43, 269-272.

Jones, A.T. (1935) The discovery of difference tones. Amer. Phys. Teacher 3, 49-51.

Kim, D.O., Molnar, C.C. and Matthews, J.W. (1980) Cochlear mechanics: nonlinear behavior in two-tone responses as reflected in cochlear-nerve-fiber responses and in ear-canal sound pressure. J. Acoust. Soc. Am. 67, 1704-1721.

Mountain, D.C. (1980) Changes in endolymphatic potential and crossed olivocochlear bundle stimulation alter cochlear mechanics. Science 210, 71-72.

Nuttall, A.L. and Dolan, D.F. (1990) Inner hair cell responses to the $2f_1$-f_2 intermodulation product. J. Acoust. Soc. Am. 87, 782-790.

Nuttall, A.L., Dolan, D.F. and Avinash, G. (1989) Laser Doppler vibrometer measurements of basilar membrane motion in the guinea pig. Soc. for Neurosci. Abst. 15, 209.

Nuttall, A.L., Dolan, D.F.and Avinash, G. (1990) Laser Doppler velocimetry of basilar membrane vibrations. Hear. Res. (submitted).

Patuzzi, R., Sellick, P.M. and Johnstone, B.M. (1984) The modulation of the sensitivity of the mammalian cochlea by low frequency tones. III. Basilar membrane motion. Hear. Res. 13, 19-27.

Patuzzi, R., Yates, G.K. and Johnstone, B.M. (1989) Outer hair cell receptor current and sensorineural hearing loss. Hear. Res. 42, 47-72.

Rhode, W.S. (1971) Observations of the vibration of the basilar membrane in squirrel monkeys using the Mössbauer technique. J. Acoust. Soc. Am. 49, 1218-1231.

Rhode, W.S. (1977) Some observations on two-tone interaction measured with the Mössbauer effect. In: Psychophysics and Physiology of Hearing, (Eds: Evans, E.F. and Wilson, J.P.) Academic Press, London, pp. 27-38.

Robles, L., Rhode, W.S. and Geisler, C.D. (1976) Transient response of the basilar membrane measured in squirrel monkeys using the Mössbauer effect. J. Acoust. Soc. Am. 59, 926-939.

Robles, L., Ruggero, M.A. and Rich, N.C. (1986a) Basilar membrane mechanics at the base of the chin-

chilla cochlea. I. Input-output functions, tuning curves, and response phases. J. Acoust. Soc. Am. 80, 1364-1374.

Robles, L., Ruggero, M.A. and Rich, N.C. (1986b) Mössbauer measurements of the mechanical response to single-tone and two-tone stimuli at the base of the chinchilla cochlea. In: Peripheral Auditory Mechanisms (Eds: Allen, J.B., Hall, J.L., Hubbard, A., Neely, S.T. and Tubis, A.) Springer, Berlin, pp. 121-128.

Robles, L., Ruggero, M.A. and Rich, N.C. (1989) Nonlinear interactions in the mechanical response of the cochlea to two-tone stimuli. In: Cochlear Mechanisms. Structure, Function and Models (Eds: Wilson, J.P. and Kemp, D.T.) Plenum Press, pp. 369-375.

Ruggero, M.A. and Rich, N.C. (1990a) Application of a commercially-manufactured Doppler-shift laser velocimeter to the measurement of basilar-membrane vibration. Hear. Res., in press.

Ruggero, M.A. and Rich, N.C. (1990b) Systemic injection of furosemide alters the mechanical response to sound of the basilar membrane. (In: this volume).

Ruggero, M.A., Rich, N.C., Robles, L. and Shivapuja, B.G. (1990) Middle-ear response in the chinchilla and its relationship to mechanics at the base of the cochlea. J. Acoust. Soc. Am. 87, 1612-1629.

Sellick, P.M., Patuzzi, R. and Johnstone, B.M. (1982) Measurement of basilar membrane motion in the guinea pig using the Mössbauer technique. J. Acoust. Soc. Am. 72, 131-141.

Siegel, J.H., Kim, D.O. and Molnar, C.E. (1982) Effects of altering organ of Corti on cochlear distortion products f_2-f_1 and $2f_1$-f_2. J. Neurophysiol. 47, 303-328.

Smoorenburg, G.F. (1972) Combination tones and their origin. J. Acoust. Soc. Am. 52, 615-632.

Smoorenburg, G.F., Gibson, M.M., Kitzes, L.M., Rose J.E. and Hind, J.E. (1976) Correlates of combination tones observed in the response of neurons in the anteroventral cochlear nucleus of the cat. J. Acoust. Soc. Am. 59, 945-962.

Wilson, J.P. and Johnstone, J.R. (1973) Basilar membrane correlates of the combination tone $2f_1$-f_2. Nature 241, 206-207.

Zurek, P.M. and Sachs, R.M. (1979) Combination tones at frequencies greater than the primary tones. Science 205, 60-602.

Zwicker, E. (1955) Der ungewohnliche Amplitudengang der nichtlinearen Verzerrungen des Ohres. Acustica 5, 67-74.

Comments and discussion

Lyon

You have attempted to maximize sensitivity to the $2f_1$-f_2 DP by placing it at the CF (determined by single tones) of the cochlear location under measurement. But nonlinear travelling-wave models predict that the primaries (above CF in this configuration) will cause a downward shift of the frequency of maximal sensitivity to as much as a half octave below CF. When you instead placed the high-side ($2f_2$-f_1) DP at CF, the low-side ($2f_1$-f_2) DP at 0.75 CF was found at an absolute level as much as 20 dB above other DPs you observed.

Do you have any comments on this large DP well below CF, or an alternate interpretation ?

Is this shift possibly the reason that the DP was not found with your earlier Mössbauer technique ?

Figure for Lyon's question to Robles

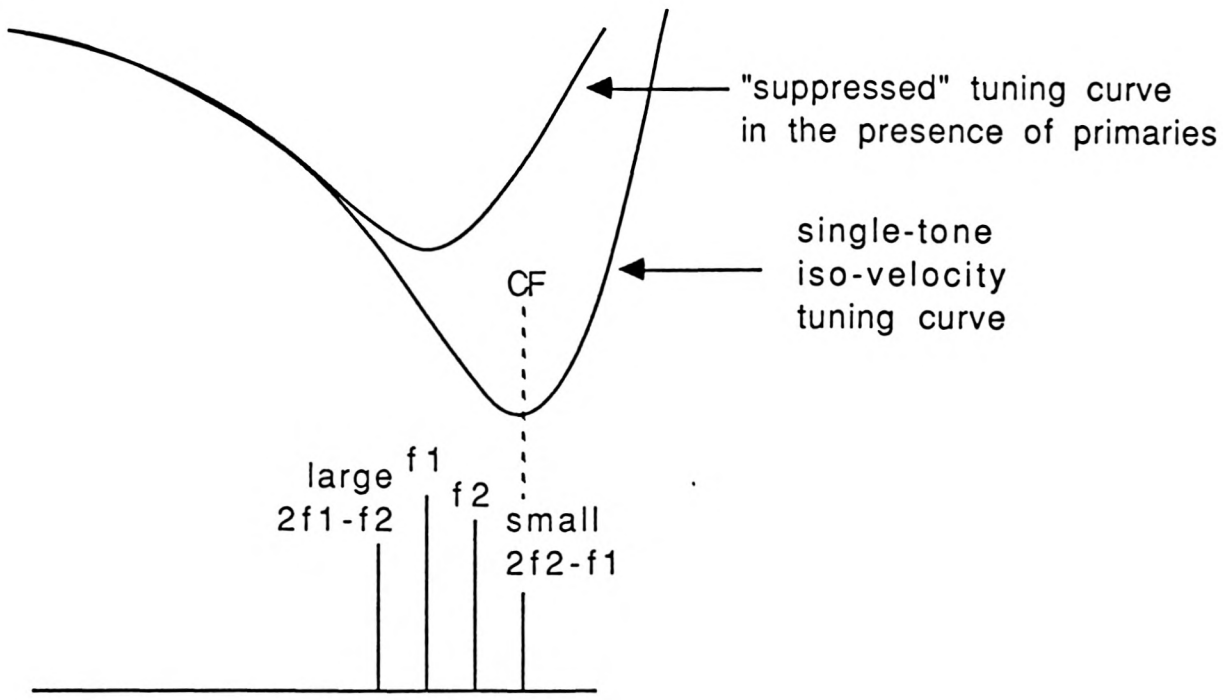

Comments and discussion

Robles

We agree with your suggestion that DP levels may be influenced by possible basilar-membrane tuning alterations caused by suppression. Indeed, we have demonstrated that mechanical tuning changes, including a downward shift of the frequency of maximal sensitivity, do occur in the presence of a suppressor (Rich et al., 1990); such changes are similar to those induced by furosemide injection (see Fig. 3, Ruggero and Rich, this volume).

Regarding the first question: we think you somewhat misinterpreted one of the slides in the oral presentation of this paper (not show in this publication). The $2f_1$-f_2 DP absolute level did not exceed the $2f_2$-f_1 DP level by 10 dB. In the experiment to which you refer (L17), with $2f_2$-f_1 at CF and $2f_1$-f_2 at 0.75 CF, the $2f_1$-f_2 DP absolute level actually exceeded that of the $2f_2$-f_1 DP by only 5 dB at primary levels of 80 dB; at other stimulus intensities the $2f_1$-f_2 DP was, in fact, 5-14 dB smaller than the $2f_2$-f_1 DP. The result at 80 dB SPL, with the $2f_1$-f_2 DP being larger than the $2f_2$-f_1 DP, could be explained by a shift of the tuning curve toward lower frequencies at high stimulus levels (i.e., for high isoresponse criteria) or by greater suppression at the original CF (i.e., $2f_2$-f_1) than at other frequencies (e.g., $2f_1$-f_2) as you suggest.

As to the second question: we think that the main reason why DPs were not demonstrated using the Mössbauer technique is the difficulty in measuring responses to multitonal stimuli with that technique.

Reference

Rich, N.C., Robles, L., and Ruggero, M.A. (1990). Two-tone suppression in the basilar membrane of the chinchilla (in preparation).

SYSTEMIC INJECTION OF FUROSEMIDE ALTERS THE MECHANICAL RESPONSE TO SOUND OF THE BASILAR MEMBRANE

Mario A. Ruggero and Nola C. Rich

Department of Otolaryngology,
University of Minnesota, 2630 University Ave. S.E.,
Minneapolis, MN 55414, U. S. A.

Introduction

A widely-held view of mammalian cochlear function is that the basilar membrane and the outer hair cells sustain a bidirectional (feedback) relationship, such that basilar membrane vibrations induce receptor potentials in outer hair cells which, in turn, boost the mechanical response of the basilar membrane at low sound levels in a frequency-selective manner [e.g., Kemp, 1978; Kim et al., 1980; Weiss, 1982; Davis, 1983; for recent review, see Dallos, 1988]. Most evidence for this hypothesis is not based on recordings of basilar membrane responses, but rather on the study of the effects of cochlear manipulations, including stimulation of the efferent system and destruction of hair cells, upon the responses to sound of cochlear afferents [e.g., Kim et al., 1980; Wiederhold and Kiang, 1970; Dallos and Harris, 1978; Liberman and Dodds, 1984; Kiang et al., 1986] and inner hair cells [Brown et al., 1983], and upon otoacoustic emissions [Anderson and Kemp, 1979; Mountain, 1980; Siegel and Kim, 1982; Hubbard and Mountain, 1983; Guinan, 1986; Mountain and Hubbard, 1989]. The discovery of *in vitro* motility of isolated outer hair cells provides additional circumstantial evidence [e.g., Brownell et àl., 1985; Ashmore, 1987]. The only *direct* support for the hypothesis (i.e., involving measurements of basilar membrane responses) has come from the observations that surgical manipulations that are necessary for recording basilar membrane vibrations frequently lead to cochlear dysfunction [Khanna and Leonard, 1982] and that, when such manipulations leave the cochlea initially relatively intact, deterioration of mechanical responses can be induced by acoustic trauma [Patuzzi et al., 1984] and also occurs with the passage of time and/or death [Rhode, 1973; Sellick et al., 1982; Robles et al., 1986]. However, while consistent with the view that the state of the organ of Corti influences the mechanical behavior of the basilar membrane, these observations fail to identify the relevant cellular elements because they are based on cochlear insults that are nonspecific and irreversible.

Here we present evidence that it is the outer hair cells which are responsible for linking cellular activity to the mechanical response of the basilar membrane. Our

approach consisted of studying the effect upon the basilar membrane's response to sound of a specific and reversible manipulation of the cochlea, namely furosemide-induced reduction of the endocochlear potential [Chodynicki and Kostrzewska, 1974; Brusilow, 1976; for review, see Rybak, 1982] and hair-cell receptor potentials [Mathog et al., 1970; Goldman et al., 1973]. Since it is highly unlikely that supporting cells of the organ of Corti are sensitive in any manner to the endocochlear potential, alterations of basilar membrane mechanics caused by furosemide must be interpreted as resulting from disruption of transduction currents, implying that the hair cells are able to influence basilar membrane mechanics. We shall argue that inner hair cells may be excluded from such role, therefore singling out the outer hair cells as the organ of Corti elements which control the sensitive, nonlinear and frequency-tuned mechanical response of the basilar membrane to sound.

Methods

The vibrational response to sound of the basilar membrane was recorded in the basal turn of the cochleae of anesthetized chinchillas. The procedures used in our laboratory for recording from the basilar membrane have been documented in detail elsewhere [Robles et al., 1986; Ruggero and Rich, 1990 a and b] and are only outlined here. The left external auditory meatus was removed to permit placement of a plastic speculum, part of a sound-stimulus delivery-and-monitoring system (which includes an earphone and a probe microphone), in close proximity to the tympanic membrane. Sound stimuli were generated by a computer-controlled waveform generator [Ruggero and Rich, 1983]. The left auditory bulla was widely opened to allow access to the cochlea. The physiological state of the cochlea was assessed by determining compound action potential (CAP) thresholds, by means of a round-window electrode, at frequencies close to the characteristic frequency (CF: the stimulus frequency to which an auditory structure is most sensitive) of the basilar membrane recording site, which was always in the range 7-10 kHz. Two methods were used to record the vibration of the basilar membrane: the Mössbauer technique [Robles et al., 1986] and laser vibrometry [Ruggero and Rich, 1990 a and b]. Both techniques required making a hole in the otic capsule and placing either a gamma source or glass microbeads on the basilar membrane. The basilar membrane velocity was derived from the motion-induced Doppler frequency shift of either gamma radiation (with the Mössbauer technique) or reflected light (with laser vibrometry).

Results

Basilar membrane responses to tone pips at CF and at 1 kHz and to clicks (in experiments involving laser vibrometry) were recorded at several intensities before and after intravenous injections of furosemide. In addition, CAP thresholds were determined periodically to ascertain the effectiveness of the injection in reducing cochlear responses. Measurements were obtained from three animals using the Mössbauer technique and from two others by means of laser vibrometry.

Upon intravenous administration of furosemide (50 mg; approximately 100

mg/kg) to chinchilla L14 there was an immediate and large decrement in the magnitude of basilar membrane responses to near-CF (9 kHz) tone pips (Fig. 1): the peak velocity diminished from 464 um/s to 78 um/s (i.e., nearly 16 dB) within the first 15 min following injection. Subsequently, responses grew gradually back to their original magnitude, being fully recovered (475 um/s) by 106 min.

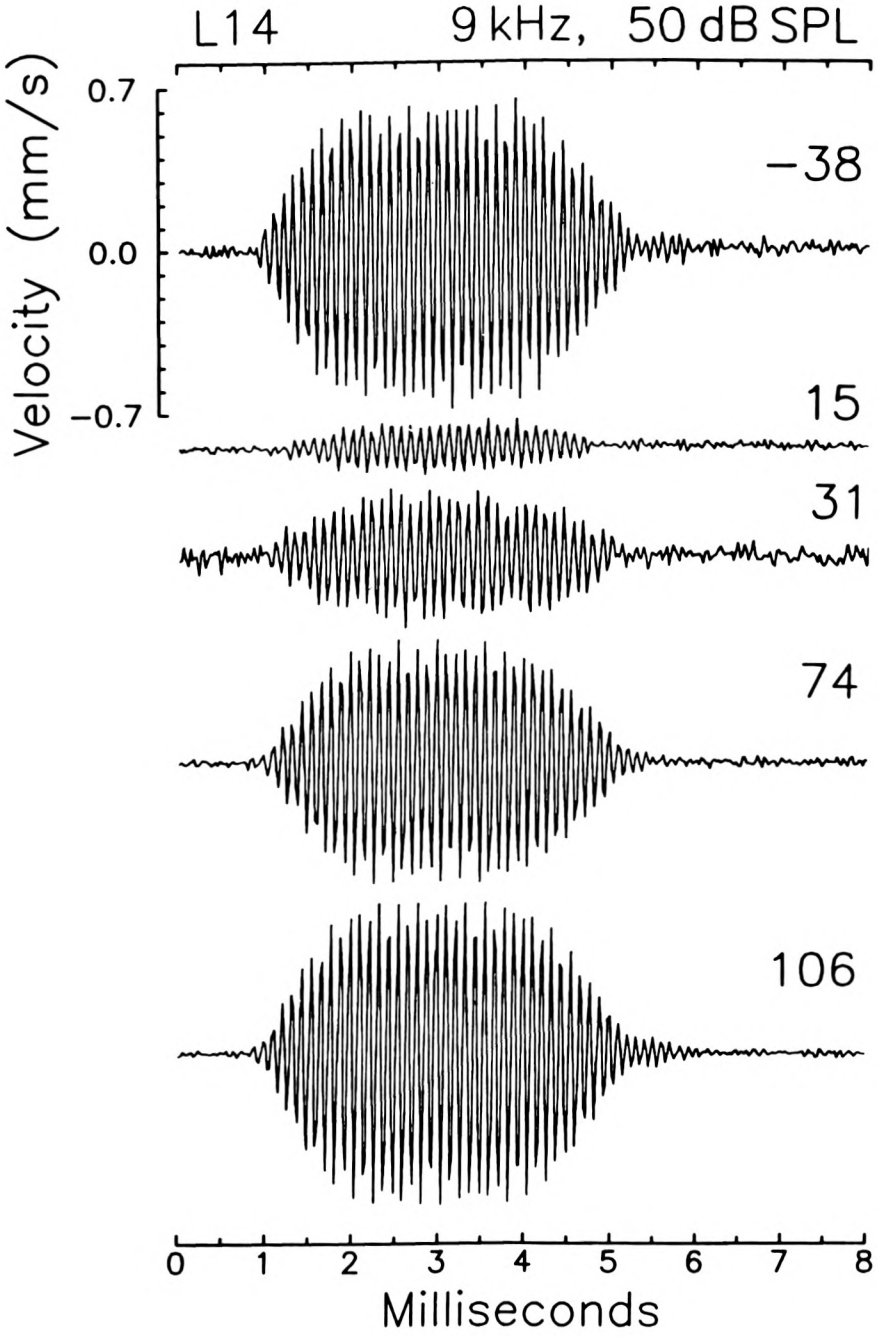

FIGURE 1 Effect of an intravenous furosemide injection upon basilar membrane responses to 9-kHz, 50-dB SPL tone pips. Each waveform, recorded with laser vibrometry in animal L14, represents the average velocity response to 1024 presentations of a 3.8 ms tone burst. Time of data collection (in minutes relative to injection time) is indicated next to each tracing. Note the large response decrement within the first 15 min following furosemide injection and the subsequent gradual recovery, which is complete at 106 min.

The effect of furosemide depended on both stimulus frequency and level. Figure 2 compares input-output functions, measured in animal M156 at various post-injection times, for tone pips at CF (8.9 kHz) and at a frequency much lower than CF (1 kHz). For low level CF tone pips, furosemide caused an immediate response reduction equivalent to a decrement in stimulus level of some 20-25 dB; at higher stimulus levels, the response reduction was smaller. Thus, the input-output curves changed from being highly compressive (i.e., growing at rates substantially lower than linear) at moderate levels to being nearly linear at all levels. With the passage of time, both response sensitivity and nonlinearity of growth reappeared progressively, so that at about 1 hour post-injection the CF input-output curve approached within a few dB pre-injection values. In contrast with the strong effects on the nonlinear CF responses, furosemide had no significant effect on the linear responses to 1-kHz tone pips.

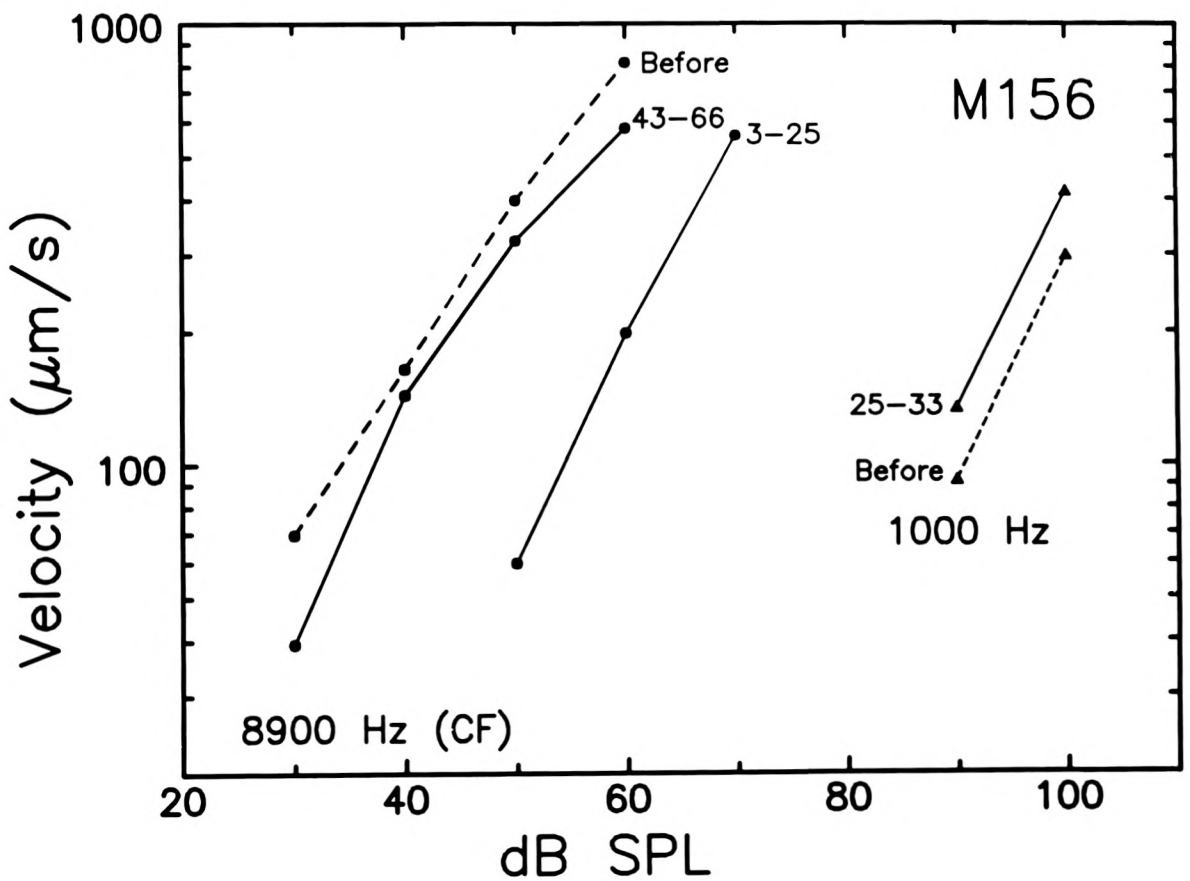

FIGURE 2 Input-output curves for the response of one basilar membrane site to tones immediately preceding and following an intravenous furosemide injection. The abscissa indicates stimulus intensity (in dB SPL, re 0.0002 dyn/cm^2); the ordinate indicates peak basilar membrane velocity, in units of um/s. Responses are shown for a high-frequency tone (9 kHz) and for a 1-kHz tone. The high frequency tone corresponded to the characteristic frequency (CF) of the basilar membrane site. Following the furosemide injection, input-output curves at CF were transiently displaced toward higher stimulus levels, the displacements being largest for low-level responses. In contrast, responses to the 1-kHz tone were hardly altered. Recordings were made using the Mössbauer technique.

In order to study in more detail the frequency dependence of the effects of furosemide, clicks were used as stimuli and the basilar membrane responses (recorded with laser velocimetry) were Fourier transformed to obtain velocity frequency spectra. In Fig. 3, a pre-injection spectrum (continuous line) is contrasted with frequency spectra of responses obtained immediately following a furosemide injection (long-dash line) or after partial recovery (short-dash line). The effect of furosemide was strongly frequency dependent: the largest decrement in response sensitivity occurred near CF, while spectral components sufficiently below CF were unaffected. Thus, the frequency-selective decrease in sensitivity resulted in a decrease in the sharpness of frequency tuning. Equivalent CF-specific response reductions were demonstrated by measuring isovelocity tuning curves (in one cochlea, not shown here) using tone-pip stimuli: near-CF responses were reduced by as much as 30 dB, while responses at the tuning curve tail were unaffected.

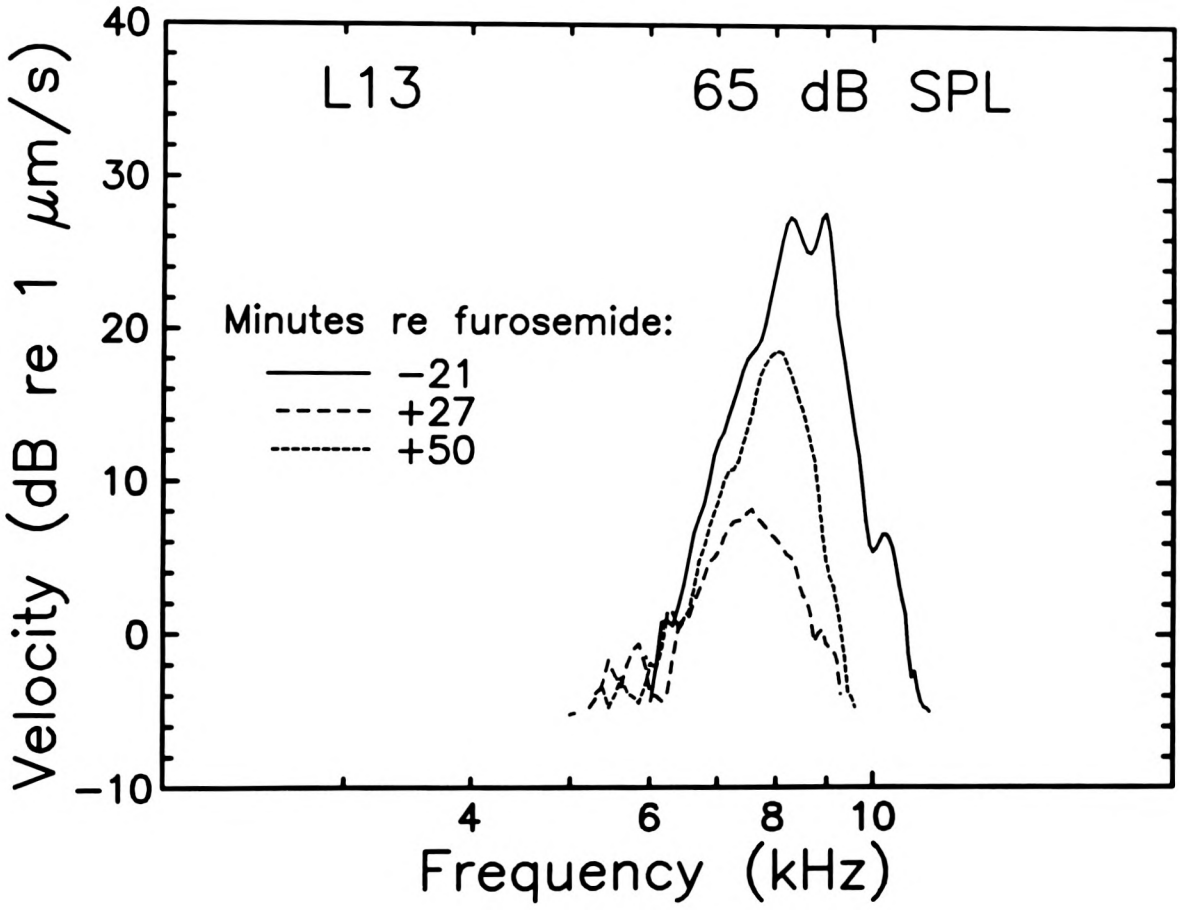

FIGURE 3 Effect of furosemide injection upon the frequency dependence of responses of basilar membrane L13 to clicks. The velocity-magnitude frequency spectra were obtained by Fourier transformation of the time-domain responses, recorded using laser vibrometry. The abscissa indicates frequency; the ordinate indicates spectral magnitude in units of um/s. Three curves are displayed: one representing responses immediately preceding furosemide injection (continuous line), a second obtained soon after the injection (long-dash line), and a third obtained at a time when substantial recovery had occurred (short-dash line). Note that the largest effect of furosemide is at frequencies near CF and that there is little effect at frequencies sufficiently lower than CF.

Discussion

The effects of furosemide injection upon the basilar membrane's mechanical response to sound, including changes in frequency selectivity and level dependence, are similar to those of death or surgical cochlear trauma [Sellick et al., 1982; Robles et al., 1986]. This suggests that death, surgical trauma and furosemide injection all result in permanent or transient alterations of the same agents that control the magnitude, frequency tuning and nonlinear response growth of basilar membrane motion. We argue that these agents are the outer hair cells.

Upon systemic (intravenous) injection of furosemide (a "loop-inhibiting" diuretic), there is a rapid, dose-dependent and reversible decrease of the large (80 mV) positive electrical potential normally present in the endolymph-filled scala media of the cochlea [Chodynicki and Kostrzewska, 1974; Brusilow, 1976]. Because the transduction currents across the apical surfaces of the hair cells are proportional to the sum of the endocochlear potential and the potential that exists across the hair cells' basolateral surfaces [Davis, 1965; Russell, 1983], there is a concurrent reduction in the receptor potentials of hair cells [Mathog et al., 1970; Goldman et al., 1973]. It is therefore not surprising that the thresholds of responses of Type-I cochlear afferents, which innervate exclusively inner hair cells, should be elevated by furosemide [Evans and Klinke, 1982; Sewell, 1984]. What is of greater interest is that the threshold elevation is much larger at each afferent's CF than at other frequencies. Since the sharp frequency tuning of cochlear inner hair cells and cochlear afferents has its origin in the frequency tuning of the basilar membrane [Khanna and Leonard, 1982; Sellick et al., 1982; Robles et al., 1986], the frequency dependence of furosemide effects upon cochlear-afferent responses has been interpreted as reflecting a corresponding reduction in the magnitude of basilar membrane vibration, itself resulting from the disruption of the feedback of outer hair cells upon the basilar membrane [Mountain et al., 1983; Patuzzi et al., 1989].

The present findings conclusively show that, indeed, basilar-membrane vibration is reduced by furosemide, and that the organ of Corti plays a crucial role in determining the basilar membrane's responses to sound. More specifically, our findings implicate the outer hair cells as mediating the effect of furosemide on basilar membrane motion. Although other interpretations are possible, they do not seem seriously tenable. Of the cells in the organ of Corti, only the outer hair cells are suitable as links between the change of endocochlear electrical potential and alterations in basilar-membrane motion: only the outer hair cells can act as both sensory receptors and as motors capable of controlling the basilar-membrane vibrations. There is ample evidence that hair cells are the cochlear mechanoreceptors, that their receptor potentials are importantly determined by the endocochlear potential [Davis, 1965; Russell, 1983] and, in fact, that cochlear microphonics (which reflect the receptor potentials of outer hair cells) are reduced by furosemide injections [Mathog et al., 1970; Goldman et al., 1973]. In contrast, no comparable evidence exists for any of the supporting cells of the organ of Corti[1]. Regarding motor-like capabilities, several reports have explicitly singled out the outer hair cells as the *only* organ of Corti cells that respond to a variety of stimuli, including electrical currents, by generating

mechanical forces capable of changing their length *in vitro* [Brownell et al., 1985; Ashmore, 1987] and, probably, of pushing or pulling the basilar membrane *in vivo*. Additionally, the position of inner hair cells is extremely unfavorable for exerting force on the basilar membrane: they are located on the edge of the bony spiral lamina and their stereocilia are only weakly attached to the tectorial membrane or do not contact it at all [Lim, 1986]. In contrast, outer hair cells are located centrally in the organ of Corti, where the basilar membrane undergoes its largest excursion, and their stereocilia are firmly connected to the tectorial membrane.

Acknowledgments

We were principally supported by NIH (NIDCD) Grants DC-00110 and DC-00419, and also by smaller grants from the Minnesota Medical Foundation and the Lions 5M Hearing Research Endowment. We thank W. D. Ward for his helpful comments on this paper.

References

Anderson, S. D. and Kemp, D. T. (1978) The evoked cochlear mechanical response in laboratory primates. Arch. Otorhinolaryngol. 224, 47-54.

Ashmore, J. F. (1987) A fast motile response in guinea-pig outer hair cells: the cellular basis of the cochlear amplifier. J. Physiol. (Lond.) 388, 323-347.

Brown, M. C., Nuttall, A. L. and Masta, R. I. (1983) Intracellular recordings from cochlear inner hair cells: effects of stimulation of the crossed olivocochlear efferents. Science 222, 69-72.

Brownell, W. E., Bader, C. R., Bertrand, D. and de Ribaupierre, Y. (1985) Evoked mechanical responses of isolated cochlear outer hair cells. Science 227, 194-196.

Brusilow, S. W. (1976) Propanolol antagonism to the effect of furosemide on the composition of endolymph in guinea pigs. Can. J. Physiol. Pharmacol. 54, 42-48.

Chodynicki, S. and Kostrzewska, A. (1974) Wplyw furosemidu i kwasu etakrynowego na potencjal endolimfatyczny swinki morskiej (Effects of furosemide and ethacrynic acid on the endolymph potential in guinea pigs). Otolaryngol. Pol. 28, 5-8.

Dallos, P. (1988) Cochlear neurobiology: some key experiments and concepts of the past two decades. In: Auditory Function: Neurobiological Bases of Hearing (Eds: Edelman, G. M., Gall, W. E. and Cowan, W. M.) Wiley, N.Y., pp. 153-188.

Dallos, P. and Harris, D. M. (1978) Properties of auditory nerve responses in absence of outer hair cells. J. Neurophysiol. 41, 365-383.

Davis, H. (1965) A model for transducer action in the cochlea. In: Cold Spring Harb. Symp. Quant. Biol. 30, 181-189.

Davis, H. (1983) An active process in cochlear mechanics. Hear. Res. 9, 79-90.

Evans, E. F. and Klinke, R. (1982) The effects of intracochlear and systemic furosemide on the properties of single cochlear nerve fibres in the cat. J. Physiol. (Lond.) 331, 409-428.

Goldman, W. J., Bielinski, T. C. and Mattis, P. A. (1973) Cochlear microphonic potential response of the dog to diuretic compounds. Toxicol. Appl. Pharmacol. 25, 259-266.

Guinan, J. J., Jr. (1986) Effect of efferent neural activity on cochlear mechanics. Scand. Audiol. Suppl. 25, 53-62.

Hubbard, A. E. and Mountain, D. C. (1983) Alternating current delivered into the scala media alters sound pressure at the eardrum. Science 222, 510-512.

Kemp, D. T. (1978) Stimulated acoustic emissions from within the human auditory system. J. Acoust. Soc. Am. 64, 1386-1391.

Khanna, S. M. and Leonard, D. G. B. (1982) Basilar membrane tuning in the cat cochlea. Science 215, 305-306.

Kiang, N. Y. S., Liberman, M. C., Sewell, W. F. and Guinan, J. J. (1986) Single unit clues to cochlear mechanisms. Hear. Res. 22, 171-182.

Kim, D. O., Molnar, C. E. and Matthews, J. W. (1980) Cochlear mechanics: nonlinear behavior in two-tone responses as reflected in cochlear-nerve-fiber responses and in ear-canal sound pressure. J. Acoust. Soc. Am. 67, 1704-1721.

Liberman, M. C. and Dodds, L. W. (1984) Single-neuron labeling and chronic cochlear pathology. III. Stereocilia damage and alterations of threshold tuning curves. Hear. Res. 16, 55-74.

Lim, D. J. (1986) Functional structure of the organ of Corti: a review. Hear. Res. 22, 117-146.

Mathog, R. H., Thomas, W. G. and Hudson, W. R. (1970) Ototoxicity of new and potent diuretics. Arch. Otolaryngol. 92, 7-13.

Mountain, D.C. (1980) Changes in endolymphatic potential and crossed olivocochlear bundle stimulation alter cochlear mechanics. Science 210, 71-72.

Mountain, D. C. and Hubbard, A. E. (1989) Rapid force production in the cochlea. Hear. Res. 42, 195-202.

Mountain, D. C., Hubbard, A. E. and McMullen, T. A. (1983) Electromechanical processes in the cochlea. In: Mechanics of Hearing (Eds: de Boer, E. and Viergever, M. A.) Delft Univ. Press, Delft, The Netherlands, pp. 119-126.

Patuzzi, R., Johnstone, B. M. and Sellick, P. M. (1984) The alteration of the vibration of the basilar membrane produced by loud sound. J. Acoust. Soc. Am. 13, 99-100.

Patuzzi, R. B., Yates, G. K. and Johnstone, B. M. (1989) Outer hair receptor currents and sensorineural hearing loss. Hear. Res. 42, 47-72.

Rhode, W. S. (1973) An investigation of post-mortem cochlear mechanics using the Mössbauer effect. In: Basic Mechanisms in Hearing (Ed: Møller, A. R.) Academic Press, New York, pp. 49-63.

Robles, L., Ruggero, M.A. and Rich, N.C. (1986) Basilar membrane mechanics at the base of the chinchilla cochlea. I. Input-output functions, tuning curves, and response phases. J. Acoust. Soc. Am. 80, 1364-1374.

Ruggero, M. A. and Rich, N. C. (1983) Chinchilla auditory-nerve responses to low-frequency tones. J. Acoust. Soc. Am. 73, 2096-2108.

Ruggero, M. A. and Rich, N. C. (1990a) Application of laser velocimetry to the measurement of basilar membrane vibrations. J. Acoust. Soc. Am. 87, S101.

Ruggero, M. A. and Rich, N. C. (1990b) Application of a commercially-manufactured Doppler-shift laser velocimeter to the measurement of basilar-membrane vibration. Hear. Res., in press.

Russell, I. J. (1983) Origin of the receptor potential in inner hair cells of the mammalian cochlea - evidence for Davis' theory. Nature 301, 334-336.

Russell, I. J. and Sellick, P. M. (1978) Intracellular studies of hair cells in the mammalian cochlea. J. Physiol. (Lond.) 284, 261-290.

Rybak, L. P. (1982) Pathophysiology of furosemide ototoxicity. J. Otolaryngol. 11, 127-133.

Sellick, P.M., Patuzzi, R. and Johnstone, B.M. (1982) Measurement of basilar membrane motion in the guinea pig using the Mössbauer technique. J. Acoust. Soc. Am. 72, 131-141.

Sewell, W.F. (1984) The effects of furosemide on the endocochlear potential and auditory-nerve fiber tuning curves in cats. Hear. Res. 14, 305-314.

Siegel, J.H. and Kim, D.O. (1982) Efferent neural control of cochlear mechanics? Olivocochlear bundle stimulation affects cochlear biomechanical nonlinearity. Hear. Res. 6, 171-182.

Weiss, T. (1982) Bidirectional transduction in vertebrate hair cells; a mechanism for coupling mechanical and electrical processes. Hear. Res. 7, 353-360.

Wiederhold, M. L. and Kiang, N. Y. S. (1970) Effects of electric stimulation of the crossed olivocochlear bundle on single auditory-nerve fibers in the cat. J. Acoust. Soc. Am. 48, 950-965.

[1]Small receptor potentials recordable intracellularly from supporting cells are not accompanied by membrane resistance changes and are believed to result from electrotonic spread from adjacent hair cells [Russell and Sellick, 1978].

Section 7

General Cochlear Models

MODELING THE NOISE DAMAGED COCHLEA

Jont B. Allen

Acoustics Research Dept., AT&T Bell Labs
Murray Hill, NJ 07090, USA

Introduction

The purpose of this paper is to present a specific model (Allen, 1980) of the cochlea which replicates normal cat threshold neural tuning curves. This model is first introduced as a linear passive model. In the process of fitting the model to the neural data, it was discovered that changes in the basilar membrane stiffness could modify the model cilia frequency response in a manner similar to the noise damaged neural tuning curves of Liberman and Dodds (1984). Liberman and Dodds found that the tips of the tuning curves become elevated by more than 40 dB, and the tails become hypersensitive by about 10 dB, after a noise trauma that damages the outer hair cells. After recording tuning curves from the noise damaged cells, they found a systematic loss of outer and/or inner hair cells associated with the noise trauma neurons. They then correlated the hair cell loss to the frequency response of the associated tuning curves. In this paper we model the Liberman and Dodds noise damaged tuning curves by associating the loss of normal outer hair cells with a decrease in the basilar membrane stiffness (increased compliance).

We believe that the compressive and frequency dependent cochlear nonlinearities that have been observed in the basilar membrane response and in inner and outer hair cell receptor potentials (for a review see Allen, 1988) are a related phenomenon, and we propose a model for the nonlinear cochlea based on this approach. In this model, the outer hair cell length changes, which occur during cell depolarization (Brownell *et al.* 1985), dynamically increase the basilar membrane compliance. The effect of this dynamically modified compliance would be a compression of the dynamic range of the basilar membrane motion, and therefore of the excitation to the inner hair cells. This nonlinearity is important to compress the dynamic range of the acoustic signal to match that of the inner hair cells.

This model is being offered as a physically realizable alternative to the active (negative-resistance) cochlear amplifier model of Neely and Kim (1983).

Neural Excitation Patterns

One of the basic problems in cochlear modeling is the determination of the model parameters from physical data in a systematic way. Frequency domain models give a response along the basilar membrane for a given input-signal frequency, whereas the experimental data (neural tuning curves) to be matched are functions of frequency for a given position along the basilar membrane. To side step this computational problem, it is possible to transform the neural tuning curve data to place. These place tuning curves are called *excitation patterns* in the literature. This transformation represents a major simplification of the data-fitting process. If the neural excitation patterns are accurately fitted by the model in the place domain for several well separated frequencies, then the frequency tuning data should fit as well.

The transformation to excitation patterns is best understood by example. Fig. 1 shows a family of normal cat tuning curves collected by Liberman. Liberman has also measured the

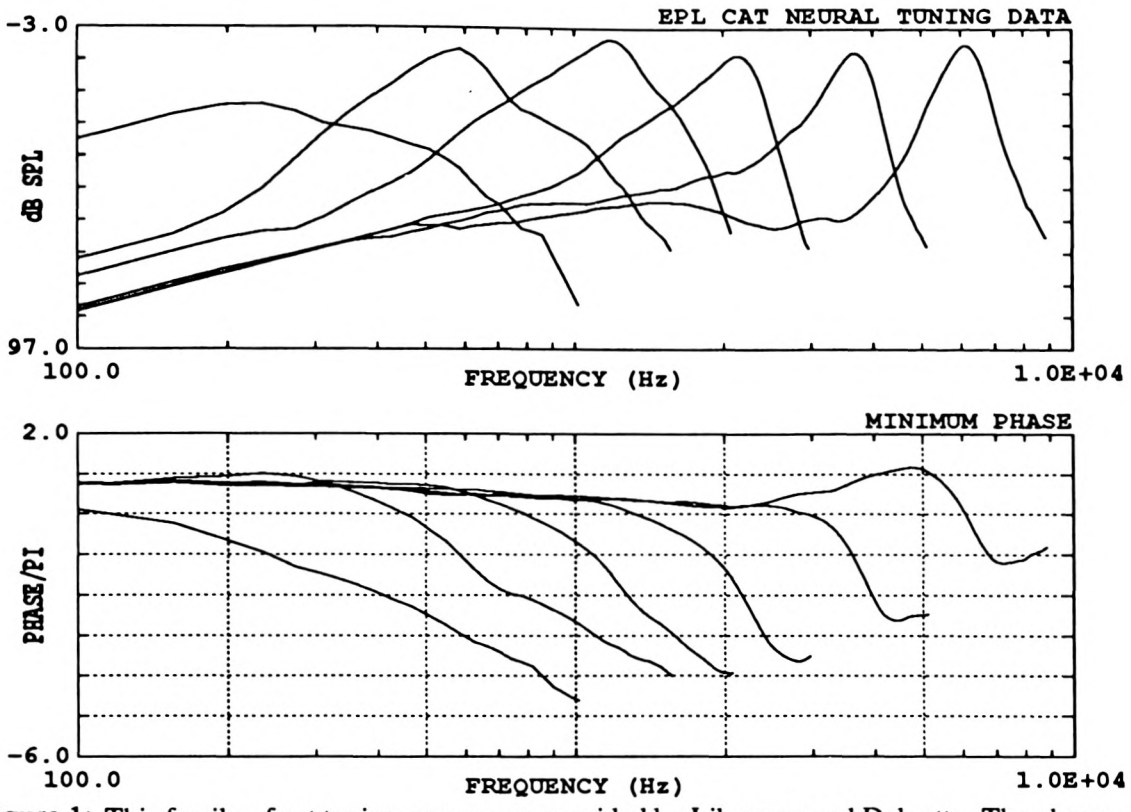

Figure 1: This family of cat tuning curves was provided by Liberman and Delgutte. The phase was generated by the Fourier Transform minimum phase method.

relation between the characteristic frequency (CF) and position on the basilar membrane $f_{CF}(x)$. Our procedure then is the following. First compute the phase for each tuning curve using the minimum phase method. The complex frequency responses are then loaded into the response matrix $\Theta(x_i, f_j)$, where x_i is the index that labels each tuning curve, and f_j is frequency. To find x_i, look across frequency to find $f_{CF}(x_i)$, the frequency of the maximum of $|\Theta(x_i, f_j)|$. Then use $f_{CF}(x)$ to determine x_i, the row index for each tuning curve, from the f_{CF} of the row. The excitation pattern is then $\Theta(x_i, f_j)$ vs. x_i for any given f_j, as shown in Fig. 2. These threshold response are for single tones as a function of position along the basilar membrane. The lower panel of Fig. 2 shows the derived phase along the basilar membrane for a given frequency. Since this phase was generated from the tuning curves using the minimum phase method, it is not necessarily the phase that one would measure neurally. The models, however, approximately match this phase. The close match demonstrates that the models approximately have a minimum phase response.

Modeling the Tuning Curve Data

In this section we show model fits to the neural excitation patterns of Fig. 2. The macromechanical model is the two-dimensional model of Sondhi (1979). The micromechanical model being used is the resonant tectorial-membrane model described in [Allen, 1980; Allen, 1988]. The basilar membrane to cilia transfer function $H_T(x, \omega)$ is used to modify the basilar membrane displacement response to give the cilia displacement. The difference between the 1980 model and the one here is in our choice of model parameters and the addition of a resistive element to the basilar membrane impedance. The comparison of the model to the neural data was made using a simple middle ear model.

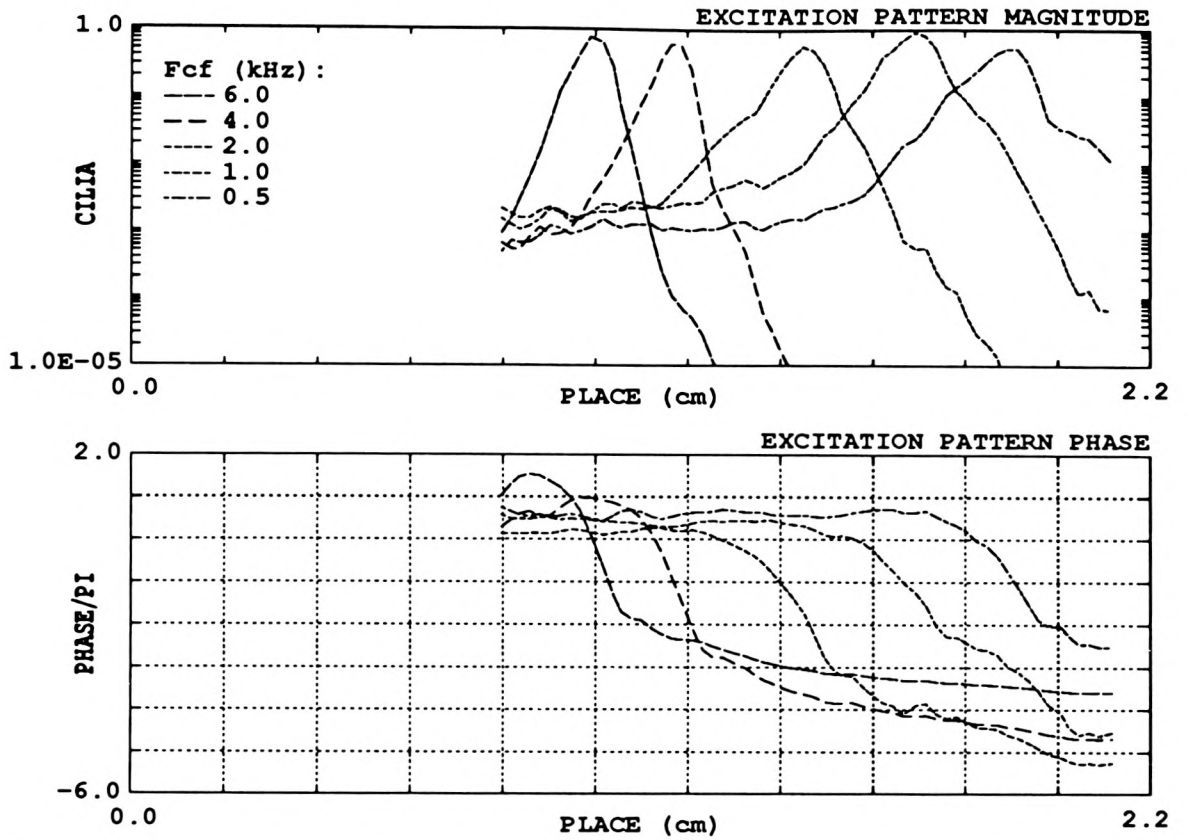

Figure 2: Transforming neural data tuning curves to place gives excitation patterns. These are more readily compared to model responses, since the model also gives excitation patterns for each input frequency.

THE TRANSDUCTION FILTER

The transduction filter $H_T(x,\omega)$ is defined as the transfer function, assumed here to be linear, between the basilar membrane displacement and the inner hair cell stereocilia displacement. In this paper $H_T(x,\omega)$ consists of three parts, which we call $G(x)$, $H_{TM}(x,\omega)$, and $H_{TR}(\omega)$. *First* is the lever action of the transduction gain $G(x)$, which is defined as the ratio of the cilia displacement to the BM displacement, under the condition that $k_c << k_T$. In Allen (1980) a formula was given for this gain (Eq's. 5 and 6) in terms of the physical variables. The estimate of G used here was heuristically determined in the process of fitting the neural data. It is desirable to have a large value of the transduction gain to increase the hair cell excitation. However, a large value of G seemed inconsistent with fitting the data. *Second*, is the effect of the elastic coupling between the limbus and the tectorial membrane $k_T(x)$. This elastic element introduces a pole and a zero into the transfer function, as described in Allen (1980, Eq. 13), and shown in Fig. 3, upper right hand panel. *Third* $H_{TR}(\omega)$ is defined as a first order high pass filter which represents the viscous fluid layer driving the stiffness-dominated inner hair cell stereocilia. H_{TR} is the transfer function developed between the tectorial membrane to reticular lamina (TM-RL) shear displacement and the cilia displacement, coupled via fluid viscosity. This component of the transduction filter is given by

$$H_{TR}(\omega) = \frac{j\omega}{j\omega + 2\pi f_c}. \quad (1)$$

If the inner hair cell cilia were attached to the underside of the tectorial membrane, then this highpass filtering action would not be present since there would be no slip condition. From the above equation, at low frequencies the cilia respond with the velocity of the shear, whereas at high frequencies, the cilia follow the TM-RL shear displacement. In the model,

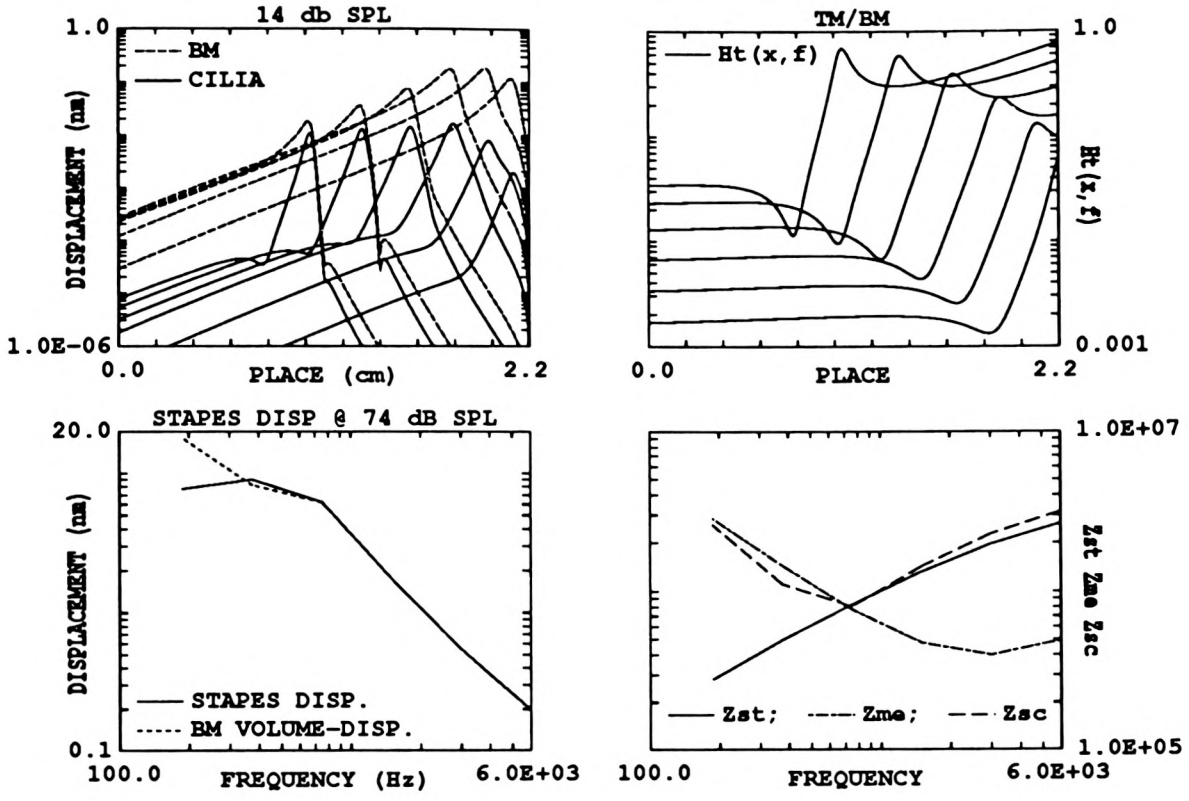

Figure 3: Model responses for octave frequencies between 6 kHz and 182.5 Hz, assuming an eardrum pressure of 14 dB SPL.

$f_c = 5.0$ kHz. As may be seen from the model response in the upper right panel of Fig. 3, the cilia move with the TM-RL shear-displacement for frequencies above f_c, and with the shear-velocity below f_c (Dallos, 1984).

Putting the three factors together gives the transduction filter

$$H_T(x,s) \;=\; G(x)\, H_{TR}(s)\, H_{TM}(x,s) \tag{2}$$

shown in Fig. 3 upper right panel.

SUMMARY OF MODEL EXCITATION RESPONSES

A summary of the model responses is given in Fig. 3. The upper left panel shows the model basilar membrane center-line and cilia rms displacements at octave frequencies between 6.0 kHz and 187.5 Hz at 14 dB SPL. The basilar membrane displacement is derived from the per unit length volume-displacement by dividing by the basilar membrane width. The lower left panel shows the stapes rms displacement at 74 dB SPL. Also shown in this panel is the volume integral of the basilar membrane displacement. The stapes volume-displacement and the basilar membrane volume-displacement should be equal at all frequencies. Because of the boundary conditions that have been assumed at the helicotrema, these two integrals are not exactly the same (Puria and Allen, 1990). The difference between them is due to fluid flow through the model helicotrema. The lower right panel shows the stapes input impedance Z_{sc}, the ossicle impedance Z_{me}, and their sum Z_{st}, which is proportional to the eardrum impedance.

In Fig. 4 the dashed lines give the model cilia excitation patterns, magnitude and phase, at the frequencies 0.5, 1.0, 2.0 4.0 and 6.0 kHz. The units in the upper panel are in nanometers (nm), and correspond to 74 dB-SPL constant pressure in the model ear canal. The solid lines are the neural data from Liberman. The amplitude scaling for the neural curves is arbitrary, but all curves are scaled by the same factor. The lower panel shows the

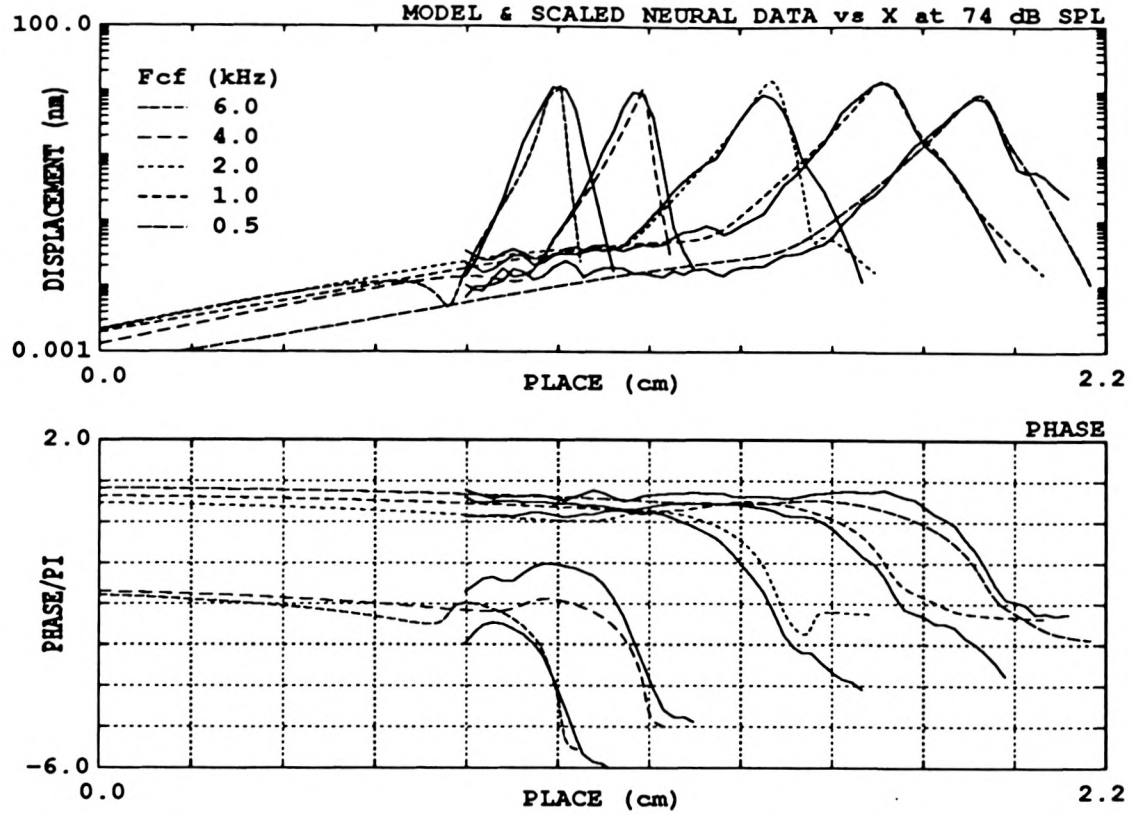

Figure 4: The solid curves are the neural data of Liberman and the dashed lines are the model responses in nanometers for a 74 dB SPL stimulus.

excitation pattern phase for the model (dashed lines) and of the neural data (solid lines) for the octave frequencies. The 4.0 and 6.0 kHz phase curves have been displaced down by $2\pi n$, where n is an integer, to separate them for clarity of plotting. The neural data is the same as shown in Fig. 2. The most significant deviation between the model and the neural data is in the phase curves for the 4 kHz tuning curves where the curves are π radians apart below CF (at 0.5 cm). There is also a trend for the model data to show a slightly greater phase lag than the neural minimum-phase result. This effect may also be seen by comparing Fig. 1 to Fig. 5.

Model Tuning Curves

After computing the model response at 7 locations along the basilar membrane for a large number of frequencies we find the results shown in Fig. 5. This figure should be compared to Fig. 1. An important degree of freedom that remains in comparing these curves is the threshold sensitivity of the model hair cell. For both Fig. 4 and 5 we would like to know if the sensitivity of the BM at the characteristic frequency (f_{CF}) is realistic. A discussion of the sensitivity question may be found in Hudspeth (1983). Denk and Webb (1989) have shown that hair cells transduce their cilia Brownian motion. The magnitude of this motion depends on the real part of the mechanical impedance of the stereocilia *in situ*. Hair cell sensitivity is an important and open question that has caused many to speculate on the need for a cochlear amplifier in the basilar membrane (Neely and Kim, 1983; Mountain and Hubbard, 1989; Patuzzi *et al.* 1989). Estimates of cilia displacements are complicated by the uncertainty introduced by the unknown transduction filter. It is not known if inner hair cells are velocity or displacement sensitive in vivo. Dallos (1984) has estimated that there is a velocity to displacement transition with a transition frequency of about 1 kHz. In the present model we assume a similar velocity to displacement as described in Eq. 1, but with $f_c = 5.0$ kHz.

It is assumed here that the rate threshold for the cat corresponds to an eardrum pressure

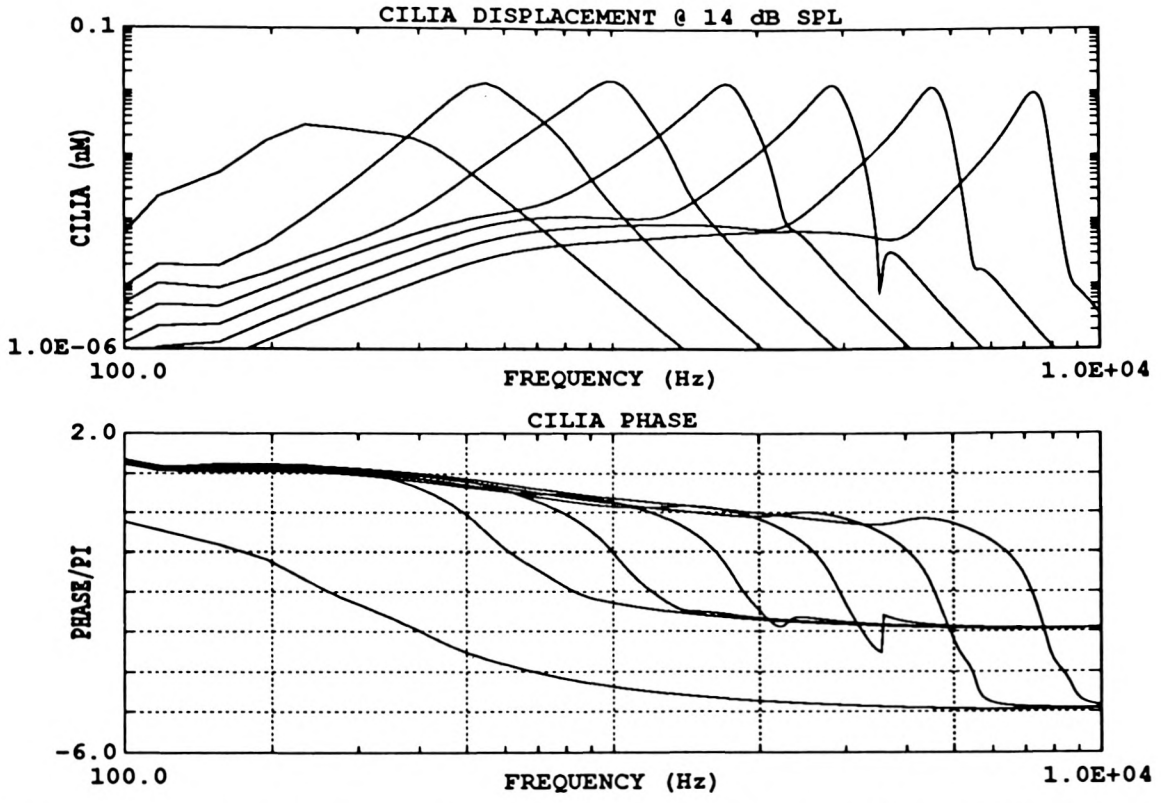

Figure 5: Once the model parameters have been determined, it is practical to compute the frequency tuning curves at points along the basilar membrane. These tuning curves are shown here, and should be compared to Fig. 1. As before, the upper panel is the cilia displacement in nanometers for a stimulus level of 14 dB SPL. The lower panel is the corresponding phase.

of 14 dB SPL. From Fig. 3, the model BM motion is 120 pm at the CF of 1 kHz and 14 dB SPL. The stapes displacement at 1 kHz for the model is 3.5 picometers at 14 dB-SPL. This means that the model basilar membrane has a gain of 31 dB at 1 kHz. Threshold displacements as low as 0.1 nm (100 pm) for cilia displacements have previously been estimated by Hudspeth, A.J. (1983). Nuttal *et al.* (1990) found basilar membrane displacements of 0.5 nm at 35 dB for his most sensitive animals. They also showed BM displacement data for several animals that showed a nonlinear input-output response growth at 80 pm for 50 dB SPL. Sellick *et al.* (1983) estimated the BM threshold at 350 pm, while Robles *et al.* (1986) have estimated the BM threshold at 1.9 nm.

THE BASILAR MEMBRANE STIFFNESS

During the parameter fitting process it was found that the basilar membrane stiffness was much more sensitive than other parameters in its effect on the basilar membrane tuning curve. Fig. 6 shows this effect. In this figure the basilar membrane stiffness was modified by a relative factor of 0.3 to 1.0 times the normal value (the value that gave a match to the tuning curve data). From this figure one may see that the tip of the model tuning curve becomes less sensitive by 40 dB and the tail of the model tuning curve is more sensitive by about 10 dB. There are several reasons for these changes in the model. First, as the stiffness decreases, the CF shifts toward the base. This means that the CF is shifting into the 'zero' (f_z) of the resonant tectorial membrane transfer function. Because of the presence of the zero, the CF threshold rises dramatically. A second important effect is the hyper-sensitive tails of the tuning curve. As the volume of fluid motion at the CF is reduced, the volume-motion in the tail increases because the net fluid motion must remain constant, as required by conservation of fluid mass. These model results should be compared to those of Liberman for noise damaged cochlea.

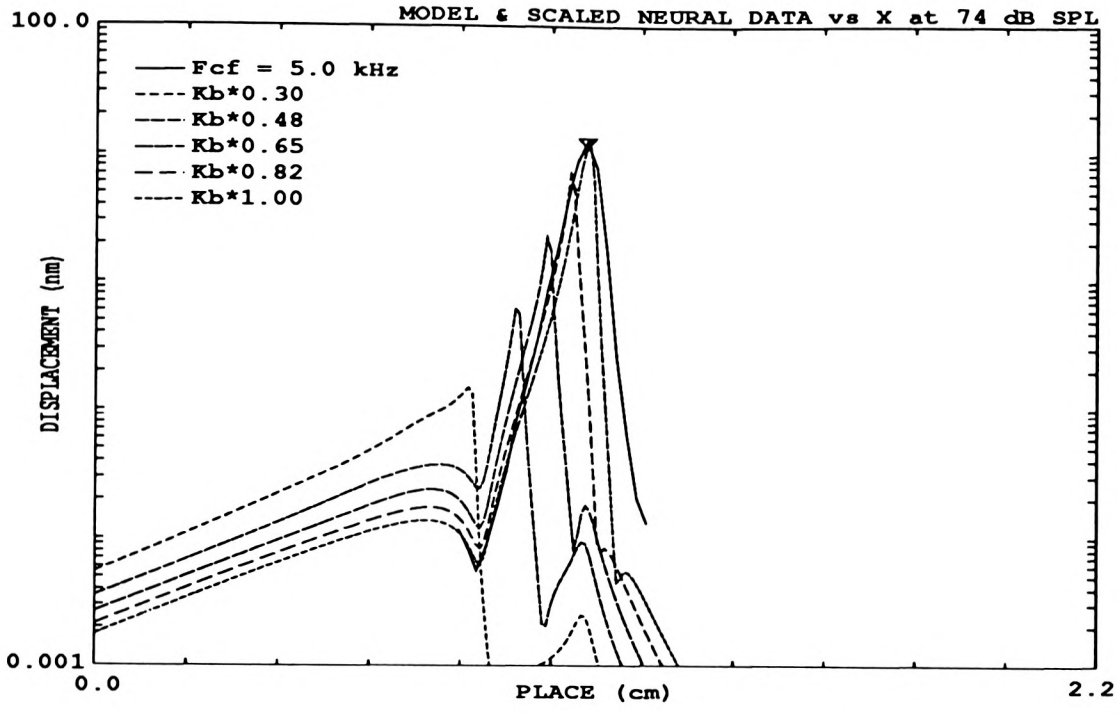

Figure 6: For an input frequency of 5.0 kHz, $K_{BM}(x)$ was varied from 30% to 100% of its normal value. This response should be compared to the tuning curves for damaged outer hair cell as found by Liberman.

Discussion: A Nonlinear Cochlear Model

A nonlinear version of this model remains to be explored, and an approach toward this end is described next. As the basilar membrane displacement increases with level, the depolarization of the outer hair cell increases due to the increased shearing of the sterocilia of the outer hair cell at the higher input levels. We propose that as the cell depolarizes, the induced hair cell shortening *reduces* the basilar membrane stiffness in the way assumed in Fig. 6. The published sensitivity of the hair cell length changes is 20 nm/mv (Santos-Sacchi and Dilger 1987). In Fig. 6 the stiffness changes are uniform along the basilar membrane, whereas in the nonlinear model they would be signal dependent and thus nonuniform. Since the stiffness variations would be low-pass filtered by the membrane capacitance of the outer hair cells, the stiffness variations would not follow the signal on a cycle-by-cycle basis. In this sense, the model could be characterized as a nonlinear parametric model. If the stiffness variations at high frequencies (e.g. 10-20 kHz) do not follow the signal waveform, then the term 'cochlear amplifier' does not apply to this class of model. It is an 'active' model in the usual electrical engineering sense, just as the Davis model of the hair cell is 'active.' However, this use of the term 'active' is not what is usually meant in cochlear modeling, where the term is frequently used interchangeably with the term 'cochlear amplifier', implying gain on a cycle by cycle basis. The details following the cell depolarization which lead to the basilar membrane stiffness change are presently unknown and we have assumed here that such a dependence is plausible. To study the site of the nonlinearity in a more systematic way, it may be helpful to model the frequency response of the $2f_1 - f_2$ distortion product for constant f_2. These distortion products may be modeled using quasi-linear techniques by introducing voltage sources in series with K_{BM} to represent the generation of the nonlinear components. From the equivalent model of the micromechanical circuit (Allen, 1980, Fig. 10), a source in series with K_{BM} would see the series impedance of the tectorial membrane, which has a minimum at f_z. This suggests that the nonlinearity might have maximum coupling to the fluid at this frequency.

A little analysis shows that this would give a maximum of the distortion product amplitude when $2f_1 - f_2 = f_z$. First we argue that the distortion product is generated at, or near, x_2, which is defined as the f_2 place. Next we define $\beta(x) = f_z(x_2)/f_2(x_2)$ as the ratio of f_z to f_2 at x_2. It follows that the distortion product amplitude will have its maximum at $f_2/f_1 \simeq 2.0/(1+\beta)$. For β in the range of 0.7 to 0.5, as it is in this model, this would give a best frequency ratio of 1.18 to 1.33, which is close to the range of observed maximum values (Wilson, 1980).

References

Allen, Jont B. (1980). "Cochlear micromechanics - A physical model of transduction," J. Acoust. Soc. Am. **68**(6) 1660-1670.

Allen, Jont B. (1988). "Cochlear signal processing," *Physiology of the Ear*, edited by A. F. Jahn and J. Santos-Sacchi, Raven Press, New York, 243-270.

Brownell, W.E., Bader, C.R., Bertran,D., and de Rabaupierre, Y. (1985). "Evoked mechanical responses of isolated cochlear outer hair cells," *Science*, **227** 194-196.

Dallos, Peter (1984). "Some electrical circuit properties of the organ of Corti. II. Analysis including reactive elements," Hearing Research **14** 281-291.

Denk, W. and Watt, W.W. (1989). "Thermal-noise-limited transduction observed in mechanosensory receptors of the inner ear," Physical Review Letters **63** 207-210.

Hudspeth, A. J. (1983). "Mechanoelectrical Transduction by Hair Cells in the acousticolateralis Sensory System," *Annu. Rev. Neurosci.*, **6** 187-215.

Liberman, M. C. and Dodds, L. (1984). "Single Neuron Labeling and Chronic Cochlear Pathology III: Stereocilia Damage and Alterations of Threshold Tuning Curves," Hearing Research **16** 55-74.

Mountain, D.C., and Hubbard, A.E. (1989). "Rapid force production in the cochlea," Hearing Research 42 195-202.

Neely, S.T. and Kim, D. O. (1983). "An active cochlear model showing sharp tuning and high sensitivity," Hearing Research. **9** 123-130.

Nuttal, F., Dolan, D. F., and Avinash, G. (1990). "Doppler Vibrometer Measurements of Basilar Membrane Motion in the Guinea Pig," abstract 293, poster 23, 13th ARO Midwinter Meeting.; See paper in this proceedings.

Patuzzi, R. B., Yates, G. K., and Johnstone, B. M. (1989). "Outer hair cell receptor current and sensorineural hearing loss," Hearing Research 42 47-72.

Puria S., and Allen, Jont B. (1990). "A Parametric Study of the Cochlear Input Impedance," J. Acoust. Soc. Am., In Press

Robles, L., Ruggero, M.A., Rich, N.C. (1986). "Basilar membrane mechanics at the base of the chinchilla cochlea. I. Input-output functions, tuning curves, and response phases," J. Acoust. Soc. Am. **80** 1364-1374.

Santos-Sacchi, J. and Dilger J. P. (1987). "Whole cell currents and mechanical responses of isolated outer hair cells," Hearing Research **35**, 143-150.

Sellick, P.M., Patuzzi, R., and Johnstone, B.M. (1983). "Comparison between the tuning properties of inner haircells and basilar membrane motion," Hearing Research **10** 93-100.

Sondhi, M. M. (1979). "Method for computing motion in a two-dimensional cochlear model," J. Acoust. Soc. Am.**63** 1468-1477

Wilson, J.P. (1980). "The combination tone, $2f_1 - f_2$, in psychophysics and ear-canal recording," in *Psychophysical and Physiological and Behavioral studies in Hearing*, edited by G. van den Brink and F. A. Bilsen, Delft Univ. Press.

Comments and discussion

LYON

In your first step, you convert iso-response tuning curves to "excitation patterns" that appear to be in terms of an iso-intensity situation. This would be a sensible transformation for a linear system, such as your model, but how can it be interpreted for a system with a strong input-output compression nonlinearity, such as the cochlea from which the data were taken ?

ALLEN

I agree with your observation which you make in your paper that the frequency dependent compression of the type that has been observed in the basilar membrane response will have an impact on the response characteristics as the input level is varied. These nonlinear properties make the job of modeling BM responses much more difficult. The question then is one of the philosophy of how to go about this difficult task. Two points need to be made about this.

The first point goes back to my paper in Keele (Allen, 1988) where I discussed the three regions of the amplitude and frequency space where we see different nonlinear behavior. Observations of basilar membrane nonlinearities are considerably reduced in the apical region of the cochlea (for example, for frequencies below 4 or 5 kHz and for levels below about 60 to 65 dB-SPL.) Evidence for this statement is documented in my Keele paper. It follows that the effects you describe are most important in the base of the cochlea, which I have not attempted to modeled for this conference. As I said in Keele, we must be very careful about not generalize the effects we see in the base of the cochlea to the apex region.

Second, in a nonlinear system it is helpful if one can hold the signal to the nonlinear element constant when specifying the systems response. In the case of the basilar membrane, there is not one nonlinear element but a nearly continuous distribution of nonlinear elements. In the case of neural tuning curves, such as I have been trying to match, we have not only the basilar membrane nonlinearity, but also the hair cell rate level nonlinearity. In making a tuning curve one attempts to minimize the nonlinear effect of the inner hair cell transduction nonlinearity by measuring the locus of pressures as a function of frequency that produce a constant output firing rate. The analogous measurement in the case of basilar membrane measurements would be to hold the excitation to the nonlinear elements constant. To the best of our present knowledge, this nonlinear element is the outer hair cell, which is controlled by the receptor voltage. Since the experimenter does not have direct control of this voltage, the basilar membrane velocity or displacement is typically help constant. This implies that the nonlinearity is varying over the course of the measurement, which greatly complicates both the interpretation and modeling of the measurement.

WAVE-PROPAGATION MODES AND BOUNDARY CONDITIONS FOR THE ULFENDAHL-FLOCK-KHANNA PREPARATION

Egbert de Boer

Laboratory of Auditory Physics, Dept. KNO
Rm D2-210, Academic Medical Centre
Meibergdreef 9, 1105 AZ Amsterdam
the Netherlands

Introduction -- the 'sandwich model'

Let us consider, in a simplified way, the cross-section of one cochlear turn. If Outer Hair Cells (OHC's) can exert forces, they can do this in essentially two ways. In the first way the cilia actively move the Tectorial Membrane (TM) and in doing so, set also the Basilar Membrane (BM) into motion. Because of the relatively small stiffness of the cilia (Strelioff and Flock, 1984) and, especially, the tectorial membrane (TM) (Zwislocki and Cefaratti, 1989) this would be unlikely. In the second way the Organ of Corti (OC) is deformed by the OHC's, either by lengthening-shortening (Ashmore, 1987) or via tilting (Gitter and Zenner, 1988). On both sides of the OC strictly local deformations can occur (displacements over only a part of the width) as well as uniform or over-all deformations (displacements over the entire width). Elsewhere it has been shown that local deformations couple very weakly to the movements of the cochlear fluids (de Boer, 1990). Coupling with uniform displacements will be the topic studied in the present paper.

Let us especially consider certain results obtained in the Ulfendahl-Flock-Khanna (UFK) preparation (Ulfendahl et al., 1989). In this in vitro preparation the cochlea and the middle ear are excised, an opening to measure vibrations is made at the apical end of the cochlea and the preparation is, up to the tympanic membrane, immersed in fluid. In one experiment the movements of the BM were found to be of a much smaller amplitude than those of the Reticular Lamina (RL) (Khanna et al., 1989a). In another experiment vibration amplitude and phase were measured along a track in the radial direction (Khanna et al., 1989b). The amplitude of vibration of the RL was found to vary in this direction but the phase remained nearly constant. These findings suggest that the OC is periodically compressed and expanded in such a way that the cross-sectional area also varies periodically.

In the model to be described the OC is considered to be contained between two abstract 'membranes', RL and BM, that can execute independent movements. We assume that both membranes remain parallel to one another, non-uniform movements are not considered. The cross-section of the so-obtained cochlea model - the 'sandwich model' - is drawn in Fig. 1. The two membranes, BM and RL, are shown as straight lines (both in their equilibrium positions and in deflected states). The OHC's are situated between the

two membranes. On their upper ends they are anchored in the RL. On the side of the BM they are attached to supporting cells, Deiters' cells. In the simplest possible representation the Deiters' cells are assumed to be rigid and the influence of the phalangeal processes is neglected. Then the only thing the OHC's can do is to displace the two membranes with respect to one another. This will cause the cross-sectional area of the OC to vary and fluid to be moved inside the OC channel, an effect that definitely has to be taken into account.

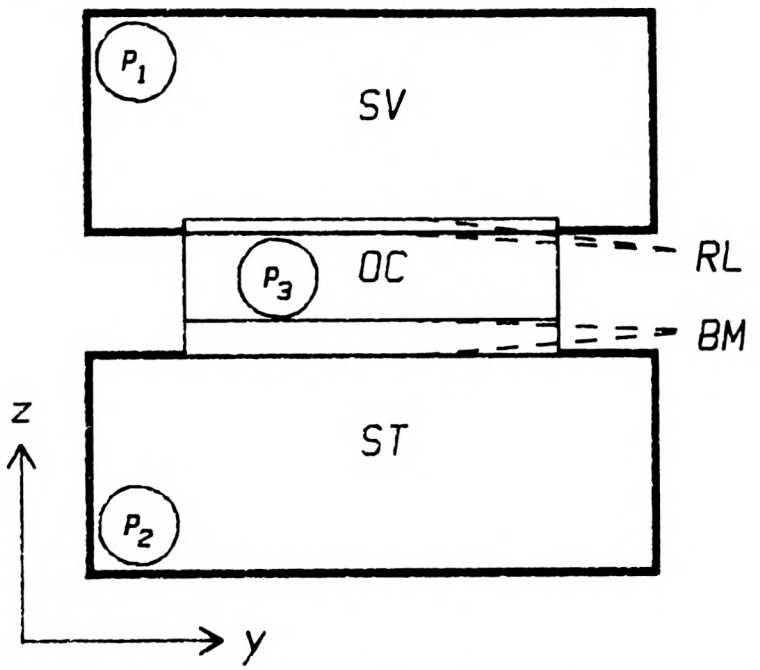

FIGURE 1 Cross-section of one cochlear turn stylized to form the 'sandwich model'. The Organ of Corti (OC) is considered as the third fluid channel.

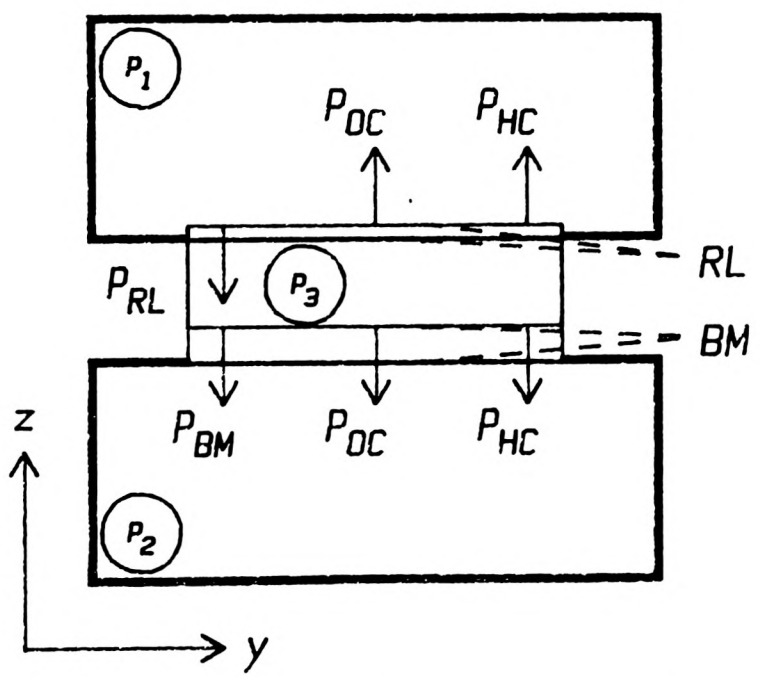

FIGURE 2 As Fig. 1, with pressures exerted by membranes and hair cells added.

Model equations — hydrodynamics, membrane and hair-cell dynamics

In a conventional model of the cochlea p_1 and p_2 are anti symmetrical. This is not so in the sandwich model considered in this paper, the pressures p_1 and p_2 are independent variables and their sum is not necessarily zero. A third pressure, p_3 in Fig. 1, has to be included and the hydrodynamics of the sandwich model is therefore more complex than in a classical model.

Let us assume, for simplicity, that long waves can travel in the channels and along the membranes of the model. This implies that the main fluid movements occur in the x-direction, perpendicular to the plane of the figure and that all fluid pressures are only functions of x.

Let us first consider channel 1. Conservation of fluid volume and Newton's law lead to the following two equations:

$$A_1 \frac{d v_{x1}}{d x} = b\, V_{RL} \tag{1-a}$$

and

$$\frac{d p_1}{d x} = -i\, \omega D_1\, v_{x1} \tag{1-b}$$

where ω is 2 π times the frequency f, v_{x1} is the point velocity of the fluid in the x direction, A_1 the cross-sectional area of the channel, b the width and v_{RL} the velocity of the RL, and D_1 the density of the fluid. Combination of these equations gives the fluid equation for channel 1 as

$$\frac{d^2 p_1}{d x^2} = -\frac{i\, \omega D_1}{h} v_{RL} \tag{2}$$

where the effective height h is introduced for A_1/b. For the fluid in the lower channel (scala tympani) a similar equation can be derived:

$$\frac{d^2 p_2}{d x^2} = +\frac{i\, \omega D_1}{h} v_{BM} \tag{3}$$

where v_{BM} is the velocity of the BM. The effective height is assumed to be the same. It is straightforward to write down the fluid equation for channel 3:

$$\frac{d^2 p_3}{d x^2} = -i\, \omega D_3 \frac{v_{BM} - v_{RL}}{h_3} \tag{4}$$

where h_3 is the effective height of this channel. The quantity D_3, the fluid density, is now a complex number, it should have a substantial imaginary part to represent frictional losses inside the OC. For simplicity we will make D_3 equal to D_1 and absorb the

imaginary component of D_3 into h_3 by making h_3 complex. The imaginary part of h_3 should then be negative. Note that the magnitude of h_3 is much smaller than h, by a factor between 10 and 40.

Substitution of eqs. (2) and (3) into eq. (4) gives:

$$\frac{d^2 p_3}{d x^2} = - \frac{h}{h_3} \frac{d^2}{d x^2} (p_1 + p_2) \tag{5-a}$$

and this equation can directly be integrated twice to yield (the two integration constants involved are zero):

$$p_3 = - \frac{h}{h_3} (p_1 + p_2) \tag{5-b}$$

We next consider the pressures acting on the (deflected) membranes, in Fig. 2 they are indicated by arrows and double-subscripted symbols. The associated impedances are:

ZBM: the impedance with which the BM is attached to the walls of the cochlea,
ZRL: the impedance with which the RL is attached to the outer walls, and
ZOC: the impedance with which RL and BM are attached to each other.

The dependence of these impedances on x and the radial frequency ω is not specifically indicated.

The relations between membrane pressures and velocities are:

$$p_{BM} = Z_{BM} \, v_{BM} \tag{6}$$

$$p_{RL} = Z_{RL} \, v_{RL} \tag{7}$$

$$p_{OC} = Z_{OC} (v_{BM} - v_{RL}) \tag{8}$$

The two remaining pressures, p_{HC}, are produced by the motility of the OHC's. It will be assumed that the OHC's are stimulated by way of their cilia. Because the cilia are partly imbedded in the tectorial membrane which slides in the radial direction over the RL, the OHC response will be related to the velocity v_{RL}. This is written in the form:

$$p_{HC} = Z_{HC} \, v_{RL} \tag{9}$$

where the parameter Z_{HC} has the meaning of a transfer impedance. Relation (9) is linear, it is assumed to hold true for the small amplitudes we are considering here. In the semi static case Z_{HC} would have the form of the reactance of a stiffness (in this representation negative). Some form of high-frequency cut- off should be incorporated in Z_{HC} because of the influence of hair-cell membrane capacitance and other limitations on OHC motility speed.

For the equilibrium of pressures at the two membranes the following equations can be written down:

$$p_{HC} + p_{OC} + p_3 = p_1 + p_{RL} \tag{10}$$

and

$$p_{HC} + p_{OC} + p_{BM} + p_3 = p_2 \tag{11}$$

By substitution of earlier equations the following model equations are obtained:

$$\frac{(ad - bc)}{E}\frac{d^2 p_1}{dx^2} = d\,p_1 - b\,p_2 + (b - d)\,p_3 \tag{12}$$

and

$$\frac{(ad - bc)}{E}\frac{d^2 p_2}{dx^2} = -c\,p_1 + a\,p_2 + (c - a)\,p_3 \tag{13}$$

with the parameters given by:

$$\begin{aligned} E &= i\omega D_1 / h \\ a &= Z_{OC} + Z_{RL} - Z_{HC} \\ b &= Z_{OC} \\ c &= Z_{OC} - Z_{HC} \\ d &= Z_{OC} + Z_{BM} \end{aligned} \tag{14}$$

Wave propagation — the basic 'modes' of the model

Because the sandwich model is a fourth-order system four types of wave are possible, four eigen functions, or modes. To simplify understanding all parameters are assumed to be constant and Z_{RL} is made zero. In each of the eigen function solutions p_2 and p_1 have a constant ratio, let us call this α ($\alpha = p_2/p_1$). For each possible value of α the two equations (12) and (13) must be equivalent, this condition leads to the following quadratic equation to be obeyed by α:

$$\left(Z_{OC} - \frac{h}{h_3} Z_{BM}\right)\alpha^2 + \left(-\frac{h}{h_3} Z_{BM} - Z_{BM} - Z_{HC}\right)\alpha + Z_{HC} - Z_{OC} = 0 \tag{15}$$

Neglecting all terms except those with h/h_3 gives a much simpler form:

$$\alpha^2 + \alpha + \frac{Z_{OC} - Z_{HC}}{(h / h_3) Z_{BM}} = 0 \tag{16}$$

In good approximation the two roots of this equation are:

$$\alpha_1 = -1 + \frac{Z_{OC} - Z_{HC}}{(h / h_3) Z_{BM}} \tag{17}$$

and

$$\alpha_2 = - \frac{Z_{OC} - Z_{HC}}{(h / h_3) Z_{BM}} \tag{18}$$

To each of the roots correspond two modes of wave propagation, one in each direction of propagation. We will only consider waves that travel 'to the right', i.e., in the direction of increasing x, so only two of the four modes are left, one for each root.

The first root, $\alpha = \alpha_1$, is very close to $\alpha = -1$, valid for the 'classical' case. If α were exactly equal to -1, it is only the BM impedance that governs the wavenumber. This mode can thus be called the 'BM mode'. Because of the large value of h/h_3 the OHC's cannot contribute materially to the wave pattern in this mode.

The second root, α_2, seems more promising in this respect. The approximate wave equation which corresponds to this root reads:

$$\frac{d^2 p_1}{d x^2} = \frac{i \omega D_1}{Z_{OC} - Z_{HC}} \frac{h}{h_3} p_1 \tag{19}$$

in which we recognize the equation for a long-wave cochlear model, where a modified form of the hair-cell transfer impedance is playing the part of the partition impedance and h_3 that of the scala height. Since α_2 is small, nearly all wave activity is taking place in the OC and the upper channel and the BM is hardly moving. We will describe this solution as the 'OC mode'. It is likely that this is the principal mode observed in the UFK preparation.

Boundary conditions and tuning

The sandwich model will, under actual conditions, show a linear combination of the modes of the system. Which combination will arise, depends on the boundary conditions. One may describe the working condition of the cochlea in the UFK preparation as follows. The vibrating tympanic membrane sets up a compression wave in the fluid. This wave will reflect against the fluid surface; it will present a large mass-like impedance to the tympanic membrane. With increasing distance from the membrane the fluid velocity will decrease rapidly.

Let us first consider the entry port at the extreme apical end of the cochlea ($x = L$) - this port is open in the UFK preparation. The sound field in the fluid surrounding the opening is nearly homogeneous hence at this point the pressures and velocities in the two main channels can be taken as equal. Therefore, the cochlea is not excited from this entry port. It is immaterial whether the third channel is open or not at this point.

Let us next consider the impedance relations at the windows. Seen from inside the cochlea the impedance of the fluid outside is large and mass-like, and probably much larger in magnitude than the impedance associated with any of the wave modes. Hence the windows are driven by velocity sources.

The movement of the stapes will be similar to the movement of the tympanic membrane but it will have a somewhat reduced amplitude due to the lever action of the

ossicles. The round window will move with the fluid around it. Due to the spreading-out of the fluid wave the velocity of the round window will be (much) smaller than that of the stapes. This corresponds approximately to the required drive for the second mode, the OC mode. Hence, it is this mode which is excited with the largest amplitude, and the observed response will be dominated by it.

As a matter of fact, it is fairly easy to demonstrate this property by solving eqs. (12) and (13) for parameters that vary with x and using the just-described boundary conditions. It then turns out that it is not difficult to simulate the type of response obtained by Khanna et al. (1989a) in the UFK preparation *). It is even not necessary to include BM mass to achieve a satisfactory response. The findings will be reported in more detail later. It is recalled from eq. (19) that $(Z_{OC} - Z_{HC})$ is the main controlling impedance for the OC mode.

A general experience with parameter manipulation in the sandwich model is that the OC mode is very susceptible to damping in the third channel. Simulation of the response obtained by Khanna et al. (1989a) is only possible when the resistive terms are kept small. For the low frequencies employed in these experiments this is entirely reasonable. However, it is to be doubted whether the same type of response can exist for frequencies well above 1 kHz. For this reason it is questionable whether the data obtained in the UFK preparation can be used to predict what happens at higher frequencies, or in more basal turns of the cochlea.

It should be stressed again that in the theoretical results for the OC mode Z_{OC} and (Z_{HC}) are playing equivalent parts. If the interpretation in terms of the sandwich model is correct, this leads to the conclusion that it is not possible to find out which of the two impedances is the most important one in the response of the UFK preparation. Or, in different terms, it is not possible to ascertain that OHC's are really active in this preparation. Only further physiological experiments can provide the answer.

*) A demonstration program for a PC/AT can be obtained from the author.

References

Ashmore, J.F. (1987) A fast motile response in guinea-pig outer hair cells: the cellular basis of the cochlear amplifier. J. Physiol. (Lond.) 388, 323-347.

Boer, E. de. (1990) Can shape deformations of the Organ of Corti influence the travelling wave in the cochlea? Hearing Res.44, 83-92.

Gitter, A.H. and Zenner, H.-P. (1988) Auditory transduction steps in single inner and outer hair cells. In: Basic Issues in Hearing (Eds: Duifhuis, H., Horst, J.W. and Wit, H.P.), Acad. Press, London, pp. 32-39.

Khanna, S.M., Flock, Å. and Ulfendahl, M. (1989a) Comparison of the tuning of outer hair cells and the basilar membrane in the isolated cochlea. Acta Otolaryng. (Stockh.) Suppl. 467, 151-156.

Khanna, S.M., Flock, Å. and Ulfendahl, M. (1989b) Changes in cellular tuning along the radial axis of the cochlea. Acta Otolaryng. (Stockh.) Suppl. 467, 163-173.

Strelioff, D. and Flock, Å. (1984) Stiffness of sensory-hair bundles in the isolated guinea pig cochlea. Hear. Res. 15,19-28.

Ulfendahl, M., Flock, Å. and Khanna, S.M. (1989) A temporal bone preparation for the study of cochlear micromechanics at the cellular level. Hear. Res. 40, 55-64.

Zwislocki, J.J. and Cefaratti, L.K. (1989) Tectorial membrane II:Stiffness measurements in vivo. Hear. Res. 42, 211-227.

ON DIPOLES AND THE RADIATING MEMBRANE

J.S.C. van Dijk

Institute of Phonetic Sciences
University of Amsterdam, Herengracht 338, 1016 CG Amsterdam, The Netherlands

Introduction

In this work we shall assume that the basilar membrane is found at the real axis of the complex z-plane. The membrane is surrounded by a fluid. The hydrodynamical pressure p depends on space and time. The actual pressure p(x,0,t) at the membrane consists of a known part which results from a forced fluid flow and an unknown disturbance. The unknown pressure is often called the radiation pressure.
If mechanical properties at a point x of the membrane are represented by a simple harmonic oscillator and we assume zero initial conditions, the Laplace transform of the pressure-deflection ratio can be written as

$$m (s^2 + 2 \delta(x) s + \omega_0^2(x)) \eta(x,s) = - 2 p(x,0,s) \quad . \tag{1}$$

$\eta(x,s)$ and $p(x,s)$ respectively are the transformed membrane deflection and pressure at x. The right member of (1) represents the pressure difference across the membrane at x. m is the effective mass and $\omega_0(x)$ the resonance frequency of the oscillator. $\delta(x)$ is a damping parameter which models internal oscillator losses.
The coupling between membrane and surrounding structures or fluid is expressed by means of the Euler equations to which a frictional force proportional to the velocity has been added (Van Dijk, 1976). At the membrane the transform of this coupling reads

$$(\rho s^2 + \lambda s) \eta(x,s) = - \frac{\partial p(x,0,s)}{\partial n} \quad . \tag{2}$$

ρ is the density of the fluid; n stands for the normal to the membrane at x and λ is the constant of proportionality which models the amount of external friction near the membrane. Damping parameters are chosen according to

$$\delta(x) = \sin \varepsilon_1 \omega_0(x) \quad \text{and} \quad \lambda = \rho \varepsilon_2 \omega \quad , \tag{3}$$

in which ε_1 and ε_2 are small positive numbers. ω denotes the circular frequency. Zeros of the left member of both (1) and (2) are at the left of the imaginary axis of the complex s-plane. For reasons of convenience we shall turn this plane a quarter of a turn to the left.

This is accomplished by putting w=is. From (1), (2), (3) and w=is follows that the pressure at the membrane obeys the equation

$$\frac{\partial p(x,w)}{\partial n} = \nu \left(\frac{w}{\omega_0(x) + w \exp(-i\varepsilon_1)} - \frac{w}{\omega_0(x) - w \exp(+i\varepsilon_1)} \right) p(x,w) \quad , \tag{4}$$

in which

$$\nu = \mu \left(1 + i \frac{\varepsilon_2 \omega}{w} \right) \quad \text{and} \quad \mu = \frac{\rho}{m \cos \varepsilon_1} \quad . \tag{5}$$

In the next section we solve eq. (4). Some good and bad properties of its solution will be discussed. Details are given in Van Dijk (1989). It will appear that near resonance it is necessary to reinvestigate eq. (1). This will be done in section 'model 2'. Subsequently, we will give some consequences concerning modeling.

Model 1

Gummer and Johnstone (1983) showed that there is reason to approximate $\omega_0(x)$ as a linear decreasing function along the membrane. We shall assume that the basilar membrane coincides with the negative real axis of the z-plane. Its high frequency side points to minus infinity and its low frequency part is near the origin. In consequence of this we define $\omega_0(x)$ according to

$$\omega_0(x) = Q|x| \quad , \quad -\infty < x < 0 \quad . \tag{6}$$

Insertion of (6) in (4) yields

$$\frac{\partial p(x,w)}{\partial n} = \nu \left(\frac{w}{Qx + w \exp(+i\varepsilon_1)} - \frac{w}{Qx - w \exp(-i\varepsilon_1)} \right) p(x,w) \quad . \tag{7}$$

We shall look at (7) as an equation in the complex z-plane which is applicable at the negative real axis. For the sake of simplicity we shall restrict ourselves to real values of w. The right member of (7) has singularities (points of resonance) at

$$z_1 = -\frac{w}{Q} \exp(+i\varepsilon_1) \, , \quad z_2 = +\frac{w}{Q} \exp(-i\varepsilon_1) \quad . \tag{8}$$

z_1 and z_2 depend on the sign of w. Therefore we distinguish among w= |w| and w= - |w|. We first consider the case w= |w|. z_1 and z_2 are points below the real axis. In consequence of this, we propose to conceive the pressure in (7) as the boundary value of a function p(z,w) which is analytic in the upper halfplane Im $z \geq 0$. In (7) the abscissa comprises the scaling factor Q/|w|. We shall assume that the unknown ordinate includes the same scaling factor. Therefore we replace in (7) the normal n by Qy/|w|. From these considerations readily follows that the solution of (7) reads

$$i \ln p(z,w) = \nu \ln \frac{z - z_1}{z - z_2} + C \ . \qquad (9)$$

z_1 and z_2 are given by (8) in which w= |w|. p(z,w) is regular in the upper halfplane and bounded for $z \rightarrow \infty$. Due to its analytic behaviour in the upper halfplane, the pressure satisfies Laplace's equation. That means, p(z,w) is the pressure in an incompressible inviscous fluid. The constant C can be used to fit p(z,w) to a prescribed pressure at any point of the membrane. In the sequel we shall omit this and similar constants.
Next we consider the case w= - |w|. According to (8), z_1 and z_2 are points in the upper halfplane and we have to approach the real axis from the lower halfplane. In this way the complex conjugate counterpart of p(z,w) is found.
z= - |x|, $-\infty < x < 0$; y=0, represents a point of the membrane. If this point is introduced in (9) we find with the help of (6) and (8) that, at the membrane, (9) is a special case of

$$\ln p(x,w) = - i \nu \ln \frac{\omega_0(x) - w \exp(+i\varepsilon_1)}{\omega_0(x) + w \exp(-i\varepsilon_1)} \ , \qquad (10)$$

in which $\omega_0(x)$= Q|x|, $-\infty < x < 0$. The same expression is found in the complex conjugate case. Thus (10) does not depend on the sign of w.
Let us return to the complex s-plane by inserting w=is in (10). Scaling of s with $\omega_0(x)\cos\varepsilon_1$ yields

$$\ln p(s) = i \nu \ln \frac{s + \tan \varepsilon_1 - i}{s + \tan \varepsilon_1 + i} \ . \qquad (11)$$

ν follows from (6). Characteristics of ln|p(s)| and arg(p(s)) are given in Fig.1a and 1b for s=iω ($\omega < 0$). At resonance the amplitude of the pressure is (almost) discontinuous and the phase weakly singular. These effects are unnatural and will be removed in the next section.

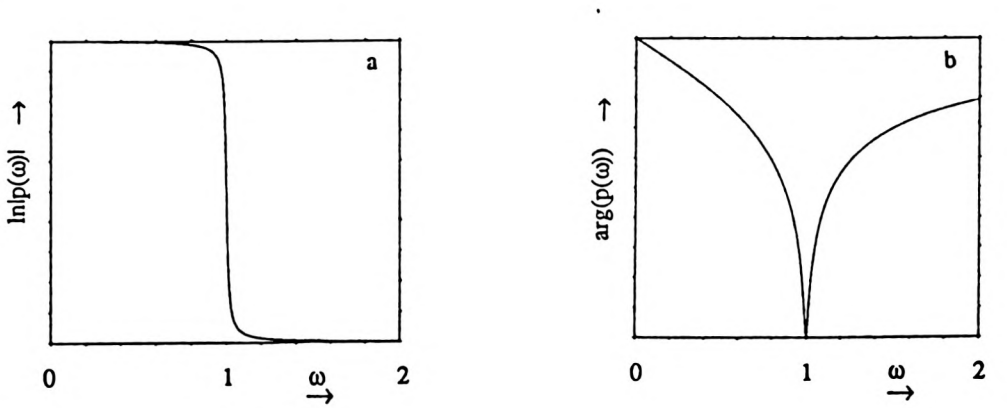

FIGURE 1 Normalized amplitude and phase characteristics of the pressure (11) at the axis s=iω ($\omega > 0$). Damping parameters are close to zero.

From (11) follows that at $\omega=0$ ($s=i\omega$; $\varepsilon_1, \varepsilon_2 << 1$) :

$$\lim_{\omega \to 0} \frac{d \arg(p(\omega))}{d\omega} \approx -2\mu \ .$$

This means that the scaled delay time of the pressure equals 2μ. Re-scaling and application of $\omega_0=k(x)/m$ yields

$$\tau(x) \approx \frac{2\mu}{\omega_0(x) \cos \varepsilon_1} = 2\frac{\rho}{\sqrt{m\, k(x)}} \ ,$$

where μ is according to (5). k(x) is the stiffness of the oscillator at x. The scaled delay time τ is visible in the impulse response (Fig. 2a) which follows from (11). The straight line in Fig. 2b is a plot of $\tau(x)$ as a function of $f_0(x)=\omega_0(x)/2\pi$ with $\mu=20$. The dots are cochlear nerve delay times for the chinchilla as a function of the 'best frequency' of the nerve-fibre (Ruggero, 1987).

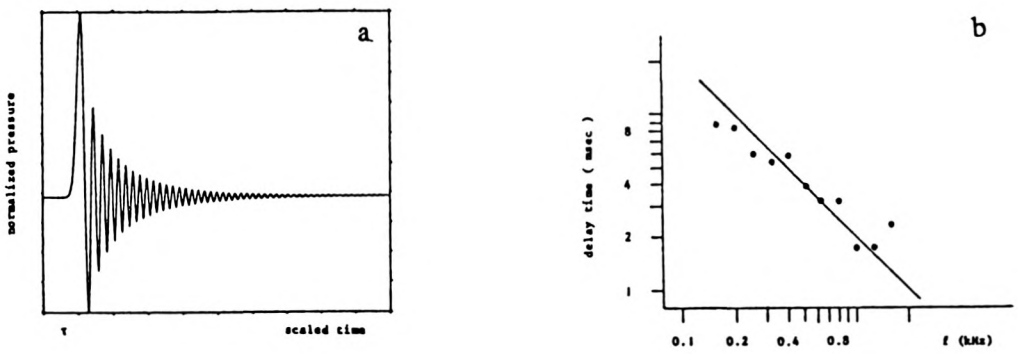

FIGURE 2 Fig. 2a: the scaled delay time $\tau = 2\mu$ is visible in the impulse response which follows from (11). Fig. 2b: the delay time $\tau(x)$ -straight line - and cochlear nerve delay times for the chinchilla after Ruggero and Rich (1987).

Model 2

Let us consider a small strip of the membrane. Subsequent membrane fibres are characterized by a harmonic oscillator. The oscillators are centered around x_0. The width of the strip is 2c (Fig. 3). First we assume that there is no coupling between adjacent fibres. Then, if a unit force is excerted at x_0, only the oscillator at x_0 will show a deflection. In reality membrane fibres are covered with soft structures. Besides, the organ of Corti covers an important part of the membrane. In that case the unit force at x_0 is spread about evenly over a small region of the membrane.

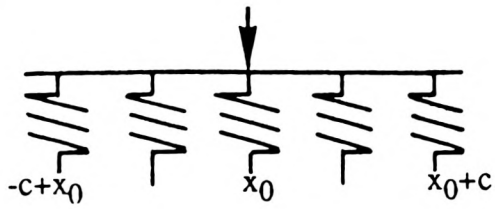

FIGURE 3 If we excert a unit force at x_0, all membrane oscillators in a small region $|x - x_0| < c$ determine the actual deflection at this point.

This implies that the pressure within that region is about 1/2c. For the effective deflection η_{eff} at x_0 we propose the expression

$$\eta_{eff} = \frac{1}{2cm} \int_{x_0+c}^{x_0-c} \frac{dx}{s^2 + 2\delta(x) + \omega_0^2(x)} , \tag{12}$$

so that the deflection-pressure ratio equals the integral in (12). Often membrane fibres are modelled as bars with appropriately chosen boundary conditions. If we use the concept of a function of Green as the sum of normalized eigenfunctions, a similar reasoning leads to the same result. If the point of resonance belongs to the region of integration in (12), the integrand has two simple poles. After decomposition of the fraction in (12) and integration of the result, we are led to a system of dipoles in the x-domain. If the point of resonance is outside the limits of integration, in principle the first model remains valid. In the sequel we shall omit all scaling factors and restrict ourselves to model behaviour near the region of resonance. This can be done by studying the dipole equivalent of (7) in a normalized shape. The equation reads

$$H(z) \frac{\partial p}{\partial n} - p = 0 , \; -\infty < x < 0 ; \; y = 0 , \tag{13}$$

in which

$$\frac{1}{H(z)} = \nu \left(\ln \frac{z - z_1}{z - z_2} - \ln \frac{z - z_3}{z - z_4} \right) . \tag{14}$$

ν is given by (5). The singular points are below the real axis and are given by

$$\begin{aligned} z_1 &= - \exp(+i\varepsilon_1) - c & z_2 &= - \exp(+i\varepsilon_1) + c \\ z_3 &= + \exp(-i\varepsilon_1) - c & z_4 &= + \exp(-i\varepsilon_1) + c . \end{aligned} \tag{15}$$

For the same reasons as have been pointed out in the previous section, we decide to write the solution of (15) as

$$\begin{aligned} i \ln p(z) = {} & \nu (z-z_1) \ln (z-z_1) - \nu (z-z_2) \ln (z-z_2) \\ & - \nu (z-z_3) \ln (z-z_3) + \nu (z-z_4) \ln (z-z_4) . \end{aligned} \tag{16}$$

Plots of $\ln|p(z)|$ and $\arg(p(z))$ at the membraneous part of the real axis are given in Fig. 4.

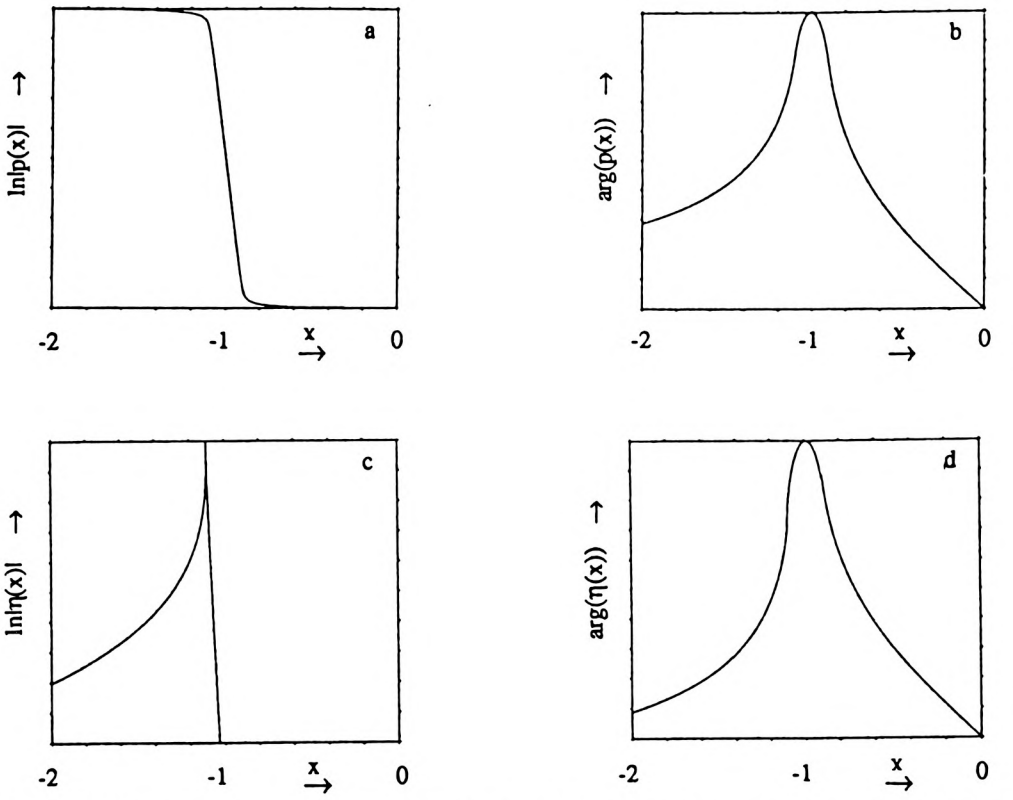

FIGURE 4 Normalized amplitude (a) and phase (b) behaviour of the pressure (16) along the membrane for - 2 < x < 0. The region of resonance is: | x + 1 | < c, with c = 0.1. The next two figures show the amplitude (c) and phase (d) behaviour of the deflection. Note that the shift between the peak at resonance and the place at which the phase is maximal, is about c = 0.1. Even at vanishing values of the damping parameters, the phase of the pressure and deflection remains bounded.

These figures correspond to positive values of w which represent negative values of the frequency ω. Between the poles of the dipole, the amplitude of the pressure rapidly diminishes to a low level in a continuous way. Independent of the damping the phase remains bounded. Its range mainly depends on c and ν. Typical values of this range are 7π - 8π. The last two plots in Fig.4 show amplitude and phase characteristics of the deflection which follow from (13), (14) and (16). After re-scaling of the variables in (16), the pressure at a certain point x of the membrane can be studied as a function of the normalized frequency. It appears that the delay time in model 2 is about the same as in the model 1.

Model 3

Zwislocki (1965) showed that phase plateaus originate from a turning point in a second order equation for the pressure. It is easy to derive such an equation. For, assume that the mean scala height h is sufficiently small (Fig.5) and that the fluid velocity normal to a bony wall (y = h) vanishes. Then we have

$$p_{yy} \approx \frac{p_y(h) - p_y(0)}{h} = -\frac{1}{h} p_y(0) \ . \qquad (17)$$

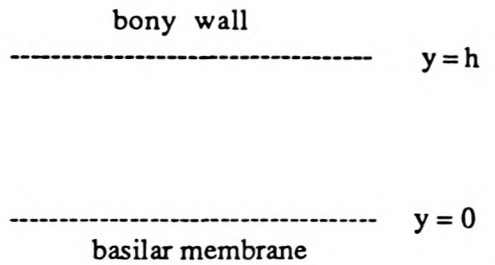

FIGURE 5 If the scala height h is sufficiently small, the rate of change of the fluid velocity in the y - direction is proportional to the velocity of the membrane.

If the fluid in the scala obeys Laplace's equation , i.e. $p_{yy} = - p_{xx}$, we find from (13) and (17) that

$$p_{zz} + G(z)\, p = 0 \; ; \; G(z) = - \frac{1}{hH(z)} \; , \; - \infty < x < 0 \; ; \; y = 0 \; . \qquad (18)$$

(18) is Zwislocki's equation. G(z) - which follows from (14) and (18) - defines a turning region between the poles of the dipole. The fall of the pressure within that region is rather mild. In consequence of this, the resonance curve for the magnitude of the deflection shows a small second 'resonance' peak (Fig. 6).

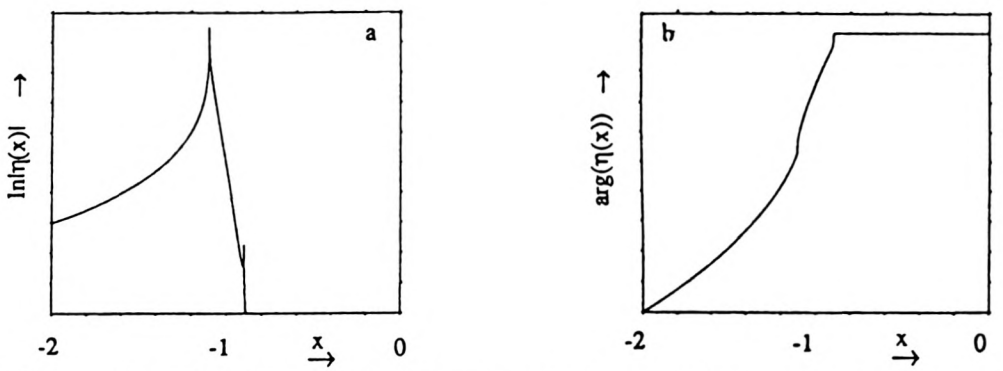

FIGURE 6 Normalized amplitude (a) and phase (b) behaviour of the membrane deflection according to (18). The distance between the dipoles determines the slope after resonance. The shift between the main resonance peak and the place at which the phase plateau occurs, is about 2c with c = 0.1.

Within the turning region the change of phase of G(z) is rather whimsical. This results in a 'disturbance' in the phase characteristic of the deflection near resonance. In order to overcome this evil, we propose a linear approximation to the change of phase within the turning region. This can be accomplished by application of elaborate membrane oscillator models. However, from Fig. 4a and Fig. 4b follows that a possible candidate can be written as

$$F(z) = C \exp(- \alpha f(z)) \; , \qquad (19)$$

in which f(z) is the right member of (16). C is a constant and α controls the magnitude of the change of phase within the turning region. The next figure is a plot of characteristics of the membrane deflection, which follows from Zwislocki's equation and

membrane oscillators of the kind (19) in the lossless case. The constant C has been determined experimentally.

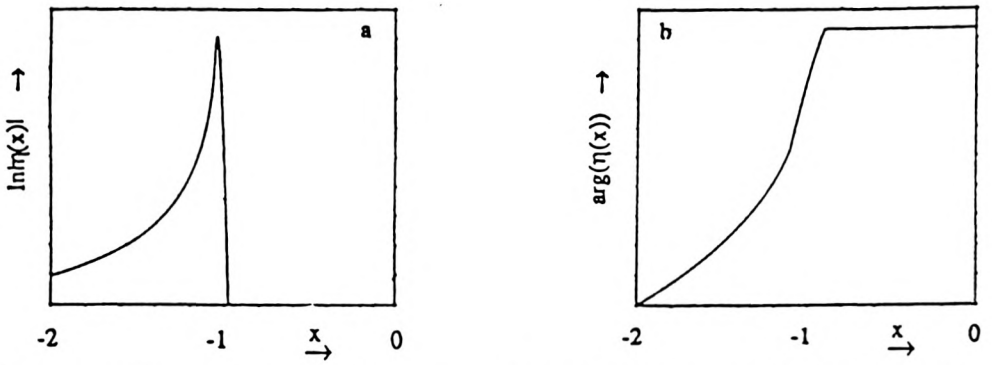

FIGURE 7 'Near resonance' behaviour. Normalized amplitude (a) and phase (b) of the membrane deflection in the lossless case. Membrane oscillators are given by (19). The dipole distance 2c = 0.1.

Conclusions

The present way of modelling shows that application of elementary mathematics rapidly leads to membrane models which possess several good (and bad) properties. Model parameters can be ascribed to separate physical effects. Far from resonance, simple oscillators can be used to model the main properties of basilar membrane fibres. However, if we assume that the internal damping of a membrane fibre is negligible, most models suffer from catastrophic resonance at at least one point of the membrane. We introduced a region of resonance, marked by the poles of a dipole. Within that region it is possible to describe behaviour of elaborate membrane oscillators which suppress infinite resonance. Near resonance the peak of the deflection has been shifted towards the high frequency side of the membrane. After resonance these models lead to phase plateaus. It seems to be meaningful to distinguish between 'near resonance' and 'far from resonance' descriptions of membrane oscillators and to combine the separate approximations in one model. In order to arrive at a better understanding of what happens at resonance, the physical background of (19) has to be investigated.

Acknowledgements

We thank René van Egmond who provided help throughout this work.

References

Dijk, J.S.C. van (1976) On the hydrodynamics of the inner ear. Theoretical part. A mathematical model. Acustica 35, 190 - 201.

Dijk, J.S.C. van (1989) Notes on cochlear filtering. In: Proceedings 13 Inst. of Phonetic Sciences, Amsterdam, pp. 133 - 143.

Gummer, A.W. and Johnstone, B.M. (1983) State of stress within the basilar membrane: a re-evaluation of the basilar membrane misnomer. Hearing Research 12, 353 - 366.

Ruggero, M.A. and Rich, N.C. (1987) Timing of spike initiation in cochlear afferents: dependence on the side of innervation. J. Neurophysiol. 58, 379 - 403.

Zwislocki, J.J. (1965) Analysis of some auditory characteristics. In: Handbook of Mathematical Psychology (Eds: Luce, R.D. et al). John Wiley, New York.

APPROXIMATE EVALUATION OF COCHLEAR MODEL TUNING FROM THE WAVE DEVELOPMENT GRAPH

S. M. Novoselova

V.A. Steklov Mathematical Institute
Academy of Sciences of the USSR
Leningrad, 191011, USSR

Introduction

The simplest direct results of most numerical and hemi-analytical models are the wave development graphs. To compare the model results with experimental data, the theoretical tuning curve must be calculated. For this aim, the exterior cycle over the stimulating frequency must be included into the program, and the complex matrix of responses $R(\omega, x) = A(\omega, x) \exp(i\phi(\omega, x))$ must be obtained.

The visual similitude of cochlear tuning curves and wave development graphs can be seen in model results, as well as in Békésy's classical experimental data (1960). If this similitude may be proved analytically, then comparison of model and experimental results becomes much more simple.

Formulation of the problem

Consider a complex matrix $R(\omega, x)$ of cochlear model responses. If the columns of this matrix are the wave development curves, the lines are the tuning curves. Let us choose any pair of column and line, such that their peaks are at the same characteristic frequencies (Fig. 1a, 1b). The longitudinal cochlear axis x may be scaled in main eigenfrequencies ω_0 of the basilar membrane cross sections:

$$\omega_0(x) = \frac{\pi^2}{b^2(x)} \sqrt{\frac{D(x)}{\mu(x)}}$$

where $b(x)$ is the width of the basilar membrane, $D(x)$ is the transverse component of basilar membrane stiffness, and $\mu(x)$ is the mass density of the section. For simplicity, stiffness and mass are assumed to be constant in the transverse direction.

In the points of maxima, which are at the same characteristic frequency, amplitudes and phases of both curves are equal. (See Figs. 1a and 1b.) Let us agree to name the amplitude curves similar in some regions around the peaks if the amplitudes are also equal

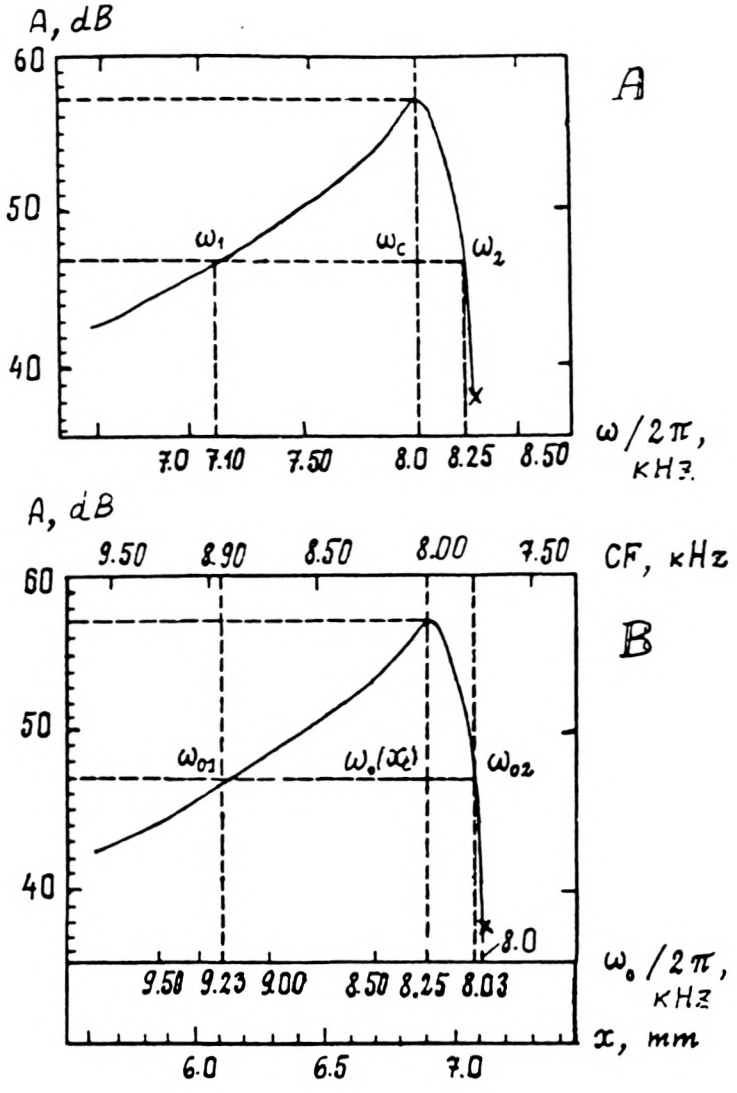

FIGURE 1 Comparison of the tuning (A) and the wave development (B) curves, with peaks, located at the same characteristic frequency.

at equal distances from the peaks, in frequency and eigenfrequency domains, to the left and to the right from the peaks respectively.

If the size of the region of similitude is large enough, the analogue of the Q-factor may be introduced at the amplitude-vs-eigenfrequency graph:

$$Q_{N\,\mathrm{dB}}(\omega_0) = \frac{\omega_0(x_c)}{|\omega_{01} - \omega_{02}|} \tag{1}$$

This magnitude will approximate the standard Q-factor in the frequency domain:

$$Q_{N\,\mathrm{dB}} = \frac{\omega_c}{|\omega_1 - \omega_2|} \tag{2}$$

where:

$$| \omega_1 - \omega_t | = | \omega_{01} - \omega_0 (x) |$$

$$| \omega_2 - \omega_t | = | \omega_{02} - \omega_0 (x_c) | \tag{3}$$

$$\Delta \omega_0 = \omega_0 (x_c) - \omega_t \ll \omega_t \tag{4}$$

Thus, the problem is to verify the similitude of small vicinities of the peaks in frequency and eigenfrequency domains.

Solution

In some hemi-analytical cochlear models, the approximate analytical expressions for amplitude and phase functions in a narrow vicinity of the peak can be obtained (de Boer and Viergever, 1982). However, these expressions are still too complicated. A more effective way is to consider some equations that entirely determine cochlear response amplitude and phase.

Such a set of equations may be, for example, the eiconal and transport equations, or the expression for the Lagrangian function of the model.

Consider a simple two-chambered, three-dimensional cochlear model. Let the mass density $\mu (x)$ and the transverse stiffness $D (x)$ be constant in each cross section, while the longitudinal stiffness is zero. The fluid in the channels is slightly viscous. Upper and lower channels are similar. The long borders of the basilar membrane are hinged.

The eiconal and transport equations may have the form (Novoselova, 1985) :

$$G (\omega, x) = \frac{\pi^4 D (x)}{b^4 (x)} - \omega^2 \mu (x)$$

$$\frac{16 \rho \omega^2 b (x) \coth (\xi H)}{p^2 L (x) \xi} \left(1 - \frac{\mu \xi^2}{2 \rho} \sqrt{\frac{i \nu}{\omega}} \right) = 0 \tag{5}$$

$$W (\omega, x) = \frac{\text{Const}}{\frac{\partial G}{\partial \xi}} \tag{6}$$

Here $L (x)$ and $H (x)$ are the width and the height of cochlear channels respectively, ρ and ν are mass density and viscosity of perilymph, $\xi (\omega, x)$ and $W (\omega, x)$ are the wave number and complex amplitude of the travelling wave.

Two unknowns in these equations are $\xi (\omega, x)$ and $W (\omega, x)$. They are related to the cochlear response function $R (\omega, x) = A (\omega, x) \exp (i \phi (\omega, x))$ through the equations :

$$A (\omega, x) = | W | \exp \left(\int_0^x \text{Im} (\xi) \, dx \right)$$

$$\phi (\omega, x) = - \int_0^x \mathrm{Re} (\xi) \, dx + \mathrm{Arctan} \left(\mathrm{Im} (W) / \mathrm{Re} (W) \right)$$

It may be seen, that the solution of the transport equation (6) is entirely determined by the solution of the eiconal equation. So, only the last one must be investigated.

The numerical computations show, that in the vicinity of the peak, Re (ξH) >> 2.7 and Coth (ξH) =1.

Let us transform further the expression (5) :

$$G (\omega, \omega_0 (x)) = \frac{G (\omega, x)}{\mu (x)}$$

$$= \omega_0^2 (x) - \omega^2 - \omega^2 \frac{\psi (x)}{\xi} + \omega^{3/2} r (x) \xi \qquad (7)$$

where :

$$\psi (x) = \frac{16 \rho b (x)}{\pi^2 \mu (x) L (x)} \quad , \quad r (x) = \frac{8 b (x) \sqrt{i \nu}}{\pi^2 L (x)} \qquad (8)$$

The amplitudes under consideration are thus determined finally by the solutions $\xi(\omega,\omega_0(x))$ of the equation (7). In close vicinity of the peak points, the function $G(\omega,\omega_0(x))$ may be represented by the Taylor series :

$$G (\omega, \omega_0 (x_c)) = G (\omega_c, \omega_0 (x_c)) + \left. \frac{\partial G}{\partial \omega} \right|_{\omega = \omega_c} d \omega + \ldots \qquad (9)$$

$$G (\omega_c, \omega_0 (x)) = G (\omega_c, \omega_0 (x_c)) + \left. \frac{\partial G}{\partial \omega_0} \right|_{\omega_0 = \omega_0 (x_c)} d \omega_0 + \ldots \qquad (10)$$

where :

$$\frac{\partial G}{\partial \omega} = - 2 \omega_c - 2 \omega_c \frac{\psi (x_c)}{\xi} + \frac{3}{2} \omega_c^{1/2} r (x_c) \xi \qquad (11)$$

$$\frac{\partial G}{\partial \omega_0} = 2 \omega_0 (x_c) - \omega_c^2 \frac{1}{\xi} \left. \frac{\partial \psi (x)}{\partial \omega_0} \right|_{x = x_c} + \omega_c^{3/2} \left. \frac{\partial r (x)}{\partial \omega_0} \right|_{x = x_c} \xi \qquad (12)$$

The partial derivatives may be transformed :

$$\frac{\partial \psi}{\partial \omega_0} = \frac{\partial \psi / \partial x}{\partial \omega_0 / \partial x} \qquad \frac{\partial r}{\partial \omega_0} = \frac{\partial r / \partial x}{\partial \omega_0 / \partial x} \qquad (13)$$

Most of the cochlear parameters are the approximate exponents of x :

$$b(x) = b_0 \exp(\beta x) \qquad D(x) = D_0 \exp(-c x)$$
$$\mu(x) = \mu_0 \exp(m x) \qquad L(x) = L_0 \exp(-l x) \tag{14}$$

Then the functions $\psi(x)$ and $r(x)$ are exponents too :

$$\psi(x) = \psi_0 \exp\left(\left(\beta + l - m\right)x\right) \qquad \psi_0 = \frac{16\, r\, b_0}{\pi^2 \mu_0 L_0}$$
$$r(x) = r_0 \exp\left(\left(\beta + l\right)x\right) \qquad r_0 = \frac{8\, b_0 \sqrt{i\,\nu}}{\pi^2 L_0} \tag{15}$$
$$\omega_0(x) = \omega_0(0) \exp\left(-\frac{4\beta + c + m}{2} x\right) \qquad \omega_0(0) = \frac{\pi^2}{b_0^2}\sqrt{\frac{D_0}{\mu_0}}$$

Thus the derivatives may be found :

$$\frac{\partial \psi}{\partial x} = \left(\beta + l - m\right)\psi \qquad \frac{\partial r}{\partial x} = \left(\beta + l\right) r$$
$$\frac{\partial \omega_0}{\partial x} = -\frac{\omega_0}{2}\left(4\beta + c + m\right) \tag{16}$$

Substitution of the expressions (13) and (16) into equation (12) yields :

$$\frac{\partial G}{\partial \omega_0} = 2\,\omega_0(x_c) + 2\,\frac{\omega_t^2\,\psi(x_c).\left(\beta + l - m\right)}{\omega_0(x_c).\left(4\beta + c + m\right)\xi} - 2\,\frac{\omega_t^{3/2}\, r(x_c)\left(\beta + l\right)}{\omega_0(x_c).\left(4\beta + c + m\right)}\,\xi \tag{17}$$

This expression may be transformed :

$$\frac{\partial G}{\partial \omega_0} = 2\,\omega_t\left(1 + \frac{\Delta\omega_0}{\omega_t}\right) + 2\,\frac{\omega_t\,\psi(x_c)}{\xi}\left(1 - \frac{\Delta\omega_0}{\omega_t}\right)(1 - \alpha_1)$$
$$- \frac{3\sqrt{\omega_t}\, r(x_c)}{2}\left(1 - \frac{\Delta\omega_0}{\omega_t}\right)(1 - \alpha_1)\,\xi \tag{18}$$

where

$$\alpha_1 = \frac{3\beta + c + 2m - l}{4\beta + c + m} \qquad \alpha_2 = \frac{8\beta + 3c + 3m - 4l}{3\left(4\beta + c + m\right)}$$

Let $d\omega_0 = -d\omega$. If the parameters $\Delta\omega_0 / \omega_c$, α_1 , α_2 are made less than 1, then the approximate equality of the expressions (9) and (10) is proved. Consider these parameters. The ratio $\Delta\omega_0 / \omega_c$ is really much less then 1 always within physiological values of friction. Coefficient α_2 seems to be reliably less than 1, but parameter α_1 may be as large as 1 if m is approximately as large as β. However, it may be expected

that the term including α_1 is much less than the first term of the right-hand part of equation (18). Indeed, the expression $\psi(x) / \xi(\omega,x)$ is the ratio between the energy E_f of the cochlear fluid and the kinetic energy E_k of the partition :

$$E_f = \frac{2\,\rho\,\omega^2\,W^2\,b^2\coth(\xi H)}{\pi^2 L\,\xi} \qquad E_k = \frac{\omega^2\,W^2\,\mu\,b}{8} \tag{19}$$

The expressions for the energies are taken from Novoselova (1985).

It has been shown by Tonndorf (1957) experimentally, and it may be easily verified numerically for each theoretical model, that the ratio between fluid and partition kinetic energies falls to zero when the wave approaches the peak position:

$$\frac{E_f(x)}{E_k(x)} \to 0 \qquad \text{when} \qquad x \to x_c$$

If this ratio is small, the error in the second term of equation (18) is not essential.

Conclusions

Thus if these next conditions hold :

$$d\,\omega_0 \quad \text{is small} \quad \Leftrightarrow |\,\omega_{01} - \omega_{02}\,| \ll \omega_0(x_c) \Leftrightarrow Q_{N\,dB} \gg 1$$

$$\alpha_1 \ll 1 \qquad \frac{\Delta\,\omega_0}{\omega_t} \ll 1 \qquad \frac{E_f(x_c)}{E_k(x_c)} \ll 1$$

then the amplitude curves are similar in frequency and eigenfrequency domains in regions $(\omega_{01}\,,\,\omega_{02}\,)$, where ω_1 and ω_2 are determined by expressions (3) and expression (1) is the approximate evaluation of the Q-factor (2).

References

Békésy, G. von (1960). Experiments in Hearing. McGraw-Hill, New York.

Boer, E. de, and Viergever, M.A. (1982). Validity of the Liouville-Green (or WKB) method for cochlear mechanics. Hearing Res. 8, 131-155.

Novoselova, S.M. (1985). Three chambered cochlear model. In: Mathematical problems in wave propagation theory (Ed. Babich, V.M.) 15, 133-143, 'Nauka', Leningrad, USSR (In Russian; English translation by Plenum Publishing Corporation).

Tonndorf, J. (1957). Fluid motion in cochlear models. J. Acoust. Soc. Am, 29, 558-568.

THE FRACTAL DOUBLY STOCHASTIC POISSON POINT PROCESS AS A MODEL FOR THE COCHLEAR NEURAL SPIKE TRAIN

Malvin C. Teich, Robert G. Turcott, and Steven B. Lowen

Department of Electrical Engineering, Columbia University, and
Fowler Memorial Laboratory, Columbia College of Physicians & Surgeons,
New York, NY 10027, USA

Introduction

It has been shown that the neural spike trains transmitted along primary fibers in the cochlear nerve can be described by a dead-time-modified fractal point process (Teich, 1989). These spike trains manifest highly irregular firing rates, irregularly shaped pulse-number distributions (even when the number of samples is large), and fractional power-law behavior in the Fano-factor time curve with a fractional power-law exponent that appears to depend on the level of stimulation (Teich and Khanna, 1985; Teich and Turcott, 1988; Teich, Johnson, Kumar and Turcott, 1990).

This fractal behavior is not manifested over short time scales (<100 msec), so it will not be revealed by certain types of measurements, such as pulse-interval distributions and post-stimulus time histograms. Point-process models based on such measures may therefore be used with confidence only for modeling short-term effects. Indeed, the dead-time-modified Poisson point process model (Cox, 1962) has achieved its success in this domain.

In this paper we show that a particular type of fractal point process that we have developed, the dead-time-modified fractal doubly stochastic Poisson point process (FDSPP), exhibits behavior that is consistent with all of the experimental statistics of spontaneous and pure-tone driven VIIIth-nerve action potentials examined to date. FDSPPs are generally not members of the renewal family of processes; rather, they are generated as a result of long-term fractal correlations. Particular attention is devoted to two specific examples of this process: the fractal-shot-noise-driven (FSND) DSPP and one of its special cases, the fractal-Gaussian-noise-driven (FGND) DSPP (Lowen and Teich, 1989, 1990). This particular process can arise from physiologically plausible nerve-spike generation models, as indicated briefly at the end of this paper.

Because refractoriness in the auditory nerve, as elsewhere in the nervous system, has both absolute and relative components (Teich and Diament, 1980; Teich, 1985), it is appropriate to modify the FDSPP by "sick time" rather than dead time. Nevertheless, a suitable approximation is provided by dead time

(Prucnal and Teich, 1983), particularly since our principal interest lies in phenomena with time scales > 100 msec. All of the processes described in this paper are therefore modified by dead time, although for simplicity this will not be explicitly stated.

Identification of the Neural Point Process

The sequence of action potentials recorded from spontaneously firing and driven adult-cat high-frequency auditory nerve fibers has been used to construct a number of experimental measures, including the pulse-interval distribution (PID), pulse-number distribution (PND), Fano-factor time curve (FFC), serial count correlation coefficient (SCC), and normalized range (R/S). The collection of these statistics provides a rather comprehensive picture of the underlying neural spike train and enables us to make reasonable conjectures about the point process that describes these events (Teich, Turcott and Lowen, 1990).

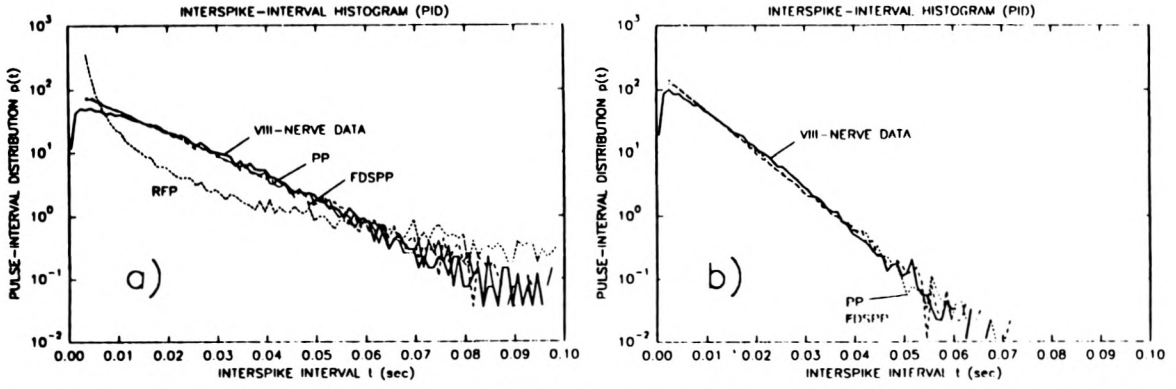

FIGURE 1 a) Pulse-interval distribution (PID) for 405 sec of data from a spontaneously firing high-frequency auditory nerve fiber (Unit A) with mean interspike interval $<t>$ = 15.3 msec and dead time $\tau_d \approx 3$ msec (solid curve). Also shown are the results of simulations for three theoretical models, all of which incorporate a fixed dead time: the Poisson point process (PP), the renewal fractal point process (RFP), and the fractal doubly stochastic Poisson point process (FDSPP). The model parameters are chosen to give approximately the same mean interspike interval and refractoriness as the data. Additional parameters used in the RFP simulation are $\alpha = 0.7$ and $\tau_c = 100$ sec. These values were selected so that the point process would exhibit fractal behavior over the time scales of interest, and yet avoid excessively large intervals which leads to computational difficulty in estimating the various statistical measures. Additional parameters used in the FDSPP simulation are $\alpha = 0.65$ and $\tau_f = 400$ msec. The PP and the FDSPP fit the data, but the RFP does not.
b) PID for 800 sec of data for this same fiber, but now in response to a pure-tone stimulus applied at the characteristic frequency (CF) of the unit. The mean interspike interval $<t>$ = 8.9 msec and the dead time $\tau_d \approx 2$ msec (solid curve). The reduced mean interevent time is reflected in the greater negative slope on this semi-logarithmic plot. The PID for the RFP closely resembles that shown in a) and is therefore not illustrated. Again the simulated FDSPP (modified by fixed dead time), with model parameters chosen to given approximately the same mean interspike interval, refractorines, fractal dimension ($\alpha = 0.86$), and fractal onset time ($\tau_f = 40$ msec) as the data, provides a good fit.

The PID, PND, and FFC are, by now, well-known statistics that have been described in detail elsewhere (Teich and Khanna, 1985; Teich and Turcott, 1988; Teich, 1989). The SCC and R/S provide estimates of the degree of serial correlation in the data set. The SCC gives the correlation between the numbers of neural spikes in adjacent counting periods, and is generally a function of the counting time T. The R/S measure reflects correlations among collections of large numbers of interspike intervals. It has the advantage of being a valid measure even when the data exhibit extremely long-term correlations, as well as large (or infinite) variance; these are characteristics that can cause a process to appear nonstationary and are consequently deleterious to standard measures (Mandelbrot, 1983).

We have compared these experimental statistics with those predicted by several theoretical models, including a dead-time-modified Poisson point process (PP), a dead-time-modified renewal fractal point process (RFP), and a dead-time-modified fractal doubly stochastic Poisson point process (FDSPP). We have performed simulations using various forms of this latter process, and found that both the FSND-DSPP and the FGND-DSPP exhibit behavior that accords with all of these statistics. The PP and RFP, in contrast, do not.

The PP is well-known. As shown in Fig. 1, it gives rise to PIDs that agree well with both spontaneous and driven data. However, as illustrated for spontaneous firings in Fig. 2, its PND ($T=1$ sec) is narrower than that that of the data, while its FFC and SCC remain flat for large times rather than increasing with T, and rescaled range analysis leads to the $k^{1/2}$ law rather than the steeper curve that describes the data. The PP fails to described the driven data in the same way.

Because the RFP is less well-known, we provide a brief discussion of its behavior. A renewal point process with interevent times governed by the hyperbolic distribution is invariant to certain scaling transformations (Mandelbrot, 1965), and therefore exhibits fractal characteristics. Its pulse-interval distribution $p(t)$ is

$$p(t) = \begin{cases} A t^{-u}, & \tau_d \le t \le \tau_c \\ 0, & \textit{otherwise}. \end{cases} \qquad (1)$$

The quantity A normalizes the distribution, and is a function of the other parameters. As shown in Fig. 1, its PID exhibits a reduction of interspike intervals with values near the mean and a concurrent enhancement of long and short intervals, relative to that of the Poisson. Because of its renewal and fractal nature, we refer to this process as the renewal fractal point process (RFP).

Such large-variance interspike intervals can lead to long-term spike correlations. Even though the interspike intervals of the RFP are independent, the numbers of spikes occurring in successive counting periods of fixed time T are not. For example, with the decreased proportion of intermediate interspike intervals, given a low number of spikes in a particular counting period we know with high probability that this period fell within a long interspike interval. Because of this the following counting period is also likely to fall within the same interspike interval, and is therefore also likely to register a low number of

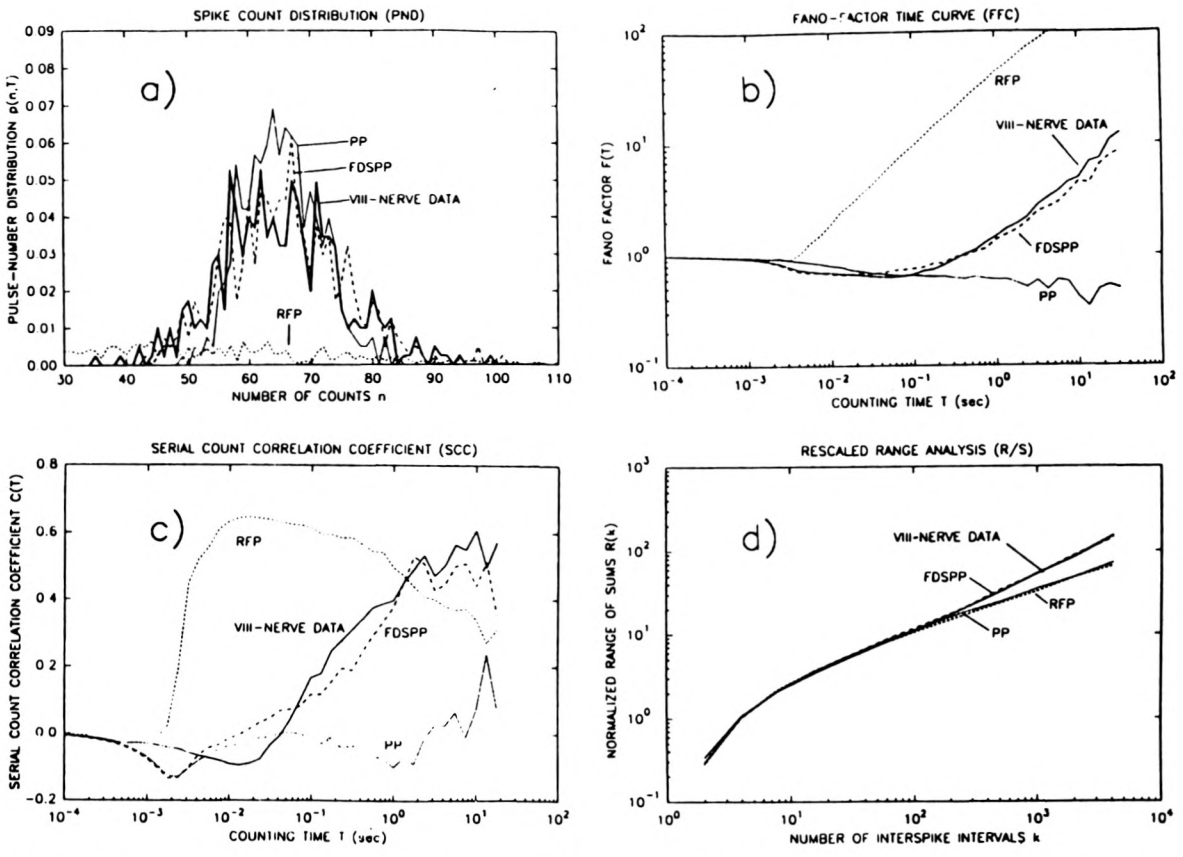

FIGURE 2 a) Pulse-number distribution (PND) constructed from the same spontaneous spike train as the PID shown in Fig. 1a, using a counting time $T = 1$ sec (solid curve). The PND is the probability $p(n,T)$ of observing n spikes in the observation time T, versus the number of spikes n. PNDs from simulations of the three theoretical models are also shown. The model parameters are chosen to give the same mean count as the data. The PND obtained from the FDSPP resembles the data. On the other hand, the PND obtained from the PP is narrower than the data while that obtained from the RFP is far broader than the data. b) The Fano-factor time curve (FFC) is constructed from the PND; it is the ratio of the count variance to the count mean for different counting times T. For VIII-nerve data, $F(T)$ typically grows in power-law fashion as T^{α} $(0 < \alpha < 1)$ for sufficiently large counting times, implying a power-law normalized coincidence rate and a power-law form for the power spectral density at low frequencies (Teich, 1989). Again the FFC obtained from the FDSPP resembles the data quite closely whereas the FFCs of the PP and the RFP deviate substantially from it, even though the latter does exhibit power-law behavior. c) The serial count correlation coefficient (SCC) gives the correlation between the numbers of neural spikes in adjacent counting periods, and is in general a function of T. For the PP, $\alpha = 0$ so that $C(T) = 0$ as is evident in the figure for sufficiently large counting times (the dip in the curve in the vicinity of 2 msec, which arises from dead time, would be moderated were sick time used instead). Once again the SSC obtained from the FDSPP closely resembles the data while the SSCs associated with the PP and the RFP deviate substantially from it. In the domain of counting times where the Fano-factor time curve behaves as T^{α}, $C(T)$ plateaus at the value $2^{\alpha} - 1$ as required by the relation between these parameters. d) Whereas the SSC reflects correlations between successive counts, the R/S parameter reflects correlations among interspike intervals. This measure is obtained by first estimating the interval mean and standard deviation in a block of interspike inervals of size k. For each of the k intervals, the difference between the value of the interval and the mean value is obtained and the result is successively added to a cumulative sum. The range is defined as the difference between the maximum and minimum values achieved within the cumulative sum, and this is normalized by the sample standard deviation to give $R(k)$. The normalized range of sums $R(k)$ is estimated for increasing values of k and plotted against k. With $R(k)$ proportional to k^h, $h > 0.5$ indicates positive correlation, $h < 0.5$ indicates negative correlation, and $h = 0.5$ indicates uncorrelated intervals (Hurst, 1951; Feller, 1951). The renewal nature of the PP and RFP cause $R(k)$ to behave as $k^{1/2}$; the data and the results from the FDSPP rise more steeply, indicating positive correlation for collections of large numbers of interspike intervals.

spikes. On the other hand, if a large number of spikes is registered in a particular counting period, it is unlikely that this counting period contains a long interspike interval and, since short interspike intervals are far more likely, it is highly probable that the following spike number will also be large. Indeed, sample functions of this point process have a strongly clustered appearance. Expanding the time scale surrounding a cluster of spikes generally reveals subclusters. For the Poisson process, on the other hand, the exponential nature of the interevent-time distribution, along with the independence of successive intervals, guarantees that the spike counts are independent.

The independence of the interspike intervals of the RFP leads to the same R/S behavior as the Poisson, as is evident in Fig. 2d. At the same time, the correlation among successive counts is apparent in the serial count correlation coefficient shown in Fig. 2c. It is this correlation that gives rise to the very broad pulse-number distribution shown in Fig. 2a and a Fano-factor time curve that increases with T in power-law fashion, as illustrated in Fig. 2b. As is evident from Figs. 1 and 2, the RFP does not model the data well.

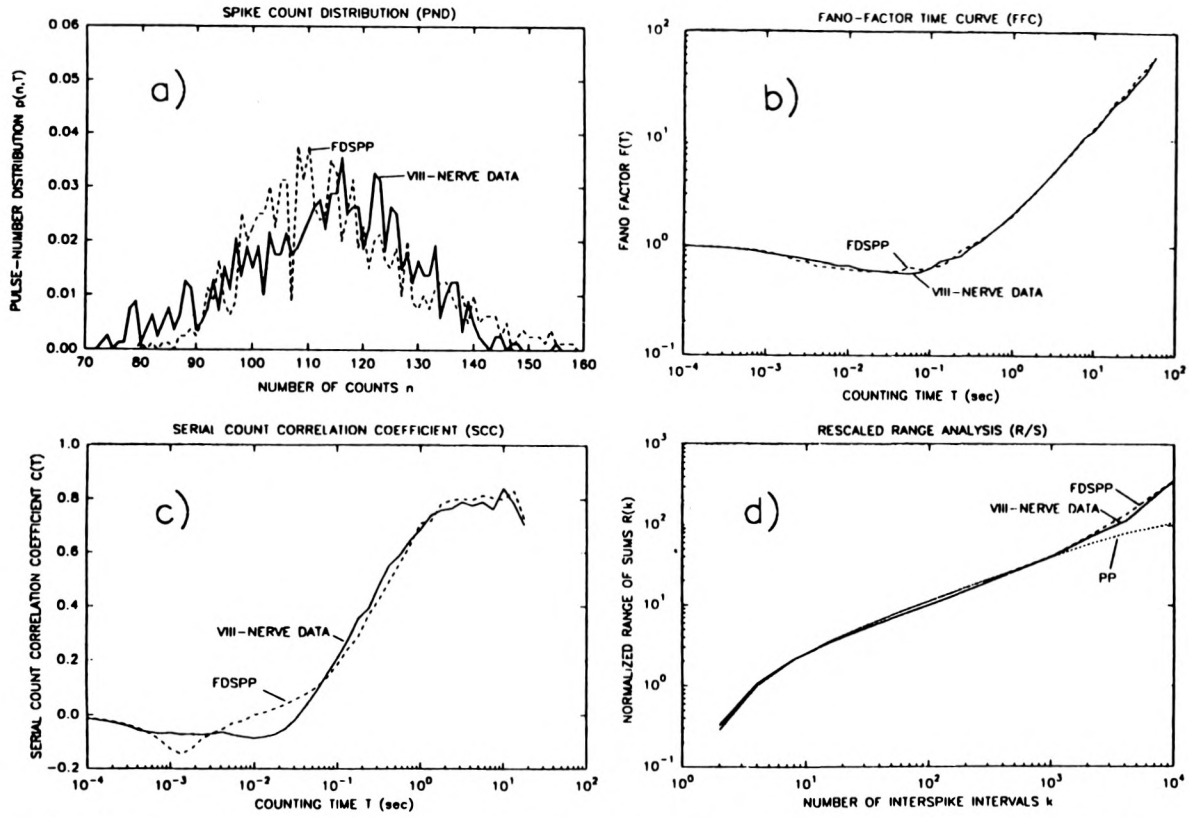

FIGURE 3 a) PND (T = 1 sec), b) FFC, c) SCC, and d) R/S constructed from the same 800-sec driven spike train as that used in Fig. 1b for the PID. The renewal processes are not represented since their behavior is similar to that presented in Fig. 2. The fractal dimension revealed by the slope of the FFC curve is approximately α = 0.86, which is greater than the value observed in Fig. 2b for spontaneous firing (α = 0.65). The increased FFC exponent is reflected in a larger count-correlation estimate, as is evident in the SCC curve (compare with Fig. 2c). The increase in α and $C(T)$ under stimulation has been observed in all VIII-nerve fibers examined to date. All of the measures constructed from a simulated FDSPP, with the same parameters as reported in Fig. 1b, resemble the neural-spike data quite closely.

In contrast, the FDSPP, and in particular the FSND-DSPP and the FGND-DSPP, give results that are largely indistinguishable from the experimental statistics that we have examined both for spontaneous firings (Fig. 2) and for driven firings (Fig. 3), and we identify it as the point process that characterizes the auditory neural spike train (Teich, Turcott and Lowen, 1990). Its behavior arises from long-term fractal rate correlations which can be removed by randomly shuffling the interspike intervals, as shown in Figs. 4 and 5 for spontaneous and driven data respectively.

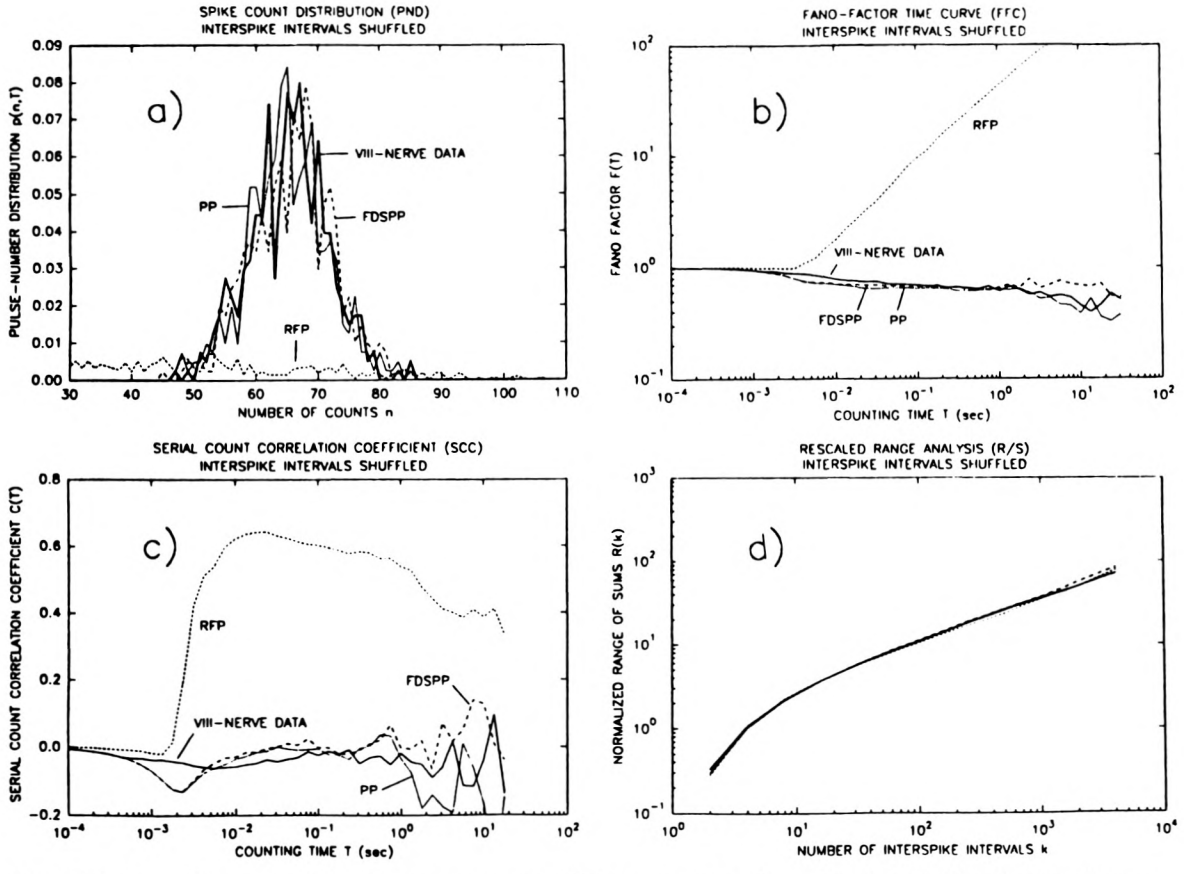

FIGURE 4 Same as Fig. 2 (spontaneous firings) except that the interspike intervals were randomly shuffled for both the experimental and simulated spike trains before constructing these measures. Several observations merit mention. First, measures constructed from the PP and RFP are not altered by shuffling. This is as expected since both are renewal processes which, by definition, have independent and identically distributed interspike intervals. Second, measures constructed from the VIII-nerve data are altered substantially by shuffling, which provides unequivocal evidence that the auditory neural events are not describable by a renewal process. Third, measures constructed from the FDSPP behave in the same way as measures constructed from the data, providing additional evidence that it is a good model for the neural point process. Finally, the results for the data and the FDSPP are indistinguishable from those of the PP after random shuffling. The shuffling removes the long-term fractal rate correlations, leaving a residue of intrinsically irreducible fluctuations, which is simply the dead-time-modified homogeneous Poisson point process. This result is consistent with the data provided in Fig. 1a where it was demonstrated that the PID for the VIII-nerve data, the FDSPP, and the PP are essentially the same.

It is of interest to note that the FFC exponent α (i.e., the fractal dimension) increases when the unit is driven, as does the serial count correlation coefficient for long counting times as reflected in the SCC curve. All of the VIII-nerve fibers we have examined to date, when presented with pure-tone stimuli, reveal an increase in the value of the fractal dimension, correlation coefficient, and firing rate (Teich, Johnson, Kumar and Turcott, 1990).

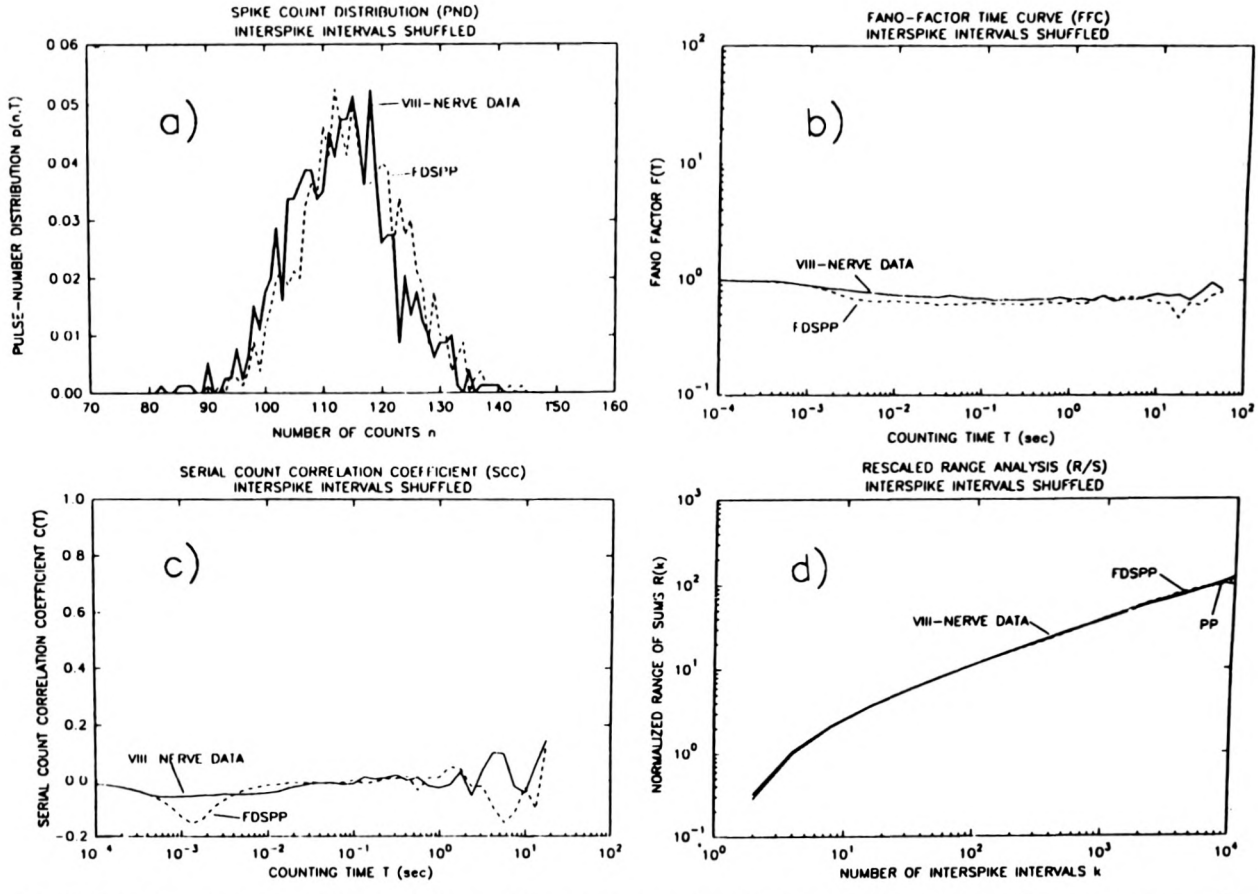

FIGURE 5 Same as Fig. 3 (driven firings) except that the interspike intervals were randomly shuffled for both the experimental and simulated spike trains before constructing these measures. As with the spontaneous data, measures constructed from the VIII-nerve data are altered substantially by shuffling, which provides confirming evidence that the auditory neural events are not describable by a renewal process. Measures constructed from the FDSPP behave in the same way as those constructed from the data, so that this model appears to be suitable for discribing the neural point process in the presence of a pure-tone stimulus as well as in its absence . The shuffled results for both the data and the simulation are indistinguishable from those of a Poisson point process since shuffling the intervals is simular to generating a renewal point process using the PID, and the PID of both the data and the FDSPP are approximately exponential.

On Possible Origins of the Fractal Behavior

The underlying fractal behavior of the VIII-nerve spike train could originate at any of a number of peripheral loci (Teich, 1989) including nonlinear cellular vibrations in the Organ of Corti (Teich, Khanna and Keilson, 1989), chaotic oscillations of the membrane potential, neurotransmitter diffusion, and fractal ionic channel openings and closings. The FDSPP turns out to be useful for modeling several of these possibilities.

Acknowledgment

This work was supported by the National Science Foundation.

References

Cox, D.R. (1962) Renewal Theory. Methuen, London.

Feller, W. (1951) The asymptotic distribution of the range of sums of independent random variables. Ann. Math. Stat. 22, 427-432.

Hurst, H.E. (1951) Long-term storage capacity of reservoirs. Trans. Amer. Soc. Civil Eng. 116, 770-808.

Lowen, S.B. and Teich, M.C. (1989) Generalised 1/f shot noise. Electron. Lett. 25, 1072-1074.

Lowen, S.B. and Teich, M.C. (1991) Fractal shot-noise-driven doubly stochastic Poisson point process. Submitted for publication.

Mandelbrot, B.B. (1965) Self-similar error clusters in communication systems and the concept of conditional stationarity. IEEE Trans. Commun. Tech. 13, 71-90.

Mandelbrot, B.B. (1983) The Fractal Geometry of Nature. Freeman, New York.

Prucnal, P.R. and Teich, M.C. (1983) Refractory effects in neural counting processes with exponentially decaying rates. IEEE Trans. Syst. Man Cybern. SMC-13, 1028-1033.

Teich, M.C. (1985) Normalizing transformations for dead-time-modified Poisson counting distributions. Biol. Cybern. 53, 121-124.

Teich, M.C. (1989) Fractal character of the auditory neural spike train. IEEE Trans. Biomed. Eng. 36, 150-160.

Teich, M.C. and Diament, P. (1980) Relative refractoriness in visual information processing. Biol. Cybern. 38, 187-191.

Teich, M.C. and Khanna, S.M. (1985) Pulse-number distribution for the neural spike train in the cat's auditory nerve. J. Acoust. Soc. Am. 77, 1110-1128.

Teich, M.C. and Turcott, R.G. (1988) Multinomial pulse-number distributions for neural spikes in primary auditory fibers: Theory. Biol. Cybern. 59, 91-102.

Teich M.C., Khanna, S.M. , and Keilson, S.E. (1989) Nonlinear dynamics of cellular vibrations in the organ of Corti. Acta Otolaryngologica Suppl. 467, 265-279.

Teich, M.C., Johnson, D.H., Kumar, A.R., and Turcott, R.G. (1990) Rate fluctuations and fractional power-law noise recorded from cells in the lower auditory pathway of the cat. Hear. Res. 46, 41-52.

Teich, M.C., Turcott, R.G., and Lowen, S.B. (1990) Identification of the point process characterizing the auditory neural spike train. Assoc. Res. Otolaryngol. Abst. 155, 141.

THE IMPEDANCE OF THE ORGAN OF CORTI

George Zweig

Hearing Research Laboratory, Signition Inc.
P.O. Box 1020, Los Alamos, NM 87544-1020, USA

Introduction

In previous papers (Zweig 1987, 1988) the impedance of the organ of Corti was deduced from measurements of basilar membrane motion. That impedance is the starting point for this paper. The power transfer between the organ of Corti and its harmonic traveling waves is calculated. The time delays of forces presumed to originate in outer hair cells are estimated.

Theoretical assumptions

THE PRIMARY ASSUMPTION

In the low-amplitude linear regime the velocity V of a section of the organ of Corti is related to the pressure difference P across that section by an impedance $Z \equiv P/V$. Assume that Z is the sum of a passive and an active impedance:

$$Z \equiv Z_{\rm p} + Z_{\rm a}.$$

Assume that $Z_{\rm p}$ acts like a conventional harmonic oscillator,

$$Z_{\rm p} = i\omega M_{\rm p}(x) + R_{\rm p}(x) + K_{\rm p}(x)/i\omega,$$

with corresponding characteristic angular frequency and damping:

$$\omega_{\rm cp}(x) \equiv \sqrt{K_{\rm p} M_{\rm p}} \text{ and } \delta_{\rm p}(x) \equiv R_{\rm p}/\sqrt{K_{\rm p} M_{\rm p}}.$$

Assume that $Z_{\rm a}$ is the sum of a fast-acting positive-feedback impedance and a slow-acting negative-feedback impedance:

$$Z_{\rm a} \equiv Z_{\rm f} + Z_{\rm s} \equiv \frac{K_{\rm f}(x) e^{-i\psi_{\rm f}(x)\omega/\omega_{\rm cp}(x)}}{i\omega} + \frac{K_{\rm s}(x) e^{-i\psi_{\rm s}(x)\omega/\omega_{\rm cp}(x)}}{i\omega},$$

where $K_{\rm f}$ and $K_{\rm s}$ are the strengths, and $\psi_{\rm f}/\omega_{\rm cp}$ and $\psi_{\rm s}/\omega_{\rm cp}$ the time delays, of the fast- and slow-acting feedback forces. $\psi_{\rm f}$ and $\psi_{\rm s}$ are positive since those forces are delayed in time. The time delay of the fast-acting force is chosen so that

$$0 < |\psi_{\rm f}\,\omega/\omega_{\rm cp}| \lesssim \psi_{\rm f} \ll 1 \ll \psi_{\rm s}, \tag{1}$$

which allows the term $e^{-i\psi_f\omega/\omega_{cp}}$ in Z_f to be expanded in powers of its argument. Keeping the first three terms in the expansion yields,

$$Z_f \approx i\omega M_f(x) + R_f(x) + K_f(x)/i\omega, \text{ where } M_f = \frac{K_f\psi_f^2}{2\omega_{cp}^2} \text{ and } R_f = -\frac{K_f\psi_f}{\omega_{cp}}.$$

The total shunt impedance becomes:

$$Z \approx i\omega M(x) + R(x) + K(x)/i\omega + K(x)\rho e^{-i\psi\omega/\omega_c(x)}/i\omega, \tag{2}$$

where

$$M = M_p + M_f,\ R = R_p + R_f,\ K = K_p + K_f,\ K\rho = K_s, \text{ and } \psi/\omega_c = \psi_s/\omega_{cp}.$$

The characteristic angular frequency ω_c and net damping δ are defined by:

$$\omega_c \equiv \sqrt{K/M}, \text{ and } \delta \equiv \frac{R}{\sqrt{KM}} = \frac{\delta_p - \rho_f\psi_f}{\sqrt{(1+\rho_f)(1+\rho_f\psi_f^2/2)}}, \text{ where } \rho_f \equiv K_f/K_p.$$

Assume that δ is negative. The three inequalities $\delta < 0 < (\delta_p, \psi_f)$ imply

$$\rho_f > 0, \text{ or } K_f > 0. \tag{3}$$

(The possibility of introducing a stiffness component having a transduction delay of several microseconds has been considered by Neely (1983). This stiffness component differs from that introduced here by virtue of its magnitude, which is never large enough to give the oscillator a net negative damping. For Neely's model, $\delta > 0$ and $K_s = \rho = 0$.)

SECONDARY ASSUMPTIONS

Approximate scaling symmetry. Assume (Zweig, 1975; Gummer et al 1987) that all circuit elements are functions only of $s(x,\omega) \equiv i\omega/\omega_c(x)$, $\omega_c(x) = \omega_{c0}e^{-x/l}$.

Eq. (2) for Z becomes

$$Z \approx \frac{\omega_{c0}M_0(s^2 + \delta s + 1 + \rho e^{-\psi s})}{s},$$

or

$$Z \approx \frac{\omega_{c0}M_0(1+\rho)}{s} e^{(\delta-\psi\rho)s/(1+\rho)} \prod_{n=-\infty}^{\infty}{}' (1 - \frac{s}{s_n})e^{s/s_n},$$

where s_n are the zeros of $Z(s)$, $s_n^* = s_{-n}$, and the prime on the product symbol indicates that the $n = 0$ term is absent.

Zeros of the shunt impedance and zeros of its derivative. In order to get a transfer function with a peak that is *both* tall and broad, assume that two zeros of $Z(s)$ coincide, $s_k = s_{k+1} \equiv s_c$, and lie on the imaginary s axis. Then, $Z(s_c) = 0$ and $Z'(s_c) \equiv dZ(s)/ds\,|_{s=s_c} = 0$. The real and imaginary parts of those

two complex equations yield four equations from which s_c, δ, ρ, and ψ are estimated. If $x = x_n \equiv 2\pi(\frac{3}{4} + \frac{n}{2} - \epsilon_n)$ is the n^{th} positive root of $x = \tan x$, $n = 0, 1, ...$, then

$$s_c = i/\sqrt{1 + 2/x_n^2},\ \psi = ix_n/s_c,\ \delta = -2/\psi,\ \text{and}\ \rho = (-1)^n i s_c \delta \sqrt{1 + 1/x_n^2}.$$

(Only the roots with positive imaginary parts are listed.) For example, for $n = 2$, $x_2 = 10.90$, $s_c = 0.992i$,

$$\psi/2\pi = 1.75,\ \delta = -0.182,\ \text{and}\ \rho = 0.181. \tag{4}$$

With those values $Z = Z_p + Z_a$ is just stable (Z has a double pole on the imaginary s axis). The existence of both a fast positive-feedback force and a slow negative-feedback force leading to a net negative damping δ were assumed because that combination yields the simplest stable time-delay system with $Z' \approx 0$ at the characteristic frequency point.

Cochlear geometry. Assume that the long-wavelength approximation is valid (the wavelength of the traveling wave is large compared to the height of the scalae). Then the pressure P is uniform within each transverse section of the cochlea and the geometry is effectively one dimensional. P obeys the transmission-line equation:

$$\frac{d^2P}{ds^2} - \frac{1}{\lambda^2}P = 0, \tag{5}$$

where $\lambda^2 = s^2 Z/l^2\overline{Z}$ and $\overline{Z}$ is the longitudinal impedance of the cochlea (Zweig, 1988).

Longitudinal impedance. Assume that $\overline{Z}(s)$ is inertial, i.e., $\overline{Z} = s\omega_{c0}\overline{M}_0$, where $\overline{M}_0$ is constant. Then the analytic structure of $P(s)$ is determined by the location of the zeros of $sZ(s) \propto s^2 + \delta s + 1 + \rho e^{-\psi s} \propto \lambda^2$.

WKB approximation. Assume that $|d\lambda/ds| \ll 1$ so that the WKB approximation may be used to find the pressure from Eq. (5). The transfer function T, which is proportional to sP/λ^2, becomes:

$$T \propto \frac{s}{\lambda^{3/2}(s)} e^{-\int_{s_0}^{s} ds'/\lambda(s')}, \tag{6}$$

where

$$\lambda^2(s) = \frac{s^2 + \delta s + 1 + \rho e^{-\psi s}}{(4N)^2},\ \text{and}\ (4N)^2 \equiv l^2\overline{M}_0/M_0. \tag{7}$$

Comparison between theory and experiment

Rhode's measurements of basilar membrane motion were extrapolated to a small constant velocity to obtain an empirical estimate of the transfer function (Zweig 1988). Figure 1 shows a fit of $T(s)$ (Eqs. (6) and (7)) to that empirical transfer function. The parameters used were:

$$\psi/2\pi = 1.742,\ \delta = -0.1217,\ \rho = 0.1416,\ N = 5.24,\ \text{and}\ \omega_c/2\pi = 7.89\text{kHz}, \tag{8}$$

in qualitative agreement with Eq. (4). Note that a negative value for δ is essential for the fit. The combination $Z'(i) \approx 0$ and $Z(i) \approx 0$ gives a transfer function

that is high and broad near $s = i$, as observed. The value $n = 2$ (Eq. (4)) is necessary and sufficient to create the low frequency plateau in the transfer function that presumably corresponds to the "tail" of the tuning curve (Zweig 1987, 1988). The zeros of $Z(s)$ are shown in Fig. 2.

The conclusions of this paper can be obtained without assuming that the wavelength is large compared to the height of the scalae (Zweig 1990). In a calculation where all other assumptions were kept but the pressure was allowed to vary in each transverse section with the distance from the organ of Corti, the fit to the transfer function was somewhat improved. This is not surprising because that two-dimensional model contains an extra free parameter (the ratio of the wavelength to the height of the scalae). A good fit to the transfer function is obtained in either the one- or two-dimensional model if the derivative of the shunt impedance vanishes near the characteristic frequency point.

Discussion

FINDING THE WAVELENGTH FROM THE TRANSFER FUNCTION

The impedance $Z = l^2\overline{Z}\lambda^2/s^2$ may be estimated directly from experiment by using $\overline{Z} \propto s$ and determining λ^2 from measurements of $T(s)$. Eq. (6) may be converted into a differential equation for $\lambda(s)$ by differentiating both sides with respect to s, yielding

$$\lambda = -\left(1 + \frac{3}{2}\frac{d\lambda}{ds}\right) \Big/ \left(\frac{d\ln(T/s)}{ds}\right). \tag{9}$$

That equation may be solved iteratively by exploiting the gradual spatial variation of the mechanical parameters, $|d\lambda/ds| \ll 1$. The resulting expressions for the real and imaginary parts of $(4N\lambda)^2$ are shown in Fig. 3. Note that near the characteristic frequency point (when $\omega/2\pi \approx 7.9$kHz corresponding to $s_c \approx i$), $\lambda^2 \approx 0$ and $\lambda^{2\prime} \approx 0$, implying $Z \approx 0$ and $Z' \approx 0$ at that point, as discussed above.

INTERPRETING Im $\{\lambda^2\}$ IN TERMS OF POWER TRANSFER

The time-average power transfer per unit length to the traveling wave from the organ of Corti is given by

$$< w(x,\omega) > = \frac{1}{2}\frac{d}{dx}\mathrm{Re}\{U^*(x,\omega)P(x,\omega)\}, \text{ or}$$

$$< w(s(x,\omega)) > \propto -\mathrm{Im}\{\lambda^2(s(x,\omega)\}|T(s(x,\omega))|^2/|s(x,\omega)|,$$

where the wave travels towards the helicotrema, $U = -(l\omega_{c0}\overline{M}_0)^{-1}dP/ds$ is the volume velocity, and the proportionality constant is positive. The magnitude of the time-average power transfer per unit length is largely determined by $|T|^2$ (Fig. 1) while the direction of flow is fixed by the sign of $\mathrm{Im}\{\lambda^2\}$. A negative imaginary part for λ^2 means that power is being transferred to the wave from the organ of Corti. In the bottom panel of Fig. 3, $\mathrm{Im}\{\lambda^2(x,\omega)\}$ is drawn as a function of $f \equiv \omega/2\pi$ for a fixed point x on the basilar membrane (corresponding to $\omega_c(x)/2\pi \approx 7.9$kHz).

Since $\mathrm{Im}\{\lambda^2\} < 0$ for all ω except for $\omega \approx \omega_c(x)$, a traveling wave of angular frequency ω passing by x picks up energy about that point unless $\omega \approx \omega_c(x)$. When $\omega \approx \omega_c(x)$, it absorbs energy instead. The power transfer to the traveling wave is greatest for frequencies just below the frequency at which no power transfer occurs ($\mathrm{Im}\{\lambda^2\} = 0$).

The assumption of scaling allows the abscissa in Fig. 3 to be reexpressed in terms of $\beta \equiv -is = \omega/\omega_c(x)$. Then, that figure may be taken to represent $\mathrm{Im}\{\lambda^2(s(x,\omega))\}$ as a function of x for fixed angular frequency ω. Note that $\beta \approx 0$ corresponds to $x = 0$ and $\beta \approx 1$ corresponds to the characteristic frequency point, i.e. the position x at which $\omega_c(x)/2\pi \approx 7.9$kHz. It is easy to show that the power transfer to the wave per unit β is proportional to the product of $|T/\beta|^2$ (the square of the curve given in the top panel of Fig. (1) divided by β^2) and $-\mathrm{Im}\{\lambda^2\}$ (the negative of the curve given in the bottom panel of Fig. 3). The function $|T/\beta|^2$ is expected to be nonzero but finite at $\beta = 0$. The traveling wave first absorbs and then deposits energy as it moves down the cochlea from the stapes to its point of maximum velocity. All the power is deposited in a small region near $\beta = 1$. Most of the power is pumped into the traveling wave just before it is absorbed.

Note that *Fig. 3 demonstrates that the cochlea is active,* i.e. the cochlea creates mechanical energy in one region in order to absorb it in another.

The buildup of power in the traveling wave is reminiscent of the power buildup of a light wave in a laser where the mechanically active cochlear elements play the role of the electrically excited laser molecules (Zweig 1989). Unlike a laser, the transfer of power to the wave increases at an exponential rate whose rate constant itself increases dramatically as the wave travels down the cochlea. While this acceleration of the rate of power transfer occurs, the sign of the imaginary part of λ^2 passes through zero, the direction of power flow is abruptly reversed, and all the accumulated power is deposited in a small section of the organ of Corti where the detection of sound at low sound pressure levels presumably occurs.

Predictions and suggestions for future experiments

PARAMETER VALUES FOR THE POSITIVE-FEEDBACK FORCE

The shift in characteristic frequency ω_c from the passive value ω_{cp} caused by the fast-acting positive-feedback force is given by the ratio

$$\zeta \equiv \omega_c/\omega_{cp} = \sqrt{(1+\rho_f)/(1+\rho_f\psi_f^2/2)}.$$

The inequalities $\psi_f < \sqrt{2}$ and $\rho_f > 0$ (Eqs. (1) and (3)) imply $\zeta > 1$. Therefore in accord with observation (Rhode 1973), active forces increase the characteristic frequency from its passive value.

The positive-feedback parameters ρ_f and ψ_f may be written in terms of δ, ζ, and δ_p:

$$\rho_f = \frac{A + \sqrt{A^2 + B^2}}{2\gamma}, \text{ and } \psi_f = \frac{\sqrt{2}}{\zeta}\left(1 - \frac{\zeta^2 - 1}{\rho_f}\right)^{\frac{1}{2}},$$

where

$$A \equiv \zeta^2 - 1 - \delta\sigma, \text{ and } B \equiv \sqrt{2\gamma}\sigma,$$

with

$$\gamma \equiv \left(1 - \frac{\delta^2}{2}\right), \text{ and } \sigma \equiv \zeta\delta_p - \delta.$$

Because the value of δ_p is currently very uncertain, ρ_f and ψ_f cannot be computed. Inequalities for ρ_f and ψ_f involving only ζ and δ may, however, be easily obtained and predict intervals in which ρ_f and ψ_f must lie:

$$\zeta^2 - 1 < \rho_f, \text{ and } \frac{-\delta\zeta}{\zeta^2 - 1} < \psi_f < \frac{\sqrt{2}}{\zeta},$$

where $-\delta \ll 1$ has been used. For example, taking $\zeta = 1.5$ and $\delta = -0.12$ gives:

$$1.25 < \rho_f, \text{ and } 1/7 < \psi_f < 1.$$

The corresponding limits on the fast-delay time ψ_f/ω_{cp} are:

$$2.5\mu s < \psi_f/\omega_{cp} < 20\mu s.$$

Including uncertainties in ζ, that delay is predicted to lie between 1.5 and 30 μs.

Measurement of two transfer functions, one in an animal with a normal active cochlear system, the other in the same animal with its active system disabled, would test the primary assumption and permit a determination of ρ_f and ψ_f (Zweig 1988). Measurement of the two corresponding impulse responses would provide consistency checks. Measurement of the fast-delay time of outer hair cell forces would permit comparison with the fast-delay time ψ_f/ω_{cp} computed from the transfer function measurements.

Acknowledgements

Support was provided by DARPA/AFOSR contract N00014-86-C-0399.

References

Zweig, G. (1987) The mechanics of hearing. Invited paper, Nonlinearity in Biology and Medicine, Seventh Annual International Conference of the Center for Nonlinear Studies, Los Alamos National Laboratory.

Zweig, G. (1988) Finding the impedance of the organ of Corti. Submitted to J. Acoust. Soc. Am.

Neely, S.T. (1983) The cochlear amplifier. In: Mechanics of Hearing (Eds: de Boer, E. and Viergever, M.A.) Nijhoff/Delft U.P., Delft, The Netherlands, 111-118.

Zweig, G. (1975) Basilar membrane motion. In: Cold Spring Harbor Symposium on Quantitative Biology, vol. XL, Cold Spring Harbor, 619-633.

Gummer, A.W., Smolders, J.W.T., and Klinke, R. (1987) Basilar membrane motion in the pigeon measured with the Mössbauer technique. Hear. Res. 29, 63-92.

Zweig, G. (1990) A two-dimensional model of cochlear mechanics. (In preparation.)

Zweig, G. (1989) Auditory speech preprocessors. In: Proceedings of the DARPA Speech and Natural Language Workshop, Morgan Kauffman, San Mateo, 229-235.

Rhode, W.S. (1973) An investigation of post-mortem cochlear mechanics using the Mössbauer effect. In: Basic Mechanisms in Hearing (Ed: Moller, A.) Academic Press, New York, 49-67.

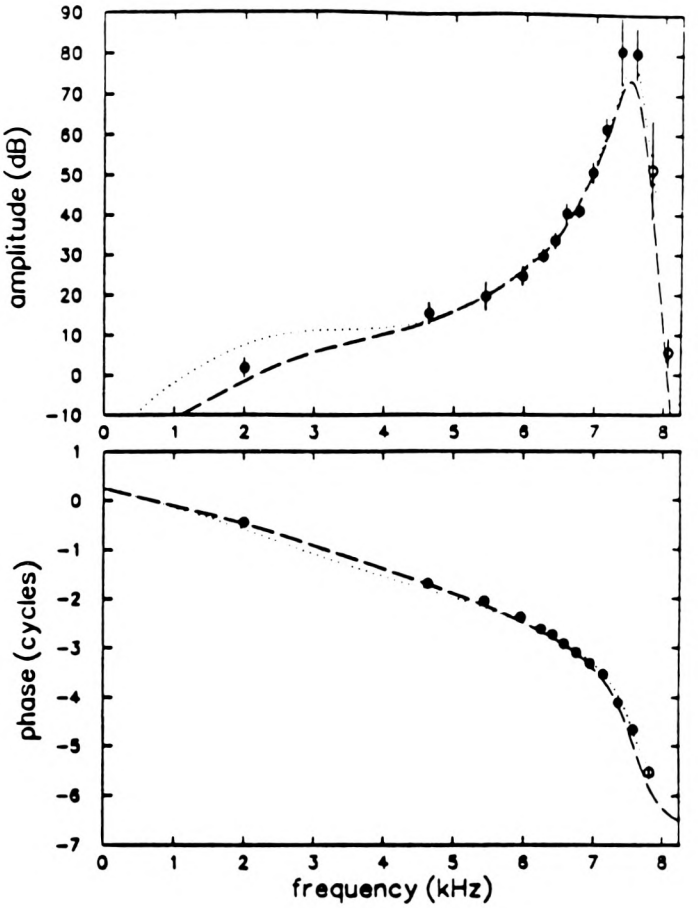

Figure 1: The amplitude and phase of the transfer function T (dotted lines) corresponding to Eqs. (6), (7), and (8) are compared with extrapolated measurements (circles) of basilar membrane motion. The transfer function (dashed line), derived from the empirical $\hat{\lambda}$ found by iterating Eq. (9), is shown for comparison. The empirically determined $(4N\hat{\lambda})^2$ is shown in Fig. 2.

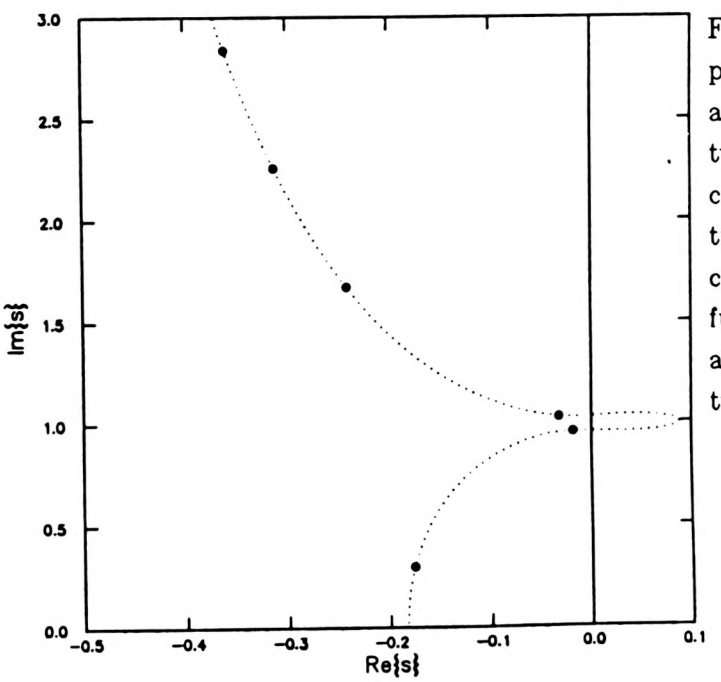

Figure 2 The real and imaginary parts of the zeros s_n in the region around $s = i$ $(Z(s_n) = 0)$. The two zeros located very near $s = i$ create the peak of the transfer function while the zero at smaller $|s|$ creates a plateau in the transfer function (Zweig 1987, 1988) presumably related to the "tails" of neural tuning curves.

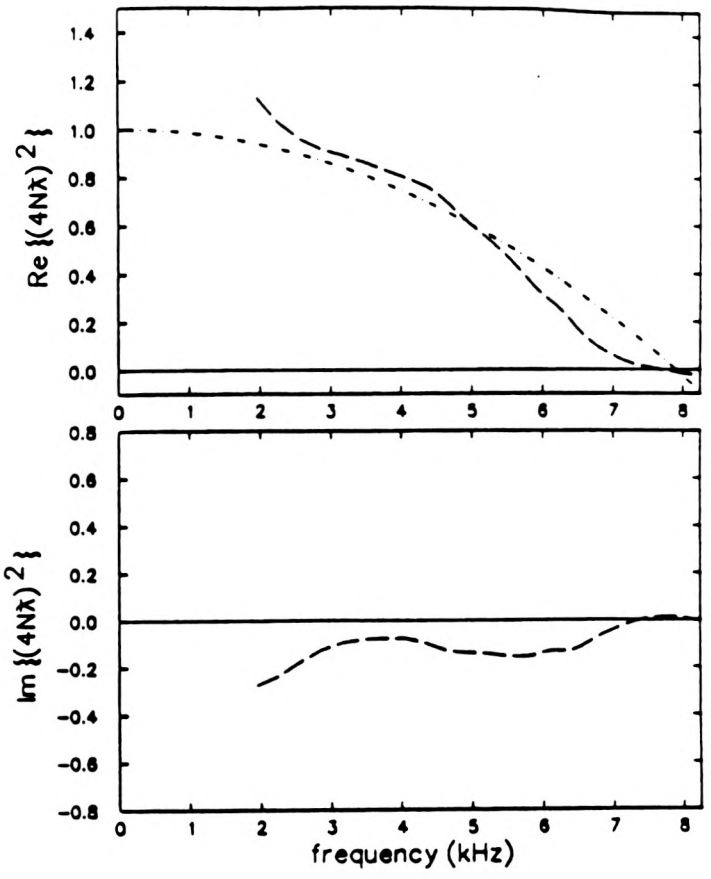

Figure 3 The real and imaginary parts of $(4N\lambda)^2$ found from the data by solving Eq. (9) iteratively are given by the dashed line. The dot-dashed line appearing in the top figure is a quadratic function of frequency and corresponds to a simple passive impedance of the form Z_p. For the bottom figure, that same passive impedance predicts a straight line with *positive* slope δ_p passing through the origin. The empirically determined $\mathrm{Im}\{\lambda^2\}$ would be better fit, on the average, with a straight line having a small negative slope corresponding to a negatively damped oscillator (with damping constant $\delta \approx -0.12$). Although $\mathrm{Im}\{\lambda^2\} < 0$ almost everywhere, the motion is stable for all frequencies (all zeros of $\lambda^2(s)$ are in the left half of the complex s plane).

Section 8

Nonlinear Models

IMPLEMENTATION OF A NONLINEAR WAVE-DIGITAL-FILTER COCHLEAR MODEL

David H. Friedman

The MITRE Corporation, Bedford, MA 01730, USA

Introduction

Research on the physiology of hearing over the past decade strongly suggests that wave propagation in the cochlea is affected by an active nonlinear regeneration mechanism. One published nonlinear cochlear modeling study (Deng and Geisler, 1987) presents results (Figure 9 of the reference) linking the nonlinearity to an apparent enhancement of speech sounds in broadband noise, in comparison to equivalent results without the nonlinearity. If such an effect can be verified and understood in general terms, it would be of significant value for improving intelligibility in speech recognition and in aids to the deaf, and perhaps for other signal recovery applications as well.

In order to verify this effect computationally, a cochlear model is needed in which the nonlinearity can be incorporated. In particular, the model should allow for signal intermodulation products to be reinjected into the wave medium, to propagate bidirectionally as waves identical in form to those in the external sound stimulus (Kim, 1986). This rules out a filter-bank or cascaded-amplifier structure with unidirectional signal flow, in place of one based on an explicit representation of cochlear wave mechanics.

It has been pointed out that the wave digital filter technique gives a realization directly equivalent to an analog network, in which the voltages and currents can correspond in turn to underlying physical variables. This work applies that approach to a model based on local cochlear micromechanics with two degrees of freedom, which yields responses similar in shape to typical physiological tuning curves, and allows over 40 db variation in peak response level under control of a single nonlinear resistive element per section.

Derivation of Cochlear Model

We view the cochlea as a duct partitioned lengthwise by the basilar membrane (BM), on which is situated the organ of Corti (OC), and above which rests the tectorial membrane (TM). The BM, OC and TM together are referred to as the cochlear partition. Vibration of the BM is considered to result in a shear motion

between the OC and TM which deflects the cilia of the inner hair cells, resulting in excitation of afferent nerve fibers. In the model presented here, the differential velocity of this motion (as a function of time and distance from the base) is taken as the output; the hair-cell transduction and neural excitation stages are not included.

The modeling of cochlear mechanics generally begins with the writing of differential equations to describe the wave motion of the BM and adjacent fluid. An approach applicable to 1-D models is to represent the discretized differential equations by an electrical network resembling a lumped equivalent to a transmission line, with voltage and current corresponding to pressure and volume velocity, and inductance, resistance and capacitance representing mass, viscosity and stiffness respectively. Among the various discrete-time realization methods available, Strube (1985) has pointed out that the wave digital filter (WDF) technique is computationally efficient and preserves the identification of elements and variables in the prototype analog network, which in turn correspond to physical quantities.

Strube's 1985 model considered only the motion of the BM, with a single degree of freedom yielding a single local resonant mode. The network itself consists of N cascaded sections each of the form shown in Figure 1(a), with each section representing a constant distance increment D along the basilar membrane. The parameters of the n-th section are determined by the following physical quantities at a distance $x_n = nD$ from the base, expressed here in typical units:

D = distance increment per section (mm)
ρ = fluid density ($\mathrm{mg/mm^3}$) = 1 for H_2O
p_n = trans-BM pressure ($\mathrm{mg/mm\,sec^2}$)
i_n = volume velocity of perpendicular BM and fluid motion ($\mathrm{mm^3/sec}$)
j_n = volume velocity of longitudinal fluid motion ($\mathrm{mm^3/sec}$)
A_n = mean cross-section of scalae ($\mathrm{mm^2}$)
b_n = effective width of BM (mm)
M_{bn} = effective mass per unit BM area ($\mathrm{mg/mm^2}$)
V_{bn} = resistance (viscosity) per unit BM area ($\mathrm{mg/mm^2\,sec}$)
S_{bn} = elastance (stiffness) per unit BM area ($\mathrm{mg/mm^2\,sec^2}$)

with A_n, b_n, M_{bn}, V_{bn}, S_{bn} varying with x_n so as to establish a given frequency-to-place mapping. For the simple case of a straight-line logarithmic mapping, all of the preceding quantities vary exponentially with x_n according to the general rule $F_n = F(x_n) = F_0 \exp(F' \cdot x_n)$, allowing the model to be fully specified by paired parameters A_0, A'; etc. The actual component values for the n-th section are determined as

$$L_{sn} = 2\rho D/A_n \quad (\mathrm{mg/mm^4}) \qquad R_{bn} = V_{bn}/b_n D \quad (\mathrm{mg/mm^4\,sec})$$
$$L_{bn} = M_{bn}/b_n D \quad (\mathrm{mg/mm^4}) \qquad C_{bn}^{-1} = S_{bn}/b_n D \quad (\mathrm{mg/mm^4\,sec^2})$$

where $b_n D$ ($\mathrm{mm^2}$) is the effective BM area for the n-th section; the linear (not volume) BM velocity at x_n is then $\dot{\phi}_n = i_n/b_n D$, where we write ϕ for displacement.

One approach to improving the model, arrived at through apparently separate lines of reasoning by Allen (1980), Neely and Kim (1986), and Zwislocki (Zwislocki and Kletsky, 1979), is to introduce a second degree of freedom to the micromechanics

of the cochlear partition: independent motion of the TM is permitted, and the BM-TM differential shear velocity taken as the output. The general form for the network section is then as shown in Figure 1(b), with the following additional elements determined in an analogous manner:

M_{tn} = effective mass of TM, per unit BM area (mg / mm^2)
V_{tn} = resistance of TM, per unit BM area (mg / mm^2 sec)
S_{tn} = elastance of TM, per unit BM area (mg / mm^2 sec^2)
V_{cn} = resistance of BM-TM coupling, per unit BM area (mg / mm^2 sec)
S_{cn} = elastance of BM-TM coupling, per unit BM area (mg / mm^2 sec^2)
$L_{tn}, R_{tn}, C_{tn}^{-1}, R_{cn}, C_{cn}^{-1} = 1/b_n D$ times above quantities respectively.

In contrast to Figure 1(a), where the elements can be directly identified with the parameters of the BM, here a complete physical interpretation of the network would require detailed knowledge of the complex *in vivo* micromechanical behavior of the cochlear partition. In the absence of this, we "make do" with association of the resonant modes of the network section with those of the cochlear partition as a whole; the "BM" and "TM" identification of the symbolic quantities listed above, and of the corresponding branches in the figure, is therefore only nominal, hence the use of quotes in the figure and henceforth. The currents i_{bn} and i_{tn} may accordingly represent different linear combinations of, rather than the actual, BM and TM motion. The output of the n-th stage of the model is the current i_{cn} of the "BM-TM coupling" branch, corresponding to the "differential" velocity $\dot{\phi}_{cn} = i_{cn}/b_n D$. Figure 1(c) shows the typical sinusoidal response, with parameters adjusted so that (1) the series resonance of the "TM" branch produces the dip to the left of the peak, typically at about half the peak frequency; (2) the series resonance of the "BM" branch at f_{bn} coincides with the parallel resonance of the lower two branches. With these conditions, the height of the peak can be adjusted over a considerable range (e.g., 40 db) by varying R_{bn}, the resistive element of the "BM" branch.[1]

[1] Strube later similarly extended his model to include independent TM motion. He found that, with TM parameters adjusted to give behavior as in Figure 1(c), a regenerative force applied differentially between BM and TM (as via the cilia of the outer hair cells) would cause the TM to break into oscillation before the response of the BM was significantly affected, as the regeneration loop gain was increased. He therefore reasoned that, for the regeneration to be effective, the force must act on the BM alone, *e.g.*, as a shear or bending moment within the OC (Strube, 1986). A likely mechanism is suggested by the longitudinal tilt of the outer hair cells relative to the phalangeal processes: the elongation/contraction motile response of an individual OHC might give rise to a longitudinally-spaced pair of opposing perpendicular forces on the BM, yielding a net force distribution vs. x as $d\dot{\phi}(x)/dx$, where $\dot{\phi}(x)$ is the displacement acting on the cilia of an OHC at x. This differs from $\dot{\phi}(x)$ in that the sign depends on propagation direction; thus forward waves could be amplified while reflected waves are attenuated, enabling a greater increase in peak response level before onset of standing-wave patterns indicating incipient oscillation. Attempts to incorporate this scheme in the model have thus far resulted in short-wavelength instability; the likely cure – a spatial or temporal low-pass filtering mechanism – remains to be justified physiologically.

Implementation of Model

While the theory of the wave digital filter cannot be presented here for lack of space, an extensive survey of the topic is given by Fettweis (1986). Essentially, an analog network is mapped into the discrete-time domain by a bilinear frequency transformation, such that an infinite analog frequency corresponds to the Nyquist frequency $F_s/2$ in the digital domain, where F_s is the sampling frequency:

$$\frac{\omega_d}{2F_s} = \tan^{-1}\frac{\omega_a}{2F_s} \tag{1}$$

where ω_a and ω_d represent corresponding frequencies for the analog prototype and digital equivalent networks respectively, with $\omega_a \approx \omega_d$ at low frequencies. This also suggests that if the frequency map is to be assumed essentially linear, F_s should be taken sufficiently high that the signal spectrum of interest falls below the point of significant departure from the above approximation.

Applying the WDF technique to the single network section of Figure 1(b) yields a set of equations in a "forward" variable u_n, a "backward" variable u'_n, and a delay variable $x_{*n} = z^{-1}x'_{*n}$, $y_{*n} = z^{-1}y'_{*n}$ for each capacitive or inductive element respectively, where z^{-1} represents a one-sample delay. Coefficients of the equations are expressed in terms of an arbitrary resistive scaling factor W_0, which represents an external series source resistance, and similar scaling factors and dimensionless coefficients α_n, etc. embodying the element values:

$$\begin{aligned}
W_{an} &= 1/(2F_sC_{cn}) + R_{cn}, & \alpha_n &= 1/(2F_sC_{cn}W_{an}) \\
W_{bn} &= 1/(2F_sC_{tn}) + 2F_sL_{tn}, & \beta_n &= 1/(2F_sC_{tn}W_{bn}) \\
W_{cn} &= W_{bn} + R_{tn}, & \gamma_n &= W_{bn}/W_{cn} \\
W_{dn} &= W_{an}\|W_{cn}, & \delta_n &= W_{dn}/W_{an} \\
W_{en} &= 1/(2F_sC_{bn}) + 2F_sL_{bn}, & \zeta_n &= 1/(2F_sC_{bn}W_{en}) \\
W_{fn} &= W_{dn} + W_{en}, & \kappa_n &= W_{dn}/W_{fn} \\
W_{gn} &= W_{fn} + R_{bn}, & \lambda_n &= W_{fn}/W_{gn} \\
W_{hn} &= W_{n-1} + 2F_sL_{sn}, & \mu_n &= W_{n-1}/W_{hn} \\
W_n &= W_{gn}\|W_{hn}, & \nu_n &= W_n/W_{hn}
\end{aligned} \tag{2}$$

where $A\|B = 1/(1/A + 1/B)$, applied sequentially for $n = 1, 2, \ldots, N$. The order of evaluation for the entire network (cascade of N sections) is:

(a) u_n in terms of u_{n-1} and the delay outputs (unprimed), for $n = 1, \ldots, N$ ("forward" phase);
(b) u'_n in terms of u_n (apical termination);
(c) u'_{n-1}, the output ϕ_{cn} and the delay inputs (primed), in terms of u_{n-1}, u'_n and delay outputs, for $n = N, \ldots, 1$ ("backward" phase).

The actual equations are as follows: for (a), for the n-th section,

$$u_n = (1-\nu_n)[(1-\delta_n)\cdot(x_{tn} - x_{cn} - y_{tn}) - y_{bn} + x_{cn} + x_{bn}] + \nu_n \cdot (y_{sn} + u_{n-1}) \tag{3}$$

For (b), a resistive termination R_N is implemented by taking

$$u'_N = \frac{R_N - W_N}{R_N + W_N} u_N \tag{4}$$

For (c), for each section, a series of subexpressions are written first:

$$\begin{aligned} t_{1n} &= y_{tn} - x_{tn} + x_{cn} & t_{4n} &= (1-\delta_n)\cdot t_{1n} + t_{2n} \\ t_{2n} &= y_{sn} + y_{bn} - x_{cn} - x_{bn} + u_{n-1} & t_{5n} &= (1+\nu_n)\cdot t_{4n} + t_{3n} \\ t_{3n} &= -y_{sn} + u'_n - u_{n-1} & t_{6n} &= (1-\nu_n)\cdot t_{4n} - t_{3n} \end{aligned} \tag{5}$$

allowing the main equations for the n-th section to be written as

$$x'_{cn} = \alpha_n[\kappa_n\lambda_n \cdot t_{5n} - 2(1-\delta_n)\cdot t_{1n}] + x_{cn} \tag{6a}$$
$$x'_{tn} = \beta_n\gamma_n(\kappa_n\lambda_n \cdot t_{5n} + 2\delta_n \cdot t_{1n}) + x_{tn} \tag{6b}$$
$$y'_{tn} = (1-\beta_n)\gamma_n(\kappa_n\lambda_n \cdot t_{5n} + 2\delta_n \cdot t_{1n}) - y_{tn} \tag{6c}$$
$$x'_{bn} = \zeta_n(1-\kappa_n)\lambda_n \cdot t_{5n} + x_{bn} \tag{6d}$$
$$y'_{bn} = (1-\zeta_n)(1-\kappa_n)\lambda_n \cdot t_{5n} - y_{bn} \tag{6e}$$
$$y'_{sn} = (1-\mu_n)\cdot t_{6n} - y_{sn} \tag{6f}$$
$$u'_{n-1} = u_{n-1} - \mu_n \cdot t_{6n} \tag{6g}$$
$$\dot{\phi}_{cn} = \frac{2F_s}{S_{cn}} \cdot (x'_{cn} - x_{cn}) \tag{6h}$$

At each sample time, the network state is evaluated as follows. First, u_0 is set to $P_0/2$, where P_0 is the present-sample driving "pressure" value (effectively applied through the resistance W_0), and equation (3) is applied sequentially to each section, $n = 1, \ldots, N$. Next, (4) is applied to obtain u'_N from u_N. Finally, (5) and (6) are applied sequentially as a group for each $n = N, \ldots, 1$, updating the individual section outputs and delays as well as producing a reflected signal component u'_0 at the input. The actual present-sample input pressure and linear velocity values are then given by $p_0 = u_0 + u'_0$ (mg / mmsec^2) and $\dot{\phi}_0 = (u_0 - u'_0)/W_0A_0$ (mm / sec) respectively; the ratio of their phasors yields the actual input impedance $Z_0(\omega)$ (mg / mm^2 sec) for the steady-state sinusoidal case. The input-output response of $\dot{\phi}_{cn}$ to either p_0 or $\dot{\phi}_0$ is then similarly the respective (dimensionless, if the latter) phasor ratio. If $W_0A_0 << Z_0$, then $p_0 \approx P_0$, while if $W_0A_0 >> Z_0$, then $\dot{\phi}_0 \approx P_0/W_0A_0$, either way allowing the response to be found at a predetermined input level.

Incorporation of Nonlinearity

The cochlear nonlinearity may be roughly represented as a negative component in the overall local damping of the cochlear partition, which increases sensitivity near threshold but saturates some 40 db higher. It has already been mentioned that, with appropriate values for the other elements, the peak height of the (linear) response curve could be varied significantly by adjusting R_{bn}; the most likely

network placement therefore seems to be in the role of R_{bn}, as a resistance with a small or negative resting value, which effectively increases to a large positive limit with increasing instantaneous magnitude of the controlling signal variable.

Correct identification of the controlling variable requires better understanding of the active effect producing the nonlinearity. For the model, likely choices are the "BM" velocity and displacement, corresponding to i_{bn} and its time integral. To avoid creating delay-free loops, $R_{bn}(t)$ cannot be made a same-sample-time function of any variable in the model. However, by exploiting the equivalence of the WDF to an analog network with reactive elements, derivatives may be extracted (subject to a magnitude error increasing with frequency, due to the nonlinear frequency mapping of (1)) and used to predict the value one sample ahead. Thus, taking the "BM" displacement ϕ_{bn} as example, the following present-sample equivalences may be derived:

$$\phi_{bn} = (x'_{bn} + x_{bn})/S_{bn} \tag{7a}$$

$$\begin{aligned}\dot{\phi}_{bn} &= (x'_{bn} - x_{bn}) \cdot 2F_s/S_{bn} \\ &= (y'_{bn} - y_{bn})/2F_s M_{bn}\end{aligned} \tag{7b}$$

$$\ddot{\phi}_{bn} = (y'_{bn} + y_{bn})/M_{bn} \tag{7c}$$

With $T_s = 1/F_s$, this leads to a predictor such as

$$\hat{\phi}_{bn}(t + T_s) = \phi_{bn}(t) + T_s\dot{\phi}_{bn}(t) + \frac{1}{2}T_s^2\ddot{\phi}_{bn}(t) \tag{8}$$

allowing $R_{bn}(t)$ to be calculated at each sample time as a function of the $\hat{\phi}_{bn}(t)$ found on the previous sample. Similarly, if $\dot{\phi}_{bn}$ is taken as the controlling variable, we might use

$$\hat{\dot{\phi}}_{bn}(t + T_s) = \dot{\phi}_{bn}(t) + T_s\ddot{\phi}_{bn}(t) \tag{9}$$

More generally, a combination of these, which we write as $\chi_n(t + T_s)$, would be taken, and R_{bn} determined as

$$R_{bn}(t) = \{V_{bn} + (U_{bn} - V_{bn})f[\chi_n(t)]\}/b_n D \tag{10}$$

where U_{bn} represents the "BM" resistance per unit area with the regenerative process fully active; $f(\chi_n)$ decreases monotonically from $f(0) = 1$ to $f(\pm\infty) = 0$ with increasing $|\chi_n|$, giving $R_{bn} = U_{bn}/b_n D$ (a small or negative value) at rest and $R_{bn} = V_{bn}/b_n D$ at saturation. Once the new present-sample R_{bn} is determined, it is then made effective in the network by changing λ_n and W_{gn}. This, however, affects μ_n, W_{hn}, ν_n, and W_n as well, both for the current section and all sections downstream, requiring that the R_{bn} update (and recalculation of the affected parameters) be done on the "forward" phase of each sample-time calculation, prior to applying (3) for each section, using (predicted) values for χ_n calculated and stored during the preceding "backward" phase.

As a demonstration of the nonlinearity, we have attempted to duplicate some data from Zwicker (1981) for psychophysical cancellation of the combination tone

$F_c = 2F_1 - F_2$ by a human subject, with the nonlinearity defined by taking $f(\chi_n) = 1/\sqrt{1+\chi_n^2}$ where

$$\chi_n^2 = [(\hat{\dot{\phi}}_{bn})^2 + (0.1 \cdot \omega_{bn}\hat{\phi}_{bn})^2]/\dot{\phi}_{ref}^2 \tag{11}$$

with $\omega_{bn} = \sqrt{S_{bn}/M_{bn}}$, and $\dot{\phi}_{ref}$ set to 10^4 times the arbitrary 0 db "SPL" input velocity level. The cancellation tone was iteratively adjusted in amplitude and phase so as to reduce the F_c output level by 40 db or more at a point slightly apical to its peak place. Results for one case are shown in Figure 2. The curves match well in level, although those for the model show flatter asymptotic slopes to either side of the peak. Phase values (not shown) generally varied as -2 degrees per db of A_1.

Acknowledgment

This work was sponsored by the Rome Air Development Center, RADC/IRAA.

References

Allen, J. B. (1980) Cochlear micromechanics – a physical model of transduction. J. Acoust. Soc. Am. 68(6), 1660-1670.

Deng, L. and Geisler, C. D. (1987) A composite auditory model for processing speech sounds. J. Acoust. Soc. Am. 82(6), 2001-2012.

Fettweis, A. (1986) Wave digital filters: theory and practice. Proc. IEEE 74(2), 270-327.

Kim, D. O. (1986) A review of nonlinear and active cochlear models. In: Peripheral Auditory Mechanisms (Eds: J. B. Allen, et. al.) Springer-Verlag, 239-249.

Neely, S. T. and Kim, D. O. (1986) A model for active elements in cochlear mechanics. J. Acoust. Soc. Am. 79(5), 1472-1480.

Strube, H. W. (1985) A computationally efficient basilar-membrane model. Acustica, 58, 207-214.

Strube, H. W. (1986) Cochleare Mikromechanik und aktive Prozesse. In: Fortschritte der Akustik, DAGA '86 Proceedings.

Zwicker, E. (1981) Dependence of level and phase of the $(2F_1 - F_2)$ cancellation tone on frequency range, frequency difference, level of primaries and subject. J. Acoust. Soc. Am. 70(5), 1277-1288.

Zwislocki, J. J. and Kletsky, E. J. (1979) Tectorial membrane: a possible effect on frequency analysis in the cochlea. Science 204, 639-641.

Parameters for Figures 1 and 2 (units as given earlier):

$F_s = 24000$ Hz $\quad N = 500$ sections $\quad D = .066$ mm/section

$W_0 = 10^7$ (for $W_0 A_0 >> Z_0$, constant-velocity drive)

$R_N = 500$ (apical termination)		$A_0 = 1$	$A' = 0$
$b_0 = .08$	$b' = .05$	$M_{b0} = .06$	$M_b' = 0$
$U_{b0} = -1600$	$U_b' = -.165$	$V_{b0} = 12000$	$V_b' = -.20$
$S_{b0} = 9.6 \cdot 10^8$	$S_b' = -.32$	$M_{t0} = .006$	$M_t' = 0$
$V_{t0} = 90$	$V_t' = -.16$	$S_{t0} = 6 \cdot 10^6$	$S_t' = -.32$
$V_{c0} = 150$	$V_c' = -.16$	$S_{c0} = 9 \cdot 10^7$	$S_c' = -.32$

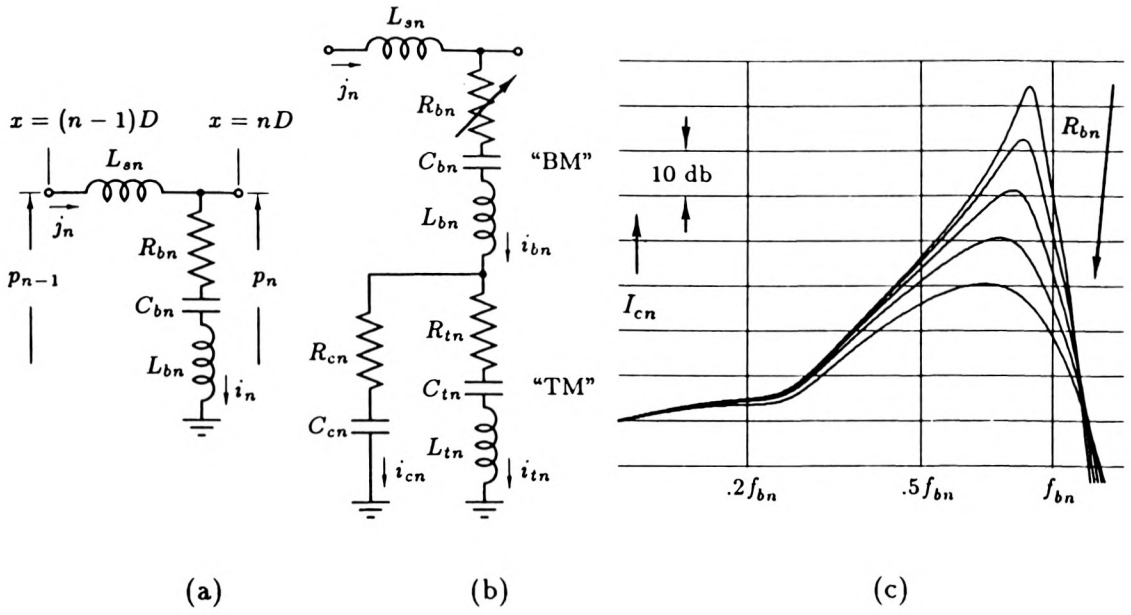

FIGURE 1 (a) Section n of one-degree-of-freedom transmission-line model. (b) Corresponding form for two-degree-of-freedom model. (c) Typical amplitude *vs.* frequency of velocity-ratio response for two-degree-of-freedom model.

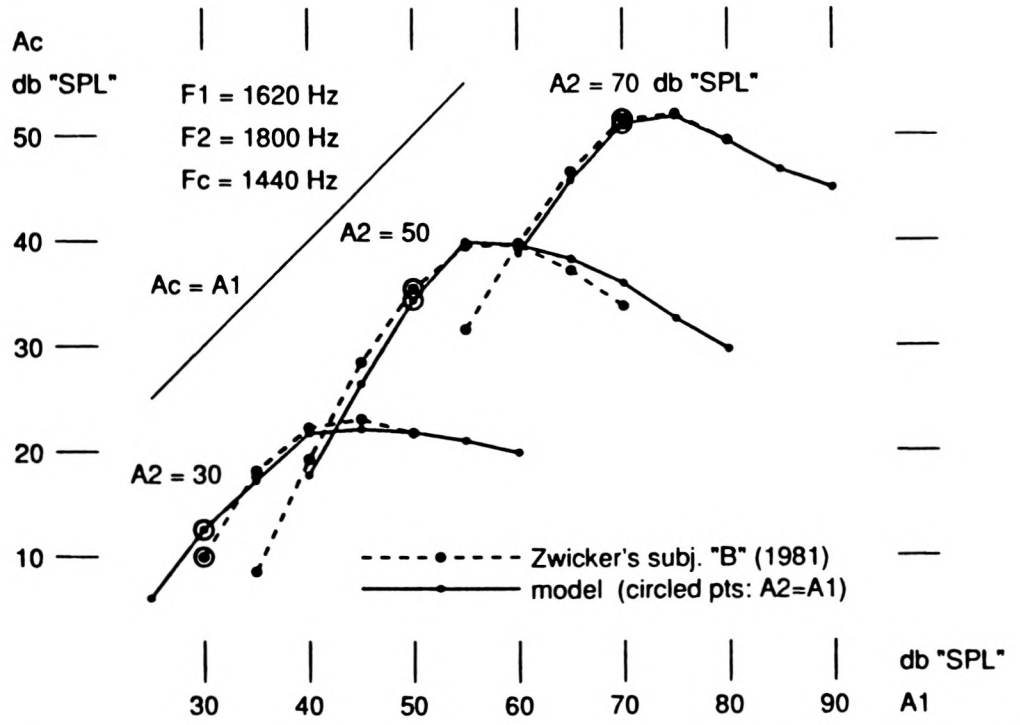

FIGURE 2 Comparison of combination-tone cancellation results for model and human subject (Zwicker, 1981) with $F_1 = 1620$ Hz, $F_2 = 1800$ Hz, $F_c = 2F_1 - F_2 = 1440$ Hz and corresponding amplitudes A_1, A_2, A_c relative to (for model) arbitrary 0 db "SPL" level. Curves show A_c as function of A_1 for $A_2 = 30$, 50, 70 db.

NONLINEAR TRANSMISSION LINE MODEL CAN PREDICT THE STATISTICAL PROPERTIES OF SPONTANEOUS OTOACOUSTIC EMISSIONS

Miriam Furst

Department of Electronic Systems, Faculty of Engineering
Tel-Aviv University
Tel-Aviv 69978
Israel

Introduction

Cochlear transmission line models were first introduced in order to account for von Bekesy's observations (von Bekesy, 1960) regarding the basilar membrane traveling wave properties (Zwislocky, 1950; Peterson and Bogert 1950). Those pioneer models assumed that the cochlear mechanics is linear as those were the experimental results at that time.

Psychophysical experiments in which the combination tone were discovered at levels near threshold (Goldstein, 1967) followed by the discovery of nonlinear behavior of basilar membrane motion (Rhode, 1971) encourage introducing nonlinearities in the transmission line model (e.g. Hubbard and Geisler, 1972; Kim et al., 1973; Hall, 1974; Nilsson and Moller, 1977). The type of nonlinearity that was included in those models was an increase in the cochlear partition friction as a function of the basilar membrane velocity. Those models were successful in predicting several nonlinear phenomena such as widening the tuning curve as a function of the stimulus level, combination tones existence, and two-tone suppression for frequency above the characteristic frequency (CF). In order to account for the phase properties of the combination tones as measured in psychophysics (Goldstein et al. 1978) another nonlinear element was added to the transmission line model, a nonlinear increase in cochlear partition stiffness as a function of the cochlear partition displacement (Furst and Goldstein, 1982).

The discovery of cochlear emissions (Kemp, 1978) raised the question if those phenomena can be explained by a transmission line model. Furst and Lapid (1988) showed that the properties of acoustic distortion products (ADP) can be predicted by the nonlinear transmission line model, including the discrepancy between animal and human data (Zurek, 1985). The nonlinear transmission line model was not adequate in order to predict the other two types of emissions, spontaneous otoacoustic emissions (SOAE) and click evoked emissions (CE). Those emissions were predicted by Furst and Lapid (1988) by introducing a non continuous resistance along the cochlear length. They proposed that such discontinuity can occur if the connection between the basilar membrane and tectorial membrane via the cilia of the outer hair cells is not uniform along the cochlear length. Thus, resistance mismatch between adjacent points along the cochlea evoke emissions. This model was very successful in predicting the huge variability in the emission spectrum among different individuals. The appearance of SOAE as a very narrow-band

noise was predicted by the model when Gaussian noise sources were added to each section in the cochlear partition. The two observations that SOAE can be suppressed by an external tone and to suppress a low level external tone (Widin and Rabinowitz, 1984) were both predicted by the model. Due to the nonlinear stiffness, the experimentally observed variability in SOAE frequency and amplitude (Zurek, 1981), were also predictable by the model.

The capability of the nonlinear transmission line model to predict the statistical properties of SOAE were carefully tested by several investigators (Wit, 1989; Furst, 1989; Talmadge et al., 1989). Bialek and Wit (1984) showed that amplitude distribution of strong SOAEs have a minimum at zero. They proved that such a distribution can be generated by an oscillator driven by a noise source, but will not be generated by a filtered noise. Talmadge et al. (1989) showed that nonlinear elements in the nonlinear transmission line model are not adequate for producing amplitude distribution with a minimum at zero. Therefore, they conclude that passive transmission line model can not predict all the properties of SOAE and active elements should be included (i.e. Van der Pol oscillator) in the cochlear model.

Active Nonlinear Transmission Line Model

In the present paper we present a modification of the transmission line model, where a negative feedback is included in each section of the transmission line. The purpose of such a feedback is to amplify the cochlear partition displacement in response to low level stimuli. Such a mechanism was suggested by several investigators as the outer hair cells contribution to the cochlear mechanics (e.g. Neely and Kim, 1986; Zwicker, 1986). This modification is expressed in the model in the term for the cochlear partition resistance (R_i). The resistance of the i'th section in the transmission line is defined as:

$$R_i = R_i^{(0)} - R_i^{(1)}\left(1 - \varepsilon I_i^2\right) \tag{1}$$

where $R_i^{(0)}$ represents the basilar membrane resistance, $R_i^{(1)}$ represents the outer hair cells contribution to the cochlear partition resistance, and I_i represents the cochlear partition velocity. The two terms in the definition of the cochlear partition resistance can be regarded as: (1) the passive, linear and invulnerable component ($R_i^{(0)}$); and (2) the nonlinear, active vulnerable component.

For simplicity, we define the relation between $R_i^{(0)}$ and $R_i^{(1)}$ by:

$$R_i^1 = \gamma R_i^{(0)} \tag{2}$$

where γ represents the amplification term. When $\gamma < 1$ the equation for the cochlear partition resistance becomes

$$R_i = \widehat{R}_i^{(0)}\left(1 + \delta I_i^2\right) \tag{3}$$

where $\widehat{R}_i^0 = \left(1 - \gamma\right) R_i^{(0)}$ and $\delta = \gamma\varepsilon / \left(1 - \gamma\right)$. Equation (3) is similar to the term used for the resistance in the passive nonlinear transmission line model. Thus, the active transmission line model represents a stable cochlea when $\gamma < 1$, and is similar to the

passive transmission line model. It is most likely that most normal cochleas are stable, and therefore all the predictions of the passive model will be obtained by the stable active model.

In the previous version of the model (Furst and Lapid, 1988), click evoked emission and spontaneous otoacoustic emission were detectable only in cochleas with nonuniform resistance, where the nonuniformity was related to the outer hair cells. Following the same rational, we introduce nonuniformity in the present version of the model through the amplification term. We define

$$\gamma = \gamma_i = \gamma_0 E_i \tag{4}$$

where E_i represents the nonuniformity of the cochlea, and γ_0 is the initial amplification term. In a uniform cochlea $E_i = 1$, for every i.

When at a certain point along the cochlea $E_i > 1$, and γ_i at that point becomes greater than 1, negative resistance is obtained. As a result, the amplifier becomes unstable and limit cycle oscillations are generated which are reflected back to the ear canal.

CEs and small SOAEs can be predicted by the model also when the cochlea is stable. When at a certain point along the cochlea $E_i > 1$ but $\gamma_i < 1$, the system is stable. Still, a significant mismatch between the resistance of adjacent points might occur which will cause reflection of a narrow band noise.

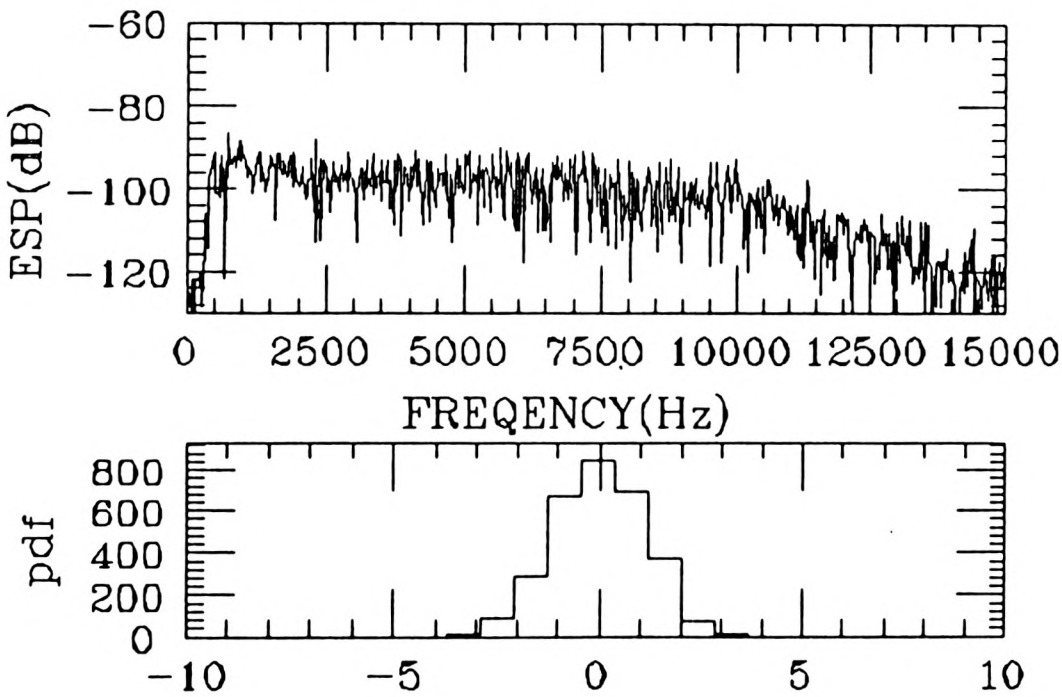

FIGURE 1 ESP calculated by the model for a uniform cochlea. The upper panel represents the ESP spectrum and the lower panel represents the calculated pdf.

The Statistical Properties of SOAE

In order to demonstrate the model prediction as regard to the statistical properties of SOAE, we calculated the ear canal sound pressure (ESP) for 40 ms when no stimulus was presented to the cochlea. Both the amplitude spectrum of the response and the probability density function were calculated. The amplitude spectrum was obtained by applying FFT on the 40 ms calculated ESP which allowed 25 Hz resolution in the frequency domain. The probability density function (pdf) was derived by dividing the calculated ESP into 20 intervals where 10 were for positive values and the other 10 for negative values, followed by counting the number of time instances in which each interval occurred.

Figure 1 represents a uniform cochlea, for every i , γ_i = 0.9. The output spectrum resembles white noise and the pdf has the expected Gaussian shape with a maximum at zero.

Figure 2 represents a nonuniform cochlea, at i = 80: γ_i = 1.1111*0.9, while for every other i , γ_i = 0.9. Note that for every i including i =80, $R_i^{(0)} > R_i^{(1)}$, and therefore the transmission line is stable. At the ESP spectrum a clear peak is seen at 4575 Hz, which is the frequency that corresponds to the nonuniform region. However the pdf of this output has a maximum at zero, which corresponds to narrow band Gaussian noise as can be expected from passive nonlinear transmission line model.

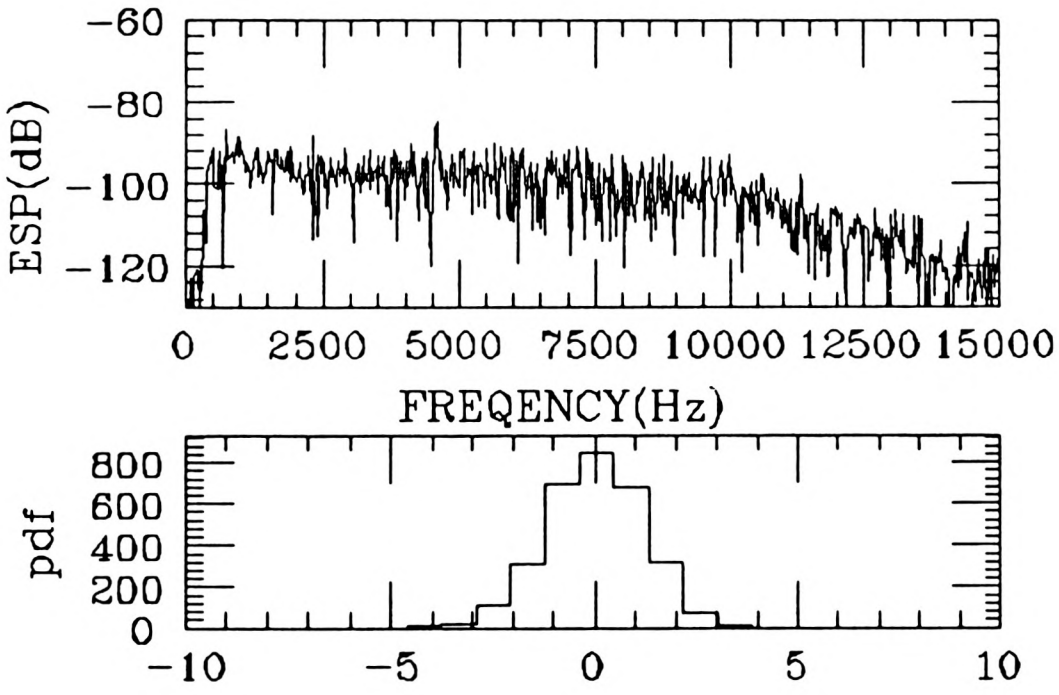

FIGURE 2 Same as Figure 1 for a nonuniform stable cochlea.

Figure 3 represents an unstable nonuniform cochlea, at i = 80 γ_i = 1.5*0.9 which determines a negative resistance at that point. A limit cycle oscillator is generated at i = 80 whose voltage is reflected back to the ear canal. The ESP spectrum has a distinct

peak (40 dB above the background noise), and the pdf has a minimum at zero as can be expected from a source that acts like a limit cycle oscillator.

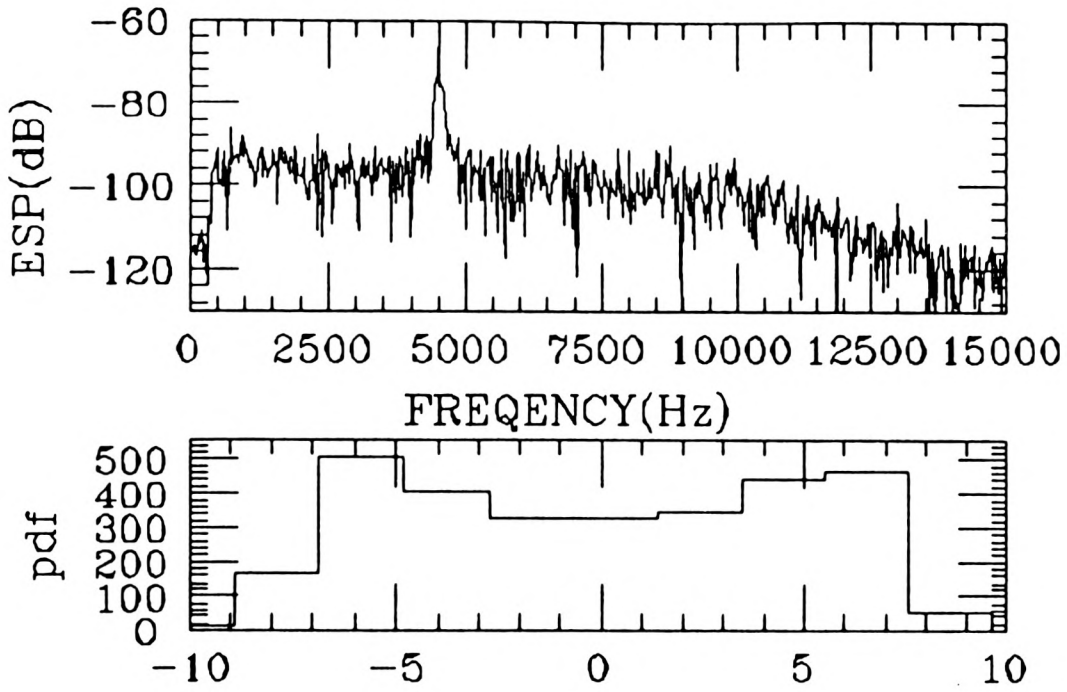

FIGURE 3 Same as Figure 1 for a nonuniform unstable cochlea.

Discussion

In the present paper we have modified the nonlinear transmission line model (Furst and Lapid 1988) in order to account for the statistical properties of strong SOAEs (Bialek and Wit, 1984; Wit, 1986; Long et al., 1988). The nonlinear term in the cochlear partition resistance have been changed to a nonlinear amplifier. The model predicts that strong SOAEs are generated when at a certain point along the cochlea an amplifier becomes unstable. The unstable amplifier produces limit cycle oscillations which are reflected back to the ear canal.

However, weak SOAEs and CEs can be generated also when all amplifiers are stable but there is a resistance mismatch between adjacent points along the cochlea. When all the amplifiers are stable the model can be regarded as passive and identical to the previous version of the model because then the cochlear partition resistance is positive at all times. All the cochlear emission properties that were predicted by the previous version of the model are valid in the modified model. Among them are the variability in emission properties in different human subjects and the differences between human and animals; the growth of the acoustic distortion product whenever its frequency or its primary frequency are involved with either CE or SOAE.

This study has demonstrated the need of including a feedback loop in cochlear models. However, it suggests that there is no need for an active model in the sense of its ability to inject energy at each point along the cochlea. The cochlea can be modeled as a series of coupled amplifiers rather than a series of coupled oscillators.

Even though, transmission line model for the cochlea is quite limited in the sense that it neglects the complicated structure of the organ of Corti, we find it a very useful tool for testing possible mechanisms in the cochlea before more complete and complicated models for the cochlea are developed.

References

Bekesy, G. (1960). Experiments in hearing , McGraw-Hill, New-York.

Bialek, W., and Wit, H.P. (1984). Quantum limits to oscillator stability: Theory and experiments on acoustic emissions from the human ear, Physics Letters 104A, 173-178.

Furst, M. (1989). Reply to 'Comment on: A cochlear model for acoustic emissions' J. Acoust. Soc. Am. 85, 2217 (1989), J. Acoust. Soc. Am. 85, 2218-2220.

Furst, M. and Lapid, M. (1988). A cochlear model for acoustic emissions, J. Acoust. Soc. Am., 84, 222-229.

Furst, M. and J.L.Goldstein (1982). A cochlear nonlinear transmission-line model compatible with combination tone psychophysics, J. Acoust. Soc. Am. 72, 717-726.

Goldstein, J.L. (1967). Auditory nonlinearity, J. Acoust. Soc. Am. 41, 676-689.

Goldstein, J.L., Buchsbaom, G., and Furst M. (1978). Compatibility between psychoacoustical and physiological measurements of aural combination tones, J. Acoust. Soc. Am. 63, 474-485.

Hall, J.L. (1974). Two tone distortion products in a nonlinear model of the basilar membrane, J. Acoust. Soc. Am. 56, 1818-1828.

Hubbard, A. E. and Geisler, C. D. (1972). A hybrid computer model of the cochlear partition, J. Acoust. Soc. Am., 51, 1895-1903.

Kemp, D.T. (1978). Stimulated acoustic emissions from within the human auditory system, J. Acoust. Soc. Am. 64, 1386-1391.

Kim, D.O., Molnar, C.E., and Pfeiffer, R.R. (1973). A system of nonlinear differential equations modeling basilar membrane motion J. Acoust. Soc. Am. 54, 1517-1529.

Long, G.R., Tubis, A., Jones. K.L., and Sivaramakrishnan, S. (1988). Modification of the external tone synchronization and statistical properties of spontaneous otoacoustic emissions by aspirin consumption, in Basic Issues in Hearing, edited by H. Duifuis, J.W. Horst and H.P. Wit (Acdemic Press, London), pp. 93-100.

Neely, S.T., and Kim, D.O. (1986). A model for active elements in cochlear biomechanics, J. Acoust. Soc. Am. 79, 1472-1480.

Nilsson, H. G. and Moller, A.R. (1977). Linear and nonlinear models of the basilar membrane motion, Biol. Cyber. 27, 107-112.

Peterson, L. and Bogert, B. (1950). A dynamical theory of the cochlea, J. Acoust. Soc. Am. 22, 369-381.

Rhode, W.S. (1971). Observations of the vibration of the basilar membrane in squirrel monkeys using the Mossbauer technique, J. Acoust. Soc. Am. 49. 1218-1231.

Talmadge, C., Tubis, A., and Long, G.R. (1989). Some implications of nonlinear passive models of spontaneous otoacoustic emissions, J. Acoust. Soc. Am. 86, S44–S45.

Widin, G.P. and Rabinowitz, W.M. (1984). Interaction of spontaneous oto-acoustic emissions and external sounds, J. Acoust. Soc. Am. 76, 1713-1720.

Wit, H.P. (1986). Statistical properties of strong spontaneous emission, in Peripheral Auditory Mechanics, edited by J.B. Allen, J.L. Hall, A.E. Hubbard, S.T. Neely, and A. Tubis (Springer Verlag, Berlin), pp. 221-228.

Wit, H.P. (1989). Comment on 'A cochlear model for acoustic emissions' J. Acoust. Soc. Am. 84, 222-229 (1988)], J. Acoust. Soc. Am. 85, 2217.

Zurek, P.M. (1985). Acoustic emissions from the ear: A summary of results from humans and animals, J. Acoust. Soc. Am. 78, 340-344.

Zurek, P.M. (1981). Spontaneous narrowband acoustic signals emitted by human ears, J. Acoust. Soc. Am. 69, 514-523.

Zwicker, E. (1986). Otoacoustic emissions in a nonlinear cochlear hardware model with feedback, J. Acoust. Soc. Am. 80, 154-162.
Zwislocki, J.J. (1950). Theory of the acoustical action of the cochlea, J. Acoust. Soc. Am. 22, 778-784.

MATHEMATICAL ANALYSIS OF A NONLINEAR MODEL FOR HYBRID FILTERING IN THE COCHLEA

Julius L. Goldstein

Central Institute for the Deaf, St. Louis, MO 63110, USA

Introduction

It has been established over the past decade that intact outer hair cells (OHC) are responsible for the sensitive tips of cochlear tuning curves (reviews by Davis, 1983; Kim, 1986; Kiang et al., 1986; Dallos, 1988; Hudspeth, 1989). The most common view is that the OHCs do not add a distinct filter system, but modify the passive hydromechanical response of the cochlea to provide a single enhanced system (Neely and Kim, 1983; Geisler, 1986; Zwicker, 1986). The hypothesis of two distinct filter systems, however, provides straightforward accounts (Goldstein, 1990) for strong suppression of CF responses by lower frequency stimuli (Abbas and Sachs, 1976; Duifhuis, 1980; Costalupes et al., 1987), and for simple-tone interference phenomena (Kiang and Moxon, 1972; Gifford and Guinan, 1983; Liberman and Kiang, 1984). Recent observations by Brundin et al. (1989) of mechanical tuning by isolated OHCs support the view that the OHCs operate as distinct electromechanical filters. We are developing a hybrid filter model that quantitatively represents the nonlinear mechanical response of the basilar membrane at each place in terms of two nonlinearly interacting bandpass nonlinearity (BPNL) filters (Goldstein, 1989, 1990). This work revives and provides a new perspective on the significance of earlier work in modeling cochlear nonlinear responses as BPNL signal processing (Goldstein, 1967; Engebretson and Eldredge, 1968; Schroeder, 1969; Pfeiffer, 1970; Sachs, 1975; Duifhuis, 1976, 1980; Johnstone, 1980; Geisler, 1985). Earlier questions on the physical basis of BPNL response characteristics are now answered by extensive experimental evidence that nonlinear mechanical response of the basilar membrane is responsible for cochlear frequency tuning and is the major source of extracochlear nonlinear phenomena (Rhode, 1971; Sellick et al., 1982; Patuzzi et al., 1984; Robles et al., 1986, 1989). Both analytic and computational methods are useful for developing the multiple-BPNL (MBPNL) model of basilar-membrane hybrid response. The computational method provides the detailed model responses required to establish the model's ability to account for complex experimental data (Goldstein, 1990). The analytic method provides insight on the global properties of the model and guides the detailed studies (Duifhuis, 1976; Goldstein, 1989). In this paper we present a basic perturbation analysis of the MBPNL model, and highlight several issues.

THE MBPNL MODEL

The MBPNL filter model is intended to represent the complex rapid waveform compression observed and inferred in basilar membrane mechanics. Each location along the basilar membrane is represented with an MBPNL frequency analyzing filter, with place dependent "center" frequency (CF), that drives the proximal inner hair cells. This

basic version of the model represents localized processing and ignores propagating distortion products. Predictions of this model provide benchmarks for the adequacy of localized processing to account for salient properties of suppression phenomena, and its inadequacy for combination tones (Goldstein, 1990).

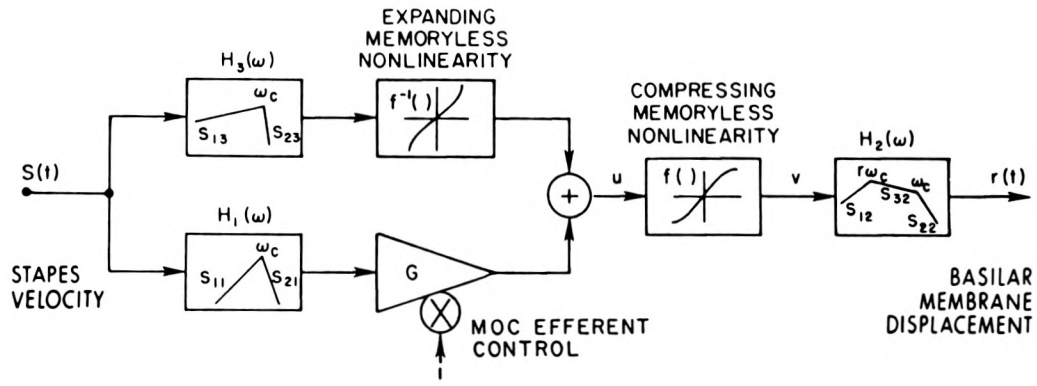

FIGURE 1 Multiple-bandpass-nonlinearity (MBPNL) filter model of hybrid response by the basilar membrane.

Figure 1 (Goldstein, 1990) defines the MBPNL nonlinear hybrid model. The lower signal processing path (H_1-H_2) is a compressive BPNL filter that represents the sensitive, narrowband and compressive tip of basilar-membrane tuning curves. The upper signalling path (H_3-H_2) is a "linear" BPNL filter that represents the insensitive, broadband linear tail response of basilar-membrane tuning. Nonlinear interaction between the two signalling paths was formulated to account for the strong suppression produced by low frequency tones (Abbas and Sachs, 1976; Duifhuis, 1980). As in the BPNL model, the same signalling paths are responsible for suppression and excitation (Pfeiffer, 1970; Duifhuis, 1976). A compressor input consisting of small and large signals will yield a response with a suppressed (i.e., smaller) representation of the small signal than obtained in response to the small signal alone. Because of the presence of the post-compressor filter (H_2), the MBPNL response can have a larger representation of the smaller compressor input signal.

The properties of the compressive transducer are central in the mathematical analysis of the model. Some form of compression was originally inferred on the basis of extracochlear studies (Goldstein, 1967; Pfeiffer, 1970). Power-law compression was later proposed (Smoorenburg, 1972; Duifhuis, 1976) as an approximation of compression observed on the basilar membrane (Rhode, 1971). It is supported by later observations (cited above), except that linear response near threshold has been clearly demonstrated. Linearity near the origin justifies a simpler mathematical analysis of the transducer response than is possible with the ideal power-law transducer. We have defined the modified power-law transducer given by eq. (1).

$$f(u) = u_+[\{1+(u/u_+)^k\}^{\upsilon} - 1]^{1/k},\ u \geq 0,\ 0 < \upsilon \leq 1 \qquad (1)$$

$$= -u_-[\{1+(-u/u_-)^k\}^{\upsilon} - 1]^{1/k},\ u < 0$$

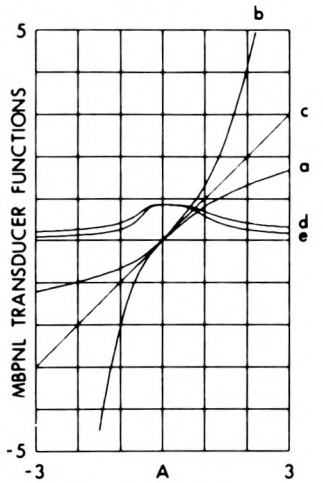

FIGURE 2 MBPNL normalized transducer functions.

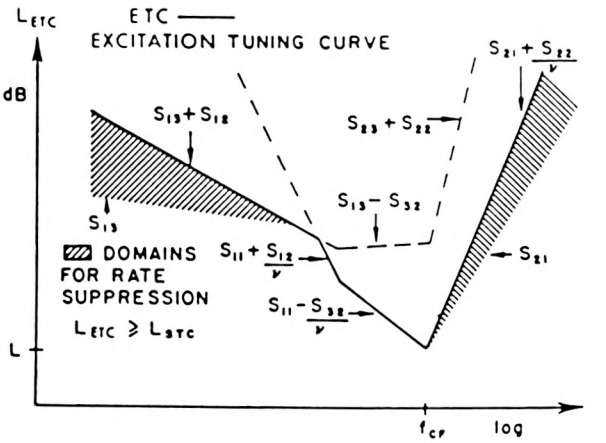

FIGURE 3 Composite tuning curves for excitation and suppression.

The transducer defined by eq. (1) is linear near the origin, being $f(u) = \upsilon^{1/k} u$. Asymmetrical transducers are obtained with compression coefficients $u_- \neq u_+$. Figure 2a shows the form of the transducer function we used to represent basilar membrane responses. The compression power is $\upsilon = 1/2$, asymmetry was required, with $2u_- = u_+ = 1$, and $k = 4$ was convenient (Goldstein, 1990). The inverse transducer is obtained by replacing υ with $1/\upsilon$ in eq. (1); its form with the above parameters is shown in Fig. 2b. Both transducers in series give the linear function shown by Fig. 2c. The slope of the compressor for a given input u=A is shown by Fig. 2d; it is a monotonically decreasing function of the magnitude of A. If a small signal is added to A, then the transducer slope at A is the "small signal gain." When A is the input to the expander (i.e., $u=f^{-1}(A)$) the slope of the compressor is given by Fig. 2e, and the small signal gain at the compressor input is uniformly smaller.

Composite and sound-level dependent tuning curves for excitation and suppression are predicted by the model, as schematized in Fig. 3. Frequency selectivity is mainly determined by the preprocessing and post-compressor linear filters, while suppression only has a minor enhancing role ($S_{32} = 0$ is consistent with data examined). The sound-level dependence results from the different rates of growth with stimulus level for the two filter paths. In the healthy cochlea the CF response of the tip filter is 40-50 dB more sensitive than that of the tail filter (Kiang et al., 1970; Ryan and Dallos, 1975); this is represented by the gain of the "cochlear amplifier" (Davis, 1983). Efferent (MOC) control of the tip response is included, following Gifford and Guinan (1983).

PERTURBATION ANALYSIS

The definition of an analytic compressor function (i.e., all derivatives exist) permits the application of more routine mathematics than is possible with the ideal power-law (Duifhuis, 1989). Compressor responses to inputs defined as the sum of small and large signals can be expanded as a Taylor series (eq. 2).

$$\text{Let } u = s + L, \text{ then } f(u) = \sum_{m=0}^{\infty} (s^m/m!)\, f^{(m)}(L) \qquad (2)$$

Two kinds of large signals are of interest, periodic functions of time and random functions of time. For the former the large signal Taylor series "coefficients" can be replaced by a Fourier series, giving eq. (2a).

$$\text{Let } L(\alpha) = L(\alpha+2\pi), \text{ then } f(u) = \sum_{m=0}^{\infty} (s^m/m!) \sum_{n=0}^{\infty} F_{mn}(L)\cos(n\alpha) \qquad (2a)$$

If the large signal is a random valued function, the expected response, indicated by eq. (2b), would be of interest.

$$E[f(u)] = \sum_{m=0}^{\infty} (s^m/m!)E_m(L), \text{ where } E_m(L) \equiv E[f^{(m)}(L)] \qquad (2b)$$

These perturbation solutions are useful, because the behavior of the MBPNL model can be studied with leading-term approximations of the various response components. Several results that have been examined in detail will be described in this paper.

SMALL SIGNAL GAIN AND SUPPRESSION

Consider the MBPNL response of a CF tone that is suppressed by a second tone whose amplitude at the compressor input significantly (≈ 10 dB) exceeds the compression coefficients (u_-,u_+). Simulated MBPNL basilar membrane CF responses are shown in Fig. 4 for suppression tones transmitted via the tip path. Two very distinct response regions are obtained. As a function of level of the CF tone, the response is initially linear and then compressive at υ dB/dB. With increase in suppressor level, the suppressed CF response shifts horizontally at the rate of (1-υ) dB/dB. This model prediction (Duifhuis, 1976; Goldstein, 1989, 1990) accounts for basilar membrane data reported by Robles et al. (1989). The analytic solution for the small signal gain F_{10} describes the linear region, while the Fourier coefficient for the large signal driven response F_{01} describes the compressive response. Joining these two responses at their point of equality gives an excellent approximation of the CF response at all levels.

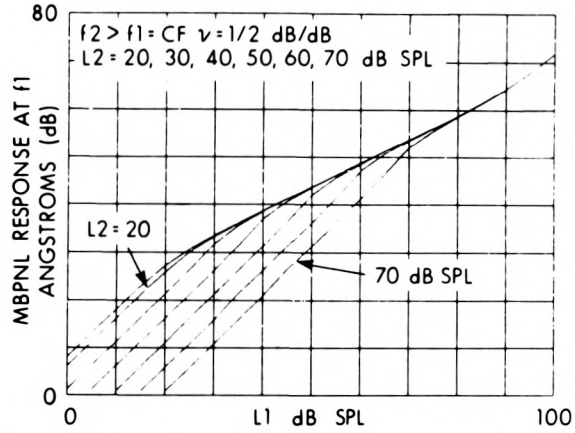

FIGURE 4 CF amplitude responses versus CF stimulus level for various fixed levels of tip-transmitted suppressor tones. υ=1/2.

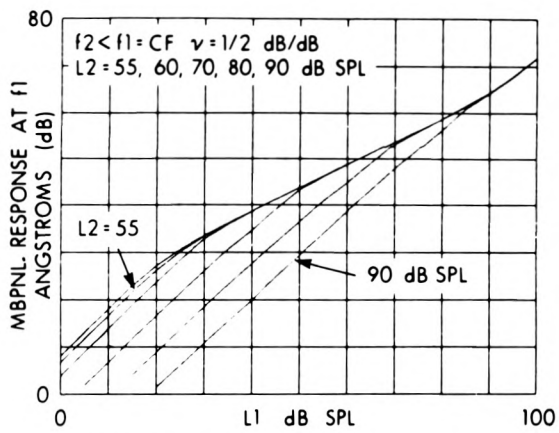

FIGURE 5 As in Fig. 4 with tail-transmitted suppressor tones.

When the suppressor tone is predominantly transmitted via the tail path, suppressed CF responses are obtained as shown in Fig. 5. Higher stimulus levels are required for suppression, but the horizontal shifts with increases in suppressor level are greater. The horizontal shifts, however are not quite as uniform as before. This nonuniform shift is illustrated more clearly with the simulation for a cube-root compression shown in Fig. 6. Here it is clear that linear growth of the small signal response given by F_{10} is generally restricted to a smaller range (< 30 dB SPL). The horizontal suppressive-shift of the small

signal gain converges to 1 dB/dB for $\upsilon < 0.5$. At higher CF stimulus levels, the horizontal shifts are greater. This behavior is the consequence of the nonsinusoidal waveform produced by the expanding transducer.

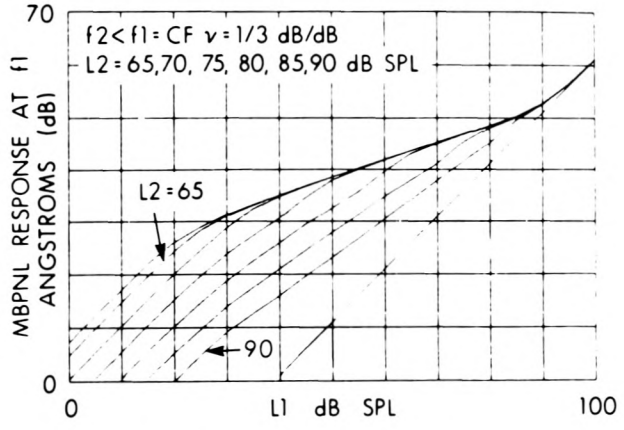

FIGURE 6 As in Fig. 5 with $\upsilon = 1/3$.

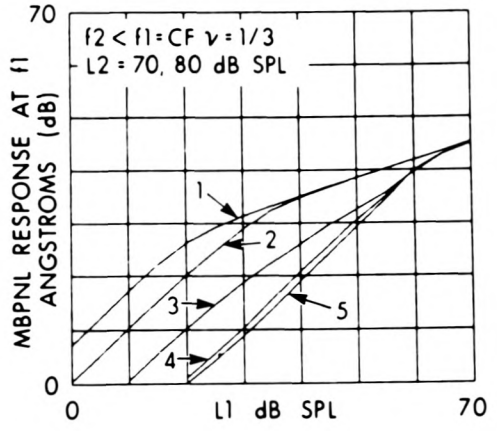

FIGURE 7 Enhancement of suppression by lowpass filtering of suppressor output. Curves 1-3 are reproduced for Fig. 6. Curves 4 and 5 are obtained for the 80 dB suppressor with 1/f and ideal lowpass filtering, respectively.

Lowpass filtering of the expander response produces a suppressed CF response that grows nearly linearly until it joins the large signal compressed response. This is shown in Fig. 7, where it is clear that 1/f lowpass filtering following the expander can have a significant effect on function. The horizontal shift of the small signal gain approaches $(1-\upsilon)/\upsilon$ dB/dB (Goldstein, 1990). It is physically plausible that some form of memory should limit the rapidity of the hybrid filter interactions, but further research is required to quantify this concept.

LINEARIZATION BY BACKGROUND NOISE

Analysis of the response to a CF tone in the presence of background noise follows eq. (2b). Similar results are obtained as with tonal suppressors. For a gaussian noise transmitted via the tip path, the CF response is linear at low levels, as predicted by the expected small signal gain E_1 in eq. (2b), and compressive at high levels, as predicted by F_{01} in eq. (2a). The horizontal shift of the small signal gain with increase in noise level is $(1-\upsilon)$ dB/dB, as for a tonal suppressor. Passing a gaussian noise through the expander produces a similar phenomenon as for a tone. The nongaussian input to the compressor produces a small signal gain with a horizontal suppression-shift that converges to 1 dB/dB for $\upsilon < 0.5$. On the other hand, if the expander output is lowpass filtered, the statistics will tend to gaussian and produce a horizontal suppression-shift of up to $(1-\upsilon)/\upsilon$ dB/dB.

It is plausible that the linear basilar membrane response found near threshold is in part caused by wideband background noise, located in the tail path before the compressor. This is consistent with the finding that tail suppression thresholds are insensitive to variation in tip gain and are uniform across auditory-nerve fibers and subjects (Schmiedt, 1982; Fahey and Allen, 1985). Thus, background noise within a "classical" hydromechanical system may linearize an inherently nonlinear electromechanical response.

PROPAGATING AND LOCAL COMBINATION TONES

MBPNL inputs consisting of periodic large and small signals, with frequencies α and β respectively, will produce responses at the combination frequencies $n\alpha+m\beta$. Leading-term approximations for the amplitudes of these responses are given by the Fourier coefficients F_{mn} along with the amplitudes from the small signal expansion. These predictions allow one to examine the plausibility of local versus propagating accounts of combination tones observed in auditory-nerve response.

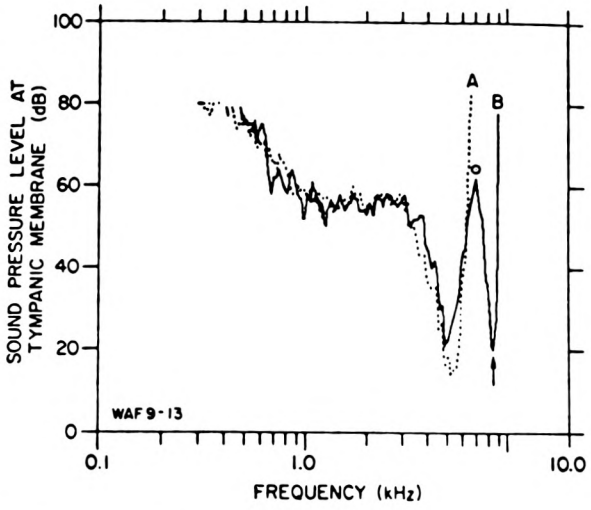

FIGURE 8 Threshold tuning curves from an auditory-nerve fiber: A) measured in quiet, and B) measured with a constant background tone of 7 kHz at 65 dB SPL (Kiang, 1984).

Data reported by Kiang (1984) that illustrate combination tones (Goldsten and Kiang, 1968) and suppression (Sachs and Kiang, 1968) for the same fiber are reproduced in Fig. 8. Curves A and B show threshold tuning curves measured in quiet and with constant background tone (65 dB SPL at 7 kHz). The presence of the constant tone causes an 8 dB suppression at the turning curve tip, and the addition of a combination tone ($2f_1$-f_2) response lobe. The two tip responses in curve B indicate that the driven suppressed response to a 20 dB SPL tone at 5.4 kHz is nearly equal to the $2f_1$-f_2 response produced by a 20 dB tone at 8.6 kHz.

Consider a possible MBPNL model for Kiang's data. The large signal at 7 kHz, which is transmitted via the tip path, is the same for both 20 dB tip stimuli in curve B. Each of these stimuli serves as the small signal compressor input, and produces similar responses at CF. If ρ is the ratio of the (lower to higher frequency) small signal amplitudes at the compressor input, then the output ratio of the two small signal responses will be $\rho(1+\upsilon)/(1-\upsilon) = 1$. With $\upsilon \approx 1/3$, we obtain $\rho \approx 0.5$. That is, the higher frequency compressor input responsible for the combination tone must be about twice as large as the CF input. It has been suggested that stagger tuning of the BPNL pre- and post-processing filters can account for tuned combination tone responses (Duifhuis, 1976; Johnstone, 1980). This explanation requires a broadly tuned preprocessing filter, and a sharply tuned postprocessing filter, which is contradicted by contemporary evidence for sharply tuned tip preprocessing filters (Sellick and Russell, 1979). We are left with the more plausible model that the combination tone is generated at a basalward site closely tuned to the higher frequency tone, and that it propagates apically to its tuned site. Further research with combination tones can yield information on the properties of the propagating medium.

Summary

Several properties of the MBPNL hybrid-filter model have been examined using perturbation analysis. 1) For sinusoidal and gaussian large signals, the small signal gains F_{10} and E_1 describe the small signal response over a large range of the small signal. This allows approximate modeling of the effects of suppression in terms of the small signal

gain coefficients. On the other hand when sinusoidal and gaussian signals are passed through the expander, the range of the small signal approximation is greatly reduced. The range of the small-signal approximation is greatly extended by introducing lowpass memory in the interaction between the MBPNL transducers, which can significantly enhance suppression. 2) The linear transducer response near the origin appears to be indistinguishable from a nonlinear transducer with background noise acting as a large signal. This suggests consideration of the plausibility that linearity is nowhere an inherent property of the healthy cochlea. 3) Both suppression and intermodulation distortion are described by the model. Auditory nerve measurements of suppression and combination tones from the same fiber (Kiang, 1984) cannot be modeled with their generation at a common location. Instead, it is more plausible to conclude that significant combination tones are propagated from basalward sites.

Acknowledgment

This research is supported by NIDCD Grant DC00737.

References

Abbas, P.J. and Sachs, M.B. (1976) Two-tone suppression in auditory-nerve fibers: Extension of a stimulus response relationship. J. Acoust. Soc. Am. 59, 112-122.

Brundin, L., Flock, A. and Canlon, B. (1989) Sound induced motility of isolated outer hair cells is frequency specific. Nature 342, 814-816.

Costalupes, J.A., Rich, N.C. and Ruggero, M.A. (1987) Effects of excitatory and nonexcitatory suppressor tones on two-tone rate suppression in auditory nerve fibers. Hear. Res. 26, 155-164.

Dallos, P. (1988) Cochlear neurobiology: Some key experiments and concepts of the past two decades. In: Auditory Function (Eds: Edelman, G.M., Gall, W.E. and Cowan, W.M.) Wiley, NY, pp. 153-188.

Davis, H. (1983) An active process in cochlear mechanics. Hear. Res. 9, 79-80.

Duifhuis, H. (1976) Cochlear nonlinearity and second filter: Possible mechanism and implications. J. Acoust. Soc. Am. 59, 408-423.

Duifhuis, H. (1980) Level effects in psychophysical two-tone suppression. J. Acoust. Soc. Am. 67, 914-927.

Duifhuis, H. (1989) Power-law nonlinearities: A review of some less familiar properties. In: Cochlear Mechanisms (Eds: Wilson, J.P. and Kemp, D.T.) Plenum Press, NY, pp. 395-401.

Engebretson, A.M. and Eldredge, D.H. (1968) Model for the nonlinear characteristics of cochlear potentials. J. Acoust. Soc. Am. 44, 548-554.

Fahey, P.F. and Allen, J.B. (1985) Nonlinear phenomena as observed at the ear canal and at the auditory nerve. J. Acoust. Soc. Am. 77, 599-612.

Geisler, C.D. (1985) Effects of a compressive nonlinearity in a cochlear model. J. Acoust. Soc. Am. 78, 257-260.

Geisler, C.D. (1986) A model for the effect of outer hair cell motility on cochlear vibrations. Hear. Res. 24, 125-131.

Gifford, M.L. and Guinan, J.J. (1983) Effects of crossed-olivocochlear-bundle stimulation on cat auditory nerve fiber responses to tones. J. Acoust. Soc. Am. 74, 115-123.

Goldstein, J.L. (1967) Auditory nonlinearity. J. Acoust. Soc. Am. 41, 676-689.

Goldstein, J.L. (1989) Updating cochlear driven models of auditory perception: A new model for nonlinear auditory frequency analyzing filters. In: Working Models of Human Perception (Eds: Elsendoorn, B. and Bouma, H.) Academic Press, London, pp. 19-57.

Goldstein, J.L. (1990) Modeling rapid waveform compression on the basilar membrane as multiple-bandpass-nonlinearity filtering. Hear. Res., in press.

Goldstein, J.L. and Kiang, N.Y.S. (1968) Neural correlates of the aural combination tone $2f_1$-f_2. Proc. IEEE 56, 981-992.

Hudspeth, A.J. (1989) How the ear's works work. Nature 341, 397-404.

Johnstone, J.R. (1980) The generation of combination tones. Hear. Res. 3, 253-256.

Kiang, N.Y.S. (1984) Peripheral neural processing of auditory information. In: Handbook of Physiology-The Nervous System III (Ed: Darian-Smith, I.) The American Physiological Society, Bethesda, MD, pp. 639-674.

Kiang, N.Y.S., Moxon, E.C. and Levine, R.A. (1970) Auditory-nerve activity in cats with normal and abnormal cochlea. In: Sensorineural Hearing Loss (Eds: Wolstenholme, G.E.W. and Knight, J.) Churchill, London, pp. 714-730.

Kiang, N.Y.S. and Moxon, E.C. (1972) Physiological considerations in artificial stimulation of the inner ear. Ann. Otol. Rhinol. Laryngol. 81, 714-730.

Kiang, N.Y.S., Liberman, M.C., Sewell, W.F. and Guinan, J.J. (1986) Single unit clues to cochlear mechanisms. Hear. Res. 22, 171-182.

Kim, D.O. (1986) A review of nonlinear and active cochlear models. In: Peripheral Auditory Mechanisms (Eds: Allen, J.B., Hubbard, A., Neely, S.T. and Tubis, A.) Springer, NY, pp. 239-249.

Liberman, M.C. and Kiang, N.Y.S. (1984) Single-neuron labeling and chronic cochlear pathology. IV. Stereocilia damage and alterations in rate- and phase-level functions. Hear. Res. 16, 75-90.

Neely, S.T. and Kim, D.O. (1983) An active cochlear model showing sharp tuning and high sensitivity. Hear. Res. 9, 123-130.

Patuzzi, R., Sellick, P.M. and Johnstone, B.M. (1984) The modulation of the sensitivity of the mammalian cochlea by low frequency tones III. Basilar membrane motion. Hear. Res. 13, 19-27.

Pfeiffer, R.R. (1970) A model for two-tone inhibition of single cochlear-nerve fibers. J. Acoust. Soc. Am. 48, 1373-1378.

Rhode, W.S. (1971) Observations of the vibrations of the basilar membrane in squirrel monkeys using the Mossbauer technique. J. Acoust. Soc. Am. 49, 1218-1231.

Robles, L., Ruggero, M.A. and Rich, N.C. (1986) Basilar membrane mechanics at the base of the chinchilla cochlea. I. Input-output functions, tuning curves and response phases. J. Acoust. Soc. Am. 80, 1364-1374.

Robles, L., Ruggero, M.A. and Rich, N.C. (1989) Nonlinear interactions in the mechanical response of the cochlea to two-tone stimuli. In: Cochlear Mechanisms (Eds: Wilson, J.P. and Kemp, D.T.) Plenum, NY, pp. 369-375.

Ryan, A. and Dallos, P. (1975) Effect of absence of outer hair cells on behavioral auditory threshold. Nature 253, 44-46.

Sachs, R.M. (1975) Perception of $2f_1$-f_2, An Auditory Distortion Product. Ph.D. Dissertation, Dept. of Audiology, Northwestern University, Evanston, IL.

Sachs, M.B. and Kiang, N.Y.S. (1968) Two-tone inhibition in auditory-nerve fibers. J. Acoust. Soc. Am. 43, 1120-1128.

Schmiedt, R.A. (1982) Boundaries of two-tone rate suppression of cochlear-nerve activity. Hear. Res. 7, 335-351.

Schroeder, M.R. (1969) Relation between critical bands in hearing and the phase characteristics of cubic difference tones. J. Acoust. Soc. Am. 46, 1488-1492.

Sellick, P.M. and Russell, I.J. (1979) Two-tone suppression in cochlear hair cells. Hear. Res. 1, 227-236.

Sellick, P.M., Patuzzi, R. and Johnstone, B.M. (1982) Measurement of basilar membrane motion in the Guinea pig using the Mossbauer technique. J. Acoust. Soc. Am. 72, 131-141.

Smoorenburg, G.F. (1972) Combination tones and their origin. J. Acoust. Soc. Am. 52, 615-632.

Zwicker, E. (1986) A hardware cochlear nonlinear preprocessing model with active feedback. J. Acoust. Soc. Am. 80, 146-153.

AUTOMATIC GAIN CONTROL IN COCHLEAR MECHANICS

Richard F. Lyon

Advanced Technology Group
Apple Computer, Inc., Cupertino, CA 95014, USA
and Computer Science Department
California Institute of Technology, Pasadena, CA 91125, USA

Introduction

Measurements of basilar membrane motion show that the cochlea has a strong compressive nonlinearity over a wide range of sound intensities, even down to low intensities where the system might be expected to be linear. Many models of cochlear hydrodynamics and micro-mechanics ignore this strong nonlinearity in order to be able to apply linear systems concepts, sometimes resulting in inappropriate interpretations of cochlear function. We propose a modeling approach based on explicitly recognizing the purpose of the strong nonlinearity as an automatic gain control (AGC) that serves to map a huge dynamic range of physical stimuli into the limited dynamic range of nerve firings.

We discuss two aspects of AGC in cochlear function. First, we cover possible AGC mechanisms and mathematical modeling techniques. These involve active outer hair cells whose properties are controlled by the efferent system, resulting in variable-gain wave propagation in the cochlea.

Second, we consider the implications of AGC-based modeling on two controversial issues in the field of cochlear function and modeling: sharpness of neural and mechanical tuning, and two-tone suppression. The single most important implication is that the linearized transfer function of the cochlea at any particular sound intensity is always much broader than an iso-response tuning curve; this fact depends very little on the other modeling details. More detailed features of iso-response tuning curve shapes (such as a notch between the tip and the tail) may depend on details of the AGC system more than on details of the transfer functions.

The physiology of medial olivocochlear efferents as mediators of a wide-dynamic-range spatially coupled binaural AGC system is discussed briefly. We propose using contralateral suppressor tones to directly assess the gain reduction effect of the efferents.

Finally, we summarize our view of cochlear function involving variable negative damping wave mechanics resulting in unsharp pseudoresonant transfer functions.

Background

By AGC we mean a mechanism for varying the sensitivity or gain of a system based on the signal level at the output of the system, so as to reduce the dynamic range of the output relative to the input. A single-input single-output system with AGC is sometimes referred to as a compressor. An AGC generally has a "gain-control loop" with a lowpass "loop filter", so that the system gain varies slowly, rather than instantaneously. An extreme form of AGC attempts to keep the output level constant, as in an AM radio receiver—we do not interpret the term AGC as implying this extreme. An AGC may either vary a "pure gain" or vary some parameter that effects an approximate gain variation coupled with other changes, such as the change of tuning sharpness in the cochlea.

Evidence for a variable-gain mechanism in cochlear function was clear in the pioneering work of Rose et al. (1971). Their data suggest "the existence of a cochlear sensitivity control mechanism which may, but perhaps need not be, mechanical in nature." Subsequent experiments to measure the mechanics of basilar membrane motion directly bear out the notion that much of the sensitivity variation occurs in the mechanical gain; the work of Robles et al. (1986) shows this effect most clearly, even below 20 dB SPL.

An early model of gain control in cochlear mechanics was proposed by Kim et al. (1973), using an instantaneously-varying damping element. This approach works fairly well for modeling many effects, and is appealing for its simplicity; it results in response characteristics similar to bandpass-nonlinearity (BPNL) models, without requiring a second filter.

In his more recent work, Kim (1984) proposes "biomechanical gain control" mediated by the efferent large medial olivocochlear neurons that innervate the outer hair cells. He provides a detailed review of anatomical and physiological evidence for his hypotheses concerning the roles of the hair-cell and nerve populations. This paper may be taken as the basis of our current views on cochlear mechanics and the need for an AGC that goes beyond the effects of the instantaneous nonlinearity.

Gain-Control Mechanisms and Models

There is plenty of evidence that the relationship between mechanical motion at the oval window and mechanical motion of the basilar membrane is nonlinear over a wide range of signal levels, with apparent gain changes in excess of a factor of 100 (40 dB) for sine waves near CF. Apparently, an active amplification of weak traveling waves gradually changes to an attenuation of strong traveling waves as the input level is increased. The coupling of the mechanical wave propagation system to the active electro-mechano-chemical system of the outer hair cells is generally presumed to provide the mechanism for the variable gain, though details remain to be worked out. Other mechanisms may also provide gain variation, as in the stapedial reflex changing the gain of the middle ear, and depletion of neurotransmitters changing the transduction gain of the inner hair cells. Mechanisms at all levels of the sensory nervous system cooperate to

map a wide range of real-world signals into more-or-less "invariant" neural representations, but in this paper we focus only on the gain variations that occur in the mechanical propagation of waves in the cochlea.

Wave propagation in the cochlea can be described by a relationship between complex wavenumber, place, and frequency, when the system is behaving linearly. Nonlinear and adaptive effects can be included in the wavenumber relations for a linearized approximation that applies to a particular state of the parameters (e.g. a particular gain vs. frequency setting that is the result of a particular steady-state stimulus). This type of analysis is easiest if there are no instantaneous nonlinearities, so that the system is short-time linear. The complex wavenumber encodes the spatially varying wavelength as well as the varying energy gain or loss seen by the traveling wave. A varying negative imaginary part of the wavenumber yields a varying-height gain peak in the overall "pseudoresonant" transfer function from the input to any chosen place. Varying the peak gain by changing the wavenumber will inherently vary the shape of the transfer function as well, though the shape and position of the peak may change only slightly compared to the large peak height variations.

Physically-based models of the cochlear mechanics generally involve expressions for the force exerted on the fluid by the cochlear partition (basilar membrane), sometimes in the form of a complex impedance. The force may include terms for membrane stiffness, tension, mass, and losses. A loss term that exerts a force proportional to membrane velocity may model viscous loss in a boundary layer at the membrane, at least approximately. Varying the magnitude of the loss term, and in particular letting it be negative, is typically the way to include a variable gain to model active and adaptive outer hair cells. Terms other than the loss may also be used to provide an active gain, as in Mountain's (1983) "active-stiffness" model.

Since frequencies above CF need to be attenuated, it is important that the loss term change from negative to positive near CF. If a pure negative damping (or negative viscosity) term is used, another loss mechanism must be introduced to attenuate high frequencies. Lyon and Mead (1988) have proposed a hypothetical force proportional to the rate of change of longitudinal curvature of the partition, which provides a loss that rises steeply with frequency or wavenumber and eventually overwhelms the gain from the negative viscosity term. Mountain's active-stiffness model, on the other hand, uses a first-order lowpass function in converting displacement to force, so that for low frequencies it is a stiffness, and for frequencies above its corner it provides nearly ninety degrees of phase shift to convert the force to an active gain; the magnitude of the active gain declines with frequency, so that a fixed passive loss term eventually dominates at high frequencies. Whether either of these models accurately describes the physics of the cochlear partition with active outer hair cells is not yet clear, but both seem to be at least qualitatively reasonable.

In modeling cochlear hydrodynamics with an active gain mechanism, the nature of the nonlinear relationship between signal level and gain is still a huge open question. Modeling both the static and dynamic aspects of the gain adaptation can be quite challenging, and there is often not enough experimental data to support a choice of model parameters. In many cases, modelers elect to forego the complexity of a dynamic gain-control loop, and settle for an instantaneous compressive nonlinearity in the active gain

mechanism. This leaves the efferent system without a functional role in the model, which does not seem reasonable. An understanding of cochlear function will almost certainly require attention to both types of nonlinear compression.

Implications for Sharpness and Suppression

The single most important implication of AGC in the cochlea is the difference in sharpness between (sharp) iso-response tuning curves and (unsharp) iso-intensity response curves or equivalent linearized transfer functions. This difference is clear in much of the experimental data in the field of hearing, whether measured in cochlear mechanics or in nerve responses. However, this difference in sharpness has not generally been interpreted as the simple result of an AGC, and indeed many modelers still make the mistake of trying to match model transfer functions to iso-response data.

Mechanical data of Robles et al. (1986) from the Mössbauer technique clearly indicate the effect of nonlinear amplitude compression on tuning curve sharpness. The BM input-output level functions of their Figure 1 emphasize the amplitude compression for frequencies near CF, rather than tuning. Our Figure 1 shows the same data as two types of tuning curves. Notice that the iso-velocity curve is considerably sharper, by any measure, than even the sharpest low-level transfer function, and much sharper than the higher-level transfer functions that are in effect over much of the range of measurement. We have shown the same effect in simulation of nonresonant models of cochlear mechanics with adaptive negative damping as the AGC (Lyon and Mead 1988).

Iso-response curves have been the most popular way to characterize tuning sharpness for many years. Because iso-response measurements require input levels changing over many orders of magnitude, gain control mechanisms are pushed to their extremes. For frequencies off CF, the input level must be raised to compensate for the falling transfer function gain, and raised more to counteract the gain reduction caused by raising the input level; hence, the skirts are pushed up sharply. Very near the tip, however, the system may in some cases operate below the level that starts to cause a gain reduction. Then within a few dB of the tip, the shapes should agree fairly closely. Indeed, Evans (1977) reported good agreement in the shapes of iso-rate tuning curves and revcor-derived transfer functions, but only within 10 dB of the tips and only for the lowest stimulus levels. Some modelers have accepted his data as evidence that these two types of curves should agree, but this interpretation is especially suspect in the light of clearly-established input-output nonlinearities.

In addition to single-tone data, Robles et al. (1986) present input-output relations in the presence of a second (suppressor) tone above CF. The tone above CF does not cause much response itself, but reduces the gain to tones near CF by more than 10 dB. When the suppressor is significantly more intense than the probe tone, it determines the gain of the system, resulting in a linear input-output relationship to the weaker probe tone in a region where the system was nonlinear when the probe tone was presented alone. These suppression effects are exactly as would be expected from an AGC-based model.

For suppressor tones below CF, two-tone suppression is still very important (mechanical data are not yet published on this, but Ruggero says it's true). Models with

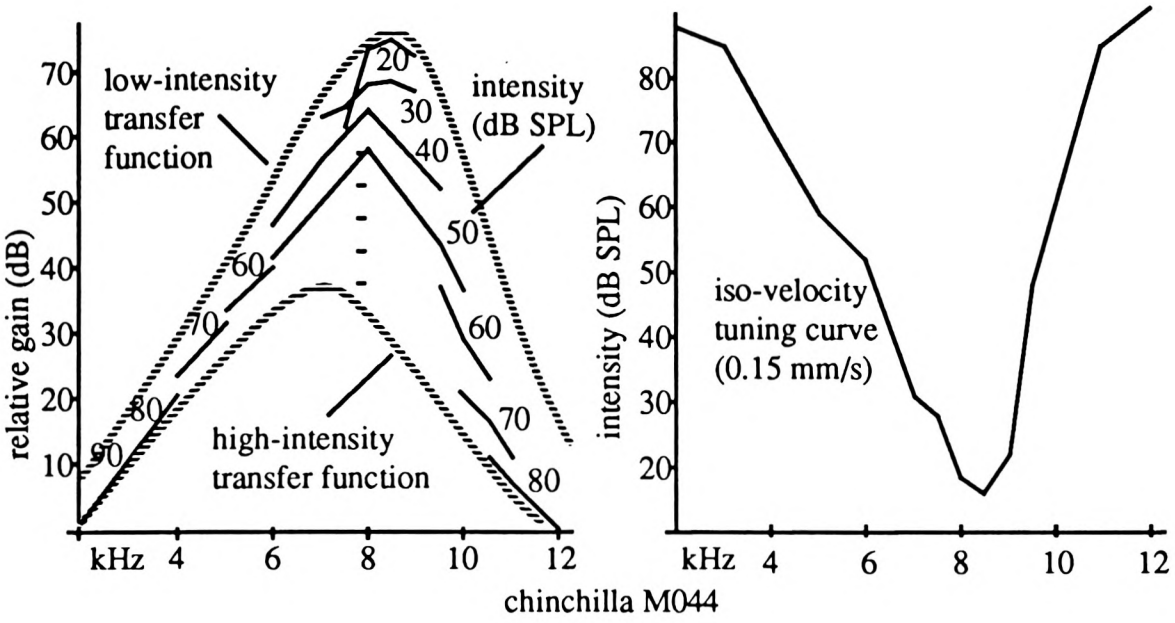

FIGURE 1 Iso-intensity data and approximated curves (left) and iso-velocity data (right) re-plotted from Figure 1 of Robles *et al.* (1986). Notice that the iso-intensity data show an input-output compression of about 2:1 near CF; that is, each 10 dB increase in input intensity causes a 5 dB decrease in the mechanical gain of the cochlea. This compression results in the iso-velocity curve being significantly sharper than even the sharpest of the transfer functions.

instantaneously-varying damping elements do not reproduce this effect, but models with AGC can, under appropriate conditions. In order for this effect to occur, it is necessary that the gain-control feedback from places responsive to the lower frequency also serve to reduce the gain at more basal places, which are sensitive to the higher frequency. We have referred to this cross-place or cross-channel inhibition as "coupled AGC" (Lyon 1982). In the wave propagation model, coupling from a high-frequency place to a low-frequency place is inherent, since waves must travel through the former to the latter. Coupling in the other direction must be provided by having the gain-control feedback signals connect to places more basal than the places whose output they are responsive to. This same cross-coupling toward the base results in significant steepening of the low-side skirt of the iso-response curves, and may contribute the notch below CF that is sometimes modeled as a micro-mechanical antiresonance.

Models with per-channel uncoupled AGC mechanisms will not do at all well in reproducing sharp tuning curves or two-tone suppression; a "lateral" gain reduction is crucial in modeling these effects.

The data in Figure 1 are not as complete as we would like, and our approximated curves are subject to significant error. Better measurements from the laser Doppler velocimeter technique will soon be available to resolve remaining uncertainties. In particular, by using both transient (click) and steady-state (tone and noise) stimuli, it should be possible to separate out the compressive effect due to instantaneous nonlinearities from that due to an efferent-mediated gain-control loop. It should also be possible to measure the small-signal gain reduction in one cochlea due to a suppressor

presented contralaterally, presuming there is such an effect.

Active outer hair cells have often been invoked to explain tuning sharpness in excess of that implied by linearized passive models of cochlear mechanics. From the above discussion we hope to make it clear that active gain is not sufficient to produce realistic tuning curves—adaptive compressive control of the gain is required in addition. Both sharp pure-tone tuning and two-tone suppression must be the result of nonlinear compression in cochlear mechanics, whether that compression results from instantaneous nonlinear elements or efferent feedback or both.

When an AGC-based modeling approach is used, sharp enough iso-response curves can be obtained without postulating a resonance based on a large basilar membrane mass; the iso-velocity data of Robles et al. (1986) is reasonably well matched using a two-dimensional wave analysis and zero mass (Lyon and Mead 1988). Contrast this approach to the use of long-wave one-dimensional analysis with a large membrane mass, which has been popular because the transfer functions are sharp enough to match iso-response data directly, ignoring nonlinearities.

Physiology of Cochlear AGC

Liberman (1986) has reported that efferent fibers in the cochlear nerve are typically almost as sharply tuned as afferents, but some are tuned for ipsilateral tones and some are tuned for contralateral tones. In addition, these fibers often have a dynamic range between threshold and saturation of 70 dB or more. He also found that these efferent fibers innervate several outer hair cells near the place corresponding to their CF. All of these observations are exactly what would be expected for the feedback path that controls the mechanical gain of the cochlea, presuming that the outer hair cells provide a controllable negative damping. Let us consider these observations one at a time.

1. The relatively small number of efferent fibers probably carry amplitude information aggregated from groups of the more numerous afferent fibers, thereby causing a slight smearing of the tuning curves.

2. The gains of the two cochleas are probably coupled, so the inter-aural intensity differences are not compressed as much as average intensities, to facilitate using such cues for localization. Such coupling would imply tuning to sounds in either ear, whether via separate units or binaurally-sensitive units.

3. The range over which the firing rates of the efferent fibers should be non-saturating should be about the same as the range of intensities for which the efferent-mediated compressive nonlinearity is active. This scheme is much more economical of fibers than the multiple levels of thresholds of quickly-saturating units often seen in the afferent system.

4. Fibers that inhibit the gain only very near the region of the CF of the corresponding afferents (whose activity is being used to control the gain) would yield a minimum of spatial coupling. A more broadly-coupled AGC is probably preferred, so that local spectral contrasts will not be compressed so much. Coupling the efferent to places more basal than the corresponding afferents will also give more control of the gain, since signals being detected travel through that region. Coupling toward the base

also gives suppression of tones at CF by lower frequencies, and steepens the low-side skirt of tuning curves, perhaps even adding a "notch" below CF. The observed spatial spread of up to nearly an octave in distance seems reasonable.

Measurements of cochlear mechanical response in the presence of a contralateral suppressor tone would be a good way to directly assess efferent-mediated gain control.

A View of Cochlear Function

Building on the AGC-based modeling approach, we have assembled a view of cochlear function that we believe is reasonably self-consistent and in agreement with much of the experimental data in the field. Many of the pieces of this view are not generally accepted, and indeed do not appear to be correct within modeling paradigms without AGC and too heavily dependent of linear analysis. In particular, the following items characterize our currents views:

1. Near CF, the cochlea operates mainly in the short-wave region, rather than in the long-wave region. The long-wave region does not contribute significantly to neural response, except perhaps in the low-frequency tails.

2. The mass of the cochlear partition is negligible, except perhaps near the base, and the tension of the cochlear partition is also negligible. Membrane stiffness and fluid mass interact to form a dispersive wave propagation system without resonance.

3. The hydrodynamic system of the cochlea is not highly tuned (in the sense of being highly frequency selective or resonant), and the best frequency for a place is quite level dependent.

4. Sharp iso-response tuning curves are the result of an AGC operating in conjunction with a broadly tuned hydrodynamic system—no "second filter" or other tuned sharpening mechanism is needed to model cochlear tuning as seen in either the mechanics or the neural firings.

5. A bandpass filterbank to model cochlear response ought to be designed as a cascade, rather than as a parallel bank of independent filters, in order to achieve a realistic amplitude and group-delay response, to model propagation of distortion products, and to conserve on computation.

6. A model of the active adaptive cochlea must be extremely nonlinear over a wide range of signal level, mainly to effect dynamic range compression.

7. Odd-order distortion products in the hydrodynamic system are audible under special conditions, and are maximum for cochlear input power levels comparable to or a little higher than the power that can be supplied by the outer hair cells.

8. Viscosity of the cochlear fluid is negligible except at a boundary layer at the basilar membrane. That is, very little energy is dissipated in the bulk of the fluid, but as the wave collapses onto the membrane in the short-wave region, energy is dissipated into the membrane and into fluid drag along the membrane.

9. Outer hair cells act approximately like a negative boundary layer viscosity, adding a force to the membrane proportional to its velocity, for frequencies below CF. The transition from negative damping to positive damping is not sharply tuned.

10. In the normally-functioning cochlea, energy travels in one direction—standing

waves, acoustic emissions, and reflections may be neglected except in pathologies.

This approach has been the basis of our work on cochlear modeling applied to speech recognition, including custom VLSI digital and analog implementations of cochlear models.

Conclusions

The progress of scientific research is generally accelerated through the use of good models to guide the design and interpretation of experiments. A key element missing from most auditory models in recent years is a dynamic AGC. We believe it is now important to include such an AGC element to help resolve some of the controversies in the hearing field, such as questions of sharpness of tuning. We propose that neurophysiologists might do well to devote more effort to answering the many open questions concerning the details of cochlear mechanical gain variation, in order to contribute to the development of a comprehensive and realistic model of hearing.

References

Evans, E.F. (1977), "Frequency Selectivity at High Signal Levels of Single Units in Cochlear Nerve and Nucleus." In: *Psychophysics and Physiology of Hearing* (Eds: Evans, E.F. and Wilson, J.P.) Academic Press, London, pp. 185–192.

Kim, D.O., Molnar, C.E. and Pfeiffer, R.R. (1973), "A system of nonlinear differential equations modeling basilar-membrane motion." J. Acoust. Soc. Am. **54:**1517–1529.

Kim, D.O. (1984). "Functional Roles of the Inner- and Outer-Hair Cell Subsystems in the Cochlea and Brainstem." In: *Hearing Science* (Ed: Berlin, C.) College-Hill Press, San Diego, pp. 241–261.

Liberman, M.C., and Brown, M.C. (1986), "Physiology and anatomy of single olivocochlear neurons in the cat." *Hearing Res.* **24**:17–36.

Lyon, R.F. (1982), "A Computational Model of Filtering, Detection, and Compression in the Cochlea." *Intl. Conf. on Acoust., Speech, and Sig. Proc.*, IEEE, Paris, pp. 1282–1285.

Lyon, R.F. and Mead, C. (1988), "An Analog Electronic Cochlea." *IEEE Trans. Acoust., Speech, and Sig. Proc.* **36**: 1119–1134.

Mountain, D.C., Hubbard, A.E., and McMullen, T.A. (1983), "Electromechanical Processes in the Cochlea," In: *Mechanics of Hearing* (Eds: de Boer, E. and Viergever, M.A.) Martinus Nijhoff, The Hague, pp. 119–126.

Robles L., Ruggero, M.A. and Rich, N.C. (1986). "Mössbauer measurements of the mechanical response to single-tone and two-tone stimuli at the base of the chinchilla cochlea." In: *Peripheral Auditory Mechanisms* (Eds: Allen, J.B. et al.) Springer-Verlag, New York, pp. 121–128.

NON-LINEARITY IN A COMPUTATIONAL MODEL OF THE RESPONSE OF THE BASILAR MEMBRANE

Ray Meddis, Michael J. Hewitt, Trevor M. Shackleton

Speech and Hearing Laboratory, Department of Human Sciences,
University of Technology, Loughborough, LE11 3TU, UK.

Introduction

We are interested in modelling human response to speech signals with particular reference to selective attention. We intend that our models should use principles derived from anatomy and physiology as far as possible. Accordingly, a balance has to be struck between available computational power and the need to model all the important subsidiary processes such as middle- and outer- ear effects, basilar membrane response, inner hair-cell response, interactions among neurons in the brainstem nuclei, etc.. Despite the computational overhead of taking it into account, the nonlinearity of the response of the inner ear to sound is important to an understanding of human speech processing for at least two reasons. Firstly, we know that distortion products influence pitch perception - the so-called second effect of pitch shift (Schouten *et al.*, 1962) - and pitch is an important element in the segregation of sounds. Secondly, the nonlinear response of the cochlea has important implications for the representation of speech sounds (Miller and Sachs, 1983).

Modelling the mechanical filtering effect of the basilar membrane has a long history (Zwislocki, 1980) and many nonlinear models have been produced. However, to the best of our knowledge, convenient and reliable algorithms which accept an arbitrary input and generate acceptable outputs are either not available or are still in an experimental stage of development. We, therefore, undertook to modify an existing digital filter bank in such a way as to meet the requirements of our situation.

We needed ;

1) asymmetrical filters whose asymmetry increases as stimulus level is increased,
2) filters whose centre frequency changes with stimulus amplitude,
3) filters whose outputs include distortion products such as combination tones which may have been generated at a remote site on the simulated membrane,
4) filters which demonstrate realistic two-tone suppression,

For sample references see (e.g. Johnstone, *et al,* 1986; Kim *et al,* 1980; Robles *et al,* 1986; Sachs and Kiang, 1968).

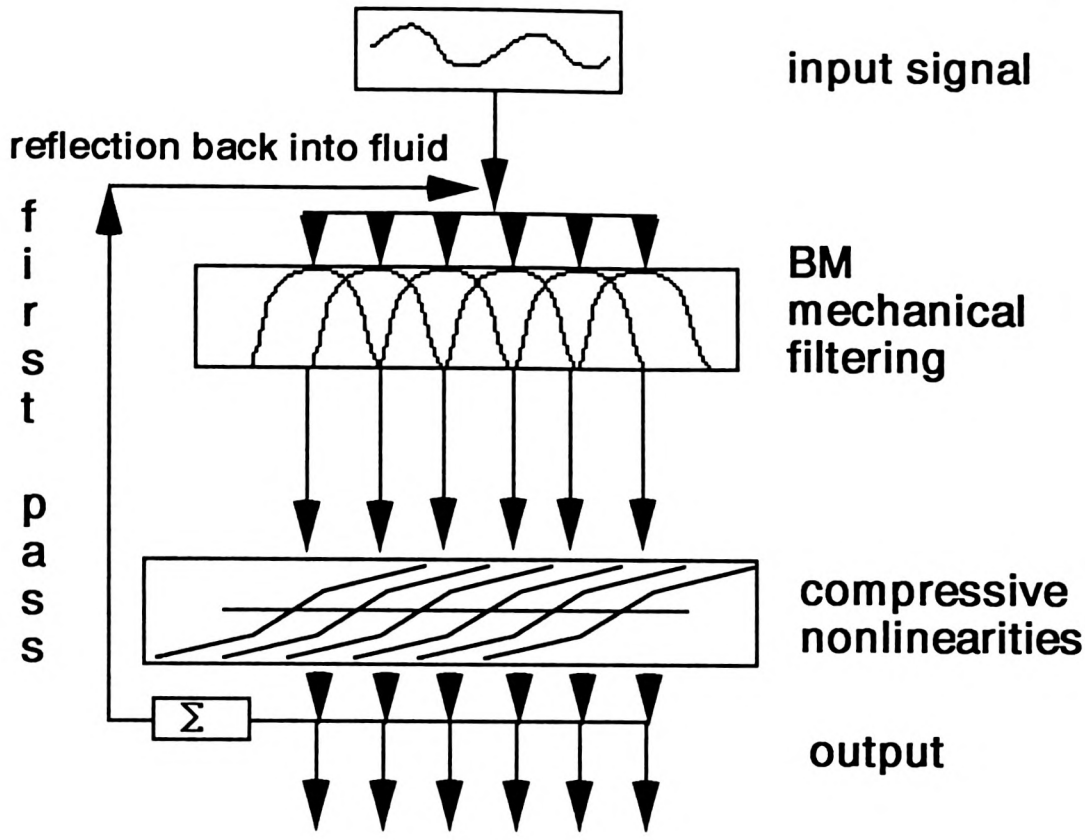

FIGURE 1 Flow diagram for the model.

Basic principles

In building the model, we have been guided by broadly agreed anatomical and physiological principles in the development of our algorithms but we did not aim to produce an explicitly macromechanical model of the cochlea. The following basic ideas characterise the system:

1. As a first approximation, the basilar membrane acts as a passive, symmetrical filter applied to the signal input velocity function.

2. The response of the BM is subject to a compression function which operates only above some value near 30 dB SPL. Below that level, the system is linear. Compression applies only to that part of the signal which exceeds 30 dB.

3. The BM is tightly coupled with the cochlea fluid so that the response of the membrane is fed back into the fluid.

4. The compressed output of each filter is virtually simultaneously available throughout the fluid (because of the high velocity of sound in the cochlear fluid). It therefore forms a new signal which replaces the original input and is subject to mechanical filtering in its turn.

5. The final output from the filters is the result of a recursive process of filtering, compression, recombination, filtering, etc..

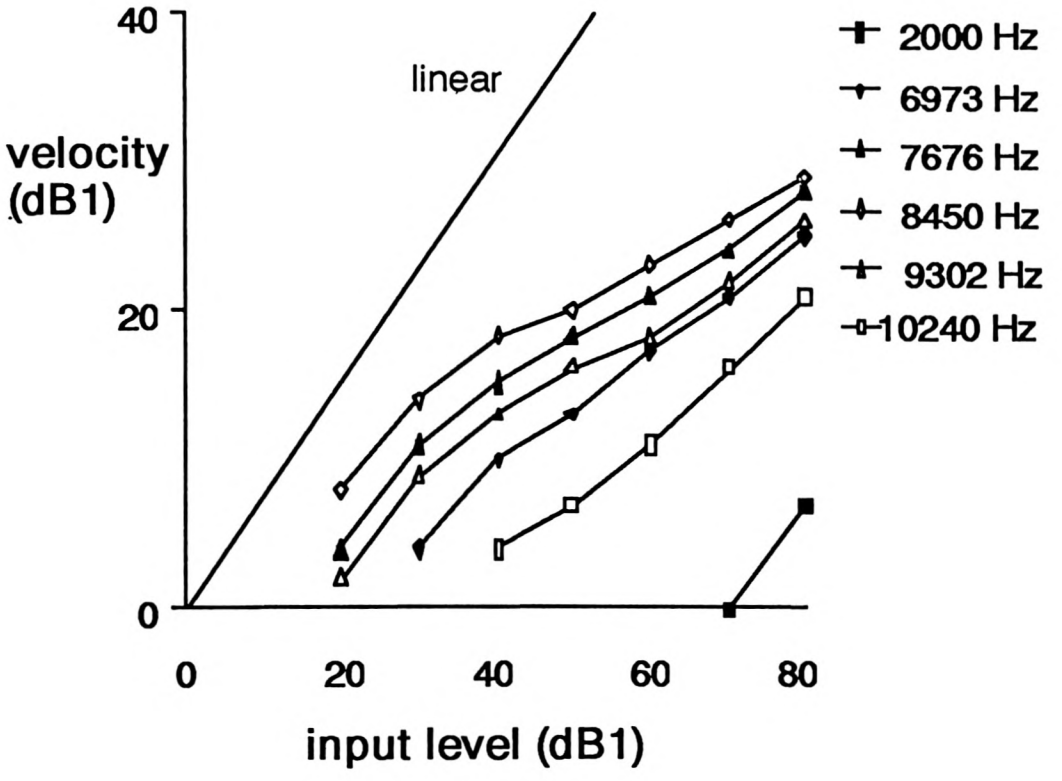

FIGURE 2 Input / output functions for a filter with CF 8450 Hz at six stimulus frequencies.

Implementation

The input signal is processed initially by a bandpasss filter bank. This consists of digital gammatone filters supplied to us by John Holdsworth and Roy Patterson, Cambridge, UK. The filters are linear, symmetrical and straight-sided. They have equivalent rectangular bandwidths (ERBs) which are based upon human psychophysical 'tuning curves' (Patterson and Moore, 1986) being wider at higher frequencies. In the results given below, we use 128 overlapping filters with centre frequencies equally spaced on an ERB-rate scale between 80 Hz and 8000 Hz. All calculations are based on a 40-kHz sample rate. The input to the system is a simple number sequence representing the acoustic stimulus. Levels are given as dB1 relative to rms=1.

The output of each of the 128 filters is then individually compressed

$$R(t) = [b + a / [1+k |x(t)|]] x(t) \quad (1)$$

where $|x(t)|$ is the modulus of the instantaneous velocity of the stimulus, $R(t)$ is the instantaneous compressed output velocity and a,b & k are parameters of the model. $a = 0.5$ and b varies with filter center-frequency, $b = 250/cf$. At low stimulus levels a dominates the compression function, while at high levels b dominates it. k influences the stimulus level at which b begins to dominate the output. In what follows, k *is* set to .034 which implies that a dominates the function below 30 dB1 and b dominates it above this level.

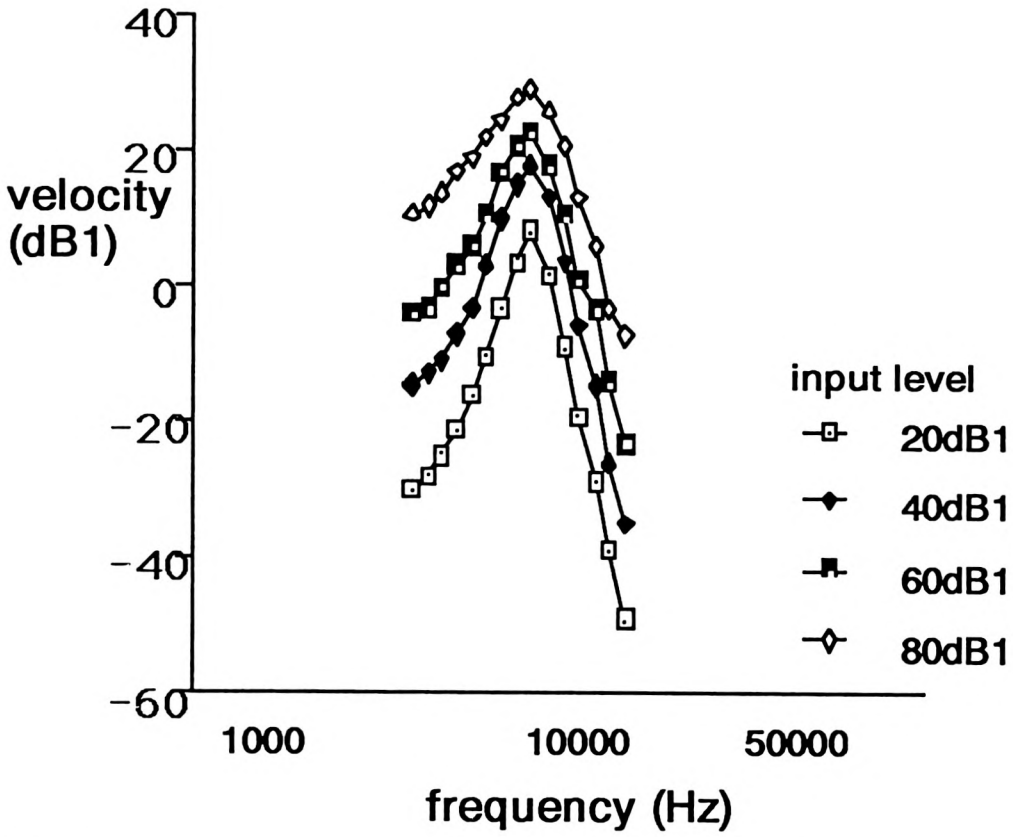

FIGURE 3 The amplitude of basilar membrane displacement plotted as a function of

The 128 filtered and compressed signals are then added together and notionally reflected back into the cochlea fluid to create a new input signal for the filterbank. The recombined signal is fed into the filter bank and the individual output from each filter is compressed once more, as described above. We could continue indefinitely with the recursion but the results below are based on only two passes through the filter bank and compression stages.

The output from the second pass through the model can be examined directly to show the resulting characteristics of the filter / compression system. Alternatively, it may be used as input to an inner hair-cell simulation leading to spike generation in a simulated auditory nerve fiber (e.g. Meddis *et al;* 1990).

No attempt is made to simulate the frequency attenuation effects of the middle ear. As a consequence these stimuli are effectively applied at the oval window. This makes it easier to compare the model output with other results in the literature.

Results

Figure 2 shows the input/output function for a single filter with a center frequency (CF) of 8.45 kHz. Values are given for a range of frequencies as a function of stimulus level. Stimuli with frequencies close to CF show a nonlinear response above 30 dB1. As stimulus

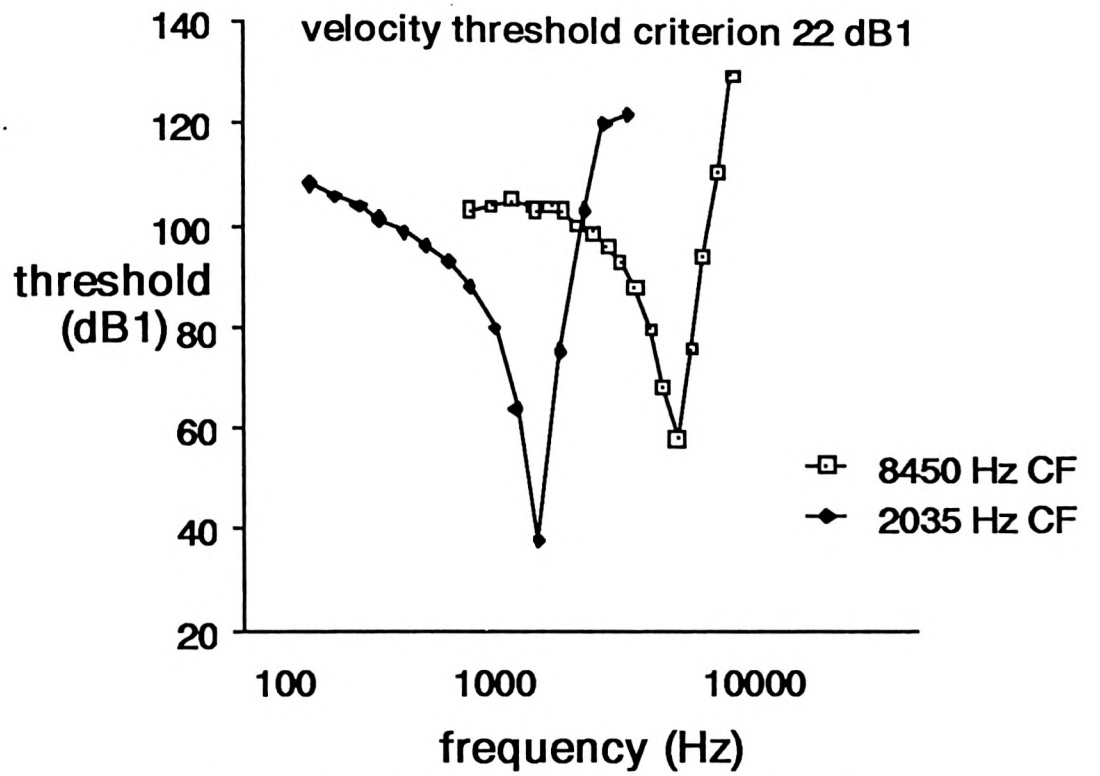

FIGURE 4 Iso-velocity tuning curves at two centre frequencies

frequency departs from CF, the response is increasingly linear. At very high stimulus amplitudes at CF the output rises 2.5 dB for each 10 dB input increase in agreement with the data of Robles *et al.* (1986).

Figure 3 shows the input/output relationships in the form of filter functions. The filter function clearly develops a wider passband at higher stimulus levels. The best frequency of the filter, however, does not change appreciably as we had hoped.

Figure 4 shows the 22 dB1 isovelocity curve at at center frequencies 2 kHz and 8.45 kHz. At 2 kHz there is little compression and the isovelocity curve closely resembles the inverse of the linear filter function except at the extreme low frequency tail. At 8.45 kHz center frequency the compression is greater and this causes the curve to move slightly upwards. The reduced compression at lower frequencies gives rise to a distinct shelf in the low frequency region in agreement with most observations of AN fiber tuning curves.

Figure 5 shows two-tone suppression effects at the location with center frequency 8.45 kHz. A 40 dB1 probe tone was played continuously at CF while a test tone was varied in frequency and intensity. The shaded area represents the frequencies and levels capable of suppressing the response to the probe tone by more than 1 dB. At 80 dB1, the greatest suppression observed was 5.6 dB at 12 kHz.

Figure 6 shows a Fourier analysis of the outputs of the filter bank / compression system in response to a two-tone stimulus (f1=2.17kHz; f2=2.79 kHz) presented to the model at 80

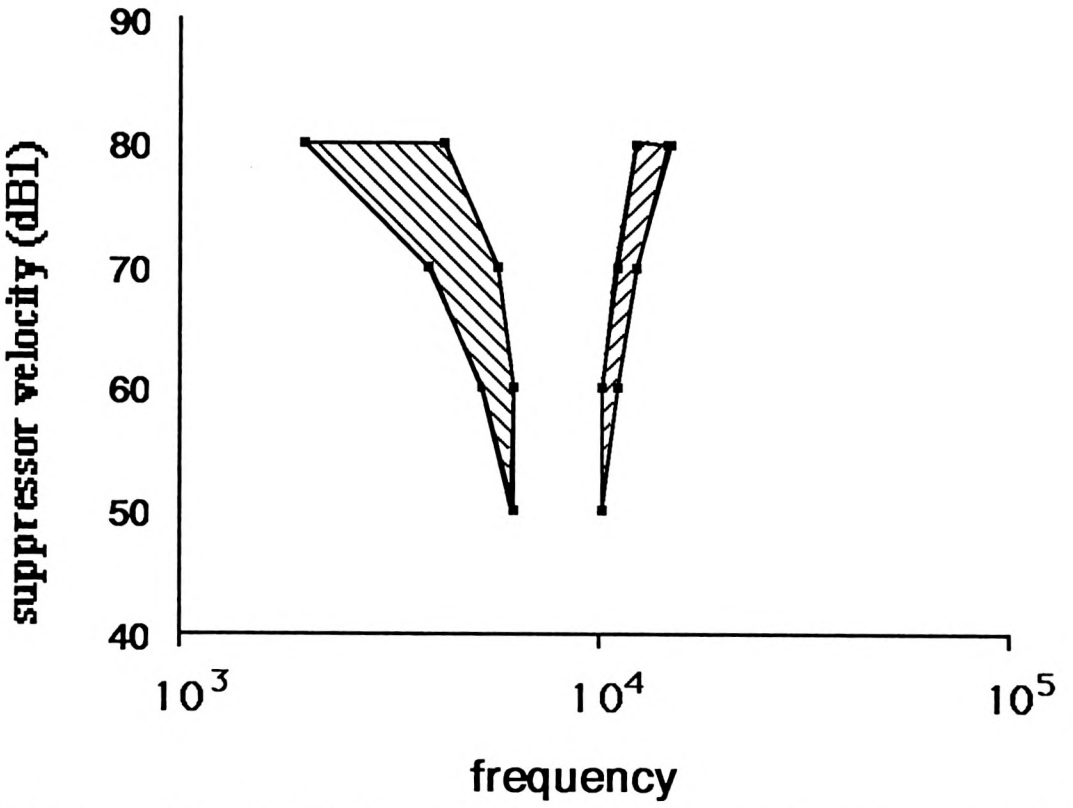

FIGURE 5 Two-tone inhibition at the output of a filter with best frequency (BF) of 2 kHz. The probe tone at BF was held constant at 40 dB

dB1. This example has been chosen to be as closely comparable to the investigation of Kim *et al* (1980). They presented two tones simultaneously and recorded auditory nerve events from a range of fibres having different best frequencies. A Fourier transform was applied to the period histograms for each fibre. Figure 6 presents the Fourier transform value for four frequencies; f1, f2, f2-f1 and 2f1-f2 at a range of estimated positions along the simulated basilar membrane. The latter two frequencies represent distortion products which we might expect to be present.

The cubic difference tone (2f1-f2) is clearly present at the location of its best frequency. The difference tone is also present but much weaker relative to the other components. Note that, unlike Kim *et al,* we have not normalised the Fourier transform

Comments

The nonlinear filtering has achieved many of our original objectives and looks to be well placed to operate as a front end for a peripheral auditory computational model. There is much room for further fine tuning of the system, but we are confident that the model has many useful features in the application areas for which it is intended. The digital filterbank supplied to us is fast in operation. The compression routines and the need to pass through the filters

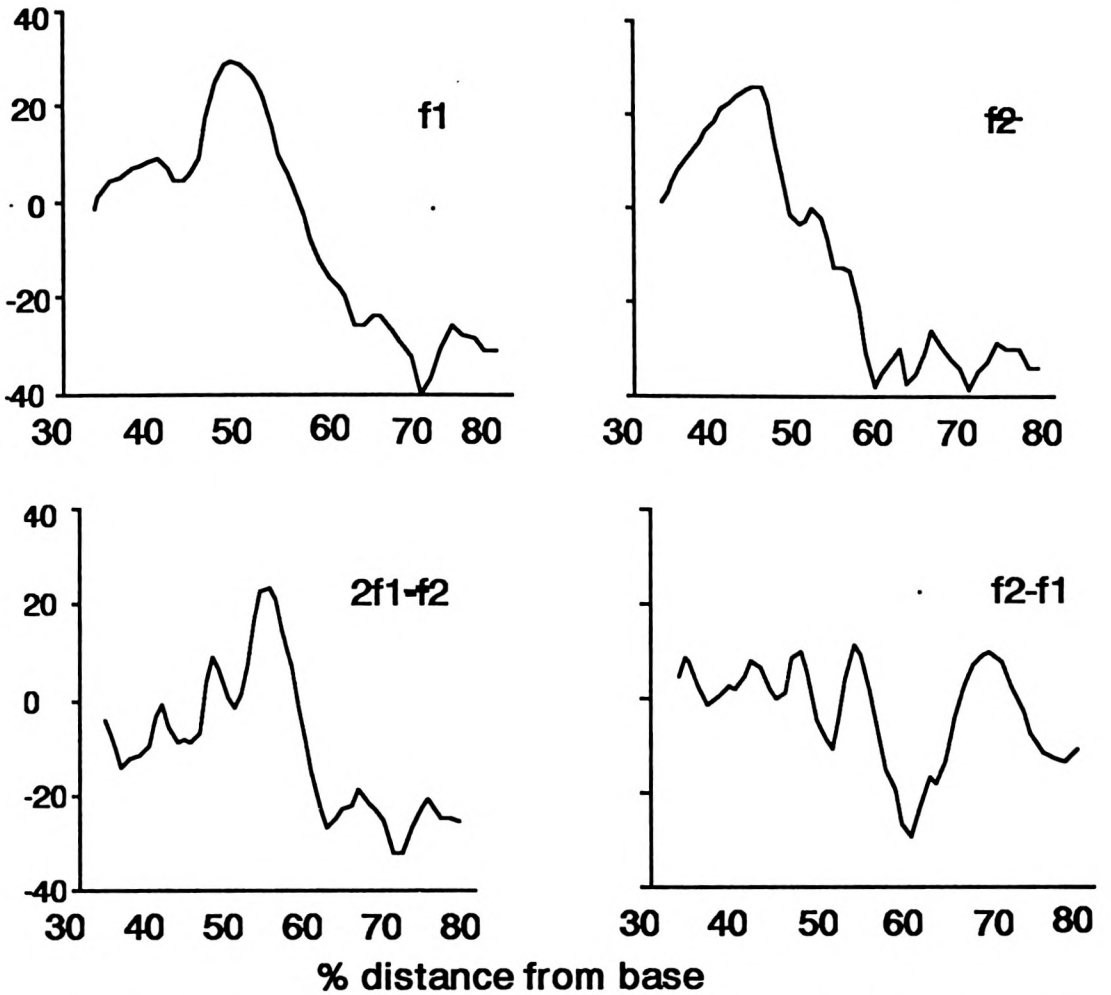

FIGURE 6 Simulation of Kim *et al's* (1980) investigation. The x-axis shows the per cent distance along the basilar membrane from the stapes. The y-axis shows the Fourier transform coefficient at the frequency indicated. 2f1-f2 (1550 Hz) is the cubic difference distortion product and f2-f1 (620 Hz) is the difference tone.

twice means that this processing stage is about three times slower than a linear version. Nevertheless, processing time is far from prohibitive and, after optimisation should be even more acceptable.

The process of parameter optimisation continues for the present. In particular, we would like to be able to simulate the shift in filter best frequency as stimulus level is raised.

Our model has many fundamental similarities with the BPNL (bandpass nonlinear) model (see Duifhuis, 1976), although there are important differences, In our model the signal is filtered, is then compressed and then passed through a second filter in much the same way as the BPNL model. Many of the properties of the model can be ascribed to this structural similarity. Of course, the BPNL system has filters of different widths and the signal outputs from its first set of filters are not combined before being fed into the second set of filters. This sharing of compressed filter-output before the second filter stage is responsible for allowing distortion products to find their way into remote filters.

The model is essentially neutral over the issue of whether the system is active or passive. The compression function would represent an amplifier if the parameter *a* were greater than one. The model demonstration described here used a value of 0.5 for this parameter making this implementation passive.

Acknowledgements

Much background advice was given by Alan Palmer and Ian Winter at the Institute of Hearing Research, Nottingham, UK. The digital filters supplied by Roy Patterson and John Holdsworth were, of course, an important contribution. Early versions of the model were run using a digital filter bank supplied by Martin Cooke of Sheffield University, UK. This work was supported by a grant from the Science and Engineering Research council.

References

Duifhuis, H. (1976) 'Cochlear nonlinearity and the second filter', J. Acoust. Soc. Am., 59, 408-423.

Johnstone, B.M., Patuzzi, R. and Yates, G.K. (1986) 'Basilar membrane measurements and the travelling wave,' Hearing Research, 22, 147-153.

Kim, D.O., Molnar, C.E. and Mathews, J.W. (1980) 'Cochlear mechanics: Nonlinear behaviour in two-tone responses as reflected in cochlear-nerve-fibre responses and in ear-canal sound pressure,' J.Acoust. Soc. Am. 67, 1704-1721.

Miller, M.I. and Sachs, M.B. (1983) 'Representation of stop consonants in the discharge patterns of auditory nerve fibres' J. Acoust. Soc. Am., 74, 502-517.

Meddis. R., Hewitt, M.J. and Shackleton, T.M. (1990) 'Implementation details of a computational model of the inner hair-cell/auditory-nerve synapse,' J. Acoust. Soc., Am. 87, 1813-1818.

Patterson, R.D. and Moore, B.C.J. (1986) 'Auditory filters and excitation patterns as representations of frequency resolution', in Frequency Selectivity in Hearing, ed. Moore, B.C.J. Academic, London.

Robles, L., Ruggero, M.A. and Rich, N.C. (1986) 'Basilar membrane mechanisms at the base of the chinchilla cochlea. I input-output functions, timing curves and response phases,' J. Acoust. Soc. Am. , 80, 1364- 1374

Sachs, M.B. and Kiang, N.Y.S. (1968) 'Two tone inhibition in auditory nerve fibers,' J. Acoust. Soc. Am., 43, 1120-1128.

Schouten, J.F., Ritsma, R.J. and Cordozo, B.J. (1962) 'Pitch of the residue', J. Acoust. Soc. Am. 34, 1418-1424.

Zwislocki, J.J. (1980) 'Five decades of research on cochlear mechanics,' J. Acoust. Soc. Am. 80, 1364-1374.

LEVEL DEPENDENCE OF THE LATENCY OF COCHLEAR TRANSIENTS

Stephen T. Neely

Boys Town National Research Hospital
555 North 30th Street, Omaha, NE 68131, USA

Introduction

An important consequence of the fact that cochlear mechanics are nonlinear is that the latency of the auditory nerve response to transient sounds is level dependent. Specifically, the latency of the neural response decreases as the sound level increases. The *cochlear component* of the latency of human auditory brainstem responses (ABR) to tone-burst stimuli has been shown to consistently decrease by about 38% for every 20 dB increase in the level of the stimulus (Neely *et al.*, 1988). Moreover, this consistent latency decrease with level holds over a wide range of tone-burst frequencies and intensities.

The level dependence of the latency of cochlear transients can be simulated in an active, nonlinear model of cochlear mechanics by applying a saturating nonlinearity to the feedback force associated with outer hair cells (Neely, 1989). The reason that this nonlinearity in the model causes the latency to vary with level in the same manner as observed in the human ABR data is not obvious. It must be that either (1) the *place* along the cochlear partition associated with the generation of the neural response changes with stimulus level or (2) the *velocity* of the transient signal along the cochlear partition varies with level.

In this paper, we examine how the cochlear place and velocity change with level with the objective of determining which has the greater influence on the latency of the neural response. The model results presented here suggest that the primary reason for the level dependence of the neural response is an increase in cochlear velocity with level.

Methods

Tone-burst stimuli were presented to an active, nonlinear, time-domain model of cochlear mechanics. The tone-bursts were Blackman-windowed tones at 4 frequencies (0.5, 1, 2, and 4 kHz) and 4 levels at each frequency (20, 40, 60, and 80 dB peSPL). The stimulus level is specified as the peak pressure at the eardrum in decibels *re* 28.28 μPa. The model response to each of the 16 stimuli was computed for 20 msec beyond onset of the stimulus.

The model equations and mathematical notation generally follow that of Neely and Kim (1986). A change was made in the representation of cochlear fluid mass in order to

simulate the decrease in scala height from base to apex. This modification improved the coupling of the cochlea to the middle ear, but did not significantly affect the latency of cochlear responses.

In order to facilitate comparison of model results with human ABR data, the model parameters were chosen so that the frequency-to-place map along the cochlear partition would be similar to a human cochlea. A time-domain formulation of the model equations was used so that the parameter controlling the force generated by the outer hair cells could vary with time to simulate a saturating nonlinearity.

Two overall measures of the model's response were recorded at each time step: (1) the locus of mechanical input to the inner hair cells (LOMI) was defined as the center of motion along the cochlear partition at each point in time; (2) the whole nerve response (WNR) was defined as the sum of the output of all inner hair cells at each point in time. These overall measures are described in more detail below.

FLUID MASS

A one-dimensional (transmission line) approximation of cochlear fluid mechanics can be written as

$$\frac{d^2}{dx^2} P_d(x) = \frac{2\rho}{H} \ddot{\xi}_p(x) \tag{1}$$

where P_d is the difference in pressure across the cochlear partition (CP), ξ_p is the average displacement across the width of the CP, H is the height of the scalae, and ρ is the density of the fluid. The dots above ξ_p indicate derivatives with respect to time. A finite-difference approximation of the spatial derivative in x results in the following equation

$$2P_d(x) - P_d(x-\Delta) - P_d(x+\Delta) = -\frac{2\rho\Delta^2}{H} \ddot{\xi}_p(x) \tag{2}$$

where $\Delta = L/(N-1)$ is a small distance along the CP over which the mechanical properties of the cochlea are lumped as a single section.

Equation (1) was derived with the assumption of constant scala height; however, the fact that the scala height decreases from base to apex has been shown to have an important influence on cochlear input impedance (Puria and Allen, 1990; Shera and Zweig, 1990). The decrease in scala height causes the effective fluid mass to increase from base to apex. In this lumped-element, transmission-line representation of the cochlea, we can identify the fluid mass as

$$m_f = \frac{2\rho\Delta^2}{H} . \tag{3}$$

The effect of decreasing scala height can be approximated by making m_f an exponentially

TABLE I. Model parameter values (cgs units).

$k_1(x) = 4 \cdot 10^8 e^{-3x}$ (dyn · cm^{-3})	$L = 3.5$ (cm)
$c_1(x) = 960 e^{-1.4x}$ (dyn · sec · cm^{-3})	$H = 0.1$ (cm)
$m_1(x) = 0.004$ (gm · cm^{-2})	$W = 0.1$ (cm)
$k_2(x) = 2 \cdot 10^8 e^{-3.2x}$ (dyn · cm^{-3})	$d_m = 10^{-7}$ (cm)
$c_2(x) = 2000 e^{-1.4x}$ (dyn · sec · cm^{-3})	$\rho = 1$ (dyn · cm^{-3})
$m_2(x) = 0.037$ (gm · cm^{-2})	$b = 1$
$k_3(x) = 2.25 \cdot 10^8 e^{-3.2x}$ (dyn · cm^{-3})	$g = 1$
$c_3(x) = 0$	$N = 409$
$k_4(x) = 4.5 \cdot 10^8 e^{-3.1x}$ (dyn · cm^{-3})	
$c_4(x) = 0$	

increasing function of x

$$m_f = \frac{2\rho\Delta^2}{H} e^x . \tag{4}$$

The model results presented in this paper use Eq. (4) to represent the fluid mass. This improves the coupling of the cochlea to the middle ear in the model by decreasing the reactive (imaginary) component of the cochlear input impedance at low frequencies. This does not, however, significantly affect the latency of cochlear transients.

PARTITION IMPEDANCE

The fluid pressure difference P_d and partition displacement ξ_p are also related by the micromechanics of the cochlear partition. Two mechanical degrees-of-freedom are represented in the partition mechanics within each lumped section, so that the fluid pressure difference across the cochlear partition is related to the velocity of the cochlear partition by a partition impedance Z_p

$$P_d(x) = Z_p(x)\dot{\xi}_p(x) \tag{5}$$

$$Z_p = (g/b)\,[Z_1 + (Z_2(Z_3 - \gamma Z_4))/(Z_2 + Z_3)] \tag{6}$$

where $Z_1 = m_1 s + c_1 + k_1/s$, $Z_2 = m_2 s + c_2 + k_2/s$, $Z_3 = c_3 + k_3/s$, and $Z_4 = c_4 + k_4/s$ are impedance functions specified in the frequency domain, $s = i\omega$. The term Z_4 in the partition impedance represents a feedback force from the outer hair cells (OHC), implementing the hypothetical *cochlear amplifier*. The model parameter values are listed in Table I. The parameter γ controls the magnitude of the influence of the cochlear

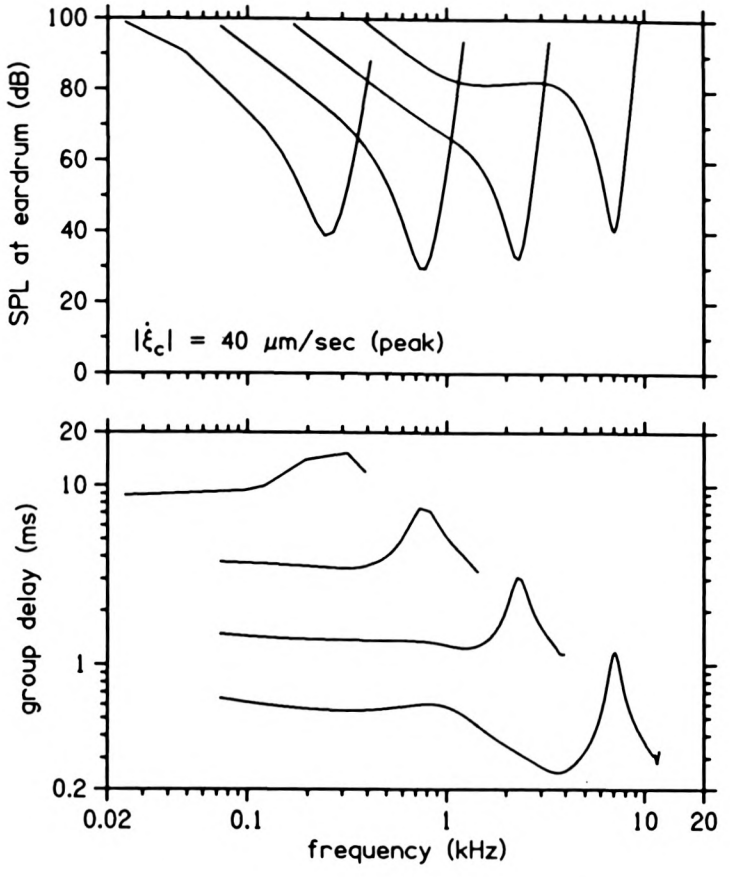

FIGURE 1 Iso-velocity tuning curves from the linear, time-domain model. The stimulus was a wide-band click presented to a simple earphone and coupler model. The linear, time-domain model response was computed for 40 msec beyond onset of the stimulus. The hair-cell velocity $\dot{\xi}_c$ at four places (corresponding to 20, 40, 60 and 80 percent distance from the base) was Fourier transformed along with the pressure at the eardrum to obtain the curves in this figure. In the upper panel the curves indicate the pressure needed at the eardrum to elicit a criterion velocity $\dot{\xi}_c$ = 40μm/sec . The lower panel shows the group delay of hair cell velocity relative to the eardrum pressure at the same four places. Group delay is defined as minus the slope of the phase with respect to frequency.

amplifier; it is constant in the frequency-domain and linear, time-domain formulations of the model and varies with time in the nonlinear, time-domain model.

For a given set of model parameters (and appropriate boundary conditions), we can use these equations to solve for P_d and ξ_p in either the frequency or time domain. For comparison with experimental data, we also identify the shearing displacement between the tectorial membrane and reticular lamina as

$$\xi_c = (g/b)\,[Z_2/(Z_2+Z_3)]\,\xi_p \tag{7}$$

The displacement ξ_c represents the mechanical input to the outer hair cells and the velocity $\dot{\xi}_c$ represents the mechanical input to the inner hair cells. Velocity was chosen as the input to inner hair cells because the iso-velocity tuning curves looked more like typical cat neural- threshold tuning curves than did the iso-displacement tuning curves.

The iso-velocity tuning curves in Fig. 1 were obtained by taking Fourier transforms of 40 msec impulse responses with $\gamma = 1$ in the time-domain model. This represents the linear version of the model. The remaining figures in this paper show "nonlinear" model results for the case in which γ was a time-varying parameter

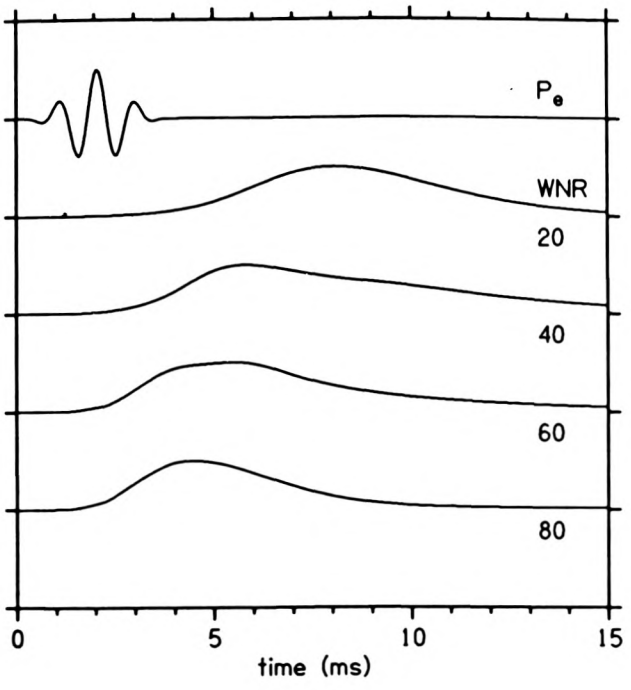

FIGURE 2 Pressure at eardrum P_e and whole-nerve response (WNR) to 1-kHz tone-bursts and four sound pressure levels. The numbers in the figure indicate the peak sound pressure at the eardrum in decibels re 28.28 μPa (peSPL). Similar results were obtained at 0.5, 2, and 4 kHz. Note that the latency of the WNR decreases as the level of the stimulus increases. The vertical scale in this figure is arbitrary. Each trace was normalized separately to the same maximum value.

$$\gamma = \begin{cases} 1, & |\xi_c| \le d_m \\ d_m/|\xi_c|, & |\xi_c| > d_m \end{cases} \tag{8}$$

making the model results dependent on the level of the stimulus. This definition of γ is equivalent to saturation of the OHC feedback force for displacements ξ_c greater than d_m (Neely, 1989).

MEASURES OF MODEL RESPONSE

The transient response within the cochlea moves as a wave packet. The locus of mechanical input to the inner hair cells (LOMI) is a measure of the location of the transient signal along the cochlear partition that was designed to track the center of the region where $\dot{\xi}_c$ was greatest. It was computed by weighting each place by the value of $\dot{\xi}_c^2$ at that place. This definition was convenient for assigning a single place to the transient signal at each time step, but is not critical to the conclusions about cochlear latency.

The whole nerve response (WNR) was computed by applying $\dot{\xi}_c$ to a simple inner hair cell model consisting of a half-wave rectifier and "leaky" integrator at each position along the cochlear partition. The time-constant of the integrator was 0.5 msec. The outputs of all integrators were summed (with equal weighting) to produce the WNR.

Results

An example of the time course of the WNR is shown in Figure 2 for the 1-kHz tone-burst at each of the 4 levels. The latency of the WNR can be measured either to (1) the peak

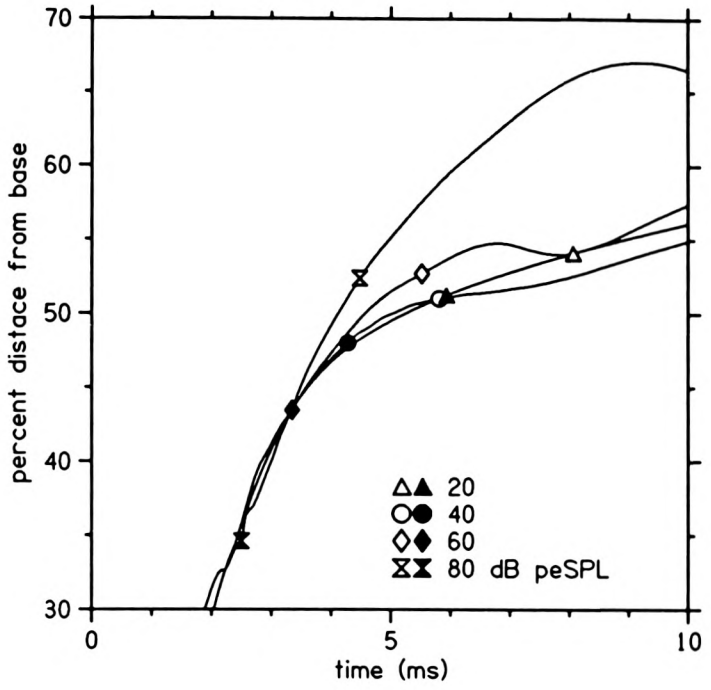

FIGURE 3 Locus of mechanical input to the inner hair cells (LOMI) and whole nerve response (WNR). The lines in this figure indicate the place at which the mechanical input to the outer hair cells is greatest based on using ξ^2_c as a weighting factor. The closed symbols indicate the time of WNR onset and the open symbols indicate the time of WNR peak. Note that the WNR peak latency at 40 dB (open circle) does not follow the trend of the other open symbols. This is due to the flattened shape of the peak of the WNR shown in Figure 2.

(maximum value) of the WNR or (2) the onset (maximum positive slope) of the WNR. Both the peak and onset latency of the WNR clearly decrease in Figure 2 as the level of the stimulus is increased. At the lowest and highest levels, the onset of the WNR precedes the peak by about 2 msec. The time difference between the onset and the peak of the WNR is largely accounted for by the difference in time between the onset and peak of the stimulus which is also 2 msec for the 1-kHz tone-burst. The onset of the WNR is probably a better measure of cochlear latency.

The latency of the WNR varies with level primarily because the time-course of the LOMI varies with level. The LOMI describes the center of activity along the cochlear partition at each point in time. In Figure 3, we see that the LOMI reaches the 1-kHz characteristic place (about 55% distance from the stapes) faster at the 80 dB level than at the 20 dB level. The velocity of the LOMI (observed as the slope of the lines in Figure 3) becomes level dependent at about 45% distance from the stapes.

We can define the place along the cochlear partition primarily responsible for the generation of the WNR as the location of the LOMI when the WNR reaches its peak value. For the 1-kHz tone-burst, this place is at 52.4% when the level is 80 dB and 54.1% when the level is 20 dB. This small change in place accounts for only a small part of the total peak latency change. Most of the change in the WNR peak latency is due to the change in velocity of the LOMI.

At each of the four levels the WNR onset latency decreases with increasing level except in one case: the 20 dB level at 4 kHz. The mechanical input to the outer hair cell may have been too small in this case to be affected by the saturating nonlinearity. The onset latency of the WNR is shown in Figure 4 for each of the 16 stimuli. The corresponding latency for the human cochlea at the same 4 levels based on analysis of human ABR data (Neely, *et al.* 1988) is represented by the dotted lines in Figure 4. In general, dependence of the WNR onset latency on level and frequency is similar to the cochlear component of the human ABR latency.

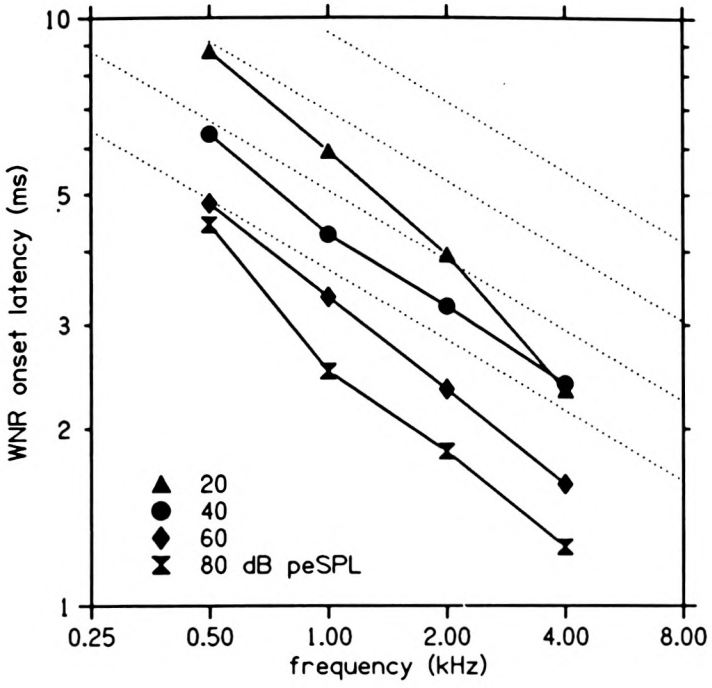

FIGURE 4 Frequency and level dependence of the WNR onset latency. The onset of the WNR was defined as the point in time corresponding to the maximum positive slope of the WNR. The dotted lines show the corresponding latency values for the human cochlea at the same four levels. These lines are based on extracting the cochlear component from human ABR latency data (Neely, *et al.*, 1988).

Discussion

COMPARISON WITH EXPERIMENT

The latency of the onset of transient responses recorded in single auditory nerve fibers also decreases as the level of the stimulus increases; however, the latency decrease may appear to be discontinuous. Post-stimulus time (PST) histograms recorded from single nerve fibers typically show several distinct peaks (Kiang, *et al.*, 1965). The latency of each individual peak does not change much with stimulus level, but earlier peaks observed at high levels are not present al low level. Thus, the onset of the transient response decreases abruptly as the stimulus level increases whenever an earlier peak becomes large enough to be observed. Similar behavior can be seen in the model results for the simulated neural response, but are not presented in this paper. The onset latency of WNR response shows more continuous variation with stimulus level because the distinct peaks seen in the response at a single place are not seen when the responses from all places are combined.

The estimates of human cochlear latency represented by the dotted lines in Figure 4 were obtained by subtracting 5 msec from measurements of the latency of ABR wave V using tone-bursts. This 5 msec is attributed to neural synaptic and propagation delay which is relatively independent of stimulus intensity and frequency (Neely, *et al.*, 1988). The model parameters could be adjusted to improve the agreement between the model results and the human latency data. In particular, the fact that the slopes of the lines in Figure 4 are greater for the model than for the human data suggests that the stiffness of the cochlear partition in the model should decrease less from base to apex.

CONCLUSIONS

The most important observation in this paper is that the latency of the WNR decreases with level mostly because the transient response moves faster along the cochlear partition near the characteristic place (for the frequency of the tone-burst) as the level increases. The

change in "the place primarily responsible for generation of the WNR" contributes much less to the change in latency than does the change in velocity of the LOMI. The fact that the frequency and level dependence of the WNR onset latency resembles that of the human ABR data suggests that this explanation may also apply to the human cochlea.

Because the cochlear velocity is determined primarily by the stiffness of the cochlear partition, these results also suggest that the stiffness of the cochlear partition is nonlinear and varies significantly with level in the vicinity of the characteristic place.

FUTURE DIRECTIONS

The method used to integrate the time-domain formulation of the equations is the same as used by Allen and Sondhi, 1980. Using a bilinear transformation of the frequency domain formulation to obtain the time-domain formulation would improve the correspondence between the frequency-domain and time-domain solutions and also improve the computational efficiency (Michel, 1989).

The nonlinear model requires that the time-varying parameter γ provide essentially a hard-limiting function for displacements greater than 1 nm. This displacement is small compared with displacements at the threshold of hearing and may need to be increased. Other more gradual limiting functions should be investigated, such as $\gamma = 1/(1 + (\dot{\xi}_c/d_m)^2)$.

Recent observations of outer-hair-cell motility suggests that these cells are intrinsically tuned to a place appropriate frequency (Brundin, *et al.*, 1989). The model equations describing the micromechanics of the cochlear partition could be reformulated to reflect this observation.

References

Allen, J.B. and Sondhi, M.M. (1979) A cochlear mechanical model of transduction. In: Psychophysical, physiological, and behavioral studies in hearing (Eds: van den Brink, G. and Bilsen, F.A.) Delft Univ. Press, Netherlands, pp 85-95.

Brundin, L., Flock, Å., Canlon, B. (1989). Sound induced motility of isolated outer hair cells is frequency-specific. Nature **342**, 814-816.

Kiang, N.Y.-S., Wanatabe, T., Thomas, E.C., and Clark, L.F. (1965). Discharge patterns of single fibers in the Cat's Auditory Nerve. M.I.T. Research Monograph No. 35., Technology Press, Cambridge, Mass., pp 32-43.

Michel, D. (1989) A model for peripheral auditory preprocessing. In: Cochlear Mechanisms (Eds: Wilson, J.P. and Kemp, D.O.) Plenum Press, London, pp 425-434.

Neely, S.T. (1989) Transient responses in an active, nonlinear model of cochlear mechanics. In: Cochlear Mechanisms (Eds: Wilson, J.P. and Kemp, D.O.) Plenum Press, London, pp 106-113.

Neely, S.T. and Kim, D.O., (1986) A model for active elements in cochlear biomechanics. J. Acoust. Soc. Am. **79**, 1472-1480.

Neely, S.T., Norton, S.J., Gorga, M.P., and Jesteadt, W. (1988) Latency of auditory brainstem responses and otoacoustic emissions using tone-burst stimuli. J. Acoust. Soc. Am. **83**, 652-656.

Puria, S. and Allen, J.B. (1990) A parametric study of cochlear input impedance. J. Acoust. Soc. Am. (submitted).

Shera, C.A. and Zweig, G. (1990) A symmetry suppresses the cochlear catastrophe. (in preparation).